An electrochemical investigation on the mechanisms of interfacial interactions of a xanthate collector on PGM surfaces in the presence of ions

Lucia Dzinza

A thesis submitted to the Faculty of Engineering and the Built Environment, University of Cape Town, in fulfilment of the requirements for the degree of Doctor of Philosophy in Chemical Engineering

February 2023

Declaration

I know the meaning of plagiarism and I declare that the work on which this thesis is based is my own work, except where acknowledgements indicate otherwise. Neither part nor the whole document has been submitted for any other degree in this institution or any other university. I, therefore, authorise the University to reproduce for the purpose of research either the whole or any portion of the contents in any manner whatsoever.

Signed by candidate

Lucia Dzinza

10 February 2023

Acknowledgements

First and foremost, I would like to express my profound gratitude to my main supervisor, Associate Professor Kirsten Corin. To say 'thank you' is an understatement. Had it not been for you, I wouldn't have taken up this doctorate degree, we both know that for sure. I had made up my mind, it was either taking up a doctorate degree with you or looking for a job after obtaining my master's degree. Instead, you chose to trust me with this exciting opportunity. You have been there every step of the way, when the going got tough, you have been extremely understanding and made sure I was in a better space to get going. You made sure I walked on the right path in my research project and provided me with excellent guidance. Your brilliant management skills are out of this world. Nothing can dim the light that shines from within you.

A special thanks to my co-supervisor, Dr Margreth Tadie. For always being there when I needed your support. For showing me the light in electrochemistry when I felt I was hitting against a wall. For responding to all, if I may say 'all' my messages, no matter what time of the day it was. For opening up my mind when I felt it had reached a limit. For your sisterly love. Your great support will never be forgotten.

I would like to give my deepest appreciation to Jordy Dinga. Thank you for going out of your way to assist me with the electrochemistry equipment in times that I faced challenges with our CMR equipment. Thank you for making time to clarify on some electrochemistry sections that I needed help with. In addition, I would like to thank Kathija Shaik, for being always willing to ask your supervisor, on my behalf, for any electrochemistry equipment that I needed. I would also like to extend my thanks to Dr. Thandazile Moyo, for making time to respond to and discuss some aspects of electrochemistry.

I must thank Shireen Govender, for being proactive in her duties as the CMR laboratory manager. You made sure I was adequately equipped for the smooth running of my research. Thanks to Lorraine Nkemba for being a great lab mate and ensuring that I had all I needed in the lab to get going with my research. I will surely miss those chats. Thank you, Kenneth Maseko, for ensuring that my equipment was locked up safely without being tempered with.

I would like to highlight three exceptional people in my life. My mom, Margaret Dzinza and my big sisters, Irene Dzinza and Enelesi Dzinza. You have been my biggest support system. Every time I fell you never deserted me, you reached out to me with your gentle hands, made sure that I

got back on my feet, and I was ready to flourish. Mum, thank you for not giving up on us even when the going got tough in life. Thank you for educating us and for helping us to reach our dreams. I wish dad was here to see me wrap up my doctorate degree. This would have made him happy. He will always occupy a special place in my heart. Thank you, dad, for your precious contribution to my life. Irene, you know I run out of words every time I want to explain how you have immensely contributed to the success of my life. Thank you for the invaluable support, advice and guidance that has shaped me into the individual that I am today. To my best friend, Enelesi, thank you for your unconditional love, you have given me room not to only approach you as my sister but as my best friend. Thank you for giving me the shoulder to lean on. Most of all thank you for your amazing support.

To my brother, Cliff Dzinza. Thank you for the career guidance and brotherly love. To Beeslay Dzinza, thank you for the brotherly love.

My life would not be the same if it hadn't been for my three roses, Talicia Nyausaru, Charlcy Nyausaru and Chardley Nyausaru. I will always refer to you all as my pillars of strength. I love you so much and thank you for giving me an amazing motherly role. You gave me enough strength to pull through my PhD journey.

To my husband Charles, thank you for your undying support.

I would like to give my deepest appreciation to the South African Minerals to Metals Research Institute (SAMMRI) and the Department of Science and Technology (DST) for their financial support. It was an honour to be one of the chosen recipients of these two scholarships. I am indebted to the funders for providing me with financial independence throughout my PhD journey.

Finally, but most importantly, I would like to thank the Almighty God for the many blessings and for giving me the strength to conquer adversity.

List of publications and conferences

An electrochemical investigation on the mechanisms of interfacial interactions of a xanthate collector on PGM sulphide mineral surfaces in the presence of electrolytes. L. Dzinza, M. Tadie and K.C. Corin. *Paper 135*. IMPC Asia-Pacific Conference 2022, Melbourne, Australia and online, Online-Oral presentation*: XXXI International Mineral Processing Congress Proceedings,* 22 - 24 August 2022.

An electrochemical investigation on the mechanisms of interfacial interactions of a xanthate collector on PGM sulphide mineral surfaces in the presence of electrolytes. L. Dzinza, M. Tadie and K.C. Corin. SAIMM (Mine-Impacted Water Conference), Online-Oral presentation, 12 – 13 October 2022.

Synopsis

Water is a vital transport and process medium used in mineral processing. Fresh water is substantially utilized as an ideal flotation media in the froth flotation process (Rao et al., 2016). However, the mining sector is impelled to save on the consumption of fresh water and reduce waste discharge owing to limited freshwater supply (Ridoutt and Pfister, 2010), stringent environmental regulations (Amezaga et al., 2011) and the increase in water demand among multiple users (Rijsberman, 2006). To improve water efficiency, the use of impure primary water supplies and process water recycling has been implemented in flotation circuits. Generally, the recycling of process water is executed from tailings dams, thickener overflows, and dewatering and filtration units. The recycling of process water has been considered to be advantageous as it reduces freshwater consumption, lowers waste discharge and reduces volumes of reagents required in flotation circuits (Muzenda, 2010). However, recycled process water has been found to exhibit increased concentrations of typical contaminants such as colloidal matter, metal ions, sulphates, sulphites, thiosalts, calcium, magnesium, sodium, potassium and residual floatation reagents. These contaminants affect the process water quality, which plays a vital role in flotation efficiency.

Though a significant amount of work has been done on the effects of water quality on the flotation of valuable minerals, many studies have focussed on base metal sulphides and the use of bench-scale techniques. Literature speculates that ions in process water hinder the interaction between xanthate collectors and valuable minerals, hence, contributing to a decrease in flotation recoveries (Kirjavainen et al., 2002, Boujounoui et al., 2015). The findings in literature have been deduced without an understanding of the underlying mechanisms of interaction between xanthate collectors and mineral surfaces in the presence of ions. Accordingly, literature still holds a lack of understanding on how ions affect the adsorption of xanthate collectors on mineral surfaces. This study, therefore, seeks to unpack the underlying mechanisms of interfacial interactions between ions with PGMs and the subsequent adsorption kinetics of a xanthate collector.

This study investigated the effects of Ca^{2+}, Mg^{2+}, SO_4^{2-}, $S_2O_3^{2-}$ and Na^{+} ions at increasing ionic strength, on the adsorption of SIBX on synthetic PdS and $PdTe_2$ minerals. The selection of the minerals was based on the need to give an insight into the differences in reactivities of the very floatable minerals (PdS) and the difficult-to-float minerals ($PdTe_2$), with SIBX in the presence of ions. The mechanisms in question were examined by electrochemical techniques at laboratory scale. Rest potential measurements were used to determine the interactions of ions and/or SIBX

on the PGM surfaces. Cyclic voltammetry was employed to determine the redox reactions that occur on the PGM surfaces in the absence and presence of ions and SIBX. Ultimately, electrochemical impedance spectroscopy was used to demonstrate the adsorption mechanisms of SIBX in the absence and presence of the investigated ions.

The rest potential measurements generally displayed an increase in the extent of interactions between the investigated ions with the palladium minerals, with an increase in ionic strength. An inverse relationship was exhibited on the extent of interactions between the ions and PdS, and the extent of interaction between SIBX and PdS. Divalent ions displayed higher interactions with the palladium minerals than the monovalent ions investigated. All salts were found to demonstrate a decrease in the rest potential for PdS at all concentrations except for $MgSO_4$, which increased the rest potential at 5 SPW and 10 SPW. Final rest potentials for most conditions were observed to be above the equilibrium potential of dixanthogen formation except for $Na_2S_2O_3$ at 3 SPW, 5 SPW and 10 SPW, and $CaCl_2$ at 1 SPW. Dixanthogen formation was most likely favoured on PdS for the conditions with final rest potentials above the equilibrium potential of dixanthogen formation.

With regard to the $PdTe_2$ mineral, it was found that most ions enhanced the interaction between SIBX and $PdTe_2$. Contrary to the findings of PdS, it was found that most salts exhibited an increase in rest potential on $PdTe_2$ except for $Na_2S_2O_3$. Final rest potentials for all conditions investigated were observed to occur above the equilibrium potential of dixanthogen formation except for $Na_2S_2O_3$ at all ionic strengths, $MgCl_2$ at 10 SPW and NaCl at ionic strengths of 3 SPW, 5 SPW and 10 SPW. The latter conditions show that the formation of a metal-xanthate on $PdTe_2$ was favoured. Generally, for both minerals, NaCl displayed the least interaction.

It was found that increasing the ionic strength of salts, generally decreased the rate of dixanthogen formation on PdS. On the contrary, SIBX interacted more with $PdTe_2$ at an increase in the ionic strength of salts. This observation favoured the formation of either a metal-xanthate or dixanthogen at a slower rate.

Additionally, it was determined that the adsorption of ions investigated occurred via interfacial charge transfer kinetics, where an ion exchange mechanism has been proposed in the case of the divalent anions. In the case of divalent cations, it was presumed that the ions dissociate in solution and precipitate upon their interaction with the palladium minerals to hydroxides and/or carbonates. This study has shown that the mechanism of adsorption of ions on palladium minerals is heavily influenced by the type of mineral surface onto which the ions adsorb. The extent of

interaction of ions with palladium minerals together with their corresponding oxidation products can be determined by the mineral type and the salt type and its ionic strength.

Moreover, it was denoted that an electrochemical system that consists of salts at the palladium mineral surfaces can best be described by a resistor, R_s in series with a parallel circuit of a capacitor, C_{dl}, representing the electrical double layer and a resistor indicating R_{ct}. For an electrochemical system with both salt and SIBX, it has been surmised that an equivalent circuit consisting of a resistor, R_s, in series with a parallel circuit of a capacitor, C_c, representing a coating layer formed on the palladium surfaces as a result of the adsorption and oxidation od SIBX and a capacitor, C_{dl}.

This work has shown that the mechanisms of interactions between xanthates and PGMs in the absence and presence of salts can be successfully determined using electrochemical techniques. An understanding of such mechanisms developed from the interactions of Ca^{2+}, Mg^{2+}, SO_4^{2-}, $S_2O_3^{2-}$ and Na^+ ions with SIBX on PGM minerals will help alleviate flotation problems caused by the troublesome ions. An understanding of the mechanisms proposed by this study will act as a diagnostic tool for developing flotation strategies that will maximize flotation recoveries where water quality is concerned.

Abbreviations and Nomenclature

AC	Alternating current
I_0	Amplitude of current
$CaCO_3$	Calcium carbonate
$Ca(Cl)_2$	Calcium chloride
$Ca(OH)_2$	Calcium hydroxide
Ca^{2+}	Calcium ion
C	Capacity of double layer
C_d	Capacity of diffuse layer
C_i	Capacity of stern layer
R_{ct}	Charge transfer resistance
R_c	Coating resistance
CV	Cyclic voltammetry
^0C	Degrees Celsius
DC	Direct current
$Na_2B_4O_7.10H_2O$	Di-sodium tetraborate decahydrate
X_2	Dixanthogen
C_{dl}	Double layer capacitance
EIS	Electrochemical Impedance Spectroscopy
θ	Fractional coverage
Hz	Hertz
Z_{imag}	Imaginary impedance
Z	Impedance
$Mg(Cl)_2$	Magnesium chloride
Mg^{2+}	Magnesium ion
$MgSO_4$	Magnesium sulphate
$PdTe_2$	Merenskyite
MX	Metal xanthate
μm	Micrometer
mg/L	Milli grams per litre

mV	Milli volts
mV/s	Milli-volts per second
M	Molarity
PdO	Palladium oxide
$PdCO_3$	Palladium carbonate
Ppm	Parts per million
Ø	Phase angle
PGE	Platinum group elements
PGM	Platinum group metals
R_p	Polarization resistance
KCl	Potassium chloride
Z_{real}	Real impedance
E^0	Reduction potential
I_t	Response signal
E_{OCP}	Rest potential/ open circuit potential
Ag/AgCl	Silver/silver chloride
NaCl	Sodium chloride
Na^+	Sodium ion
SIBX	Sodium iso-butyl xanthate
$Na_2S_2O_3$	Sodium thiosulphate
K_{sp}	Solubility product
R_s	Solution resistance
SHE	Standard Hydrogen Electrode
σ_0	Surface charge
ψ_0	Surface potential
SO_4^{2-}	Sulphate ion
SPW	Synthetic plant water
1SPW	Synthetic plant water with ionic strength of 0.0242 M
3SPW	Synthetic plant water with ionic strength of 0.0727 M
5SPW	Synthetic plant water with ionic strength of 0.1212 M
10SPW	Synthetic plant water with ionic strength of 0.2426 M

$S_2O_3^{2-}$	Thiosulphate ion
V	Volts
PdS	Vysotskite
X^-	Xanthate ion

Table of Contents

Declaration i

Acknowledgements ii

List of publications and conferences iv

Synopsis v

Abbreviations and Nomenclature viii

List of Tables xvii

List of Figures xviii

1. Introduction 1

1.1 Background 1

1.2 Scope of Study 3

2. Literture review 5

2.1 Geology of the Bushveld Complex 5

2.2 Crystal structures of palladium minerals 7

2.2.1 Palladium Sulphide (Vysotskite) 8

2.2.2 Palladium Telluride (Merenskyite) 9

2.3 Flotation behaviour of PGMs 11

2.3.1 Reactivity and Flotation behaviour of PGM Sulphides 13

2.3.2 Reactivity and Flotation behaviour of PGM Tellurides 18

2.4 Adsorption mechanisms of xanthate collectors on mineral surfaces 21

2.4.1 The influence of xanthate collector and mineral type 25

2.4.2 Adsorption mechanisms of xanthates in PGMs 28

2.5 Mineral- Solution interfaces and the electrical double layer 30

2.6 Effect of ions on the adsorption of xanthate collectors 34

2.7 Electrochemical techniques 36

2.7.1 Rest potential technique 36

2.7.2 Cyclic Voltammetry 39

2.7.3 Electrochemical Impedance Spectroscopy 42

Electrolyte resistance 44

Double layer capacitance 44

Polarization resistance 45

Charge transfer resistance 45

Diffusion 45

2.8 Summary of Literature 49

3. Research Objectives 51

3. 1 Objectives 51

3.2 Key Questions 51

3.3 Hypothesis 51

4. Experimental methods 53

4.1 Validation 53

4.2 Reagents Preparation 53

4.3 Electrochemical measurements 54

4.3.1 Equipment 54

4.3.1 Working electrode preparation 56

4.3.2 Rest Potential measurements 57

4.3.3 Cyclic Voltammetry measurements 57

4.3.4 Electrochemical Impedance Spectroscopy 57

5. Results: Rest Potential Measurements 59

5.1 Validation 59

5.2 Reproducibility 60

5.3 Rest Potential measurements for PdS 62

5.3.1 Effect of $S_2O_3^{2-}$ ions 63

5.3.2 Effect of SO_4^{2-} ions 64
5.3.3 Effect of Mg^{2+} ions 64
5.3.4 Effect of Ca^{2+} ions 64
5.3.5 Effect of Na^{+} ions 65
5.4 Rest Potential measurements for $PdTe_2$ 66
5.4.1 Effect of $S_2O_3^{2-}$ 66
5.4.2 Effect of SO_4^{2-} 67
5.4.3 Effect of Mg^{2+} 67
5.4.4 Effect of Ca^{2+} 67
5.4.5 Effect of Na^{+} 68
5.5 Key Findings 68
6. Results: Cyclic Voltammetry Measurements 70
6.1 Validation 70
6.2 Reproducibility 72
6.3 Voltammograms for PdS 74
6.3.1 Effect of $Na_2S_2O_3$ 74
6.3.2 Effect of $MgSO_4$ 76
6.3.3 Effect of $MgCl_2$ 78
6.3.4 Effect of $CaCl_2$ 80
6.3.5 Effect of NaCl 82
6.3.6 Effect of 1 SPW of salts 84
6.3.7 Effect of 3 SPW of salts 86
6.3.8 Effect of 5 SPW of salts 88
6.3.9 Effect of 10 SPW of salts 90
6.4 Voltammograms for $PdTe_2$ 93
6.4.1 Effect of $Na_2S_2O_3$ 93

6.4.2 Effect of $MgSO_4$ 95
6.4.3 Effect of $MgCl_2$ 97
6.4.4 Effect of $CaCl_2$ 99
6.4.5 Effect of NaCl 101
6.4.6 Effect of 1 SPW of salts 103
6.4.7 Effect of 3 SPW of salts 106
6.4.8 Effect of 5 SPW of salts 109
6.4.9 Effect of 10 SPW of salts 112
6.5 Key findings 115
7. Results: Electrochemical Impedance Spectroscopy 116
7.1 Validation 116
7.2 Reproducibility 117
7.3 EIS for $PdTe_2$ 118
7.3.1 Effect of $Na_2S_2O_3$ 118
7.3.2 Effect of $MgSO_4$ 123
7.3.3 Effect of $MgCl_2$ 128
7.3.4 Effect of $CaCl_2$ 133
7.3.5 Effect of NaCl 137
7.3.6 Effect of salts at 1 SPW 141
7.3.7 Effect of salts at 3 SPW 146
7.3.8 Effect of salts at 5 SPW 150
7.3.9 Effect of salts at 10 SPW 155
7.4 EIS for PdS 159
7.4.1 Effect of $Na_2S_2O_3$ 159
7.4.2 Effect of $MgSO_4$ 164
7.4.3 Effect of salts at 1 SPW 168

7.4.4 Effect of salts at 3 SPW 172

7.4.5 Effect of salts at 5 SPW 176

7.4.6 Effect of salts at 10 SPW 180

7.5 Modelling of EIS data 184

7.6 Key Findings 186

8. Discussion 187

8.1 Reactions of Palladium minerals in the absence of salts and SIBX 187

8.1.1 Reactions of PdS 187

8.1.2 Reactions of $PdTe_2$ 188

8.2 Reactions of Palladium minerals with SIBX 189

8.2.1 Reactions of PdS with SIBX 189

8.2.2 Reactions of $PdTe_2$ with SIBX 190

8.2.3 Surface coverage of SIBX on $PdTe_2$ 192

8.3 Effect of $Na_2S_2O_3$ on adsorption of SIBX on palladium minerals 193

8.4 Effect of $CaCl_2$ on adsorption of SIBX on palladium minerals 197

8.5 Effect of $MgCl_2$ on adsorption of SIBX on palladium minerals 201

8.6 Effect of $MgSO_4$ on adsorption of SIBX on palladium minerals 205

8.7 Effect of NaCl on adsorption of SIBX on palladium minerals 211

8.8 Equivalent circuit 215

8.9 Summary 215

9. Conclusions 219

10. Recommendations 223

References 224

APPENDICES 233

Appendix A 233

Rest potential measurements 233

Appendix B 263

Cyclic voltammetry measurements 263

Appendix C 264

Calculations for surface coverage of SIBX on $PdTe_2$ 264

Appendix D 266

Electrochemical Impedance Spectroscopy: 266

List of Tables

Table 2.1: Vysotskite crystallography 9

Table 2.2: Merenskyite crystallography 10

Table 2.3: Physical characteristics and recovery behaviour of different PGM classes 13

Table 2.4: Correlation between mineral semi-conductor type and collector species 26

Table 2.5: Rest potentials for various minerals. 38

Table 2.6: Relationship between circuit and impedance equivalent values 47

Table 4.1: Cyclic voltammetry parameters 57

Table 4.2: Electrochemical impedance spectroscopy parameters 58

Table 6.1: Key findings for cyclic voltammetry measurements 115

Table 7.1: Key findings for electrochemical impedance results 186

List of Figures

Figure 1.1: Schematic diagram representing scope of this study……4

Figure 2.1: Geological map of the Bushveld Complex ……..6

Figure 2.2: Crystal structure of vysotskite. Sourced from . 8

Figure 2.3: a) Braggite mineral b) Cooperite crystal 9

Figure 2.4: Crystal structure of merenskyite 10

Figure 2.5: a) Merenskyite mineral b) Borovskite 10

Figure 2.6: Percentages of locked and liberated PGMs in samples A and B of UG-2 ore. 12

Figure 2.7: Flotation recoveries for different PGM phases 12

Figure 2.8: Eh-pH diagrams of the system S-O-H 15

Figure 2.9: Eh-pH diagram for the system Pd-S-H_2O 16

Figure 2.10: Voltammograms for PdS in the absence and presence of 6.24×10^{-4} S.E.X collector. 17

Figure 2.11: Eh-pH diagrams of the system Te-O-H 19

Figure 2.12: Generic structure of a xanthate collector 22

Figure 2.13: Solubility product of different metal xanthates 24

Figure 2.14: Voltammograms for a galena mineral surface at a pH of 9.2 in ethyl xanthate 27

Figure 2.15: Dissolution of ferric hydroxide and formation of dixanthogen of a pyrite surface. 28

Figure 2.16: Voltammograms for $PdTe_2$ in the absence and presence of SEX at 6.25×10^{-4} M. 29

Figure 2.17: Voltammograms for PdS in the absence and presence of SEX at 6.25×10^{-4} M. 30

Figure 2.18: Electrical double layer . 31

Figure 2.19: Coordination of calcium, sulphate and thiosulphate ions on a pyrrhotite surface 35

Figure 2.20: Applied potential, where E_S and E_f are switching potentials . 40

Figure 2.21: Cyclic voltammogram resulting from the potential sweep in Figure 2.20. 41

Figure 2.22: Voltammograms for Pd-Bi-Te electrode in 0.05 M $Na_2B_4O_7$ solution. 42

Figure 2.23: Sinusoidal current response in a pseudo-linear system. 43

Figure 2.24: Bode and Nyquist plots . 46

Figure 2.25: Equivalent cell for a single electrochemical cell 47

Figure 4.1: Experimental set-up for electrochemical measurements 55

Figure 4.2: Schematic diagram for the experimental set-up for electrochemical measurements 55

Figure 4.3: Palladium working electrodes (a) PdS b) $PdTe_2$ 56

Figure 5.1: Rest potential measurements for palladium minerals in sodium ethyl xanthate collector. 60

Figure 5.2: Rest potentials for PdS mineral in $MgSO_4$ at 10 SPW 61

Figure 5.3: Rest potentials for $PdTe_2$ mineral in NaCl 62

Figure 5.4: Final rest potentials and changes in rest potentials for PdS 63

Figure 5.5: Final rest potentials and changes in rest potentials for $PdTe_2$. 66

Figure 6.1: Cyclic voltammograms for PtS in aerated solutions in the absence and presence of S.E.X 71

Figure 6.2: Voltammetric response for PdS in the absence and presence of S.E.X. 72

Figure 6.3: Cyclic voltammograms for $PdTe_2$ electrode in $Na_2S_2O_3$ (5 SPW) with SIBX 73

Figure 6.4: Cyclic voltammograms for $PdTe_2$ electrode in $MgCl_2$ (5 SPW) 73

Figure 6.5: Cyclic voltammograms for PdS in the absence and presence of $Na_2S_2O_3$ at increasing ionic strength 74

Figure 6.6: Cyclic voltammograms for PdS in the absence and presence of $Na_2S_2O_3$ at increasing ionic strength with SIBX. 75

Figure 6.7: Cyclic voltammograms for PdS in the absence and presence of $MgSO_4$ at increasing ionic strength 76

Figure 6.8: Cyclic voltammograms for PdS in the absence and presence of $MgSO_4$ at increasing ionic strength with SIBX 77

Figure 6.9: Cyclic voltammograms for PdS in the absence and presence of $MgCl_2$ at increasing ionic strength 78

Figure 6.10: Cyclic voltammograms for PdS in the absence and presence of $MgCl_2$ at increasing ionic strength with SIBX 79

Figure 6.11: Cyclic voltammograms for PdS in the absence and presence of $CaCl_2$ at increasing ionic strength 80

Figure 6.12: Cyclic voltammograms for PdS in the absence and presence of $CaCl_2$ at increasing ionic strength with SIBX 81

Figure 6.13: Cyclic voltammograms for PdS in the absence and presence of NaCl at increasing ionic strength 82

Figure 6.14: Cyclic voltammograms for PdS in the absence and presence of NaCl at increasing ionic strength with SIBX 83

Figure 6.15: Cyclic voltammograms for PdS in the absence and presence of $Na_2S_2O_3$, NaCl, $MgSO_4$, $MgCl_2$ and $CaCl_2$ at 1 SPW 84

Figure 6.16: Cyclic voltammograms for PdS in the absence and presence of $Na_2S_2O_3$, NaCl, $MgSO_4$, $MgCl_2$ and $CaCl_2$ at 1 SPW with SIBX 85

Figure 6.17: Cyclic voltammograms for PdS in the absence and presence of $Na_2S_2O_3$, NaCl, $MgSO_4$, $MgCl_2$ and $CaCl_2$ at 3 SPW 86

Figure 6.18: Cyclic voltammograms for PdS in the absence and presence of $Na_2S_2O_3$, NaCl, $MgSO_4$, $MgCl_2$ and $CaCl_2$ at 3 SPW with SIBX 87

Figure 6.19: Cyclic voltammograms for PdS in the absence and presence of $Na_2S_2O_3$, NaCl, $MgSO_4$, $MgCl_2$ and $CaCl_2$ at 5 SPW 88

Figure 6.20: Cyclic voltammograms for PdS in the absence and presence of $Na_2S_2O_3$, NaCl, $MgSO_4$, $MgCl_2$ and $CaCl_2$ at 5 SPW with SIBX 89

Figure 6.21: Cyclic voltammograms for PdS in the absence and presence of Na_2S2O_3, NaCl, $MgSO_4$, $MgCl_2$ and $CaCl_2$ at 10 SPW 90

Figure 6.22: Cyclic voltammograms for PdS in the absence and presence of $Na_2S_2O_3$, NaCl, $MgSO_4$, $MgCl_2$ and $CaCl_2$ at 10 SPW with SIBX 92

Figure 6.23: Cyclic voltammograms for $PdTe_2$ in the absence and presence of $Na_2S_2O_3$ at increasing ionic strength. 93

Figure 6.24: Cyclic voltammograms for $PdTe_2$ in the absence and presence of $Na_2S_2O_3$ at increasing ionic strength with SIBX 94

Figure 6.25: Cyclic voltammograms for $PdTe_2$ in the absence and presence of $MgSO_4$ at increasing ionic strength 95

Figure 6.26: Cyclic voltammograms for $PdTe_2$ in the absence and presence of $MgSO_4$ at increasing ionic strength with SIBX 96

Figure 6.27: Cyclic voltammograms for $PdTe_2$ in the absence and presence of $MgCl_2$ at increasing ionic strength 97

Figure 6.28: Cyclic voltammograms for $PdTe_2$ in the absence and presence of $MgCl_2$ at increasing ionic strength with SIBX 98

Figure 6.29: Cyclic voltammograms for $PdTe_2$ in the absence and presence of $CaCl_2$ at increasing ionic strength 99

Figure 6.30: Cyclic voltammograms for $PdTe_2$ in the absence and presence of $CaCl_2$ at increasing ionic strength with SIBX 100

Figure 6.31: Cyclic voltammograms for $PdTe_2$ in the absence and presence of NaCl at increasing ionic strength 101

Figure 6.32: Cyclic voltammograms for $PdTe_2$ in the absence and presence of NaCl at increasing ionic strength with SIBX 102

Figure 6.33: Cyclic voltammograms for $PdTe_2$ in the absence and presence of $Na_2S_2O_3$, NaCl, $MgSO_4$, $MgCl_2$ and $CaCl_2$ at 1 SPW 103

Figure 6.34: Cyclic voltammograms for $PdTe_2$ in the absence and presence of $Na_2S_2O_3$, NaCl, $MgSO_4$, $MgCl_2$ and $CaCl_2$ at 1 SPW with SIBX 104

Figure 6.35: Cyclic voltammograms for $PdTe_2$ in the absence and presence of $Na_2S_2O_3$, NaCl, $MgSO_4$, $MgCl_2$ and $CaCl_2$ at 3 SPW 106

Figure 6.36: Cyclic voltammograms for $PdTe_2$ in the absence and presence of $Na_2S_2O_3$, NaCl, $MgSO_4$, $MgCl_2$ and $CaCl_2$ at 3 SPW with SIBX 107

Figure 6.37: Cyclic voltammograms for $PdTe_2$ in the absence and presence of $Na_2S_2O_3$, NaCl, $MgSO_4$, $MgCl_2$ and $CaCl_2$ at 5 SPW 109

Figure 6.38: Cyclic voltammograms for $PdTe_2$ in the absence and presence of $Na_2S_2O_3$, NaCl, $MgSO_4$, $MgCl_2$ and $CaCl_2$ at 5 SPW with SIBX 110

Figure 6.39: Cyclic voltammograms for $PdTe_2$ in the absence and presence of $Na_2S_2O_3$, NaCl, $MgSO_4$, $MgCl_2$ and $CaCl_2$ at 10 SPW 112

Figure 6.40: Cyclic voltammograms for $PdTe_2$ in the absence and presence of $Na_2S_2O_3$, NaCl, $MgSO_4$, $MgCl_2$ and $CaCl_2$ at 5 SPW with SIBX 113

Figure 7.1: Bode plots for pentlandite 117

Figure 7.2: Nyquist plots for $PdTe_2$ in the presence of $CaCl_2$(1SPW) with SIBX 118

Figure 7.3: Nyquist plots for $PdTe_2$ in the presence of $Na_2S_2O_3$ at increasing ionic strength 118

Figure 7.4: Bode plots of Z_{mod} versus log frequency for $PdTe_2$ in the presence of $Na_2S_2O_3$ at increasing ionic strength. 119

Figure 7.5: Bode plots of phase angle versus log frequency for $PdTe_2$ in the presence of $Na_2S_2O_3$ at increasing ionic strength. 119

Figure 7.6: Nyquist plots for $PdTe_2$ in the absence and presence of $Na_2S_2O_3$ at increasing ionic strength in SIBX 121

Figure 7.7: Bode plots of Z_{mod} versus log frequency for $PdTe_2$ in the absence and presence of $Na_2S_2O_3$ at increasing ionic strength with SIBX. 121

Figure 7.8: Bode plots of phase angle versus log frequency for $PdTe_2$ in the absence and presence of $Na_2S_2O_3$ at increasing ionic strength with SIBX 122

Figure 7.9: Nyquist plots for $PdTe_2$ in the presence of $MgSO_4$ at increasing ionic strength in SIBX. 123

Figure 7.10: Bode plots of Z_{mod} versus log frequency for $PdTe_2$ in the presence of $MgSO_4$ at increasing ionic strength with SIBX. 124

Figure 7.11: Bode plots of phase angle versus log frequency for $PdTe_2$ in the presence of $MgSO_4$ at increasing ionic strength. 124

Figure 7.12: Nyquist plots for $PdTe_2$ in the absence and presence of $MgSO_4$ at increasing ionic strength with SIBX. 125

Figure 7.13: Bode plots of Z_{mod} versus log frequency for $PdTe_2$ in the absence and presence of $MgSO_4$ at increasing ionic strength with SIBX. 126

Figure 7.14: Bode plots of phase angle versus log frequency for $PdTe_2$ in the absence and presence of $MgSO_4$ at increasing ionic strength with SIBX. 126

Figure 7.15: Nyquist plots for $PdTe_2$ in the presence of $MgCl_2$ at increasing ionic strength. 128

Figure 7.16: Bode plots of Z_{mod} versus log frequency for $PdTe_2$ in the presence of $MgCl_2$ at increasing ionic strength. 128

Figure 7.17: Bode plots of phase angle versus log frequency for $PdTe_2$ in the presence of $MgCl_2$ at increasing ionic strength 129

Figure 7.18: Nyquist plots for $PdTe_2$ in the absence and presence of $MgCl_2$ at increasing ionic strength with SIBX. 130

Figure 7.19: Bode plots of Z_{mod} versus log frequency for $PdTe_2$ in the absence and presence of $MgCl_2$ at increasing ionic strength with SIBX. 131

Figure 7.20: Bode plots of phase angle versus log frequency for $PdTe_2$ in the absence and presence of $MgCl_2$ at increasing ionic strength with SIBX. 131

Figure 7.21: Nyquist plots for $PdTe_2$ in the presence of $CaCl_2$ at increasing ionic strength. 133

Figure 7.22: Bode plots of Z_{mod} versus log frequency for $PdTe_2$ in the presence of $CaCl_2$ at increasing ionic strength. 133

Figure 7.23: Bode plots of phase angle versus log frequency for $PdTe_2$ in the presence of $CaCl_2$ at increasing ionic strength. 134

Figure 7.24: Nyquist plots for $PdTe_2$ in the absence and presence of $CaCl_2$ at increasing ionic strength with SIBX. 135

Figure 7.25: Bode plots of Z_{mod} versus log frequency for $PdTe_2$ in the absence and presence of $CaCl_2$ at increasing ionic strength with SIBX. 135

Figure 7.26: Bode plots of phase angle versus log frequency for $PdTe_2$ in the absence and presence of $CaCl_2$ at increasing ionic strength with SIBX. 136

Figure 7.27: Nyquist plots for $PdTe_2$ in the presence of NaCl at increasing ionic strength. 137

Figure 7.28: Bode plots of Z_{mod} versus log frequency for $PdTe_2$ in the presence of NaCl at increasing ionic strength. 137

Figure 7.29: Bode plots of phase angle versus log frequency for $PdTe_2$ in the presence of NaCl at increasing ionic strength. 138

Figure 7.30: Nyquist plots for $PdTe_2$ in the absence and presence of NaCl at increasing ionic strength with SIBX.....139

Figure 7.31: Bode plots of Z_{mod} versus log frequency for $PdTe_2$ in the absence and presence of NaCl at increasing ionic strength with SIBX 139

Figure 7.32: Bode plots of phase angle versus log frequency for $PdTe_2$ in the absence and presence of NaCl at increasing ionic strength with SIBX.....140

Figure 7.33: Nyquist plots for $PdTe_2$ in the presence of $Na_2S_2O_3$, NaCl, $CaCl_2$, $MgSO_4$, $MgCl_2$ at 1 SPW 141

Figure 7.34: Bode plots of Z_{mod} versus log frequency for $PdTe_2$ in the presence of $Na_2S_2O_3$, NaCl, $CaCl_2$, $MgSO_4$, $MgCl_2$ at 1 SPW.....142

Figure 7.35: Bode plots of phase angle versus log frequency for $PdTe_2$ in the presence of $Na_2S_2O_3$, NaCl, $CaCl_2$, $MgSO_4$, $MgCl_2$ at 1 SPW 142

Figure 7.36: Nyquist plots for $PdTe_2$ in the absence and presence of $Na_2S_2O_3$, NaCl, $CaCl_2$, $MgSO_4$, $MgCl_2$ at 1 SPW with SIBX.....143

Figure 7.37: Bode plots of Z_{mod} versus log frequency for $PdTe_2$ in the absence and presence of $Na_2S_2O_3$, NaCl, $CaCl_2$, $MgSO_4$, $MgCl_2$ at 1 SPW with SIBX.....144

Figure 7.38: Bode plots of phase angle versus log frequency for $PdTe_2$ in the absence and presence of $Na_2S_2O_3$, NaCl, $CaCl_2$, $MgSO_4$, $MgCl_2$ at 1 SPW with SIBX 144

Figure 7.39: Nyquist plots for $PdTe_2$ in the presence of $Na_2S_2O_3$, NaCl, $CaCl_2$, $MgSO_4$, $MgCl_2$ at 3 SPW 146

Figure 7.40: Bode plots of Z_{mod} versus log frequency for $PdTe_2$ in the presence of $Na_2S_2O_3$, NaCl, $CaCl_2$, $MgSO_4$, $MgCl_2$ at 3 SPW.....146

Figure 7.41: Bode plots of phase angle versus log frequency for $PdTe_2$ in the presence of $Na_2S_2O_3$, NaCl, $CaCl_2$, $MgSO_4$, $MgCl_2$ at 3 SPW 147

Figure 7.42: Nyquist plots for $PdTe_2$ in the absence and presence of $Na_2S_2O_3$, NaCl, $CaCl_2$, $MgSO_4$, $MgCl_2$ at 3 SPW with SIBX.....148

Figure 7.43: Bode plots of Z_{mod} versus log frequency for $PdTe_2$ in the absence and presence of $Na_2S_2O_3$, NaCl, $CaCl_2$, $MgSO_4$, $MgCl_2$ at 3 SPW with SIBX.....148

Figure 7.44: Bode plots of phase angle versus log frequency for $PdTe_2$ in the absence and presence of $Na_2S_2O_3$, NaCl, $CaCl_2$, $MgSO_4$, $MgCl_2$ at 3 SPW with SIBX 149

Figure 7.45: Nyquist plots for $PdTe_2$ in the presence of $Na_2S_2O_3$, NaCl, $CaCl_2$, $MgSO_4$, $MgCl_2$ at 5 SPW 150

Figure 7.46: Bode plots of Z_{mod} versus log frequency for $PdTe_2$ in the presence of $Na_2S_2O_3$, NaCl, $CaCl_2$, $MgSO_4$, $MgCl_2$ at 5 SPW.....151

Figure 7.47: Bode plots of phase angle versus log frequency for $PdTe_2$ in the presence of $Na_2S_2O_3$, NaCl, $CaCl_2$, $MgSO_4$, $MgCl_2$ at 5SPW……..…….151

Figure 7.48: Nyquist plots for $PdTe_2$ in the absence and presence of $Na_2S_2O_3$, NaCl, $CaCl_2$, $MgSO_4$, $MgCl_2$ at 5 SPW with SIBX……...152

Figure 7.49: Bode plots of Z_{mod} versus log frequency for $PdTe_2$ in the absence and presence of $Na_2S_2O_3$, NaCl, $CaCl_2$, $MgSO_4$, $MgCl_2$ at 5 SPW with SIBX.....153

Figure 7.50: Bode plots of phase angle versus log frequency for $PdTe_2$ in the absence and presence of $Na_2S_2O_3$, NaCl, $CaCl_2$, $MgSO_4$, $MgCl_2$ at 5 SPW with SIBX. 153

Figure 7.51: Nyquist plots for $PdTe_2$ in the presence of $Na_2S_2O_3$, NaCl, $CaCl_2$, $MgSO_4$, $MgCl_2$ at 10 SPW 155

Figure 7.52: Bode plots of Z_{mod} versus log frequency for $PdTe_2$ in the presence of $Na_2S_2O_3$, NaCl, $CaCl_2$, $MgSO_4$, $MgCl_2$ at 10 SPW 155

Figure 7.53: Bode plots of phase angle) versus log frequency for $PdTe_2$ in the presence of $Na_2S_2O_3$, NaCl, $CaCl_2$, $MgSO_4$, $MgCl_2$ at 10 SPW. 156

Figure 7.54: Nyquist plots for $PdTe_2$ in the absence and presence of $Na_2S_2O_3$, NaCl, $CaCl_2$, $MgSO_4$, $MgCl_2$ at 10 SPW with SIBX.....157

Figure 7.55: Bode plots of Z_{mod} versus log frequency for $PdTe_2$ in the absence and presence of $Na_2S_2O_3$, NaCl, $CaCl_2$, $MgSO_4$, $MgCl_2$ at 10 SPW with SIBX.....157

Figure 7.56: Bode plots of phase angle versus log frequency for $PdTe_2$ in the absence and presence of $Na_2S_2O_3$, NaCl, $CaCl_2$, $MgSO_4$, $MgCl_2$ at 10 SPW with SIBX 158

Figure 7.57: Nyquist plots for PdS in the presence of $Na_2S_2O_3$ at increasing ionic strength.....159

Figure 7.58: Bode plots of Z_{mod} versus log frequency for PdS in the absence and presence of $Na_2S_2O_3$ at increasing ionic strength 160

Figure 7.59: Bode plots of phase angle versus log frequency for PdS in the presence of $Na_2S_2O_3$ at increasing ionic strength 160

Figure 7.60: Nyquist plots for PdS in the absence and presence of $Na_2S_2O_3$ at increasing ionic strength with SIBX.....162

Figure 7.61: Bode plots of Z_{mod} versus log frequency for PdS in the absence and presence of $Na_2S_2O_3$ at increasing ionic strength with SIBX 162

Figure 7.62: Bode plots of phase angle versus log frequency for PdS in the absence and presence of $Na_2S_2O_3$ at increasing ionic strength with SIBX.....163

Figure 7.63: Bode plots of Z_{mod} versus log frequency for PdS in the presence of $MgSO_4$ at increasing ionic strength.....164

Figure 7.64: Bode plots of Z_{mod} versus log frequency for PdS in the presence of $MgSO_4$ at increasing ionic strength 164

Figure 7.65: Bode plots of phase angle versus log frequency for PdS in the presence of $MgSO_4$ at increasing ionic strength……165

Figure 7.66: Nyquist plots for PdS in the absence and presence of $MgSO_4$ at increasing ionic strength with SIBX.....166

Figure 7.67: Bode plots of Z_{mod} versus log frequency for PdS in the absence and presence of $MgSO_4$ at increasing ionic strength with SIBX. 166

Figure 7.68: Bode plots of phase angle versus log frequency for PdS in the absence and presence of $MgSO_4$ at increasing ionic strength with SIBX. 167

Figure 7.69: Nyquist plots for PdS in the presence of $Na_2S_2O_3$ and $MgSO_4$ at 1 SPW. 168

Figure 7.70: Bode plots of Z_{mod} versus log frequency for PdS in the presence of $Na_2S_2O_3$ and $MgSO_4$ at 1 SPW.....168

Figure 7.71: Bode plots of phase angle versus log frequency for PdS in the presence of $Na_2S_2O_3$ and $MgSO_4$ at 1 SPW 169

Figure 7.72: Nyquist plots for PdS in the absence and presence of $Na_2S_2O_3$ and $MgSO_4$ at 1 SPW with SIBX.....170

Figure 7.73: Bode plots of Z_{mod} versus log frequency for PdS in the absence and presence of $Na_2S_2O_3$ and $MgSO_4$ at 1 SPW with SIBX.....170

Figure 7.74: Bode plots of phase angle versus log frequency for PdS in the absence and presence of $Na_2S_2O_3$ and $MgSO_4$ at increasing ionic strength with SIBX.....171

Figure 7.75: Nyquist plots for PdS in the presence of $Na_2S_2O_3$ and $MgSO_4$ at 3 SPW 172

Figure 7.76: Bode plots of Z_{mod}versus log frequency for PdS in the presence of $Na_2S_2O_3$ and $MgSO_4$ at 3 SPW.....172

Figure 7.77: Bode plots of phase angle versus log frequency for PdS in the presence of $Na_2S_2O_3$ and $MgSO_4$ at 3 SPW 173

Figure 7.78: Nyquist plots for PdS in the absence and presence of $Na_2S_2O_3$ and $MgSO_4$ at 3 SPW with SIBX.....174

Figure 7.79: Bode plots of Z_{mod} versus log frequency for PdS in the absence and presence of $Na_2S_2O_3$ and $MgSO_4$ at 3 SPW with SIBX 174

Figure 7.80: Bode plots of phase angle versus log frequency for PdS in the absence and presence of $Na_2S_2O_3$ and $MgSO_4$ at 3 SPW with SIBX.....175

Figure 7.81: Nyquist plots for PdS in the presence of $Na_2S_2O_3$ and $MgSO_4$ at 5 SPW 176

Figure 7.82: Bode plots of Z_{mod} versus log frequency for PdS in the presence of $Na_2S_2O_3$ and $MgSO_4$ at 5 SPW.....176

Figure 7.83: Bode plots of phase angle versus log frequency for PdS in the presence of $Na_2S_2O_3$ and $MgSO_4$ at 5 SPW 177

Figure 7.84: Nyquist plots for PdS in the absence and presence of $Na_2S_2O_3$ and $MgSO_4$ at 5 SPW with SIBX……..178

Figure 7.85: Bode plots of Z_{mod} versus log frequency for PdS in the absence and presence of $Na_2S_2O_3$ and $MgSO_4$ at 5 SPW with SIBX 178

Figure 7.86: Bode plots of phase angle versus log frequency for PdS in the absence and presence of $Na_2S_2O_3$ and $MgSO_4$ at 5 SPW with SIBX 179

Figure 7.87: Nyquist plots for PdS in the presence of $Na_2S_2O_3$ and $MgSO_4$ at 10 SPW 180

Figure 7.88: Bode plots of Z_{mod} versus log frequency for PdS in the presence of $Na_2S_2O_3$ and $MgSO_4$ at 10 SPW. 181

Figure 7.89: Bode plots of phase angle (o) versus log frequency for PdS in the presence of $Na_2S_2O_3$ and $MgSO_4$ at 10 SPW 181

Figure 7.90: Nyquist plots for PdS in the absence and presence of $Na_2S_2O_3$ and $MgSO_4$ at 10 SPW with SIBX 182

Figure 7.91: Bode plots of Z_{mod} versus log frequency for PdS in the absence and presence of $Na_2S_2O_3$ and $MgSO_4$ at 10 SPW with SIBX 183

Figure 7.92: Bode plots of phase angle versus log frequency for PdS in the absence and presence of $Na_2S_2O_3$ and $MgSO_4$ at 10 SPW with SIBX 183

Figure 7.93: Physical model of palladium minerals in an electrolyte solution 184

Figure 7.94: Equivalent circuit model for fitting EIS data in the presence of salts. 184

Figure 7.95: Equivalent circuit model for fitting EIS data in the presence of salts and SIBX. 185

Figure 8.1: Divalent palladium xanthate 190

Figure 8.2: Fractional coverage of SIBX on $PdTe_2$ in the absence and presence of salts at increasing ionic strength. 193

Figure 8.3: Bode plots of Z_{mod} versus log frequency for PdS in the presence of SIBX only and $Na_2S_2O_3$ at increasing ionic strength 195

Figure 8.4: Bode plots of Z_{mod} versus log frequency for $PdTe_2$ in the presence of SIBX only and $Na_2S_2O_3$ at increasing ionic strength 195

Figure 8.5: Eh-pH diagrams of a Ca-O-H system. 198

Figure 8.6: Bode plots of Z_{mod} versus log frequency for $PdTe_2$ in the presence of SIBX only and $CaCl_2$ at increasing ionic strength 201

Figure 8.7: Magnesium species diagram 202

Figure 8.8: Bode plots of Z_{mod} versus log frequency for $PdTe_2$ in the presence of SIBX only and $MgCl_2$ at increasing ionic strength 204

Figure 8.9: Eh-pH diagrams of a S-O-H system 207

Figure 8.10: Bode plots of Zmod versus log frequency for PdS in the presence of SIBX only and $MgSO_4$ at increasing ionic strength 209

Figure 8.11: Bode plots of Zmod versus log frequency for $PdTe_2$ in the presence of SIBX only and MgSO4 at increasing ionic strength 209

Figure 8.12: Eh-pH diagram illustrating a Na-O-H system..... 212

Figure 8.13: Bode plots of Zmod versus log frequency for $PdTe_2$ in the presence of SIBX only and NaCl at increasing ionic strength. 214

Figure 8.14: An illustration of the mechanisms of interaction of ions and xanthate collectors on PdS...217

Figure 8.15: An illustration of the mechanisms of interaction of ions and xanthate collectors on $PdTe_2$.. 218

1. Introduction

1.1 Background

South Africa has been established to be the world's largest producer of platinum group of minerals (PGMs), with more than 80% of the world's PGM reserves (Jones, 1999). The Bushveld Complex is a prominent natural reserve in South Africa that is well known for its overwhelming deposits of PGMs. It is comprised of three different ore bodies, the Merensky Reef, the Upper Group 2 (UG2) chromitite and the Platreef ore body. Typically, the distribution of platinum and palladium within the PGMs in the three ore bodies is approximately 55 % and 32 %, 44 % and 46 % and 46 % and 30 %, respectively with 15% being comprised of other metals (Cawthorn, 1999).

On a broader perspective, PGMs can be classified into metals, intermetallic compounds, and alloys with Fe, Pb, Sn, Ni, Hg and Cu, with some PGMs that are formed with Bi, Te, As, Sb and S. The largest class of PGMs are complexes of sulphides, followed by arsenides and tellurides (Daltry and Wilson, 1997). Of interest to this study are palladium sulphides and tellurides, in which the PGM tellurides have been reported to constitute 20-45 % of PGMs in the Platreef (Shackleton et al., 2007).

Palladium is one of the most abundant platinum metals, which is considered as the most expensive precious metal. It has special characteristics that make it indispensable for industrial applications such as catalytic converters, dental alloys, coating printed circuit components, multilayer ceramic capacitors and so forth.

Most research has focused on the flotation behaviour of base metal sulphides due to their association with PGMs. However, the assumption that PGMs are associated with base metal sulphides was disputed by the work of Penberthy et al. (2000), who conducted an extensive study that proved that 50% of PGMs are liberated during milling. Notwithstanding the significant quantities of PGMs in the Bushveld Complex and their economic value, very limited research has investigated the flotation behaviour of PGMs. Therefore, this study seeks to examine the reactions that occur on PGM surfaces during the flotation process, from an electrochemical perspective.

Froth flotation is an essential process that recovers valuable minerals from non-valuable material (Wills and Napier-Munn, 2006). For successful and effective flotation performance, it is pivotal to apply suitable conditions that will selectively modify the surface of desired minerals to enhance

their hydrophobicity or modify the surface of unwanted material to depress them. Therefore, chemical reagents such as collectors, depressants, activators and modifiers can be administered into the pulp phase to achieve this purpose. From the aforementioned list of chemical reagents used in the flotation process, this study focusses on xanthate collectors.

Xanthate collectors are surfactants used to modify the surface wettability of mineral surfaces by adsorbing at the solid-liquid interface (Chang et al., 2018). Most studies have accepted that xanthate collectors are highly selective in the flotation of base metal sulphides (Usul and Tolun, 1974, Leppinen, 1990, Buckley et al., 2003) whilst a few of the flotation studies on PGMs have shown a strong interaction that transpires between PGMs and xanthate collectors (Vermaak et al., 2005, Shackleton et al., 2007). The interaction of xanthate collectors with mineral surfaces has been accepted to occur through an electrochemical mechanism (Janetski et al., 1977, Woods, 1996a, Vermaak et al., 2004, Tadie et al., 2015a). The mechanisms in which xanthate collectors adsorb onto mineral surfaces has been a topic of interest for the past decades (Allison et al., 1972, Ertekin et al., 2016), and still remains an interesting topic to date. The manner in which xanthate collectors interact with mineral surfaces is dependent on conditions applied to a flotation system, in which the ions found in process water have been found to play a significant role.

The accumulation of ions in process water comes from the need to recycle water from the flotation circuits due to the increase in social demand and scarcity of fresh water in countries such as South Africa. The presence of ions in process water has been reported to either enhance the flotation performance of valuable minerals or have a detrimental effect on flotation recoveries (Corin et al., 2011, Manono et al., 2018, October et al., 2020). The effect of ions has been determined to be type and concentration dependent. High ion concentrations have been determined to inhibit the adsorption of xanthate collectors on mineral surfaces (Wang et al., 2015). Mg^{2+} ions have been reported to have a depressing effect on flotation recoveries at 50 ppm and the presence of Ca^{2+} ions were reported to have a reduced effect compared to Mg^{2+} ions, both of which were found to have a depressing effect on sphalerite recoveries. In addition, it was observed that the ions did not hinder the uptake of xanthate collector, implying that the ions would have most likely competed with xanthate ions for adsorption on the mineral surface (Lascelles et al., 2001). These findings were in agreement with the findings of Hodgson and Agar (1989) and Ikumapayi et al. (2012), where Ca^{2+}, SO_4^{2-} and $S_2O_3^{2-}$ ions were postulated to compete with xanthate ions for adsorption on active sites on pentlandite and galena, respectively. Studies have shown that in the presence of ionic species the species formed within the flotation process pH range are the precipitated surface oxidized compounds (Wang et al., 2015, Hirajima et al., 2016, Flores-Álvarez et al., 2017), which

are hydrophilic in nature and are generally expected to have a negative impact on the flotation performance of valuable minerals. However, ionic species like Na^+, have been observed to enhance the adsorption of xanthate collector ions on minerals like magnetite as a result of the ability of Na^+ ions to reduce the negative charge on the mineral surface, thereby facilitating the adsorption of collector ions (Potapova et al., 2010).

Despite several publications that have reported on the effects of ions on the adsorption of xanthate collectors on base metal sulphides, the mechanisms involved have not been examined from an electrochemical perspective. Therefore, this study seeks to make use of electrochemical techniques to explore the extent to which xanthate collectors adsorb onto PdS and $PdTe_2$ mineral surfaces in the presence of ions and the potential redox reactions at play. Ultimately, their interfacial adsorption mechanisms with respect to the resistive and capacitive behaviour of the investigated mineral's electrical double layer were examined.

1.2 Scope of Study

This study examines the electrochemical behavior of selected ions with an increase in ionic strength on the adsorption of SIBX on palladium sulphide (PdS) and palladium telluride ($PdTe_2$) mineral surfaces. The extent to which Ca^{2+}, Mg^{2+}, SO_4^{2-}, $S_2O_3^{2-}$ and Na^+ ions at increasing ionic strengths interact with PdS and $PdTe_2$ minerals and their subsequent effect on the interaction of SIBX with the palladium minerals was explored by rest potential measurements. Cyclic voltammetry measurements were applied to characterize redox reactions that occur at increasing ionic strengths of Ca^{2+}, Mg^{2+}, SO_4^{2-}, $S_2O_3^{2-}$ and Na^+ ions in the absence and presence of SIBX on PdS and $PdTe_2$ mineral surfaces. Ultimately, electrochemical impedance spectroscopy measurements were performed to evaluate the mechanisms involved when SIBX is adsorbed on PdS and $PdTe_2$ mineral surfaces in the absence and presence of Ca^{2+}, Mg^{2+}, SO_4^{2-}, $S_2O_3^{2-}$ and Na^+ ions at increasing ionic strengths.

Each electrochemical measurement was validated with previous work in literature. Experimental parameters such as temperature, pH and concentration of SIBX were kept constant whilst the ionic strength of Ca^{2+}, Mg^{2+}, SO_4^{2-}, $S_2O_3^{2-}$ and Na^+ was varied at 0.0242 M, 0.0727 M, 0.1212M and 0.2426 M.

A schematic representation of the scope of this work is shown in Figure 1.1. The inputs of this study are highlighted in orange, green and red whereas the outputs are highlighted in purple.

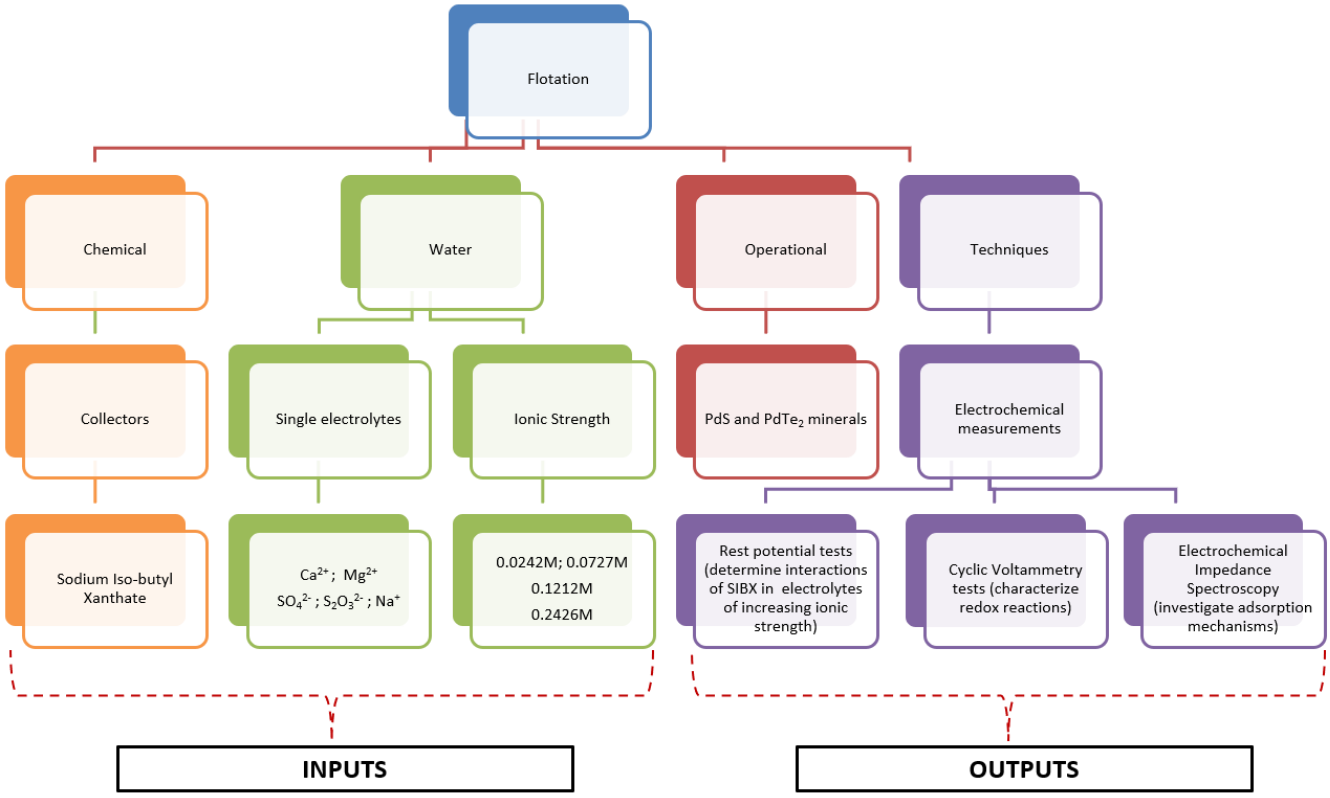

Figure 1.1: Schematic diagram representing scope of this study

2. Literature review

2.1 Geology of the Bushveld Complex

The Bushveld Complex in South Africa is considered to have originated from a vast eruption of magma from deep within the Earth's mantle. An estimated volume of 1 million km^3 magma that covered a diameter of at least 300 km in diameter and approximately 8 km in depth, slowly cooled and different types of minerals hardened and accumulated into sub-horizontal layers (Cawthorn, 2010). The intermittent eruption of the hot magma resulted in a cycle of cooling, hardening of minerals and generated a repetition of the mineral layering (Cawthorn, 1999).

The Bushveld Complex is classified into three groups of rocks namely ultramafic and mafic layered rocks known as the Rusternburg Layered Suite (RLS), ultramafic and mafic sills that encroach the country rocks underlying the RLS and granophyre's and granites that envelop the RLS (Barnes et al., 2004). The RLS is stratigraphically divided into five zones (Figure 2.1); the Marginal zone, the Lower Zone which consists of peridotites and pyroxenites igneous rocks, the Critical zone which comprises of the chromitite, pyroxenite and norite igneous rocks and ultimately the Main and Upper zones that contain cyclic units of the gabbronorites, anorthosites and magnetite which are overlapped by diorite igneous rocks. The top of the Critical zone holds the platinum bearing horizons (Merensky, Upper Group Chromite number 2 (UG-2) and Plat reefs). The RLS is exposed around the margins of the Bushveld Complex in areas known as lobes. These are subdivided into the western, eastern and northern lobes (Figure 2.1), where most of the essential magmatic sulphide and PGE deposits are found (Zientek et al., 2010).

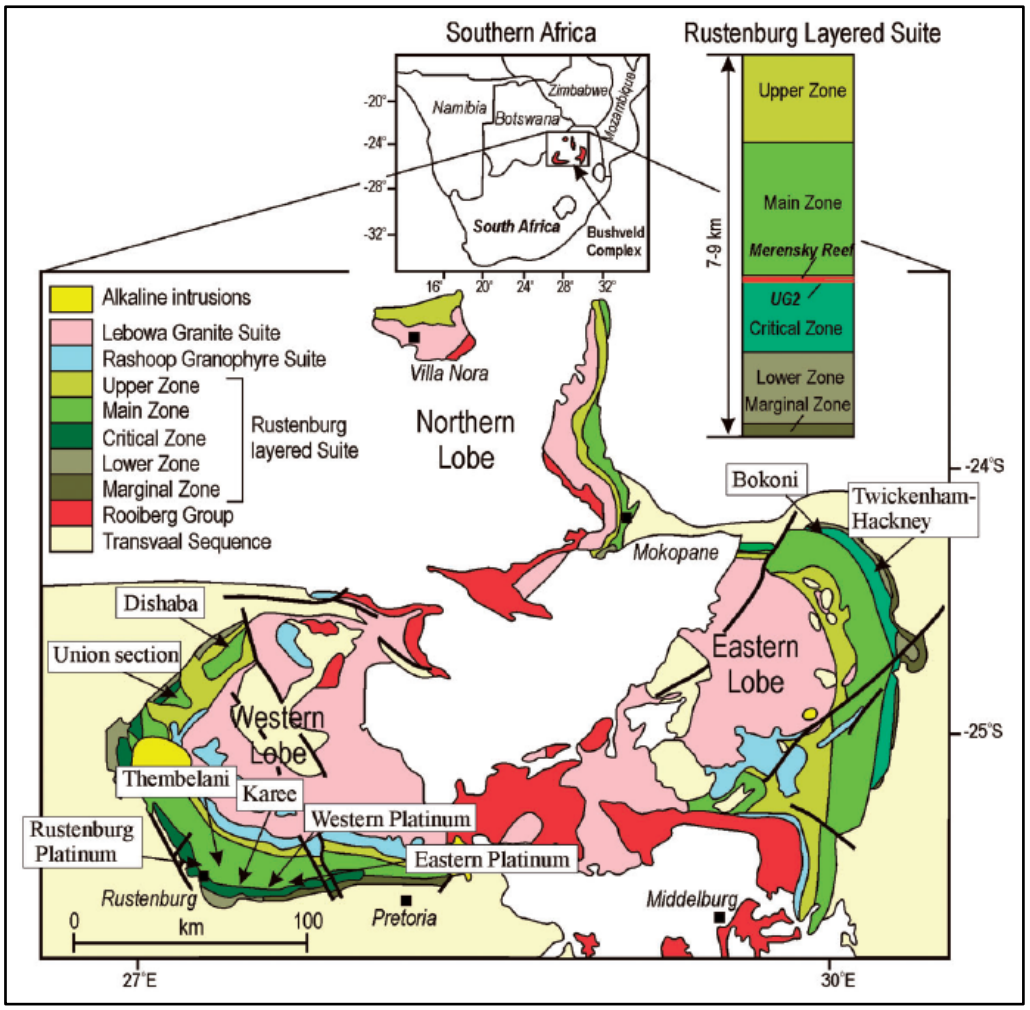

Figure 2.1: Geological map of the Bushveld Complex (Latypov et al., 2015).

The northern lobe hosts the Platreef, which is a 10 - 300 m thick collection of PGE rich pyroxenites and gabbros, that emerges from the base of the lobe and stretches for over 30 km along strike north of Mokopane (McDonald et al., 2005). The Platreef was discovered by Merensky in 1925, after the discovery of the Merensky Reef. The geology of the Platreef in the northern lobe has been accepted in literature to be similar to that of the Merensky Reef in the Bushveld Complex (White, 1994), partially due to the existence of sulphide mineralization associated with coarse grained pyroxenites. However, there are some differences as unveiled by the western and eastern lobes of the Complex (Manyeruke and Maier, 2005). The Platreef was formed as a result of heat and material exchange reactions that occurred between the hot magma and lime-rich floor rocks. This process resulted in the generation of abundant lime-rich minerals as well as the serpentinisation of an envelope of pyroxenites. The reef consists of an irregular distribution and value of base metal mineralization and PGE concentrations. The most common base metal sulphides that occur in the Reef include chalcopyrite, pentlandite, pyrite and pyrrhotite and the major PGMs that consist of PGE tellurides, arsenides, sulphides and alloys. The most predominant

minerals, platinum and palladium tellurides contribute ~ 20 - 45 % of PGMs in the reef, arsenides (~ 21 %), sulphides (~ 19 %) and alloys (~ 26 %). Though PGMs frequently occur bound in or on grain boundaries of base metal sulphides, some areas of this region have a high association of PGMs with silicate minerals (Schouwstra et al., 2000).

The Merensky Reef and the UG-2 are situated in the eastern and western lobes of the Bushveld Complex, near the top of the Upper Critical zone (Zientek et al., 2010). The Merensky Reef was discovered in 1924 by Dr Hans Merensky (Jones, 1999). It is a collection of chromite and sulphide-bearing pyroxenitic rocks, enriched in PGE and it is approximately 10 - 12 metres thick (Latypov et al., 2015). The reef consists of base metal sulphides and associated PGMs. The compositions of the base metal sulphides are approximately 40 % pyrrhotite, ~ 30 % pentlandite, ~ 15 % chalcopyrite and minor quantities of cubanite, millerite, pyrite and troilite. The PGM content in the Merensky Reef have been estimated to be approximately 4 to 10 g/t. The major PGMs found are braggite, sperrylite, cooperate and PGE alloys (Schouwstra et al., 2000).

Alternatively, the UG-2 reef, being a platiniferous chromitite layer lies approximately 20 - 400 metres below the Merensky horizon, thus making the PGM content in the UG-2 reef almost equivalent to that of the Merensky Reef. In this case the PGM content has been estimated to range between ~ 4.4 to 10.6 g/t (Jones, 1999). The reef consists primarily of approximately 90 % by volume, chromite, ~ 5 - 30 % pyroxene and ~ 1 - 10 % plagioclase (Vermaak, 1995). Silicates, phlogopite, biotite, the oxides: ilmenite, rutile and magnetite and base metal sulphides are found in small concentrations, with the secondary minerals being talc, quartz and serpentine. The PGMs in the UG-2 reef can be distinguished by the existence of large quantities of PGE sulphides that primarily contain cooperate, braggite and laurite. The mineral laurite preferentially associates with chromite whereas most PGMs demonstrate a preferential association with base metal sulphides. A significant quantity of alloys such as Pt-Fe alloy or various tellurides are also found. The most common base metal sulphides include pentlandite, pyrrhotite and chalcopyrite, with a grain size that hardly exceeds 30 μm whereas the PGMs in this region have been determined to have an average grain size of 12 μm (Schouwstra et al., 2000).

2.2 Crystal structures of palladium minerals

Crystal structures of minerals play a vital role in determining their properties and reactivities. Geologists use crystal structure to identify minerals present in rocks. In 1912, Max von Laue discovered the diffraction of X-rays by crystals, soon after which, diffraction methods were applied

in characterizing crystal structures of minerals (Reventos et al., 2012). Of interest to this study are the palladium minerals; PdS (vysotskite) and $PdTe_2$ (merenskyite).

2.2.1 Palladium Sulphide (Vysotskite)

Vysotskite is a mineral that belongs to the braggite (Pt, Pd, Ni)S crystal group. In 1932, minerals of this nature were first described upon their discovery in the Bushveld Igneous Complex. The group of minerals was named after William Henry Bragg and his son William Lawrence Bragg, and they were the first to be discovered using X rays.

In 1962, the mineral vysotskite was reported by Genkin and Zvyagintsev. The formula designated to it was (Pd,Ni)S, though Ni was considered to be a non-essential component. The crystal structure of the mineral was determined to be tetragonal (Figure 2.2) (Gaskell, 1936), with a similar pattern to braggite. After further analysis, both vysotskite and braggite were suggested to be isomorphous, to which the mineral vysotskite was eventually assigned the composition PdS (Cabri et al., 1978). The arrangement of palladium atoms have been determined by Patterson and Fourier analysis to resemble β-tungsten structure whereas the sulphur atoms were found to lie at almost the corners of the cube of half the linear dimensions of the unit cell (Gaskell, 1936). Vysotskite is known to be a silver-gray mineral (Figure 2.3a) with irregular grains that form inclusions in other minerals or rocks (Figure 2.3b). The crystallography of vysotskite is as shown in Table 2.1.

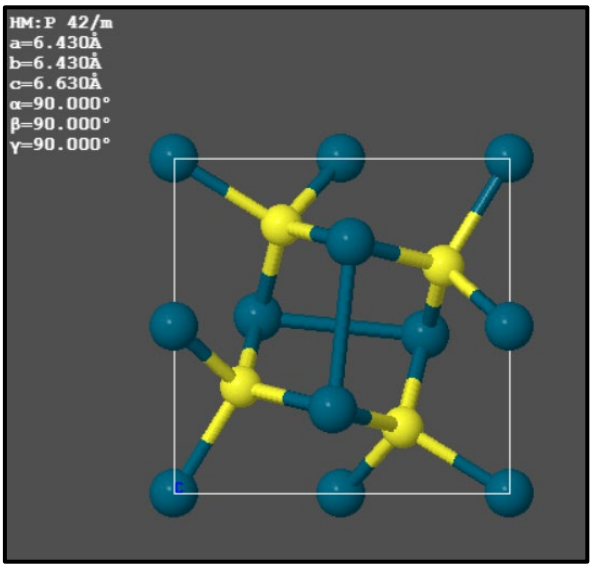

Figure 2.2: Crystal structure of vysotskite. Sourced from (Webmineral). [http://www.webmineral.com]

Table 2.1: Vysotskite crystallography (Webmineral) [http://www.webmineral.com]

Parameter	
Axial Ratios	a:c = 1:1.02652
Cell dimensions	a = 6.371, c = 6.54, Z = 5; V = 265.46 Den (Calc) = 3.96
Crystal system	Tetragonal-Dipyramidal H-M Symbol (4/m) Space Group: P $4_1/m$
X-ray diffraction	By intensity (I/I_o): 2.86(1), 2.91(1), 2.61(0.8)

a)  b) 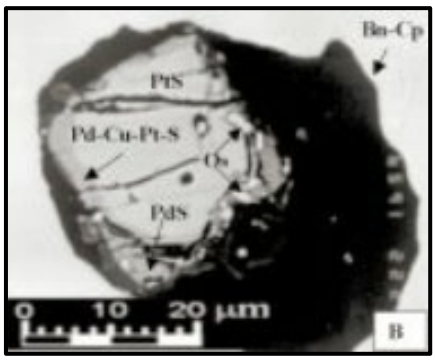

Figure 2.3: a) Braggite mineral, sourced from [http://www.assignment.com] b) Cooperite crystal surrounded by Pd-Cu-Pt-S, vysotskite phases from Scanning Electron Microscopy (SEM) analysis. Location- Pustava River placers deposit, situated within the Koryak-Kamchatka platinum-bearing belt of Alaskan-type intrusions in eastern Russia. Sourced from (Webmineral) [http://www.webmineral.com].

2.2.2 Palladium Telluride (Merenskyite)

Named after the geologist Hans Merensky, merenskyite $(Pd, Pt)(Te, Bi)_2$ was first described in 1966 for its occurrence in the Merensky Reef of the Western Bushveld Complex. It is a rare telluride/bismuthinide mineral that crystallizes into a trigonal (D'Olimpio et al., 2019) crystal structure (Figure 2.4). The structure of $PdTe_2$ has been found to exist in layers with a Pd-Te bond distance of 2.693 Å (Pell et al., 1996). It occurs as a white, grayish white mineral (Figure 2.5a), that is found as inclusions in other minerals such as chalcopyrite (Figure 2.5b). Crystallography data for merenskyite is shown in Table 2.2.

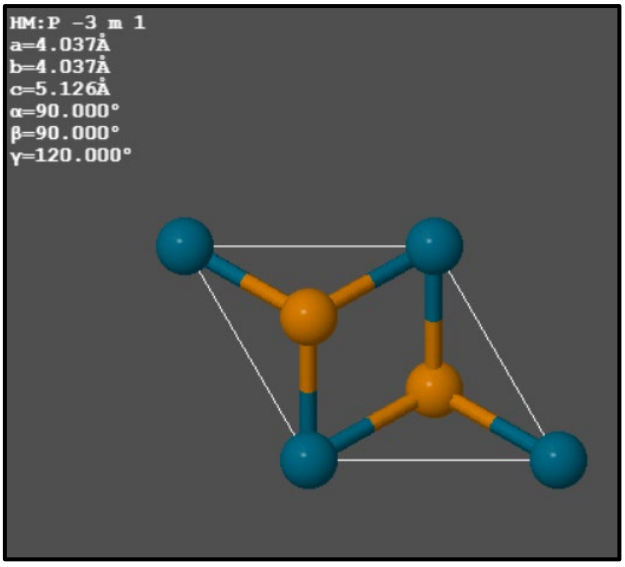

Figure 2.4: Crystal structure of merenskyite. Sourced from (Webmineral) [http://www.webmineral.com]

Table 2.2: Merenskyite crystallography (Webmineral) [http://www.webmineral.com]

Parameter	
Axial Ratios	a:c = 1:1.28833
Cell dimensions	A = 3.978, c = 5.125, Z = 1; V = 70.24 Den(Calc) = 9.14
Crystal system	Trigonal-Ditrigonal Pyramidal H-M Symbol (3m) Space Group: P 3m1
X-ray diffraction	By Intensity(I/I_O): 2.92(1), 2.1(0.6), 3.07(0.3)

a)  b) 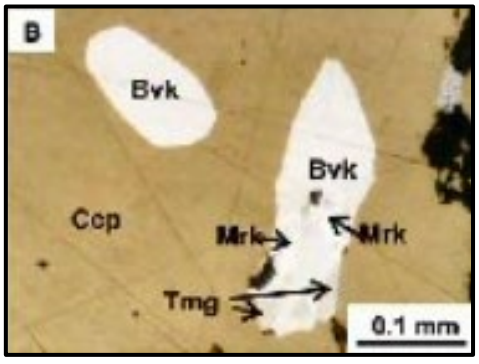

Figure 2.5: a) Merenskyite mineral. Sourced from [http://www.assignment.com] b) Borovskite (Bvk) - temagamite (Tmg) - merenskyite (Mrk) composite grain included in chalcopyrite. Location- McBratney high-grade PGE-Au occurrence, Bear Lake mafic unit, Proterozoic Flin Flon greenstone belt, Manitoba, Canada. Sourced from (Webmineral) [http://www.webmineral.com].

2.3 Flotation behaviour of PGMs

Flotation is an adaptable physico-chemical selective process in which the valuable minerals are separated from non-valuable gangue material owing to their differences in surface wettability (Wills and Napier-Munn, 2006). The theory behind this process is complex and has not been well understood up to date.

Research work on the flotation of PGMs is very limited. Most work has therefore focused on the flotation of base metal sulphides due to their good association with PGMs (Wiese et al., 2005, Manono et al., 2016). However, Penberthy et al. (2000) argued with this assumption after carrying out an extensive study on the recovery of PGMs from a UG-2 ore. It was found that milling the ore to 80 % < 75 μm liberated more than 50 % of PGM grains from the ore matrix (Figure 2.6). Hence, this significantly reduced the PGM grains that reported to the tailings. The flotation recoveries of the PGMs were determined to be dependent on grain size, mineral type and mode of occurrence. Sulphides of rhodium, platinum and palladium were identified as fast floating compared to laurite and non-sulphide platinum group minerals. The sequence in the rate of flotation of the PGMs was established to be braggite > cooperite > malanite > ferroplatinum > non-sulphide PGMs > laurite (Figure 2.7).

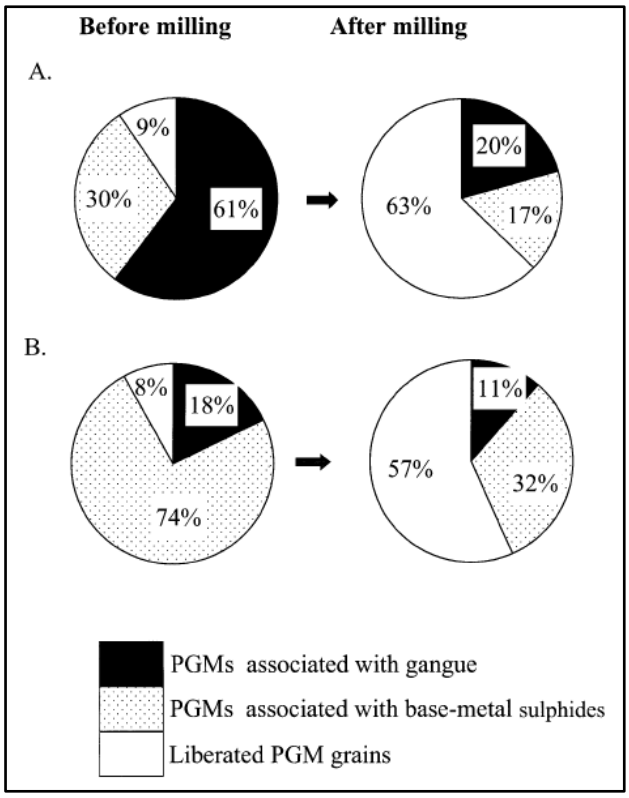

Figure 2.6: Percentages of locked and liberated PGMs in samples A and B of UG-2 ore. Sample size for each pie chart is at least 1000 PGM grains (Penberthy et al., 2000).

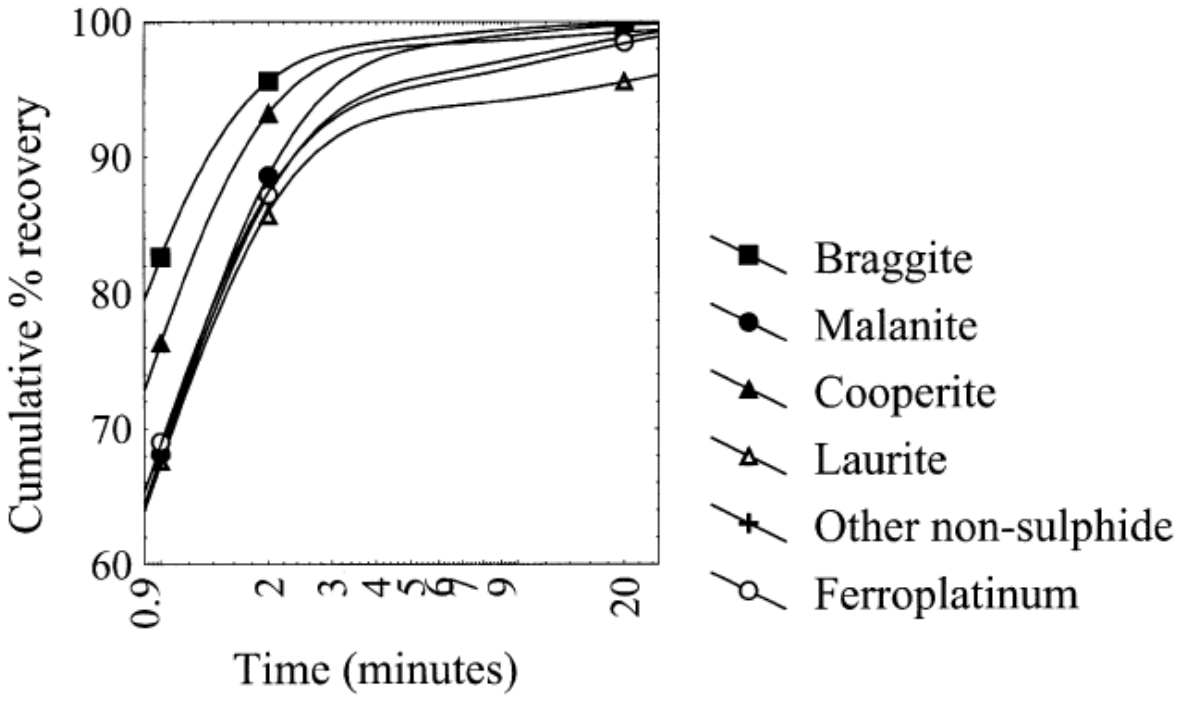

Figure 2.7: Flotation recoveries for different PGM phases (Penberthy et al., 2000).

A summary of the physical characteristics of different PGMs is shown in Table 2.3. The assumption in the flotation recoveries is that all minerals are liberated. These findings demonstrate the importance of understanding the flotation behaviour of tellurides versus sulphides.

Table 2.3: Physical characteristics and recovery behaviour of different PGM classes (Vermaak, 2005)

PGM class	Size	Density	Gravity recovery	Flotation recovery
Sulphides	Coarse	High	Good	Good
Tellurides	Variable	Low	Poor	Poor
Arsenides	Variable	Medium	Good	Good
Alloys	Coarse	Very high	Excellent	Variable
Oxides	Fine	Low	Very poor	Very poor

2.3.1 Reactivity and Flotation behaviour of PGM Sulphides

Crystal structure and crystallographic orientation play a crucial role in surface phenomena such as adsorption, catalysis etc. The tendency of the bonds in a crystal structure to acquire stable configurations is considered from their chemical behaviour and electronic properties (Gatos, 1962).

2.3.1.1 Reactivity of PGM Sulphides

The oxidation of base metal sulphides is a topic that has been extensively studied in the previous decades. However, oxidation reactions of PGM sulphides have not been given much attention. Reactions that involve the oxidation of PGM sulphides are almost similar to those of base metal sulphides, therefore it is of importance to understand the reactions involved in the oxidation of base metal sulphides. Surface oxidation products formed on mineral surfaces impact the surface hydrophobicity of minerals and hence affect their ability to float.

The oxidation of sulphides in alkaline conditions has been proposed to occur as in Equation 2.1 (Hu et al., 2009)

$$MS + nH_2O \leftrightarrow M(OH)_n + S + nH^+ + ne^- \quad \text{(Eqn. 2.1a)}$$

$$\Delta G^0 \leftrightarrow \Delta G^0_{M(OH)_n} + \Delta G^0_s - \Delta G^0_{MS} - \Delta G^0_{H_2O} \quad \text{(Eqn. 2.1b)}$$

Where ΔG^0 represents the standard free energy of reaction.

Other oxidation reactions that may occur result in the formation of oxy-sulphur species:

$$2MS + 7H_2O \leftrightarrow 2M(OH)_2 + S_2O_3^{2-} + 10H^+ + 8e^- \quad \text{(Eqn. 2.2a)}$$

$$\Delta G^0 \leftrightarrow 2\Delta G^0_{M(OH)_n} + \Delta G^0_{S_2O_3^{2-}} - \Delta G^0_{MS} - 7\Delta G^0_{H_2O} \quad \text{(Eqn. 2.2b)}$$

$$MS + 6H_2O \leftrightarrow M(OH)_2 + SO_4^{2-} + 10H^+ + 8e^- \quad \text{(Eqn. 2.3a)}$$

$$\Delta G^0 \leftrightarrow 2\Delta G^0_{M(OH)_n} + \Delta G^0_{SO_4^{2-}} - \Delta G^0_{MS} - 6\Delta G^0_{H_2O} \quad \text{(Eqn. 2.3b)}$$

If the oxidation of sulphides proceeds by Equations 2.2a and 2.3a, collectorless flotation is not expected owing to the potential corresponding to these reactions being on the upper limit at which collectorless flotation of sulphide minerals comes to an end.

It is worth noting that the type of species formed on mineral surfaces is dependent upon the pH and redox potential of the system. Eh-pH diagrams are the most suitable means of illustrating relationships that exist in reactants in aqueous systems as a function of the oxidizing potential and pH. Figure 2.8 shows a S-O-H system, in which the most stable species likely to form over a wide range of pH under standard conditions is SO_4^{2-} ions.

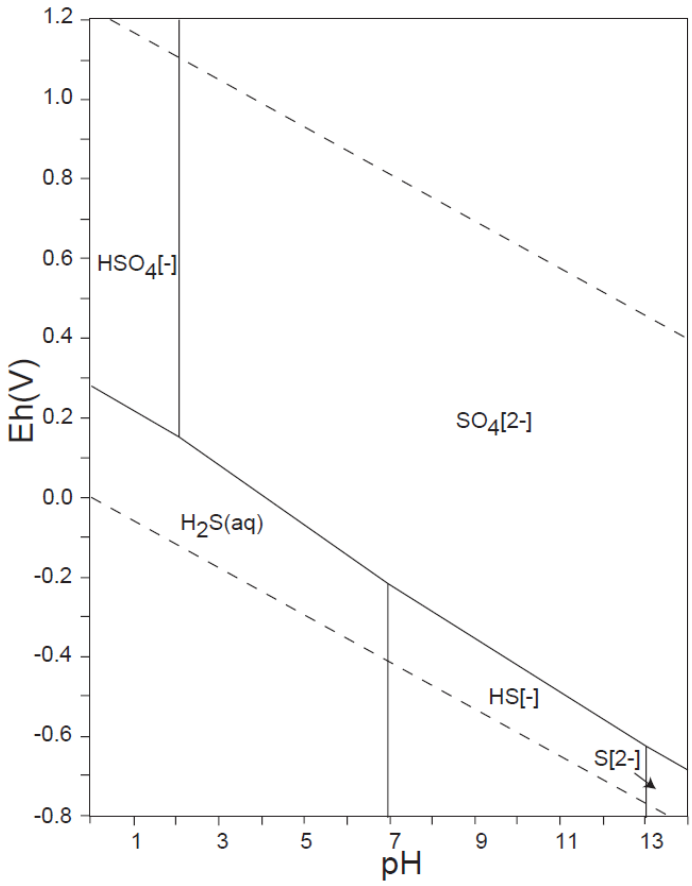

Figure 2.8: Eh-pH diagrams of the system S-O-H. Σ S = 10-10, 298.15 K, 105 Pa (Takeno, 2005).

Sulphide systems are considered to be complex in view of the fact that the equilibria Equations 2.4 to 2.7 control the stability of the species H_2S, HS^-, HSO_4^- and SO_4^{2-}. Therefore, sulphide minerals such as PtS and PdS may coexist with a solution containing these sulphur species.

$$H_2S \leftrightarrow HS^- + H^+ \quad \text{(Eqn. 2.4)}$$

$$H_2S \leftrightarrow S^0 + 2H^+ + 2e^- \quad \text{(Eqn. 2.5)}$$

$$S^0 + 4H_2O \leftrightarrow SO_4^{2-} + 8H^+ + 6e^- \quad \text{(Eqn. 2.6)}$$

$$S^0 + H_2O \leftrightarrow HSO_4^- + 7H^+ + 6e^- \quad \text{(Eqn. 2.7)}$$

Figure 2.9 shows a Pourbaix diagram for a Pd-S-H_2O system, in which the lower sulphide, PdS seems to encroach the regions where the disulphides are expected to form. The paradox of the

formation of lower sulphides from a disulphide with an increase in Eh is due to the oxidation of sulphide which more than counterbalances the reduction of the metal ion (Westland, 1981).

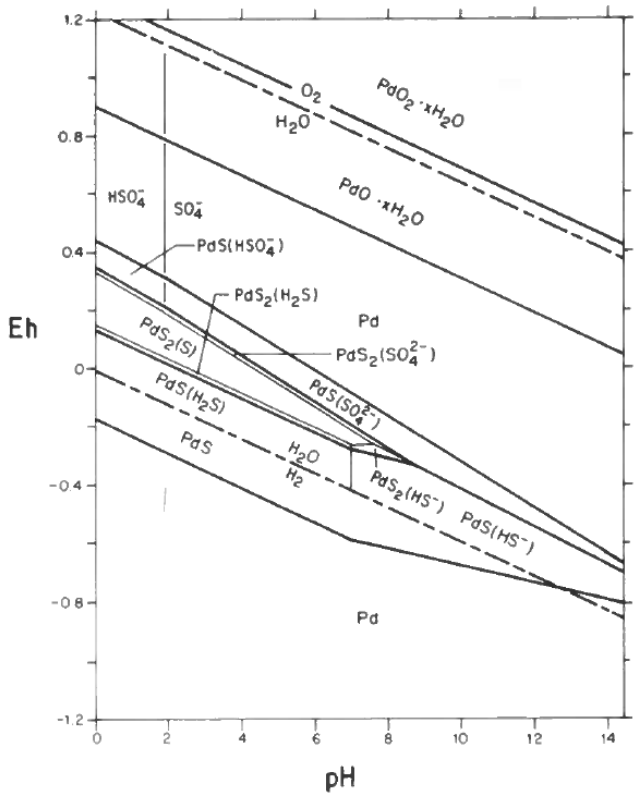

Figure 2.9: Eh-pH diagram for the system Pd-S-H_2O (Westland, 1981).

Hence, the oxidation of PdS in alkaline conditions is most likely to occur as in Equation 2.8a.

$$PdS + 4H_2O \leftrightarrow Pd + SO_4^{2-} + 8H^+ + 6e^- \quad \text{(Eqn. 2.8a)}$$

$$Eh = 0.468 - 0.0788\,pH + 0.0098\log\,[SO_4^{2-}] \quad \text{(Eqn. 2.8b)}$$

Excessive oxidation conditions are known to have a detrimental effect on the flotation performance of sulphide minerals owing to reduced collector selectivity. Hence, moderate oxidizing conditions are believed to have a beneficial effect on the formation of the hydrophobic sulphur species and on adsorption of collectors. During oxidation processes, hydrolyzed metal ions and oxidized sulphur species may re-adsorb on the sulphide mineral surfaces as thin layers or react with each other and possibly precipitate to colloidal particles. The interaction of the layers of oxidation products is suggested to be weak in nature, hydrophobic and/or electrostatic (Clarke et al., 1995).

2.3.1.2 Flotation of PGM Sulphides

The flotation of PGM sulphides is an area that has been neglected in literature. Due to their small grain size and the unavailability of PGMs for test work, previous work have successfully used synthetic samples that serve as a proxy for the PGM minerals (Shackleton et al., 2007). A comprehensive electrochemical investigation on the mechanisms of interaction of PGM minerals with collectors and copper sulphate carried out by Tadie et al. (2015a), determined that PdS and PtS minerals may react in almost a similar manner as a result of similar crystal structures. In the case of PdS, the adsorption of sodium ethyl xanthate (SEX) was observed to thermodynamically favour the formation of PdX_2 (Equation 2.9).

$$2X^- + PdS + 4H_2O \rightarrow PdX_2 + SO_4^{2-} + 8H^+ + 8e^- \qquad E = -0.226\ V \qquad \text{(Eqn. 2.9)}$$

Moreover, it was outlined that the presence of SEX enhanced the formation of anodic currents that were more positive than those generated in the absence of the collector (Figure 2.10). Notably, the anodic currents were above the dixanthogen reduction potential. It was established that the reduction of oxygen was completely inhibited due to a greater surface coverage of dixanthogen on the PdS mineral surface.

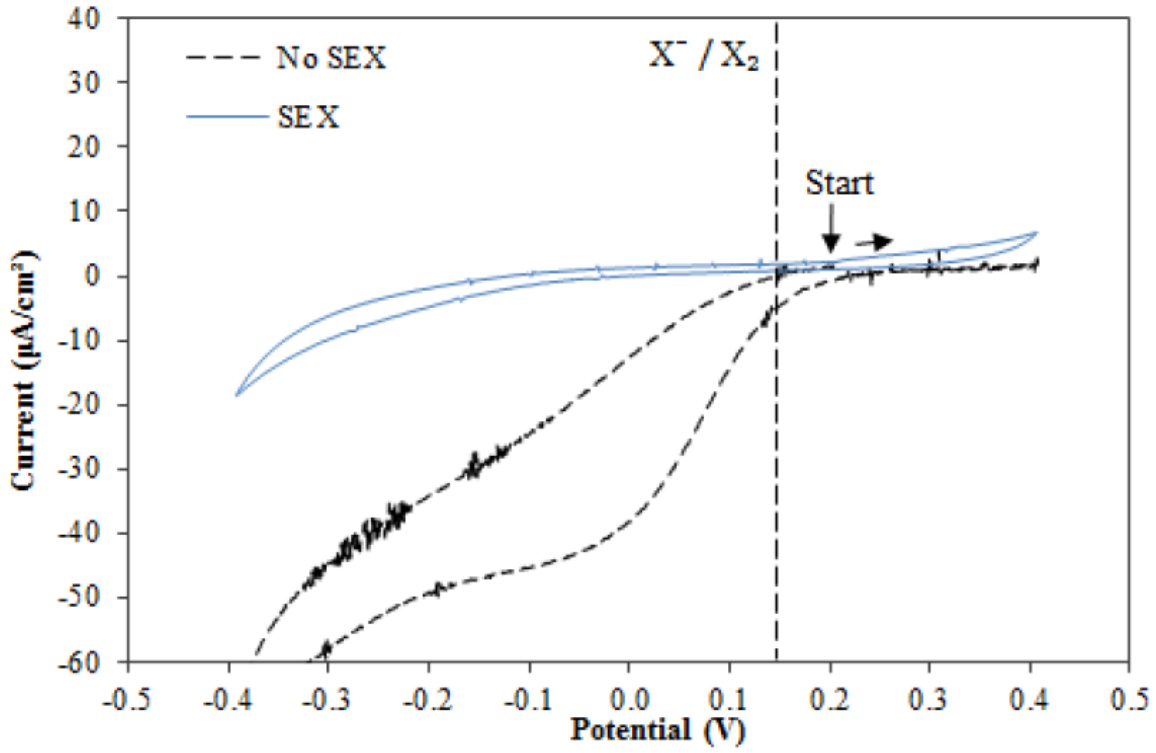

Figure 2.10: Voltammograms for PdS in the absence and presence of 6.24×10^{-4} S.E.X collector. Dotted line represents the oxidation potential for dixanthogen (0.15 V) (Tadie et al., 2015a).

In accordance with the findings mentioned above, Shackleton et al. (2007) investigated on the floatability of PdS in the absence and presence of a xanthate collector. Flotation recoveries of 64 % and 95% were obtained, respectively. This observation implies that PdS readily floats in the presence of xanthate collectors.

2.3.2 Reactivity and Flotation behaviour of PGM Tellurides

2.3.2.1 Reactivity of PGM Tellurides

Literature does not hold much information on the reactivities of PGM tellurides. However, a few publications have reported on the reactivities of Pd-bearing bismuth-tellurides (Elvy and Williams, 1996, Vermaak et al., 2005). Elvy and Williams (1996) investigated the oxidation of a Pd-Te-Bi system (PdTe, PdTeBi, PdBi). It was found that the sequence of reactivity of the Pd-Te-Bi system towards oxidation at ambient temperatures was PdTe < PdTeBi < PdBi. This observation denotes that PdTe is more resist to oxidation than PdTeBi, due to its high Te content. The most stable species formed upon the oxidation of PdTe in air has been considered to be TeO_2 (Equation 2.10) (D'Olimpio et al., 2019). In the case of PdTeBi the oxidation products formed were observed to be incongruent due to the possible migration of Te and Bi to the air/water interface to form the oxides TeO_2 and/Bi_2O_3 (Equation 2.11), despite the fact that pure Te and Bi do not oxidize readily in their pure states. However, it was observed that the oxidation of the Pd-Te-Bi system did not yield PdO at ambient temperatures, though chemisorption of oxygen is perceived to occur.

$$PdTe + xO_2 \rightarrow PdTe_{1-x} + xTeO_2 \qquad \text{(Eqn. 2.10)}$$

$$PdTeBi + \left(x + \frac{3y}{4}\right) O_2 \rightarrow PdTe_{1-x}Bi_{1-y} + xTeO_2 + (\frac{y}{2})Bi_2O_3 \qquad \text{(Eqn. 2.11)}$$

In agreement with the proposed oxidation products reported by Elvy and Williams (1996), D'Olimpio et al. (2019) further observed that TeO_2 may remain in the sub-nanometric range even after a year of exposure. However, it was found that TeO_2 is a thermally unstable species due to temperature-induced reduction. Additionally, $PdTe_2$ was observed to be thermally stable even at temperatures above 227 ^{0}C.

2.3.2.2 Flotation of PGM Tellurides

The flotation behaviour of PGM tellurides has not received much attention to date. However, very limited studies have looked into the flotation behaviour of the Pd-Bi-Te system (Vermaak et al.,

2005); and Pt, Pd tellurides (Shackleton et al., 2007, Tadie et al., 2015a) in the absence and presence of xanthate collectors.

Thermodynamic data for a Te-O-H system is shown in the Pourbaix diagram in Figure 2.11. It is shown that under standard pressure and temperature, the most stable species that forms over a very wide range of pH in a Te-O-H system is TeO_3^{2-}. An extensive electrochemical investigation carried out by Mishra et al. (1990), investigated the anodic oxidation of Te ions. The study has since proved the thermodynamic feasibility of the oxidation reaction of Te^0 to TeO_3^{2-} (Equation 2.16) under alkaline conditions.

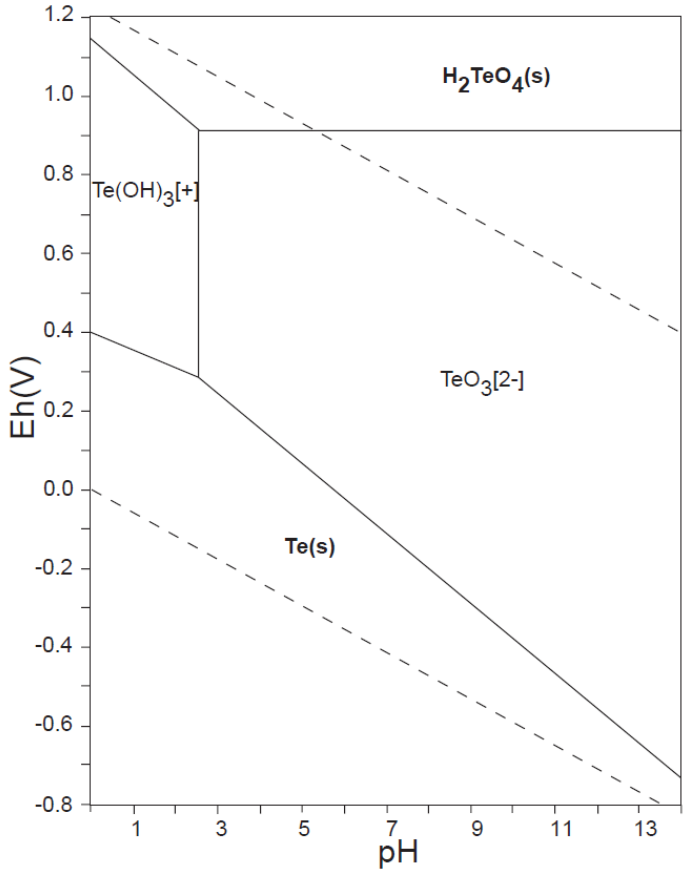

Figure 2.11: Eh-pH diagrams of the system Te-O-H. Σ Te = 10^{-10}, 298.15 K, 10^5 Pa (Takeno, 2005).

A number of chemical and electrochemical reactions in a Te-H_2O system under alkaline conditions have been proposed to occur through any of the reactions shown in Equations 2.12 to 2.19 (Mishra et al., 1990).

$$Te^0 + 2e^- \leftrightarrow Te^{2-} \qquad E = -1.38 \qquad \text{(Eqn. 2.12)}$$

$$Te^0 + Te^{2-} \leftrightarrow Te_2^{2-} \qquad \text{(Eqn. 2.13)}$$

$2Te^0 + 2e^- \leftrightarrow Te_2^{2-}$ E = -1.06 (Eqn. 2.14)

$Te_2^{2-} + 2e^- \leftrightarrow 2Te^{2-}$ E = -1.68 (Eqn. 2.15)

$TeO_3^{2-} + 3H_2O + 4e^- \leftrightarrow Te^0 + 6OH^-$ E = -0.82 (Eqn. 2.16)

$2TeO_3^{2-} + 12H^+ + 10e^- \leftrightarrow Te_2^{2-} + 6H_2O$ E = 0.25 (Eqn. 2.17)

$TeO_3^{2-} + 3H_2O + 6e^- \leftrightarrow Te^{2-} + 6OH^-$ E = -1.04 (Eqn. 2.18)

$TeO_4^{2-} + H_2O + 2e^- \leftrightarrow TeO_3^{2-} + 2OH^-$ E = -0.33 (Eqn. 2.19)

With regards to the few studies that have investigated the floatation behaviour of PGM tellurides, the oxidation products of $PtTe_2$ in alkaline conditions, have been proposed using the standard Gibbs energy of formation (Tadie et al., 2015a). It was surmised that the oxidation of $PtTe_2$ at a pH of 9.2 could most likely result in the formation of tellurite ions (Equations 2.20 & 2.21 and Figure 2.11).

$PtTe_2 + H_2O \rightarrow PtTe + TeO_3^{2-} + 6H^+ + 4e^-$ E = 0.112 V (Eqn. 2.20)

$PtTe_2 + 7H_2O \rightarrow PtO + 2TeO_3^{2-} + 14H^+ + 10e^-$ E = 0.221 V (Eqn. 2.21)

Furthermore, the oxidation of $PdTe_2$ under alkaline conditions has been proposed to exhibit a similar behaviour to $PtTe_2$. Therefore, any or all of the reactions in Equations 2.22 to 2.26 are expected to occur (Tadie et al., 2015a).

$PdO + 2TeO_3^{2-} + 14H^+ + 10e^- \rightarrow PdTe_2 + 7H_2O$ E = 0.188 V (Eqn. 2.22)

$Pd(OH)_2 + 2TeO_3^{2-} + 14H^+ + 10e^- \rightarrow PdTe_2 + 8H_2O$ E = 0.210 V (Eqn. 2.23)

$Pd^{2+} + 2TeO_3^{2-} + 12H^+ + 10e^- \rightarrow PdTe_2 + 6H_2O$ E = 0.213 V (Eqn. 2.24)

$PdTe + TeO_3^{2-} + 6H^+ + 4e^- \rightarrow PdTe_2 + 3H_2O$ E = 0.133 V (Eqn. 2.25)

$PdO + TeO_3^{2-} + 8H^+ + 6e^- \rightarrow PdTe + 4H_2O$ E = 0.226 V (Eqn. 2.26)

It has been proposed that the adsorption of ethyl xanthate on a Pd-Bi-Te system gives rise to the co-presence of xanthate and dixanthogen. Hence, the poor flotation behaviour of Pd-Bi-Te was attributed to possibly the particle size of the minerals rather than their interaction with collectors (Vermaak et al., 2005). Similarly, Shackleton et al. (2007) observed that $PtTe_2$ and $PdTe_2$ minerals readily float in the presence of SIBX, owing to the adsorption of the xanthate ions on the mineral

surfaces. However, poor recoveries or very slow flotation rates for $PtTe_2$ and $PdTe_2$, were attributed to the presence of copper ions that are administered to process water to enhance the flotation of base metal sulphides. The depressing effect of copper sulphate to the flotation recoveries of the telluride minerals was speculated to be caused by the precipitation of copper sulphate ions to $Cu(OH)_2$, was speculated to compete with SIBX for vacant active sites on the mineral surfaces, thereby inhibiting the adsorption of xanthates on telluride surfaces.

In support of the conclusions drawn by Vermaak et al. (2005) and Shackleton et al. (2007), the findings by Tadie et al. (2015a) also suggested the existence of xanthate ions on the PGM telluride mineral surfaces in the presence of xanthate collectors. It was proposed that the mechanisms of adsorption of xanthate collectors on telluride mineral surfaces involve the chemisorption of the xanthate collector ions followed by the oxidation of the adsorbed species into PtX_2 (Equation 2.27) and X_2 in the case of $PtTe_2$ and $PdTe_2$, respectively. This suggested that the mechanisms behind the adsorption of xanthate collectors on $PtTe_2$ and $PdTe_2$ are not similar. Moreover, it was observed that xanthate collectors demonstrate higher rates of oxidation on $PdTe_2$ surfaces compared to $PtTe_2$ surfaces. Generally, larger changes in potential were obtained for PGM telluride surfaces compared to their corresponding sulphides, in the presence of sodium ethyl xanthate (SEX) and sodium diethyl dithiophosphate (SEDTP) collectors. This observation was ascribed to tellurides reacting to a greater extent with the xanthate collectors than their corresponding sulphide counterparts. The higher rate of oxidation of Te was attributed to weaker bonds formed by Te owing to its lower electronegativity property compared to the S atom.

$$2X^- + PtTe_2 + 6H_20 \rightarrow PtX_2 + 2TeO_3^{2-} + 12H^+ + 10e^- \qquad \text{E} = 0.005\ \text{V} \qquad \text{(Eqn. 2.27)}$$

2.4 Adsorption mechanisms of xanthate collectors on mineral surfaces

The selective flotation of sulphide minerals has been successfully executed by the use of thiol-based collectors called xanthates (Richardson et al., 1984, Buckley and Woods, 1997, Kocabağ and Güler, 2007). The principal role of collectors is to selectively induce hydrophobicity onto desired valuable minerals. Collectors are heteropolar surfactants (Figure 2.12) that have a non-polar hydrocarbon chain that protrudes into the bulk phase thus rendering the mineral surface hydrophobic, and a polar region that interacts with the mineral surface (Wills and Napier-Munn, 2006).

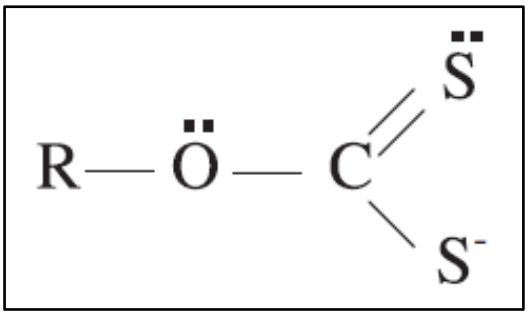

Figure 2.12: Generic structure of a xanthate collector. Where R represents an alkyl chain, in which the length and structure affects the manner in which the collector reacts.

The mechanisms of interaction between xanthates and mineral surfaces are dependent upon the collector type, nature and charge on mineral surface (Lotter and Bradshaw, 2010). Most sulphide minerals can sustain electrochemical processes due to their semiconducting property. Hence, they can either donate or accept electrons. Collectors adsorb onto mineral surfaces through physisorption or chemisorption. The concentration of species on a minerals surface, without the formation of a three-dimensional lattice characterizes an adsorption reaction.

Physisorption is generally a reversible process that is dominated by weak van der Waals bonds. Upon the occurrence of a physisorption reaction, the energy of physisorption is of the same order in magnitude as the heat of condensation. The energy released is estimated to be as low as between 20 - 60 KJ/mol, whereas the ΔH_{ads} is estimated to be less negative than -25 KJ/mol. Since the energy released is insufficient to break the bonds of the collector, the physisorbed collector molecules usually retains its identity (Persson, 1994).

Alternatively, chemisorption is characterized by chemical bonds that attach the collector ions to the active sites on a mineral surface. This interaction retains a covalent character. The collector molecule interacts with the mineral surface without movement of the metal ions from their lattice. Accordingly, a chemisorption reaction is limited to mono-layer coverage, whereas a surface chemical reaction is accompanied by movement of metal ions from their lattice, therefore generating multilayers. Additionally, the heat of chemisorption is considered to be approximately 5 - 10 times larger than that of a physisorption reaction. Thus, the energy is sufficient to break the bond of a collector molecule. Hence, the heat of adsorption is more negative than -40 KJ/mol. A chemisorption reaction is expected to be exothermic as no entropy loss occurs or possibly a small positive entropy may be observed if coordination sites of interest are hydrated. Hence, the transitional entropy of the products must be lower than the heat of adsorption of the incoming collector molecule (Persson, 1994, Bradshaw, 1997).

Early theories of collector adsorption mechanisms on sulphide mineral surfaces have been integrated by an electrochemical approach. It has been accepted that xanthate collectors adsorb onto sulphide mineral surfaces through a mixed potential. The mixed potential mechanism involves an anodic reaction where the xanthate collector transfers electrons to the mineral and a simultaneous cathodic reaction in which the reduction of oxygen (Equation 2.28) returns the charge back to the solution.

$$O_2 + 4H^+ + 4e^- \rightarrow 2H_2O \qquad \text{(Eqn. 2.28)}$$

The anodic reactions have been established to occur as one or more of the following reactions (Equations 2.29- 2.30) (Woods, 1996b).

a) Chemisorption

$$X^- \rightarrow X_{ads} + e^- \qquad \text{(Eqn. 2.29)}$$

For most mineral/collector systems, chemisorption is a thermodynamically favoured reaction, implying that it is the first reaction to transpire. The adsorbed xanthate ions go through further chemical reactions, hence forming a stable surface specie.

The rate of adsorption for xanthates can be expressed as in Equation 2.30 (Moslemi and Gharabaghi, 2016).

$$-\frac{dc_{x^-}}{dt} = kc_{x^-}\alpha - c_{O_2}\beta_{CH^+}\gamma \qquad \text{(Eqn. 2.30)}$$

Where $k = \left({}^{1}/_{V}\right)k'(A_aA_c)^{1/2}$; V is liquid volume; k' is the rate constant; A_a and A_c are surface areas for sites on which oxidation and reduction reactions occur, respectively; c_{x^-} and c_{O2} and c_{H+} are the concentrations of xanthate ions, dissolved oxygen and hydrogen ions in solution, respectively and α, β and γ are reaction orders.

b) Formation of a metal xanthate

$$MS + 2X^- + 4H_2O \leftrightarrow MX_2 + SO_4^- + 8H^+ + 8e^- \qquad \text{(Eqn. 2.31)}$$

The precipitation of insoluble salts may arise from the interaction between xanthate collectors and heavy metal ions. Solubility product is a determining factor for the precipitation of the salts (Equation 2.32 and 2.33).

$$K_{sp} = [M^{++}][X^-]^2 \qquad \text{for a divalent cation} \qquad \text{(Eqn. 2.32)}$$

Or as

$K_{sp} = [M^+][X^-]$ for a monovalent cation (Eqn. 2.33)

The solubility products for most metal xanthates are dependent upon the number of carbon atoms in the hydrocarbon group as shown in Figure 2.13. It has been inferred that precipitation of the insoluble salts is most likely to occur when the product of ionic activities is in excess of the solubility product. It is therefore a requirement that for a metal xanthate to exhibit a hydrophobic character, it should be present on the mineral surface rather than as a precipitate in the bulk solution (Chander, 1988).

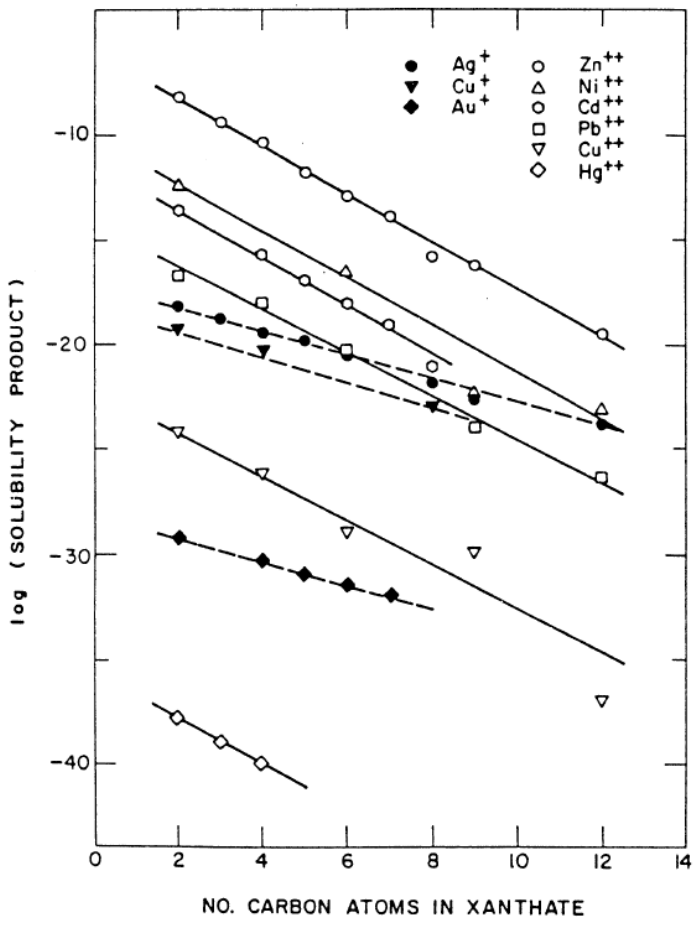

Figure 2.13: Solubility product of different metal xanthates (Aplan and Chander, 1988)

c) Formation of dixanthogen

$2X^- \leftrightarrow X_2 + 2e^-$ (Eqn. 2.34)

The anodic oxidation of a xanthate collector to dixanthogen can be represented by redox potential. Hence, the potential can be calculated by the Nernst equation (Equation 2.35) (Moslemi and Gharabaghi, 2016).

$$Eh_{X_2} = E^0_{X^-/X^2} - 0.059log[X^-] \quad \text{(Eqn. 2.35)}$$

Where E^0 is the standard redox potential for reaction in Equation 2.35. $[X^-]$ is the molar concentration of xanthate. There exists an inverse relationship between the equilibrium potential of a xanthate/dixanthogen couple and the length of hydrocarbon chain of a xanthate collector. An increase in the length of hydrocarbon chain results in a decrease in the equilibrium potential of a xanthate/dixanthogen couple. Therefore, a lower value for Eh^0 demonstrates that the type of collector readily oxidizes (Chander, 1988).

2.4.1 The influence of xanthate collector and mineral type

Electrochemical techniques and spectroscopy methods have been applied to investigate possible mechanisms involved when collectors interact with mineral surfaces (Allison et al., 1972, Tadie et al., 2015a).

It has been established that the various xanthate species formed on mineral surfaces in the presence of xanthate collectors in flotation systems, may impart some form of hydrophobicity. Amongst the proposed oxidation products formed through the oxidation of xanthates, dixanthogen is considered to impart a greater extent of hydrophobicity on mineral surfaces. Nonetheless, in the case of covellite, it was found that both dixanthogen and a metal xanthate may possibly form due to the initial formation of an unstable cupric xanthate that possibly might decompose to cuprous xanthate and dixanthogen (Allison et al., 1972). Table 2.4 shows that in the presence of xanthates, n-type semiconductors displayed the existence of dixanthogen on mineral surfaces. On the other hand, p type semiconductors were found to predominantly exhibit the presence of metal xanthates on their surfaces. However, this does not preclude the chances of having the cosorption of dixanthogen with a metal xanthate under certain conditions, though the former can be in minute quantities (Allison and Finkelsten, 1971).

Table 2.4: Correlation between mineral semi-conductor type and collector species formed on mineral surfaces

Mineral	Semi-conductor type (i)	Collector species identified (ii)
Realgar	no data	NPI
Orpiment	no data	NPI
Sphalerite	poor conductor	NPI
Stibnite	poor conductor	NPI
Cinnabar	n	NPI
Antimonite	No data	MX
Bornite	p	MX
Chalcocite	p	MX
Covellite	p	MX+ X_2 and MX (iii)
Galena	n and p	MX
Alabandite	no data	X_2
Arsenopyrite	n	X_2
Chalcopyrite	n	X_2
Molybdenite	n and p	X_2
Pyrite	n and p	X_2
Pyrrhotite	n and p (iii)	X_2

NPI represents No positive identification; MX represents metal xanthate and X_2 represents dixanthogen. i) Shuey (1975) ii) Allison et al. (1972) iii) Ackerman et al. (1986)

Woods (1971) investigated the interaction of ethyl xanthate with a galena surface using cyclic voltammetry. It was determined that a scan in the anodic direction generated an anodic peak that was assigned to the chemisorption of a monolayer of ethyl xanthate on the galena surface (Figure 2.14). An increase in anodic current that succeeded the anodic peak was assigned to the oxidation of a collector to a metal xanthate, lead ethyl xanthate and diethyl dixanthogen.

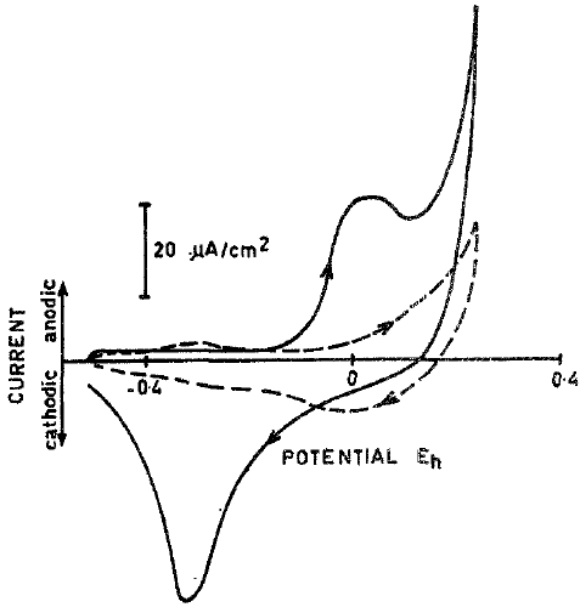

Figure 2.14: Voltammograms for a galena mineral surface at a pH of 9.2 in ethyl xanthate at 9.5×10^{-3} M (Woods, 1996b).

Pre-waves observed in the positive scan direction were an indication of a chemisorption reaction (Equation 2.36). Further studies on the oxidation of galena proposed that the initial product formed was a metal deficient sulfide, therefore implying that the reaction in Equation 2.37 is highly likely to occur in the presence of a xanthate collector (Buckley, 1996). However, this did not change the fact that a chemisorption reaction occurs at underpotentials.

$$C_2H_5OCS_2^- \rightarrow (C_2H_5OCS_2)_{ads} + e^- \quad \text{(Eqn. 2.36)}$$

$$PbS + 2xC_2H_5OCS_2^- \rightarrow xPb(C_2H_5OCS_2)_2 + Pb_{1-x}S + 2xe^- \quad \text{(Eqn. 2.37)}$$

It has been accepted that the oxidation of a sulphide mineral surface by oxygen, enhances the adsorption of xanthates (Richardson, 1995, Moslemi and Gharabaghi, 2016). In the case of pyrite, it has been determined that the existence of oxysulfides and ferric ions facilitate the formation of dixanthogen (Pecina et al., 2006). An increase in the concentration of ferrous ions increases the adsorption of xanthate ions. It was proposed that the reduction of ferric hydroxide and the oxidation of xanthate to dixanthogen occur simultaneously as shown if Figure 2.15 (Leppinen et al., 1995).

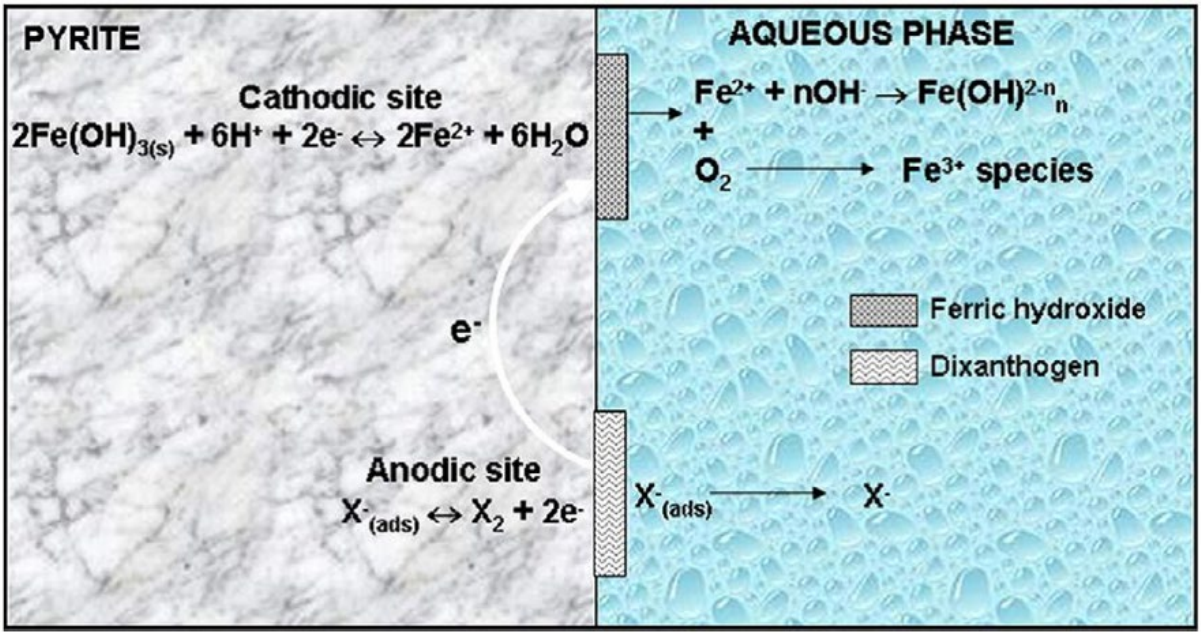

Figure 2.15: Dissolution of ferric hydroxide and formation of dixanthogen of a pyrite surface (Moslemi and Gharabaghi, 2016).

2.4.2 Adsorption mechanisms of xanthates in PGMs

A few publications have discussed the possible adsorption mechanisms of PGMs in xanthate collectors (Vermaak et al., 2004, Vermaak et al., 2005, Tadie et al., 2015a). Though some mechanisms have been proposed, this field still requires more attention.

Vermaak et al. (2004) investigated the possible mechanisms that occur in a Pd-Bi-Te system, in the presence of an ethyl xanthate. Pd-Bi-Te was anodically polarized at a potential of 0.3 V for 20 minutes in the presence of potassium ethyl xanthate. Impedance measurements showed lower capacitance values in the presence of an ethyl xanthate indicating the formation of a continuous layer on the mineral surface. The surface layer was assigned to the formation of multi-layers of dixanthogen owing to the equilibrium potential of ethyl xanthate at 1×10^{-3} M, which was measured to be 0.121 V. Furthermore, their Raman Spectroscopy studies confirmed the co-existence of xanthate with dixanthogen. This was an indication that xanthate first goes through a chemisorption reaction and the presence of dixanthogen was identified after long exposure of the mineral surface to the xanthate collector (Vermaak et al., 2005). Moreover, the presence of such hydrophobic species shows that the mineral is expected to be hydrophobic under the conditions used in the investigation, thus denoting that the low flotation recoveries for PGMs are not as a result of a lack of interaction between xanthate collectors and PGMs.

In agreement with the findings of Vermaak, (Tadie et al., 2015a), observed an anodic peak at 0.3 V for $PdTe_2$ in the presence of an ethyl xanthate (Figure 2.16). It was postulated that the two cathodic peaks observed upon their return scan, could be due to the formation of both a metal xanthate and dixanthogen on the $PdTe_2$ surface. Alternatively, it was discerned that in a PdS system in the presence of ethyl xanthate, the reduction of oxygen was almost completely inhibited (Figure 2.17). This possibly implies a slower rate of flotation for PdS than $PdTe_2$ in the presence of a xanthate collector (Shackleton, 2007). The absence of reduction peaks for PdS in the presence of the xanthate collector was proposed to be due to the presence of non-electrochemically active oxidation products that might have formed on the sulphide mineral. Additionally, it was determined that the rate of oxygen reduction for $PdTe_2$ was lower than that for PdS, hence indicating a slower rate of formation of xanthate hydrophobic species on $PdTe_2$ than on PdS.

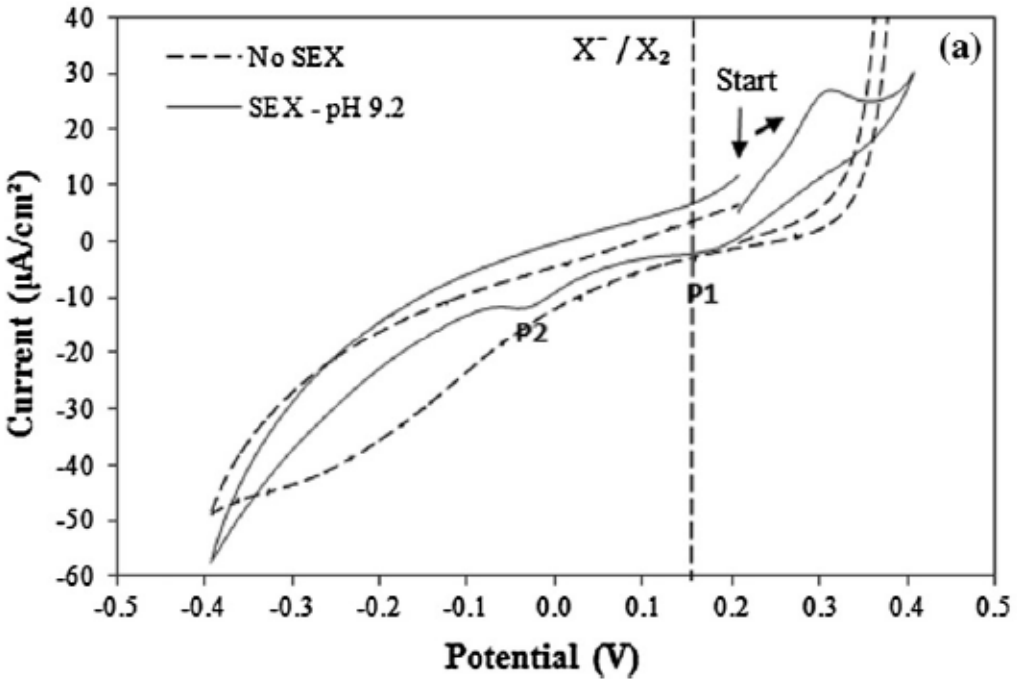

Figure 2.16: Voltammograms for $PdTe_2$ in the absence and presence of SEX at 6.25×10^{-4} M at a pH of 9.2. Vertical dotted line indicates the equilibrium potential (0.15 V) of SEX at 6.25×10^{-4} M.

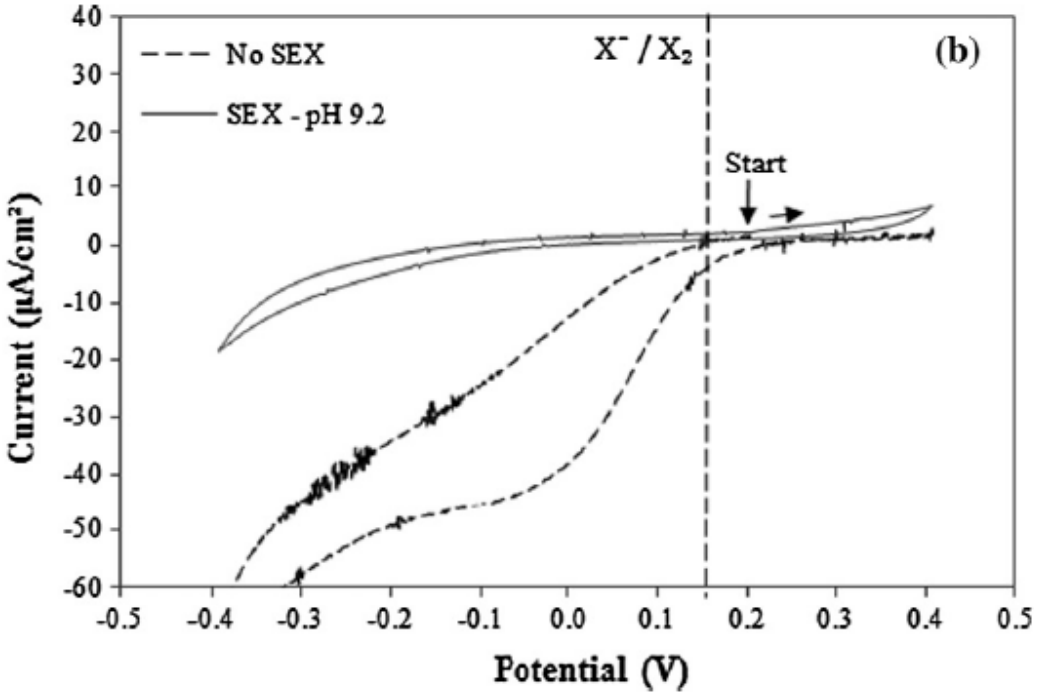

Figure 2.17: Voltammograms for PdS in the absence and presence of SEX at 6.25×10^{-4} M at a pH of 9.2. Vertical dotted line indicates the equilibrium potential (0.15 V) of SEX at 6.25×10^{-4} M.

2.5 Mineral- Solution interfaces and the electrical double layer

Adsorption mechanisms concerning minerals in aqueous conditions are controlled by an electrical double layer that is presumed to exist at the mineral-solution interface (Figure 2.18) (Fuerstenau, 1984). This model is used to visualize the ionic domain surrounding a charged colloid and in the bulk solution; and the occurrence of electrical repulsive forces. In flotation systems, the double layer is presumed to develop from charged species that migrate between the mineral and solution interface. A negatively charged mineral surface will attract the positively charged ions from the solution thereby forming a firmly attached layer of counter ions around the surface known as a Stern layer. A dynamic equilibrium develops when additional positive ions are attracted to the mineral surface but at the same time are repelled by the positively charged counter ions from the Stern layer and other positively charged ions approaching the negatively charge mineral surface. This results in the formation of a diffuse layer of counter ions. The positively charged counter-ions gradually decrease from the Stern layer until an equilibrium is reached with the counter ion concentration in the bulk solution. On the other hand, negatively charged ions gradually increase with distance as repulsive forces are screened out by positive counter-ions until an equilibrium is reached. Both the Stern and the diffuse layers form an electric double layer. The potential across the double layer decreases with an increase in distance from the surface until a potential of 0 is

reached at the boundary of the double layer (Figure 2.18). The thickness of the double layer is dependent upon ion type and concentration (Zeta-Meter Inc).

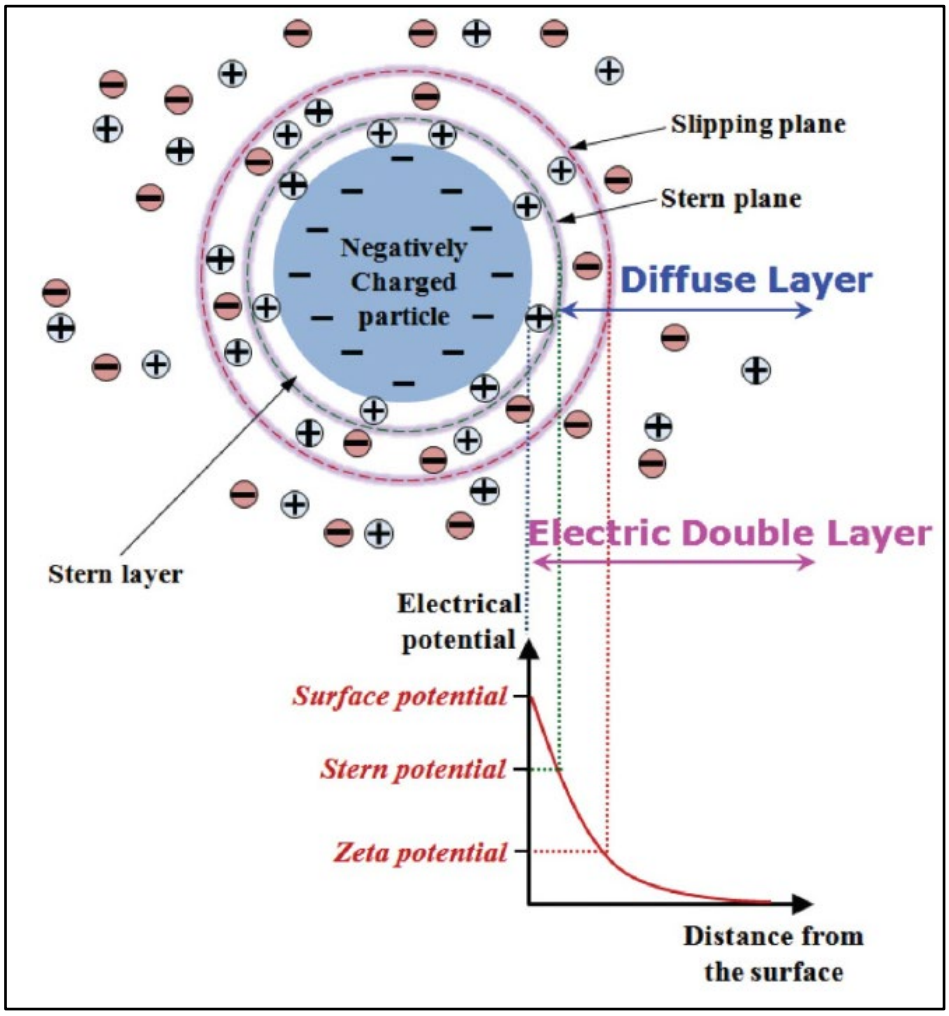

Figure 2.18: Electrical double layer (Park and Seo, 2011).

The magnitude of the Stern layer is dependent on ion hydration whereas the thickness of the diffuse layer is dependent upon the concentration of ions present in the system. Hence, the thickness of the diffuse layer, 1/k, for a symmetrical ion ($z_+ = z_- = z$), can best be described by the Debye-Huckel theory (Equation 2.38) (Fuerstenau, 1984).

$$K^2 = \frac{8\pi c z^2 F^2}{\varepsilon RT} \qquad \text{(Eqn. 2.38)}$$

Where c represents the concentration of ion in solution, ε represents the dielectric constant of the solution. In solutions of 1 - 1 valent ions, 1/k is 10^{-4}, 10^{-5}, 10^{-6} cm in length in 10^{-7}, 10^{-5} and 10^{-3} M solutions, respectively. Therefore an increase in ion concentration results in a decrease in the extension of the diffuse layer (Fuerstenau, 1984). With regards to ion size, it has been shown that

an increase in counter ion size with a decrease in ion concentration in the bulk solution, increases the electrical double layer (Bohinc et al., 2001).

The charge on the diffuse layer may be represented by the Gouy-Chapman theory (Equation 2.39) (Fuerstenau, 1984). The Gouy-Chapman theory shows an inverse relation between the adsorption density of counter ions in the diffuse layer and the concentration of ions if potentials does not change substantially.

$$\sigma_d = \sqrt{\frac{2\varepsilon RT}{\pi}}\sqrt{c}\,\sinh\left(\frac{zF\varphi_\delta}{RT}\right) \quad \text{(Eqn. 2.39)}$$

σ_d is the diffuse layer charge, ψ_δ is the potential drop to the Stern layer.

In addition to electrostatic forces, some ions strongly adsorb onto the Stern layer through other forces. Such ions are termed to be specific in adsorption. The adsorption density of such ions may be represented by a Lang-muir equation (Equation 2.40).

$$\frac{\theta}{1-\theta} = \frac{c}{55.5} exp\, -\Delta G^0_{ads}/RT \quad \text{(Eqn. 2.40)}$$

Where θ represents the fractional coverage, ΔG^0_{ads} represents the standard free energy of adsorption and $\frac{c}{55.5}$ represents mole fraction of solute in the solution.

The standard free energy of adsorption contains other adsorption terms other than the electrostatic effects, $z_\pm F\psi\delta$. It can be expressed as in Equation 2.41.

$$\Delta G^0_{ads} = z_\pm F\varphi\delta + \Delta G^0_{chem} + \Delta G^0_{CH_2} + \Delta G^0_{solv} + \Delta G^0_H + \cdots \quad \text{(Eqn. 2.41)}$$

Where ΔG^0_{chem} is the chemical bonding at the surface of the mineral, $\Delta G^0_{CH_2}$ is free energy allied to the hydrocarbon chain association at the mineral surface, ΔG^0_{solv} is the adsorption mechanism determined by hydration or solvation of ions and surfaces. ΔG^0_H represents the contribution of hydrogen bonding to the adsorption mechanism.

The extent to which the two capacitances found in series (Equation 2.42) on the double layer (the Stern layer and the diffuse layer) both dominate is dependent upon the concentration of ions in a solution. The stern layer dominates in more concentrated solutions and alternatively, the diffuse layer dominates in dilute solutions.

$$\frac{1}{C} = \frac{1}{C_i} + \frac{1}{C_d} \quad \text{(Eqn. 2.42)}$$

Where C is the capacity of the double layer. C_i is the capacity of the Stern layer and C_d is the capacity of the diffuse layer. Hence, the capacitance is increased and dominated by C_d in dilute solutions and decreased and dominated by C_i in concentrated solutions.

Additionally, the differential capacity of the diffuse layer is represented by Equation 2.43.

$$C_d = {}^{-d\sigma_d}/_{d\varphi_\delta} = \frac{K\varepsilon}{4\pi} cosh \frac{zF\varphi\delta}{2RT} \quad \text{(Eqn. 2.43)}$$

And the differential capacity of the Stern layer is given by Equation 2.44.

$$C_i = {}^{\sigma_o}/_{(\varphi_o - \varphi_\delta)} \quad \text{(Eqn. 2.44)}$$

The types of ions considered in mineral-water systems can be grouped according to their impact on the double layer (Fuerstenau, 1984). The ions can be classified as follows:

1. Potential determining ions - These ions easily pass through the mineral and water phases. A few examples of potential determining ions are Ba^{2+}, SO_4^{2-}, H^+, OH^-. These ions induce a surface charge, σ_0 and determine the magnitude of surface potential, ψ_0.
2. Surface active organic ions - These ions include organic ions that physisorb through electrostatic forces and hydrocarbon chain attachment in the Stern layer. Alternatively, these ions may also chemisorb onto the mineral surface sites.
3. Surface active inorganic ions - These inorganic ions specifically target the Stern layer and adsorb through simple electrostatic forces and forces of interaction. Examples include multivalent cations and anions that result from electrical interactions and hydrolyzed metal ions which display surface activity through solvation and chemisorption.
4. Non-surface-active indifferent ions - These are counter ions that exist in the diffuse layer and their main purpose is to maintain electrostatic neutrality. A few of the examples are K^+, Na^+, Cl^-, NO_3^- with TiO_2, Fe_2O_3.

2.6 Effect of ions on the adsorption of xanthate collectors

The presence of electrolytes has been shown to have an impact on the adsorption rate of ionic surfactants, in which the ionic strength of electrolytes has been determined to play a huge role (Atkin et al., 2001). It has been proposed that at lower ionic strengths, the adsorption rate of surfactants is increased owing to greater screening of electrostatic repulsive forces between incoming monomers and adsorbed monomers. On the other hand, at high ionic strengths, more co-ions are present to compete with the surfactant ions for the active sites on a surface, hence a reduction in adsorption rate of the surfactant ions (Atkin et al., 2001). In some instances, the presence of inorganic ions has been reported to promote the chemisorption of surfactants by providing more adsorption sites for surfactant ions (Malati, 1967). The nature of electrolyte ions has been considered to also play a vital role. Anions have been postulated to exhibit a greater depressing effect than cations of the same valence (Ofor, 1996). Additionally, divalent ions have been found to display a greater effect on collector adsorption at mineral surfaces compared to monovalent ions (Potapova et al., 2010).

In the flotation of base metal sulphides, the effect of inorganic ions has been found to be predominantly dependent upon the type of mineral/ore (Corin et al., 2011, Manono et al., 2016, October et al., 2021).

Effects of the divalent ions, Ca^{2+} and SO_4^{2-} from recycled process water on the flotation of chalcopyrite and galena were investigated by Ikumapayi et al. (2012) and Ikumapayi and Rao (2015). The ions were explored at concentrations of 186 mg/l and 153 mg/l, respectively. It was speculated that the divalent ions inhibited the adsorption on xanthate ions on both chalcopyrite and galena, due to a possible ion exchange reaction that might have occurred between xanthate ions and formed mineral oxidation products. Moreover, it was deduced that calcium ions generally had a more significant impact on the flotation recoveries of both minerals than sulphate ions. Similar observations were made by Elizondo-Álvarez et al. (2017), who used a combination of cyclic voltammetry and micro-flotation measurements to investigate the effect of 0 - 2×10^{-2} mol/L of both Ca^{2+} and SO_4^{2-} ions on galena. In addition to the conclusions drawn by Ikumapayi et al. (2012) and Ikumapayi and Rao (2015), Elizondo-Álvarez et al. (2017) highlighted that the hindrance of the ion exchange reactions between xanthate-sulphate, xanthate-carbonate and xanthate-hydroxyl results in a reduction in the hydrophobic nature of galena thereby causing a decrease in the flotation recoveries of the mineral. It was presumed that SO_4^{2-} ions form a non-uniform barrier of lead sulphate on the mineral surface. This barrier was proposed to inhibit the

interaction of xanthate ions with the active sites on the mineral surface. Furthermore, low concentrations of 0.005 mol/l for both ions did not have an effect on the recoveries of galena.

Hodgson and Agar (1989) conducted electrochemical investigations to determine if Ca^{2+}, SO_4^{2-} and $S_2O_3^{2-}$ ions at concentrations of 350 mg/l, 1 600 mg/l and 170 mg/l, respectively, were surface active on pyrrhotite and pentlandite minerals. The ions were reported to be surface active at normal process water pH and based on their bubble contact and batch flotation test work, their adsorption was proposed to reduce selectivity of mineral surfaces. In the case of pyrrhotite, it was proposed that Ca^{2+} ions coordinate onto the mineral surface via sulphur sites, whereas SO_4^{2-} and $S_2O_3^{2-}$ ions were proposed to coordinate through Fe sites and oxidized Fe sites or CaS_2 product, respectively (Figure 2.19). Additionally, $S_2O_3^{2-}$ ions were suggested to regulate the oxidation of pyrrhotite. On the other hand, Ca^{2+} ions were considered to possibly chemisorb onto the pentlandite mineral surface, thereby replacing the metal ions on the mineral. Hydrophobicity tests that were conducted showed that $S_2O_3^{2-}$ ions hindered the hydrophobicity of both minerals but preferentially depressed pentlandite.

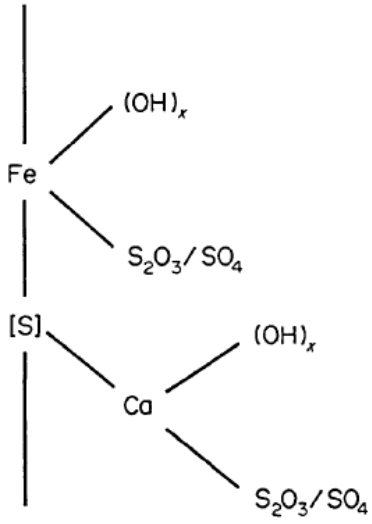

Figure 2.19: Coordination of calcium, sulphate and thiosulphate ions on a pyrrhotite surface (Hodgson and Agar, 1989).

The depressive effect of the divalent ions Ca^{2+} and Mg^{2+} have been associated with the formation of hydrophilic species, $CaCO_3$ and $Mg(OH)_2$, respectively, which inhibit the adsorption of xanthates onto mineral surfaces. However, SO_4^{2-} ions were reported to display a significant positive effect on the flotation recoveries of galena, chalcopyrite and sphalerite. The positive effect was observed to occur at concentrations above 1 500 mg/l. The effect of the SO_4^{2-} ions was attributed to the formation of slightly soluble heavy metal sulphite salts, $PbSO_4$, in the case of galena which

exhibits a K_s of $1.8*10^{-8}$ at ambient temperature in water (Boujounoui et al., 2015). These findings together with the aforementioned effect of SO_4^{2-} ions on other base metal sulphides display the essential role of ionic strength and mineral type in the adsorption mechanisms that occur on mineral surfaces, thereby affecting final flotation recoveries. In agreement with the findings of Boujounoui et al. (2015), Mg^{2+} ions were observed to exert a more significant depressive effect on the flotation of chalcopyrite and molybdenite than Ca^{2+} (Hirajima et al., 2016). In the latter study it is worth noting that the concentration of Mg^{2+} ions used was approximately seven times more than in the former study (0.0014 M). The fact that Mg^{2+} ions exhibit a negative impact on xanthate adsorption even in the lower concentration range goes on to show the great impact that these ions have on the flotation performance of valuable minerals.

(Mhonde et al., 2020) assessed the influence of ions on the adsorption of a xanthate collector using multiple linear regression. Na^+ and Ca^{2+} were determined to enhance the adsorption of a xanthate collector on sulphide mineral surfaces whereas Mg^{2+} and $S_2O_3^{2-}$ ions were suggested to reduce xanthate adsorption owing to the precipitation of hydroxides (Boujounoui et al., 2015, Hirajima et al., 2016). Oxidation products of Mg^{2+} have been proposed to passivate mineral surfaces whereas $S_2O_3^{2-}$ ions were surmised to compete with xanthate ions for active sites on mineral surfaces.

The effect of NaCl on xanthate adsorption on sphalerite surfaces was investigated by Wang et al. (2015). At low concentrations < 0.1 M, a decrease in induction time was observed with increasing ionic strength, whilst at high concentrations of NaCl > 0.1 M, induction time was observed to substantially increase with an increase in NaCl concentration. Such a phenomenon indicates the important role played by the ionic strength of inorganic ions in process water.

2.7 Electrochemical techniques

Electrochemical techniques have been used successfully for decades to give invaluable information on the possible mechanisms involved when base metal sulphides interact with flotation reagents (Allison et al., 1972, Wang and Forssberg, 1991, Ekmekçi et al., 2010b, Moslemi et al., 2011). Some electrochemical techniques that will be used in this study shall be reviewed.

2.7.1 Rest potential technique

Rest potential measurements are thermodynamic, purely electrolytic measurements that evaluate the potential difference between a working electrode and a reference electrode (Equation 2.45). Rest potential, also referred to as mixed potential or open circuit potential or zero-current potential

or corrosion potential is exhibited by sulphide minerals in flotation processes. A rest potential arises when the potential of an electrode is governed by more than one redox reaction. A mineral electrode is at its rest potential when the current due to the anodic process is equal to the current due to the cathodic process (Chander, 1988).

$$E_{OCP} = E_{WKG} - E_{REF} \quad \text{(Eqn. 2.45)}$$

Where E_{OCP} is the rest potential/open circuit potential, E_{WKG} is the potential at the working electrode and E_{REF} is the potential at the reference electrode.

Rest potentials are used to establish the state of oxidation of minerals. The work of Allison et al. (1972) shows the significance of rest potentials in determining surface oxidation products of sulphide minerals in the presence of xanthates (Table 2.5). It was deduced that the interaction of xanthates with sulphide minerals results in the formation of either dixanthogen or a metal-xanthate and not both. Furthermore, it was concluded that dixanthogen was formed as the primary product on minerals that had their rest potentials above the equilibrium potential of the dixanthogen/xanthate couple, 0.13 V. Alternatively, metal xanthate formed as the principal product in systems where the rest potentials were below the equilibrium potential of the dixanthogen/xanthate couple.

Table 2.5: Rest potentials for various minerals in 6.24×10^{-4} M KEX and corresponding oxidation species formed at a pH of 7 (Allison et al., 1972).

Mineral	Oxidation product formed	Rest potential after 10 minutes vs N.H.E
Arsenopyrite	X_2	+0.22
Pyrite	X_2	+0.22
Pyrrhotite	X_2	+0.21
Molybdenite	X_2	+0.16
Alabandite	X_2	+0.15
Chalcopyrite	X_2	+0.14
Covellite	X_2	+0.05
Bornite	MX	+0.06
Galena	MX	+0.06
Chalcocite	NPI	+0.06
Cinnabar	NPI	-0.05
Antimonite	NPI	-0.09
Orpiment	NPI	-0.1
Realgar	NPI	-0.12
Stibnite	NPI	-0.125
Sphalerite	NPI	-0.15

The effect of pH on the rest potentials of pyrite and pyrrhotite was investigated by Moslemi et al. (2011). It was found that an increase in pH decreases the rest potentials for both pyrite and pyrrhotite minerals. It was speculated that solutions of high pH values favour the formation of iron hydroxides that precipitate on the mineral surfaces thus hindering further oxidation reactions from occurring on the mineral surfaces.

Rest potential measurements have also been used to investigate the surface chemical inertness of pyrite and gold (Huai et al., 2018). In the presence of Fe^{3+} ions, pyrite and gold displayed rest potential values of 630 mV and 805 mV, respectively, where it was suggested that gold is a more noble mineral than pyrite due to its higher rest potential relative to pyrite. On the other hand, in the absence of Fe^{3+} ions, pyrite had a higher rest potential value relative to that of gold, in which it was concluded that gold is slightly more active than pyrite at a pH of 2.

Ekmekçi et al. (2010b) used rest potential measurements to investigate the differences in state of surface oxidation between different pyrrhotite electrodes at pH 7 and 10. It was determined that the rate of formation of oxidation products was higher at pH 10 than 7. At pH 10, it was shown that magnetic pyrrhotite is more reactive than non-magnetic and mixed pyrrhotite owing to its high rest potential value. It was surmised that this observation could be due to the fact that magnetic pyrrhotite has more vacancies (1 in 8 vacancies for Fe_7S_8), thus more hole type conductivity because of the Fe deficiency in its crystal structure than non-magnetic pyrrhotite which possesses 1 in 10 vacancies for Fe_9S_{10}. Hence, the greater availability of vacant sites allows for electron transfer.

An electrochemical investigation into the effects of xanthate collector type and mineral type on rest potentials was performed by (Tadie et al., 2015b). It was observed that the equilibrium potential for sodium diethyl diphosphate (SEDTP) was higher compared to that of SEX. This indicates that SEX readily oxidizes compared to SEDTP (Chander, 1988), hence all minerals that were investigated in the presence of SEDTP had their rest potentials lower than the equilibrium potential of SEDTP, implying that a metal-xanthate specie predominantly forms on the mineral surfaces. Additionally, it was proposed that SEX collector oxidizes to its dimer form on PtS and $PdTe_2$ mineral surfaces compared to PdS and $PtTe_2$ minerals.

2.7.2 Cyclic Voltammetry

Cyclic voltammetry is a versatile technique that has proven to be useful in determining redox processes that occur when minerals interact with xanthates (Woods, 1971, Hodgson and Agar, 1989, Khan and Kelebek, 2004).

In this technique, the potential applied to the working electrode is scanned linearly from E_i, where no reaction occurs at the electrode surface. The potential is then varied between switching potentials, E_s and E_f (Figure 2.20). The voltammogram shown in Figure 2.21, indicates that as the potential is scanned in the positive direction the current develops into a peak and then decays in a conventional manner. However, depending on the system at hand, the scan can be initiated in the negative direction. Hence, the current obtained is highly dependent upon movement of electroactive species from the bulk solution to the electrode surface and any electron transfer reactions that may occur. Therefore, movement of electroactive species is dominated by diffusion in a quiescent solution with a stationary electrode (Mabott, 1983).

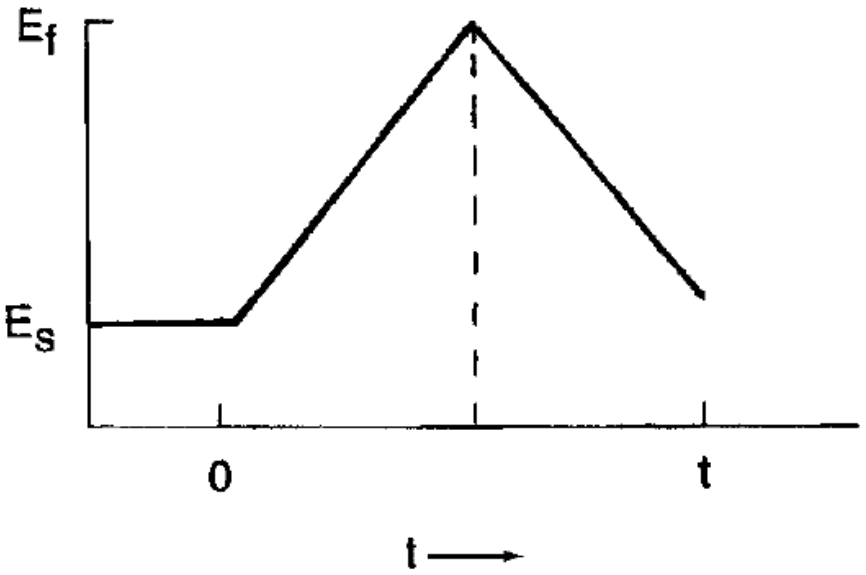

Figure 2.20: Applied potential, where E_S and E_f are switching potentials (Persson, 1994).

For the oxidation process, the electron transfer rate constant, k_r, can be expressed as a function of potential (Equation 2.46).

$$k_r = k^o \exp\left(\frac{(1-\alpha)nF}{RT}\right)(E - E^{o'}) \qquad \text{(Eqn. 2.46)}$$

Where k^o is the standard heterogeneous electron-transfer rate constant, $\propto$ is the transfer coefficient, n is the number of electrons transferred per molecule, F is the Faraday constant, R is the universal gas constant, T is temperature in Kelvin and $E^{o'}$ is the reduction potential.

On the reverse scan, the oxidized form is reduced back to the initial material and vice-versa. The electron transfer rate constant for the reduction process, k_f, can be theoretically represented by Equation 2.47.

$$k_f = k^o exp\frac{-\propto nF}{RT}(E - E^{o'}) \qquad \text{(Eqn. 2.47)}$$

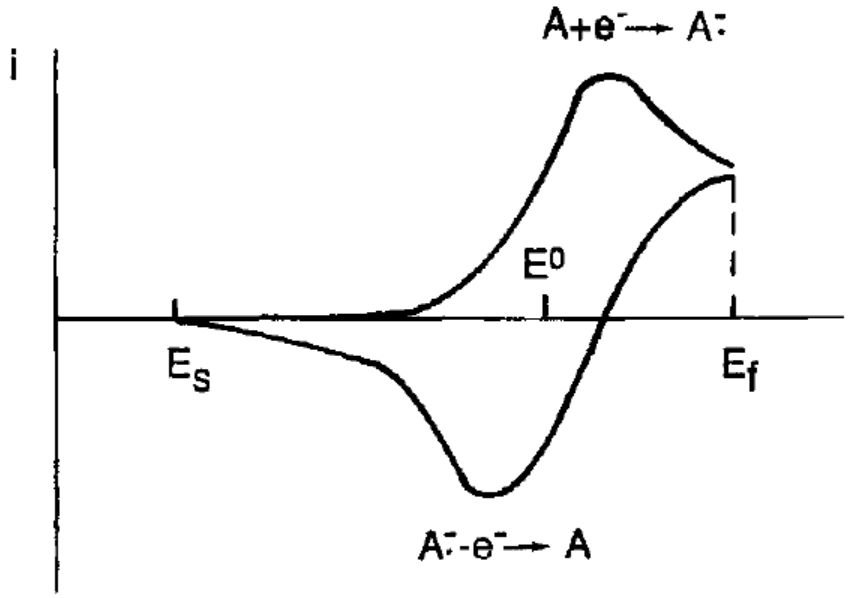

Figure 2.21: Cyclic voltammogram resulting from the potential sweep in Figure 2.20 (Persson, 1994).

A comprehensive study on the mechanisms of interaction of ethyl xanthate on platinum, gold, copper and galena electrodes was executed by Woods (1971). It was inferred that xanthate ions are adsorbed and desorbed between a potential range of -0.47 V and 0.2 V on a galena surface and that xanthate adsorption does not involve a reaction with the oxidation products formed on a galena surface. Furthermore, it was deduced that unlike xanthate, dixanthogen is not chemisorbed but is rather physisorbed on the electrodes surfaces in multilayers. The formation of dixanthogen on all electrode surfaces was concluded to occur via an adsorbed xanthate radical on the electrode surfaces. In addition, dixanthogen formation on both copper and galena electrodes was observed to occur when the intermediate adsorbed xanthate radical approaches full coverage on the electrode surfaces.

In the presence of 0.25 M potassium amyl xanthate (KAX), it was proposed that dixanthogen enhanced the hydrophobic nature of both pentlandite and pyrrhotite (Hodgson and Agar, 1989). Similar to the findings of Woods (1971), it was proposed that the formation of dixanthogen on both mineral surfaces proceeded via the oxidation of the chemisorbed xanthate ions. In another study by Hodgson and Agar (1989), where they investigated the interaction of 0.1 M xanthate on both pentlandite and pyrrhotite mineral surfaces. It was found that no anodic peaks were associated with the chemisorption of xanthate ions or formation of dixanthogen. However, lower current densities were observed in the case of pyrrhotite in the xanthate collector, thus indicating its participation in the formation of a partially passivating film.

Furthermore, a cyclic voltammetry study by Bowden (2016), indicated that the chemisorption of a xanthate collector on chalcopyrite goes via the oxidation of the mineral surface to chalcocite before proceeding to the chemisorption stage.

Vermaak et al. (2005) applied the technique in investigating the interaction of an ethyl xanthate on a Pd-Bi-Te system. In the absence of ethyl xanthate, a small anodic current was observed above 0 V, this anodic peak was associated with the oxidation of the mineral surface (Figure 2.22). In the presence of ethyl xanthate, a significant peak was noticed above 200 mV, in the anodic direction and two cathodic peaks were observed. The anodic peak was assigned to the presence of dixanthogen, and the two cathodic peaks were assigned to the reduction of dixanthogen and the reduction of mineral oxidation products formed on the mineral surface.

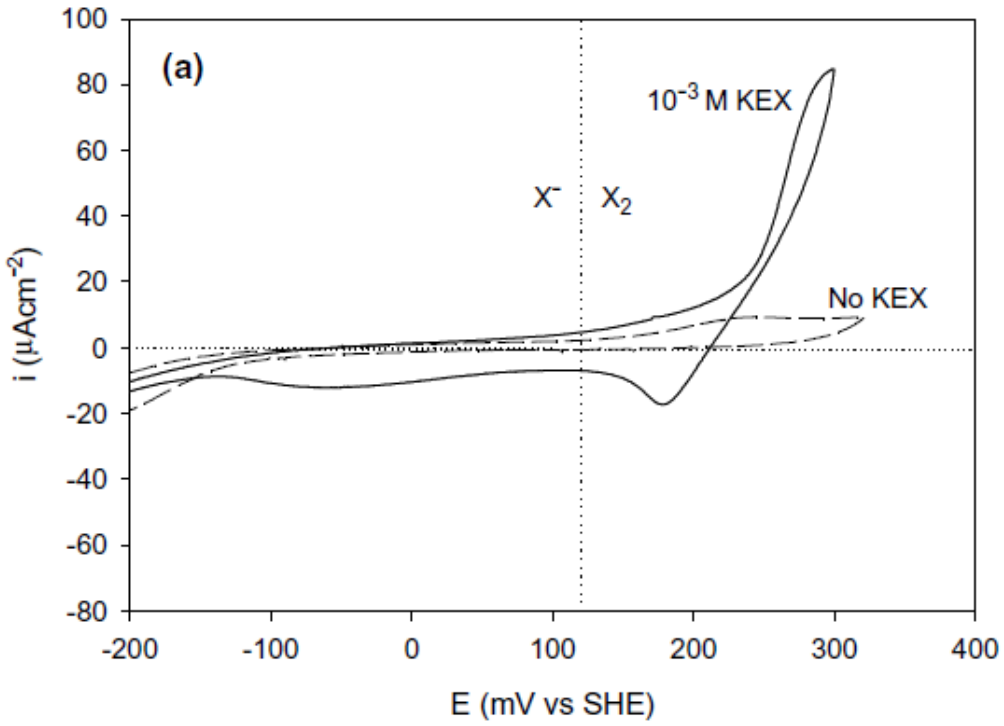

Figure 2.22: Voltammograms for Pd-Bi-Te electrode in 0.05 M $Na_2B_4O_7$ solution at 25^0C in the absence and presence of 10^{-3} M KEX (Vermaak et al., 2005).

2.7.3 Electrochemical Impedance Spectroscopy

Electrochemical Impedance Spectroscopy (EIS) is a dynamic technique used to characterize electrochemical systems and establish the contribution of electrode or electrolytic processes in such systems. EIS can give invaluable kinetic and mechanistic information which makes it a powerful tool in various applications. It has found various uses in investigating on the effects of

current, ionic strength and temperature on the electrical properties of skin (Oh et al., 1993), characterizing human skin impedance after electrical treatment for transdermal drug delivery (Clemente et al., 2013), determining electric double layer properties and protonation rates at the hematite surface (Shimizu and Boily, 2014), investigating the conductivity and dielectric properties of composite solid electrolytes (Iqbal and Rafiuddin, 2016), biological analysis and food characterization (Grossi and Riccò, 2017), monitoring corrosion of solid material (Ribeiro et al., 2015), investigating the adsorption mechanisms of flotation reagents on base metal sulphides (Ekmekçi et al., 2010a, Mu et al., 2015, Ertekin et al., 2016), just to mention but a few of its applications.

2.7.3.1 Principles of EIS

Impedance is the measure of the ability of a circuit to resist the flow of current, but unlike resistance, impedance is not limited to the simplifying properties of an ideal resistor. The principle behind EIS is that a sinusoidal small excitation potential in the range (5 - 20 mV) is applied to generate a sinusoidal current response at the same frequency but with a shift in phase angle (Figure 2.23) (Ribeiro et al., 2015).

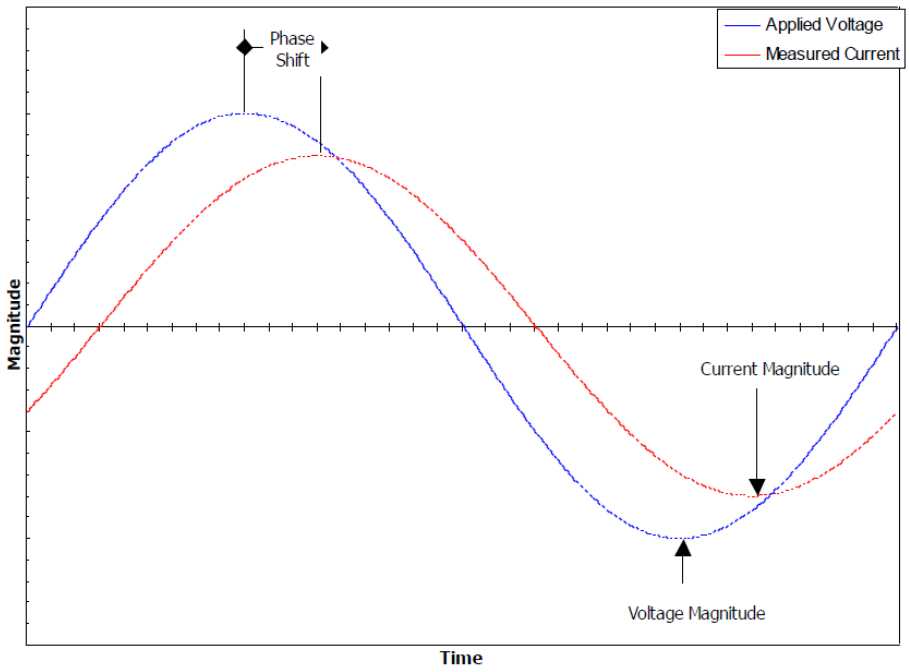

Figure 2.23: Sinusoidal current response in a pseudo-linear system (Gamry Instruments, 1989).

EIS works in the frequency domain and the technique is based on the theory that an interface can be visualized as a combination of passive electrical circuit elements, resistor, capacitor and inductor.

The excitation signal applied can be expressed as a function of time (Equation 2.48) (Chander, 1988) .

$$E_t = E_0 \sin(\omega t) \quad \text{(Eqn. 2.48)}$$

Where E_t is the potential at time t, E_0 is the amplitude of the signal and ω is angular frequency ($\omega = 2\pi f$, where f represents frequency).

Whereas, the response signal, I_t, is shifted in phase angle, $\emptyset$, and I_0 is the amplitude of the current. The response signal can be expressed as in Equation 2.49.

$$I_t = I_0 \sin(\omega t + \emptyset) \quad \text{(Eqn. 2.49)}$$

An expression that corresponds to the Ohm's Law, enables the calculation of impedance as in Equation 2.50. Therefore, impedance can be expressed as a function of magnitude, Z_0 and a shift in phase angle, $\emptyset$.

$$Z = \frac{E_t}{I_t} = \frac{E_0 \sin(\omega t)}{I_0 \sin(\omega t + \emptyset)} = Z_0 \frac{\sin(\omega t)}{\sin(\omega t + \emptyset)} \quad \text{(Eqn. 2.50).}$$

2.7.3.2 Parameters measured by EIS

Electrolyte resistance

When potential is passed through an electrolyte, the ions that exist between the working electrode and the reference electrode impede electron flow. The final potential which is determined by comparing the input potential and the output potential is used to determine the electrolyte/solution resistance, R_s. Electrolyte resistance is dependent upon the ionic concentration, type of ions, temperature of the solution and the geometry of the area in which current is carried. Since resistance is directly proportional to impedance, electrolyte resistance is therefore directly proportional to impedance (Acord, 2021).

Double layer capacitance

A double layer is formed on the interface between an electrode and its surrounding solution. The formation of the double layer is attributed to ions from the solution that interact with the electrode surface. The charged electrode surface is separated from the solution charged ions by an insulating space, usually on the order of angstroms. The separation of charges by the insulating space forms

a capacitor. Ideally, a metal immersed into an electrolyte should have a capacitor. Double layer capacitance is dependent upon the electrode potential, ionic concentration, type of ions, temperature, oxide layer, impurity adsorption and the surface texture of an electrode. Charge built up at the electrode surface is directly proportional to the surface area of the electrode surface and size of ions. Hence, double layer capacitance increases with an increase in electrode surface area (Gamry Instruments, 1989, Acord, 2021).

Polarization resistance

Polarization occurs when the potential of an electrode is forced from equilibrium by an external voltage. Polarization of an electrode causes current flow through electrochemical reactions that transpire at the electrode surface. Hence, the amount of current is controlled by kinetics of reactions and diffusion of reactants towards and away from the electrode. The impedance of current flow by the electrochemical reactions transpiring is referred to as polarization resistance (R_p) (Acord, 2021).

Charge transfer resistance

Unlike polarization resistance, charge transfer resistance is formed by a single, kinetically controlled electrochemical reaction. Charge transfer resistance does not account for a mixed potential but rather a single reaction at equilibrium. When a metal gets into contact with an electrolyte, the metal may electrolytically dissolve into the electrolyte. In the forward reaction, electrons enter the metal and alternatively metal ions diffuse into the electrolyte. This illustration explains the concept of charge transfer. Charge transfer reactions may occur at certain speeds, which are dependent upon the kind of reaction, temperature, concentration of reaction products and potential of the system (Gamry Instruments, 1989).

Diffusion

Warburg impedance is a diffusion-controlled impedance which is dependent on the frequency of the potential perturbation. Warburg impedance is inversely proportional to frequency. At high frequencies, Warburg impedance is small since diffusing reactants do not have to move very far. At low frequencies, the Warburg impedance is high since the reactants have to diffuse further.

2.7.3.3 Graphical representation

Impedance measurements are generally obtained as real Z' and imaginary Z" impedances or modulus IZI and phase angle φ as functions of frequency. Impedance data can either be presented on a Bode plot or a Nyquist plot as shown in Figure 2.24. The graphical representation of EIS data makes it possible to identify the electrical equivalent circuit elements (Lasia, 2014). Plotting the real part on the x-axis and the imaginary part on the y-axis, at different frequencies, produces a 'Nyquist plot,' also known as the Argand or Colo-Cole representation (Ribeiro et al., 2015). In the Nyquist plot, the y-axis and each point on the graph is the impedance at one frequency. The low frequency data is presented on the right and the higher frequency data on the left side of the graph, however the Nyquist plots do not indicate specific frequencies used to record any point.

Another graphical way to represent impedance data is through a 'Bode plot.' There are two types of bode plots, log IZI (magnitude) versus log f (frequency) and a phase angle versus log f plot, both can be presented on a single graph. Unlike, the Nyquist plot, Bode plots indicate frequency information (Gamry Instruments, 1989).

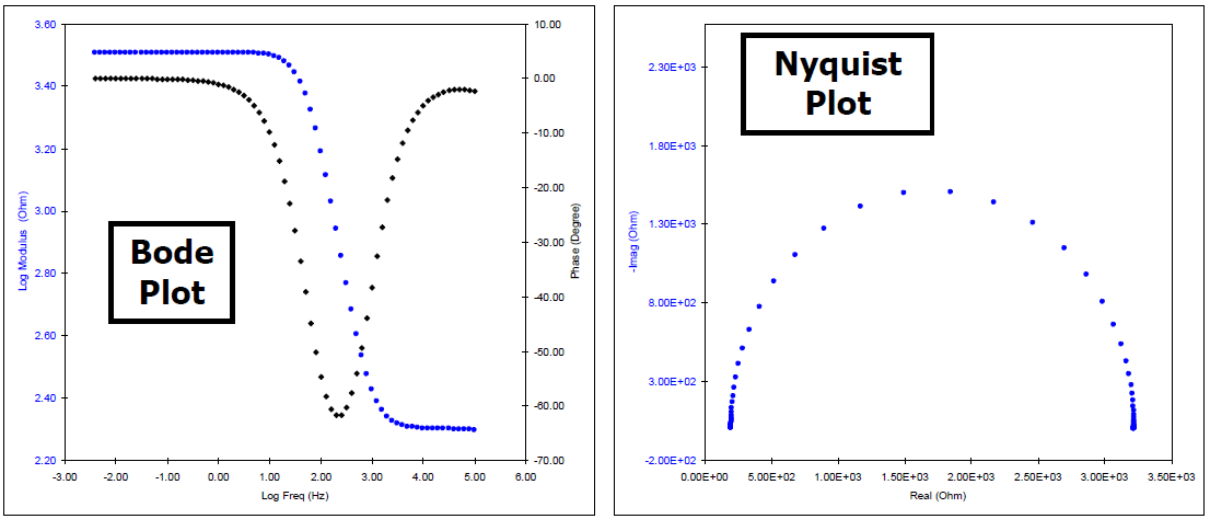

Figure 2.24: Bode and Nyquist plots (Gamry Instruments, 1989).

2.7.3.4 Equivalent circuit modelling

A physicoelectrical model is an equivalent circuit composed of various circuit elements used to interpret experimental impedance data (Figure 2.25). The conductive path of the circuit is represented by resistance, the resistor in a circuit may represent the bulk conductivity of the material or even the chemical step associated with an electrode reaction. Inductors and capacitors

are associated with space charge polarization regions, specific adsorption and electrocrystallization processes occurring at the electrode surface (Barsoukov and Macdonald, 2005).

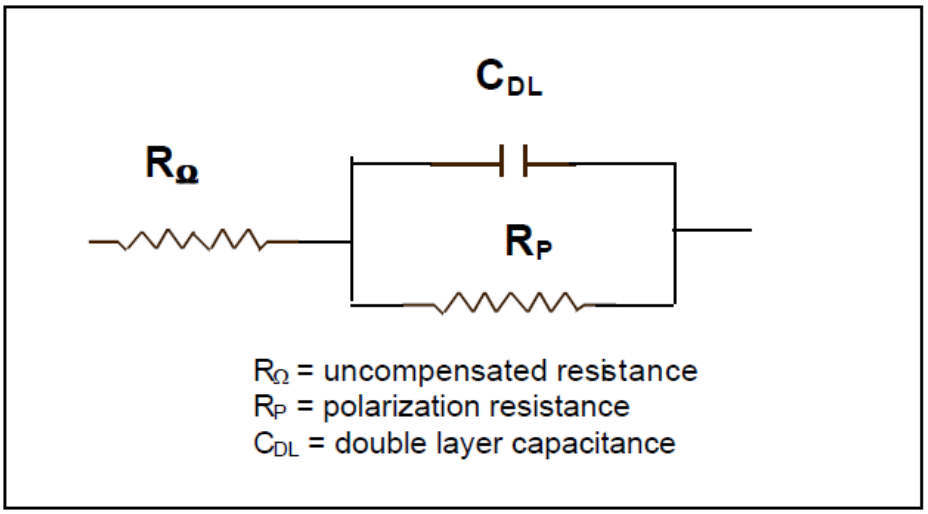

Figure 2.25: Equivalent cell for a single electrochemical cell (Ametek Scientific Instruments, 2015).

Knowledge on the impedance of common electrical elements is therefore useful and equations for their current versus voltage relationships are shown in Table 2.6.

Table 2.6: Relationship between circuit and impedance equivalent values (Gamry Instruments, 1989).

Element	Current vs Voltage	Impedance
Resistor	$E = IR$	$Z = R$
Inductor	$E = L\,di/dt$	$Z = j\omega L$
Capacitor	$I = C\,dE/dt$	$Z = 1/j\omega C$

Table 2.6 illustrates that the impedance of a resistor is independent of frequency and does not have an imaginary component. Due to the real impedance component, the current through a resistor stays in phase with the voltage across the resistor. Unlike the resistor, the impedance for an inductor is directly proportional to frequency and only has an imaginary component. Hence, the current through an inductor is phase-shifted -90 degrees with respect to the voltage. Alternatively, the impedance of a capacitor is inversely proportional to frequency. However, similar to inductors, capacitors only have an imaginary component. Consequently, the current through a capacitor is phase shifted 90 degrees with respect to voltage.

2.7.3.5 EIS applied in the flotation of base metal sulphides

EIS has proven to be a very useful tool in determining the mechanisms involved when xanthates interact with mineral surfaces (Mu et al., 2015). However, with regards to flotation studies, this technique has been applied mostly to base metal sulphides, though the only work on PGMs published thus far has looked at the Pd-Bi-Te system (Vermaak et al., 2004).

Ertekin et al. (2016) successfully used EIS to determine the rate of collector adsorption on different pyrite minerals. They associated the rate of collector adsorption to coating resistance (R_c), where it was deduced that a decrease in R_c resulted in a higher rate of collector adsorption. Additionally, Mu et al. (2015) investigated the variation of surface properties of pyrite in the presence of potassium amyl xanthate and a lignosulfonate depressant. The mechanisms proposed in the presence of the depressant were either chemisorption or physisorption of the depressant onto the pyrite surface, henceforth, forming a discontinuous layer which passivates the mineral surface and inhibits any further electrochemical reactions from occurring on the mineral surface. It was found that the presence of the depressant lowers R_{ct}, indicating that the adsorption of the depressant onto the mineral surface, prevents pyrite oxidation. The lower R_{ct} value obtained was assigned to the difficulty in charge transfer reactions that may occur between the mineral surface and the electrolyte and between the mineral and xanthate ions in solution. Therefore, this phenomenon will affect any redox reactions from occurring on the mineral surface, inhibiting the possible formation of dixanthogen.

The technique was also applied by Ekmekçi et al. (2010a) in investigating the electrochemical behaviour of different samples of pyrrhotite at pH 7 and 10, upon collector addition and copper activation. Higher impedance values were obtained at pH 10 than at 7, owing to the higher rate of oxidation on the mineral surfaces at higher pH. The addition of a xanthate collector only and the collector plus copper sulphate decreased resistance and alternatively increased capacitance values. This observation was attributed to the oxidation of xanthate to its dimer state and the reduction of copper sulphate from Cu^{2+} to Cu^{+}.

An investigation by Marape and Vermaak (2012), examined the compositional variations and electrochemical behaviour of pentlandite samples. It was found that pentlandite samples enriched with some iron content displayed lower capacitance values. This observation was proposed to be an indication of the development of either a thicker oxide layer or a layer with a smaller dielectric constant. On the other hand, pentlandite samples enriched with nickel exhibited higher capacitance

values. Hence, the variations in capacitance values were an indication of changes in electronic properties of product layers formed on the different pentlandite samples.

In a Pd-Bi-Te system, Vermaak et al. (2004) explored the electrochemical studies of the interaction between Pd-Bi-Te and ethyl xanthate. It was reported that longer exposure of Pd-Bi-Te in an ethyl xanthate at potentials above 0.2 V (SHE), created lower capacitance values. Similarly, EIS work done on base metal sulphides would assign such an observation to the growth of an oxidation layer on the mineral surface. In this regard, the Pd-Bi-Te system was observed to exhibit lower capacitance values that were assigned to the formation of dixanthogen on the mineral surface.

Changes in capacitance values in EIS measurements are due to the double layer effect and possible surface oxidation layers that form on the mineral surface. Moreover, capacitance values demonstrate the growth of any surface oxidation layers formed and differences in electronic properties of the product layers.

2.8 Summary of Literature

Water quality in flotation studies is an area that has been recently receiving attention. It has become a field of interest due to the need to recycle process water or find freshwater alternatives owing to the scarcity of water resources and the high-water usage that comes with the flotation process. Thus far, most studies have used bench scale tests (Kirjavainen et al., 2002, Ikumapayi et al., 2012, Hirajima et al., 2016), hence they have speculated on the mechanisms involved on xanthate adsorption onto mineral surfaces in the presence of ions. Moreover, previous studies have focused on the effect of water quality in both mixed-salt systems (Lisa et al., 2019; Mali et al., 2012) and single-salt systems (Lisa et al., 2021; Sinche-Gonzalez etand Fornasiero 2021). In mixed ion systems, it is difficult to distinguish the sole detrimental effects of each ion present in process water. Hence, the need to bring a fundamental understanding into single-salt systems. Additionally, water quality studies for both the mixed and single-salt systems have focussed on base metal sulphides. Therefore, PGM minerals have not received attention in this regard due to their association with base metal sulphides, despite the findings of Penberthy et al. (2000).

Electrochemical techniques have proved to be the most useful methods that can be used to investigate the interactions between mineral surfaces and flotation reagents. These techniques have been applied in obtaining important information on possible mechanisms involved when mineral surfaces interact with flotation reagents (Venter and Vermaak, 2008, Tadie et al., 2015a).

Though the effects of ions have been reported through flotation recoveries and other bench scale techniques, there is very little knowledge with regards to the mechanisms involved in the adsorption of xanthate collectors on mineral surfaces in the presence of ions. Gaining knowledge on the mechanisms involved, will act as a diagnostic tool for developing flotation strategies in maximizing recoveries by alleviating flotation problems related to water quality, which will in turn help in improving profits for the mining sector.

Henceforth, this study seeks to unpack the mechanisms of interfacial interactions between a xanthate collector and selected PGMs in the presence of specific ions at increasing ionic strength using electrochemical techniques.

3. Research Objectives

3. 1 Objectives

The objectives of this study were:

1) To determine the interactions between single salts at increasing ionic strength with palladium minerals in the absence and presence of SIBX.
2) To establish the mechanisms of interaction of SIBX with palladium minerals in the absence and presence of single salts with an increase in ionic strength.
3) To identify the effects of different salts on the adsorption of SIBX on palladium minerals.
4) To develop electrical circuit model systems for SIBX adsorption on palladium minerals in the absence and presence of single salts.

3.2 Key Questions

1) How do single salts at increasing ionic strength interact with palladium minerals?
2) How does SIBX interact with palladium minerals in the presence of single salts at increasing ionic strength?
3) What are the adsorption mechanisms involved upon interaction of SIBX with palladium minerals in the absence and presence of single salts with an increase in ionic strength?
4) How do different salts affect the interaction between SIBX and palladium minerals?
5) Which electrical circuit elements represent the mineral-water interface of the palladium mineral systems?

3.3 Hypothesis

The following hypotheses were developed:

1) In the presence of ions, electrochemically passive layers may form with an increase in ionic strength and therefore decrease the resistance and increase the capacitance of the electrical double layer. This is due to their high dielectric constants and the high net current for the ion adsorption reactions that occur on the mineral surfaces. Therefore, ions will compete for adsorption with xanthate ions on PdS and $PdTe_2$ mineral surfaces.

2) PdS and $PdTe_2$ will react with surface active ions differently. This is due to the different crystal structures that the minerals possess, which play a significant role in adsorption reactions.

4. Experimental methods

4.1 Validation

- Rest potential measurements were validated from work done by Tadie et al. (2015b). An investigation into the electrochemical interactions between platinum group minerals and sodium ethyl xanthate and sodium diethyl dithiophosphate collectors: Mixed potential study.
- Cyclic Voltammetry measurements were validated from work done by Tadie et al. (2015a). An investigation into electrochemical interactions between platinum group minerals and xanthate: Voltammetric study.
- Electrochemical Impedance Spectroscopy measurements were validated from work done by Marape and Vermaak (2012). Fundamentals of pentlandite mineralogy and its effect on its electrochemical behaviour.

4.2 Reagents Preparation

Ultra-pure water was used throughout the preparation of solutions.

SIBX, supplied by Senmin (Pty) Ltd, was used as a collector at a concentration of 6.24×10^{-4} M for all test work. A fresh 1% SIBX solution made up using ultra-pure water was prepared prior to each experimental run.

To investigate the effect of ions on the adsorption of SIBX on selected PGM minerals, sodium thiosulphate ($Na_2S_2O_3$), magnesium sulphate ($MgSO_4$), magnesium chloride ($MgCl_2$), calcium chloride ($CaCl_2$) and sodium chloride (NaCl), supplied by Sigma-Aldrich, were used. The selected salts were dissolved to ionic strengths of 0.0242 M, 0.0727 M, 0.1212 M and 0.2426 M, to simulate recycled water systems in literature (Manono et al., 2018). All salts used in this study were of analytical grade.

Di-sodium tetraborate decahydrate ($Na_2B_40_7.10H_2O$), supplied by Sigma-Aldrich, was used as a buffer. The salt was dissolved to a concentration of 0.05 M, to achieve a pH of 9.2.

4.3 Electrochemical measurements

4.3.1 Equipment

Figures 4.1 and 4.2 show the experimental setup used for the electrochemical measurements. All electrochemical measurements were conducted in a 500 ml double-jacketed electrochemical cell (1), with an outer thermostat compartment (8) programmed to keep circulating water constantly at ±25°C. The measurements were performed in an oxygen-saturated environment and at a pH of 9.2. Potentials were measured against the Ag/AgCl reference electrode (4) filled with saturated KCl, with a potential of - 0.207 V against the standard hydrogen electrode (SHE). The working electrode was screwed onto a holder that comprised a copper wire (2), insulated in a plastic casing sealed with epoxy resin. In all electrochemical measurements, the working electrode (3) was kept stationary while the buffer solution (borate solution of 0.05 M) and other reagents (6) under investigation were stirred continuously (Rest potential and EIS measurements) whereas CV measurements were carried out in quiescent solutions. A platinum wire, used as a counter electrode (5), also referred to as an auxiliary electrode was used in CV and EIS measurements, where current is expected to flow.

The PdS and $PdTe_2$ minerals used in this study were of 97.4 % and 68.7 % purity, respectively. The surface area of the PGM working electrodes was measured using ImageJ software (National Institutes of Health, Bethesda, MD, USA). The surface areas (Tables 4.1 & 4.2) for the PdS and $PdTe_2$ electrode minerals were checked regularly to determine any changes in surface area.

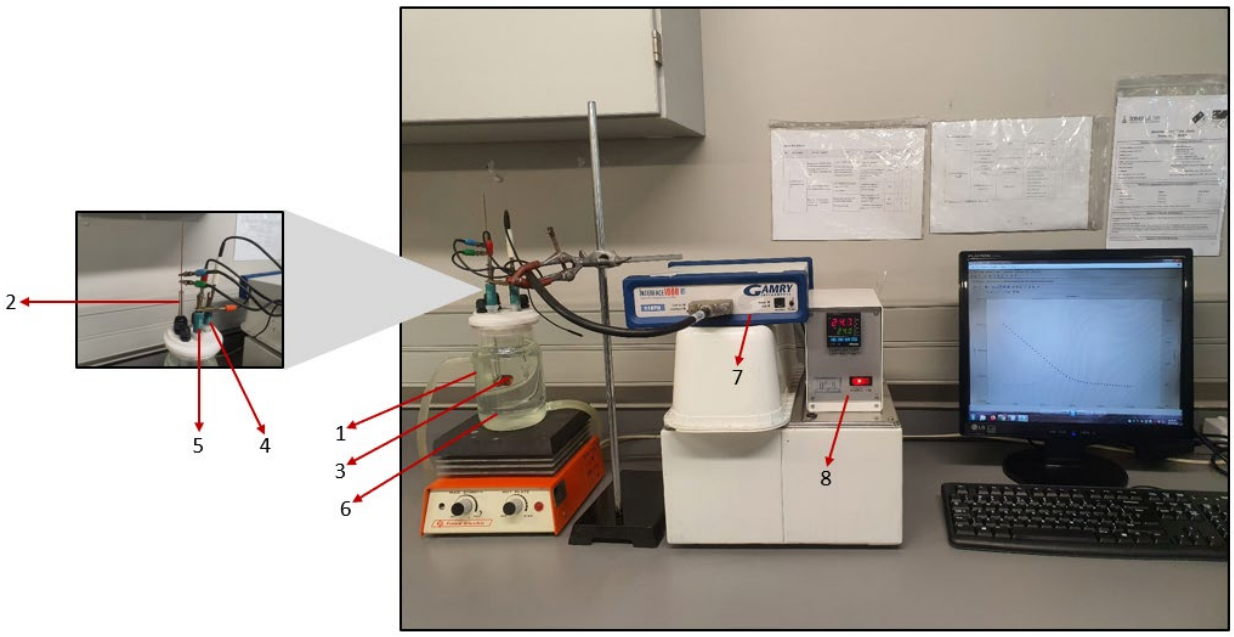

Figure 4.1: Experimental set-up for electrochemical measurements

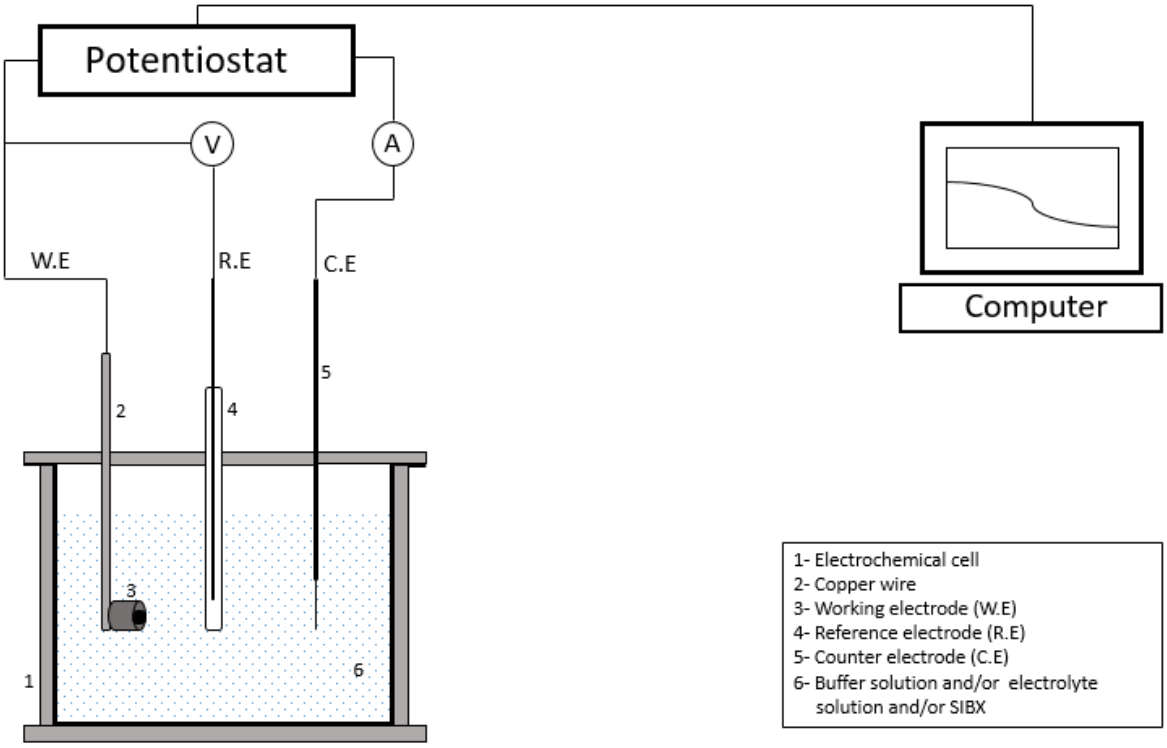

Figure 4.2: Schematic diagram for the experimental set-up for electrochemical measurements

A Gamry Instruments Reference 3000 Potentiostat (7) was used for all rest potential and cyclic voltammetry measurements. A Gamry Instruments Reference 600, which had been upgraded to the latest software, was used to conduct EIS measurements. Both of which made use of the Gamry Framework interface. The Gamry instruments were calibrated using a calibration dummy cell in a Faraday cage to enhance the accuracy of the instruments. The results obtained in all electrochemical measurements were analysed by Gamry Instruments Echem™ Analyst Software. All the data obtained were transferred to Microsoft Excel for further analysis and converted to the SHE scale.

4.3.1 Working electrode preparation

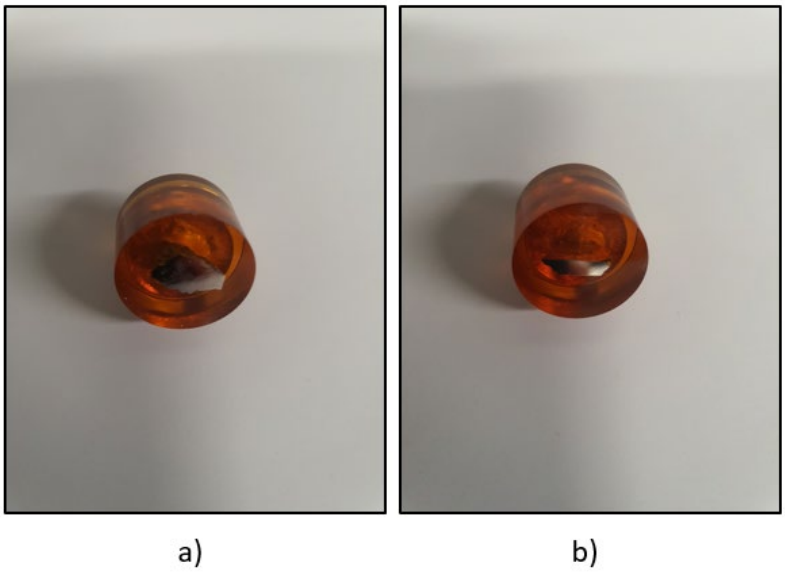

Figure 4.3: Palladium working electrodes (a) PdS b) $PdTe_2$

The working electrodes, palladium sulphide (PdS) and palladium telluride ($PdTe_2$), shown in Figure 4.3, were freshly prepared prior to each electrochemical measurement. The minerals were wet polished using alumina powder suspensions prepared from 1 μm, 0.3 μm and 0.05 μm powders, respectively. Ultra-distilled water was used to make micro-polish alumina powder suspensions. A jet of ultra-distilled water was used to thoroughly rinse the electrodes during and after polishing. A final rinse was carried out just before drying the electrodes by lightly dabbing the mineral surface with a paper towel, after which the electrodes were immediately transferred to the electrochemical cell for measurements. This polishing treatment aids in obtaining reproducible results. The alumina powders were supplied by IMP Scientific and Precision (Pty) Ltd.

4.3.2 Rest Potential measurements

In order to gain an understanding of the extent of interactions between the selected salts and/or SIBX on PdS and $PdTe_2$, rest potentials measurements were performed. A two-electrode system, Ag/AgCl reference electrode and a mounted working electrode was employed for the measurements. The electrodes were submerged into a continuously stirred buffer solution. The measurements were conducted in the absence and presence of salt solutions and SIBX. The salt solutions were dosed at volumes that corresponded to final concentrations of 0.0242 M, 0.0727 M, 0.1212 M and 0.2426 M. Each salt solution was dosed at 300 seconds, after which SIBX was dosed at 600 seconds. The total run for each experiment was 1200 seconds. Electrode potential was monitored as a function of time.

4.3.3 Cyclic Voltammetry measurements

Cyclic voltammetry measurements were conducted to characterize redox reactions occurring on the selected PGM mineral surfaces due to the adsorption of salt and xanthate ions. A conventional three-electrode system was employed, which consisted of Ag/AgCl reference electrode, mounted working electrode and platinum counter electrode. The measurements were conducted between potentials of 0.6 V to -0.6 V, at a scan rate of 15 mV/s. For each CV measurement, rest potential was initially measured, to avoid excessive initial high currents. Thereafter, the potential was scanned in the anodic direction up to the positive vertex potential (0.6 V) and the potential scan was reversed in the cathodic direction, continued until it reached the negative vertex potential (-0.6 V) and back to its rest potential. The parameters used in the cyclic voltammetry measurements are shown in Table 4.1.

Table 4.1: Cyclic Voltammetry parameters

Parameter	**PdS**	**$PdTe_2$**
Electrode Area (cm^2)	0.316	0.140
Initial Scan (V)	0.6	
Final Scan (V)	- 0.6	
Scan rate (mV/s)	15	

4.3.4 Electrochemical Impedance Spectroscopy

Electrochemical Impedance Spectroscopy measurements were employed to investigate the adsorption mechanisms of SIBX in salt solutions of increasing ionic strength. The same conventional three-electrode system used in CV measurements was also used for EIS measurements. The rest potential was taken as the direct current (DC) voltage (starting potential)

of the EIS measurements, whereas the alternating current (AC) voltage (amplitude) depended on the type of mineral used as shown in Table 4.2. The frequency range for each mineral investigated was applied as shown in Table 4.2. Parameters used in the EIS measurements are as shown in Table 4.2.

Table 4.2: Electrochemical Impedance Spectroscopy parameters

Parameter	**PdS**	**$PdTe_2$**
Electrode Area (cm^2)	0.310	0.140
Initial Frequency (Hz)	100 000	100 000
Final Frequency (Hz)	5	0.01
Amplitude (mV/rms)	12	7

5. Results: Rest Potential Measurements

Rest potential measurements were used to investigate the extent to which SIBX interacted with palladium minerals, PdS and $PdTe_2$, in the absence and presence of $Na_2S_2O_3$, $MgSO_4$, $MgCl_2$, $CaCl_2$ and NaCl at 1SPW, 3 SPW, 5 SPW and 10 SPW. The experiments were conducted in 0.05 M $Na_2B_4O_7.10H_2O$ buffer solution. The baseline case in this study was a condition with SIBX only, with no salt present.

It was presumed that the formation of dixanthogen was favoured at final rest potentials above the equilibrium potential of dixanthogen formation, whereas the formation of metal xanthate was favoured at final rest potentials below the equilibrium potential of dixanthogen formation.

5.1 Validation

Prior to the actual test work for this study, the rest potential measurements were validated from the work of Tadie et al. (2015b). Validation was performed to avoid generating inaccurate data with regard to the actual measurements for this work. Figure 5.1 illustrates similar test work performed by Tadie et al. (2015b).

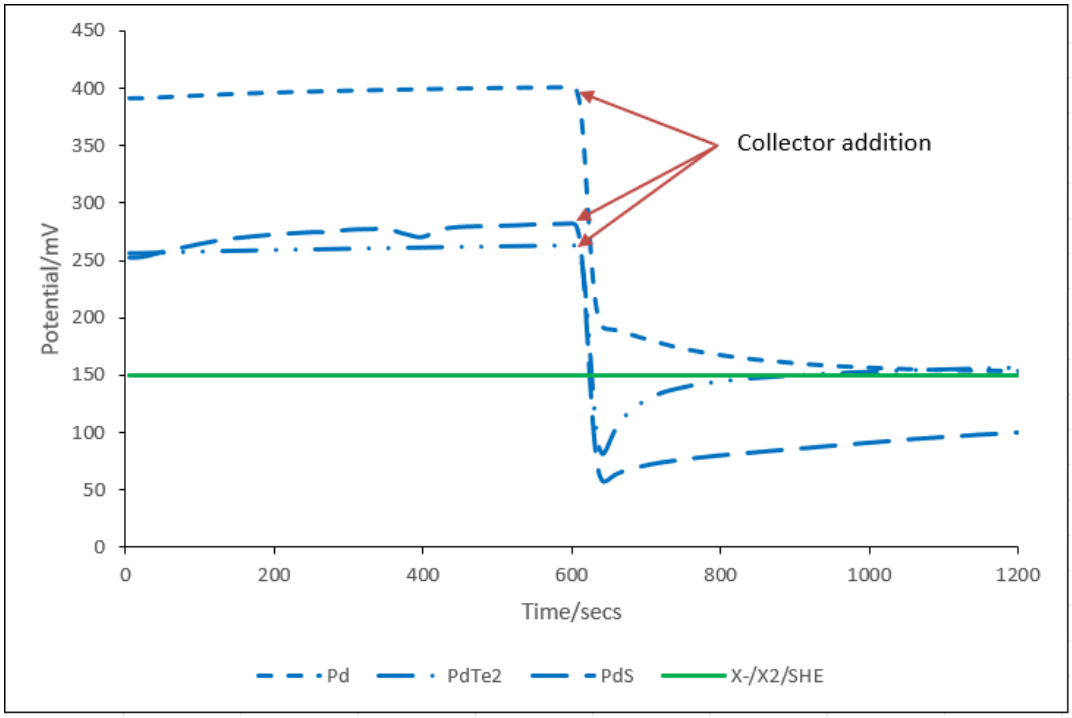

Figure 5.1: Rest potential measurements for palladium minerals in 6.24×10^{-4} M sodium ethyl xanthate collector, 0.1 M $Na_2S_2O_4$ and 0.05 M $Na_2B_4O_7.10H_2O$ at a pH of 9.2. The green line represents the oxidation potential for sodium ethyl xanthate at 6.24×10^{-4} M which was found to be 0.15 V.

Similar to the findings of Tadie et al. (2015b), this study obtained agreeable potential ranges (within ≈ 30 mV), to those that were reported, prior and after collector addition. Prior to collector addition both studies have shown that Pd displays higher potentials than $PdTe_2$ and PdS. This observation implies that Pd is more reactive than the other palladium minerals. Upon addition of collector, all palladium minerals demonstrate relatively similar rates of reduction on the mineral surfaces. Accordingly, the final rest potentials obtained for both Pd and $PdTe_2$ minerals were slightly higher than the equilibrium potential of the collector (150 mV), whereas PdS exhibited a lower final rest potential to the equilibrium potential of the collector.

5.2 Reproducibility

All experiments were performed in duplicates. For bar graphs, the precision for the tests was analyzed by a standard error analysis, represented by error bars as shown in Figures 5.4 and 5.5.

Figure 5.2 illustrates the duplicate rest potentials obtained for PdS, prior to the addition of $MgSO_4$ at 10 SPW, after the addition of the salt at 300 seconds and after the addition of SIBX at 600 seconds.

Figure 5.3 depicts the duplicate rest potentials acquired for $PdTe_2$, prior to the addition of NaCl at 3 SPW, after the addition of the salt at 300 seconds and after the addition of SIBX at 600 seconds. It has been accepted in this work that rest potential measurements between two repeats within ≈ 30 mV, were considered to be reproducible. Hence, it is shown in both Figures 5.2 and 5.3 that the potentials obtained between two repeats for each test are reproducible.

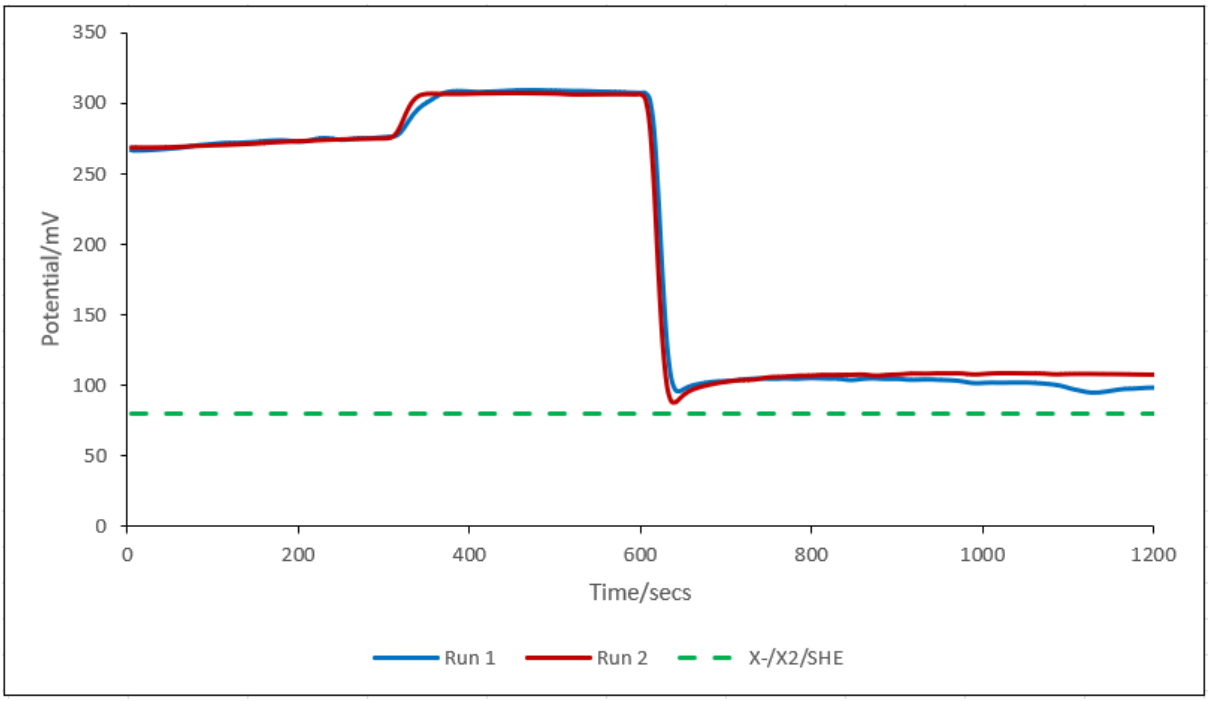

Figure 5.2: Rest potentials for PdS mineral in $MgSO_4$ at 10 SPW and in the presence and absence of 6.24×10^{-4} M SIBX. The green line represents the oxidation potential of SIBX at 6.24×10^{-4} M which is 80 mV.

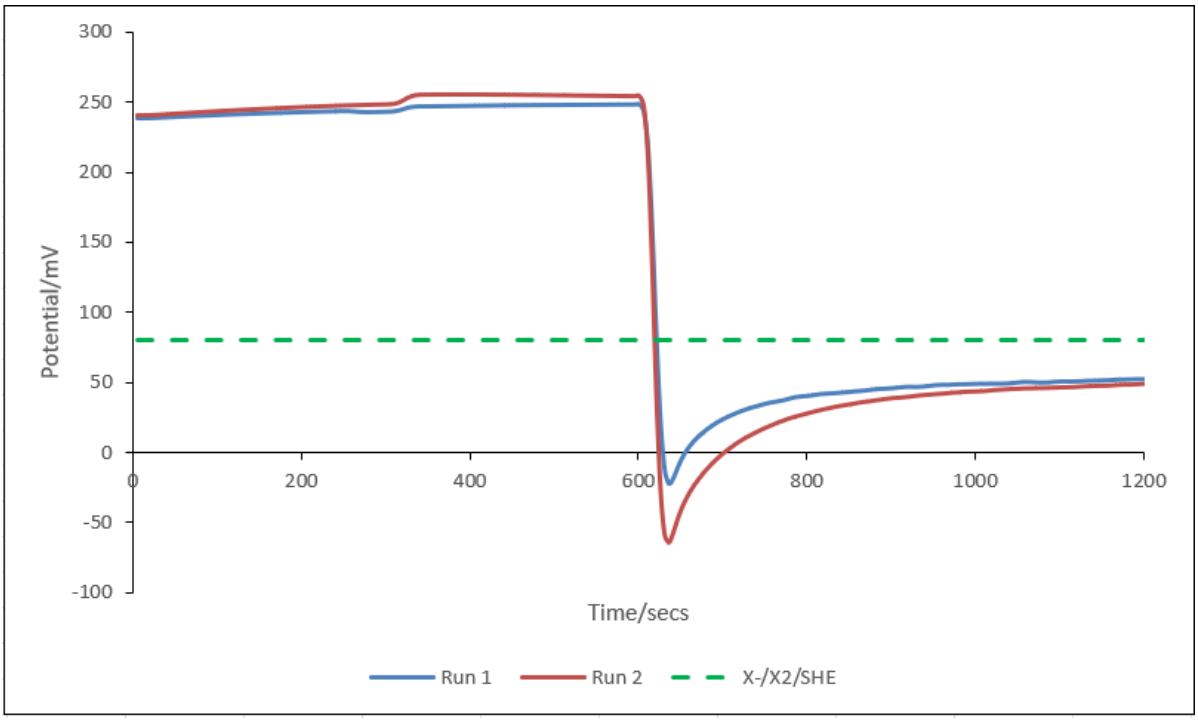

Figure 5.3: Rest potentials for $PdTe_2$ mineral in NaCl at 3 SPW and in the presence and absence of 6.24×10^{-4} M SIBX. The green line represents the oxidation potential of SIBX at 6.24×10^{-4} M which is 80 mV.

5.3 Rest Potential measurements for PdS

The difference in rest potentials as represented by the bar graphs (Figures 5.4 and 5.5), denote the extent of interaction (Tadie et al., 2015b) of either the salts at various ionic strengths (green and blue bars) and SIBX (grey bars) with the palladium minerals. In this work, the magnitude of decrease in potential was considered as the rate of reduction whereas the magnitude of increase in potential was viewed as the rate of oxidation on the palladium mineral surfaces. The full sets of data for the rest potential measurements are presented in Appendix A.

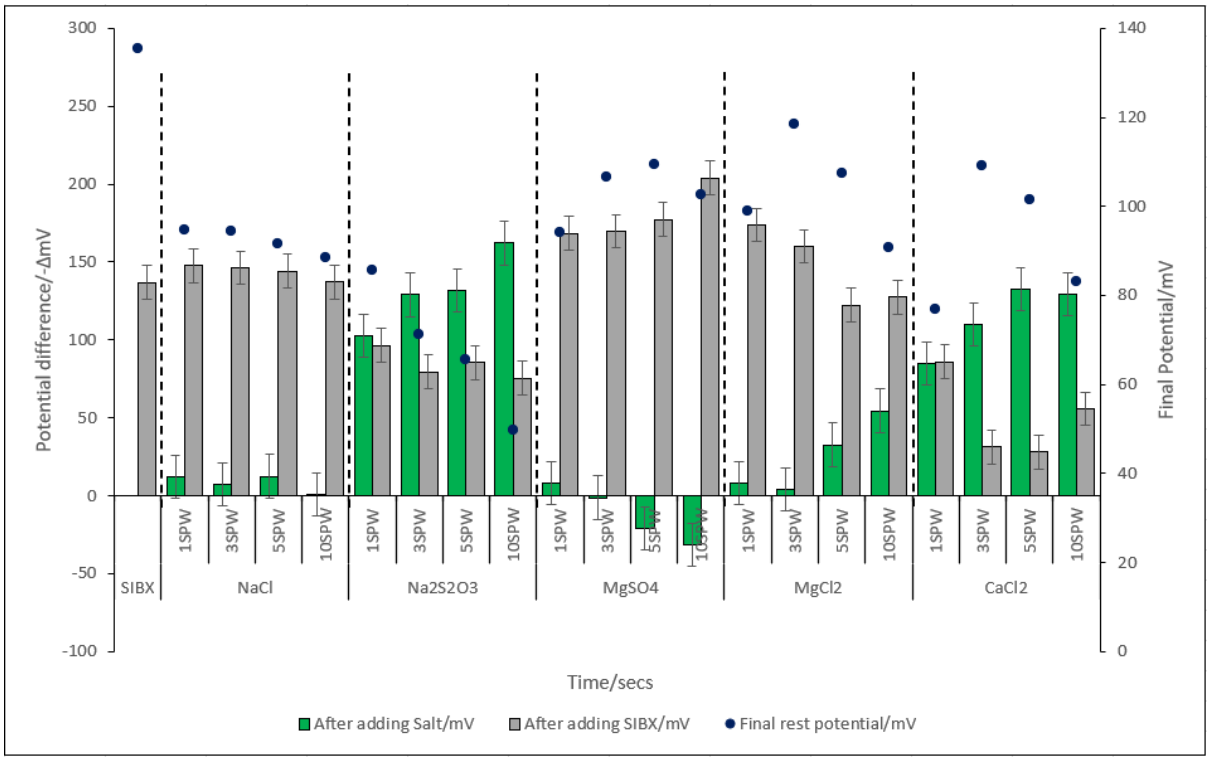

Figure 5.4: Final rest potentials (blue circles) and changes in rest potentials for PdS after addition of various salts at different ionic strengths (green bars) and SIBX at 6.24×10^{-4} M (grey bars).

Figure 5.4 depicts final rest potentials and changes in rest potentials for PdS after the addition of SIBX, in the absence and presence of salts at increasing ionic strength. A general trend was observed where an increase in the ionic strength of the salts resulted in an increase in the extent to which the salts interacted with PdS. An increase in the interaction between the salts and PdS, subsequently decreased the interaction between SIBX and the mineral surface.

5.3.1 Effect of $S_2O_3^{2-}$ ions

Compared to all other salts, $Na_2S_2O_3$ exhibited a more pronounced interaction with the PdS mineral. As the ionic strength of $Na_2S_2O_3$ increased, an increase in interaction between the salt and PdS was observed. Therefore, the rate of reduction on the PdS mineral surface was increased as indicated by the increase in potential difference with an increase in ionic strength of $Na_2S_2O_3$. Alternatively, the preceding effect of the salt decreased the extent to which SIBX interacted with PdS, indicating a decrease in the rate of reduction on the mineral surface. It was observed that as the ionic strength of the salt increased, there was a decrease in the final rest potentials. Consequently, the lowest ionic strength of $Na_2S_2O_3$, resulted in a final rest potential that was greater than the equilibrium potential for SIBX at 6.24×10^{-4} M, which was determined to be 80 mV. This denotes that dixanthogen was the most favorable oxidation product formed on the

mineral surface. An increase in the ionic strength, at 3 SPW, 5 SPW and 10 SPW, resulted in final rest potentials that were lower than the equilibrium potential of SIBX. This suggested that the formation of metal xanthate was favoured at these conditions. Generally, the extent of interaction of SIBX with $PdTe_2$ in the presence of $Na_2S_2O_3$ at all ionic strengths was less than that for the baseline case.

5.3.2 Effect of SO_4^{2-} ions

Interestingly, of all the salts, the addition of $MgSO_4$ resulted in an increase in rest potential of PdS only at higher ionic strengths, 5 SPW and 10 SPW. Hence, an increase in the ionic strength of $MgSO_4$ increased the degree of interaction between SIBX and PdS. In the lower ionic strengths, the interaction between the mineral and $MgSO_4$ was minimum. $MgSO_4$ at 3 SPW shows very low or no interaction at all with the PdS mineral, whilst the rate of reduction of the mineral surface increased in the presence of $MgSO_4$ with an increase in ionic strength. Overall, all final rest potentials at all ionic strengths were observed to be greater than the equilibrium potential of SIBX. This implies that the formation of dixanthogen was favorable (Allison et al., 1972) at all ionic strengths. However, a general increase in the final rest potentials was seen with an increase in ionic strength.

5.3.3 Effect of Mg^{2+} ions

It is apparent from Figure 5.4 that the extent to which $MgCl_2$ interacts with PdS increased with an increase in ionic strength. It is demonstrated that the rate at which PdS is reduced is increased in the presence of $MgCl_2$ at increasing ionic strength. This effect subsequently decreased the extent to which SIBX interacts with PdS, implying a decrease in the rate of reduction of PdS with an increase in ionic strength. At all ionic strengths of $MgCl_2$, it was demonstrated that final rest potentials lie above the equilibrium potential of SIBX. However, a general decrease in final rest potentials with an increase in ionic strength was exhibited. This indicates that the rate of formation of dixanthogen decreased with an increase in ionic strength. Additionally, compared with the baseline case, the lower ionic strengths (1 SPW and 3 SPW) displayed higher interactions between SIBX and PdS compared to the higher ionic strengths (5 SPW and 10 SPW).

5.3.4 Effect of Ca^{2+} ions

$CaCl_2$ displayed a high degree of interaction with PdS, though it is slightly less pronounced than that of $Na_2S_2O_3$. An increase in the ionic strength of $CaCl_2$ is directly proportional to the extent of

interaction between the salt and the PdS mineral surface. It was observed that the rate of reduction of PdS increased with an increase in ionic strength of $CaCl_2$. Alternatively, the presence of $CaCl_2$ at increasing ionic strength, decreased the degree to which PdS interacts with the SIBX collector. Accordingly, the rate at which the mineral surface was reduced decreased with an increase in ionic strength of $CaCl_2$ in the presence of SIBX. In general, final rest potentials decreased with an increase in ionic strength. Final rest potentials for 3 SPW, 5 SPW and 10 SPW were greater than the equilibrium potential of SIBX, although Figure 5.4 revealed that the final rest potential for 1 SPW was below the equilibrium potential of SIBX. It was presumed that in the presence of $CaCl_2$ at 3 SPW, 5 SPW and 10 SPW, the formation of dixanthogen was favoured whereas the formation of a metal-xanthate was favoured at the lowest ionic strength of $CaCl_2$.

5.3.5 Effect of Na^+ ions

Amongst all salts, NaCl displayed the least interaction with PdS. Unexpectedly, the highest ionic strength of NaCl showed very low or no interaction with the mineral surface. However, the rate at which PdS was reduced was generally lower in the presence of NaCl at 1 SPW, 3 SPW and 5 SPW, in comparison with other conditions investigated. To which the extent of interaction does not significantly differ with changes in ionic strength. Therefore, this had no significant impact on the interaction between SIBX and PdS. Overall, the interactions of SIBX with PdS in the presence of NaCl were comparable to the baseline case. Additionally, all final rest potentials were above the equilibrium potential for SIBX though a very slight decrease was observed with an increase in ionic strength. Presumably, the formation of dixanthogen was favoured at all ionic strengths of NaCl.

5.4 Rest Potential measurements for $PdTe_2$

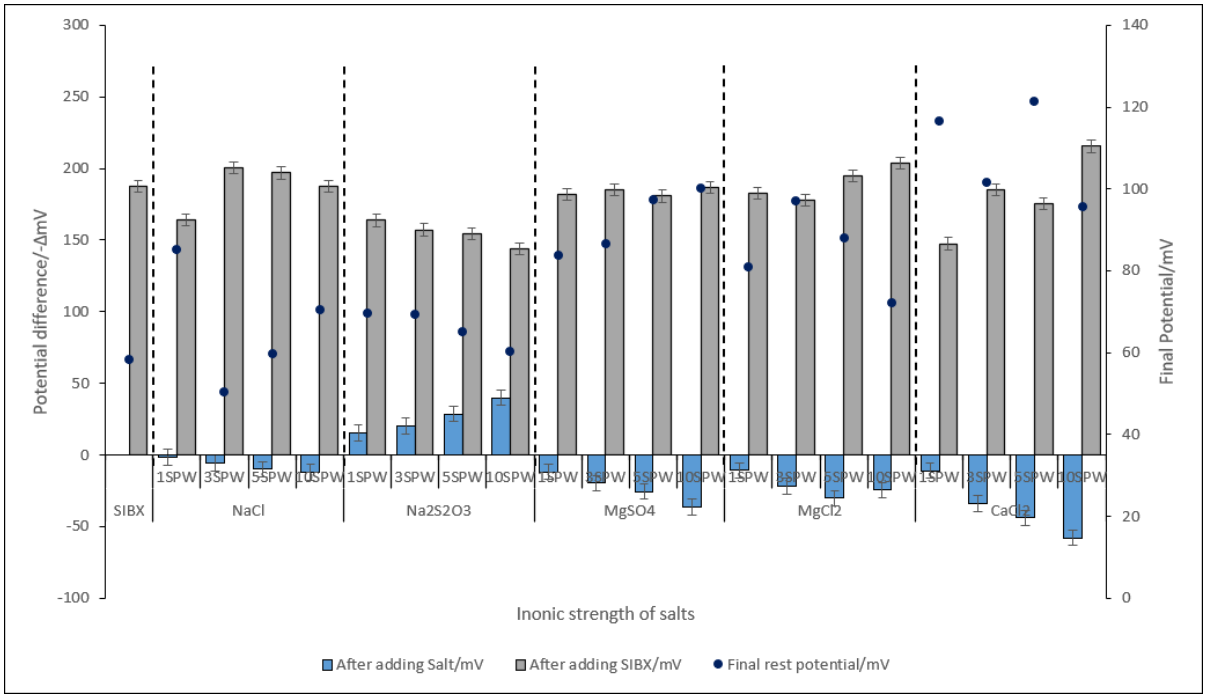

Figure 5.5: Final rest potentials (blue circles) and changes in rest potentials for $PdTe_2$ after addition of various salts at different ionic strengths (blue bars) and SIBX at 6.24×10^{-4} M (grey bars).

Figure 5.5 plots final rest potentials and changes in rest potentials for $PdTe_2$ after the addition of SIBX, in the absence and presence of salts at increasing ionic strength. Compared with PdS, $PdTe_2$ generally portrayed lower interactions with all salts. This observed effect consequently resulted in higher interactions between the SIBX collector and the $PdTe_2$ mineral. Unlike with PdS, most salts investigated enhanced the oxidation of $PdTe_2$.

5.4.1 Effect of $S_2O_3^{2-}$

In comparison with PdS, the interaction of $Na_2S_2O_3$ with $PdTe_2$ demonstrated a similar effect and trend at all ionic strengths. However, $PdTe_2$ exhibited lower interactions with $Na_2S_2O_3$ than PdS. Therefore, implying that the rate of reduction of $PdTe_2$ in the presence of $Na_2S_2O_3$ was lower than that of the PdS mineral surface. Hence, this effect subsequently displays higher interactions between SIBX and $PdTe_2$, compared to PdS, thereby suggesting that the rate of reduction of $PdTe_2$ was increased in the presence of both $Na_2S_2O_3$ and SIBX. Despite the higher interactions of SIBX on a $PdTe_2$ mineral surface, the final rest potentials obtained were interestingly lower than the equilibrium potential of SIBX at all ionic strengths. This suggests that the formation of a metal-xanthate was probably favoured at all ionic strengths of $Na_2S_2O_3$, on the $PdTe_2$ mineral surface.

5.4.2 Effect of SO_4^{2-}

It was observed in Figure 5.5 that $MgSO_4$ interacts with $PdTe_2$ in a different mechanism compared to that displayed on the PdS mineral surface at 1 SPW. However, the rate of oxidation increases in the presence of $MgSO_4$ at increasing ionic strength. The extent of interaction between SIBX and $PdTe_2$ in the presence of $MgSO_4$ was almost similar at all ionic strengths and was comparable to the baseline case. Moreover, all final rest potentials were above the equilibrium potential of SIBX, though an increase in potentials was observed with an increase in ionic strength of $MgSO_4$. This indicates that the formation of dixanthogen was most likely favoured on the $PdTe_2$ mineral surface.

5.4.3 Effect of Mg^{2+}

Unlike the interaction of $MgCl_2$ with PdS, it was evident that the interaction between $MgCl_2$ with $PdTe_2$ occurred via a different mechanism. Figure 5.5 revealed an increase in the rate of mineral oxidation with an increase in ionic strength of $MgCl_2$. Hence, increasing the ionic strength of $MgCl_2$ enhanced the interaction of SIBX on $PdTe_2$. Nonetheless, a general decrease in final rest potentials with an increase in ionic strength is demonstrated. Ultimately, all other final rest potentials were above the equilibrium potential of SIBX except for the highest ionic strength, 10 SPW. This denotes that the formation of dixanthogen was favoured on the mineral surface at ionic strengths less than 10 SPW. Moreover, the highest ionic strength presumably favoured the formation of a metal-xanthate on $PdTe_2$.

5.4.4 Effect of Ca^{2+}

Contrary to the interaction of $CaCl_2$ with PdS, the presence of $CaCl_2$ increased the rate of oxidation of $PdTe_2$. In comparison with other salts investigated, it was indicated in Figure 5.5 that an increase in the ionic strength of $CaCl_2$ resulted in higher rates of oxidation of $PdTe_2$. Thus, a general increase in interaction between SIBX and $PdTe_2$ was observed with an increase in ionic strength. Additionally, all final rest potentials obtained in the presence of $CaCl_2$ were above the equilibrium potential of SIBX, implying that the formation of dixanthogen was favoured under these conditions (Vermaak et al., 2004).

5.4.5 Effect of Na^+

The interaction between NaCl and $PdTe_2$ was shown to be minimum in comparison with other salts investigated. However, the extent of interaction between the salt and mineral surface increased with an increase in ionic strength. The rate of oxidation on the $PdTe_2$ mineral surface increased with an increase in ionic strength of NaCl. This implies that NaCl interacted with $PdTe_2$ in a different mechanism to that displayed by PdS. The extent of interaction of SIBX with $PdTe_2$ in the presence of NaCl was relatively similar to the baseline case. Additionally, the lowest ionic strength of NaCl, which showed almost no interaction between the salt and mineral surface, had a final rest potential above the equilibrium potential of SIBX. This suggests that the formation of dixanthogen was favoured at the lowest ionic strength. However, higher ionic strengths indicated that the final rest potentials were below the equilibrium potential of SIBX, therefore denoting that the formation of a metal-xanthate was favoured (Allison et al., 1972) at higher ionic strengths of NaCl.

5.5 Key Findings

- There was a general increase in the extent of interactions between the salts and the palladium minerals with an increase in ionic strength of the salts.
- In the case of PdS, the extent of interaction of the salts with the mineral surface was found to be inversely proportional to the extent of interaction between SIBX and the mineral, in the presence of the salts. All salts decreased the rest potential of PdS at all concentrations, except for $MgSO_4$ at higher ionic strengths of 5 SPW and 10 SPW. It was demonstrated that in $MgSO_4$ at 3 SPW and NaCl at 10 SPW, very low or no interactions occurred between the salts at the respective concentrations with the PdS mineral surface. All final rest potentials were observed to be above the equilibrium potential of SIBX in all salts except for $Na_2S_20_3$ at 3 SPW, 5 SPW and 10 SPW and $CaCl_2$ at 1 SPW.
- In the case of $PdTe_2$, most salts enhanced the interaction between SIBX and the mineral surface. All salts increased the rest potential of $PdTe_2$ except for $Na_2S_2O_3$. It was observed that in the presence of NaCl at 1 SPW, there was very low or no interaction between the salt and $PdTe_2$. Moreover, final rest potentials were found to be above equilibrium potential for all salts except for $Na_2S_2O_3$ at all ionic strengths, $MgCl_2$ at 10 SPW and NaCl at 3 SPW, 5 SPW and 10 SPW.
- Amongst all salts investigated, NaCl displayed the least interaction with the palladium minerals.

- The highest interaction with SIBX was exhibited in $MgSO_4$ at all ionic strengths and $CaCl_2$ at 10 SPW for PdS and $PdTe_2$, respectively.

6. Results: Cyclic Voltammetry Measurements

The key objective of conducting cyclic voltammetric measurements was to investigate the redox processes that occurred on PdS and $PdTe_2$ minerals in the absence and presence of $Na_2S_2O_3$, $MgSO_4$, $MgCl_2$, $CaCl_2$ and NaCl at 1SPW, 3 SPW, 5 SPW and 10 SPW with and without SIBX. The baseline cases presented from this technique were conditions without salts (buffer only or SIBX only).

The variations of the current as a function of potential were acquired by changing the potential linearly with time between 0.6 V to – 0.6 V vs Ag/Ag/Cl, at a scan rate of 15 mV/s for PdS and $PdTe_2$ minerals in the absence and presence of the salts at increasing ionic strength with and without SIBX. All experiments were performed in a buffer solution of pH 9.2.

6.1 Validation

Validation of cyclic voltammetry measurements was done using the work of Tadie et al. (2015a). All conditions were used as in literature and voltammograms with similar current profiles were obtained, implying that the validation was successfully performed.

Figure 6.1 displays the voltammetric response of PtS in the absence and presence of sodium ethyl xanthate (S.E.X). Similar current profiles were obtained in both this work and the validated study. It is demonstrated that in the absence of S.E.X, small anodic currents were obtained. This suggests the slow oxidation of PtS in the presence of oxygen. On the cathodic scan, a strong reduction peak is observed at a potential range < 0.1 V. An enhanced anodic activity is illustrated in the presence of S.E.X. This observation is probably due to the oxidation of the collector on the PtS mineral surface. Furthermore, the reduction peak obtained in the presence of S.E.X commenced to more negative potentials compared to those obtained in the absence of S.E.X, thereby indicating that the presence of S.E.X inhibited the reduction of oxygen on the mineral surface.

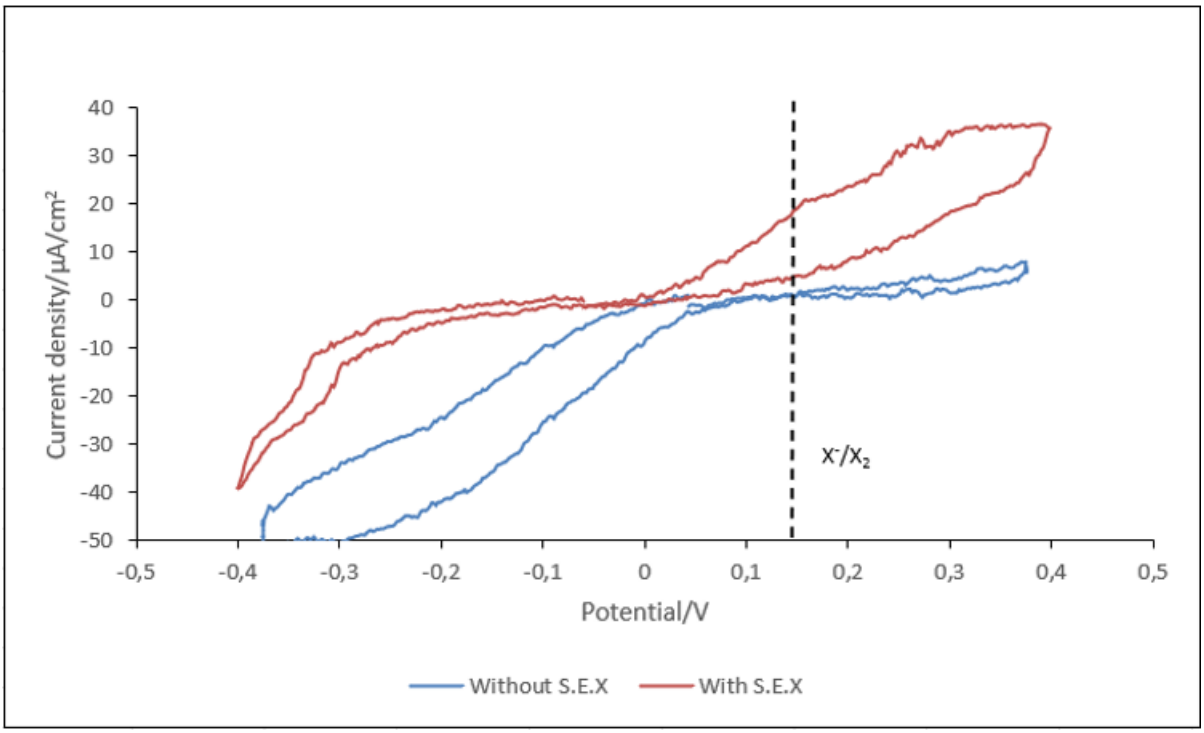

Figure 6.1: Cyclic voltammograms for PtS in aerated solutions in the absence and presence of S.E.X at a scan rate of 10 mV/s within a potential region of ± 0.4 V.

Figure 6.2 plots the voltammograms for PdS in the absence and presence of S.E.X. Small anodic currents were generated in the absence of S.E.X, whereas higher anodic currents were developed in the presence of S.E.X. The higher anodic currents obtained in the presence of S.E.X could be attributable to the oxidation of the collector on the mineral surface. In addition, a strong cathodic peak was obtained in the absence of S.E.X, probably resembling the reduction of oxygen on the mineral surface. Ultimately, the peak commenced at potentials > 0.1 V.

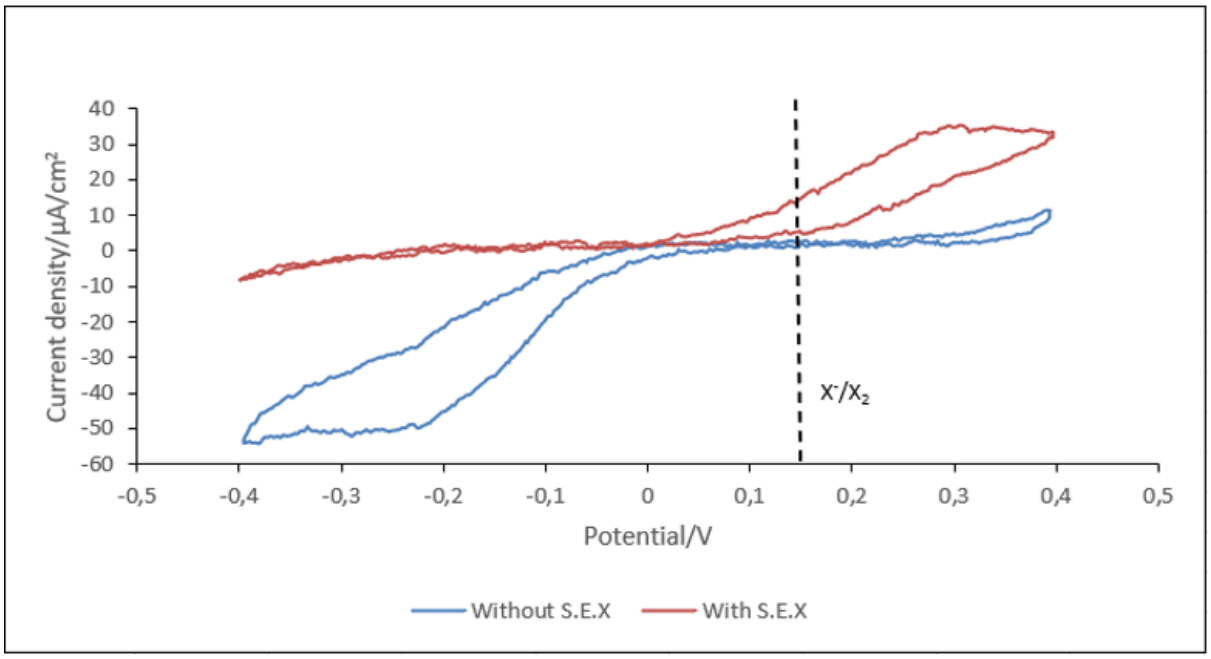

Figure 6.2: Voltammetric response for PdS in the absence and presence of S.E.X at a scan rate of 10 mV/s within a potential range of ± 0.4 V.

6.2 Reproducibility

All tests were conducted in duplicates. Due to similar current profiles that were obtained for the repeat measurements, an average for two runs was obtained for each test.

Figure 6.3 plots the cyclic voltammograms for $PdTe_2$ in $Na_2S_2O_3$ (5 SPW) with SIBX. It is evident that both runs 1 and 2 generated identical current profiles. It is clear that two anodic peaks were generated on the anodic scan. The first peak shows a steep increase in anodic currents at a potential range > 0.2 V. The second peak was developed at potentials > 0.5 V. Corresponding to the anodic peaks developed, two broad reduction peaks were observed. The cathodic peaks were observed within the potential regions of 0.2 V to – 0.15 V and – 0.15 V to – 0.6 V.

Figure 6.4 demonstrates the voltametric response of $PdTe_2$ in $MgCl_2$ at 5 SPW. The figure clearly indicates that the current profiles developed for runs 1 and 2 are similar. One prominent anodic peak was generated at potentials > 0.2 V on the positive sweep. Alternatively, on the reverse sweep, two cathodic peaks were observed within the potential regions 0 V to – 0.25 V and at potentials < 0.4 V.

The similar current profiles obtained for Figures 6.3 and 6.4 clearly indicate that the cyclic voltammetric measurements performed in this study were very reproducible.

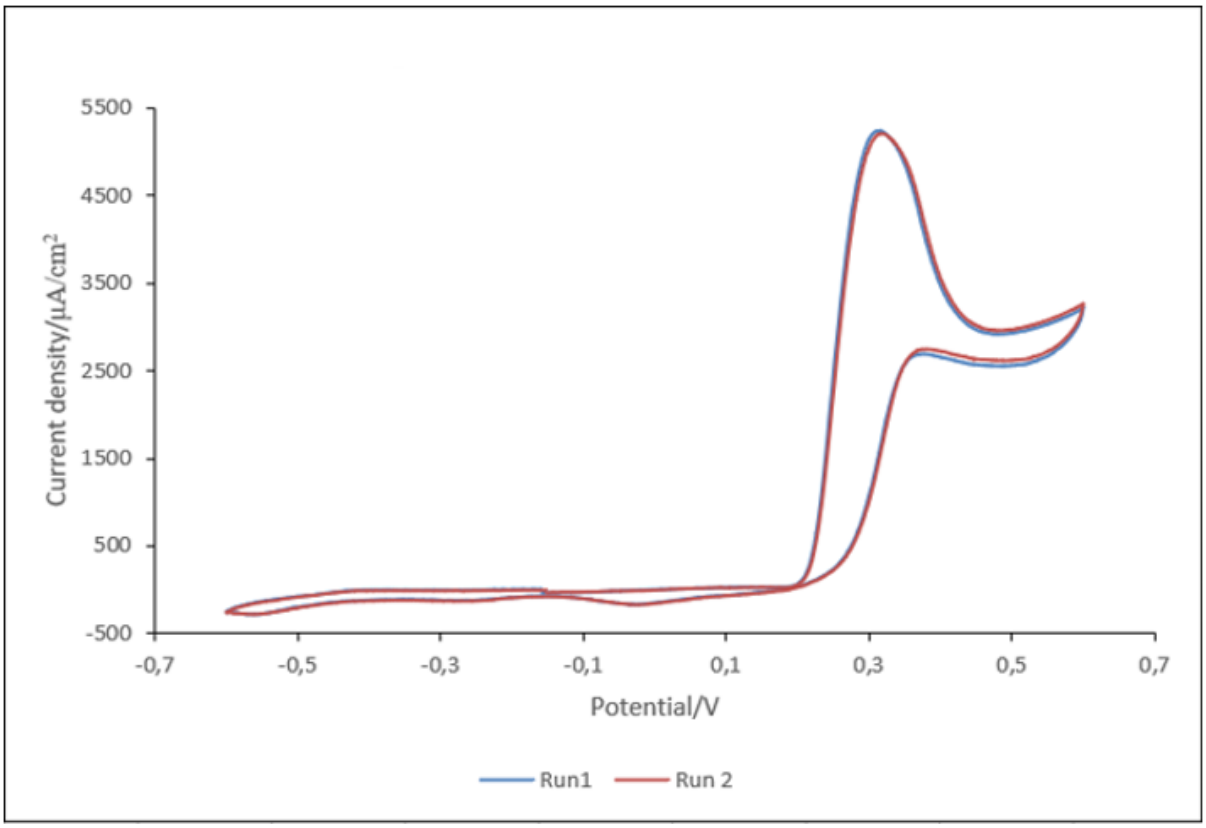

Figure 6.3: Cyclic voltammograms for $PdTe_2$ electrode in $Na_2S_2O_3$ (5 SPW) with SIBX, at a scan rate of 15 mV/s within a potential range of ± 0.6 V and at a pH of 9.2.

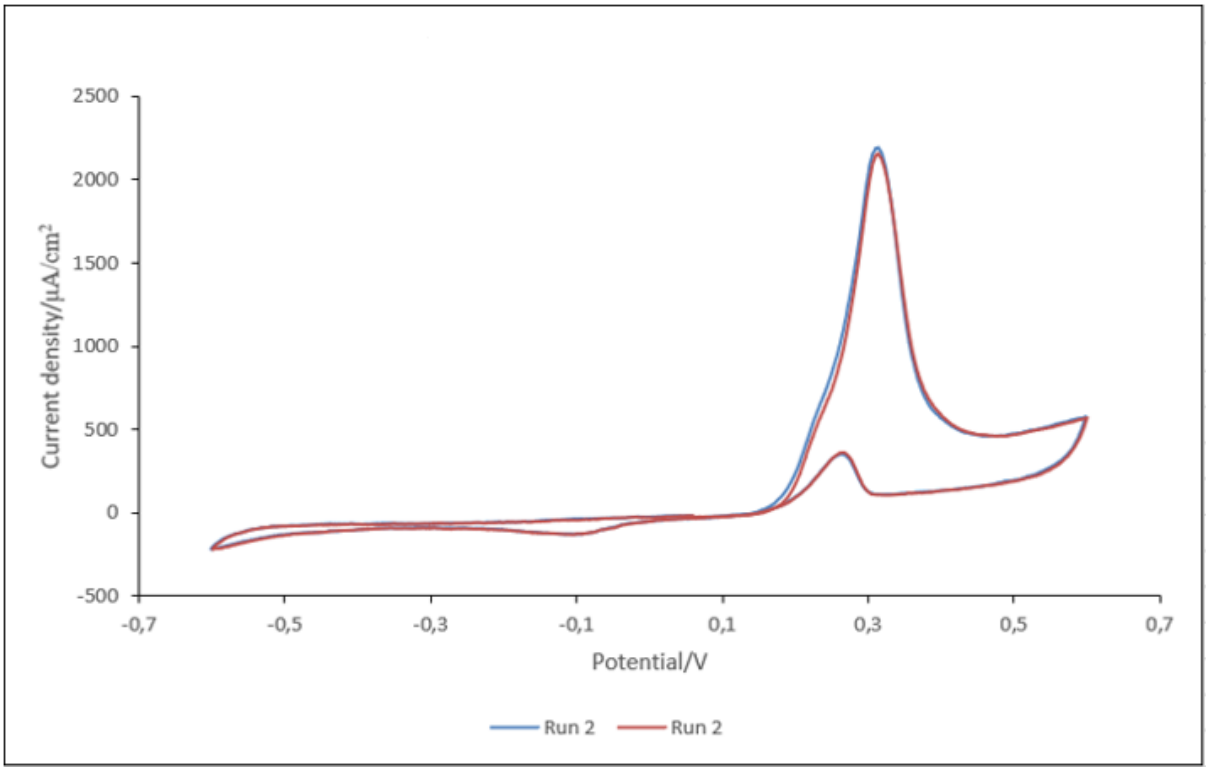

Figure 6.4: Cyclic voltammograms for $PdTe_2$ electrode in $MgCl_2$ (5 SPW), at a scan rate of 15 mV/s within a potential range of ± 0.6 V and at a pH of 9.2.

6.3 Voltammograms for PdS

6.3.1 Effect of $Na_2S_2O_3$

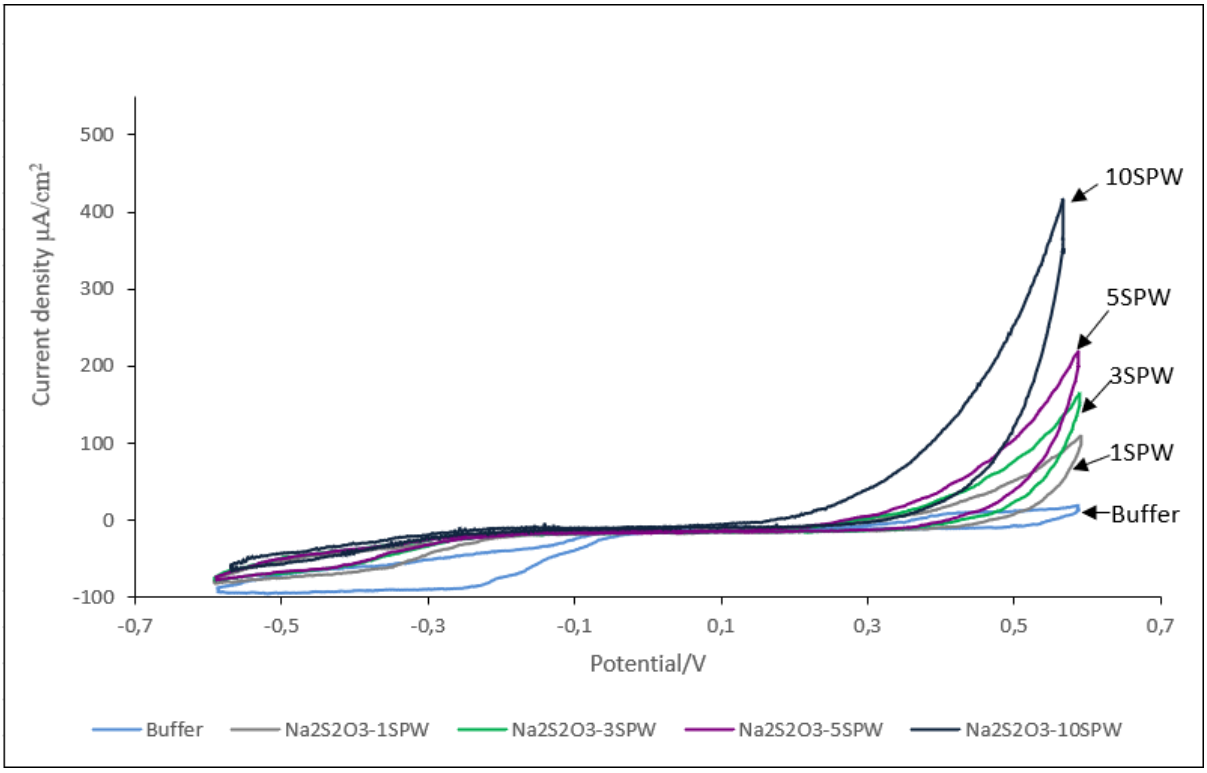

Figure 6.5: Cyclic voltammograms for PdS in the absence and presence of $Na_2S_2O_3$ at increasing ionic strength at a scan rate of 15 mV/s within a potential range of ± 0.6 V and at a pH of 9.2.

Figure 6.5 demonstrates the voltammetric response of PdS in the absence and presence of $Na_2S_2O_3$ at increasing ionic strength. On the anodic scan, one anodic current peak was observed for all conditions observed. It was noted that the anodic peak obtained in the absence of $Na_2S_2O_3$ was less pronounced than the peaks obtained in the presence $Na_2S_2O_3$. The peak was observed to appear at a potential of ≈ 0.3 V. In the presence of $Na_2S_2O_3$, an increase in ionic strength resulted in a steep increase in current densities. The current peak for $Na_2S_2O_3$ at the highest ionic strength commenced at a lower potential of 0.15 V compared to other conditions of lower ionic strength, which had current peaks commencing at higher potentials of ≈ 0.25 V. This implies that an increase in ionic strength of $Na_2S_2O_3$ slightly decreased the potential at which the anodic peaks developed. Therefore, it is clear that an increase in ionic strength of $Na_2S_2O_3$ enhances the rate of oxidation of PdS.

On the contrary, the sweep in the negative direction for the baseline case yielded a pronounced cathodic peak between the potential range of – 0.1 V to – 0.6 V. This peak could be ascribed to the reduction of oxygen on the PdS mineral surface. The presence of $Na_2S_2O_3$ noticeably inhibits the reduction of oxygen on the mineral surface (Gardner and Woods, 1979) as demonstrated by the reduction currents commencing to more negative potentials in the potential range of – 0.2 V to – 0.6 V.

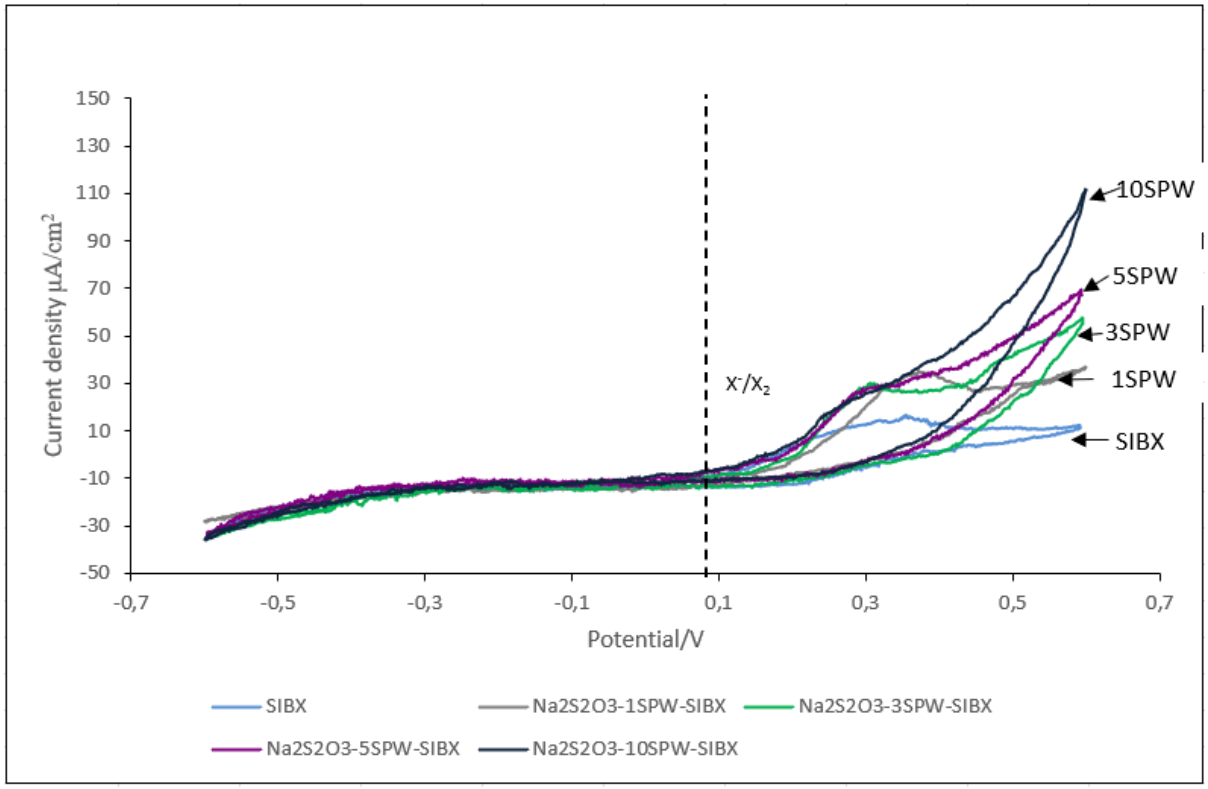

Figure 6.6: Cyclic voltammograms for PdS in the absence and presence of $Na_2S_2O_3$ at increasing ionic strength with SIBX at a scan rate of 15 mV/s within a potential range of ± 0.6 V and at a pH of 9.2. The dotted line represents the equilibrium potential of dixanthogen formation of SIBX at 6.24×10^{-4} M (0.08 V).

Though Figure 6.6 shows that the presence of $Na_2S_2O_3$ enhances the oxidation of PdS, generally the lower current densities obtained would have occurred due to the oxidation of $Na_2S_2O_3$ being inhibited by the presence of SIBX. In addition, anodic current peaks for all conditions appeared at potentials higher than the equilibrium potential of dixanthogen formation. This observation reveals that the oxidation products formed on the mineral surface are expected to be due to the formation of dixanthogen. During the subsequent negative sweep, no cathodic peaks were observed. This suggests that the oxidation products formed on the mineral surface were possibly soluble or electrochemically inactive within the potential range investigated in this study

(Tadie et al., 2015a) or possible formation of a loosely bound layer of oxidation products on PdS (Vermaak et al., 2007).

6.3.2 Effect of $MgSO_4$

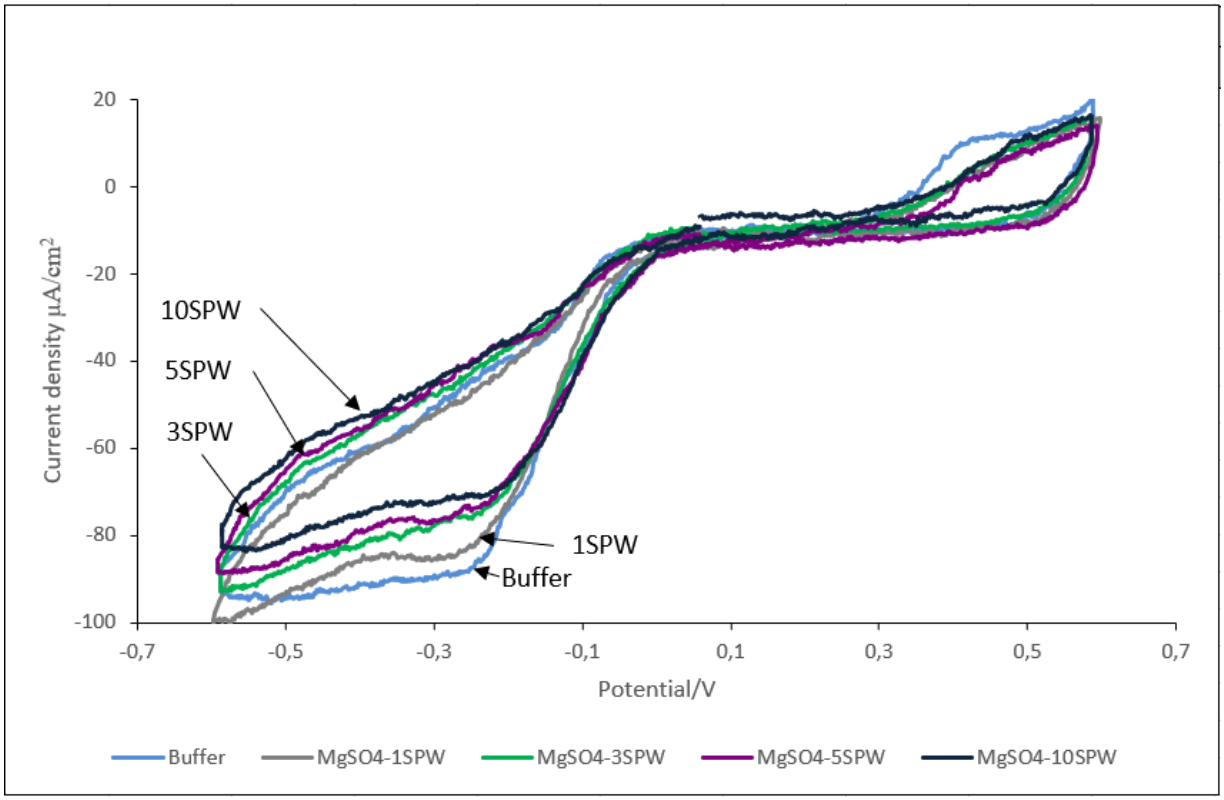

Figure 6.7: Cyclic voltammograms for PdS in the absence and presence of $MgSO_4$ at increasing ionic strength at a scan rate of 15 mV/s within a potential range of ± 0.6 V and at a pH of 9.2.

Figure 6.7 illustrates the effect of increasing the ionic strength of $MgSO_4$ on PdS mineral surface. Generally, small anodic current peaks were achieved both in the absence and presence of $MgSO_4$ at potentials above 0.3 V, owing to the slow oxidation of PdS. Overall, there was no significant difference in the anodic current densities observed.

However, on the cathodic scan, strong reduction currents were attained both in the absence and presence of $MgSO_4$. The reduction peaks may be associated with the reduction of oxygen on PdS. A slight shift in reduction currents to more negative potentials is exhibited from the baseline case with an increase in ionic strength of $MgSO_4$ within the potential range of – 0.2 V and – 0.6 V. This suggests that probably $MgSO_4$ inhibited the reduction of oxygen on PdS (Tadie et al., 2015a).

The presence of $MgSO_4$ noticeably inhibits the reduction of oxygen on the mineral surface (Gardner and Woods, 1979) as demonstrated by the reduction currents commencing to more negative potentials in the potential range of – 0.2 V to – 0.6 V.

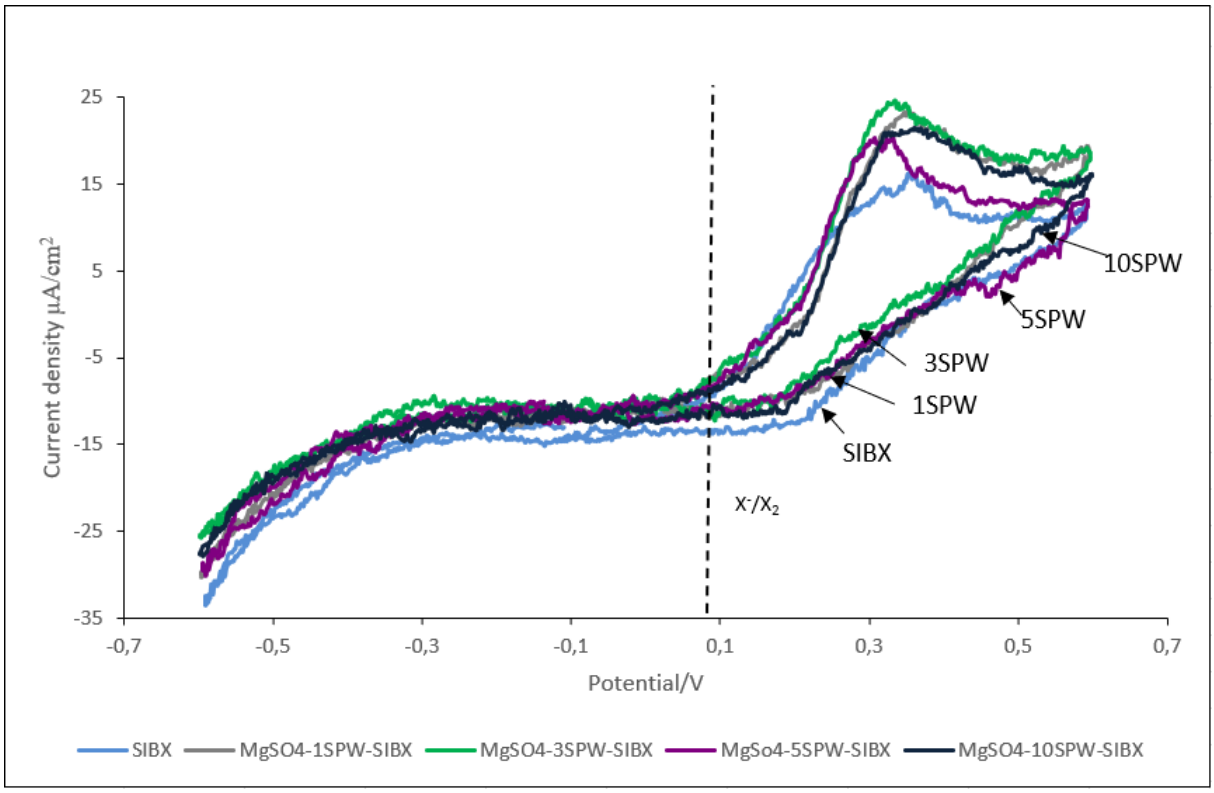

Figure 6.8: Cyclic voltammograms for PdS in the absence and presence of $MgSO_4$ at increasing ionic strength with SIBX at a scan rate of 15 mV/s within a potential range of ± 0.6 V and at a pH of 9.2. The dotted line represents the equilibrium potential of dixanthogen formation of SIBX at 6.24×10^{-4} M (0.08 V).

Figure 6.8 displays voltammograms for PdS in the absence and presence of $MgSO_4$ at increasing ionic strength with SIBX. On the anodic scan, prominent anodic currents (Vermaak et al., 2004) were generated for all conditions investigated. However, there was no significant difference between the baseline case and conditions with $MgSO_4$. The anodic peaks obtained in Figure 6.8 displayed slightly higher anodic currents compared to those shown in Figure 6.7 (without SIBX), owing to the oxidation of SIBX on the mineral surface. Furthermore, it is indicated in Figure 6.8 that the anodic peaks were above the equilibrium potential of dixanthogen formation, implying that the formation of dixanthogen could be favoured under all conditions investigated.

All conditions both in the absence and presence of $MgSO_4$ with SIBX, yielded no reduction current peaks. The absence of the reduction peaks could possibly be assigned to the formation of soluble oxidation products or electrochemically inactive products or a non-protective nature of loosely bound layer of oxidation products (Vermaak et al., 2007).

6.3.3 Effect of $MgCl_2$

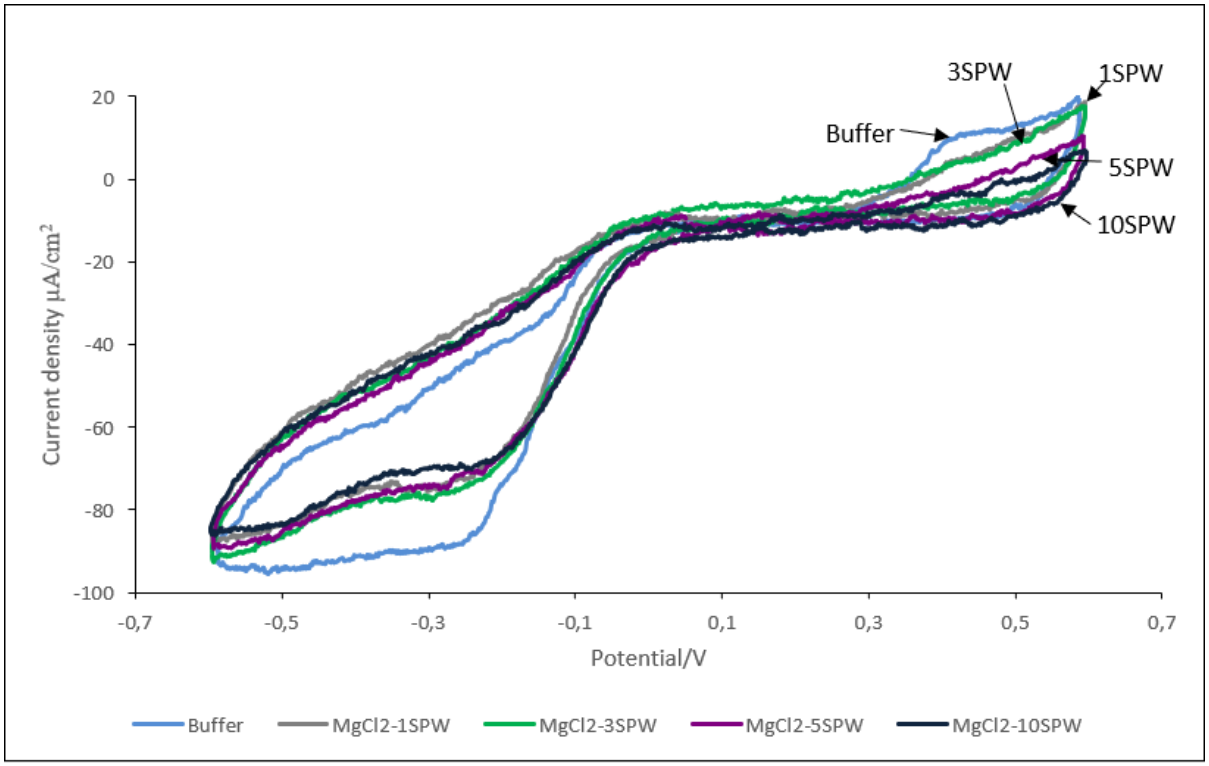

Figure 6.9: Cyclic voltammograms for PdS in the absence and presence of $MgCl_2$ at increasing ionic strength at a scan rate of 15 mV/s within a potential range of ± 0.6 V and at a pH of 9.2.

Figure 6.9 conveys voltammograms of PdS in the absence and presence of $MgCl_2$. The positive sweep perceptibly yields small anodic currents above 0.3 V, which are not significantly different. This possibly suggests the slow oxidation of PdS under the investigated conditions. Notwithstanding the non-significant differences in anodic peaks, the presence of $MgCl_2$ displayed slightly lower anodic current densities with an increase in ionic strength. Hence, indicating that an increase in ionic strength $MgCl_2$ slightly inhibits the oxidation of the PdS mineral (Gardner and Woods, 1979).

The negative sweep generated appreciable cathodic current peaks both in the absence and presence of $MgCl_2$. It is accepted that the reduction peaks obtained could be attributable to the reduction of oxygen on the mineral surface. However, a slight shift in reduction currents to more negative potentials is demonstrated in the presence of $MgCl_2$ within a potential range of – 0.1 V to – 0.6 V. This suggests a slight inhibition of $MgCl_2$ on the reduction of oxygen on the minerals surface within the potential range investigated.

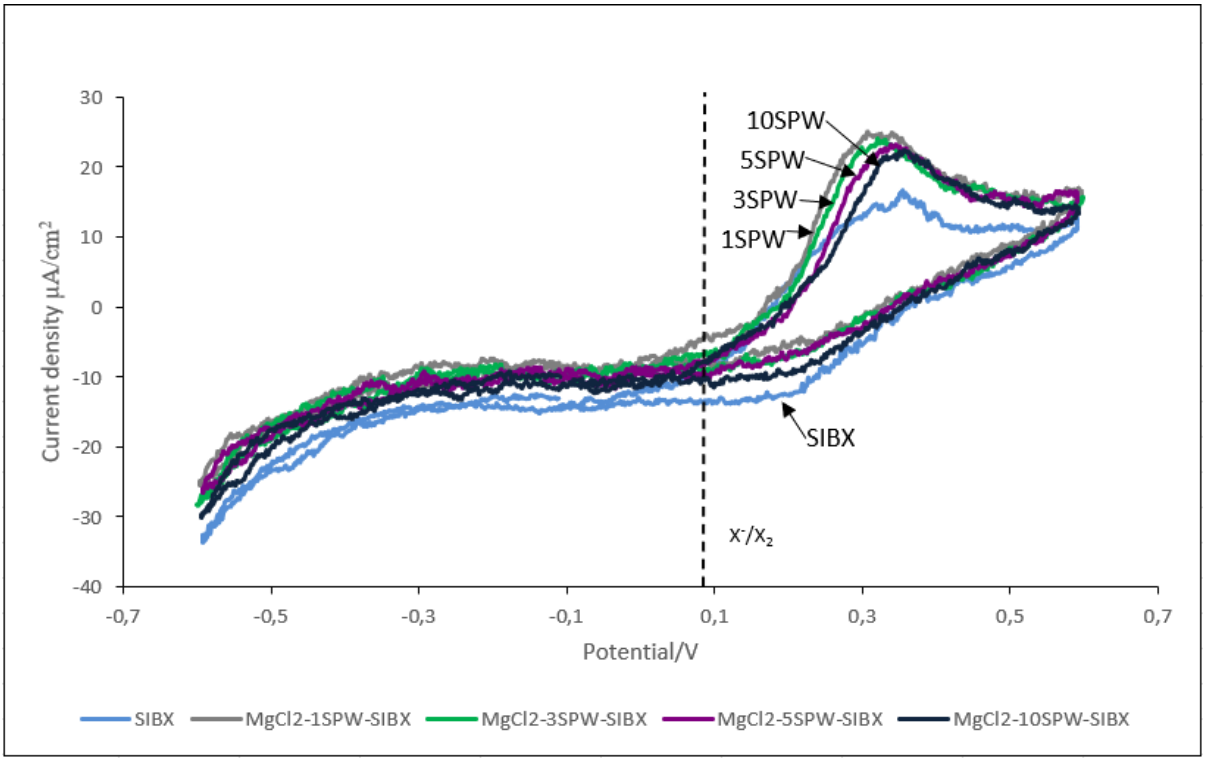

Figure 6.10: Cyclic voltammograms for PdS in the absence and presence of $MgCl_2$ at increasing ionic strength with SIBX at a scan rate of 15 mV/s within a potential range of ± 0.6 V and at a pH of 9.2. The dotted line represents the equilibrium potential of dixanthogen formation of SIBX at 6.24×10^{-4} M (0.08 V).

Figure 6.10 depicts the voltammetric response of PdS in the absence and presence of $MgCl_2$ with SIBX. The figure clearly shows the enhanced anodic activity in the presence of SIBX. For all conditions investigated, the anodic currents started to increase strongly > 0.1 V, a potential that is above the reversible potential of xanthate-di-isobutyl dixanthogen equilibrium. This observation suggests a possible formation of dixanthogen on the mineral surface under the conditions investigated. However, the baseline case displays lower current densities compared to those generated in the presence of $MgCl_2$, hence implying a slightly enhanced oxidation effect on PdS with a decrease in ionic strength of $MgCl_2$.

In contrast to the prominent oxidation peaks observed, cathodic peaks related to the reduction of the oxidized products were absent. The absence of the peaks could be as a result of the formation of soluble oxidation products or non- protective nature (loosely bound layer) (Vermaak et al., 2007) of the oxidation products formed on the mineral surface or the formation of electrochemically inactive products within the potential range investigated.

6.3.4 Effect of $CaCl_2$

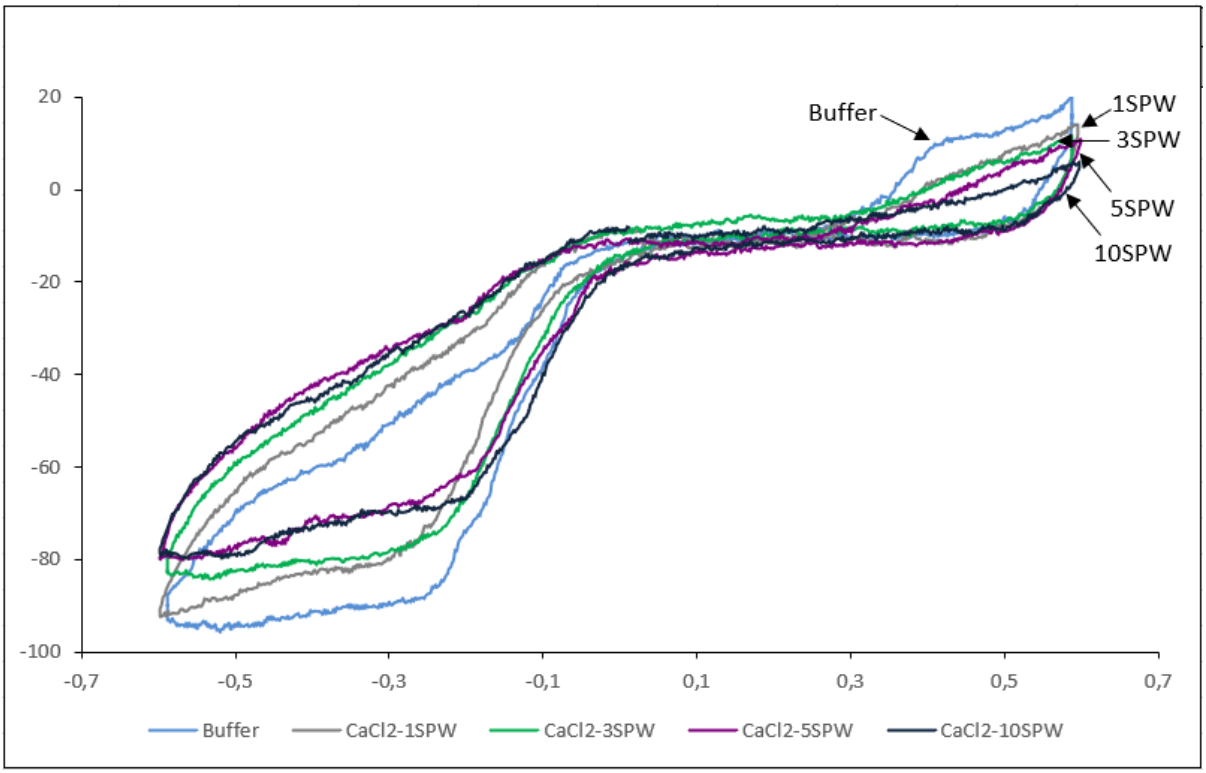

Figure 6.11: Cyclic voltammograms for PdS in the absence and presence of $CaCl_2$ at increasing ionic strength at a scan rate of 15 mV/s within a potential range of ± 0.6 V and at a pH of 9.2.

Figure 6.11 shows voltammograms for PdS in the absence and presence of $CaCl_2$ at increasing ionic strength. Small anodic currents are evident above 0.3 V, denoting the slow oxidation of PdS both in the absence and presence of $CaCl_2$. Nonetheless, slightly lower anodic current densities are observed with an increase in ionic strength of $CaCl_2$. Therefore, suggesting that the presence of $CaCl_2$ at increased ionic strengths inhibits the oxidation of PdS.

The reverse scan displayed significant reduction peaks between the potential range of 0 V to – 0.6 V. These prominent reduction peaks demonstrate the reduction of oxygen on PdS. It is apparent that an increase in ionic strength of $CaCl_2$ inhibits the reduction of oxygen on the mineral surface (Gardner and Woods, 1979), as revealed by the reduction currents commencing to more negative potentials.

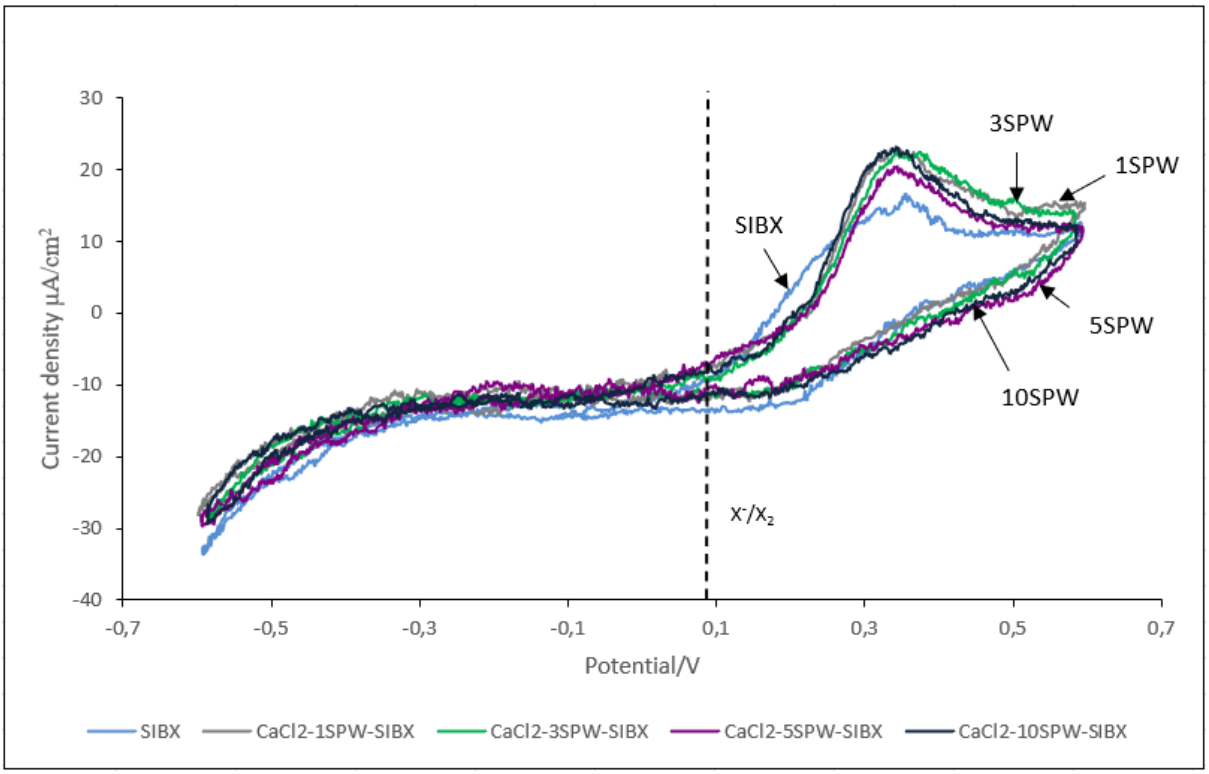

Figure 6.12: Cyclic voltammograms for PdS in the absence and presence of $CaCl_2$ at increasing ionic strength with SIBX at a scan rate of 15 mV/s within a potential range of ± 0.6 V and at a pH of 9.2. The dotted line represents the equilibrium potential of dixanthogen formation of SIBX at 6.24×10^{-4} M (0.08 V).

Figure 6.12 exhibits current-potential curves for PdS in the absence and presence of $CaCl_2$ with SIBX. Compared to Figure 6.11, higher anodic current peaks were obtained in Figure 6.12 due to the oxidation of SIBX on the mineral surface. However, the presence of $CaCl_2$ shows a slightly enhanced anodic activity (Vermaak et al., 2004) compared to the baseline case. Anodic currents are visible above the equilibrium potential of dixanthogen formation, probably reflecting the formation of dixanthogen on the mineral surface under all conditions investigated.

Conversely, on the cathodic scan, reduction peaks were absent. This observation could be attributable to the formation of soluble oxidation products or loosely bound oxidation product layer (Vermaak et al., 2007) formed on the mineral surface or the oxidation products formed might be electrochemically inactive within the potential range investigated.

6.3.5 Effect of NaCl

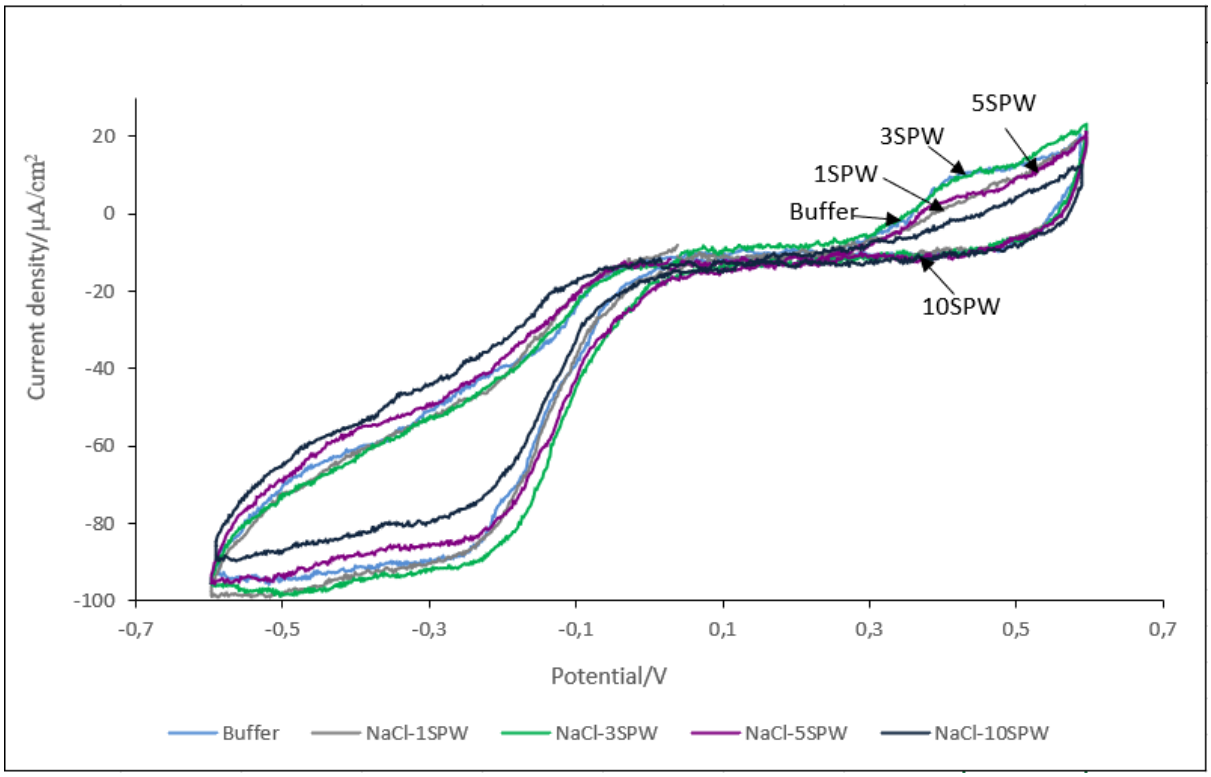

Figure 6.13: Cyclic voltammograms for PdS in the absence and presence of NaCl at increasing ionic strength at a scan rate of 15 mV/s within a potential range of ± 0.6 V and at a pH of 9.2.

Figure 6.13 plots the voltammetric response of PdS in the absence and presence of NaCl with increasing ionic strength. Similar to $MgSO_4$, $MgCl_2$ and $CaCl_2$, NaCl displayed small anodic currents that appear possibly as a consequence of the slow oxidation of PdS. Anodic activity was established to commence at a potential of 0.3 V. Interestingly, the anodic currents both in the absence and presence of NaCl do not demonstrate any significant differences.

On the reverse scan, prominent peaks were observed which could be associated with the reduction of oxygen. No trend is observed in the case of ionic strength of NaCl, however, the cathodic peaks did not show any significant difference from the reduction peak obtained for the baseline case. Hence, implying the insignificant effect of NaCl on PdS mineral.

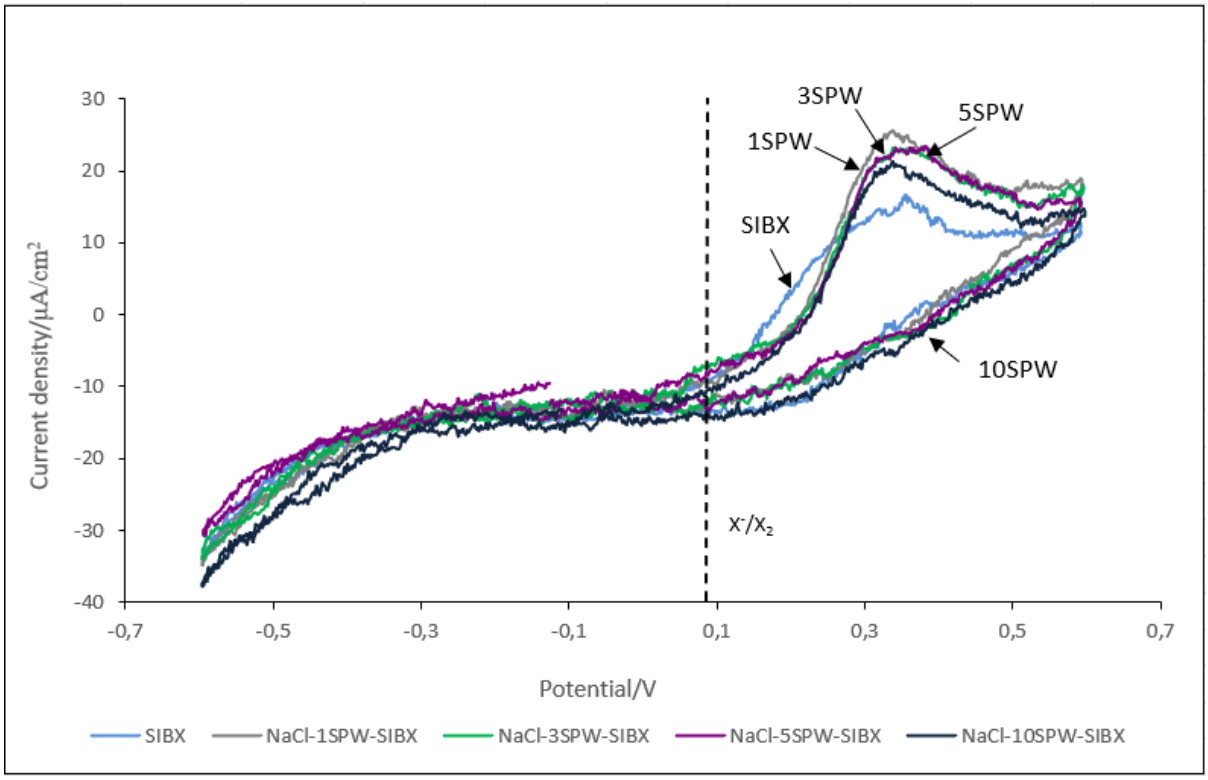

Figure 6.14: Cyclic voltammograms for PdS in the absence and presence of NaCl at increasing ionic strength with SIBX at a scan rate of 15 mV/s within a potential range of ± 0.6 V and at a pH of 9.2. The dotted line represents the equilibrium potential of dixanthogen formation of SIBX at 6.24×10^{-4} M (0.08 V).

Figure 6.14 demonstrates voltammograms for PdS in the absence and presence of NaCl with SIBX. It is evident that the anodic currents obtained in Figure 6.14 are slightly higher than those obtained in Figure 6.13, owing to the oxidation of SIBX on the PdS mineral surface. The enhanced anodic activity commenced at the potential at which the equilibrium of dixanthogen formation occurs. It is therefore expected that the conditions investigated in Figure 6.14 should give rise to the formation of dixanthogen on the mineral surface. Additionally, it is shown that the presence of NaCl on the PdS slightly enhanced the anodic activity on the mineral surface.

Alternatively, the cathodic scan did not generate any visible cathodic peaks. The absence of the peaks could be ascribed to the formation of soluble oxidation products or loosely bound oxidation product layers (Vermaak et al., 2007) to the mineral surface or the formation of electrochemically inactive oxidation products within the potential range investigated.

6.3.6 Effect of 1 SPW of salts

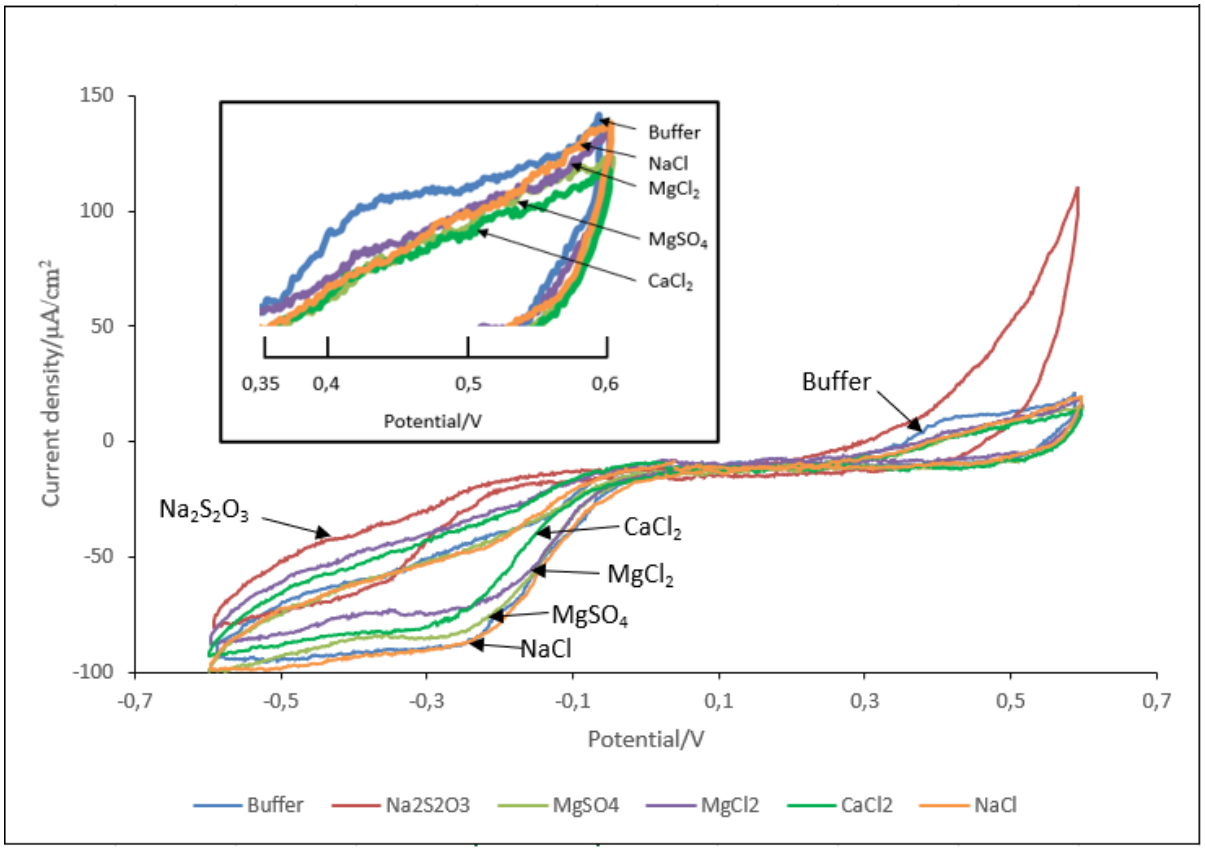

Figure 6.15: Cyclic voltammograms for PdS in the absence and presence of $Na_2S_2O_3$, NaCl, $MgSO_4$, $MgCl_2$ and $CaCl_2$ at 1 SPW at a scan rate of 15 mV/s within a potential range of ± 0.6 V and at a pH of 9.2.

Figure 6.15 illustrates cyclic voltammograms for PdS in the absence and presence of the five salts investigated in this study at 1 SPW. On the anodic scan, a broad peak is noted within the potential range of 0.35 V to 0.5 V, for the baseline case. Moreover, the baseline case showed an anodic peak which was not seen in the presence of the salts, within a potential range of 0.35 V to 0.5 V. The observed anodic peak could be associated to the oxidation of dissolved oxygen. A prominent anodic peak is displayed in the presence of $Na_2S_2O_3$ compared with other conditions. This is probably due to an enhanced oxidation effect of $Na_2S_2O_3$ on PdS. The anodic peak for $Na_2S_2O_3$ appeared at 0.2 V and continued in a wide potential range up to 0.6 V. However, the baseline case, $MgSO_4$, $MgCl_2$, $CaCl_2$ and NaCl displayed small anodic currents within a potential range of 0.3 V to 0.6 V. This observation could be attributable to the slow oxidation of PdS. Nonetheless, no significant difference in current density was observed in the presence of $MgSO_4$, $MgCl_2$, $CaCl_2$ and NaCl. The presence of $MgSO_4$, $MgCl_2$, $CaCl_2$ and NaCl at 1 SPW appears to have no effect on the electrochemical reactivity of the surface species produced in this potential range.

Strong cathodic peaks were noted on the reverse scan for all conditions investigated, which could be assigned to the reduction of oxygen on the mineral surface. It was apparent that the cathodic peak for NaCl followed a similar trend to that of the baseline case. However, cathodic peaks for $CaCl_2$ and $Na_2S_2O_3$ commenced to more negative potentials within potential ranges of – 0.15 V to – 0.6 V and – 0.2 V to – 0.6 V, respectively. Thereby, implying that the presence of $Na_2S_2O_3$ displayed a slightly higher impact in inhibiting oxygen on the mineral surface than in the presence of $CaCl_2$.

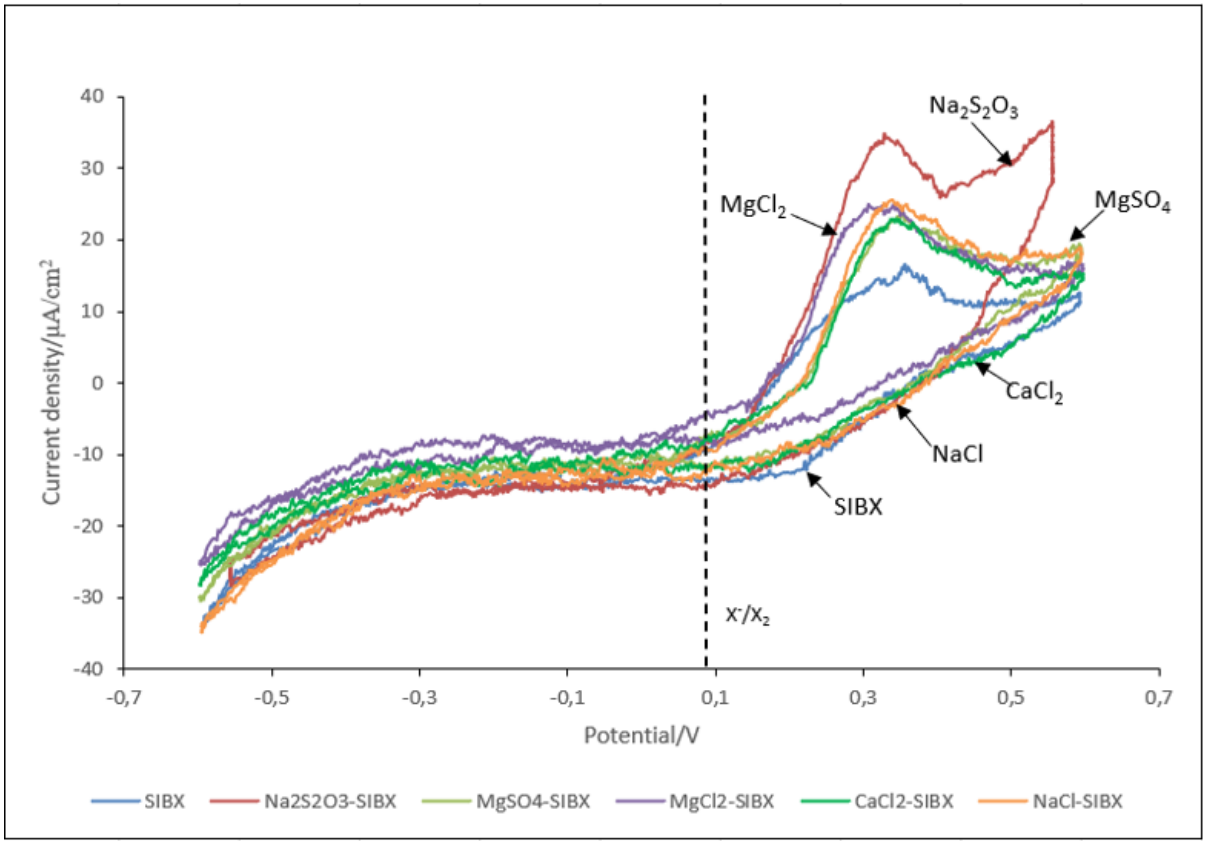

Figure 6.16: Cyclic voltammograms for PdS in the absence and presence of $Na_2S_2O_3$, NaCl, $MgSO_4$, $MgCl_2$ and $CaCl_2$ at 1 SPW with SIBX at a scan rate of 15 mV/s within a potential range of ± 0.6 V and at a pH of 9.2. The dotted line represents the equilibrium potential of dixanthogen formation of SIBX at 6.24×10^{-4} M (0.08 V).

Figure 6.16 displays the voltammetric response for PdS in the absence and presence of SIBX with $Na_2S_2O_3$, $MgSO_4$, $MgCl_2$, $CaCl_2$ and NaCl at 1 SPW. The figure clearly exhibits enhanced anodic activity imposed by the presence of SIBX. The anodic currents displayed for the baseline case were slightly lower than in the presence of salts. The presence of salts shows an enhanced anodic effect on the mineral surface. Unlike other conditions that displayed one prominent anodic peak, the presence of $Na_2S_2O_3$ yielded two significant anodic peaks, probably due to two oxidation reactions which could have occurred on the mineral surface. Additionally, anodic peaks for all the conditions

investigated commenced above the reversible potential for the oxidation of SIBX to dixanthogen, at a potential ≈ 0.1 V. The potential at which the anodic peaks appeared indicate a possible formation of dixanthogen on the mineral surface in the conditions investigated.

Contrary to the prominent anodic peaks observed, the cathodic scan did not generate any cathodic peaks under all conditions investigated. The absence of the cathodic peaks could be associated to the formation of soluble oxidation products, loosely bound oxidation product layer formed (Vermaak et al., 2007) or the formation on electrochemically inactive species within the potential region of this study.

6.3.7 Effect of 3 SPW of salts

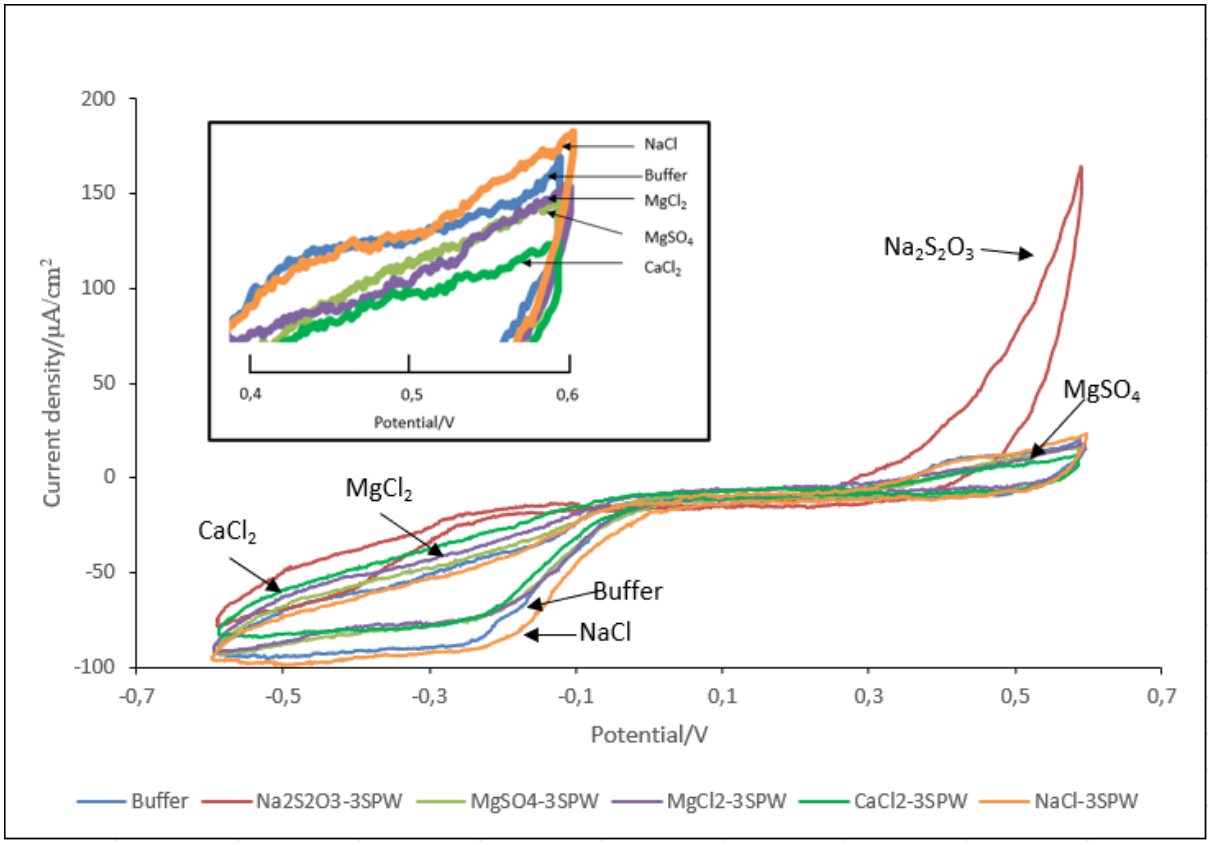

Figure 6.17: Cyclic voltammograms for PdS in the absence and presence of $Na_2S_2O_3$, NaCl, $MgSO_4$, $MgCl_2$ and $CaCl_2$ at 3 SPW at a scan rate of 15 mV/s within a potential range of ± 0.6 V and at a pH of 9.2.

Figure 6.17 reveals current-potential curves for PdS in the absence and presence of $Na_2S_2O_3$, $MgSO_4$, $MgCl_2$, $CaCl_2$ and NaCl at 3 SPW. A strong anodic peak is observed in the presence of $Na_2S_2O_3$ as compared to other conditions, with the enhanced anodic activity commencing at a potential above 0.25 V. Small anodic currents were yielded for the baseline case and in the presence of $MgSO_4$, $MgCl_2$, $CaCl_2$ and NaCl, owing to the slow oxidation of the PdS mineral surface. The

small anodic currents appeared within a broad potential range of 0.35 V to 0.6 V. The current densities obtained were not significantly different, though slightly higher anodic currents were obtained for the baseline case and in the presence of NaCl. Hence, the presence of $MgSO_4$, $MgCl_2$, $CaCl_2$ probably inhibited the oxidation on PdS, slightly.

The negative sweep, yielded prominent cathodic peaks within a potential range of 0 to – 0.6 V. The observed peaks could be ascribed to the reduction of oxygen on PdS in the absence and presence of $MgSO_4$, $MgCl_2$, $CaCl_2$ and NaCl. However, the cathodic peak generated by the presence of $Na_2S_2O_3$ appeared at more negative potentials of between – 0.25 V to – 0.6 V. The presence of $Na_2S_2O_3$ probably inhibited the reduction of oxygen on the mineral surface.

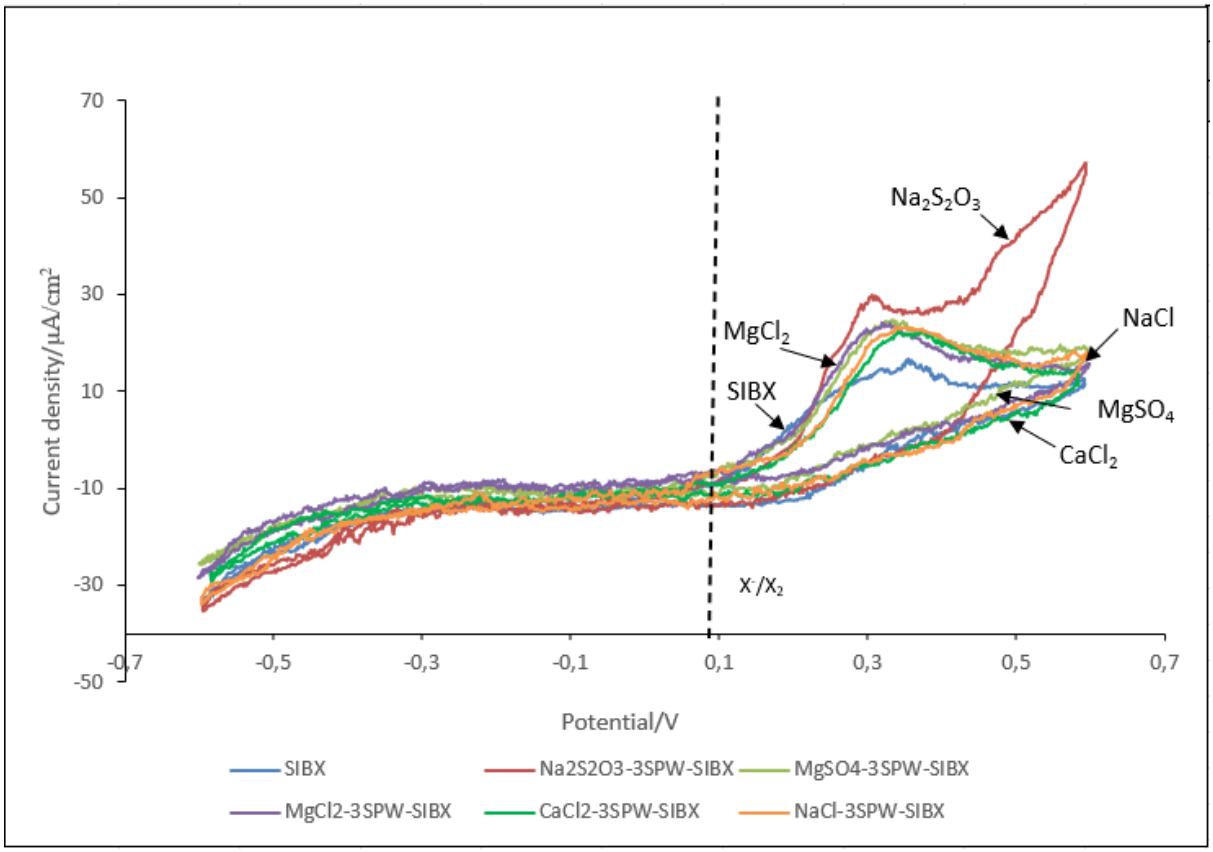

Figure 6.18: Cyclic voltammograms for PdS in the absence and presence of $Na_2S_2O_3$, NaCl, $MgSO_4$, $MgCl_2$ and $CaCl_2$ at 3 SPW with SIBX at a scan rate of 15 mV/s within a potential range of ± 0.6 V and at a pH of 9.2. The dotted line represents the equilibrium potential of dixanthogen formation of SIBX at 6.24×10^{-4} M (0.08 V).

Figure 6.18 exhibits voltammograms for PdS in the absence and presence of $Na_2S_2O_3$, $MgSO_4$, $MgCl_2$, $CaCl_2$ and NaCl at 3 SPW with SIBX. It is clear that the presence of SIBX enhances the anodic activity of the mineral surface, as indicated by the prominent anodic peaks generated. The absence of salts exhibited lower anodic activity, hence implying that the oxidation of PdS is slightly

appreciable in the presence of the salts. However, the presence of $Na_2S_2O_3$ conveyed two strong anodic peaks compared with other conditions. The first peak started at 0.2 V and continued to a potential of 0.4 V, whereas the second peak commenced at a potential of 0.45 V to 0.6 V. Overall, the anodic peaks were observed to appear above the equilibrium potential of dixanthogen, therefore depicting a possible formation of dixanthogen on the mineral surface under the investigated conditions.

Conversely, the reverse scan displayed no cathodic peaks. The observation could be attributable to the formation of loosely bound oxidation product layer (Vermaak et al., 2007) or the formation of soluble oxidation products or possibly the formation on electrochemically inactive products.

6.3.8 Effect of 5 SPW of salts

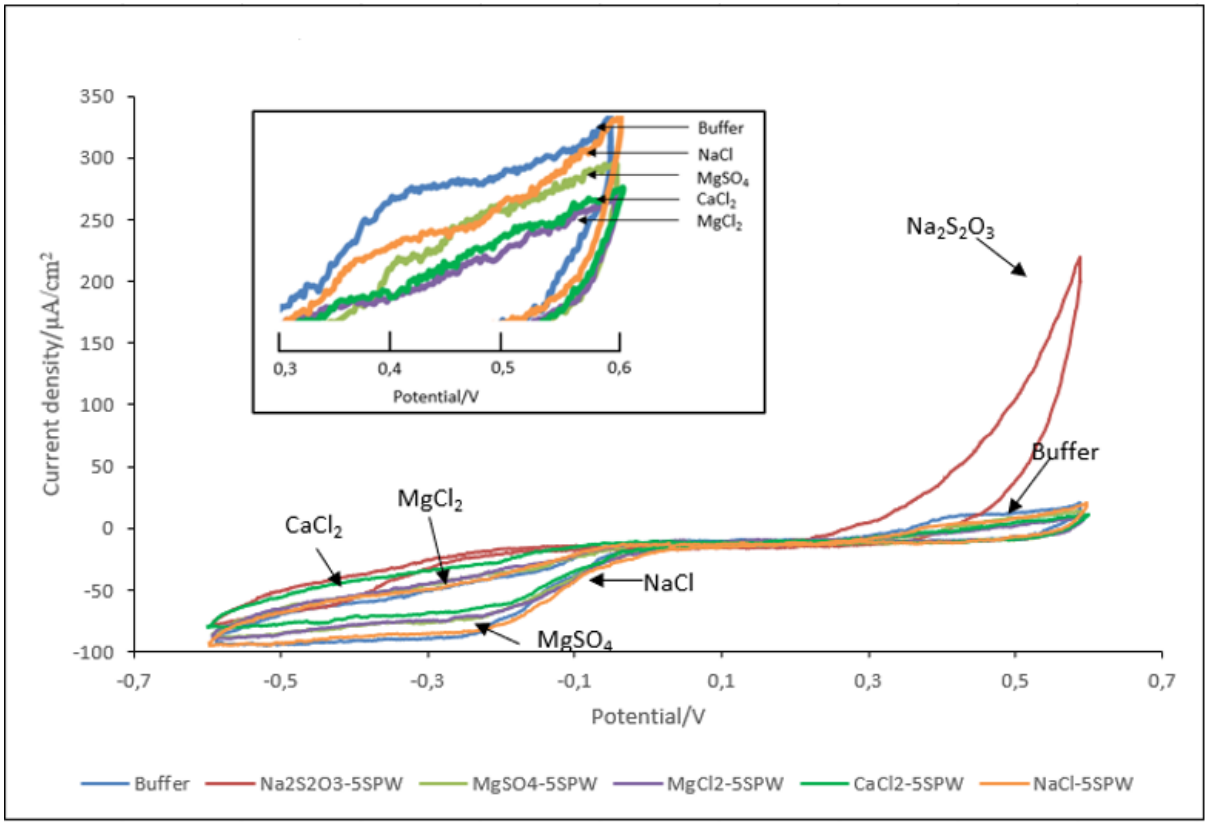

Figure 6.19: Cyclic voltammograms for PdS in the absence and presence of $Na_2S_2O_3$, NaCl, $MgSO_4$, $MgCl_2$ and $CaCl_2$ at 5 SPW at a scan rate of 15 mV/s within a potential range of ± 0.6 V and at a pH of 9.2.

Figure 6.19 plots the voltammetric response of PdS in the absence and presence of $Na_2S_2O_3$, $MgSO_4$, $MgCl_2$, $CaCl_2$ and NaCl at 5 SPW. On the anodic scan, the presence of $Na_2S_2O_3$ exhibits significantly high anodic behaviour as compared to other conditions, with the anodic peak commencing at a potential > 0.25 V. Small anodic currents were generated for the baseline case

and in the presence of $MgSO_4$, $MgCl_2$, $CaCl_2$ and NaCl, due to the slow oxidation of PdS. These small currents did not differ significantly, though the baseline case demonstrated slightly higher anodic currents. Hence, the presence of $MgSO_4$, $MgCl_2$, $CaCl_2$ and NaCl slightly inhibited the oxidation of PdS.

On the other hand, the negative sweeps displayed strong cathodic peaks in the potential range between 0 V to – 0.6 V, in the case of $MgSO_4$, $MgCl_2$, $CaCl_2$ and NaCl. The observed cathodic peaks probably reflect the reduction of oxygen on the PdS mineral surface. However, in the presence of $Na_2S_2O_3$, the cathodic peak observed commenced at – 0.2 V, therefore showing a shift to the negative potential range compared with other conditions. This suggests that the presence of $Na_2S_2O_3$ probably inhibits the reduction of oxygen on PdS (Gardner and Woods, 1979).

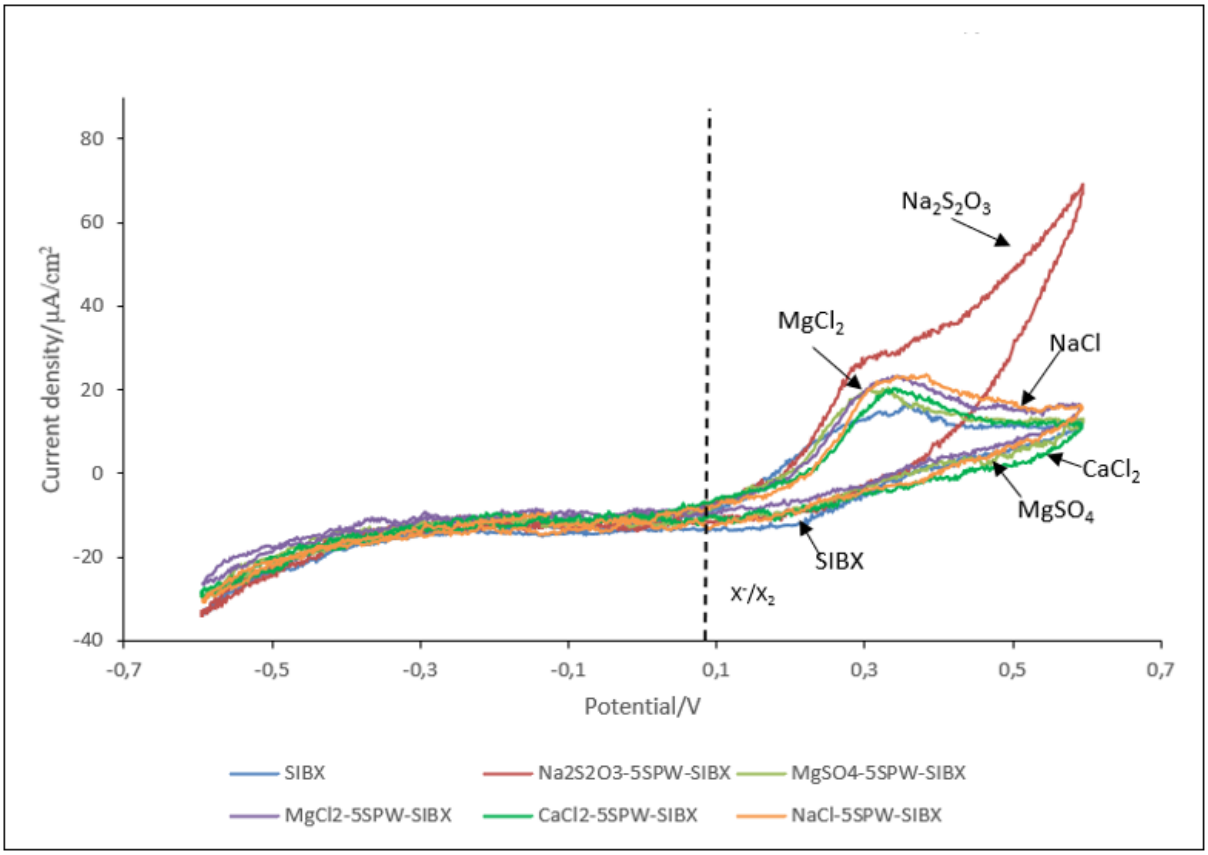

Figure 6.20: Cyclic voltammograms for PdS in the absence and presence of $Na_2S_2O_3$, NaCl, $MgSO_4$, $MgCl_2$ and $CaCl_2$ at 5 SPW with SIBX at a scan rate of 15 mV/s within a potential range of ± 0.6 V and at a pH of 9.2. The dotted line represents the equilibrium potential of dixanthogen formation of SIBX at 6.24×10^{-4} M (0.08 V).

Figure 6.20 conveys cyclic voltammograms for PdS in the absence and presence of $Na_2S_2O_3$, $MgSO_4$, $MgCl_2$, $CaCl_2$ and NaCl at 5 SPW with SIBX. It is evident that the presence of SIBX enhances the anodic behaviour of PdS, as demonstrated by the prominent anodic peaks generated.

Conditions for the baseline case and the presence of $MgSO_4$, $MgCl_2$, $CaCl_2$ and NaCl each created one prominent anodic peak, which appeared ≈ 0.15 V. It is apparent that at 5 SPW the anodic activity of PdS both in the absence and presence of $MgSO_4$, $MgCl_2$, $CaCl_2$ and NaCl does not differ significantly, hence indicating that the presence of these salts has no significant effect on the electrochemical reactivity of the surface species formed within the potential region of this study. Two oxidation current peaks can be noted in the presence of $Na_2S_2O_3$ within the potential regions of 0.25 V to 0.35 V and 0.35 V to 0.6 V.

On the cathodic scan, no cathodic peaks were observed. The absence of the reduction peaks appears to be related to the formation of electrochemically inactive oxidation species formed within the potential range investigated in this study or the formation of a loosely bound layer (Vermaak et al., 2007) of oxidation products on the mineral surface or probably the formation of soluble oxidation products.

6.3.9 Effect of 10 SPW of salts

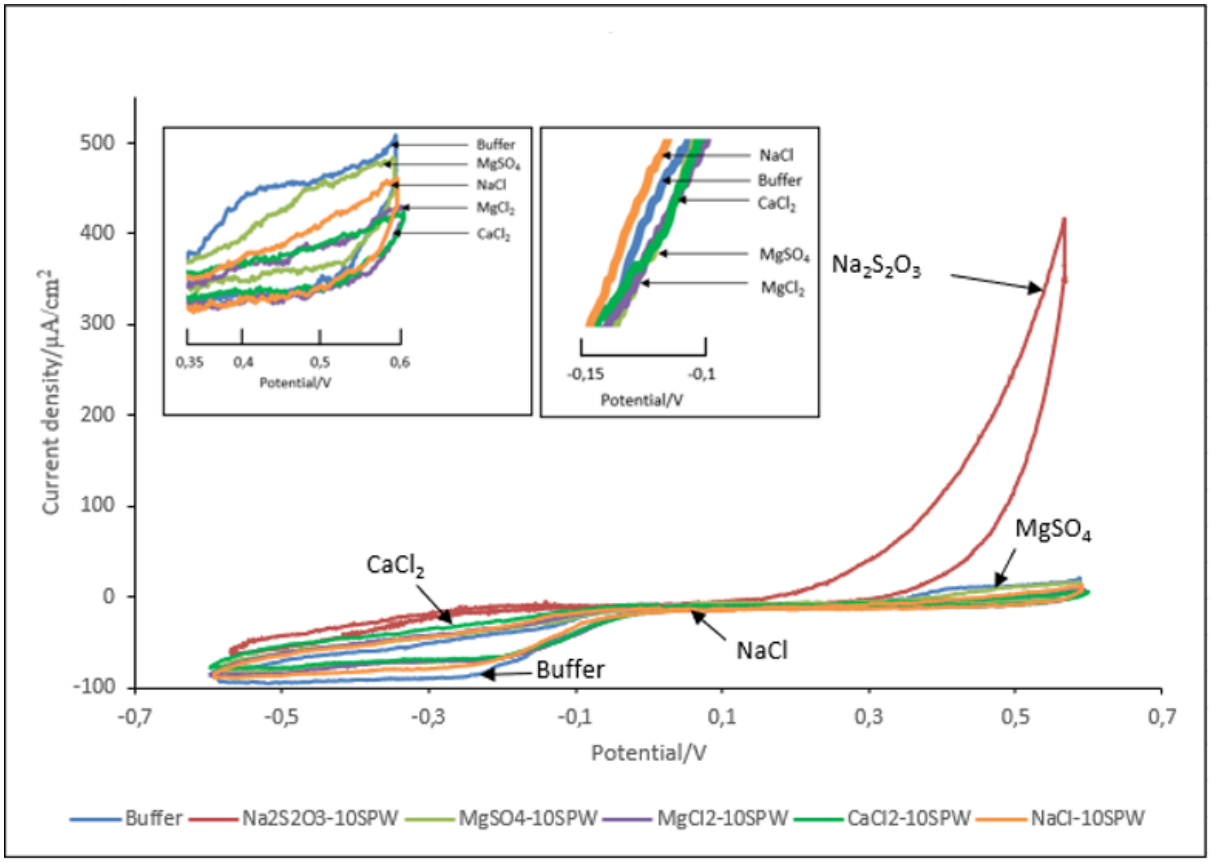

Figure 6.21: Cyclic voltammograms for PdS in the absence and presence of $Na_2S_2O_3$, NaCl, $MgSO_4$, $MgCl_2$ and $CaCl_2$ at 10 SPW at a scan rate of 15 mV/s within a potential range of ± 0.6 V and at a pH of 9.2.

Figure 6.21 illustrates cyclic voltammograms for PdS in the absence and presence of $Na_2S_2O_3$, $MgSO_4$, $MgCl_2$, $CaCl_2$ and NaCl at 10 SPW. On the positive forward sweep, the voltammogram in the presence of $Na_2S_2O_3$ was characterized by steeply rising currents, where the anodic wave commenced at ≈ 0.2 V. However, small anodic currents were obtained in the absence of salts and presence of $MgSO_4$, $MgCl_2$, $CaCl_2$ and NaCl, which are attributable to the slow oxidation of PdS. The small anodic currents are observed to start at a potential of ≈ 0.35 V. It is noticeable that the inhibition of the anodic process occurring on the PdS mineral surface increases in the order $CaCl_2$ > $MgCl_2$ > NaCl > $MgSO_4$ at the highest ionic strength.

Reduction of the oxidation products formed on the anodic processes gave rise to one cathodic peak on the subsequent negative-going scan. The cathodic peak that appeared in the absence of salts and in the presence of $MgSO_4$, $MgCl_2$, $CaCl_2$ and NaCl did not significantly differ and appeared in the potential range of 0 V to – 0.6 V. Moreover, the cathodic peak in the presence of $Na_2S_2O_3$ commenced at more negative potentials, thereby indicating that the presence of $Na_2S_2O_3$ could be considered to contribute to the inhibition of the reduction of oxygen.

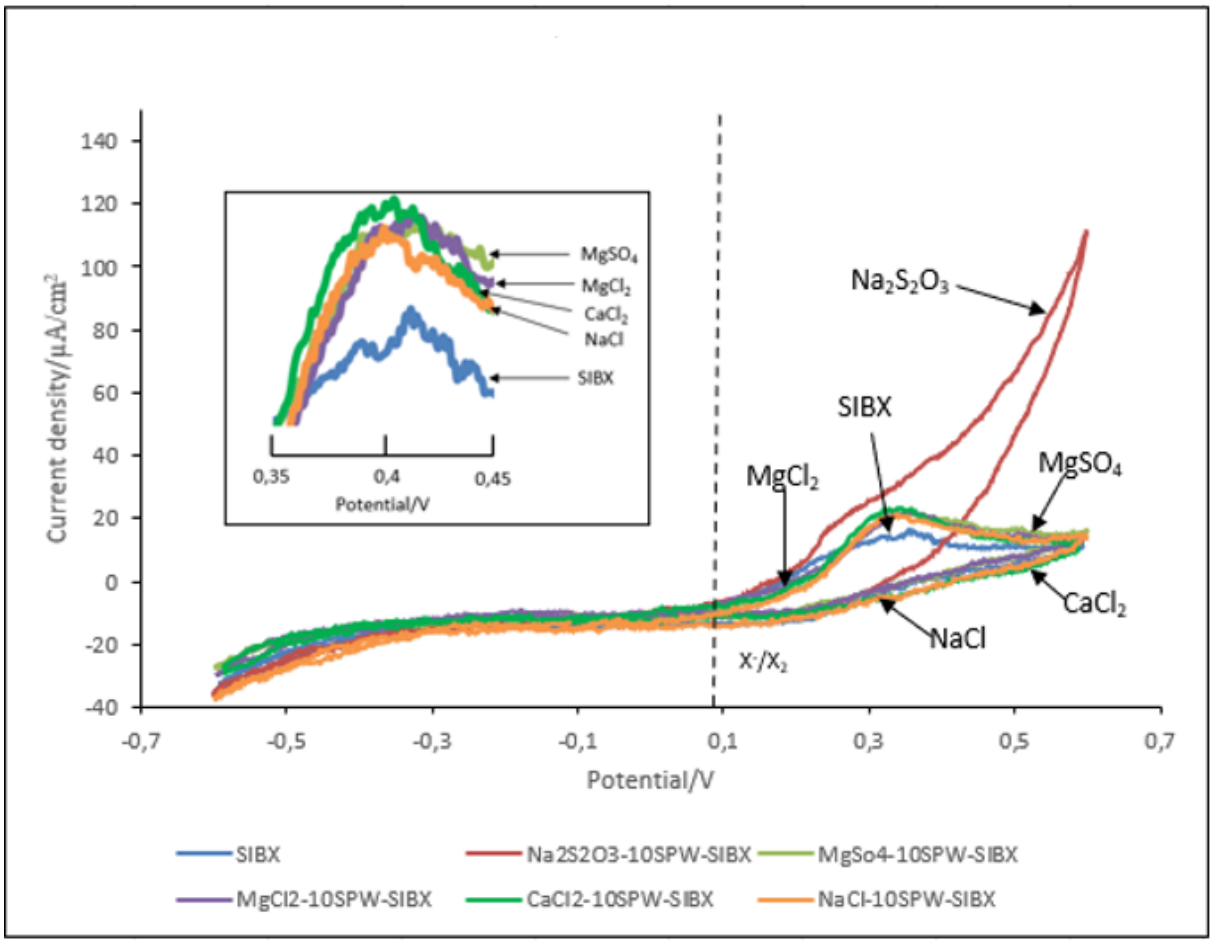

Figure 6.22: Cyclic voltammograms for PdS in the absence and presence of $Na_2S_2O_3$, NaCl, $MgSO_4$, $MgCl_2$ and $CaCl_2$ at 10 SPW with SIBX at a scan rate of 15 mV/s within a potential range of ± 0.6 V and at a pH of 9.2. The dotted line represents the equilibrium potential of dixanthogen formation of SIBX at 6.24×10^{-4} M (0.08 V).

Figure 6.22 shows voltammograms resulting from the reactions of $Na_2S_2O_3$, $MgSO_4$, $MgCl_2$, $CaCl_2$ and NaCl at 10 SPW in the presence of SIBX on PdS. The enhanced anodic activity of PdS in the presence of SIBX can be clearly observed in the figure. The anodic currents for all conditions investigated developed at a potential above the equilibrium potential of dixanthogen, thereby suggesting a possible formation of dixanthogen on PdS. However, though other conditions show the occurrence of one anodic process, the presence of $Na_2S_2O_3$ generated two anodic peaks. A steep increase in current is observed on the second peak, at more positive potentials. In addition, it is noted that the presence of $MgSO_4$, $MgCl_2$, $CaCl_2$ and NaCl slightly enhanced the anodic process that occurred on the mineral surface from the baseline case, though the effect of the salts did not significantly differ.

On the contrary, cathodic peaks related to the reduction of the oxidized species were not observed. This observation could be attributable to the formation of soluble oxidation products or the

formation of electrochemically inactive species or the formation of a loosely bound oxidation layer on the mineral surface (Vermaak et al., 2007).

6.4 Voltammograms for $PdTe_2$

6.4.1 Effect of $Na_2S_2O_3$

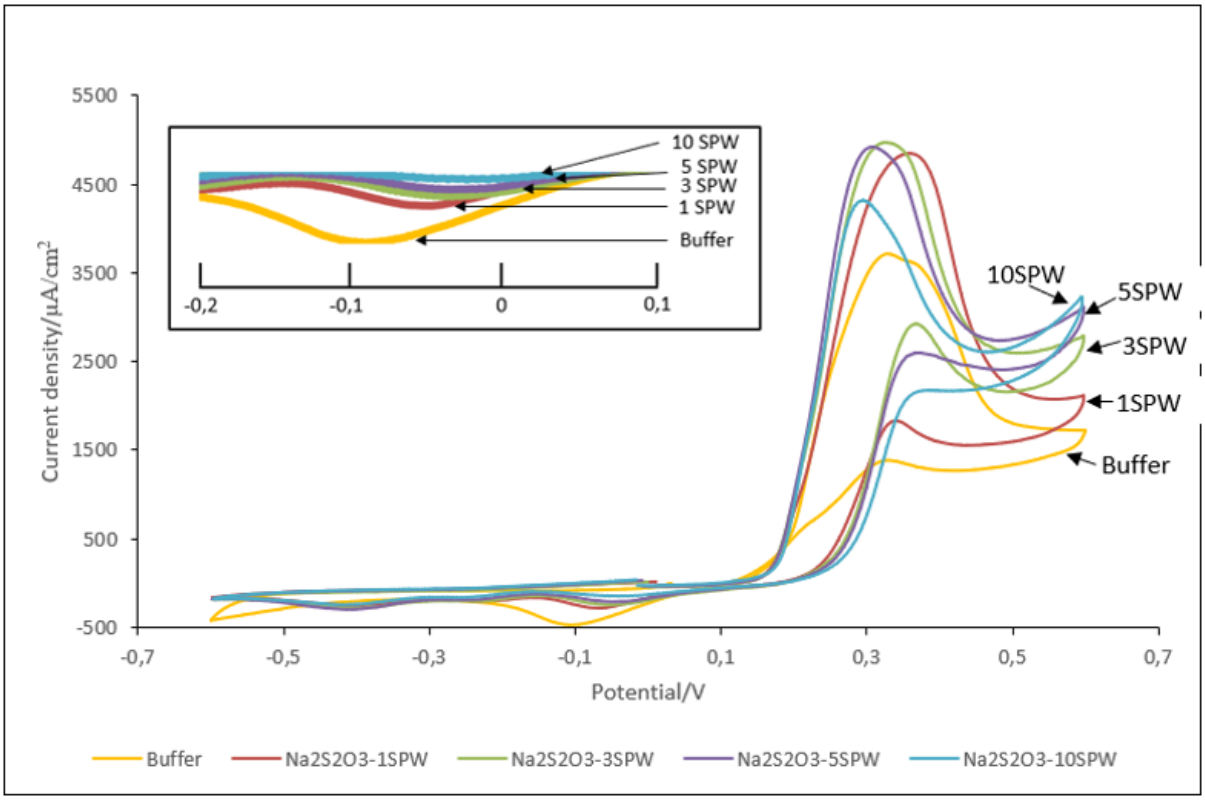

Figure 6.23: Cyclic voltammograms for $PdTe_2$ in the absence and presence of $Na_2S_2O_3$ at increasing ionic strength at a scan rate of 15 mV/s within a potential range of ± 0.6 V and at a pH of 9.2.

Figure 6.23 depicts the voltammogram response of $PdTe_2$ in the absence and presence of $Na_2S_2O_3$ with an increase in ionic strength. A steep increase in anodic currents is observed at ≈ 0.2 V for all conditions investigated. However, slightly lower anodic currents were generated for the baseline case, though two anodic peaks were observable. It is apparent that lower ionic strengths of $Na_2S_2O_3$ yielded slightly higher anodic currents that the anodic currents generated at the highest ionic strength. The figure demonstrates a second anodic process that progresses at a potential above 0.45 V, with an increase in ionic strength.

On the return scan, the baseline case produced a broad cathodic peak observed within a potential range of 0 V to – 0.2 V. The cathodic peak could be ascribed to the reduction of more than one component of oxidation products. Corresponding to the steep anodic peaks generated, it is evident

that three reduction processes transpired in the presence of $Na_2S_2O_3$, as depicted by the three cathodic peaks that appeared within a potential range of 0 V to 0.6 V. Additionally, it is visible that an increase in ionic strength of $Na_2S_2O_3$ diminishes the first cathodic peak that appeared within a potential range of 0 V to – 0.15 V. Hence, denoting an increase in the hindrance of the reduction of oxygen on $PdTe_2$, with an increase in ionic strength.

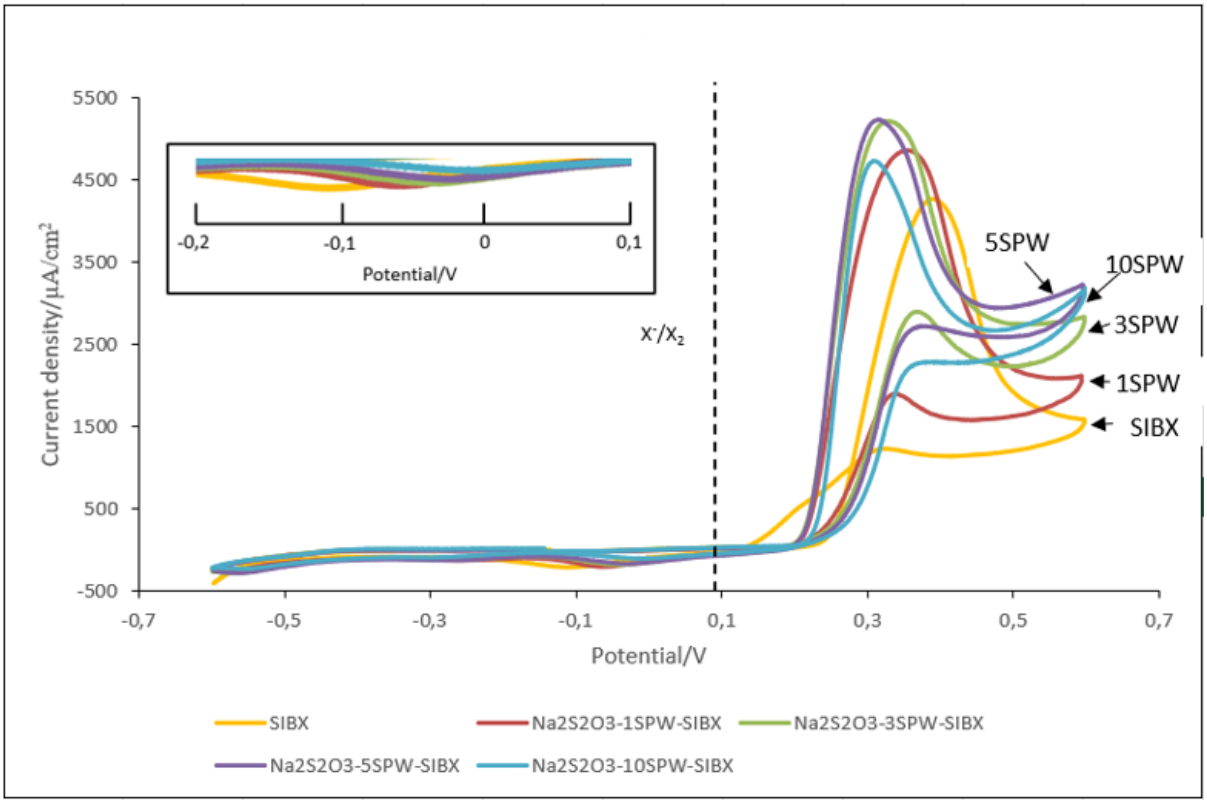

Figure 6.24: Cyclic voltammograms for $PdTe_2$ in the absence and presence of $Na_2S_2O_3$ at increasing ionic strength with SIBX at a scan rate of 15 mV/s within a potential range of ± 0.6 V and at a pH of 9.2. The dotted line represents the equilibrium potential of dixanthogen formation of SIBX at 6.24×10^{-4} M (0.08 V).

Figure 6.24 displays current-potential curves for $PdTe_2$ in the absence and presence of $Na_2S_2O_3$ with an increase in ionic strength with SIBX. Compared to Figure 6.23, the presence of SIBX enhanced the anodic activity on $PdTe_2$ to a small degree, as denoted by the slight increase in anodic currents. However, in the absence of $Na_2S_2O_3$, a shift on the anodic peak to more positive potentials was observed. The anodic current commenced at a potential of about 0.3 V. On the other hand, the presence of $Na_2S_2O_3$ clearly shows anodic currents commencing at a lower potential of ≈ 0.25 V. This suggests the enhanced oxidation effect that $Na_2S_2O_3$ imposes on $PdTe_2$. Similar to Figure 6.23, a slight decrease in anodic currents with an increase in ionic strength of $Na_2S_2O_3$ is demonstrated. Additionally, a second anodic peak is observed to develop with an increase in ionic strength. Overall, conditions investigated display prominent anodic peaks

developed at a potential significantly above the reversible potential of the xanthate-di-isobutyl-dixanthogen couple.

On the cathodic scan, one reduction peak was yielded for all conditions investigated. Interestingly, the cathodic peak in the absence of $Na_2S_2O_3$ appears at more negative potentials than in the presence of $Na_2S_2O_3$.

6.4.2 Effect of $MgSO_4$

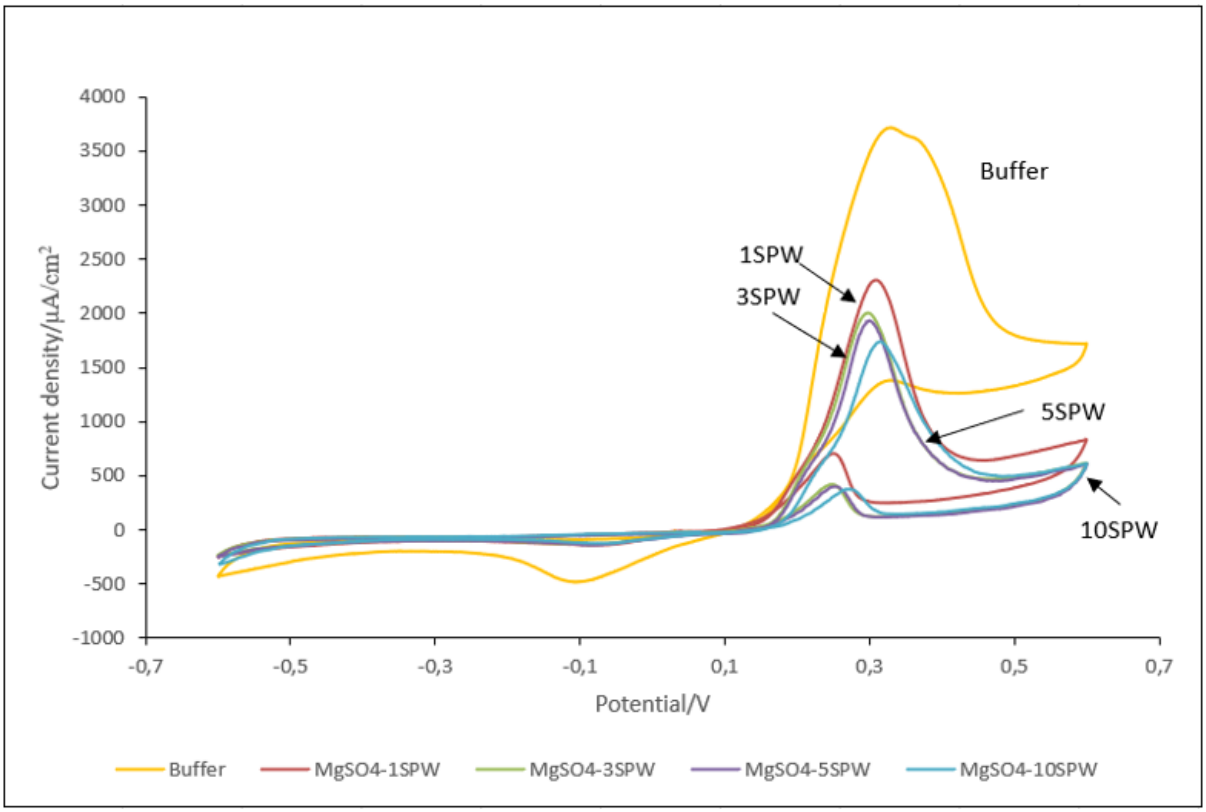

Figure 6.25: Cyclic voltammograms for $PdTe_2$ in the absence and presence of $MgSO_4$ at increasing ionic strength at a scan rate of 15 mV/s within a potential range of ± 0.6 V and at a pH of 9.2.

Figure 6.25 plots the voltammetric response of $PdTe_2$ in the absence and presence of $MgSO_4$. A steep increase in anodic current is exhibited in the absence of $MgSO_4$. The prominent anodic peak is observed to appear at a potential of > 0.2 V. The increase in the anodic current generated two anodic peaks between a potential range of 0.3 V to 0.4 V. Significantly lower anodic currents were obtained in the presence of $MgSO_4$. This suggests that the presence of $MgSO_4$ on $PdTe_2$ inhibits oxidation on the mineral surface (Gardner and Woods, 1979). Furthermore, a slight shift to more positive potentials was evident with an increase in ionic strength, owing to a possible passivation on the mineral surface, thereby creating some extent of resistance to oxidation on the mineral surface.

On the cathodic scan, one broad reduction peak is noted in the absence of $MgSO_4$. This suggests the reduction of more than one oxidation product. Contrary to the significant anodic currents obtained in the presence of $MgSO_4$, diminished cathodic peaks that shifted to less negative current densities were displayed.

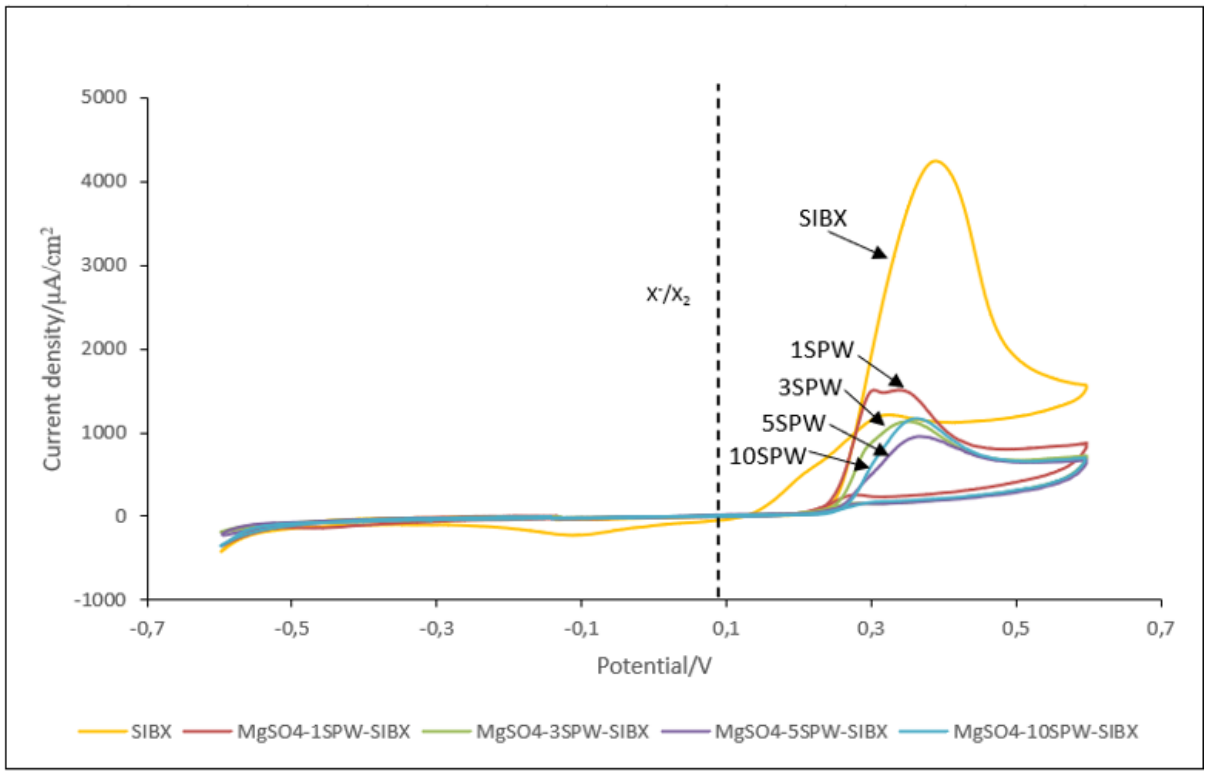

Figure 6.26: Cyclic voltammograms for $PdTe_2$ in the absence and presence of $MgSO_4$ at increasing ionic strength with SIBX at a scan rate of 15 mV/s within a potential range of ± 0.6 V and at a pH of 9.2. The dotted line represents the equilibrium potential of dixanthogen formation of SIBX at 6.24×10^{-4} M (0.08 V).

Figure 6.26 reveals cyclic voltammograms for $PdTe_2$ in the absence and presence of $MgSO_4$ with SIBX. On the positive sweep, the baseline case generated a steep increase in current with one anodic peak, due to the oxidation of SIBX on the mineral surface. However, a very significant decrease in current density is noted in the presence of $MgSO_4$. This demonstrates that the presence of $MgSO_4$ inhibits the oxidation of SIBX on $PdTe_2$. Moreover, a slight decrease in the anodic currents is evident with an increase in ionic strength, indicating that oxidation of SIBX on the mineral surface is inhibited with an increase in the ionic strength of $MgSO_4$. Unlike other conditions, it can be discerned that the lowest ionic strength, 1 SPW, gave rise to two anodic peaks which could be associated with two anodic processes occurring. Interestingly, the presence of SIBX inhibited the electrochemical reactions taking place in $MgSO_4$, thereby indicating a strong interaction between $PdTe_2$ with SIBX. This is observable in Figure 6.26, where the rate of anodic activity decreased compared to what was observed in Figure 6.25. Generally, anodic peaks for the

conditions investigated were generated above the reversible potential for the xanthate-dixanthogen couple, at a potential > 0.25 V.

On the negative sweep, a broad cathodic peak is observed between a potential range of 0.1 V to – 0.3 V for the baseline case. This observation could be attributed to the reduction of more than one component on the mineral surface. In the presence of $MgSO_4$, no cathodic peaks are noted. The absence of the reduction peaks could be associated with the formation of soluble oxidation products or the formation of electrochemically inactive products within the potential range investigated or the formation of a loosely bound layer (Vermaak et al., 2007) of oxidation products on the mineral surface.

6.4.3 Effect of $MgCl_2$

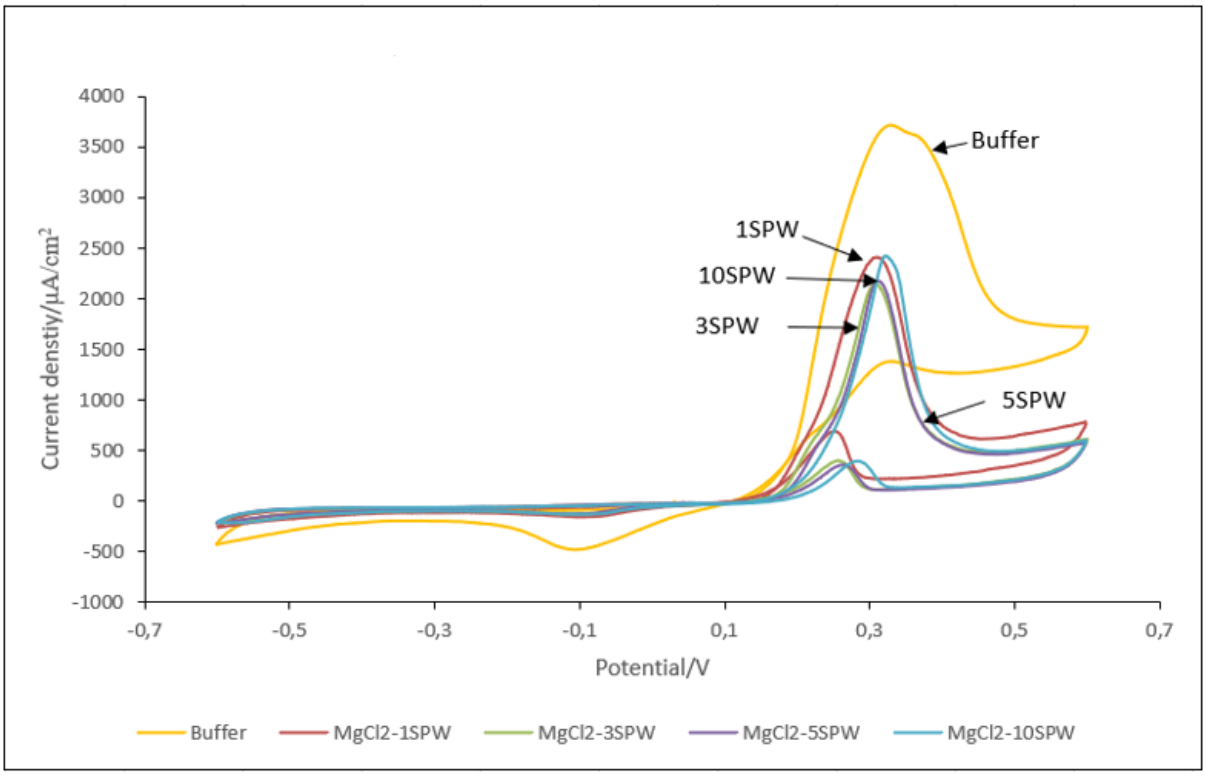

Figure 6.27: Cyclic voltammograms for $PdTe_2$ in the absence and presence of $MgCl_2$ at increasing ionic strength at a scan rate of 15 mV/s within a potential range of ± 0.6 V and at a pH of 9.2.

Figure 6.27 illustrates voltammograms for $PdTe_2$ in the absence and presence of $MgCl_2$ with an increase in ionic strength. On the positive sweep, the baseline case demonstrates an enhanced anodic activity on the mineral surface compared to the presence of $MgCl_2$. The anodic scan yielded two anodic peaks between the potential range of 0.3 V to 0.4 V. Furthermore, the presence of $MgCl_2$ generated reduced anodic activity on the mineral surface. This could suggest that the

presence of $MgCl_2$ could possibly be inhibiting the oxidation of oxygen on the mineral surface. Nevertheless, the lowest and highest ionic strengths, 1 SPW and 10 SPW, show slightly higher anodic currents compared with 3 SPW and 5 SPW. Additionally, it is noticeable that the potential at which the anodic peaks commenced, increased with an increase in ionic strength from the baseline case scenario.

Corresponding to the anodic peaks generated in the absence of $MgCl_2$, one broad cathodic peak is observed, which could be attributable to the reduction of more than one oxidation component. Contrary to the prominent anodic peaks yielded in the presence of $MgCl_2$, a small cathodic peak was observed within the potential range of 0 V to – 0.15 V. No significant difference in the current density was observed with regards to the ionic strength of $MgCl_2$.

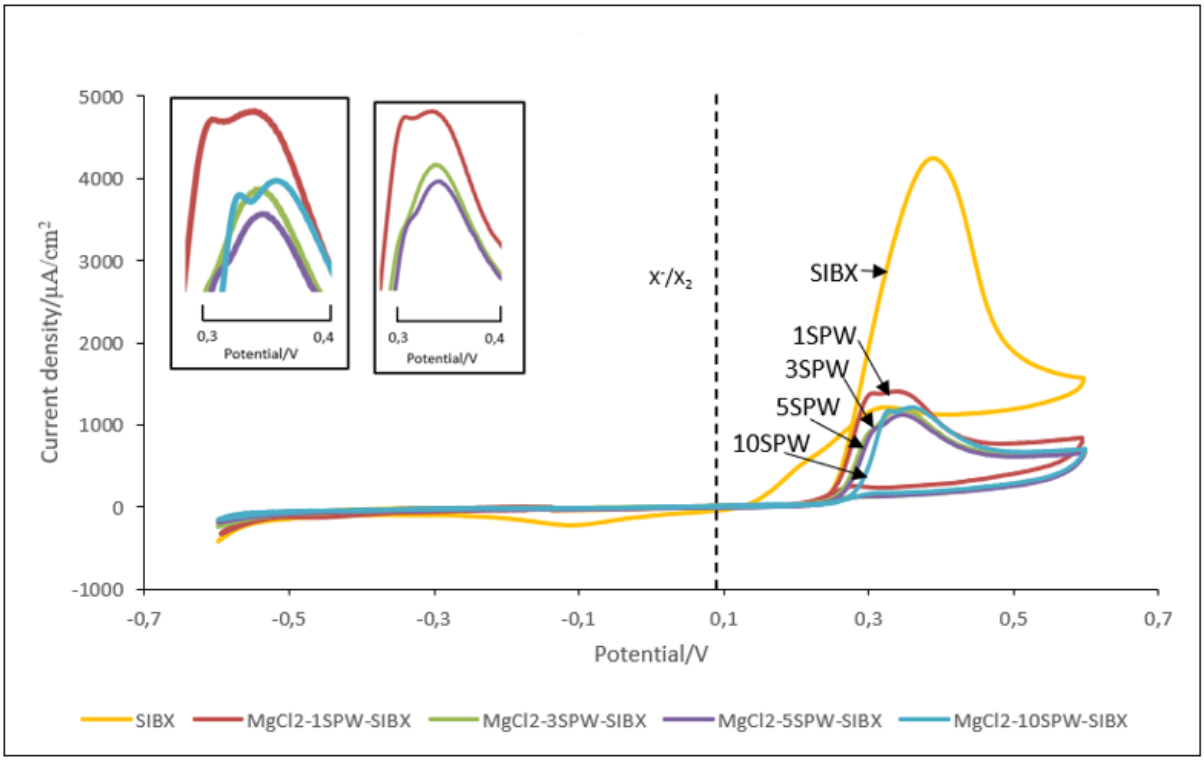

Figure 6.28: Cyclic voltammograms for $PdTe_2$ in the absence and presence of $MgCl_2$ at increasing ionic strength with SIBX at a scan rate of 15 mV/s within a potential range of ± 0.6 V and at a pH of 9.2. The dotted line represents the equilibrium potential of dixanthogen formation of SIBX at 6.24×10^{-4} M (0.08 V).

Figure 6.28 demonstrates the voltammetric response of $PdTe_2$ in the absence and presence of $MgCl_2$ with SIBX. Compared to Figure 6.27, the baseline case shows an enhanced anodic effect on the mineral surface, probably due to the oxidation of SIBX on $PdTe_2$. On the other hand, the presence of $MgCl_2$ shows reduced anodic activity on the mineral surface, as indicated by the reduced anodic currents. This suggests that the presence of $MgCl_2$ inhibits the oxidation of SIBX on the $PdTe_2$ mineral surface. Compared to Figure 6.27, the anodic peaks developed in this figure

were less pronounced. SIBX could be possibly inhibiting the electrochemical reactions occurring in the presence of $MgCl_2$, due to a strong interaction occurring between $PdTe_2$ and SIBX. In addition, it is evident that $MgCl_2$ at 1 SPW and 10 SPW displayed two anodic peaks with insignificantly different anodic currents, whereas 3 SPW and 5 SPW yielded two anodic peaks with the second peak slightly higher than the first anodic peak. Overall, all anodic peaks for all conditions investigated appear at potentials significantly above the equilibrium potential of dixanthogen, owing to the formation of dixanthogen on the mineral surface under the investigated conditions.

On the cathodic scan, one broad cathodic peak is developed with the baseline case, whereas no cathodic peaks are observed in the presence of $MgCl_2$.

6.4.4 Effect of $CaCl_2$

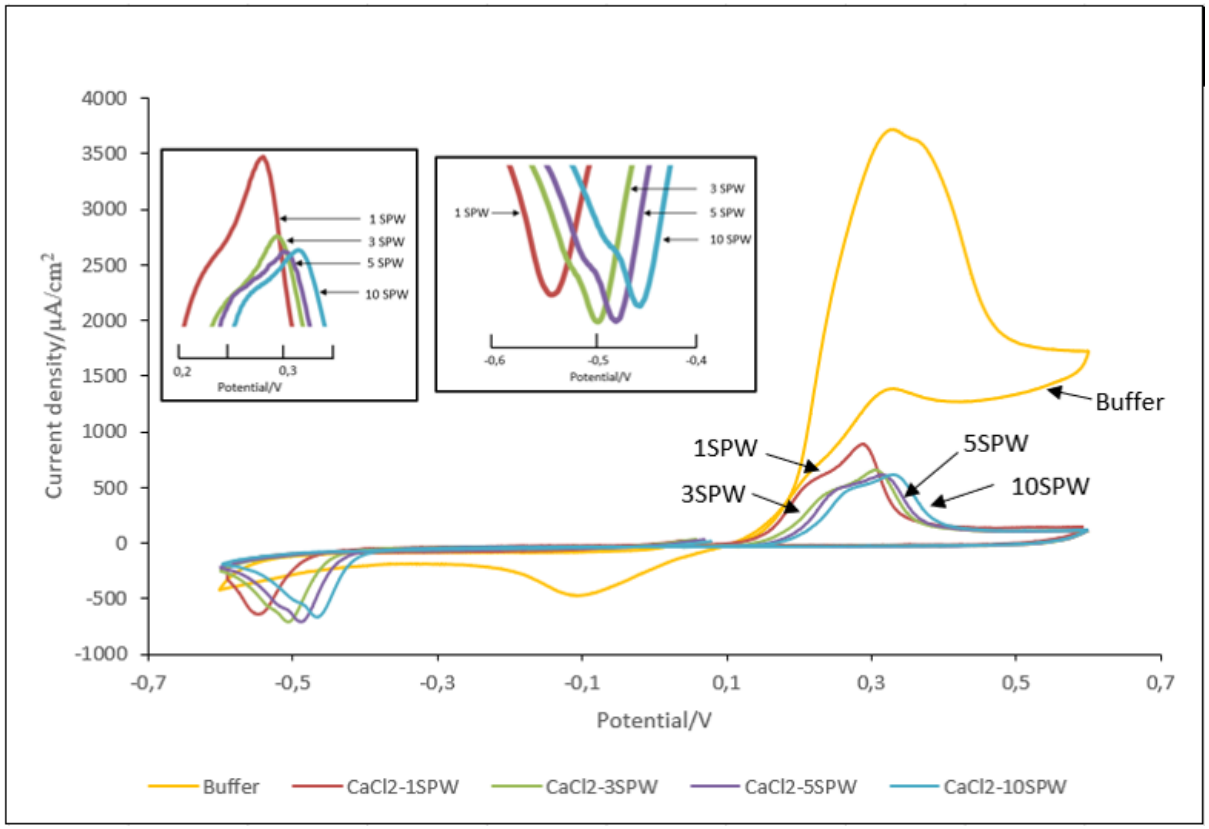

Figure 6.29: Cyclic voltammograms for $PdTe_2$ in the absence and presence of $CaCl_2$ at increasing ionic strength at a scan rate of 15 mV/s within a potential range of ± 0.6 V and at a pH of 9.2.

Figure 6.29 exhibits voltammograms of $PdTe_2$ in the absence and presence of $CaCl_2$ with an increase in ionic strength. The absence of $CaCl_2$ reveals a steep increase in anodic currents at potentials above 0.2 V. On the contrary, the presence of $CaCl_2$ displays significantly reduced anodic

activity on the mineral surface. The significantly reduced anodic activity could be attributable to a significantly high hindrance to surface oxidation in the presence of $CaCl_2$. Moreover, an increase in the potential at which the anodic currents developed was found to increase with an increase in ionic strength. Additionally, it is evident that the presence of $CaCl_2$ resulted in two anodic peaks within a potential range of 0.15 V to 0.4 V.

On the cathodic scan, it is observable that conditions in the absence of $CaCl_2$ and in the presence of $CaCl_2$ at 1 SPW yielded one reduction peak. At higher ionic strengths of $CaCl_2$, two cathodic peaks were generated. Furthermore, it is apparent that reduction currents commenced to more negative potentials with a decrease in ionic strength. Thereby implying that the reduction of oxygen was inhibited with a decrease in the ionic strength of $CaCl_2$.

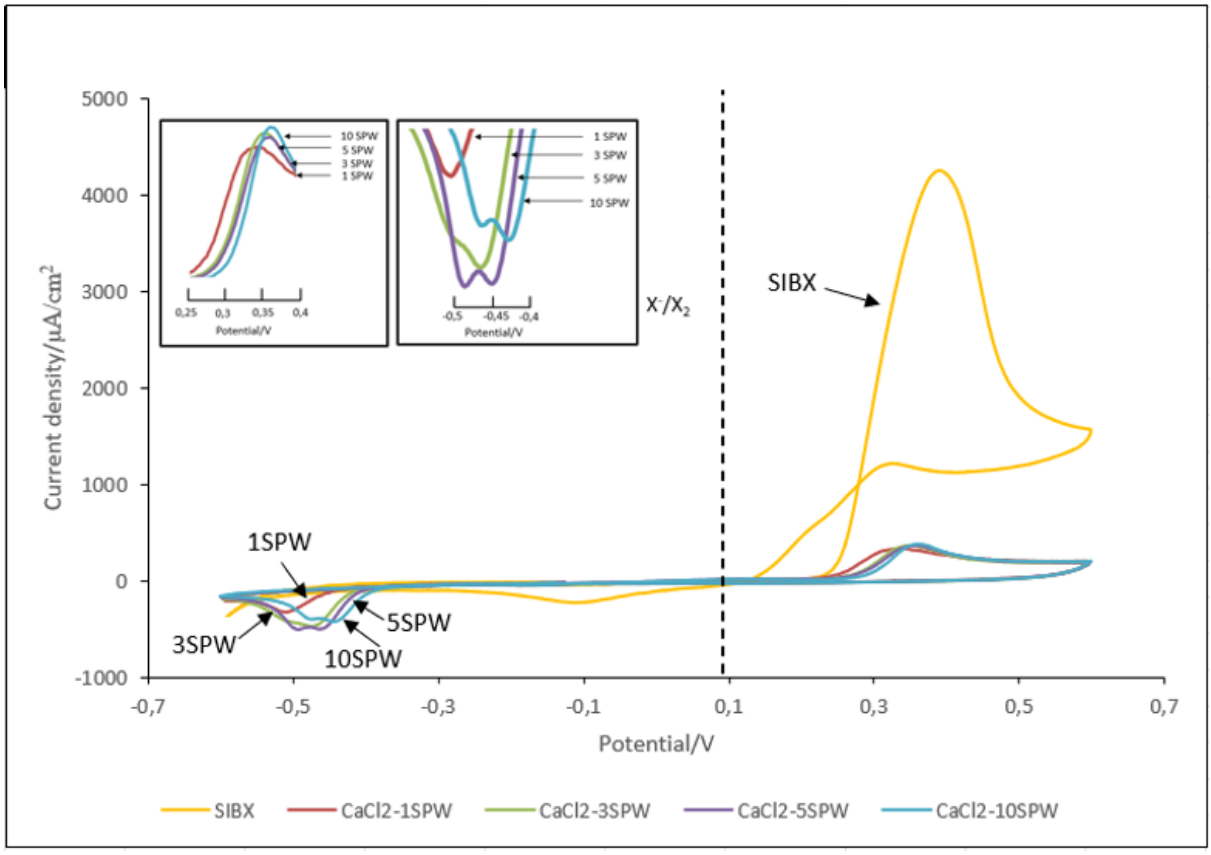

Figure 6.30: Cyclic voltammograms for $PdTe_2$ in the absence and presence of $CaCl_2$ at increasing ionic strength with SIBX at a scan rate of 15 mV/s within a potential range of ± 0.6 V and at a pH of 9.2. The dotted line represents the equilibrium potential of dixanthogen formation of SIBX at 6.24×10^{-4} M (0.08 V).

Figure 6.30 shows cyclic voltammograms for $PdTe_2$ in the absence and presence of $CaCl_2$ with increasing ionic strength in SIBX. On the anodic scan, a prominent anodic peak is observed in the absence of $CaCl_2$. The increased anodic activity on the mineral surface could be assigned to the oxidation of SIBX on the mineral surface. On the contrary, the presence of $CaCl_2$ shows

suppressed anodic activity on $PdTe_2$. The presence of $CaCl_2$ probably hinders the oxidation of SIBX on the mineral surface. Furthermore, a slight shift to positive potentials is noted with an increase in ionic strength.

On the negative sweep, it is evident that one cathodic reaction occurred in the absence of $CaCl_2$ and in the presence of $CaCl_2$ at the lowest ionic strength, whereas a second cathodic peak developed with an increase in ionic strength. Additionally, a shift to more negative potentials is observed with a decrease in ionic strength.

6.4.5 Effect of NaCl

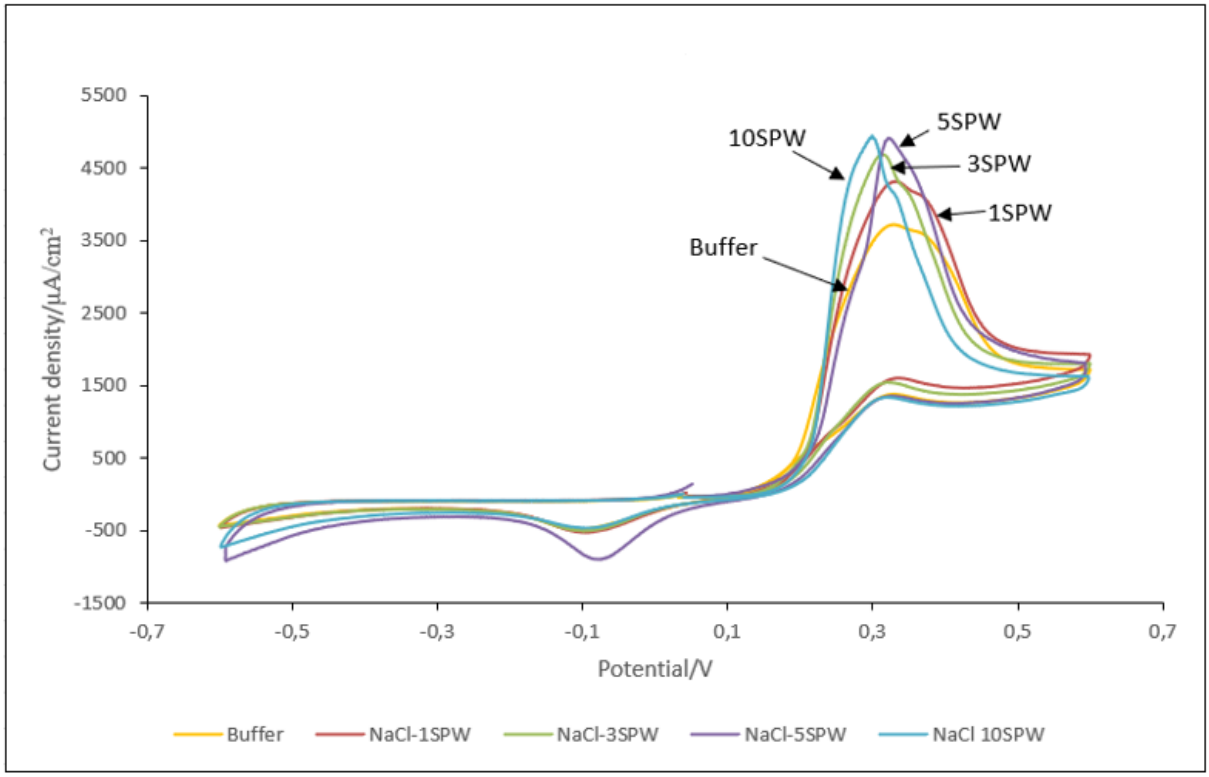

Figure 6.31: Cyclic voltammograms for $PdTe_2$ in the absence and presence of NaCl at increasing ionic strength at a scan rate of 15 mV/s within a potential range of ± 0.6 V and at a pH of 9.2.

Figure 6.31 plots the voltammetric response of $PdTe_2$ in the absence and presence of NaCl at increasing ionic strength. It is apparent that under all conditions investigated, an enhanced anodic activity is displayed on the $PdTe_2$ mineral surface above the potential of 0.2 V. The baseline case shows slightly reduced anodic currents though the anodic currents generated both in the absence and presence of NaCl do not significantly differ. It is further demonstrated that two anodic processes are most likely to occur on the mineral surface both in the absence of NaCl and at 1

SPW. Additionally, one distinct anodic peak is displayed at higher ionic strengths of 3 SPW, 5 SPW and 10 SPW.

In correspondence to the anodic currents yielded, the cathodic scan generated two cathodic peaks, one broad reduction peak was observed between 0.05 V to – 0.2 V. The second cathodic peak appeared < – 0.4 V, the peak therefore diminishes at lower ionic strengths.

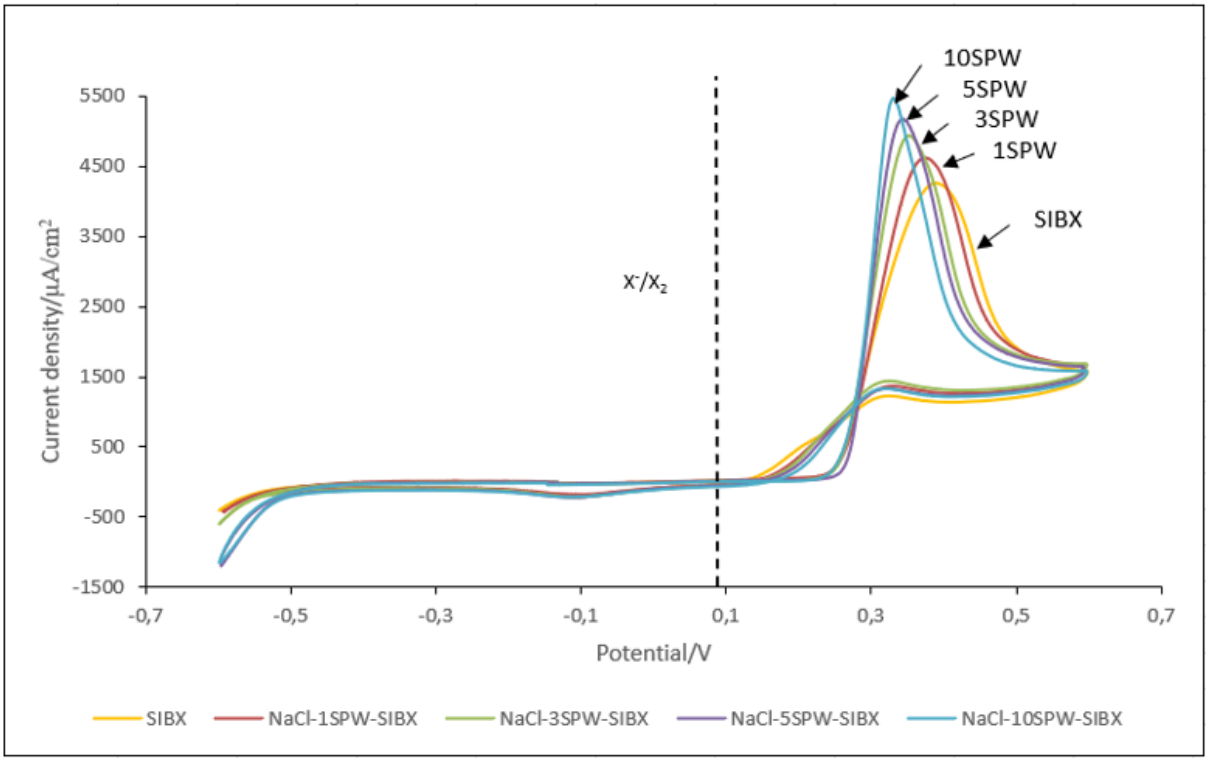

Figure 6.32: Cyclic voltammograms for $PdTe_2$ in the absence and presence of NaCl at increasing ionic strength with SIBX at a scan rate of 15 mV/s within a potential range of ± 0.6 V and at a pH of 9.2. The dotted line represents the equilibrium potential of dixanthogen formation of SIBX at 6.24×10^{-4} M (0.08 V).

Figure 6.32 displays voltammograms for $PdTe_2$ in the absence and presence of NaCl at increasing ionic strength with SIBX. For all conditions investigated, strong anodic currents developed at a potential that is significantly above the equilibrium potential of dixanthogen formation. Hence, the anodic activity on the mineral surface occurred in regions which favour the formation of dixanthogen. Slightly lower anodic currents are generated in the absence of NaCl and a slight increase in anodic activity is noted with an increase in ionic strength. Overall, compared to Figure 6.31, one distinct anodic peak is attained for all conditions investigated, with an enhanced anodic activity in the presence of SIBX. This suggests that the oxidation of SIBX most likely occurred on the mineral surface.

Alternatively, on the cathodic scan, two diminished reduction peaks appear between 0 V to – 0.25 V and < 0.5 V. The absence and presence of NaCl appears to have no significant effect on the electrochemical reactivity of the surface species formed in the potential region 0 V to – 0.25 V. Regarding the second reduction peak, the reduction currents shifted to less negative current densities with a decrease in ionic strength.

6.4.6 Effect of 1 SPW of salts

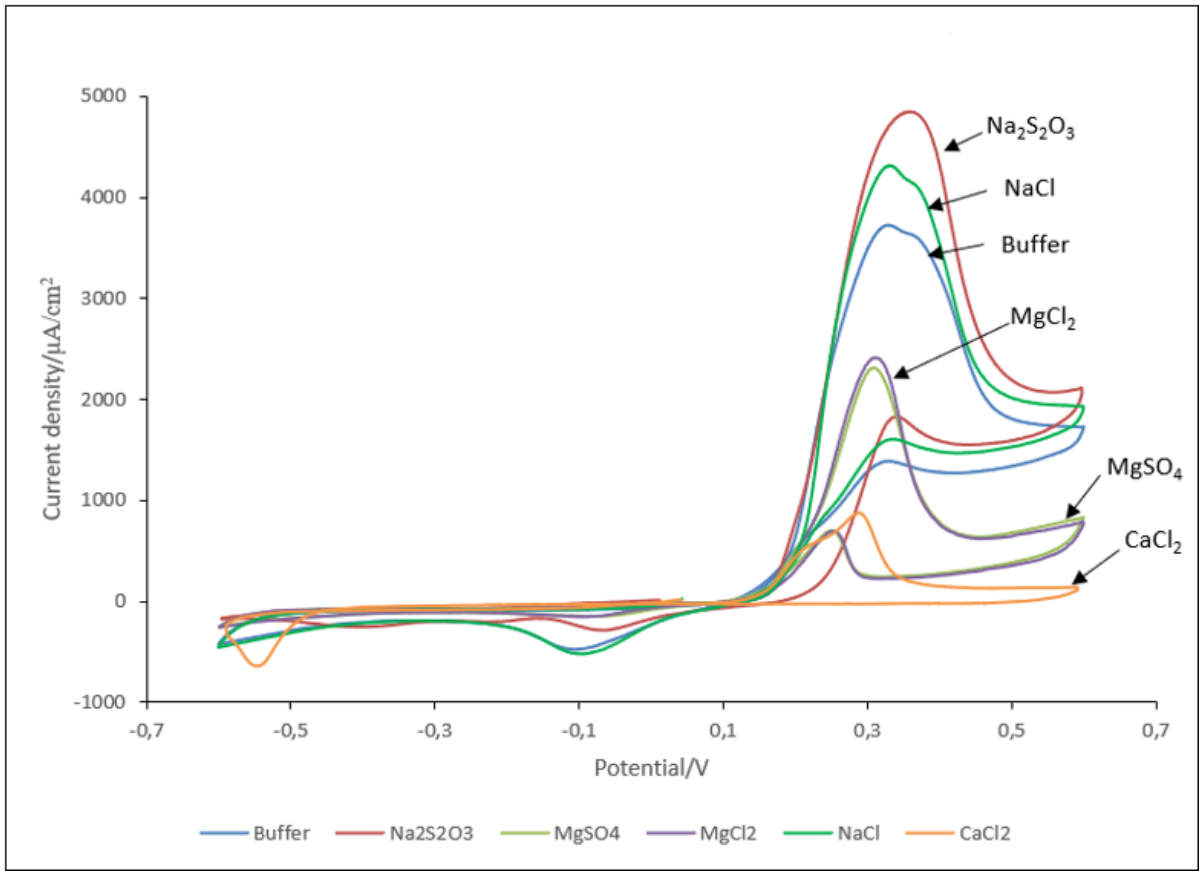

Figure 6.33: Cyclic voltammograms for $PdTe_2$ in the absence and presence of $Na_2S_2O_3$, NaCl, $MgSO_4$, $MgCl_2$ and $CaCl_2$ at 1 SPW at a scan rate of 15 mV/s within a potential range of ± 0.6 V and at a pH of 9.2.

Figure 6.33 depicts cyclic voltammograms for $PdTe_2$ in the absence and presence of NaCl, $Na_2S_2O_3$, $MgCl_2$, $MgSO_4$ and $CaCl_2$ at 1SPW. A steep increase in anodic currents is shown to occur in the following order $Na_2S_2O_3$ > NaCl > buffer > $MgCl_2$ > $MgSO_4$ > $CaCl_2$. $Na_2S_2O_3$, $MgCl_2$ and $MgSO_4$ salts exhibit one anodic peak above 0.2 V, whereas the presence of NaCl, $CaCl_2$ and the baseline case generated two anodic peaks. Furthermore, it is shown that the anodic currents for NaCl show a similar trend to the baseline case, though the currents yielded in the case of NaCl are slightly enhanced.

On the negative sweep, the presence of $Na_2S_2O_3$ generated three cathodic peaks in the potential regions of between 0.1 V to – 0.15 V, – 0.15 V to – 0.25 V and – 0.35 V to – 0.55 V. Whereas, the presence of $MgCl_2$ and $MgSO_4$ demonstrated two diminished reduction peaks within the potential ranges of 0 V to – 0.2V and < – 0.45 V. Moreover, two cathodic peaks that followed a similar trend were developed in the presence of NaCl and in the absence of salts. One of the cathodic peaks was exhibited over a broad potential region of 0.1 V to – 0.2 V and the second peak is shown to appear at potentials < – 0.45 V. Additionally, the presence of $CaCl_2$ generated one reduction peak within the region – 0.5 V to – 0.6 V.

Overall, it is evident that the currents for NaCl and those generated in the absence of salts; and currents produced in the presence of $MgCl_2$ and $MgSO_4$ followed similar trends both in the anodic and cathodic regions. This implies that the redox reactions occurring in the presence of NaCl and in the absence of salts and those that resulted from the presence of $MgCl_2$ and $MgSO_4$ could most likely be similar within the potential regions investigated.

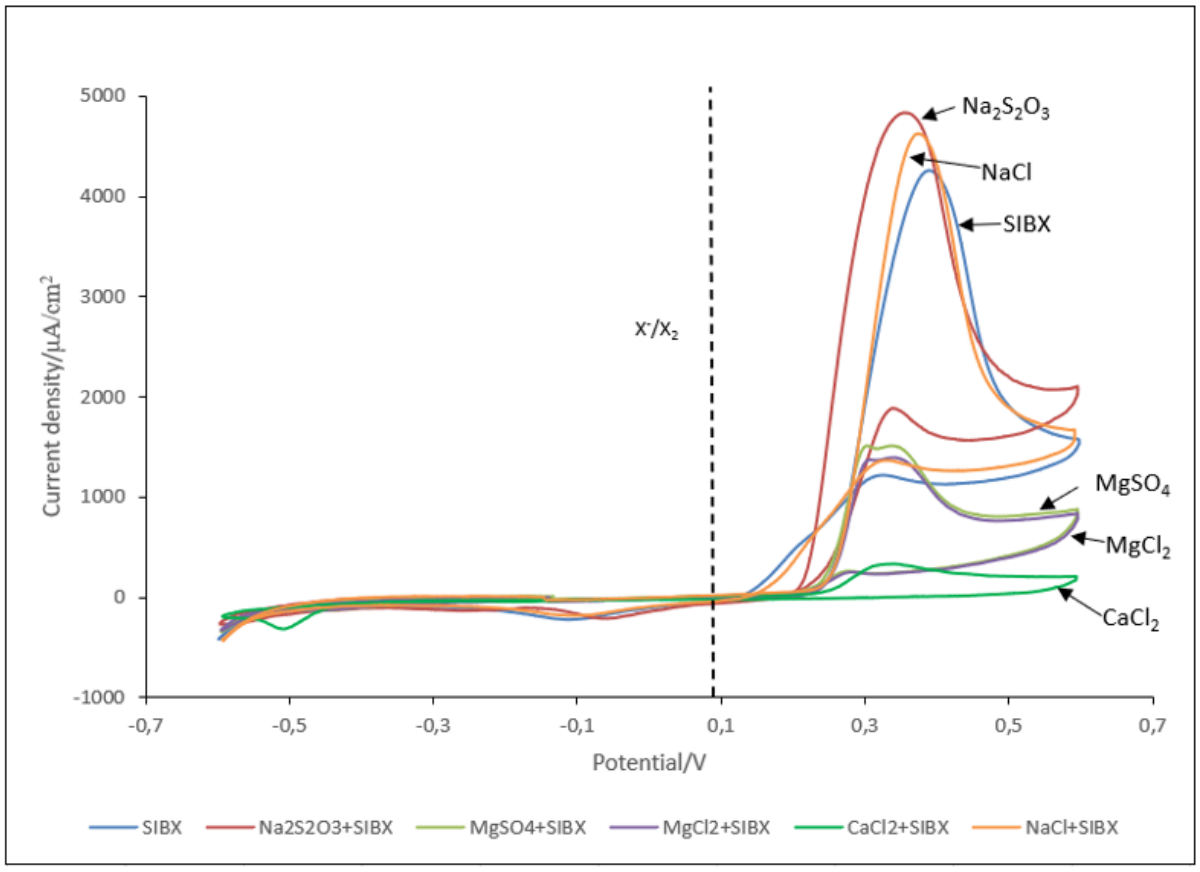

Figure 6.34: Cyclic voltammograms for $PdTe_2$ in the absence and presence of $Na_2S_2O_3$, NaCl, $MgSO_4$, $MgCl_2$ and $CaCl_2$ at 1 SPW with SIBX at a scan rate of 15 mV/s within a potential range of ± 0.6 V and at a pH of 9.2. The dotted line represents the equilibrium potential of dixanthogen formation of SIBX at 6.24×10^{-4} M (0.08 V).

Figure 6.34 presents the voltammetric response of $PdTe_2$ in the absence and presence of NaCl, $Na_2S_2O_3$, $MgCl_2$, $MgSO_4$ and $CaCl_2$ at 1SPW with SIBX. A steep increase in anodic currents is observed in the absence of salts and in the presence of NaCl and $Na_2S_2O_3$. Compared to Figure 6.33, it is clear that in Figure 6.34, the anodic activities in the case of $Na_2S_2O_3$, $MgCl_2$, $MgSO_4$ and $CaCl_2$ were slightly decreased whereas alternatively, the anodic activity both for the baseline case and in the presence of NaCl were slightly enhanced. The enhanced anodic activity on the mineral surface could be attributable to the oxidation of SIBX on $PdTe_2$ whereas the reduced anodic activity in the case of $Na_2S_2O_3$, $MgCl_2$, $MgSO_4$ and $CaCl_2$ could be associated with the fact that the presence of SIBX could possibly be inhibiting the anodic processes occurring on the mineral surface due to the presence of the salts. Interestingly, in comparison with Figure 6.33, the presence of NaCl and the baseline case displayed two anodic peaks in the absence of SIBX to one anodic peak in the presence of SIBX and in the case of $MgCl_2$ and $MgSO_4$, one anodic peak was displayed in the absence of SIBX to two anodic peaks were exhibited in the presence of SIBX. The variation in peaks therefore demonstrates the reactions occurring due to the presence SIBX. Overall, it is shown that the anodic peaks commenced at an appreciable potential from the equilibrium potential of dixanthogen formation, hence implying that the formation of dixanthogen is favoured under the investigated conditions.

On the return scan, the baseline case and the presence of NaCl displayed two cathodic peaks in the potential regions of 0.15 V to – 0.25 V and < – 0.5 V. In the presence of $Na_2S_2O_3$ three diminished reduction peaks were exhibited in the potential regions of 0.2 V to – 0.15 V, – 0.2 V to 0.35 V and < – 0.5 V. Additionally, $MgCl_2$ and $MgSO_4$ generated a similar small cathodic peak in the potential region < 0.5 V. The presence of $CaCl_2$ demonstrated one reduction peak that was portrayed within a potential range of 0.45 V to 0.55 V.

6.4.7 Effect of 3 SPW of salts

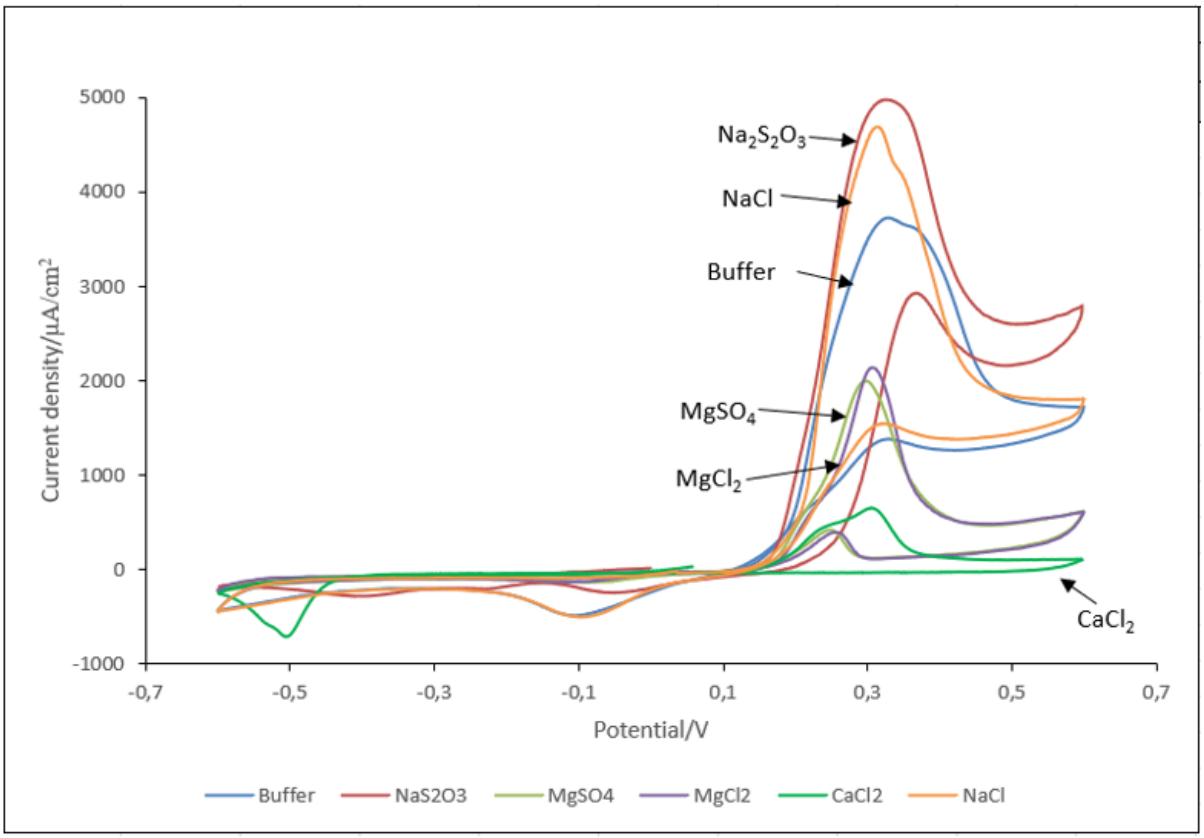

Figure 6.35: Cyclic voltammograms for $PdTe_2$ in the absence and presence of $Na_2S_2O_3$, NaCl, $MgSO_4$, $MgCl_2$ and $CaCl_2$ at 3 SPW at a scan rate of 15 mV/s within a potential range of ± 0.6 V and at a pH of 9.2.

Figure 6.35 illustrates voltammograms obtained for $PdTe_2$ in the absence and presence of NaCl, $Na_2S_2O_3$, $MgCl_2$, $MgSO_4$ and $CaCl_2$ at 3 SPW. On the positive sweep, increased anodic activities were observed in the absence of salts and in the presence of NaCl, $Na_2S_2O_3$, whereas reduced anodic currents were visible in the case of $MgCl_2$, $MgSO_4$ and more so with $CaCl_2$. Furthermore, it is clear that one prominent peak developed in the presence of $Na_2S_2O_3$, $MgCl_2$ and $MgSO_4$ salts, whereas the absence of salts and the presence of NaCl and $CaCl_2$ exhibited two anodic reactions. Overall, the anodic peak in the presence of $CaCl_2$ appeared at a lower potential of 0.15 V compared to other conditions investigated, which had anodic peaks commencing ≈ 0.2 V.

On the cathodic scan, cathodic peaks demonstrating the reduction of the oxidation species formed by each condition, are displayed. In the absence of salts, two reduction peaks are generated due to probably the reduction of oxygen and other oxidation species formed on the mineral surface. A broad cathodic peak developed within the potential range of 0.1 V to – 0.25 V and the second peak commenced from a potential of – 0.4 V. Similar reduction peaks were observed in the presence of NaCl. Corresponding to the prominent anodic peak formed in the presence of

$Na_2S_2O_3$, three reduction peaks were obtained in the potential regions of 0.1 V to – 0.15 V, – 0.15 V to – 0.25 V and – 0.3 V to – 0.55 V. Furthermore, two similar diminished reduction peaks were yielded in the presence of $MgCl_2$ and $MgSO_4$ within the potential regions of 0 V to – 0.2 V and < – 0.45 V. Ultimately, it is evident that two cathodic peaks were generated in the presence of $CaCl_2$.

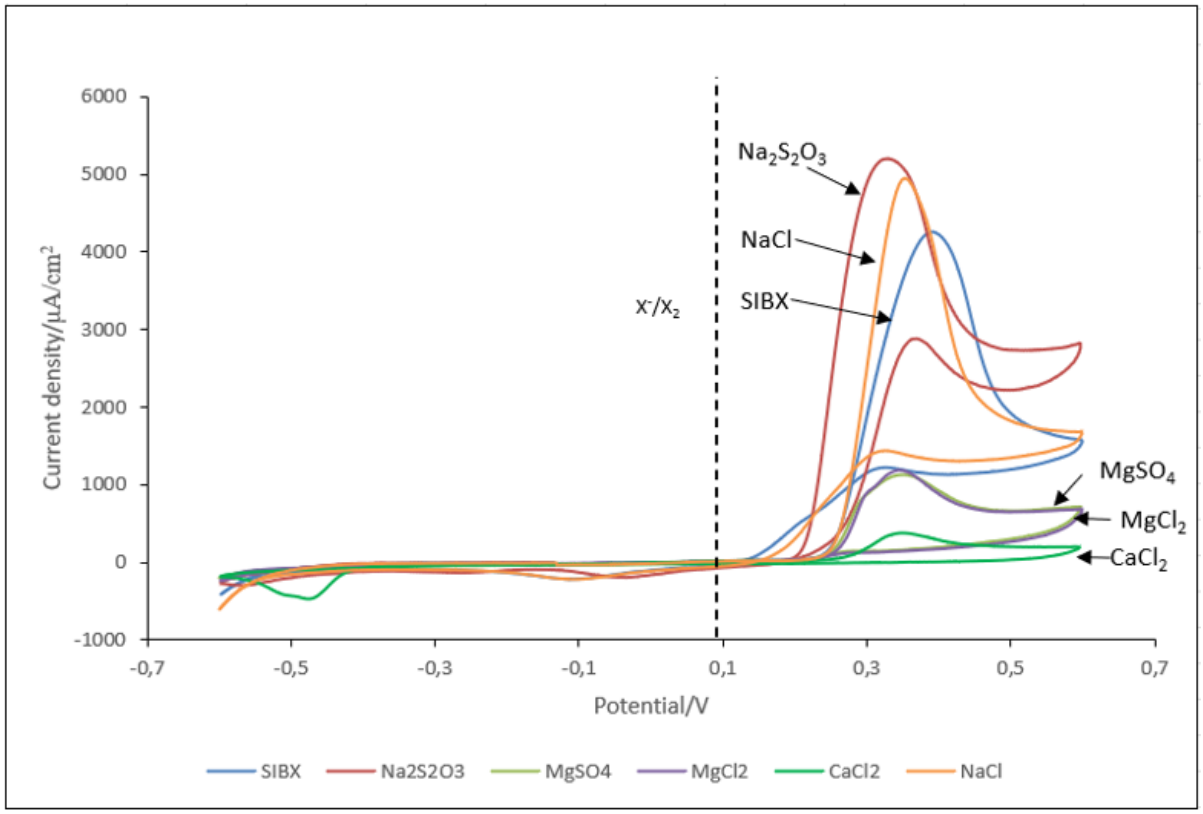

Figure 6.36: Cyclic voltammograms for $PdTe_2$ in the absence and presence of $Na_2S_2O_3$, NaCl, $MgSO_4$, $MgCl_2$ and $CaCl_2$ at 3 SPW with SIBX at a scan rate of 15 mV/s within a potential range of ± 0.6 V and at a pH of 9.2. The dotted line represents the equilibrium potential of dixanthogen formation of SIBX at 6.24×10^{-4} M (0.08 V).

Figure 6.36 exhibits cyclic voltammograms for $PdTe_2$ in the absence and presence of NaCl, $Na_2S_2O_3$, $MgCl_2$, $MgSO_4$ and $CaCl_2$ at 3 SPW in SIBX. On the positive sweep, the absence of salts and presence of NaCl and $Na_2S_2O_3$ were characterized by a steep increase in currents. However, the anodic currents in the presence of $Na_2S_2O_3$ started at lower potentials of ≈ 0.2 V, whereas a shift to more positive potentials was evident with other conditions. It is apparent that the absence of salts and the presence of NaCl resulted in one prominent anodic peak that commenced at potentials > 0.3 V. It is demonstrated that the presence of $MgCl_2$ and $MgSO_4$ yielded significantly reduced anodic currents > 0.25 V. Moreover, a pre-wave was observed in the presence of $CaCl_2$ within the potential region of – 0.05 V to 0.2 V, which could be attributable to the adsorption of

xanthate on the mineral surface. In addition, a fully developed anodic peak is noted > 0.3 V. Generally, compared to Figure 6.35 a slightly enhanced anodic activity is demonstrated in the absence of salts and in the presence of NaCl and $Na_2S_2O_3$. Alternatively, the presence of $MgCl_2$, $MgSO_4$ and $CaCl_2$ displayed slightly reduced anodic activity. The enhanced anodic activity could be ascribed to the oxidation of SIBX on $PdTe_2$, whereas the latter observation could be indicating that in the presence of SIBX, the current flow corresponding to the oxidation of $PdTe_2$ in the presence of $MgCl_2$, $MgSO_4$ and $CaCl_2$. Overall, it is shown that all anodic currents for the conditions investigated developed above the equilibrium potential of dixanthogen formation.

On the other hand, cathodic peaks corresponding to the anodic reactions that occurred on the minerals surface, were developed. The absence of salts and the presence of NaCl generated two cathodic peaks, one broad peak appeared in the potential region 0.15 V to – 0.3 V, which could be due to the reduction of more than one oxidized component. The second diminished peak developed at potentials < – 0.5 V. Furthermore, three reduction peaks were observed in the presence of $Na_2S_2O_3$ within the potential regions 0.2 V to – 0.15 V, – 0.2 V to – 0.4 V and < – 0.4 V. The presence of $MgCl_2$ and $MgSO_4$ displayed a diminished cathodic peak in the potential range < 0.5 V. Finally, the presence of $CaCl_2$ exhibited two cathodic peaks within the potential region of – 0.4 V to – 0.6 V.

6.4.8 Effect of 5 SPW of salts

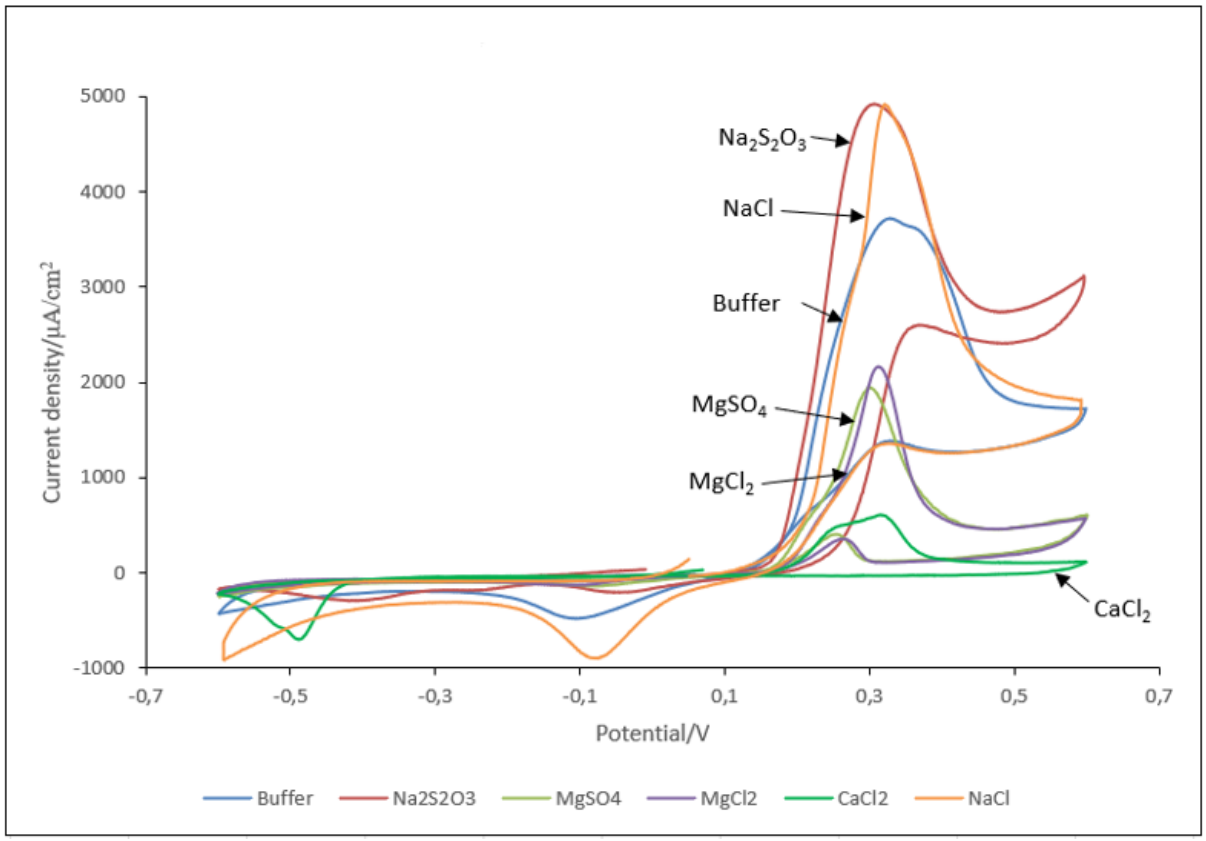

Figure 6.37: Cyclic voltammograms for $PdTe_2$ in the absence and presence of $Na_2S_2O_3$, NaCl, $MgSO_4$, $MgCl_2$ and $CaCl_2$ at 5 SPW at a scan rate of 15 mV/s within a potential range of ± 0.6 V and at a pH of 9.2.

Figure 6.37 plots the voltammetric response of $PdTe_2$ in the absence and presence of NaCl, $Na_2S_2O_3$, $MgCl_2$, $MgSO_4$ and $CaCl_2$ at 5 SPW. In the absence of salts, two anodic peaks are seen above 0.2 V. The presence of NaCl and $Na_2S_2O_3$ revealed enhanced anodic activity on the mineral surface from the baseline case. Hence, implying that the presence of NaCl and $Na_2S_2O_3$ at 5 SPW enhances the oxidation of $PdTe_2$. Conversely, the presence of $MgCl_2$, $MgSO_4$ and $CaCl_2$ exhibited lower anodic currents. In addition, anodic peaks commenced at potentials > 0.15 V for $MgCl_2$, $MgSO_4$ and $CaCl_2$, with the anodic activity in the absence of salts and in the presence $Na_2S_2O_3$ starting from > 0.2 V. Furthermore, the presence of NaCl resulted in anodic currents commencing at more positive potentials > 0.3 V. It is evident that the presence of NaCl, $Na_2S_2O_3$, $MgCl_2$ and $MgSO_4$ demonstrated one anodic peak reaction that could have occurred on the mineral surface, whereas two anodic reactions were associated with the absence of salts and with the presence of $CaCl_2$.

On the reverse scan, the baseline case generated two cathodic peaks that corresponded to the two anodic peaks formed. The peaks were developed in the potential regions 0.1 V to – 0.25 V and

< – 0.45 V. The presence of $Na_2S_2O_3$ yielded the highest number of reduction peaks. The cathodic peaks were observed in the potential regions 0.1 V to – 0.15 V; – 0.15 V to – 0.3 V and – 0.35 V to – 0.55 V. The presence of NaCl displayed two prominent reduction peaks within the potential range of 0.05 V to – 0.2 V and < 0.4 V. Two diminished cathodic peaks were seen in the presence of $MgCl_2$ and $MgSO_4$ within potential regions of 0 to – 0.2 V and < – 0.45 V. Similarly, the presence of $CaCl_2$ exhibited two cathodic peaks within the potential range of – 0.4 V to – 0.6 V.

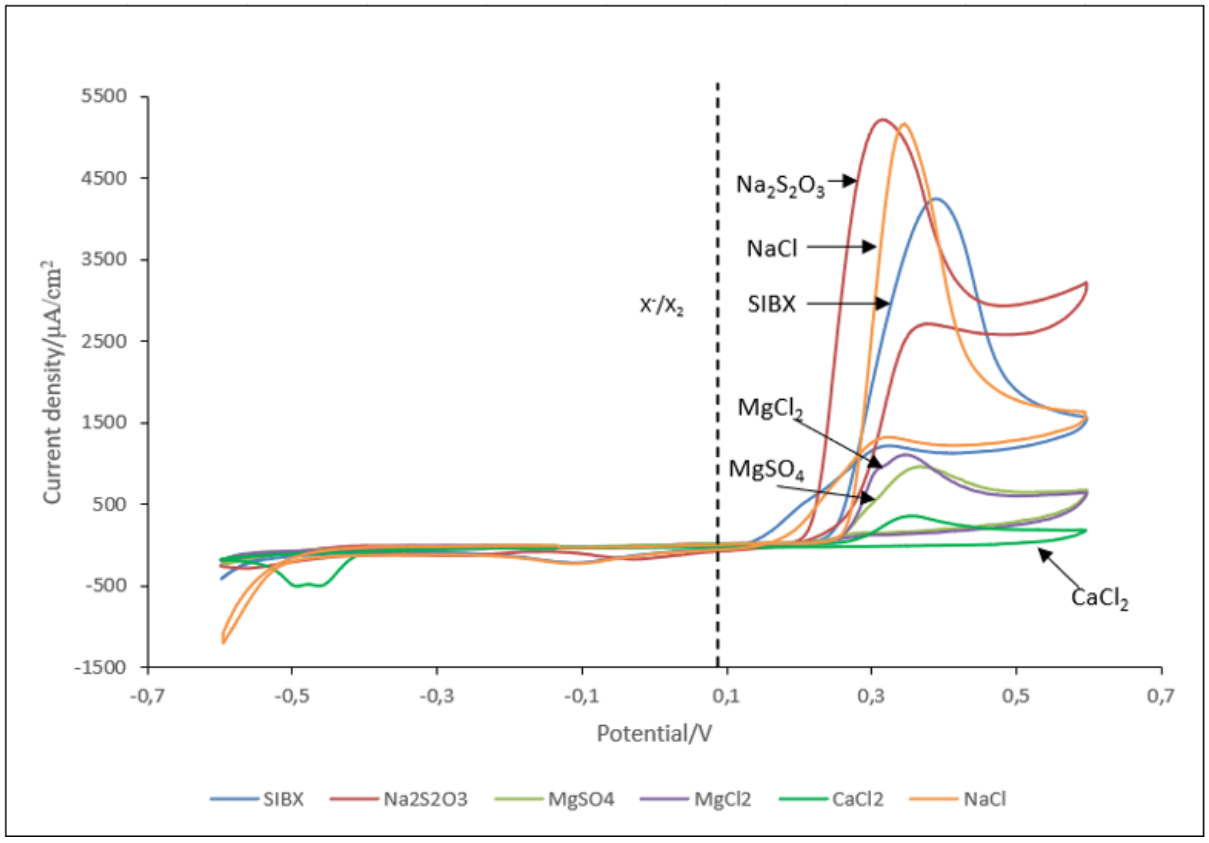

Figure 6.38: Cyclic voltammograms for $PdTe_2$ in the absence and presence of $Na_2S_2O_3$, NaCl, $MgSO_4$, $MgCl_2$ and $CaCl_2$ at 5 SPW with SIBX at a scan rate of 15 mV/s within a potential range of ± 0.6 V and at a pH of 9.2. The dotted line represents the equilibrium potential of dixanthogen formation of SIBX at 6.24×10^{-4} M (0.08 V).

Figure 6.38 demonstrates cyclic voltammograms $PdTe_2$ in the absence and presence of NaCl, $Na_2S_2O_3$, $MgCl_2$, $MgSO_4$ and $CaCl_2$ at 5 SPW in SIBX. It is discerned from Figure 6.38 that a steep increase in anodic currents is generated in the absence of salts, and in the presence of NaCl and $Na_2S_2O_3$ compared to other conditions. One significant anodic peak, which commenced at potentials > 0.3 V, was yielded in the absence of salts and in the presence of NaCl. Furthermore, the anodic currents are noted to start at slightly lower potentials in the presence of $Na_2S_2O_3$, $MgCl_2$, $MgSO_4$ and $CaCl_2$. Moreover, one anodic peak is generated in the presence of $Na_2S_2O_3$ at potentials > 0.2 V. One diminished anodic peak is yielded in the presence of $MgSO_4$ and $CaCl_2$ at potentials

> 0.25 V. Additionally, the presence of $MgCl_2$ generated two anodic peaks at similar potentials > 0.25 V. Compared to Figure 6.37, an increase in anodic currents is observed in Figure 6.38 in the absence of salts and in the presence of NaCl and $Na_2S_2O_3$, probably due to the oxidation of SIBX on the mineral surface. On the other hand, the presence of SIBX decreased the anodic activities imposed by the presence of $MgCl_2$, $MgSO_4$ and $CaCl_2$. This could suggest that the presence of SIBX inhibits the extent to which $MgCl_2$, $MgSO_4$ and $CaCl_2$ oxidize the mineral surface. Overall, it is demonstrated that under all investigated conditions, anodic peaks were generated above the equilibrium potential of dixanthogen formation.

On the cathodic scan, reduction peaks were generated for all investigated conditions. It is shown that in the absence of salts, two cathodic peaks within the potential ranges of 0.15 V to – 0.25 V and < – 0.5 V, were obtained. Moreover, the presence of $Na_2S_2O_3$ exhibited more reduction peaks than all other conditions investigated. It is apparent that three reduction peaks were generated in the presence of $Na_2S_2O_3$ within the potential ranges of 0.2 V to – 0.15 V; – 0.15 V to – 0.45 V and < 0.45 V. Two cathodic peaks were observed in the presence of $CaCl_2$ and NaCl within the potential range of – 0.4 V to – 0.6 V and 0.15 V to 0.25 V and < 0.5 V, respectively. Furthermore, the presence of $MgCl_2$ and $MgSO_4$ yielded one very small cathodic peak in the potential region < – 0.5 V.

6.4.9 Effect of 10 SPW of salts

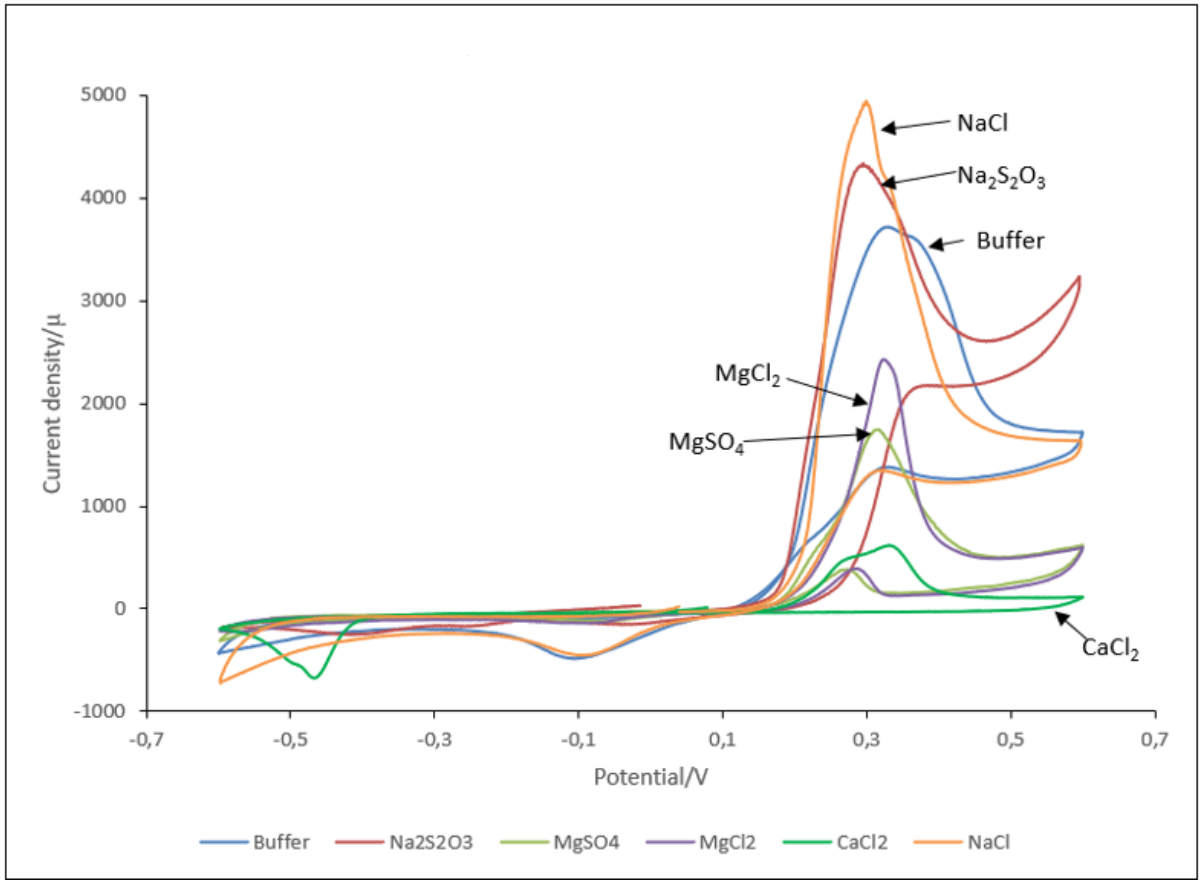

Figure 6.39: Cyclic voltammograms for $PdTe_2$ in the absence and presence of $Na_2S_2O_3$, NaCl, $MgSO_4$, $MgCl_2$ and $CaCl_2$ at 10 SPW at a scan rate of 15 mV/s within a potential range of ± 0.6 V and at a pH of 9.2.

Figure 6.39 shows voltammograms $PdTe_2$ in the absence and presence of NaCl, $Na_2S_2O_3$, $MgCl_2$, $MgSO_4$ and $CaCl_2$ at 10 SPW. Prominent anodic peaks are visible for the conditions investigated. However, the anodic activity on the mineral surface is observed to increase in the order NaCl > $Na_2S_2O_3$ > no salts > $MgCl_2$ > $MgSO_4$ > $CaCl_2$. It is noted that the baseline case and the presence of NaCl generated two anodic peaks at potentials > 0.2 V. Moreover, the presence of $Na_2S_2O_3$ yielded two anodic peaks, one prominent peak was seen between the potential region of 0.2 V to 0.4 V and the second peak commenced at potentials > 0.5 V. The presence of $MgSO_4$ achieved one anodic peak at potentials > 0.2 V. Additionally, the presence of $MgCl_2$ and $CaCl_2$ yielded anodic currents that commenced at slightly lower potentials > 0.15 V. However, the presence of $CaCl_2$ generated two anodic peaks within the potential region of 0. 15 V to 0.4 V.

The figure clearly indicates that reduction reactions of the oxidized species formed on the mineral surface occurred under the investigated conditions. The baseline case produced two cathodic peaks, one broad peak within the potential region of 0.1 V to – 0.25 V, which could be ascribed

to the reduction of oxygen. The second peak appeared at a potential range of < – 0.4 V. This peak could be attributable to the reduction of the oxidation species formed during to the interaction between the metal ions and oxygen. The prominent anodic peaks developed in the presence of $Na_2S_2O_3$ resulted in the formation of three reduction peaks within the potentials regions of 0.1 V to – 0.15 V; – 0.2 V to – 0.3 V and – 0.3 V to – 0.6 V. Two small cathodic peaks were observed in the presence of $MgCl_2$ and $MgSO_4$ within the potential regions of 0.05 V to – 0.15 V; < – 0.4 V and 0 V to – 0.2 V; < – 0.4 V, respectively. The presence of $CaCl_2$ generated two reduction peaks within the potential region – 0.4 V to – 0.6 V, the second peak appeared to be diminished. Similarly, the presence of NaCl yielded two reduction peaks within a potential range of 0.1 V to – 0.2 V and < – 0.35 V.

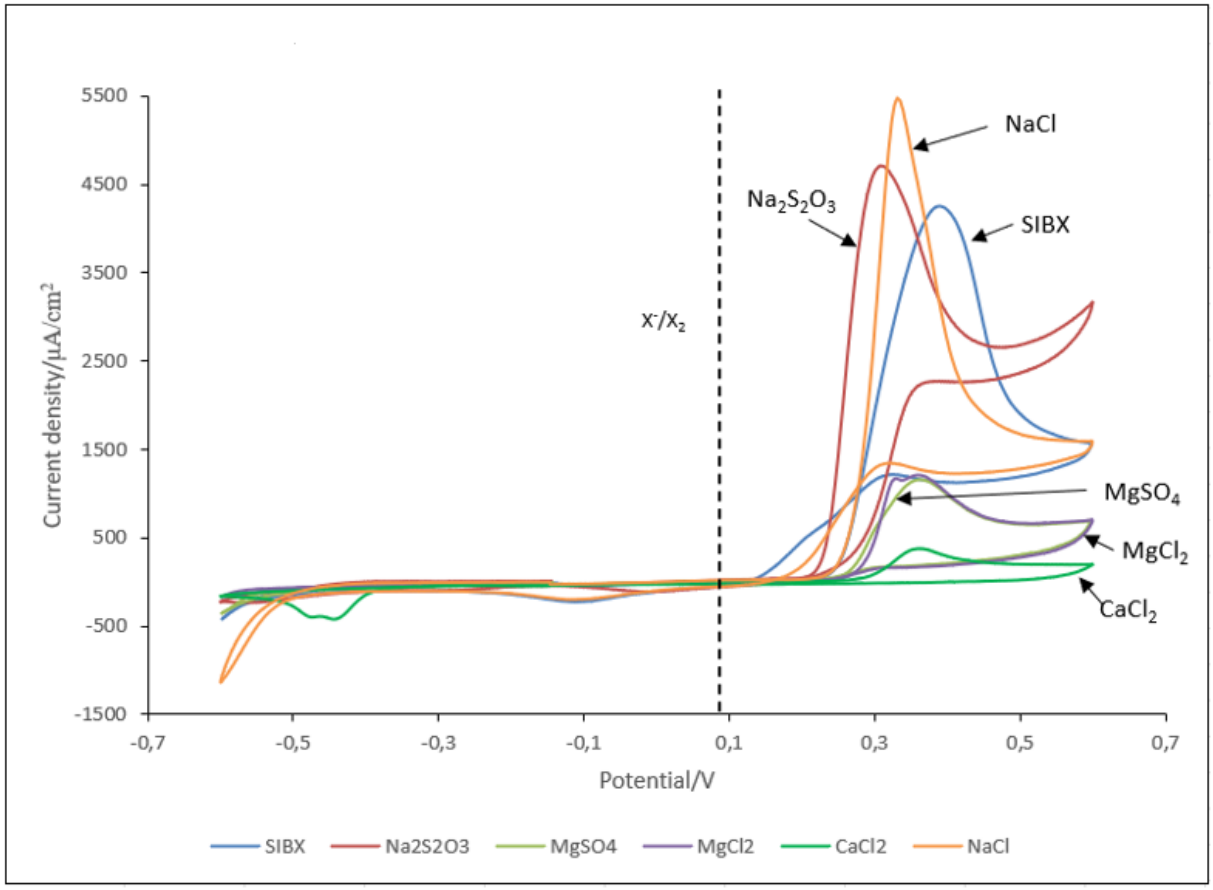

Figure 6.40: Cyclic voltammograms for $PdTe_2$ in the absence and presence of $Na_2S_2O_3$, NaCl, $MgSO_4$, $MgCl_2$ and $CaCl_2$ at 5 SPW with SIBX at a scan rate of 15 mV/s within a potential range of ± 0.6 V and at a pH of 9.2. The dotted line represents the equilibrium potential of dixanthogen formation of SIBX at 6.24×10^{-4} M (0.08 V).

Figure 6.40 presents the voltammetric response of $PdTe_2$ in the absence and presence of NaCl, $Na_2S_2O_3$, $MgCl_2$, $MgSO_4$ and $CaCl_2$ at 10 SPW in SIBX. A steep increase in anodic currents is observed especially in the absence of salts and in the presence of NaCl and $Na_2S_2O_3$.Overall, the

increase in anodic currents is found to be in the order NaCl > $Na_2S_2O_3$ > no salts > $MgCl_2$ > $MgSO_4$ > $CaCl_2$, in the presence of SIBX. Compared to Figure 6.39, it is evident that there was an increase in anodic currents, probably owing to the oxidation on SIBX on the mineral surface. An increased anodic activity is also visible in the case of NaCl and $Na_2S_2O_3$. In contrast, the presence of SIBX slightly reduced the anodic activity of $MgCl_2$, $MgSO_4$ and $CaCl_2$ on the mineral surface. This suggests that the presence of SIBX inhibits the extent to which the salts oxidize the mineral surface. Moreover, the increase in potential at which the anodic activities on the mineral surface commenced in the order $Na_2S_2O_3$ < NaCl ≈ no salts < $MgCl_2$ ≈ $MgSO_4$ < $CaCl_2$. One prominent anodic peak is generated in the absence of salts and in the presence of NaCl at potentials > 0.3 V. The presence of $Na_2S_2O_3$ yielded two anodic peaks, with one prominent peak appearing within the potential region of 0.25 V to 0.4 V. The second peak was developed at potentials > 0.45 V. The presence of $MgSO_4$ gave rise to one anodic peak which commenced > 0.25 V. Two anodic peaks were developed within a potential range of 0.3 V to 0.45 V in the presence of $MgCl_2$. The presence of $CaCl_2$ gave rise to a diminished anodic peak at potentials regions > 0.25 V.

On the negative sweep, two cathodic peaks were obtained in the potential regions of 0.15 V to – 0.25 V and < – 0.5 V, for the baseline case. The cathodic peaks are attributable to the reduction of the oxidized species formed on the mineral surface due to the oxidation of SIBX. In the presence of NaCl, two reduction peaks were seen to develop within the same potential regions to those shown for the baseline case. This implies that probably similar reactions most likely occurred on the mineral surface in the absence of the salts and in the presence of NaCl. Additionally, two broad reduction peaks were evident in the presence of $Na_2S_2O_3$ within the potential regions of 0.2 V to – 0.1 V and – 0.15 V to – 0.6 V. A small reduction peak was developed in the potential range < – 0.5 V, in the presence of $MgSO_4$ yet in the presence of $MgCl_2$, contrary to the anodic peaks generated, no cathodic peaks were formed. Ultimately, in the presence of $CaCl_2$, the reduction of the oxidation products formed gave rise to two cathodic peaks within the potential region of – 0.4 V to – 0.6 V, on the subsequent negative-going scan.

6.5 Key findings

Table 6.1: Key findings for cyclic voltammetry measurements

PdS	$PdTe_2$
• Generally high anodic activity was conveyed on the mineral surface in the presence of $Na_2S_2O_3$ compared to other salts.	• Generally higher anodic currents observed for all conditions investigated compared with currents generated for PdS.
• An increase in anodic currents was demonstrated with an increase in ionic strength, in the case of $Na_2S_2O_3$.	• The presence of $MgSO_4$, $MgCl_2$ and $CaCl_2$ clearly inhibited oxidation of oxygen and SIBX on the mineral surface, with $CaCl_2$ exhibiting a more pronounced effect.
• Small anodic currents were observed in the presence of $MgSO_4$, $MgCl_2$, $CaCl_2$ and NaCl.	• The presence of $Na_2S_2O_3$ and NaCl showed slightly enhanced anodic activity.
• No reduction peaks were displayed in the presence of SIBX for all conditions investigated.	• No reduction peaks were displayed in the presence of $MgSO_4$ and $MgCl_2$ with SIBX.
• Anodic currents in the presence of SIBX commenced at potentials above the equilibrium potential of dixanthogen formation.	• Anodic currents in the presence of SIBX commenced at potentials above the equilibrium potential of dixanthogen formation.
• Strong reduction peaks were observed in the absence and presence of salts. A shift to more negative potentials was noted with an increase in the ionic strength of the salts investigated.	• The presence of NaCl exhibited similar current profiles to the baseline cases.

7. Results: Electrochemical Impedance Spectroscopy

EIS is a technique that has been successfully used in previous studies to measure collector adsorption (Venter and Vermaak, 2008, Mu et al., 2015, Ertekin et al., 2016). It has been determined that collectors form an electrochemically passive layer which brings about changes to the resistance and conductance of a mineral surface.

In this study, EIS measurements were performed to investigate the mechanisms of interfacial interactions of five salts at increasing ionic strength in the absence and presence of SIBX with $PdTe_2$ and PdS. The mechanisms of interactions of $Na_2S_2O_3$, NaCl, $CaCl_2$, $MgSO_4$ and $MgCl_2$ at 1 SPW, 3SPW, 5 SPW and 10 SPW were determined in the case of $PdTe_2$. Owing to the similar trends generated in cyclic voltammetric responses between NaCl, $CaCl_2$, $MgSO_4$ and $MgCl_2$ with PdS, only $Na_2S_2O_3$ and $MgSO_4$ salts were explored at increasing ionic strength for EIS measurements of PdS. Substantially, the mechanisms of interactions between SIBX with $PdTe_2$ and PdS in the absence and presence of the investigated salts were determined.

The impedance spectra were obtained at OCP by applying a sinusoidal excitation signal of 7 mV/rms in the frequency range from 0.01 – 100 000 Hz for $PdTe_2$. On the other hand, a sinusoidal excitation signal of 12 mV/rms in the frequency range of 5 – 100 000 Hz were applied in the case of PdS. All measurements were performed at a pH of 9.2.

The measured EIS spectra have been displayed in the form of Nyquist plots, which represent the imaginary impedance (Z_{imag}) plotted against the real impedance (Z_{real}) and Bode plots, which illustrate Z modulus (Z_{mod}) and phase angle (^{o}) plotted versus the logarithm of frequency (Log frequency). The distance between the y-axis and the point in the high frequency domain, where the Nyquist plot commences denotes the solution resistance (R_s), whereas the radius of a semicircle on a Nyquist plot indicates charge transfer resistance (R_{ct}). However, R_{ct} is inversely proportional to the rate of electrochemical reactions occurring on an electrode surface (De Wet et al., 1995).

7.1 Validation

Validation of EIS measurements was successfully performed from the work of Marape and Vermaak (2012). Figure 7.1 shows Bode plots for pentlandite at pH 9.3 in an air saturated solution

of 0.05 M of $Na_2B_4O_7$ measured at OCP. A common response of a resistor that corresponds to R_s is displayed in the higher frequency domain, by the relatively constant and low impedance values and phase angle that approaches zero. A capacitive behaviour of the electrical double layer which is presumed to exist at the pentlandite mineral/solution interface was indicated by the linear relationship obtained between impedance and frequency which generated a slope of –1 in the medium frequency domain and phase angle of approximately – 70°. Hence, these findings are in full agreement with what was reported in literature.

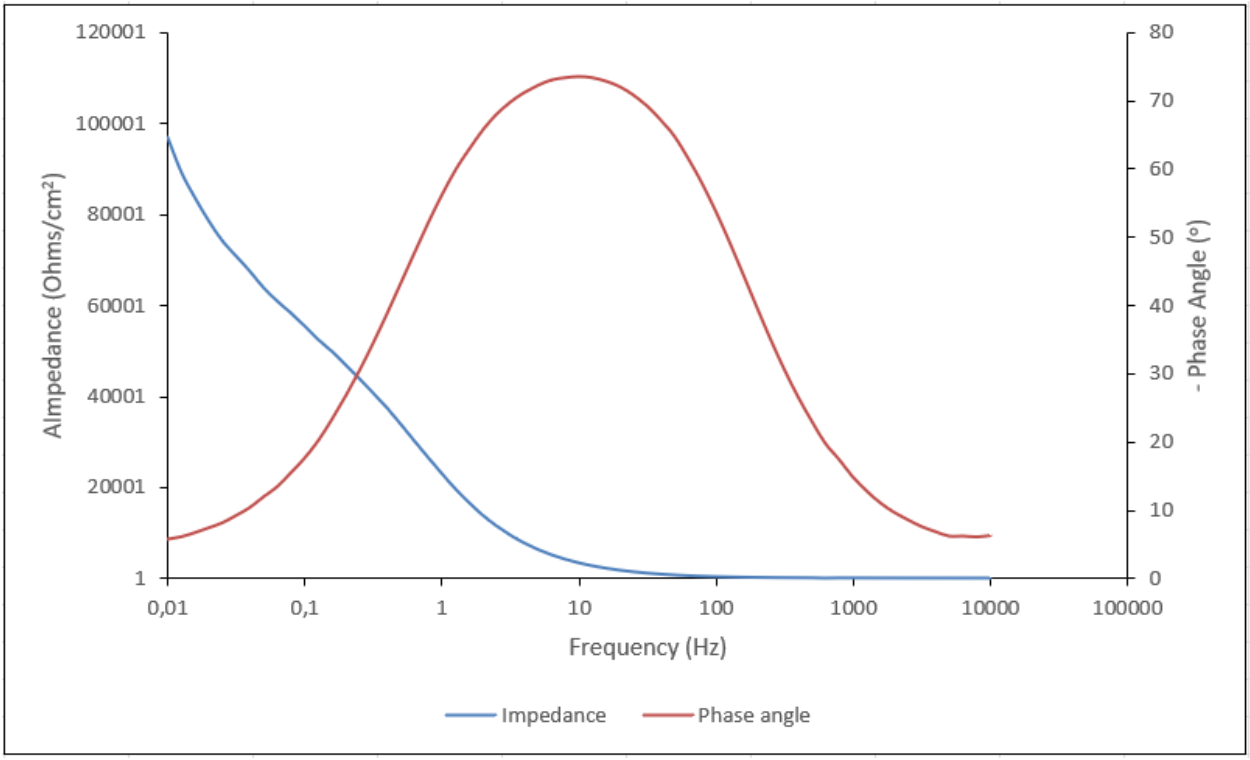

Figure 7.1: Bode plots for pentlandite at a pH of 9.3 in air saturated 0.05 M $Na_2B_4O_7$.

7.2 Reproducibility

Figure 7.2 conveys runs 1 and 2 on Nyquist plots for $PdTe_2$ in the presence of $CaCl_2$ at 1 SPW in SIBX. It is evident that the adsorption of $CaCl_2$ at 1 SPW in SIBX was controlled by interfacial charge transfer kinetics, as depicted by the incomplete semicircles (Ekmekçi et al., 2010b). It is clear that the impedance of the two runs is very similar. Therefore, the similar Nyquist plots obtained provided clear evidence that the EIS measurements performed in this study were very reproducible.

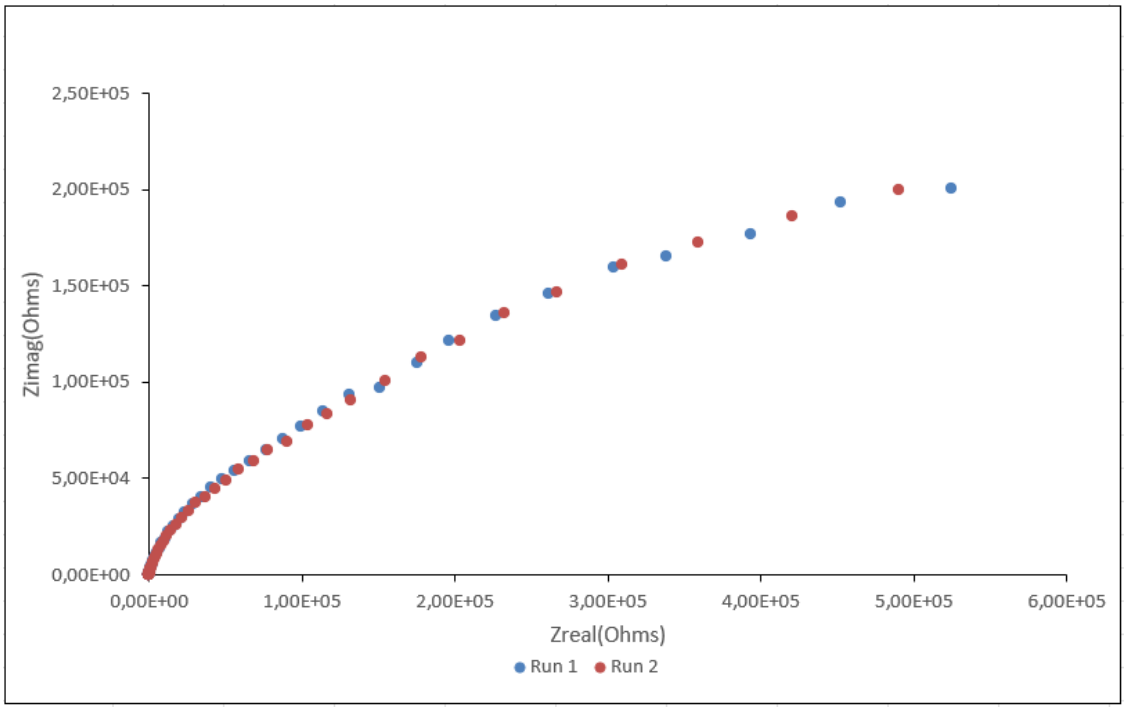

Figure 7.2: Nyquist plots for $PdTe_2$ in the presence of $CaCl_2$(1SPW) with SIBX at a pH of 9.2 in 0.05 M $Na_2B_4O_7$.

7.3 EIS for $PdTe_2$

7.3.1 Effect of $Na_2S_2O_3$

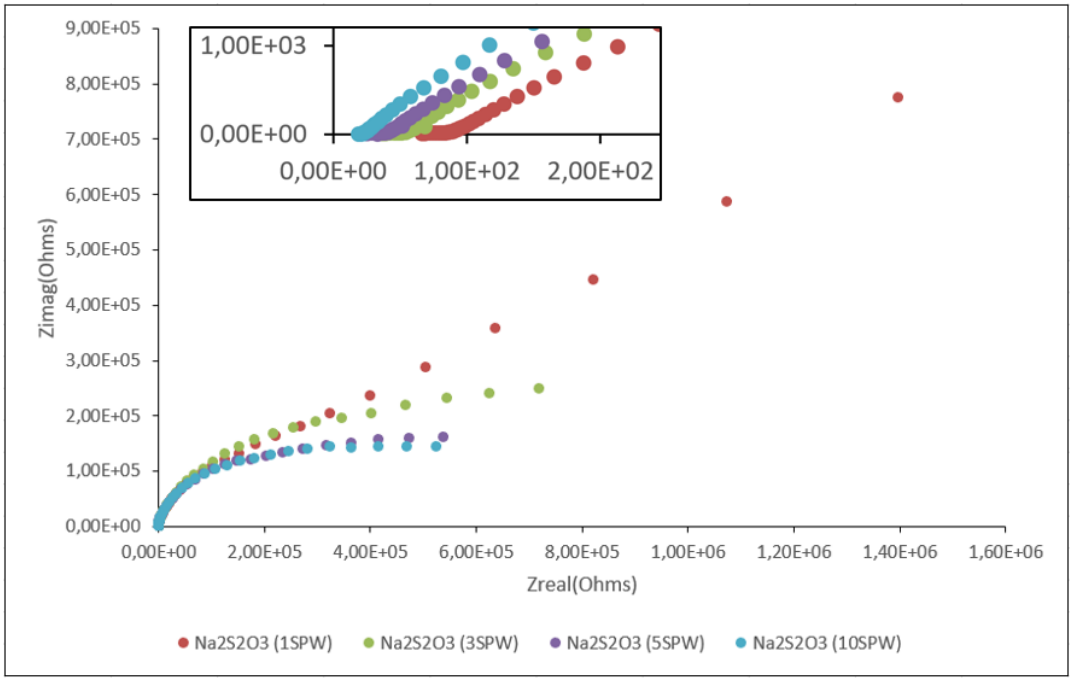

Figure 7.3: Nyquist plots for $PdTe_2$ in the presence of $Na_2S_2O_3$ at increasing ionic strength at a pH of 9.2 in O.O5 M $Na_2B_4O_7$.

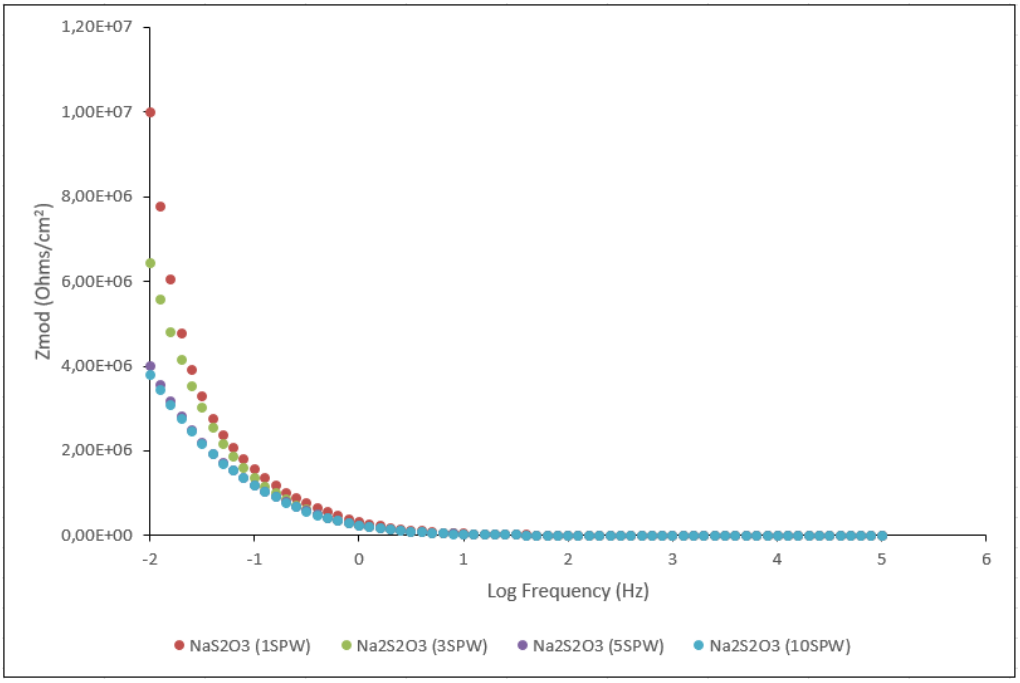

Figure 7.4: Bode plots of Z_{mod} (Ohms/cm^2) versus log frequency (Hz) for $PdTe_2$ in the presence of $Na_2S_2O_3$ at increasing ionic strength at a pH of 9.2 in O.O5 M $Na_2B_4O_7$.

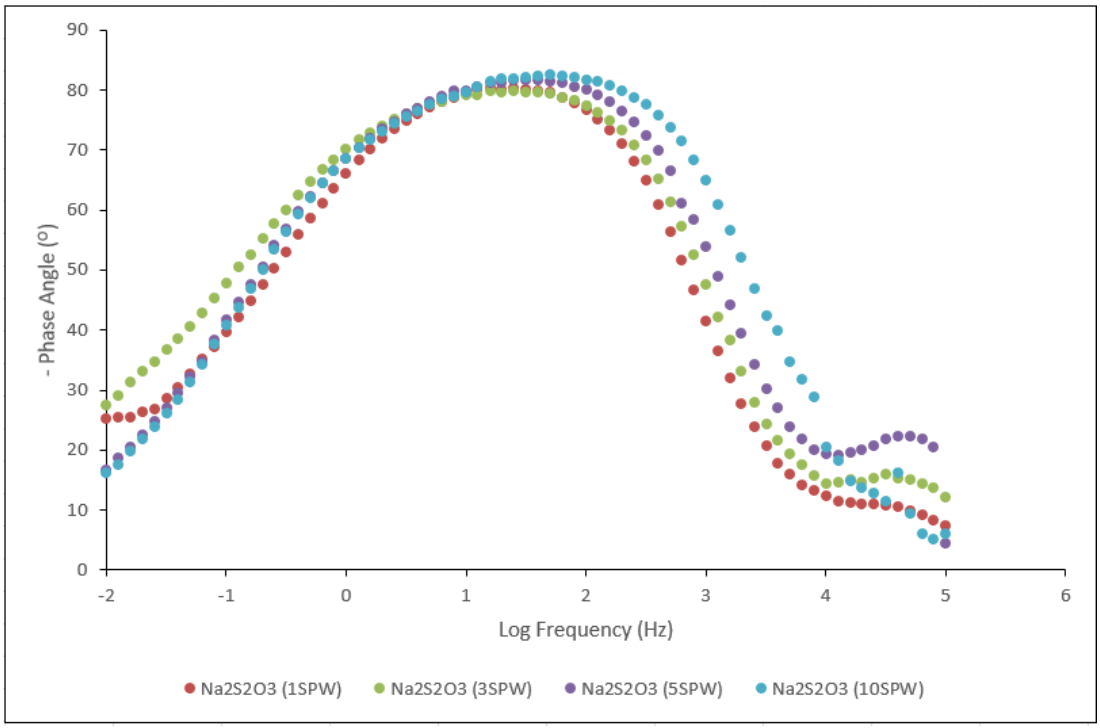

Figure 7.5: Bode plots of phase angle (°) versus log frequency for $PdTe_2$ in the presence of $Na_2S_2O_3$ at increasing ionic strength at a pH of 9.2 in O.O5 M $Na_2B_4O_7$.

Figures 7.3 to 7.5 demonstrate Nyquist and Bode plots for $PdTe_2$ in the presence of $Na_2S_2O_3$ at increasing ionic strength. It is observed on the Nyquist plot in Figure 7.3 that the radius of the semicircle for $PdTe_2$ electrode in the presence of $Na_2S_2O_3$ at the lowest ionic strength is much larger than those obtained in the presence of higher ionic strengths of $Na_2S_2O_3$. Therefore, R_{ct} was found to decrease with an increase in ionic strength of $Na_2S_2O_3$. Since R_{ct} is inversely proportional to the rate of electrochemical reactions (De Wet et al., 1995) , lower R_{ct} indicates a higher current flow for the electrochemical reactions occurring between $PdTe_2$ and the $Na_2S_2O_3$ ions (Mu et al., 2015). Thereby implying that $PdTe_2$ showed a high rate of reaction in the presence of the highest ionic strength of $Na_2S_2O_3$. It is clear that the reactions occurring on $PdTe_2$ surface in the presence of 3SPW, 5 SPW and 10 SPW $Na_2S_2O_3$, were attributed mainly to interfacial kinetics. However, at the lowest ionic strength, the impedance was attributed to interfacial kinetics at higher frequencies whereas the electron transfer occurring at lower frequencies was influenced by a diffusion-limited process. Moreover, it is illustrated that R_s decreases with an increase in ionic strength.

It is clearly shown from Figure 7.4 that the lowest Z_{mod} values were obtained at higher ionic strengths in the lower frequency range, indicating a higher rate of adsorption of $Na_2S_2O_3$ ions with an increase in ionic strength. Conversely, Z_{mod} values were higher at lower ionic strength of $Na_2S_2O_3$, suggesting higher resistance to charge transfer at lower ionic strength. Additionally, the lower Z_{mod} values demonstrate lower resistance and higher capacitive behaviour owing to higher net current for the electrochemical reactions on $PdTe_2$ mineral surface (Ekmekçi et al., 2010a). There was no significant change in the Bode plot in the intermediate frequency range in the presence of $Na_2S_2O_3$ at all ionic strengths investigated. This indicates no change in the capacitance and no continuous surface layers (Mu et al., 2015) were formed after the adsorption of $Na_2S_2O_3$ on $PdTe_2$ in this region. Furthermore, at higher frequency domain, Z_{mod} values are low and relatively constant whilst the phase angle values decrease approaching zero. This denotes a typical response of a resistor to an AC with high frequency, corresponding to R_s. Conclusively, the phase angles were found to be approximately -80^o, which denotes a capacitive behaviour of the electrical double layer (Ekmekçi et al., 2010a).

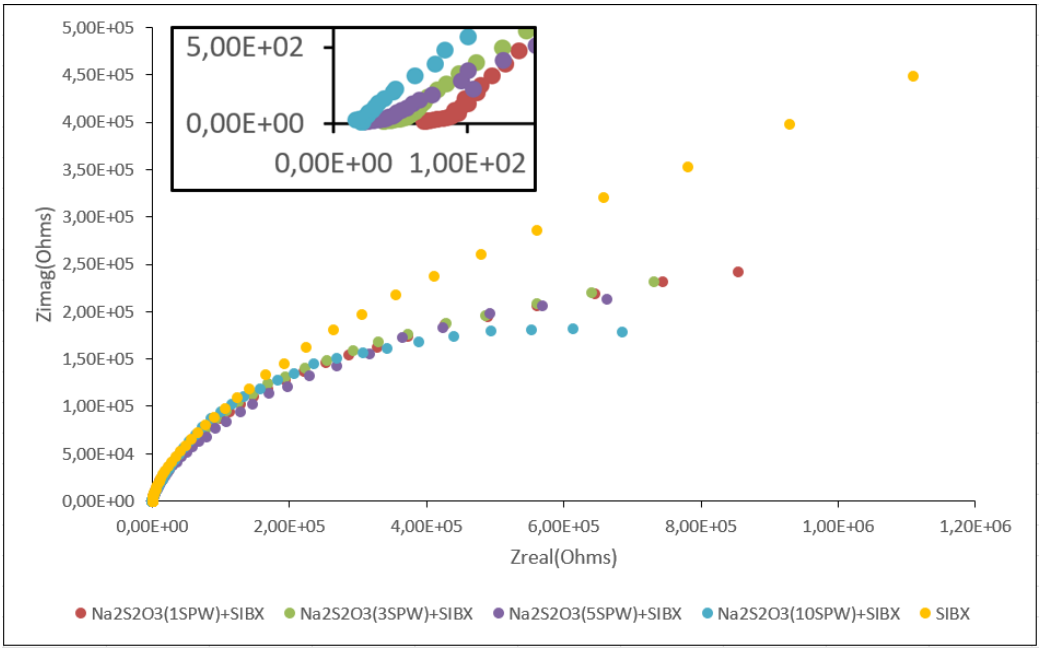

Figure 7.6: Nyquist plots for $PdTe_2$ in the absence and presence of $Na_2S_2O_3$ at increasing ionic strength in SIBX at a pH of 9.2 in O.O5 M $Na_2B_4O_7$.

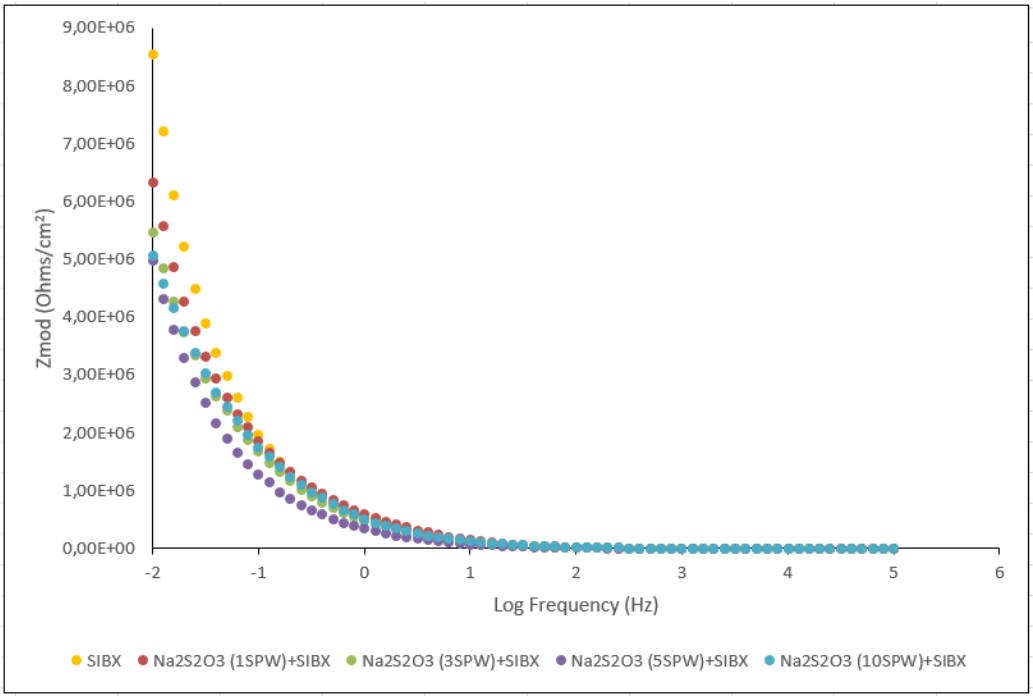

Figure 7.7: Bode plots of Z_{mod} (Ohms/cm^2) versus log frequency (Hz) for $PdTe_2$ in the absence and presence of $Na_2S_2O_3$ at increasing ionic strength with SIBX at a pH of 9.2 in O.O5 M $Na_2B_4O_7$.

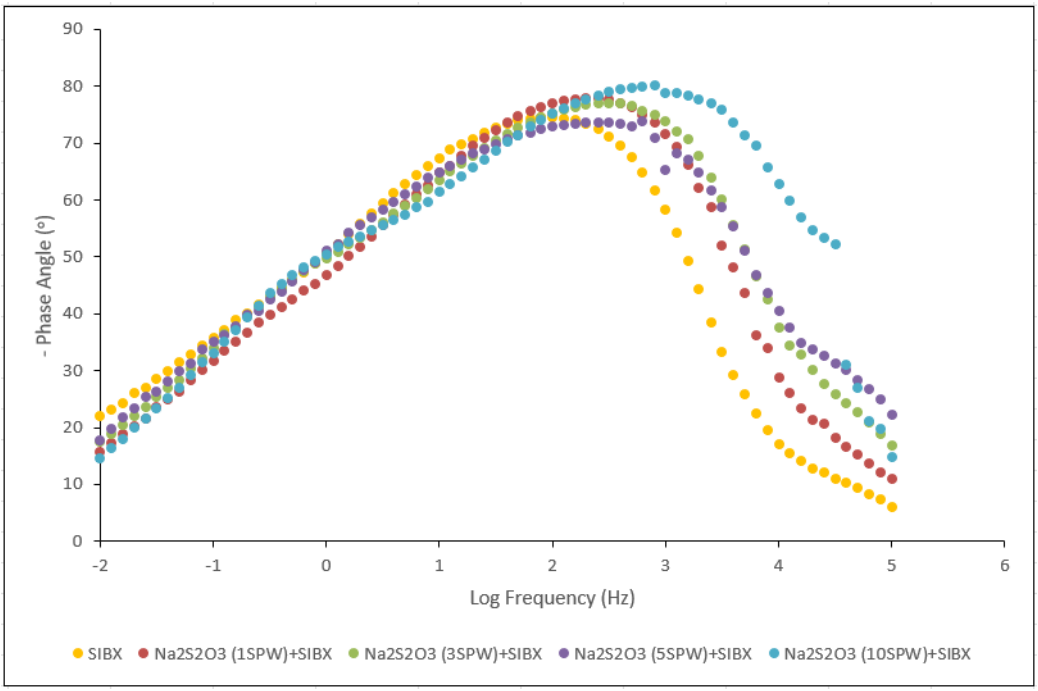

Figure 7.8: Bode plots of phase angle (°) versus log frequency for $PdTe_2$ in the absence and presence of $Na_2S_2O_3$ at increasing ionic strength with SIBX at a pH of 9.2 in O.O5 M $Na_2B_4O_7$.

Figures 7.6 to 7.8 illustrate Nyquist and Bode plots for $PdTe_2$ in the absence and presence of $Na_2S_2O_3$ at increasing ionic strength in SIBX. It is evident in Figure 7.6 that there was a pronounced decrease in R_{ct} for the lowest ionic strength in the presence of SIBX than in the absence of SIBX as indicated in Figure 7.4. The decrease in R_{ct} in the presence of SIBX is attributable to the attachment of xanthate ions on the mineral surface. The xanthate ions are oxidized to dixanthogen, thereby transferring charges to the $PdTe_2$ surface. It is evident that there was no significant change in R_{ct} both in the absence and presence of SIBX. However, Figure 7.6 displays a decrease in R_{ct} with an increase in ionic strength, though the R_{ct} for 1 SPW, 3 SPW and 5 SPW did not significantly differ. Furthermore, the Nyquist plots convey incomplete semicircles for all the conditions investigated, suggesting that the adsorption of both $Na_2S_2O_3$ and SIBX was mainly controlled by charge transfer processes (Ekmekçi et al., 2010b). This observation is supported by the low phase angle values obtained at lower frequency range. Moreover, lower R_{ct} is depicted by the highest ionic strength of $Na_2S_2O_3$ in the presence of SIBX, thereby indicating a higher rate of electrochemical reactions. On the contrary, the lower ionic strengths exhibited lower rates of reactions on the mineral surface.

It is noticeable in the Bode plots that in the low frequency region, an inverse relationship was found to exist between Z_{mod} and the frequency and the phase angles were approximately – 80 °.

This observation, therefore, correlates to the capacitive behaviour caused by the electrical double layer at the mineral/solution interface, after the adsorption of $Na_2S_2O_3$ ions and/or SIBX . Compared to Figure 7.4, interestingly, Figure 7.7 displays lower impedance values in the presence of SIBX in the lower frequency range for the lowest ionic strengths, 1 SPW and 3 SPW. This demonstrates lower resistance and higher capacitive behaviour due to a higher net current for the electrochemical reactions on the $PdTe_2$ minerals surface. The formation of hydrophilic species on the mineral surface would reduce the electrode capacitance whereas continuing electrochemical reactions involving the oxidation of xanthate to dixanthogen increase capacitance values. It is predicted that a decrease in R_{ads} and an increase in C_{ads} upon the addition of xanthates is attributable to the enhanced anodic activity due to the oxidation of xanthate to its dimer form (Ekmekçi et al., 2010a). In addition, a change in impedance in the low frequency range reveals a change in the capacitance and formation of continuous surface layers through the interaction between $PdTe_2$ with $Na_2S_2O_3$ and SIBX. On the contrary, it is observed in Figure 7.8 that in the higher frequency range, no significant change occurred because no continuous layers were formed on the $PdTe_2$ mineral surface. Overall, slightly lower Z_{mod} values were obtained with an increase in ionic strength of $Na_2S_2O_3$, thereby demonstrating the highest rates of adsorption on the mineral surface.

7.3.2 Effect of $MgSO_4$

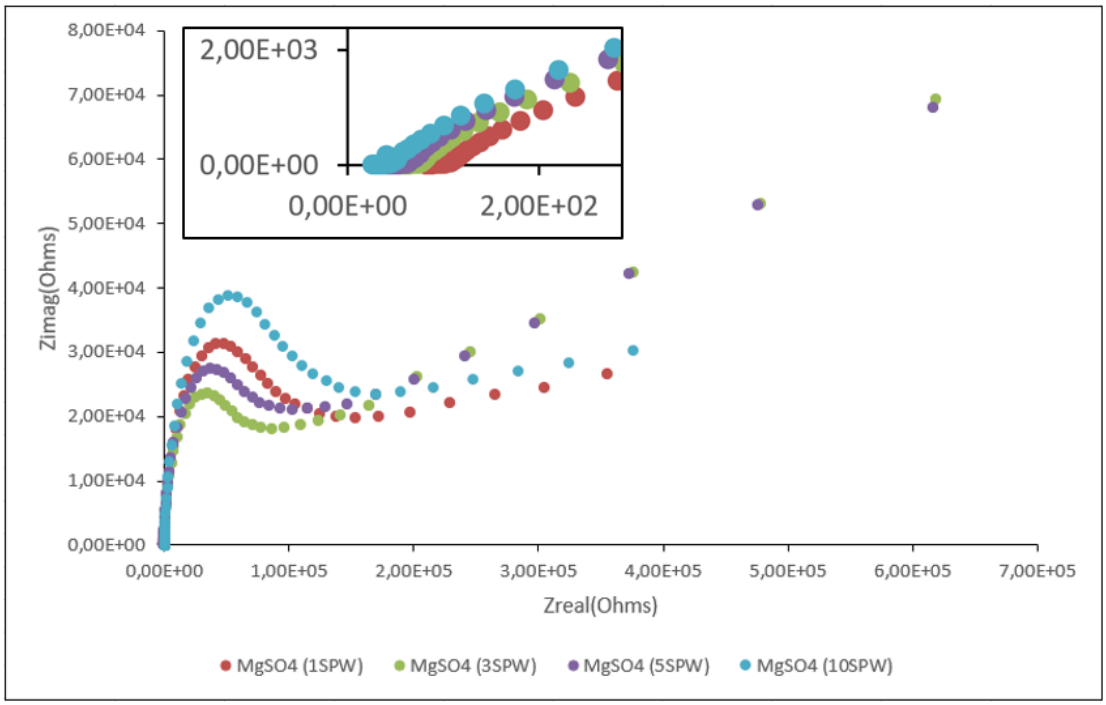

Figure 7.9: Nyquist plots for $PdTe_2$ in the presence of $MgSO_4$ at increasing ionic strength in SIBX at a pH of 9.2 in O.O5 M $Na_2B_4O_7$.

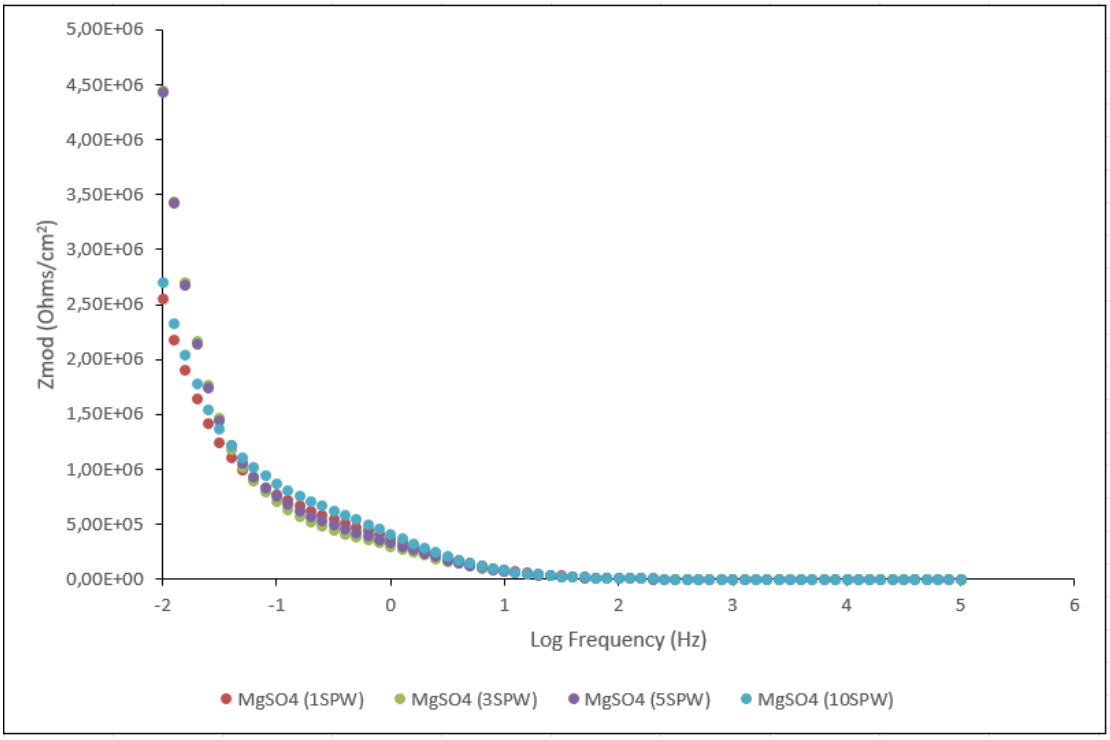

Figure 7.10: Bode plots of Z_{mod} (Ohms/cm^2) versus log frequency (Hz) for $PdTe_2$ in the presence of $MgSO_4$ at increasing ionic strength with SIBX at a pH of 9.2 in O.O5 M $Na_2B_4O_7$.

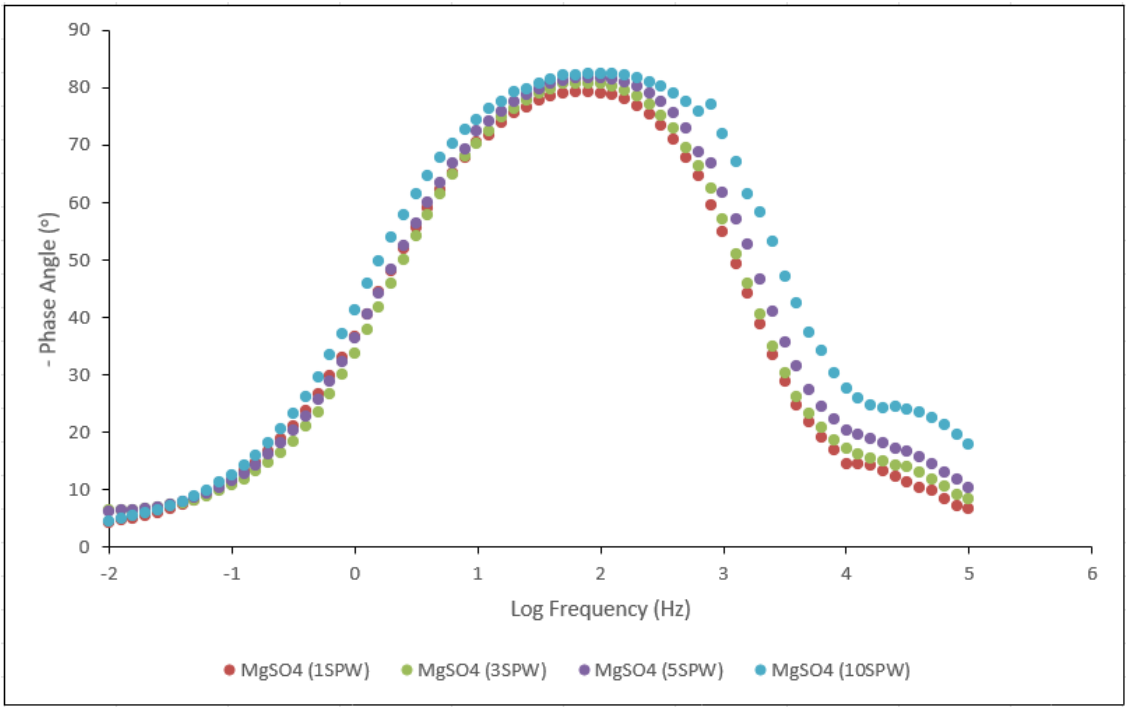

Figure 7.11: Bode plots of phase angle (°) versus log frequency for $PdTe_2$ in the presence of $MgSO_4$ at increasing ionic strength at a pH of 9.2 in O.O5 M $Na_2B_4O_7$.

Figures 7.9 to 7.11 display Nyquist and Bode plots for $PdTe_2$ in the presence of $MgSO_4$ at increasing ionic strength. It is evident in Figure 7.9 that the impedance of $PdTe_2$ in the presence

of $MgSO_4$ may be associated to interfacial kinetics in the higher frequency range. However, it is apparent that at 3 SPW and 5 SPW in the low frequency domain, the electron transfer reactions that occurred were influenced by diffusion-limited processes. Additionally, the Nyquist plot clearly shows that an increase in R_{ct} was obtained in the order of 3 SPW < 5 SPW < 1SPW < 10 SPW. Implying that a lower current occurred for the electrochemical reactions on $PdTe_2$, with a general increase in ionic strength. Moreover, a decrease in R_s is observed with an increase in ionic strength (Shimizu and Boily, 2014).

Lower Z_{mod} values are displayed at 1 SPW and 10 SPW, suggesting higher rates of adsorption (Ertekin et al., 2016) of $MgSO_4$ at the lowest and highest ionic strengths. Towards the intermediate frequency range, no significant change was observed in the Bode plot in Figure 7.10, indicating that there was no continuous formation of surface layers on the mineral surface after adsorption of $MgSO_4$. Moreover, a common response to an AC with high frequency, corresponding to R_s, was demonstrated by the Bode plots in Figures 7.10 and 7.11, where relatively constant and low Z_{mod} values were obtained in the high frequency domain whilst the phase angle decreased approaching zero.

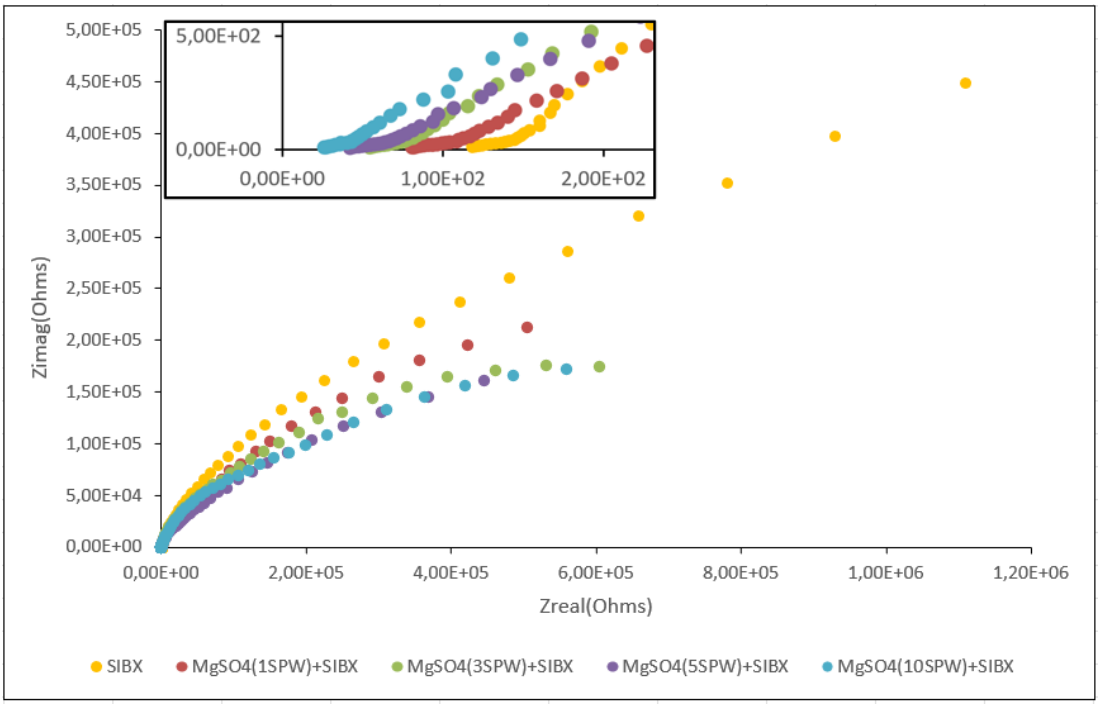

Figure 7.12: Nyquist plots for $PdTe_2$ in the absence and presence of $MgSO_4$ at increasing ionic strength with SIBX at a pH of 9.2 in 0.05 M $Na_2B_4O_7$.

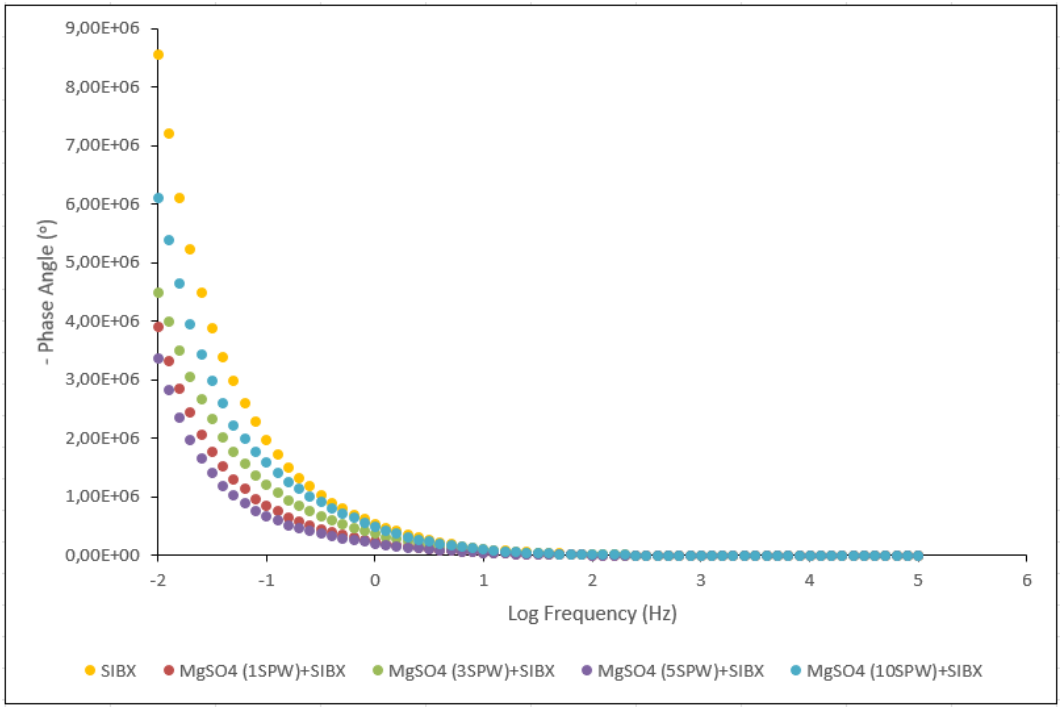

Figure 7.13: Bode plots of Z_{mod} (Ohms/cm^2) versus log frequency (Hz) for $PdTe_2$ in the absence and presence of $MgSO_4$ at increasing ionic strength with SIBX at a pH of 9.2 in O.O5 M $Na_2B_4O_7$.

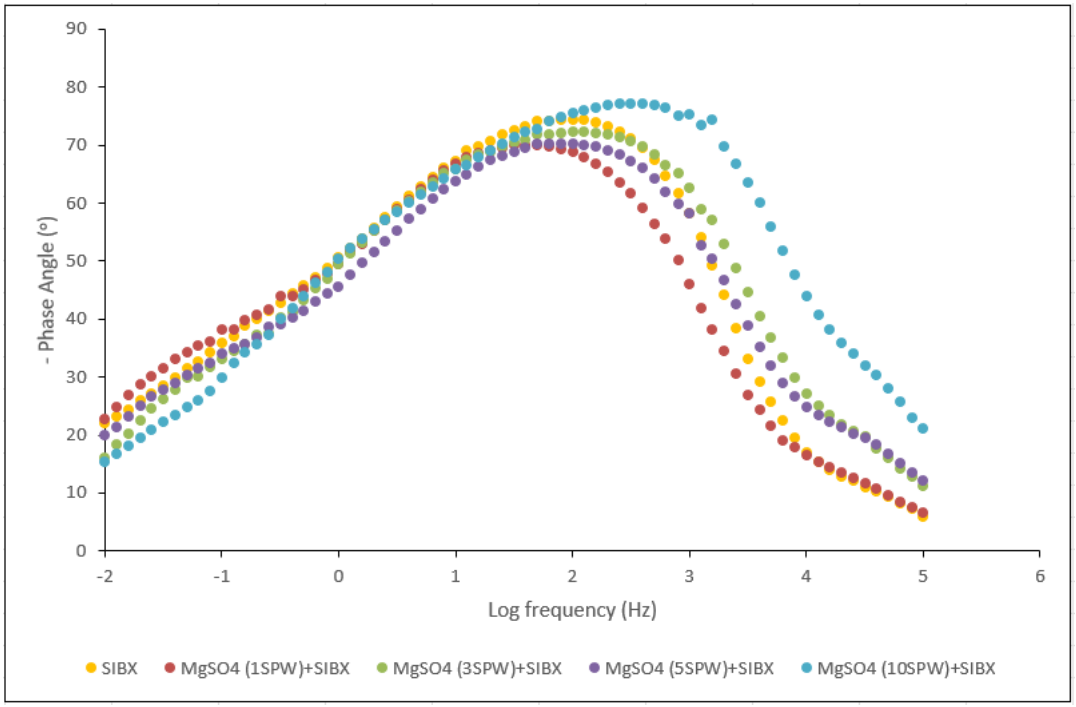

Figure 7.14: Bode plots of phase angle (°) versus log frequency for $PdTe_2$ in the absence and presence of $MgSO_4$ at increasing ionic strength with SIBX at a pH of 9.2 in O.O5 M $Na_2B_4O_7$.

Figures 7.12 to 7.14 depict Nyquist and Bode plots for $PdTe_2$ in the absence and presence of $MgSO_4$ at increasing ionic strength in SIBX. The Nyquist plot in Figure 7.12 generally displays higher R_{ct} for all conditions in the presence of SIBX compared to Figure 7.9, in the absence of SIBX. The rise in R_{ct} in the presence of SIBX indicates a lower capacitance due to lower current flow for the electrochemical reactions. This suggests the formation of a layer with a small dielectric constant due to the adsorption of SIBX on $PdTe_2$ (Mu et al., 2015). However, it is observable in Figure 7.12 that R_{ct} decreases with an increase in ionic strength. Additionally, it is apparent that the reactions occurring on the $PdTe_2$ mineral surface in the presence of SIBX are attributed mainly to interfacial kinetics. This observation is supported by the lower phase angles obtained in the lower frequency range for all ionic strengths of $MgSO_4$ in the presence of SIBX. Furthermore, a zoomed image of the Nyquist plots clearly shows a decrease in solution resistance with an increase in ionic strength. It is demonstrated further that R_s did not show any significant changes both in the absence and presence of SIBX, therefore, suggesting that R_s was not greatly affected by any chemical transformations that occurred at the $PdTe_2$ mineral surface.

It is evident in Figure 7.13 that lower Z_{mod} values were obtained in the presence of $MgSO_4$ at 5SPW. This observation denotes a strong adsorption of $MgSO_4$ at 5SPW with SIBX on the mineral surface. Z_{mod} values decreased in the order 5 SPW < 1 SPW < 3 SPW < 10 SPW. In the low frequency range, the relationship between impedance and frequency was found to be inversely proportional and phase angles were determined to be approximately – 70^o to – 80^o. This observation could be ascribed to the capacitive behaviour caused by the electrical double layer at the mineral/solution interface. Additionally, the changes in the low frequency range in impedance values at different ionic strengths of $MgSO_4$ indicate a change in capacitance of the $PdTe_2$ surface. This could be associated with the formation of significant continuous surface layers on $PdTe_2$ (Ekmekçi et al., 2010a), due to the adsorption of xanthate ions and the subsequent formation of dixanthogen. Moreover, impedance values in the low frequency range were significantly higher in $MgSO_4$ at 1 SPW, 3 SPW and 10 SPW in the presence of SIBX than in the absence of SIBX. This demonstrates higher resistance and lower capacitive behaviour due to a lower net current for the electrochemical reactions occurring on the $PdTe_2$ surface. Since double layer capacitance is dependent upon the dielectric property, upon the adsorption of SIBX, a decrease in the dielectric constant between the mineral and water interphase will therefore decrease the capacitance value. Interestingly, a decrease in impedance values was observed in $MgSO_4$ at 5 SPW in the presence of SIBX.

7.3.3 Effect of $MgCl_2$

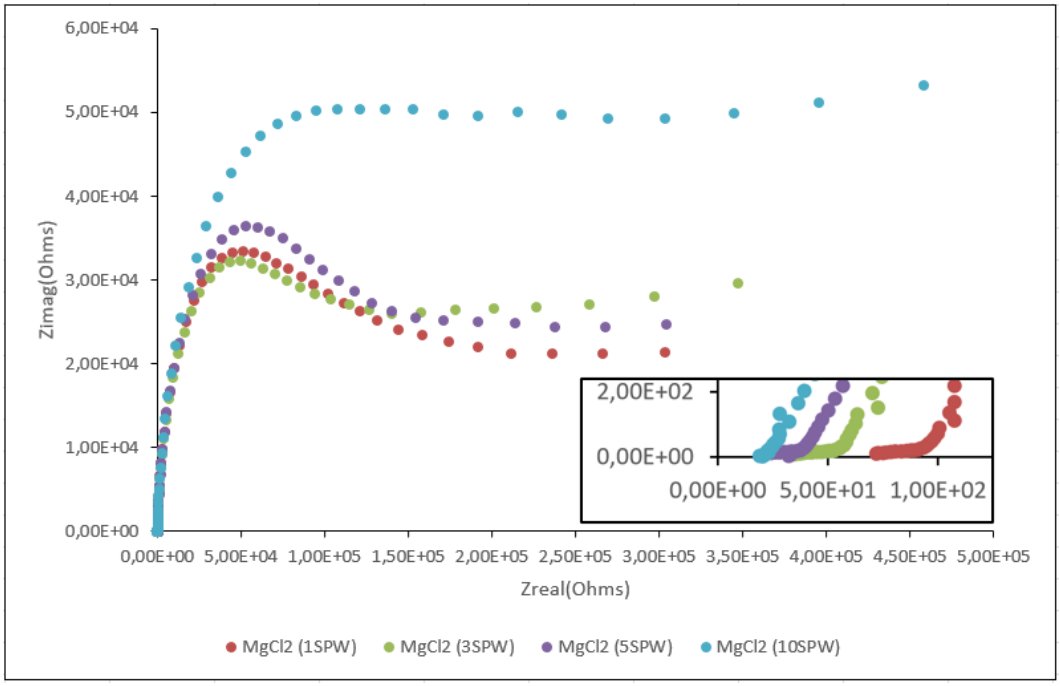

Figure 7.15: Nyquist plots for $PdTe_2$ in the presence of $MgCl_2$ at increasing ionic strength at a pH of 9.2 in O.O5 M $Na_2B_4O_7$.

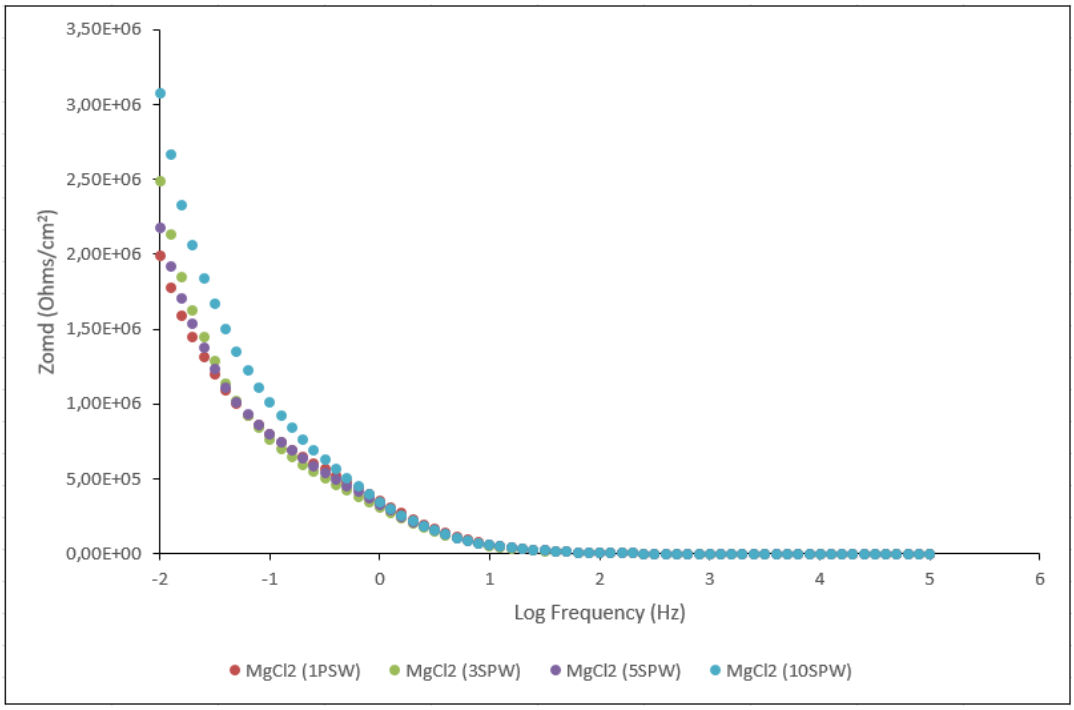

Figure 7.16: Bode plots of Z_{mod} (Ohms/cm^2) versus log frequency (Hz) for $PdTe_2$ in the presence of $MgCl_2$ at increasing ionic strength at a pH of 9.2 in O.O5 M $Na_2B_4O_7$.

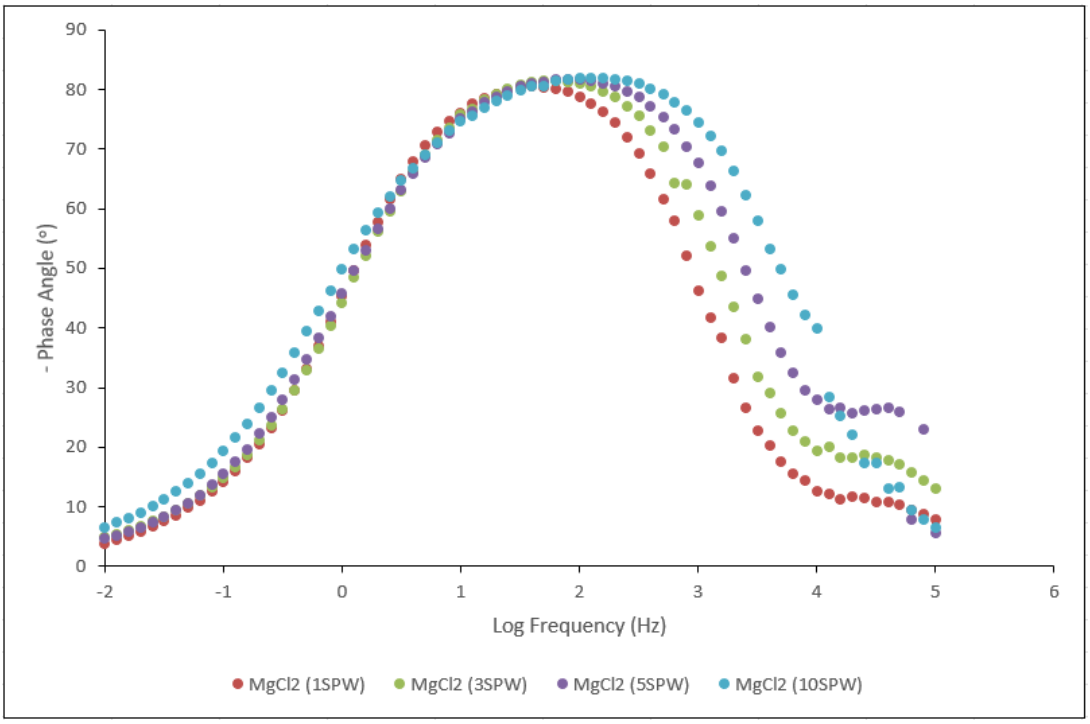

Figure 7.17: Bode plots of phase angle (°) versus log frequency for $PdTe_2$ in the presence of $MgCl_2$ at increasing ionic strength at a pH of 9.2 in O.O5 M $Na_2B_4O_7$.

Figures 7.15 to 7.17 convey Nyquist and Bode plots for $PdTe_2$ in the presence of $MgCl_2$ at increasing ionic strength. It is clear from Figure 7.15 that R_{ct} increases with an increase in ionic strength in the presence of $MgCl_2$. An increase in R_{ct} depicts a lower current flow for electrochemical reactions transpiring on the mineral surface, therefore, implying that the adsorption of $MgCl_2$ onto $PdTe_2$ hinders $PdTe_2$ oxidation to some extent. Hence, $PdTe_2$ displayed higher rates of reactions at lower ionic strengths of $MgCl_2$. In addition, it can be discerned from the Nyquist plot that R_S decreases with an increase in ionic strength. Furthermore, it is observable that the reactions occurring on the $PdTe_2$ mineral surface are due to interfacial kinetics. This observation is in agreement with the lower values of phase angles obtained in the lower frequency range, in Figure 7.17.

Higher Z_{mod} values were obtained with the highest ionic strength of $MgCl_2$ and a higher R_{ct} is expected. These observations correspond to the results observed in the Nyquist plot. Z_{mod} values increased in the order 1 SPW < 5 SPW < 3 SPW < 10 SPW, therefore, indicating that generally the rate of adsorption (Ertekin et al., 2016) of $MgCl_2$ decreased with an increase in ionic strength. Higher Z_{mod} values indicate higher resistance and lower capacitive behaviour due to lower net current for the electrochemical reactions occurring on the $PdTe_2$ mineral surface. A lower capacitance value demonstrates the development of either a thicker oxide layer or a layer with a

smaller dielectric constant. Hence, the development of a thicker oxide layer could be associated with an increase in ionic strength. Overall, it is evident that at a higher frequency domain, Z_{mod} values are low and relatively constant and concurrently the phase angles decrease approaching zero. This observation denotes a typical response of a resistor to an AC with high frequency corresponding to R_s. Phase angles of approximately – 80° were determined, thereby indicating a capacitive behaviour caused by the electrical double layer at the mineral/solution interface.

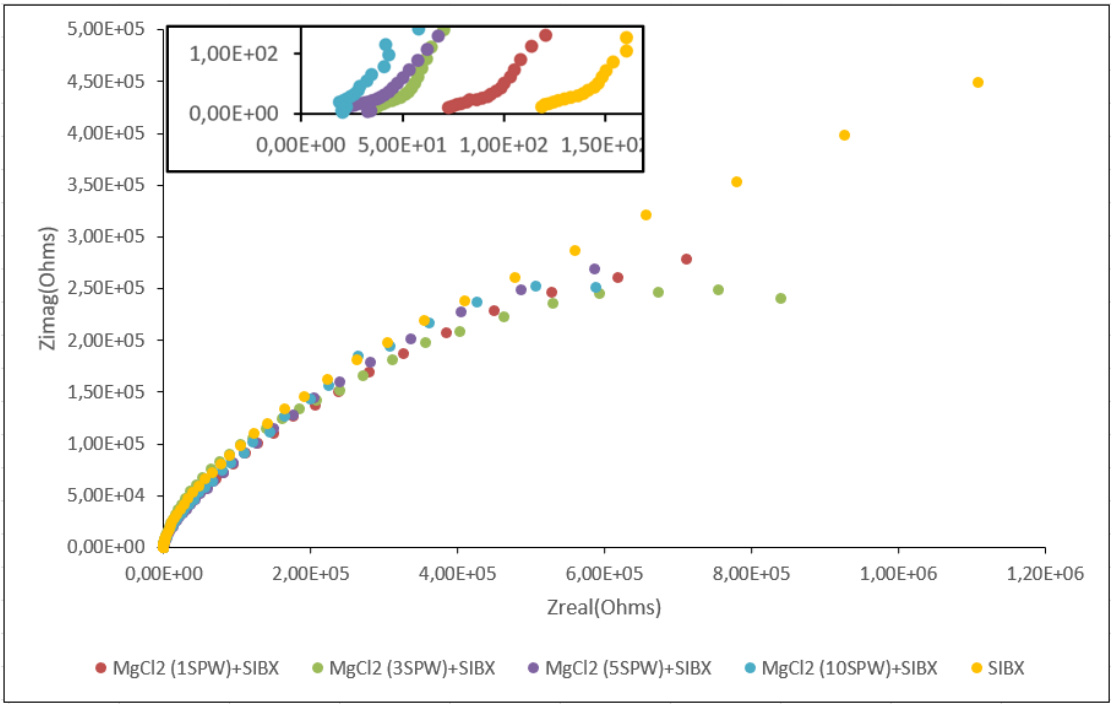

Figure 7.18: Nyquist plots for $PdTe_2$ in the absence and presence of $MgCl_2$ at increasing ionic strength with SIBX at a pH of 9.2 in O.O5 M $Na_2B_4O_7$.

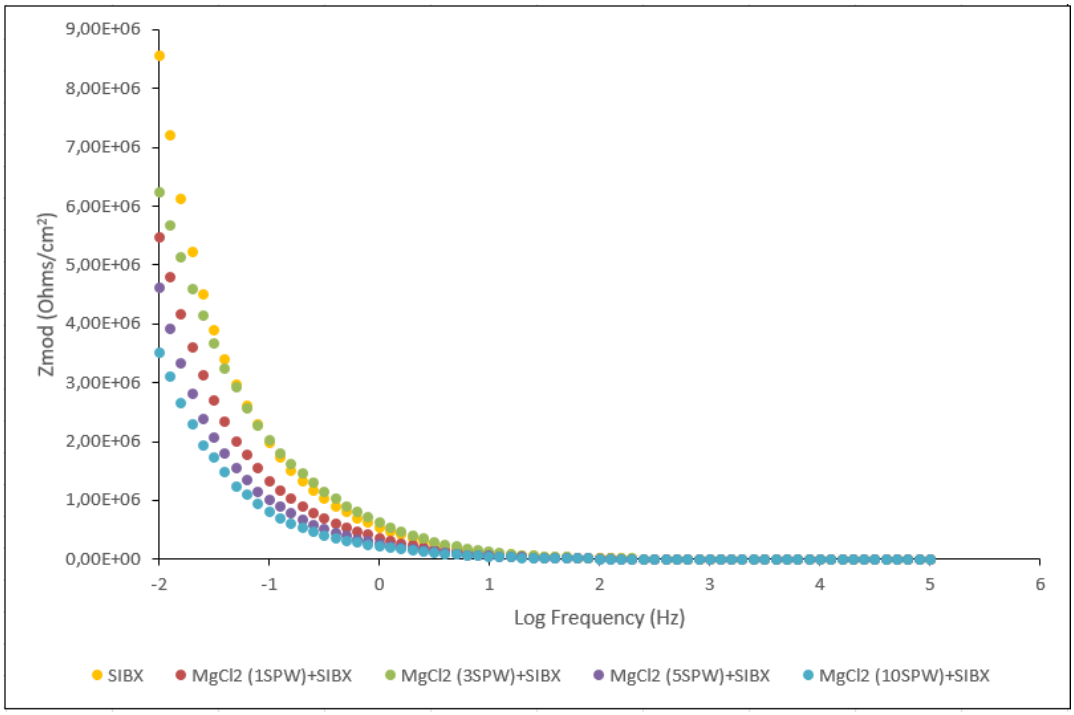

Figure 7.19: Bode plots of Z_{mod} (Ohms/cm^2) versus log frequency (Hz) for $PdTe_2$ in the absence and presence of $MgCl_2$ at increasing ionic strength with SIBX at a pH of 9.2 in O.O5 M $Na_2B_4O_7$.

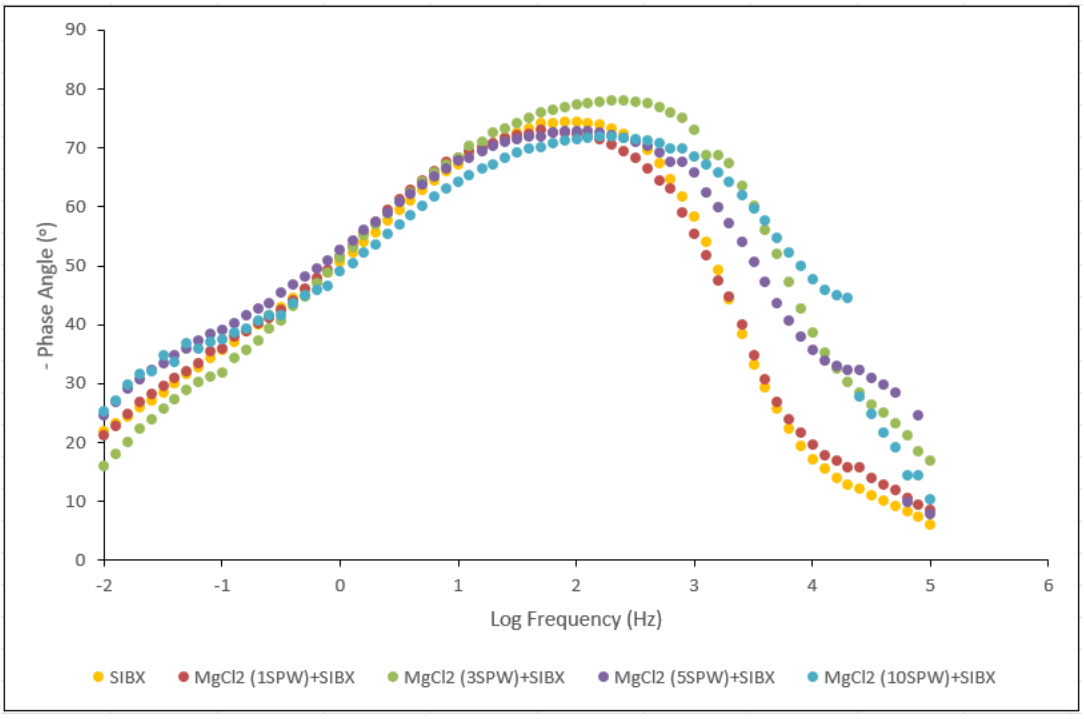

Figure 7.20: Bode plots of phase angle (°) versus log frequency for $PdTe_2$ in the absence and presence of $MgCl_2$ at increasing ionic strength with SIBX at a pH of 9.2 in O.O5 M $Na_2B_4O_7$.

Figures 7.18 to 7.20 plot Nyquist and Bode graphs in the absence and presence of $MgCl_2$ in SIBX. Generally, Figure 7.18 shows an increase in R_{ct} in the presence of $MgCl_2$ at all ionic strengths in

SIBX compared to Figure 7.15. Higher R_{ct} in the presence of SIBX implies a lower capacitance value, which could be attributable to the formation of a layer of oxidation products of SIBX or a layer with a smaller dielectric constant. It is evident in Figure 7.18 that higher R_{ct} was obtained in the absence of $MgCl_2$ than in the presence of $MgCl_2$. The higher R_{ct} illustrates a lower current flow for the electrochemical reactions occurring on the mineral surface. Hence, implying that the presence of $MgCl_2$ with SIBX increases the rate of electrochemical reactions taking place at the $PdTe_2$ mineral surface.

It is observed in Figure 7.19 that an increase in impedance values is achieved in $MgCl_2$ in the presence of SIBX than in the absence of SIBX, Figure 7.16. This observation could be attributable to the higher degree of the oxidation of SIBX that occurs on the mineral surface. However, it is clear that lower Z_{mod} values were attained with an increase in ionic strength, implying that the rate of adsorption of $MgCl_2$ with SIBX increased with an increase in ionic strength. In the low frequency domain, an appreciable difference in impedance values is seen at different ionic strengths of $MgCl_2$. This could possibly suggest the formation of significant continuous surface layers on the mineral surface due to the adsorption of xanthate ions and the formation of dixanthogen. Additionally, the higher Z_{mod} value in the absence of $MgCl_2$ denotes higher R_{ct} as shown in the Nyquist plot. Ultimately, the Nyquist plot and Bode plot showing lower phase angle indicate that the reactions occurring on the $PdTe_2$ mineral surface in $MgCl_2$ in the presence of SIBX could be associated with mainly interfacial kinetics.

7.3.4 Effect of $CaCl_2$

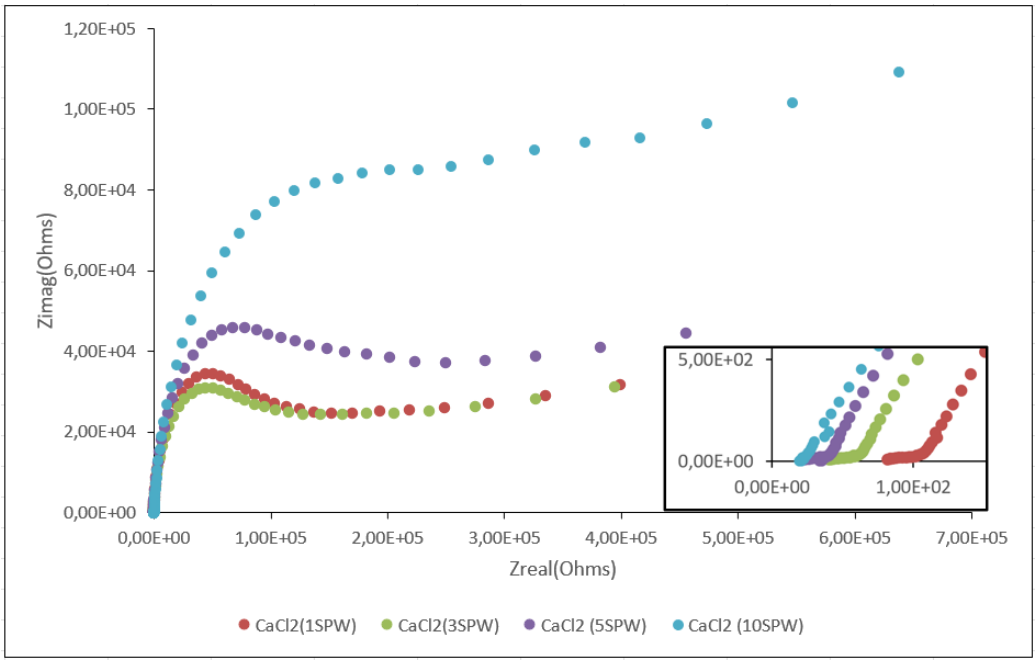

Figure 7.21: Nyquist plots for $PdTe_2$ in the presence of $CaCl_2$ at increasing ionic strength at a pH of 9.2 in O.O5 M $Na_2B_4O_7$.

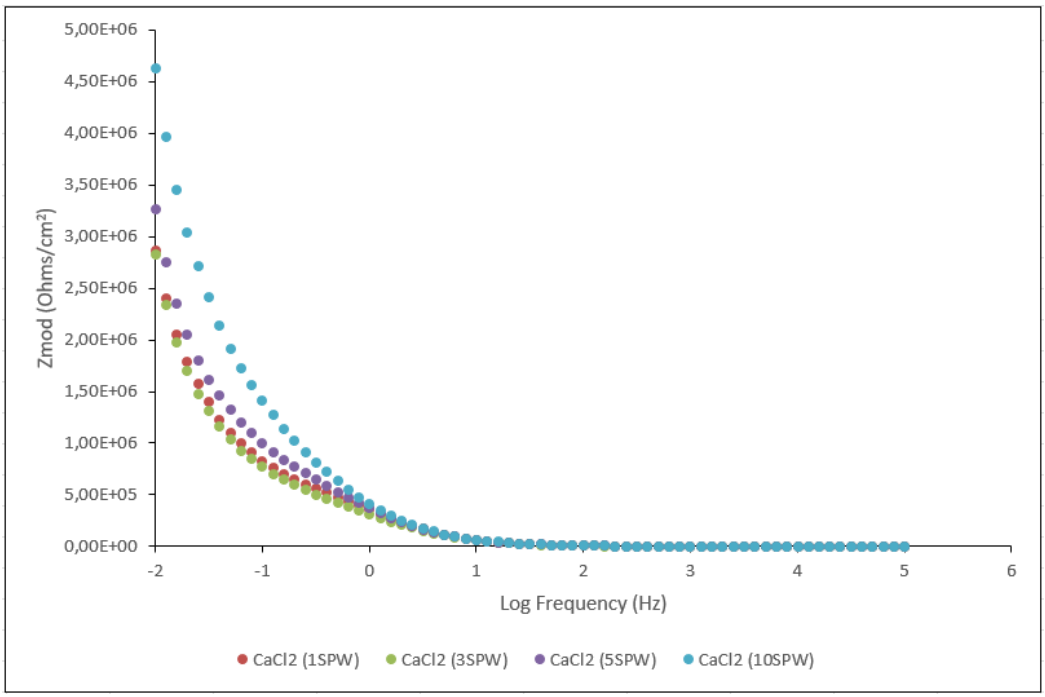

Figure 7.22: Bode plots of Z_{mod} (Ohms/cm^2) versus log frequency (Hz) for $PdTe_2$ in the presence of $CaCl_2$ at increasing ionic strength at a pH of 9.2 in O.O5 M $Na_2B_4O_7$.

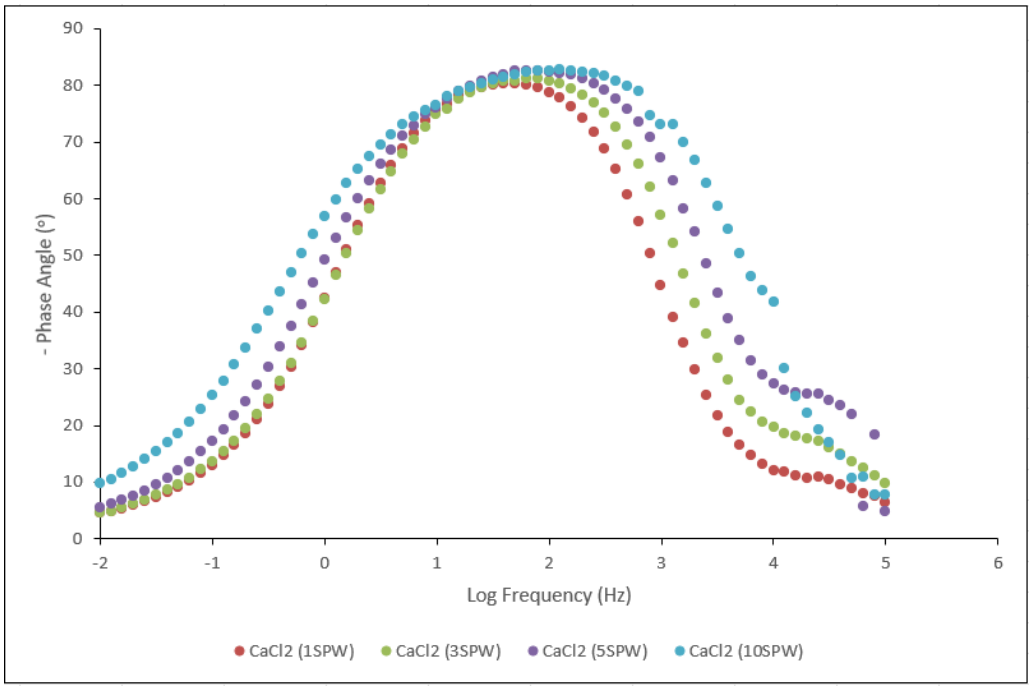

Figure 7.23: Bode plots of phase angle (°) versus log frequency for $PdTe_2$ in the presence of $CaCl_2$ at increasing ionic strength at a pH of 9.2 in O.O5 M $Na_2B_4O_7$.

Figures 7.21 to 7.23 show Nyquist and Bode plots for $PdTe_2$ in the absence and presence of $CaCl_2$ at increasing ionic strength. It is apparent in Figure 7.21 that the electron transfer reactions occurring at the $PdTe_2$ mineral surface were due to interfacial kinetics. This observation corresponds to the lower phase angles obtained in Figure 7.23. However, a clear increase in R_{ct} is shown with an increase in ionic strength. This therefore suggests lower rates of electrochemical reactions with an increase in ionic strength. Higher R_{ct} for the highest ionic strength of $CaCl_2$ is seen to correspond to the high impedance values obtained in the Bode plot in Figure 7.22. Moreover, R_s was observed to decrease with an increase in ionic strength.

Additionally, Figure 2.22 shows lower Z_{mod} values at lower ionic strengths, implying higher rates of adsorption of $CaCl_2$ on the mineral surface. A pronounced change in impedance values between $CaCl_2$ at 10 SPW and other lower ionic strengths was observed. This could be attributed to the significant difference in the formation of continuous surface layers on $PdTe_2$. The lower Z_{mod} values displayed at lower ionic strength indicate higher capacitive behaviour and higher current flow for the electrochemical reactions on the mineral surface. Furthermore, the capacitive behavior caused by the electrical double layer at the electrode/solution interface was demonstrated by the inverse relationship developed from the slopes generated towards the medium frequency range between impedance and frequency and the phase angles were determined to be

approximately - 80°. Moreover, in the higher frequency domain, it is shown that Z_{mod} values are low and relatively constant whilst the phase angle values decrease to zero.

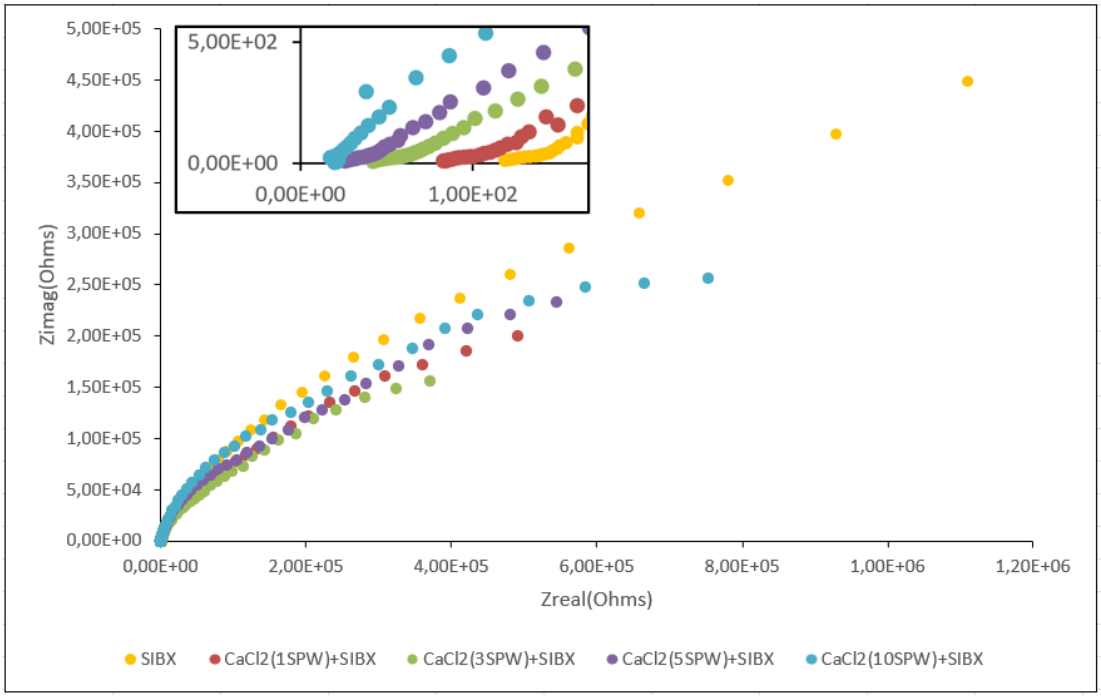

Figure 7.24: Nyquist plots for $PdTe_2$ in the absence and presence of $CaCl_2$ at increasing ionic strength with SIBX at a pH of 9.2 in O.O5 M $Na_2B_4O_7$.

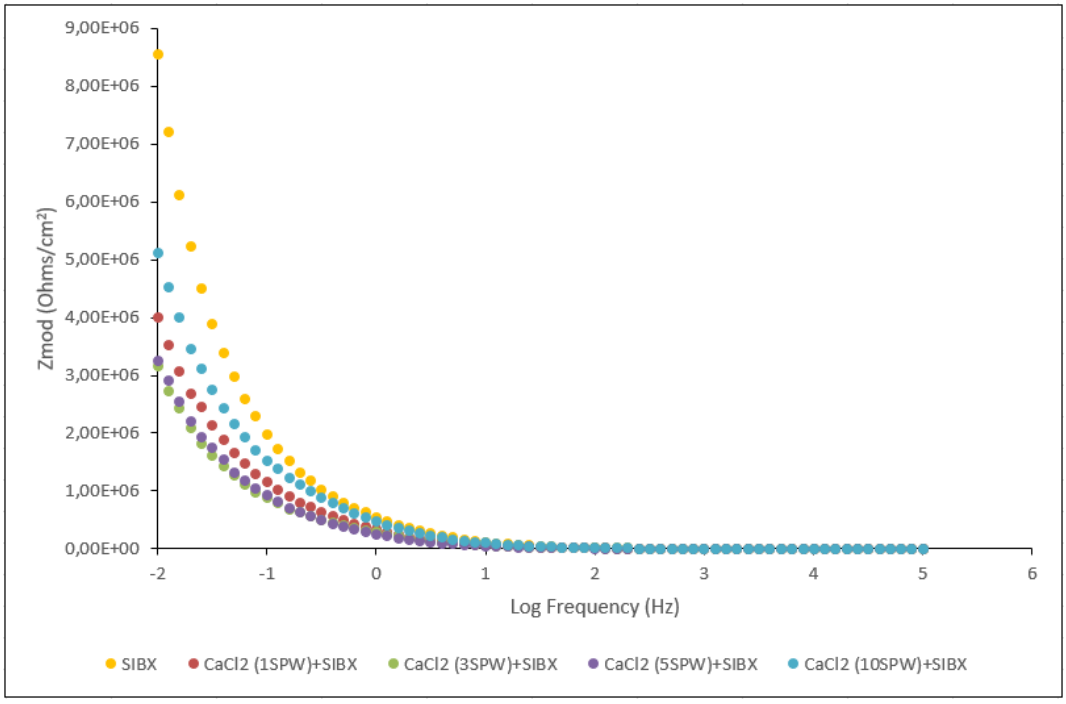

Figure 7.25: Bode plots of Z_{mod} (Ohms/cm^2) versus log frequency (Hz) for $PdTe_2$ in the absence and presence of $CaCl_2$ at increasing ionic strength with SIBX at a pH of 9.2 in O.O5 M $Na_2B_4O_7$.

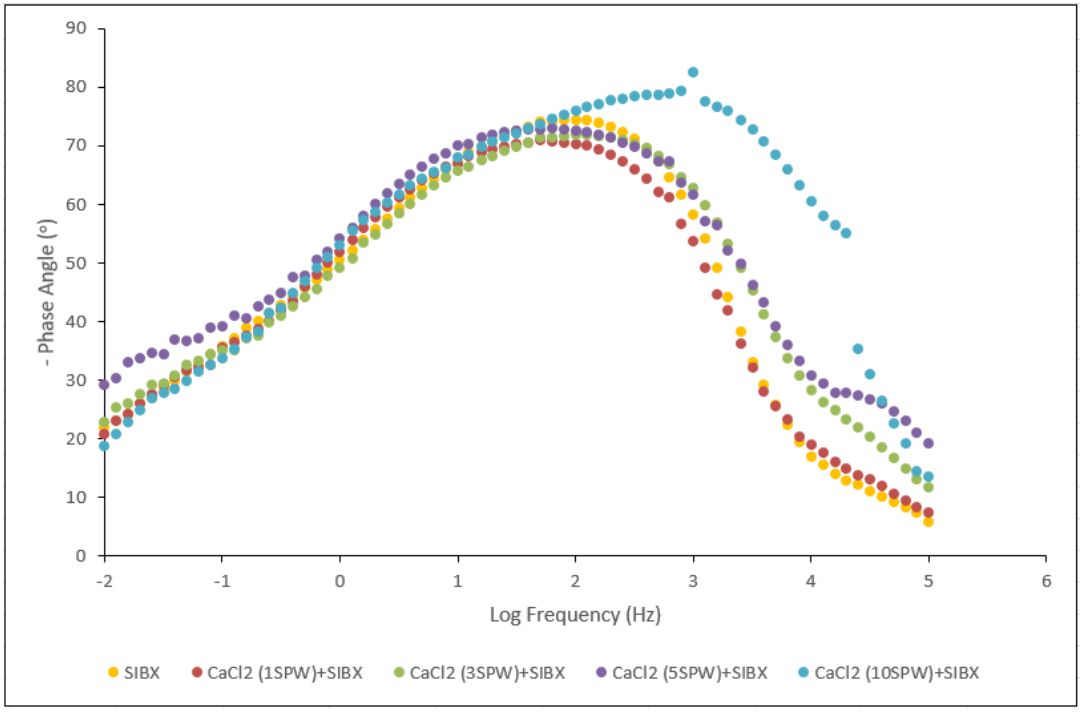

Figure 7.26: Bode plots of phase angle (°) versus log frequency for $PdTe_2$ in the absence and presence of $CaCl_2$ at increasing ionic strength with SIBX at a pH of 9.2 in O.O5 M $Na_2B_4O_7$.

Figures 7.24 to 7.26 demonstrate Nyquist and Bode plots in the absence and presence of $CaCl_2$ in SIBX. Generally, it is demonstrated in Figure 7.24 that R_{ct} for $CaCl_2$ at all ionic strengths was higher in the presence of SIBX than in $CaCl_2$ only (Figure 7.21). Higher R_{ct} values indicate lower capacitive behaviour. Lower capacitance may be associated with a lower dielectric constant due to the adsorption and oxidation of SIBX to dixanthogen on the mineral surface. However, Figure 7.24 displays a decrease in R_{ct} with a decrease in ionic strength. This suggests that $PdTe_2$ displayed higher rates of electrochemical reactions at lower ionic strengths of $CaCl_2$. Additionally, similar to other salts investigated, R_s decreased with an increase in ionic strength in the case of $CaCl_2$.

Furthermore, Figure 7.25 shows lower Z_{mod} values in the presence of $CaCl_2$ in SIBX than in SIBX only. This implies a higher rate of adsorption of $CaCl_2$ ions and SIBX. The Bode plot shown in Figure 7.25 demonstrates that adsorption of $CaCl_2$ ions on the $PdTe_2$ mineral surface inhibits the adsorption and oxidation of SIBX. Moreover, the noticeable difference in impedance values in the low frequency range indicates the formation of continuous layers owing to the presence of $CaCl_2$ and/or SIBX. Conclusively, it is important to note that the points obtained for phase angles in Figure 7.26, at the highest ionic strength looked distorted at in the higher frequency domain, this could be assigned to be precipitate formed at 10 SPW.

7.3.5 Effect of NaCl

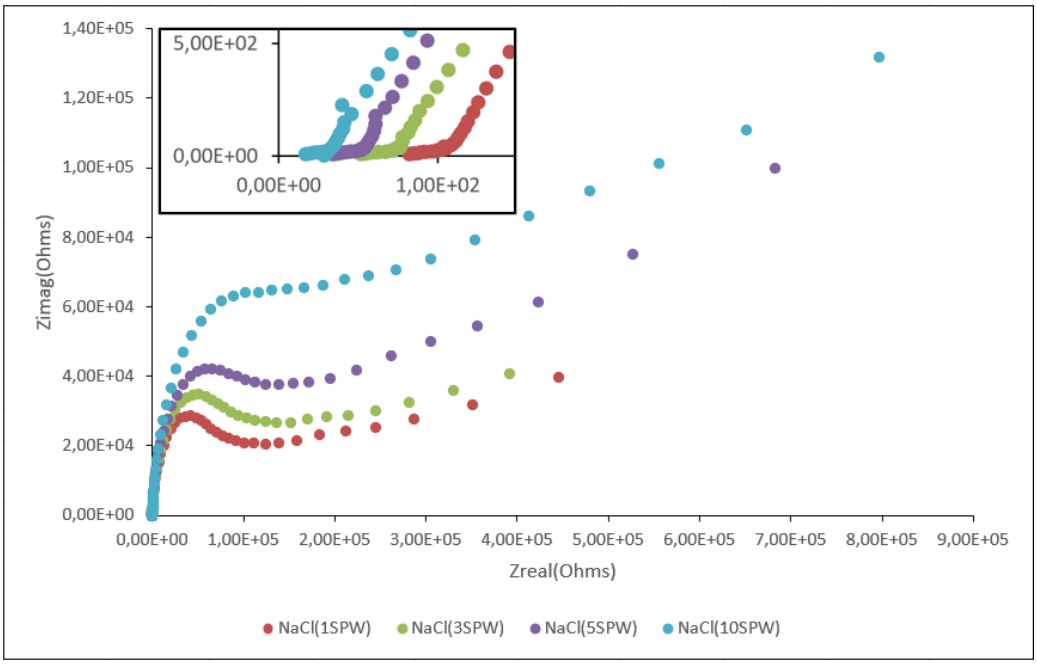

Figure 7.27: Nyquist plots for $PdTe_2$ in the presence of NaCl at increasing ionic strength at a pH of 9.2 in O.O5 M $Na_2B_4O_7$.

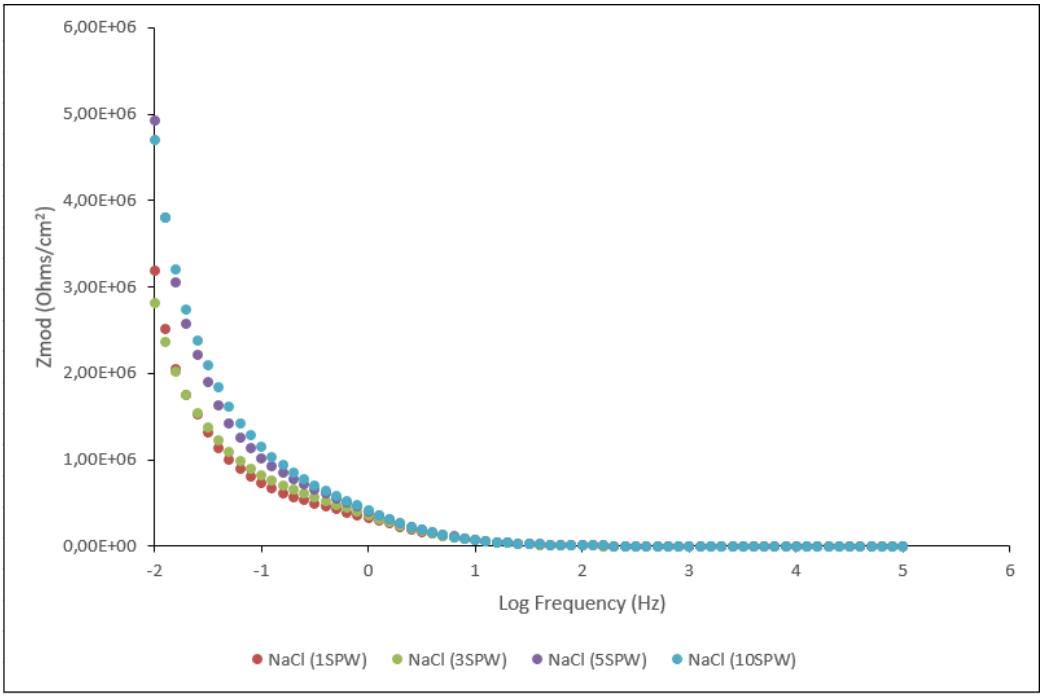

Figure 7.28: Bode plots of Z_{mod} (Ohms/cm^2) versus log frequency (Hz) for $PdTe_2$ in the presence of NaCl at increasing ionic strength at a pH of 9.2 in O.O5 M $Na_2B_4O_7$.

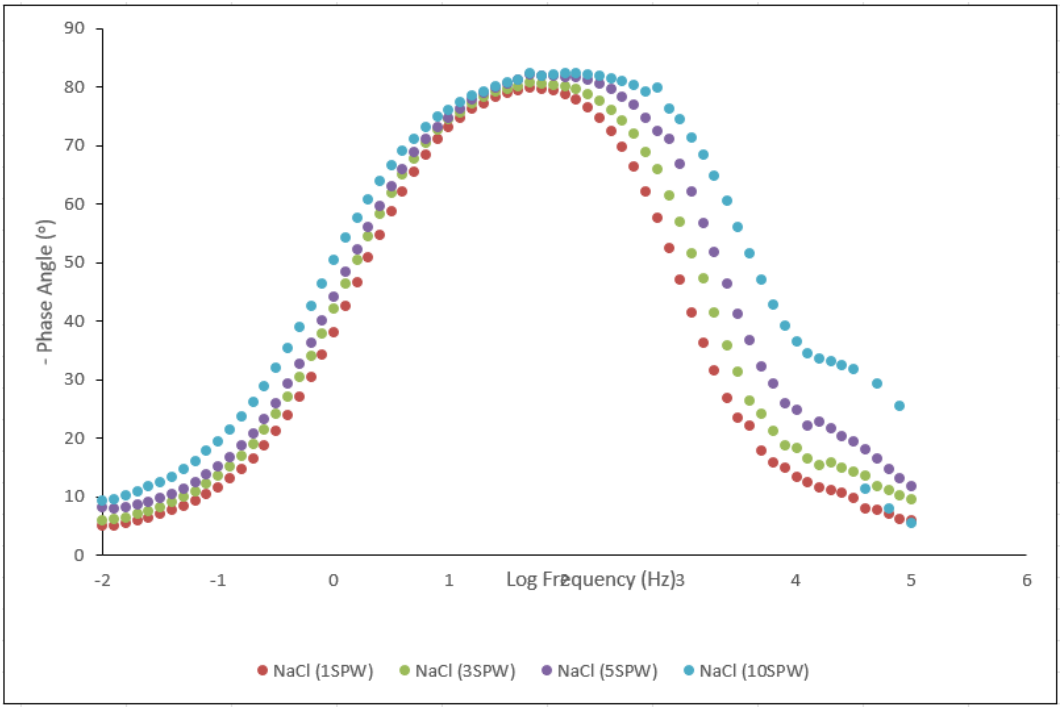

Figure 7.29: Bode plots of phase angle (°) versus log frequency for $PdTe_2$ in the presence of NaCl at increasing ionic strength at a pH of 9.2 in O.O5 M $Na_2B_4O_7$.

Figures 7.27 to 7.29 exhibit Nyquist and Bode plots for $PdTe_2$ in the presence of NaCl at increasing ionic strength. It is evident in Figure 7.27 that in the higher frequency range, impedance for $PdTe_2$ in the presence of NaCl was attributed mainly to interfacial kinetics. It is clear that in the lower frequency range at 5 SPW and 10 SPW, the electron transfer reactions occurring on the mineral surface are probably influenced by diffusion-limited processes. However, it is clearly observed that R_{ct} increases with an increase in ionic strength. Implying that an increase in ionic strength of NaCl, decreased the rate of electrochemical reactions on $PdTe_2$. Furthermore, a decrease in R_s is observable with an increase in ionic strength.

The higher impedance values obtained in Figure 7.28 at higher ionic strengths correspond to the higher R_{ct} attained in Figure 7.27. Higher impedance values indicate lower capacitive behaviour. This therefore suggests the generation of either a thicker oxide layer or a layer with a smaller dielectric constant. It is clear that the rate of adsorption of NaCl ions is higher at lower ionic strengths, as denoted by the lower impedance values. The changes in impedance values in the low frequency domain indicate the formation of continuous surface layers on the mineral surface, owing to the adsorption of NaCl ions. It is visible that at a higher frequency domain, the impedance values are very low and constant, whilst at the same time the phase angle values approach zero. This observation suggests a common response of a resistor to an AC with high frequency,

correlating to R_s. Accordingly, the phase angles at all investigated ionic strengths of NaCl were found to be approximately – 80°, hence indicating a capacitive behaviour caused by the electrical double layer.

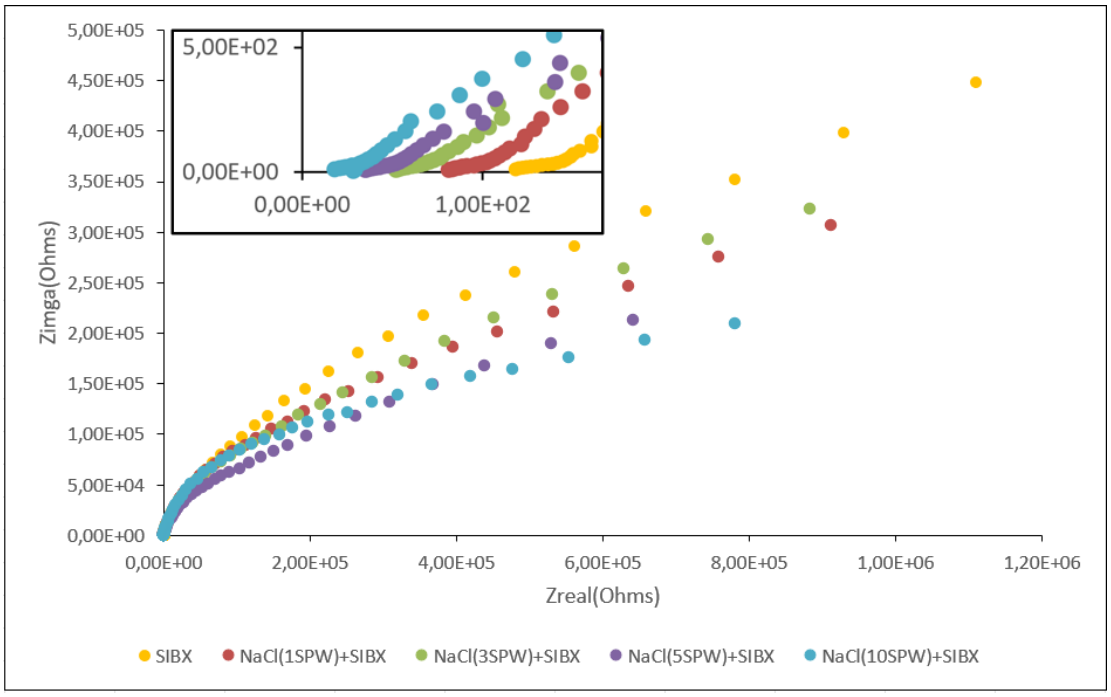

Figure 7.30: Nyquist plots for $PdTe_2$ in the absence and presence of NaCl at increasing ionic strength with SIBX at a pH of 9.2 in O.O5 M $Na_2B_4O_7$.

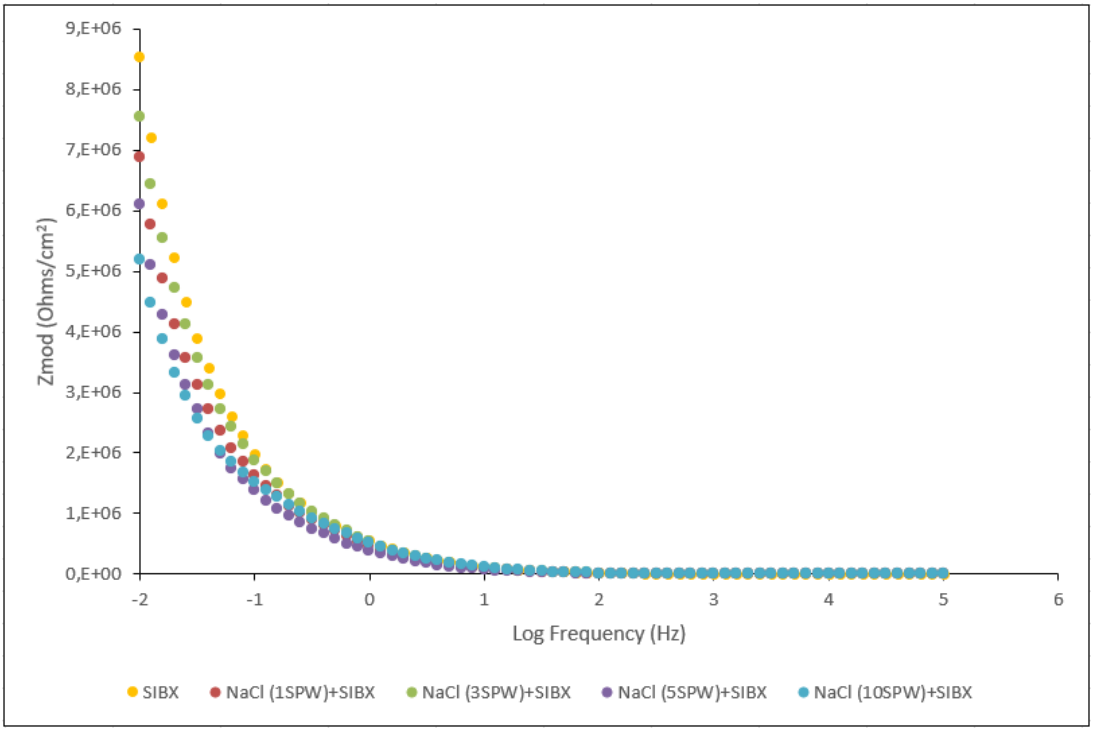

Figure 7.31: Bode plots of Z_{mod} (Ohms/cm^2) versus log frequency (Hz) for $PdTe_2$ in the absence and presence of NaCl at increasing ionic strength with SIBX at a pH of 9.2 in O.O5 M $Na_2B_4O_7$.

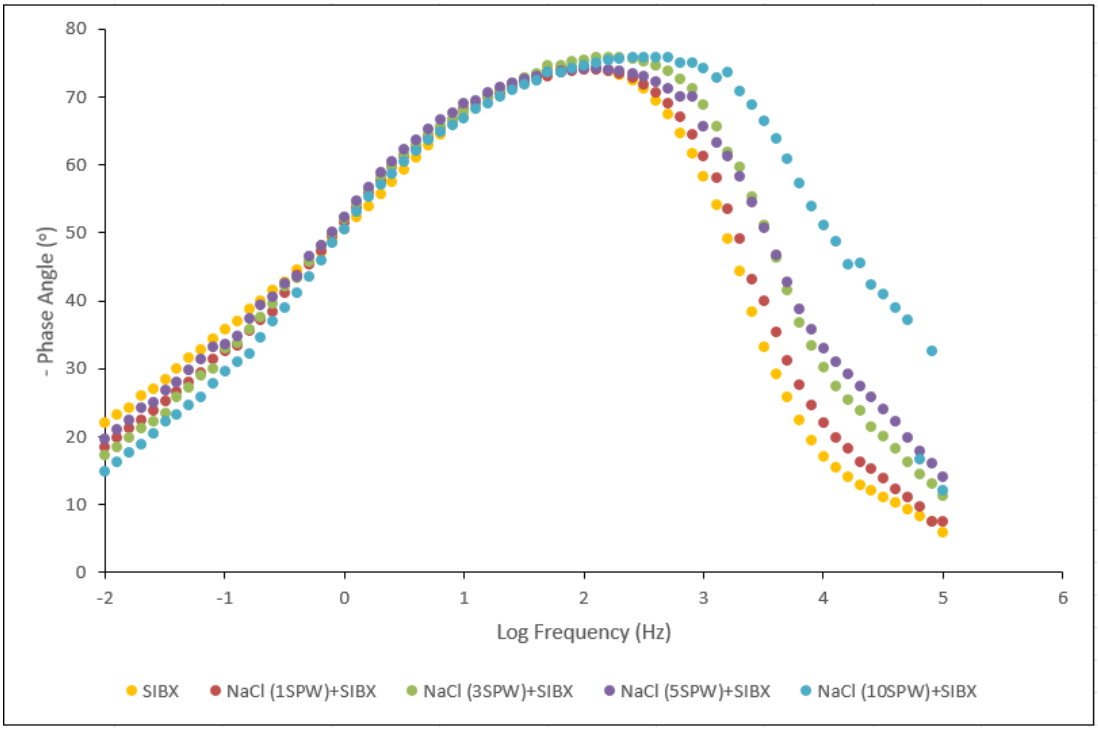

Figure 7.32: Bode plots of phase angle (°) versus log frequency for $PdTe_2$ in the absence and presence of NaCl at increasing ionic strength with SIBX at a pH of 9.2 in O.O5 M $Na_2B_4O_7$.

Figures 7.30 to 7.32 display Nyquist and Bode plots for $PdTe_2$ in the absence and presence of NaCl at increasing ionic strength in SIBX. It can be discerned from the Nyquist plot in Figure 7.30 that higher R_{ct} values were obtained in the presence of SIBX than in the absence of SIBX (Figure 7.27). The higher resistance values in the presence of SIBX correspond to lower capacitive behaviour, which could be associated with the adsorption of SIBX and generation of a surface oxidation layer due to the formation of oxidation products of SIBX on the mineral surface. Organic compounds such as xanthates are known to have smaller dielectric constants, which result in lower capacitive behaviour of $PdTe_2$. Furthermore, it is apparent that in Figure 7.30, the reactions that occurred on the mineral surface were attributable to interfacial kinetics. However, a general decrease in R_{ct} is observed with an increase in ionic strength. Implying an increase in the rate of electrochemical reactions on the $PdTe_2$ mineral surface. It is noted that the Nyquist plots in Figure 7.27 and 7.30, in the absence of SIBX and in the presence of SIBX, respectively, show no significant difference in R_s. This observation therefore indicates that R_s was not affected by the chemical transformations that occurred on the mineral surface due to the adsorption of SIBX.

The higher Z_{mod} values obtained in Figure 7.31, in the presence of SIBX only correspond to high R_{ct} values displayed in the Nyquist plot. However, a slight decrease in Z_{mod} values is observed with an increase in ionic strength of NaCl in the presence of SIBX. This suggests a high rate of

adsorption of NaCl in the presence of SIBX at higher ionic strengths. The pronounced change in impedance values in the low frequency domain implies the formation of continuous surface layers on the mineral surface as a result of the adsorption of xanthate ions and the formation of dixanthogen on the mineral surface. Ultimately, the impedance data shown in Figure 7.31 shows that the adsorption of NaCl on the $PdTe_2$ slightly inhibits the adsorption and oxidation of SIBX on the mineral surface. Moreover, the rate at which NaCl inhibits the adsorption of SIBX increases with an increase in ionic strength.

7.3.6 Effect of salts at 1 SPW

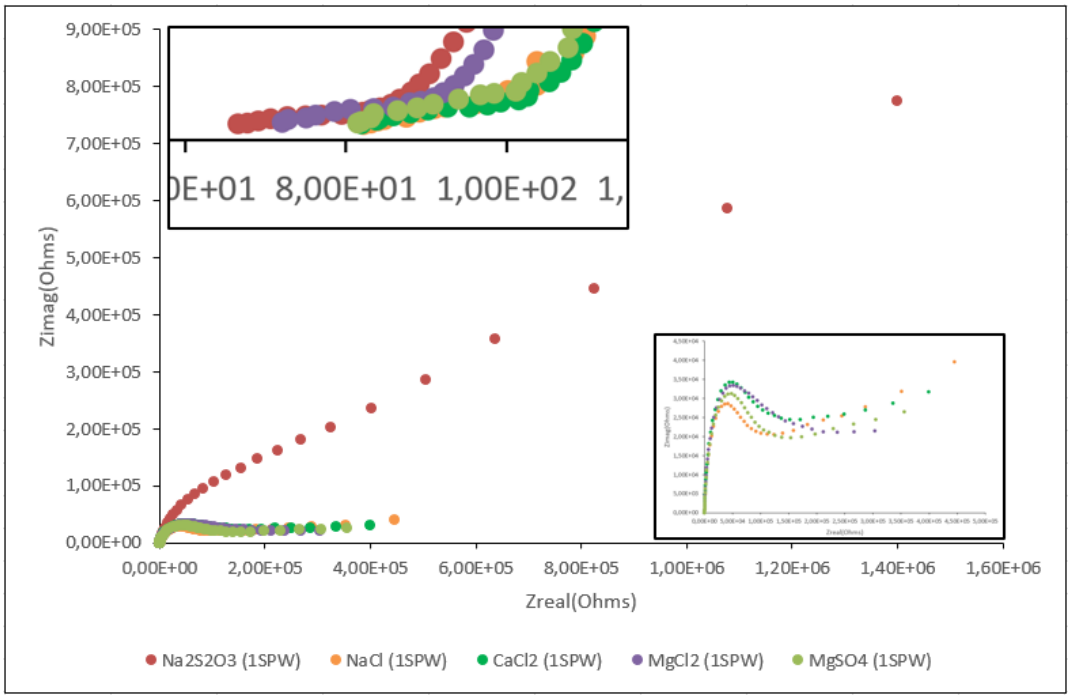

Figure 7.33: Nyquist plots for $PdTe_2$ in the presence of $Na_2S_2O_3$, NaCl, $CaCl_2$, $MgSO_4$, $MgCl_2$ at 1 SPW at a pH of 9.2 in 0.05 M $Na_2B_4O_7$.

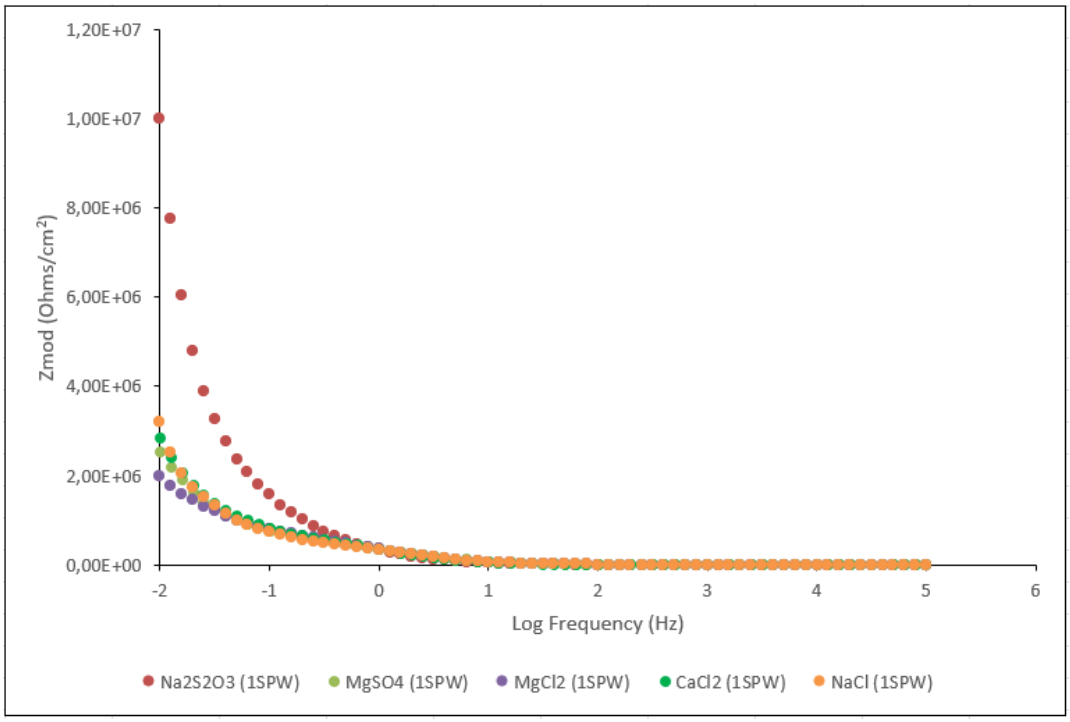

Figure 7.34: Bode plots of Z_{mod} (Ohms/cm^2) versus log frequency (Hz) for $PdTe_2$ in the presence of $Na_2S_2O_3$, NaCl, $CaCl_2$, $MgSO_4$, $MgCl_2$ at 1 SPW at a pH of 9.2 in O.O5 M $Na_2B_4O_7$.

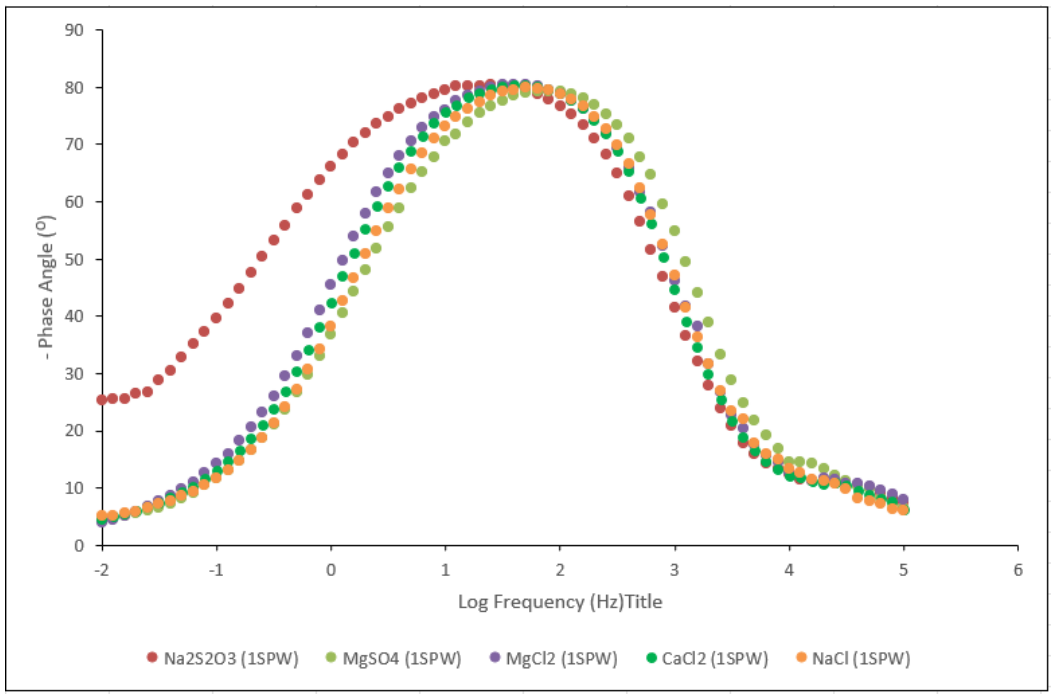

Figure 7.35: Bode plots of phase angle (°) versus log frequency for $PdTe_2$ in the presence of $Na_2S_2O_3$, NaCl, $CaCl_2$, $MgSO_4$, $MgCl_2$ at 1 SPW at a pH of 9.2 in O.O5 M $Na_2B_4O_7$.

Figures 7.33 to 7.35 show Nyquist and Bode plots in the presence of $Na_2S_2O_3$, $MgSO_4$, $MgCl_2$, $CaCl_2$ and NaCl at 1 SPW. Figure 7.33 clearly shows that $Na_2S_2O_3$ displayed a higher R_{ct} compared to other salts. This observation corresponds to the higher impedance values obtained in Figure

7.34. The Nyquist plot in Figure 7.33 further shows that impedance for all conditions investigated is dominated by interfacial kinetics. The order of decrease in R_{ct} was determined to be $Na_2S_2O_3$ > $CaCl_2$ > $MgCl_2$ > $MgSO_4$ > NaCl. $PdTe_2$ showed lower R_{ct} in the presence of NaCl, indicating better rates of reactions on $PdTe_2$ than with other salts. On the other hand, R_s was observed to decrease in the order $MgSO_4$ ≈ $CaCl_2$ ≈ NaCl > $MgCl_2$ > $Na_2S_2O_3$.

It is apparent in Figure 7.34 that in the lower frequency range, impedance increased in the order $MgCl_2$ < $MgSO_4$ < $CaCl_2$ < NaCl < $Na_2S_2O_3$, implying a decrease in the rate of adsorption of the salts on the mineral surface. Furthermore, it can be seen that in the low frequency domain, continuous surface layers formed at the same rate in the presence of $MgCl_2$, $MgSO_4$, $CaCl_2$ and NaCl. Higher impedance values indicate lower capacitive behaviour thereby indicating that a thicker oxide layer formed in the case of $Na_2S_2O_3$. Moreover, the Bode plot in Figure 7.35 shows that possibly the reactions occurring on $PdTe_2$ in the presence of $Na_2S_2O_3$ could be associated with interfacial kinetics.

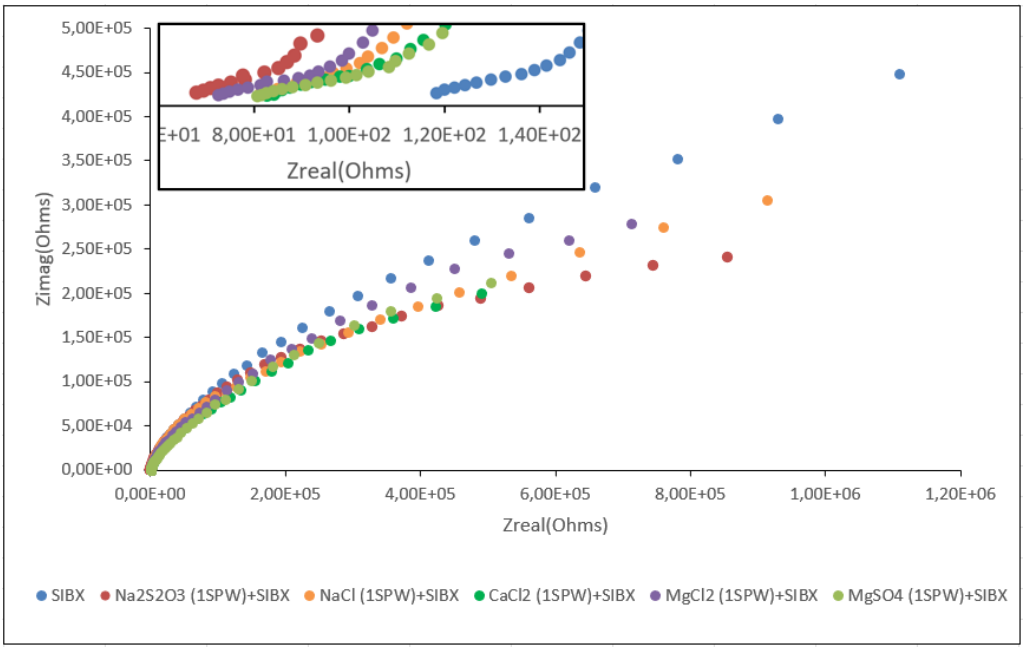

Figure 7.36: Nyquist plots for $PdTe_2$ in the absence and presence of $Na_2S_2O_3$, NaCl, $CaCl_2$, $MgSO_4$, $MgCl_2$ at 1 SPW with SIBX at a pH of 9.2 in O.O5 M $Na_2B_4O_7$.

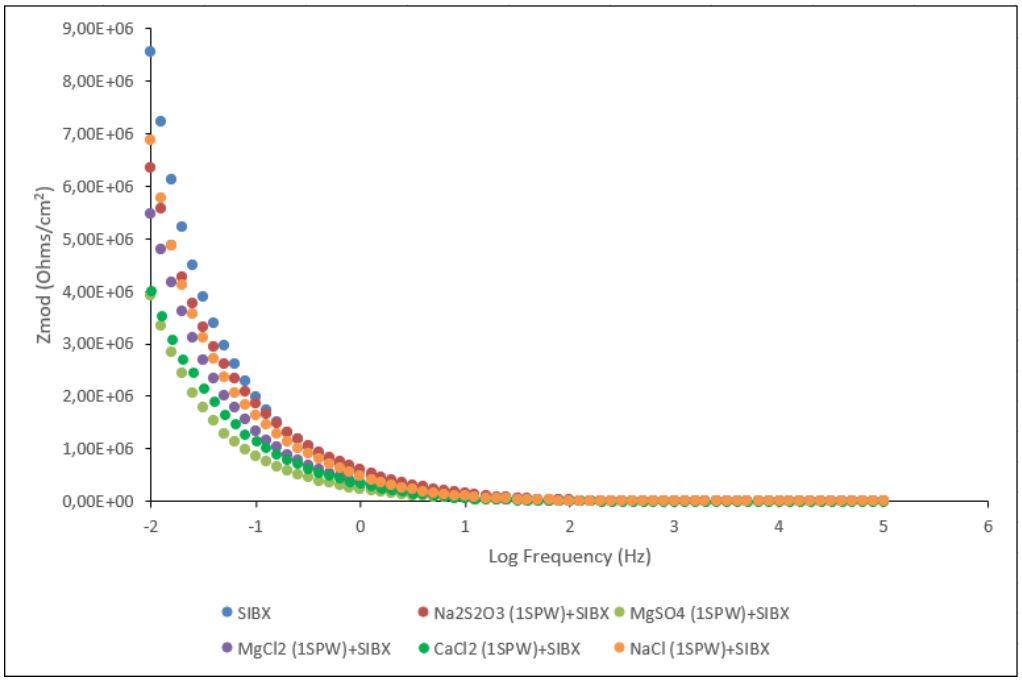

Figure 7.37: Bode plots of Z_{mod} (Ohms/cm^2) versus log frequency (Hz) for $PdTe_2$ in the absence and presence of $Na_2S_2O_3$, NaCl, $CaCl_2$, $MgSO_4$, $MgCl_2$ at 1 SPW with SIBX at a pH of 9.2 in O.O5 M $Na_2B_4O_7$.

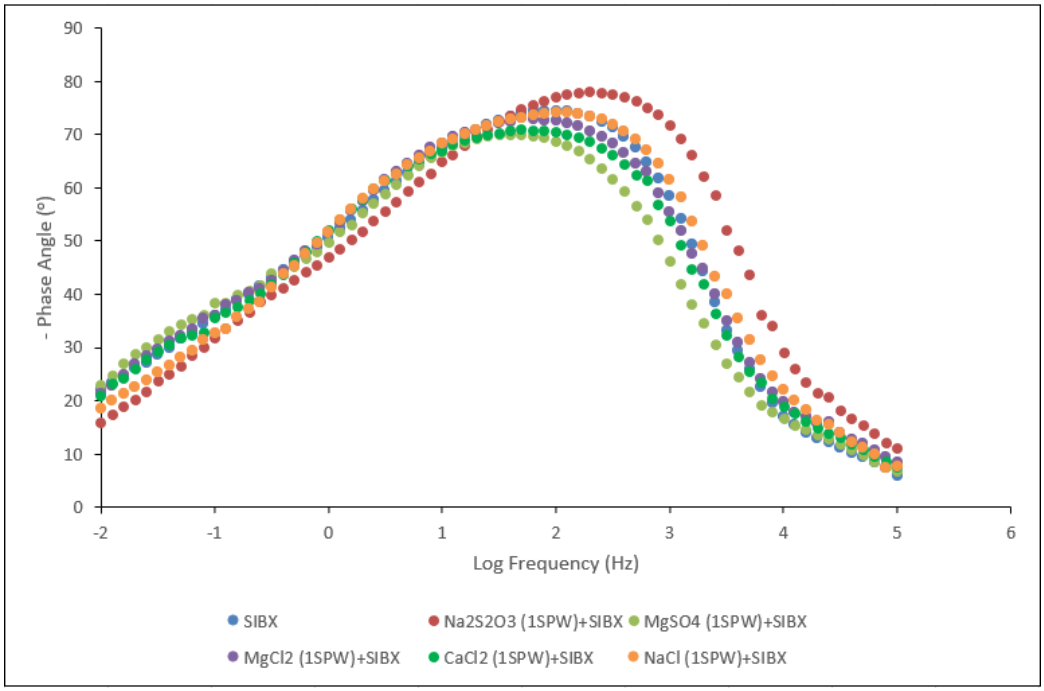

Figure 7.38: Bode plots of phase angle (°) versus log frequency for $PdTe_2$ in the absence and presence of $Na_2S_2O_3$, NaCl, $CaCl_2$, $MgSO_4$, $MgCl_2$ at 1 SPW with SIBX at a pH of 9.2 in O.O5 M $Na_2B_4O_7$.

Figures 7.36 to 7.38 display Nyquist and Bode plots in the presence of $Na_2S_2O_3$, $MgSO_4$, $MgCl_2$, $CaCl_2$ and NaCl at 1 SPW in SIBX. It is noticeable from Figure 7.36 that R_{ct} of $PdTe_2$ in the

presence of $Na_2S_2O_3$ showed a pronounced decrease in the presence of SIBX compared to Figure 7.33, in the absence of SIBX. The decrease in R_{ct} is attributable to negatively charged xanthate ions that bind onto the mineral surface and are subsequently oxidized to dixanthogen, hence, transferring charges to the $PdTe_2$ mineral surface. Consequently, the charge transfer is promoted, therefore resulting in a decrease in charge transfer resistance (Mu et al., 2015). Alternatively, an increase in R_{ct} exhibited by $MgSO_4$, $MgCl_2$, $CaCl_2$ and NaCl in the presence of SIBX compared to Figure 7.33, in the absence of SIBX, could be assigned to higher capacitive behaviour owing to a higher current flow for the electrochemical reactions occurring on the $PdTe_2$ mineral surface (Ekmekçi et al., 2010a). The R_s both in the absence and presence of SIBX, Figures 7.33 and 7.36, respectively, did not significantly differ, implying that this resistance was not affected by the chemical transformations that transpired at the mineral surface.

Figure 7.37 reveals that Z_{mod} values decrease in the order SIBX > NaCl > $Na_2S_2O_3$ > $MgCl_2$ > $CaCl_2$ > $MgSO_4$, indicating that the rate of adsorption on the mineral surface is faster in the presence of salts than in their absence. Therefore, the rates of adsorption on $PdTe_2$ increased in the order SIBX < NaCl < $Na_2S_2O_3$ < $MgCl_2$ < $CaCl_2$ < $MgSO_4$. Conclusively, the lower phase angles for all the conditions investigated, as shown in Figure 7.38, indicate that the electron transfer reactions occurring on the mineral surface are mainly attributed by interfacial kinetics.

7.3.7 Effect of salts at 3 SPW

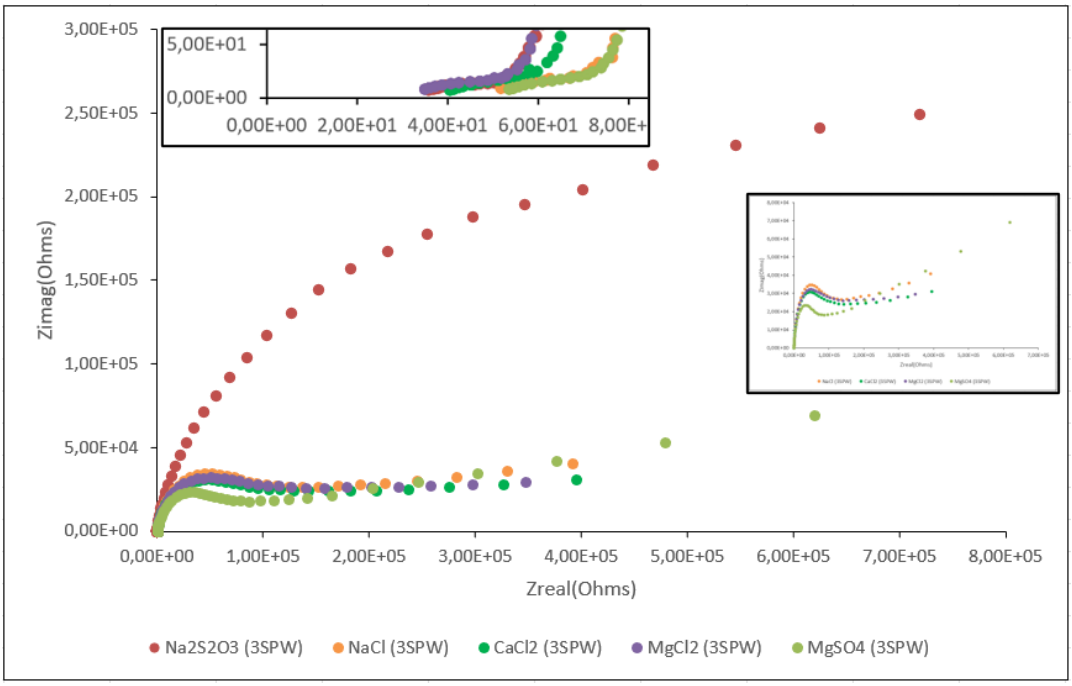

Figure 7.39: Nyquist plots for $PdTe_2$ in the presence of $Na_2S_2O_3$, NaCl, $CaCl_2$, $MgSO_4$, $MgCl_2$ at 3 SPW at a pH of 9.2 in O.O5 M $Na_2B_4O_7$.

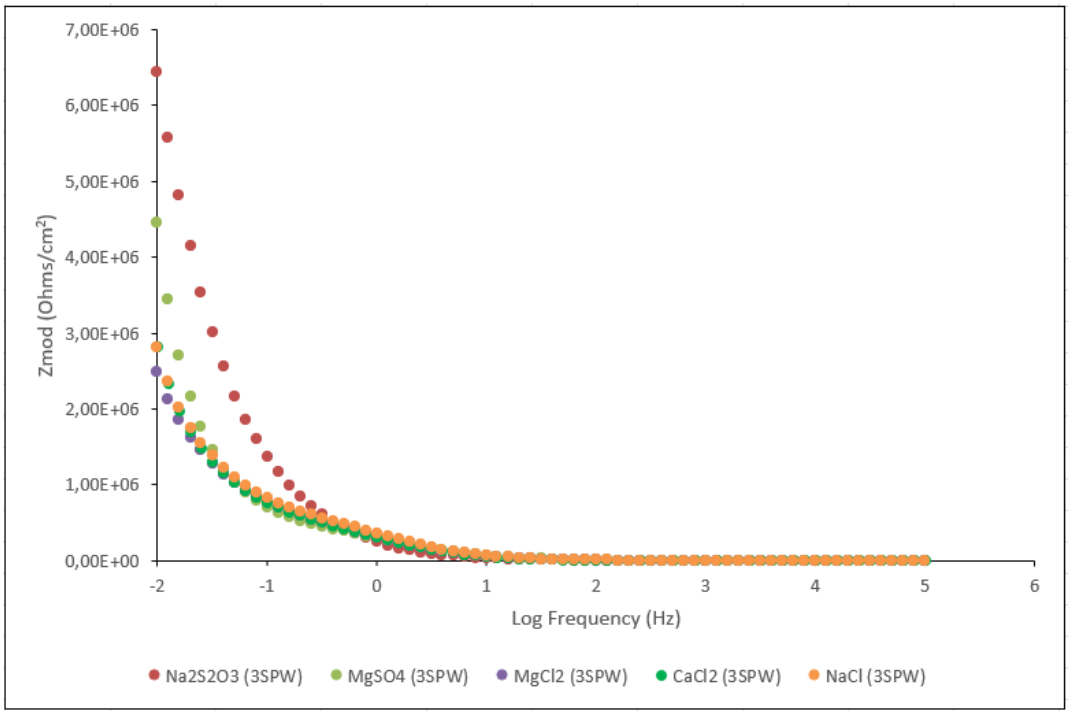

Figure 7.40: Bode plots of Z_{mod} (Ohms/cm^2) versus log frequency (Hz) for $PdTe_2$ in the presence of $Na_2S_2O_3$, NaCl, $CaCl_2$, $MgSO_4$, $MgCl_2$ at 3 SPW at a pH of 9.2 in O.O5 M $Na_2B_4O_7$.

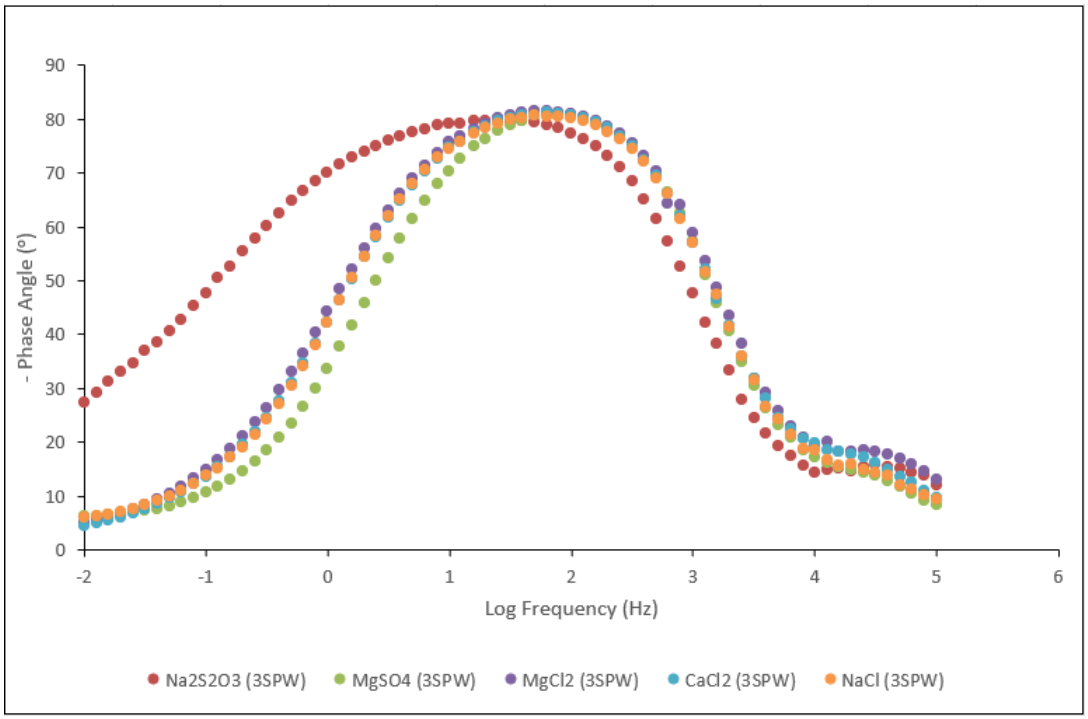

Figure 7.41: Bode plots of phase angle (°) versus log frequency for $PdTe_2$ in the presence of $Na_2S_2O_3$, NaCl, $CaCl_2$, $MgSO_4$, $MgCl_2$ at 3 SPW at a pH of 9.2 in O.O5 M $Na_2B_4O_7$.

Figures 7.39 to 7.41 depict Nyquist and Bode plots in the presence of $Na_2S_2O_3$, $MgSO_4$, $MgCl_2$, $CaCl_2$ and NaCl at 3 SPW. It is clear from Figure 7.39 that the R_{ct} for $PdTe_2$ in the presence of $Na_2S_2O_3$ was significantly higher than for other salts, therefore indicating a lower rate of electrochemical reactions on the mineral surface. A higher R_{ct} implies lower capacitance due to the formation of a thicker oxide layer or a layer with a smaller dielectric constant on the $PdTe_2$ mineral surface. Furthermore, the order of decrease in R_{ct} was observed to be $Na_2S_2O_3$ > NaCl > $MgCl_2$ > $CaCl_2$ > $MgSO_4$. In addition, the R_s was found to increase in the order $MgCl_2$ < $Na_2S_2O_3$ < $CaCl_2$ < NaCl < $MgSO_4$.

Figure 7.40 displayed lower Z_{mod} values for $MgCl_2$, $CaCl_2$ and NaCl suggesting a higher rate of adsorption on the $PdTe_2$ mineral surface. It is observable that the rate of adsorption of the investigated salts did not significantly differ. The higher Z_{mod} value obtained in the presence of $Na_2S_2O_3$ indicates higher R_{ct}, this is supported in the results observed in Figure 7.39. Moreover, the Bode plot in Figure 7.41 suggests that the electron transfer reactions on the $PdTe_2$ mineral surface occurring in the presence of all salts investigated at 3 SPW are mainly associated by interfacial kinetics. This is illustrated by a larger phase angle obtained in the presence of $Na_2S_2O_3$ than with other salts. Ultimately, it is apparent that the Bode plots show that at a higher frequency range the impedance values are low and relatively constant whilst the phase angle values approach

zero. This is typically a response expected for a resistor to an AC with high frequency, which corresponds to R_s. It is perceptible that the phase angles under the investigated conditions were determined to be approximately – 80°, which typically demonstrates a capacitive behaviour of the electrical double layer at the mineral/solution interface.

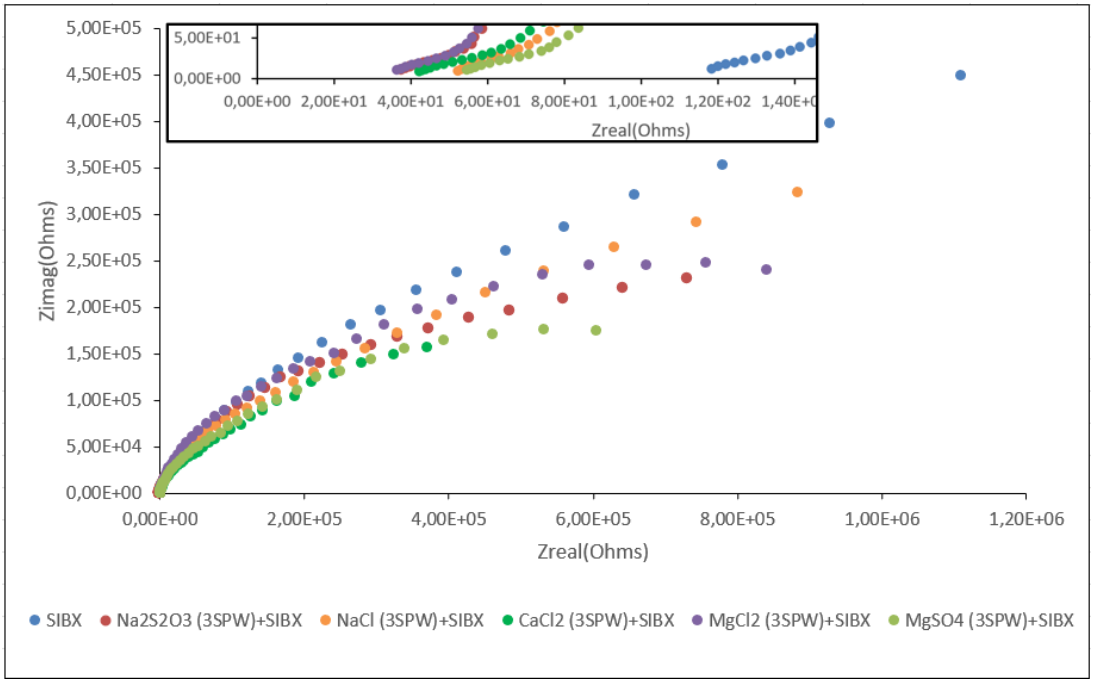

Figure 7.42: Nyquist plots for $PdTe_2$ in the absence and presence of $Na_2S_2O_3$, NaCl, $CaCl_2$, $MgSO_4$, $MgCl_2$ at 3 SPW with SIBX at a pH of 9.2 in O.O5 M $Na_2B_4O_7$.

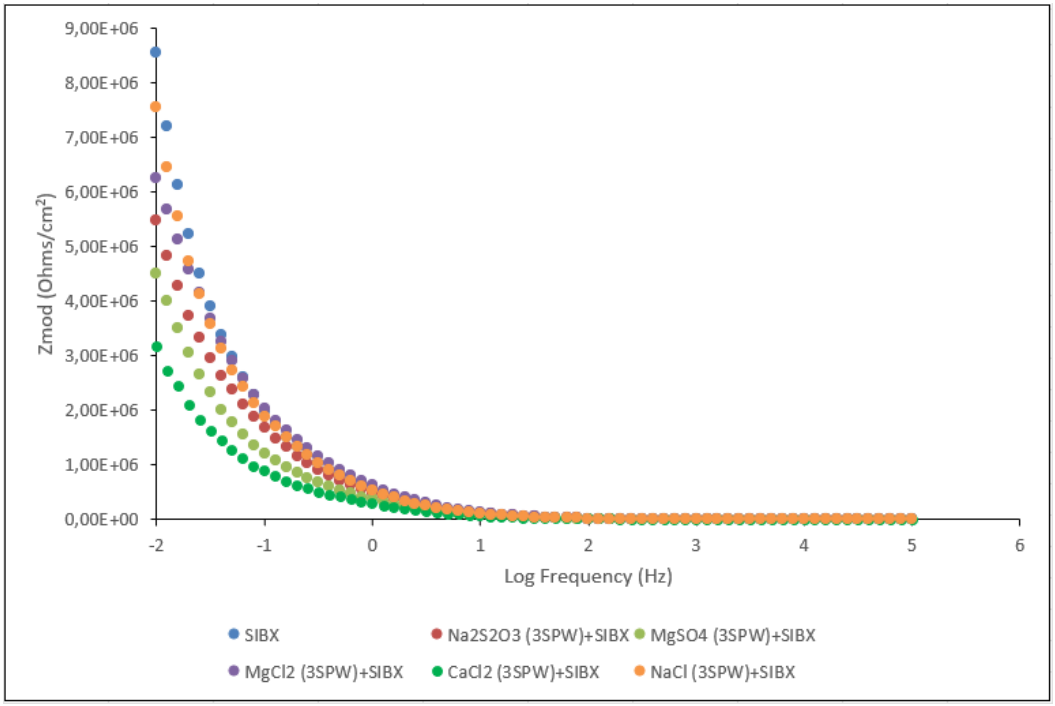

Figure 7.43: Bode plots of Z_{mod} (Ohms/cm^2) versus log frequency (Hz) for $PdTe_2$ in the absence and presence of $Na_2S_2O_3$, NaCl, $CaCl_2$, $MgSO_4$, $MgCl_2$ at 3 SPW with SIBX at a pH of 9.2 in O.O5 M $Na_2B_4O_7$.

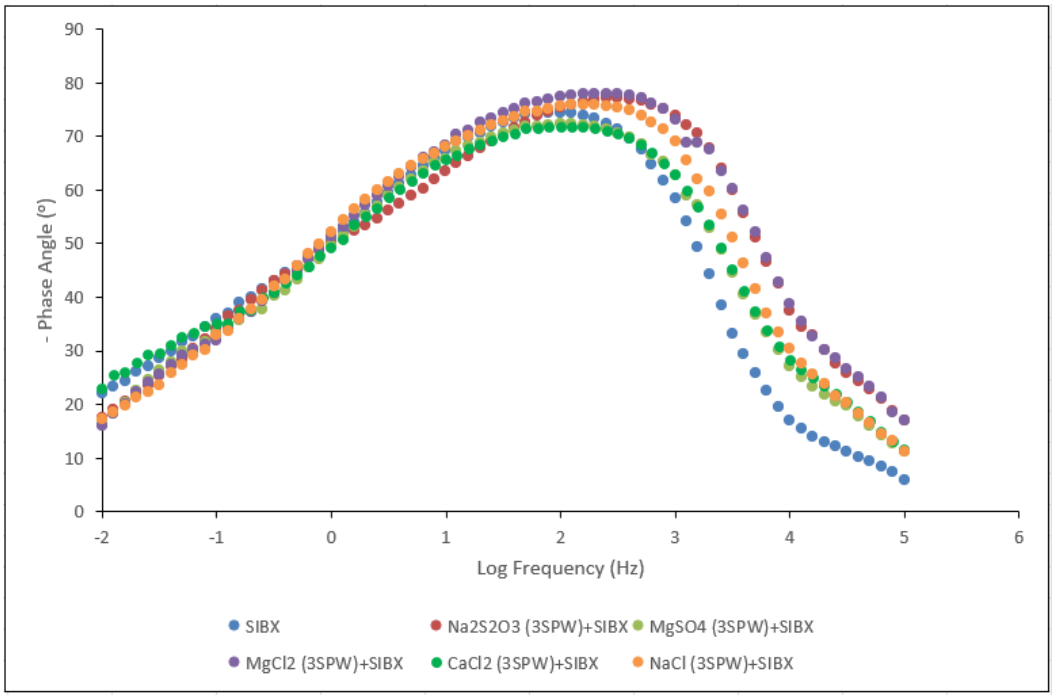

Figure 7.44: Bode plots of phase angle (°) versus log frequency for $PdTe_2$ in the absence and presence of $Na_2S_2O_3$, NaCl, $CaCl_2$, $MgSO_4$, $MgCl_2$ at 3 SPW with SIBX at a pH of 9.2 in O.O5 M $Na_2B_4O_7$.

Figures 7.42 to 7.44 exhibit Nyquist and Bode plots in the presence of $Na_2S_2O_3$, $MgSO_4$, $MgCl_2$, $CaCl_2$ and NaCl at 3 SPW in SIBX. A decrease in R_{ct} is observed in Figure 7.42 in the presence of $Na_2S_2O_3$ in SIBX than in the absence of SIBX (Figure 7.39). Figure 7.42 displays a slight decrease in R_{ct} in the presence of $Na_2S_2O_3$ in SIBX. This indicates a higher current for the electrochemical reactions on $PdTe_2$ in the presence of SIBX. In addition, the xanthate ions that attach onto the mineral surface are oxidized to dixanthogen thereby transferring charge to the mineral surface. Accordingly, the charge transfer process is achieved thereby affording a decrease in R_{ct}. However, it can be discerned from Figure 7.42 that the impedance of all conditions investigated was mainly influenced by interfacial kinetics. This observation is supported by the lower phase angles obtained in Figure 7.44. However, it is observable that R_{ct} increased in the order $CaCl_2 \approx MgSO_4 < Na_2S_2O_3 < MgCl_2 <$ NaCl < SIBX. An increase in R_{ct} indicates lower current flow for the electrochemical reactions taking place on the $PdTe_2$ mineral surface. Furthermore, a similar trend in R_s is noticeable both in the absence and presence of SIBX with the salts investigated, implying that R_s was not changed by the chemical transformations that transpired on the mineral surface in the presence of SIBX.

Generally, it was observed in the Bode plot in Figure 7.43 that adsorption on the mineral surface was faster in the presence of salts than with SIBX only. This is indicated by the decrease in Z_{mod}

values, which were found to occur in the order $CaCl_2$ < $MgSO_4$ < $Na_2S_2O_3$ < $MgCl_2$ < NaCl < SIBX. This suggests that the presence of these salts on the mineral surface inhibits the adsorption of SIBX. Additionally, the changes in impedance values in the low frequency domain in the presence of different salts were as a result of the difference in rates of formation of continuous surface layers on the mineral surface.

7.3.8 Effect of salts at 5 SPW

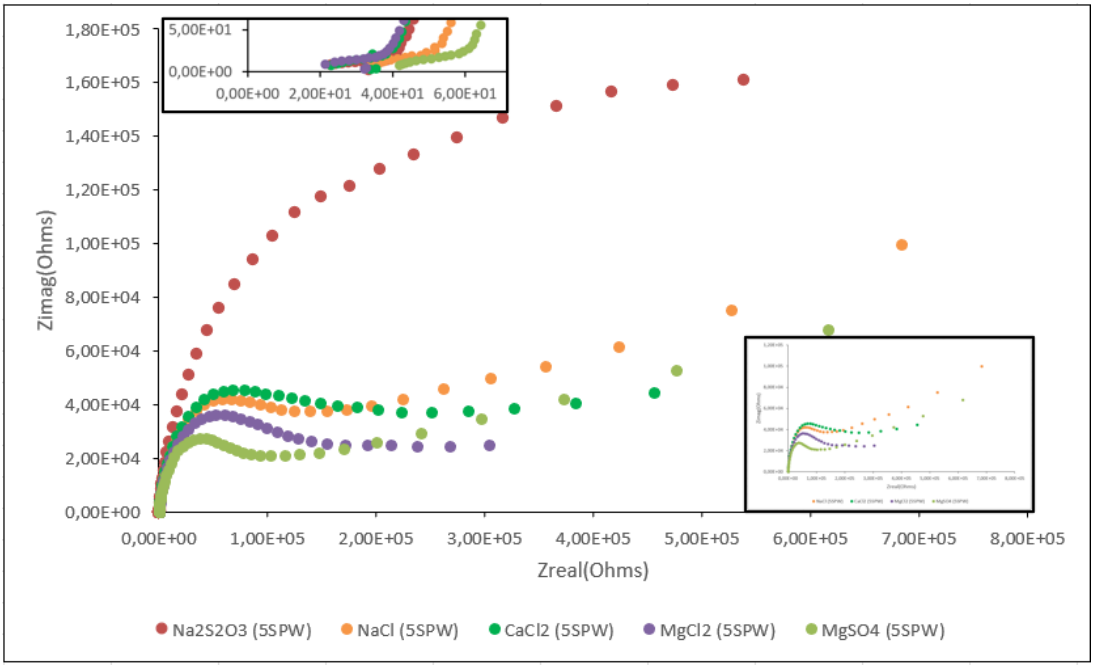

Figure 7.45: Nyquist plots for $PdTe_2$ in the presence of $Na_2S_2O_3$, NaCl, $CaCl_2$, $MgSO_4$, $MgCl_2$ at 5 SPW at a pH of 9.2 in O.O5 M $Na_2B_4O_7$.

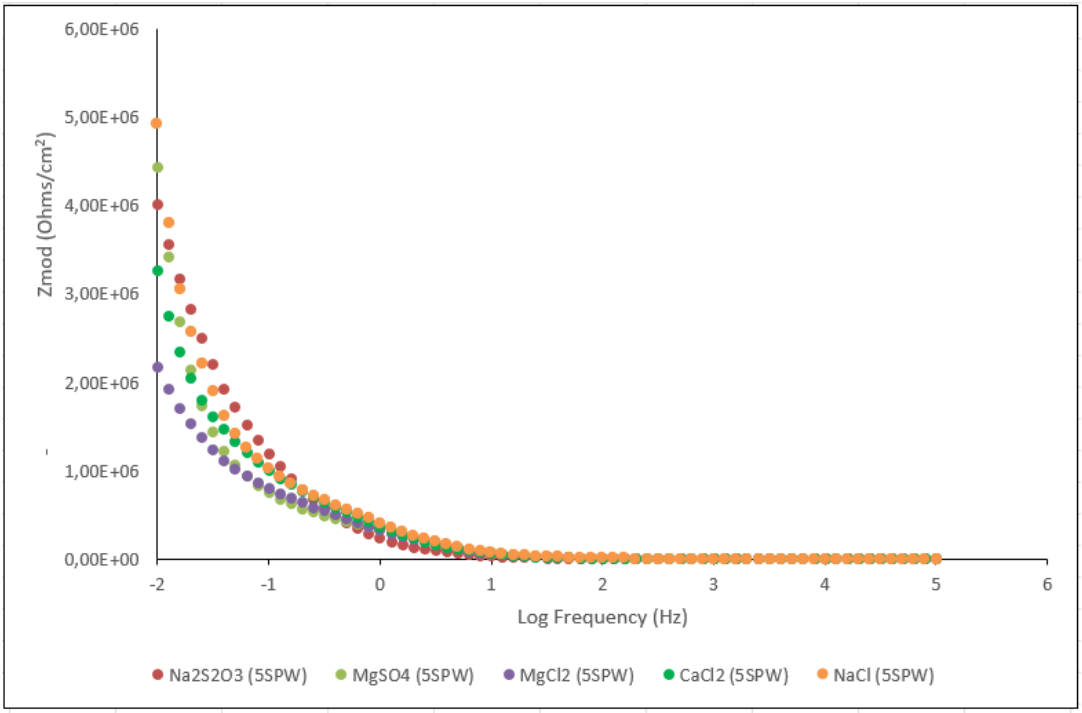

Figure 7.46: Bode plots of Z_{mod} (Ohms/cm^2) versus log frequency (Hz) for $PdTe_2$ in the presence of $Na_2S_2O_3$, NaCl, $CaCl_2$, $MgSO_4$, $MgCl_2$ at 5 SPW at a pH of 9.2 in O.O5 M $Na_2B_4O_7$.

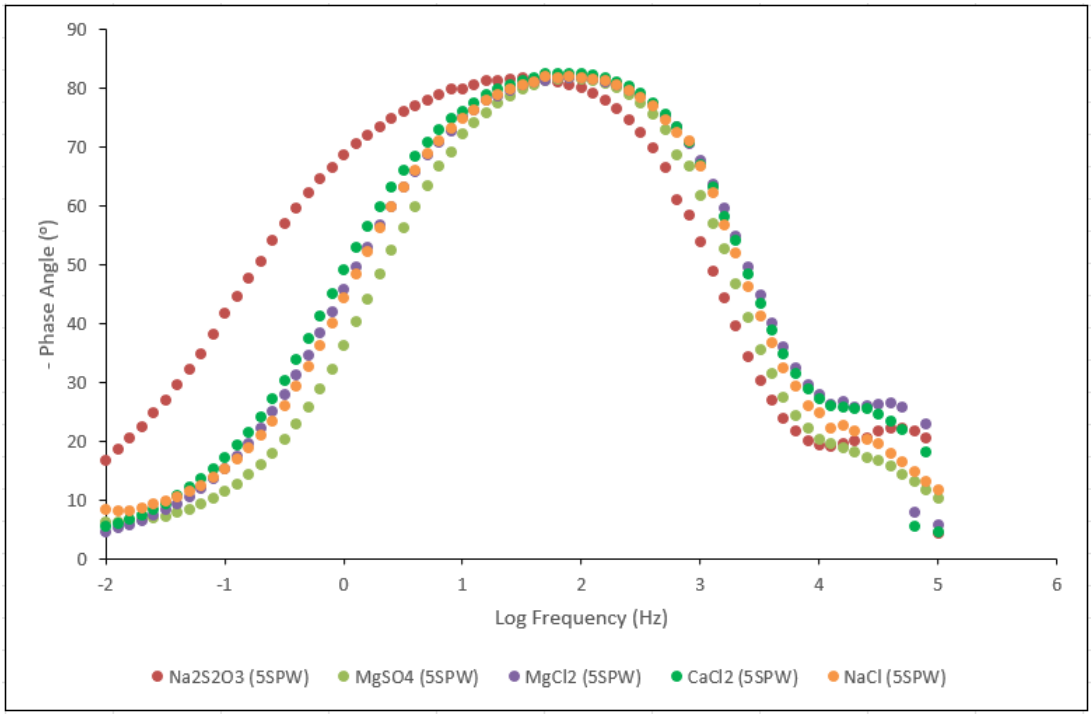

Figure 7.47: Bode plots of phase angle (°) versus log frequency for $PdTe_2$ in the presence of $Na_2S_2O_3$, NaCl, $CaCl_2$, $MgSO_4$, $MgCl_2$ at 5 SPW at a pH of 9.2 in O.O5 M $Na_2B_4O_7$.

Figures 7.45 to 7.47 convey Nyquist and Bode plots in the presence of $Na_2S_2O_3$, $MgSO_4$, $MgCl_2$, $CaCl_2$ and NaCl at 5 SPW. It is evident in Figure 7.45 that $Na_2S_2O_3$ displayed higher R_{ct} than the

other salts. However, the order of increase in R_{ct} in the presence of the salts investigated was observed to occur as in $MgSO_4$ < $MgCl_2$ < NaCl < $CaCl_2$ < $Na_2S_2O_3$. This implies lower current flow hence, a decrease in capacitance, indicating the generation of a thicker surface oxide layer. It is apparent that the impedance of $PdTe_2$ in the presence of $MgSO_4$, $MgCl_2$, $CaCl_2$ and NaCl is attributed mainly to interfacial kinetics. Additionally, R_s was found to increase in the order $MgCl_2$ ≈ $Na_2S_2O_3$ ≈ $CaCl_2$ < NaCl < $MgSO_4$.

It is clear from Figure 7.46 that Z_{mod} values increased in the order $MgCl_2$ < $CaCl_2$ < $Na_2S_2O_3$ < $MgSO_4$ < NaCl, implying a decrease in the rate of adsorption of the salts on $PdTe_2$. Moreover, from the Bode plots in Figures 7.46 and 7.47, the low and constant impedance values in the higher frequency domain and the phase angles decreasing to zero, indicate a common response of a resistor to an AC with high frequency, corresponding to R_s. The capacitive behaviour caused by the electrical double layer at the mineral/solution interface is denoted by the phase angels that were determined to be approximately – 80°.

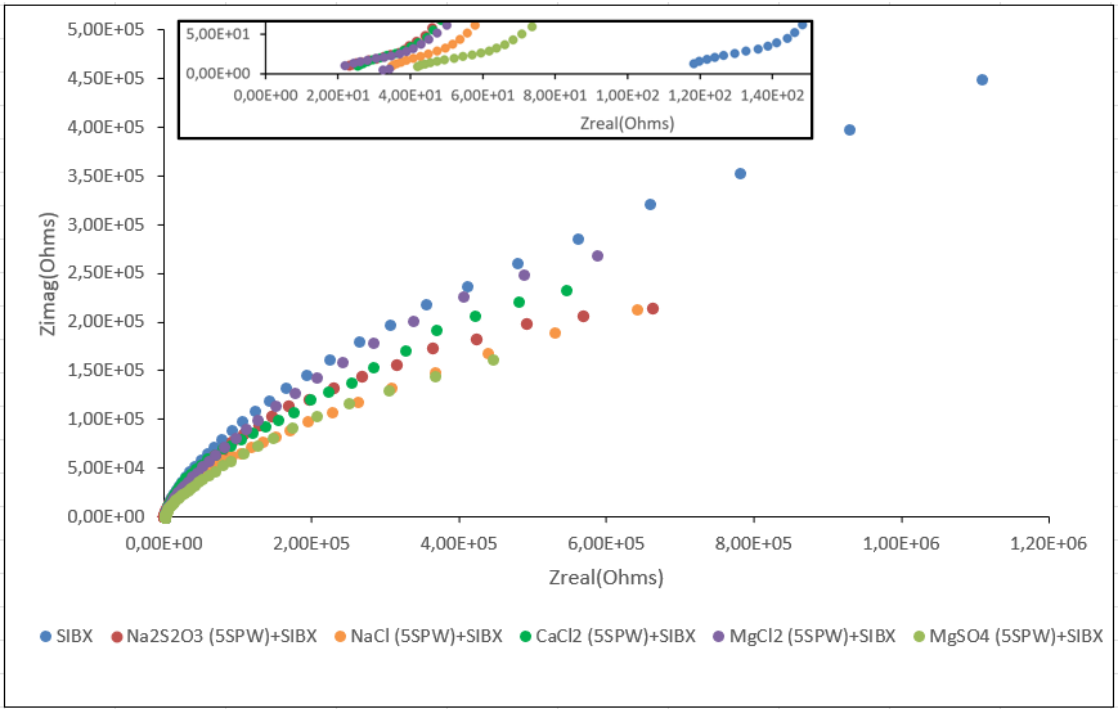

Figure 7.48: Nyquist plots for $PdTe_2$ in the absence and presence of $Na_2S_2O_3$, NaCl, $CaCl_2$, $MgSO_4$, $MgCl_2$ at 5 SPW with SIBX at a pH of 9.2 in O.O5 M $Na_2B_4O_7$.

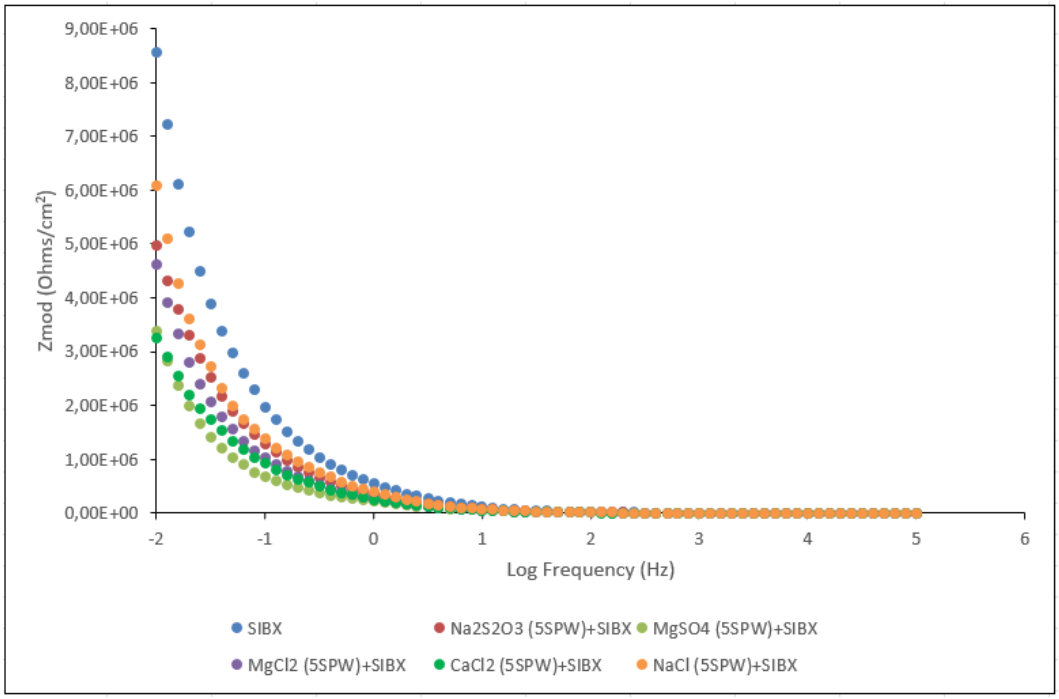

Figure 7.49: Bode plots of Z_{mod} (Ohms/cm^2) versus log frequency (Hz) for $PdTe_2$ in the absence and presence of $Na_2S_2O_3$, NaCl, $CaCl_2$, $MgSO_4$, $MgCl_2$ at 5 SPW with SIBX at a pH of 9.2 in O.O5 M $Na_2B_4O_7$.

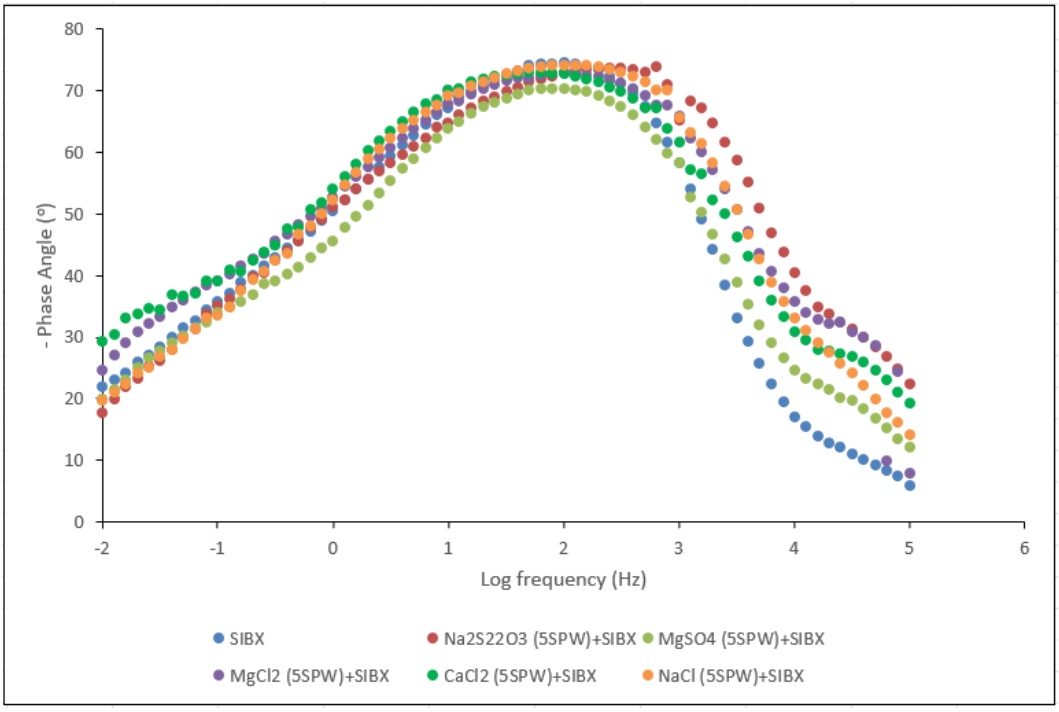

Figure 7.50: Bode plots of phase angle (°) versus log frequency for $PdTe_2$ in the absence and presence of $Na_2S_2O_3$, NaCl, $CaCl_2$, $MgSO_4$, $MgCl_2$ at 5 SPW with SIBX at a pH of 9.2 in O.O5 M $Na_2B_4O_7$.

Figures 7.48 to 7.50 demonstrate Nyquist and Bode plots in the absence and presence of $Na_2S_2O_3$, $MgSO_4$, $MgCl_2$, $CaCl_2$ and NaCl at 5 SPW in SIBX. It is evident from Figure 7.48 that the

impedance for all conditions investigated in the presence of SIBX displayed higher R_{ct} than in the absence of SIBX (Figure 7.45). Higher R_{ct} values indicate lower current flow, hence lower capacitive behaviour. The adsorption of SIBX results in lower capacitive behaviour owing to its low dielectric constant. Moreover, the addition of xanthate ions in a system may decrease capacitance as a result of the removal of the oxidation products formed on the $PdTe_2$ mineral surface (Ertekin et al., 2016). Furthermore, it is observed that R_{ct} increased in the order $MgSO_4 \approx NaCl < Na_2S_2O_3 < CaCl_2 < MgCl_2 <$ SIBX. This indicates that $PdTe_2$ is more reactive in the presence of the salts and SIBX than in the presence of SIBX only. Additionally, it is apparent that R_s was not changed both in the absence and presence of SIBX with the salts investigated.

It is apparent in Figure 7.49 that Z_{mod} values increased in the order $CaCl_2 \approx MgSO_4 < MgCl_2 < Na_2S_2O_3 < NaCl <$ SIBX, implying that the rate of adsorption on $PdTe_2$ was higher in the presence of $CaCl_2$ and $MgSO_4$ in SIBX. Generally, it was observed that the rate of adsorption on $PdTe_2$ was higher in the presence of both the salts and SIBX than in the presence of SIBX only. Thereby, indicating that the presence of salts at 5 SPW inhibited the adsorption of SIBX. The difference in impedance values in the low frequency domain indicates the different rates in the formation of continuous surface layers due to the adsorption of the investigated ions and SIBX and its oxidation to dixanthogen on the mineral surface. Ultimately, Figure 7.50 did not display much significant differences in phase angles for all the conditions investigated.

7.3.9 Effect of salts at 10 SPW

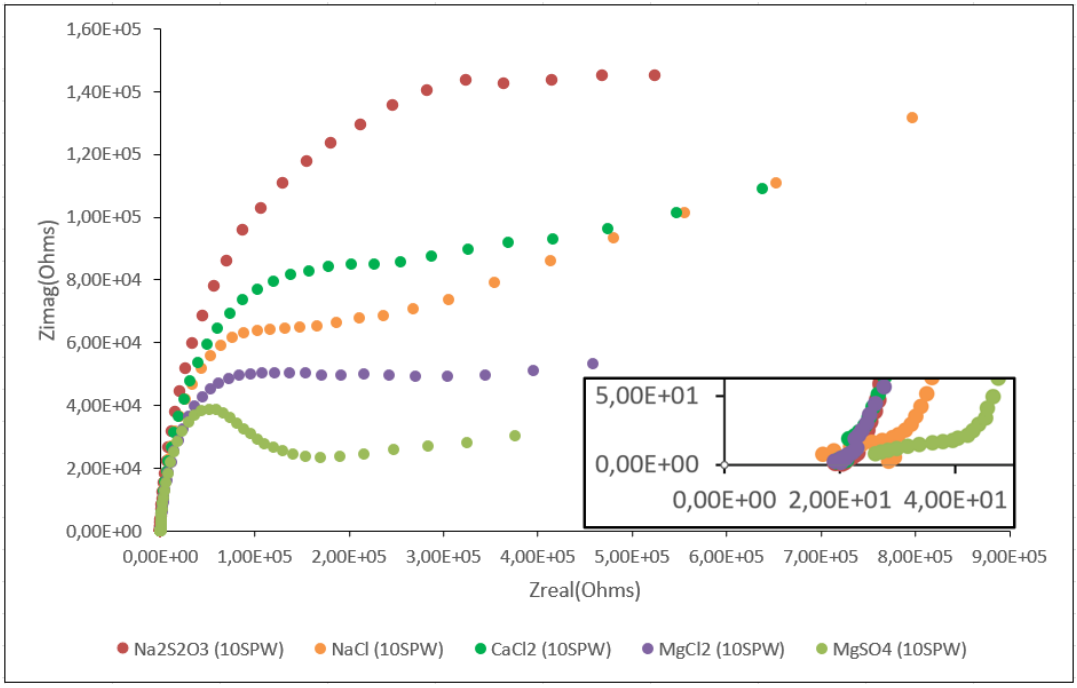

Figure 7.51: Nyquist plots for $PdTe_2$ in the presence of $Na_2S_2O_3$, NaCl, $CaCl_2$, $MgSO_4$, $MgCl_2$ at 10 SPW at a pH of 9.2 in O.O5 M $Na_2B_4O_7$.

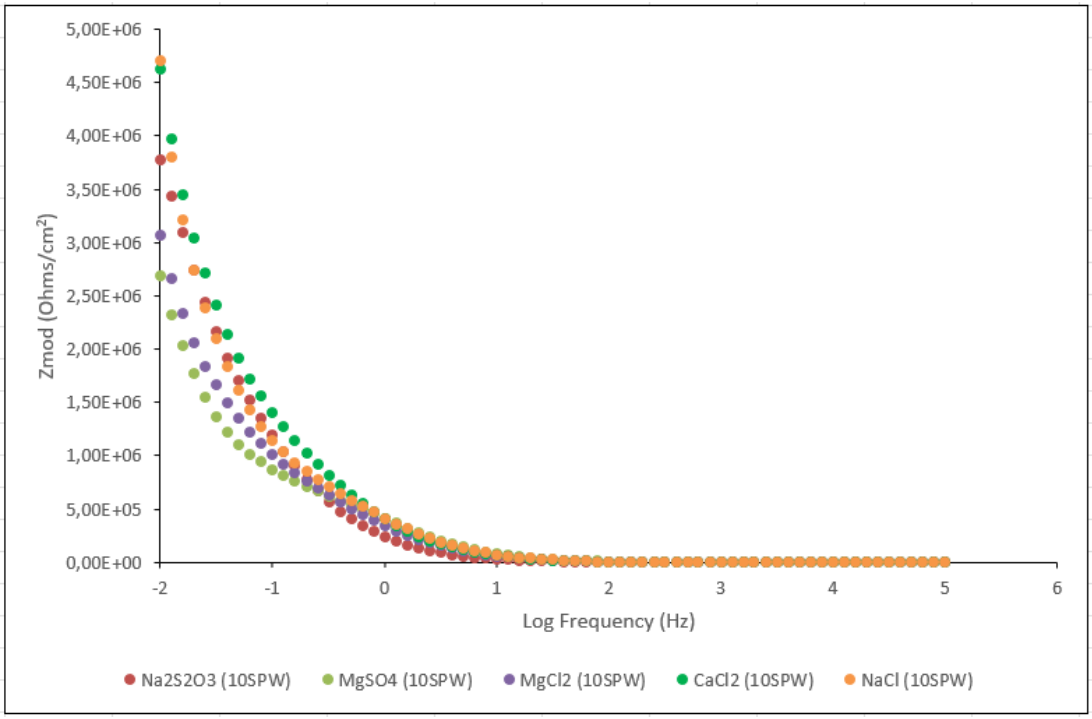

Figure 7.52: Bode plots of Z_{mod} (Ohms/cm^2) versus log frequency (Hz) for $PdTe_2$ in the presence of $Na_2S_2O_3$, NaCl, $CaCl_2$, $MgSO_4$, $MgCl_2$ at 10 SPW at a pH of 9.2 in O.O5 M $Na_2B_4O_7$.

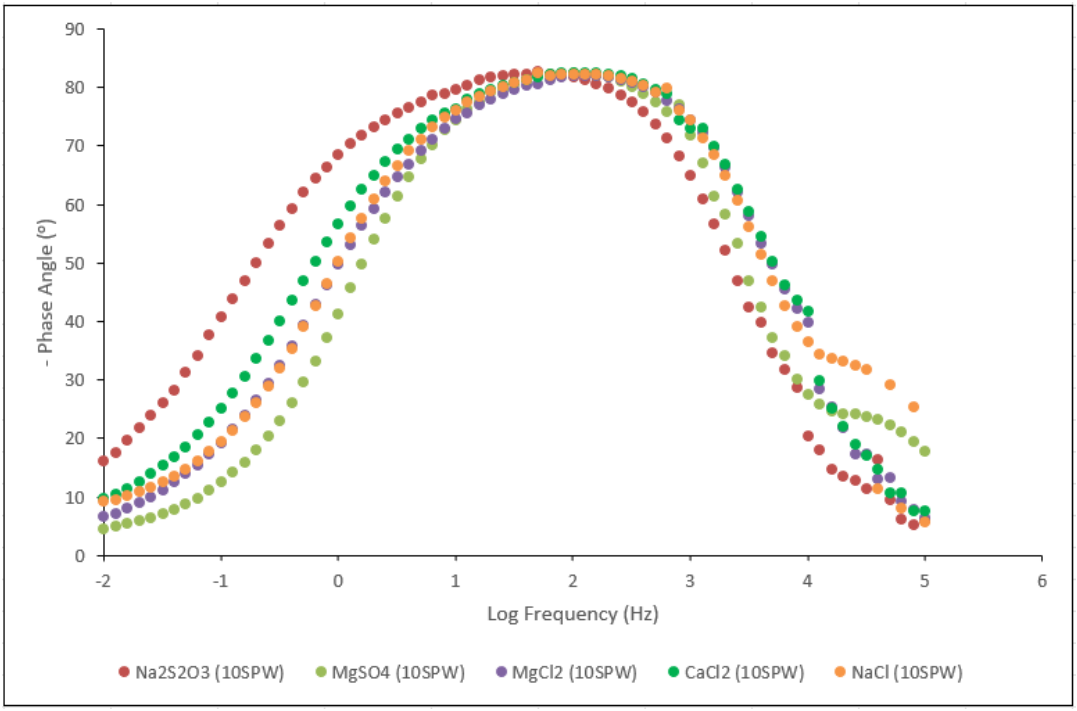

Figure 7.53: Bode plots of phase angle (°) versus log frequency for $PdTe_2$ in the presence of $Na_2S_2O_3$, NaCl, $CaCl_2$, $MgSO_4$, $MgCl_2$ at 10 SPW at a pH of 9.2 in O.O5 M $Na_2B_4O_7$.

Figures 7.51 to 7.53 plot Nyquist and Bode graphs in the presence of $Na_2S_2O_3$, $MgSO_4$, $MgCl_2$, $CaCl_2$ and NaCl at 10 SPW. It is observable from Figure 7.51 that R_{ct} for the salts investigated at 10 SPW varied significantly compared to other ionic strengths. However, the order of increase in R_{ct} was found to be $MgCl_2 < MgSO_4 < NaCl < CaCl_2 < Na_2S_2O_3$, indicating lower current flow and lower rates of reactions, hence lower capacitive behaviour with an increase in R_{ct}. This behaviour therefore suggests an increase in the thickness of an oxide layer that probably formed on the mineral surface, with an increase in R_{ct}. It is observable that the magnesium salts most likely formed the least surface layer on $PdTe_2$.It is noticeable that the reactions that took place at the mineral surface in the presence of the salts investigated at 10 SPW, were attributed to interfacial kinetics. Interestingly, at higher ionic strength the order of decrease in R_s is shown to occur in the order $NaCl < MgCl_2 \approx Na_2S_2O_3 < CaCl_2 < MgSO_4$.

Figure 7.52 shows that Z_{mod} values at the lower frequency domain decrease in the order $NaCl > CaCl_2 > Na_2S_2O_3 > MgCl_2 > MgSO_4$, thereby implying an increase in the rate of adsorption on the $PdTe_2$ mineral surface from magnesium salts to NaCl. An increase in frequency shows that the formation of continuous layers on the mineral surface did not change the capacitance. It is evident that Z_{mod} values became constant and approached zero in the higher frequency domain. Moreover,

phase angles for the conditions investigated were found to be approximately – 80°, with $Na_2S_2O_3$ showing a higher phase angle than other salts investigated.

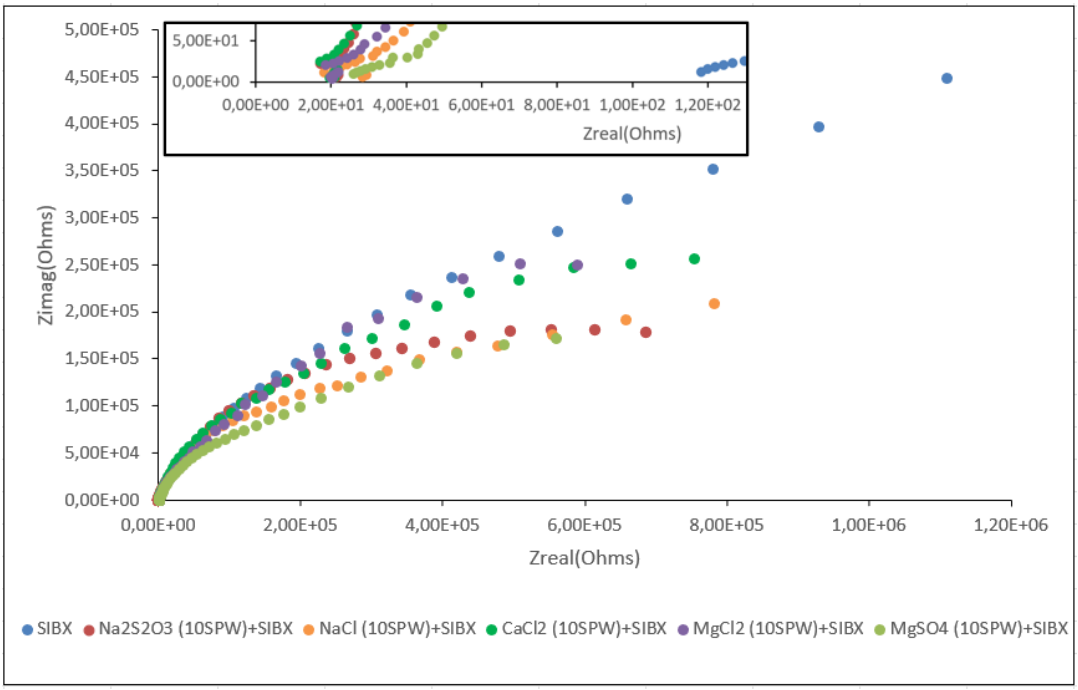

Figure 7.54: Nyquist plots for $PdTe_2$ in the absence and presence of $Na_2S_2O_3$, NaCl, $CaCl_2$, $MgSO_4$, $MgCl_2$ at 10 SPW with SIBX at a pH of 9.2 in O.O5 M $Na_2B_4O_7$.

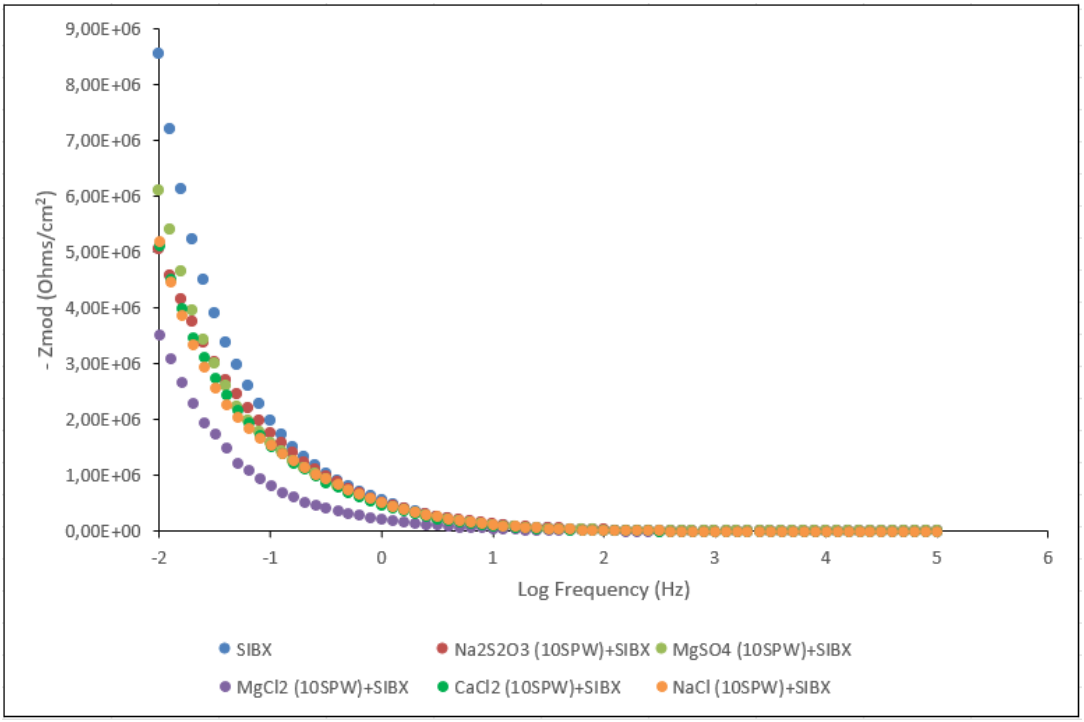

Figure 7.55: Bode plots of Z_{mod} (Ohms/cm^2) versus log frequency (Hz) for $PdTe_2$ in the absence and presence of $Na_2S_2O_3$, NaCl, $CaCl_2$, $MgSO_4$, $MgCl_2$ at 10 SPW with SIBX at a pH of 9.2 in O.O5 M $Na_2B_4O_7$.

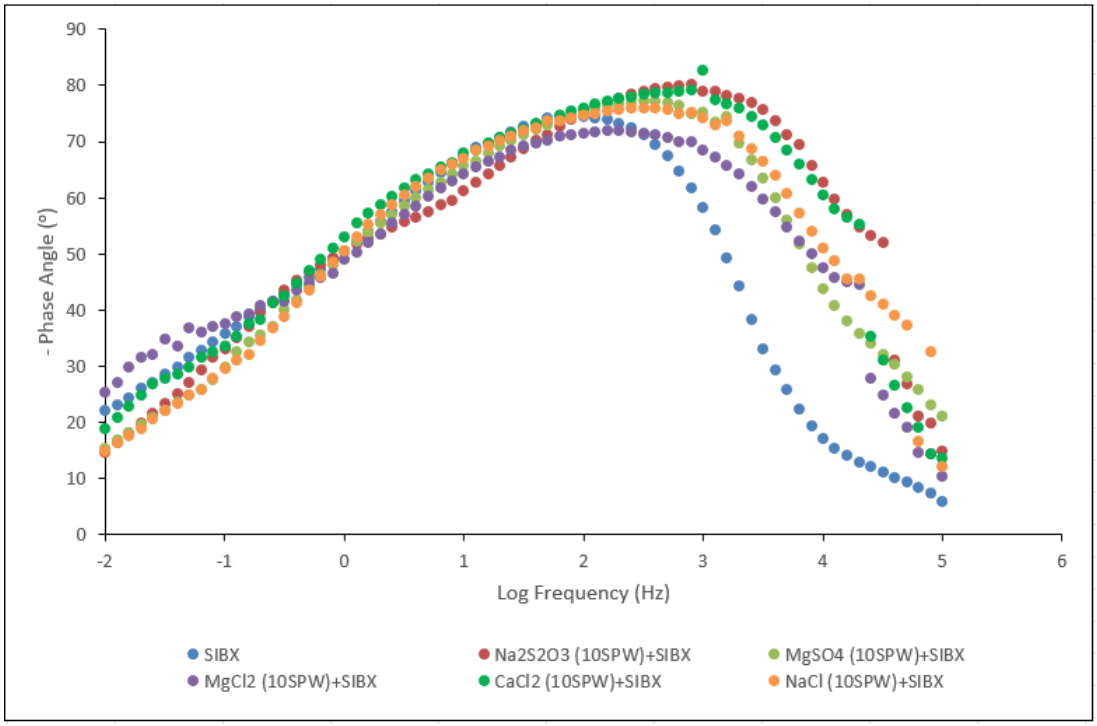

Figure 7.56: Bode plots of phase angle (°) versus log frequency for $PdTe_2$ in the absence and presence of $Na_2S_2O_3$, NaCl, $CaCl_2$, $MgSO_4$, $MgCl_2$ at 10 SPW with SIBX at a pH of 9.2 in O.O5 M $Na_2B_4O_7$.

Figures 7.54 to 7.56 exhibit Nyquist and Bode plots in the presence of $Na_2S_2O_3$, $MgSO_4$, $MgCl_2$, $CaCl_2$ and NaCl at 10 SPW in SIBX. It is observable from Figure 7.54 that R_{ct} for $PdTe_2$ in the presence of the salts investigated increased in the presence of SIBX than in the absence of SIBX (Figure 7.51). An increase in resistance would suggest lower capacitive behaviour. Since capacitance is inversely proportional to surface resistance, the adsorption of SIBX would cause a decrease in capacitance due to low dielectric constants exhibited by xanthates (around 4-8) (Mu et al., 2015). However, it is clearly observed from Figure 7.54 that SIBX only exhibited higher R_{ct} than in the presence of salts, thereby implying that the rate of reactions occurring on the mineral surface was higher in the presence of both the salts and SIBX. Furthermore, it is noticeable that R_s changes in the presence of SIBX compared to Figure 7.51, in the absence of SIBX. This implies that the chemical transformations that occurred on the mineral surface in the presence of the salts at 10 SPW with SIBX changed R_s to some extent.

Additionally, it is evident in Figure 7.55 that the rate of adsorption on $PdTe_2$ is higher in the presence of both SIBX and the salts than in the presence of SIBX only. Moreover, $MgCl_2$ in the presence of SIBX absorbs faster on the mineral surface than other salts. It is apparent that the rate at which $Na_2S_2O_3$, $MgSO_4$, $CaCl_2$ and NaCl adsorb on the mineral surface in the presence of SIBX

does not significantly differ. Ultimately, it was observed in Figure 7.56 that a capacitive behaviour of the electrical double layer was displayed for all conditions investigated.

7.4 EIS for PdS

7.4.1 Effect of $Na_2S_2O_3$

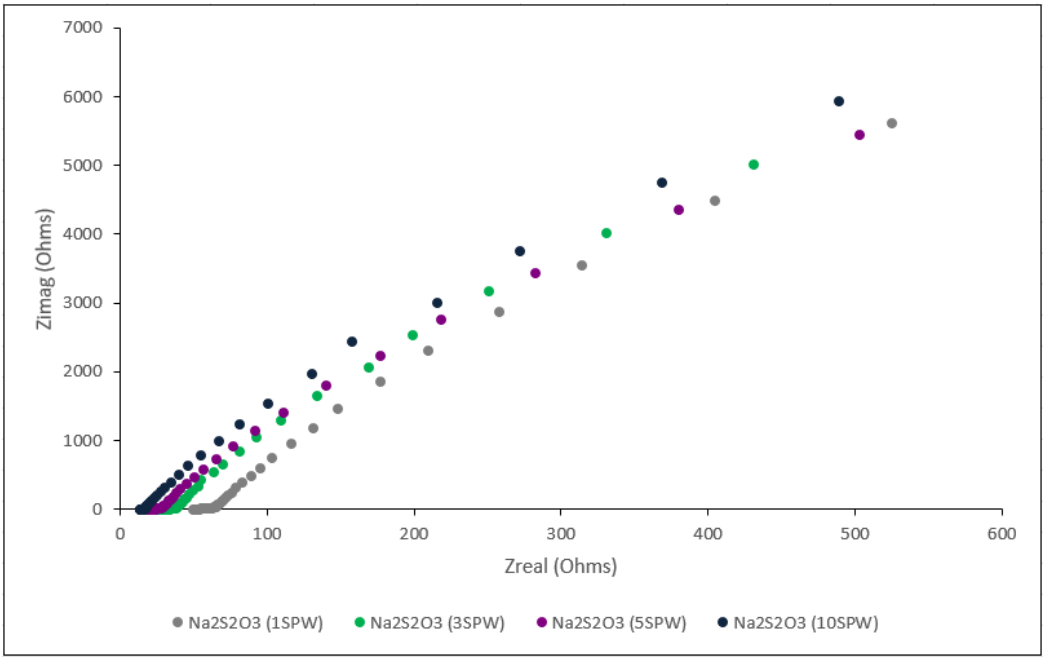

Figure 7.57: Nyquist plots for PdS in the presence of $Na_2S_2O_3$ at increasing ionic strength at a pH of 9.2 in O.O5 M $Na_2B_4O_7$.

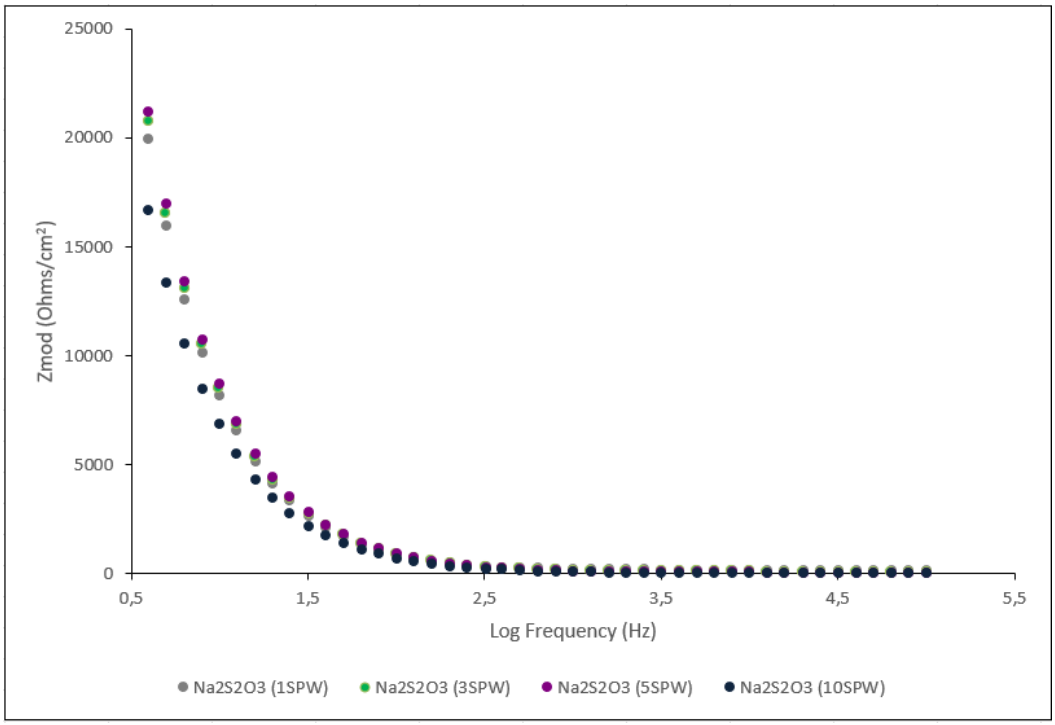

Figure 7.58: Bode plots of Z_{mod} (Ohms/cm^2) versus log frequency (Hz) for PdS in the presence of $Na_2S_2O_3$ at increasing ionic strength at a pH of 9.2 in O.O5 M $Na_2B_4O_7$.

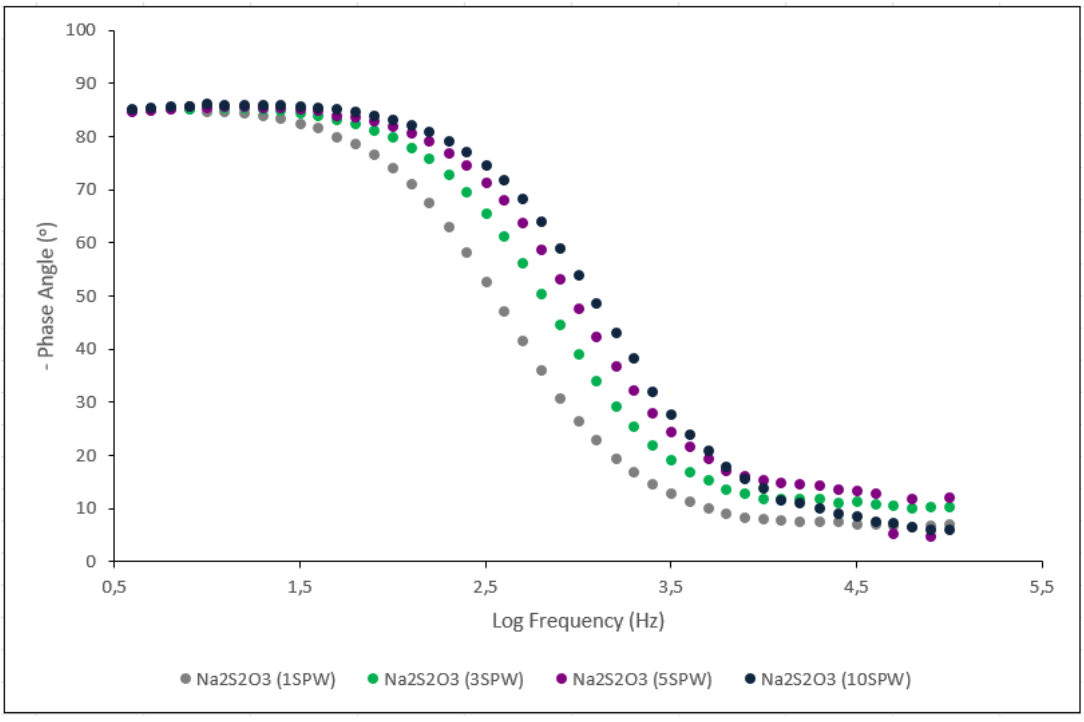

Figure 7.59: Bode plots of phase angle (°) versus log frequency for PdS in the presence of $Na_2S_2O_3$ at increasing ionic strength at a pH of 9.2 in O.O5 M $Na_2B_4O_7$.

Figures 7.57 to 7.59 display Nyquist and Bode plots for PdS in the presence of $Na_2S_2O_3$ at increasing ionic strength. It is evident from the Nyquist plot that R_{ct} increases with an increase in ionic strength. This suggests that the rate at which the electrochemical reactions occur on PdS is higher at lower ionic strengths. Moreover, it is perceived from the Nyquist plot that the reactions occurring on the mineral surface under all conditions investigated are attributed mainly to interfacial kinetics. Additionally, R_s is observed to decrease with an increase in ionic strength.

The highest ionic strength exhibits the lowest Z_{mod} value, implying higher adsorption of $Na_2S_2O_3$ compared to other ionic strengths. The rates at which $Na_2S_2O_3$ adsorbed and formed continuous surface layers on PdS did not significantly differ at 1 SPW, 3 SPW and 5 SPW. The lower impedance value obtained at 10 SPW, indicates higher capacitive behaviour due to higher current flow for the electrochemical reactions occurring on the mineral surface. It is depicted from the Bode plots that at a higher frequency range, impedance values are relatively constant and very low, whilst the phase angles decrease to zero. This observation is a common response of a resistor to an AC with high frequency and is in correspondence to R_s. The capacitive behaviour displayed by the electrical double layer is demonstrated by phase angles that were determined to be approximately – 85°. Additionally, the significant change in impedance values in the intermediate frequency domain conveys a strong decrease in the capacitive behaviour of PdS. This observation suggests the formation of continuous surface layers on the mineral surface.

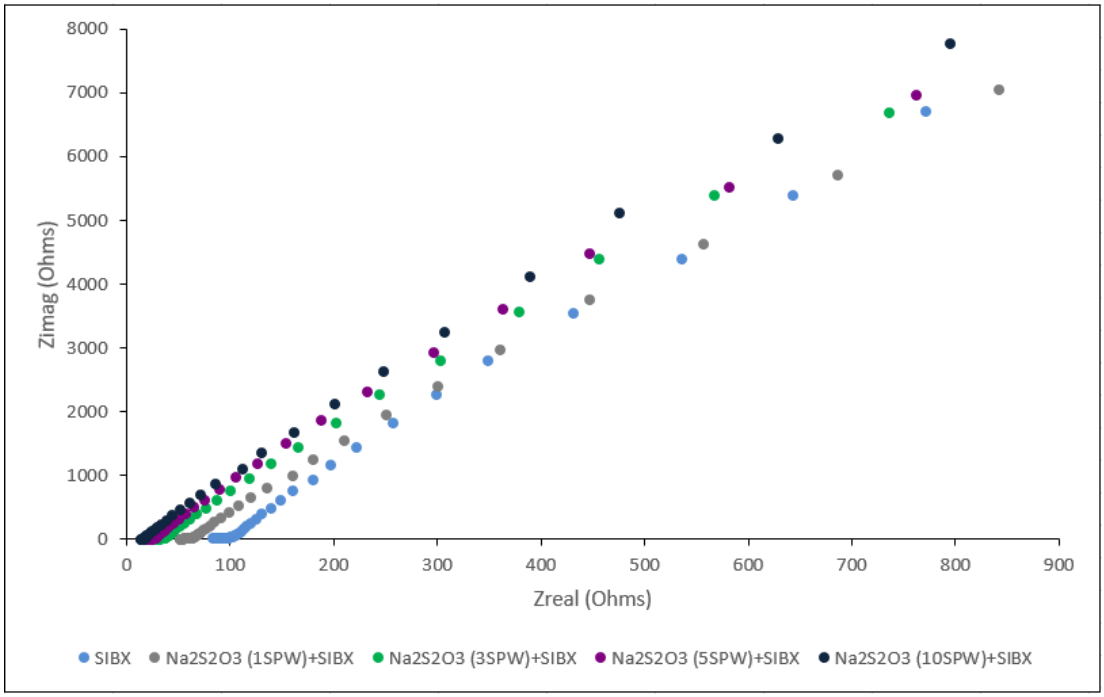

Figure 7.60: Nyquist plots for PdS in the absence and presence of $Na_2S_2O_3$ at increasing ionic strength with SIBX at a pH of 9.2 in O.O5 M $Na_2B_4O_7$.

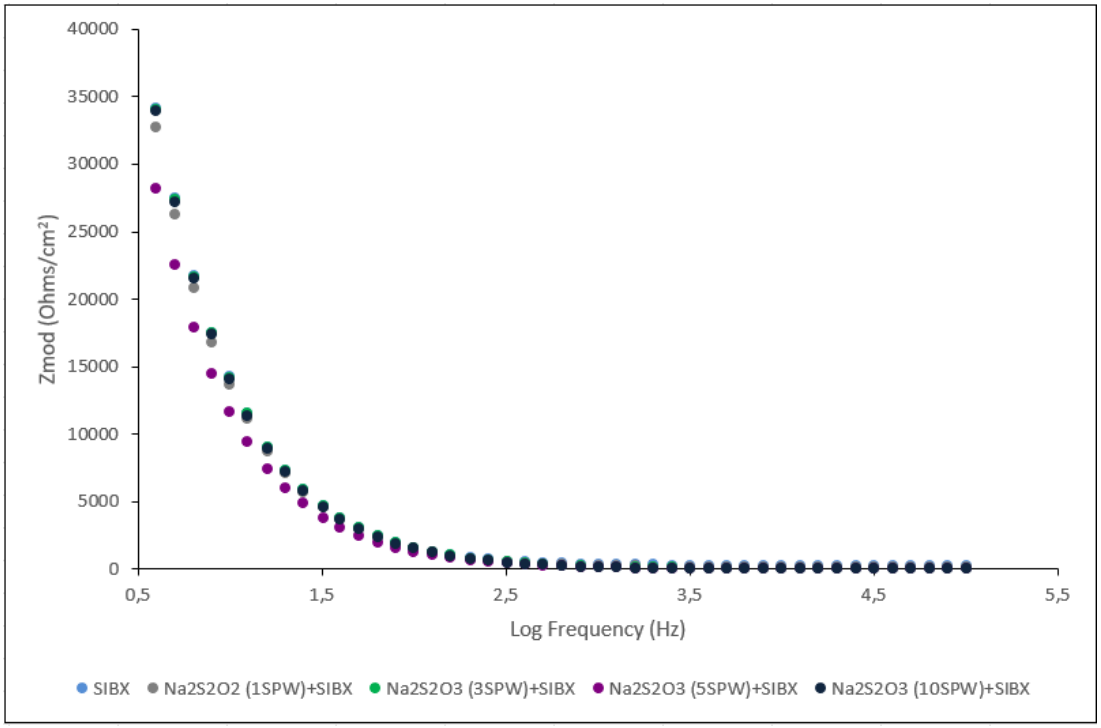

Figure 7.61: Bode plots of Z_{mod} (Ohms/cm^2) versus log frequency (Hz) for PdS in the absence and presence of $Na_2S_2O_3$ at increasing ionic strength with SIBX at a pH of 9.2 in O.O5 M $Na_2B_4O_7$.

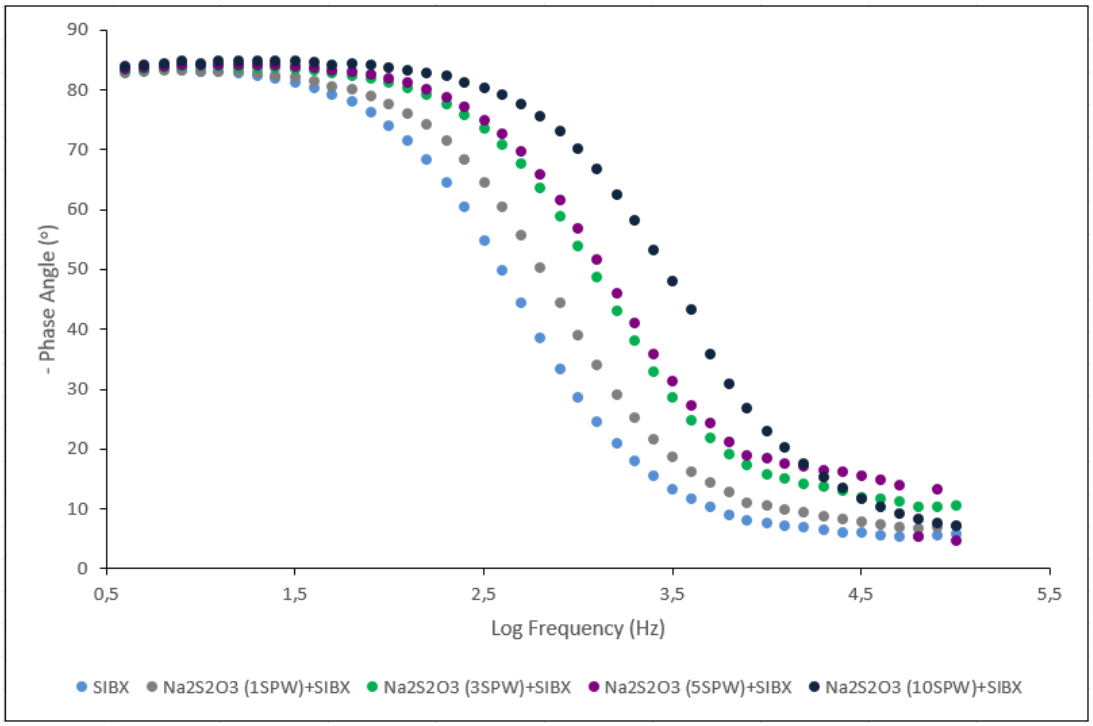

Figure 7.62: Bode plots of phase angle (°) versus log frequency for PdS in the absence and presence of $Na_2S_2O_3$ at increasing ionic strength with SIBX at a pH of 9.2 in O.O5 M $Na_2B_4O_7$.

Figures 7.60 to 7.62 show Nyquist and Bode plots in the presence of $Na_2S_2O_3$ at increasing ionic strength in SIBX. It is discernible from the Nyquist plot in Figure 7.60 that R_{ct} increases in the presence of SIBX compared to Figure 7.57. This suggests lower capacitive behaviour due to lower net current for the electrochemical reactions occurring in the presence of SIBX on PdS. Lower capacitive behaviour could be associated to the adsorption and formation of oxidation products of SIBX or the generation of a layer formed from SIBX with a smaller dielectric constant. Consequently, upon the adsorption of SIBX on PdS, the decrease in dielectric constant between the mineral surface and solution phase results in a decrease in the capacitance. Furthermore, it is observed that the electron transfer reactions that took place in the presence of all salts investigated in SIBX, where most likely influenced by diffusion- limited processes, owing to the almost linear Nyquist behaviour.

Interestingly, it is evident from Figure 7.61 that the Z_{mod} values did not significantly differ, implying that the rate at which the SIBX adsorbed on the mineral surface both in the absence and presence of salts did not differ significantly. However, the adsorption of SIBX was shown to be slightly higher in $Na_2S_2O_3$ at 5 SPW than in other ionic strengths. Phase angles of approximately – 85° were obtained, indicating a capacitive behaviour at the mineral surface/solution interface.

7.4.2 Effect of $MgSO_4$

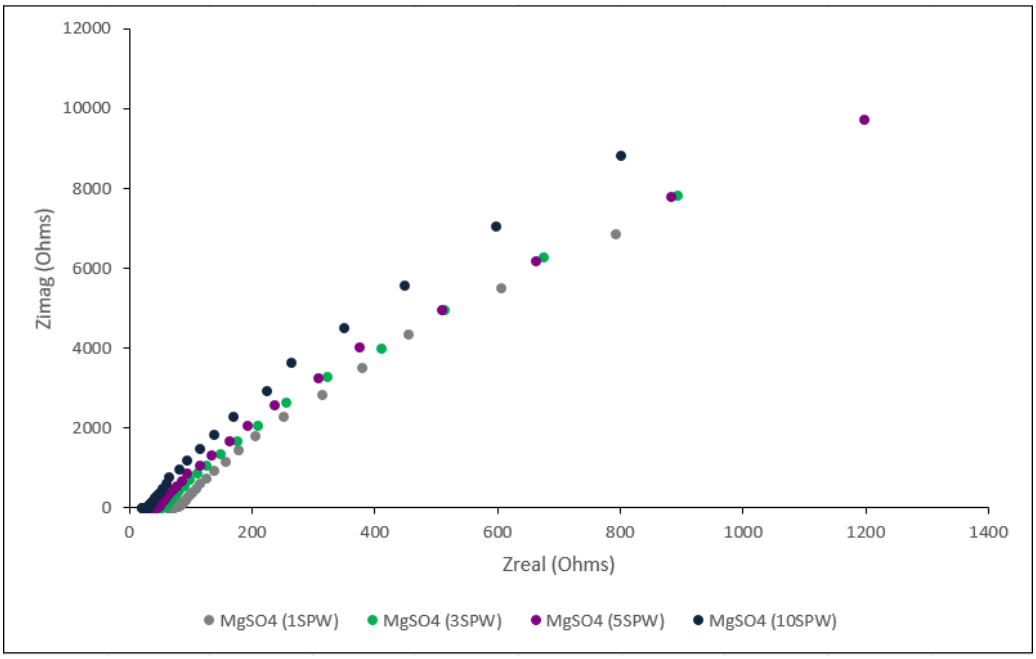

Figure 7.63: Bode plots of Z_{mod} (Ohms/cm^2) versus log frequency (Hz) for PdS in the presence of $MgSO_4$ at increasing ionic strength at a pH of 9.2 in O.O5 M $Na_2B_4O_7$.

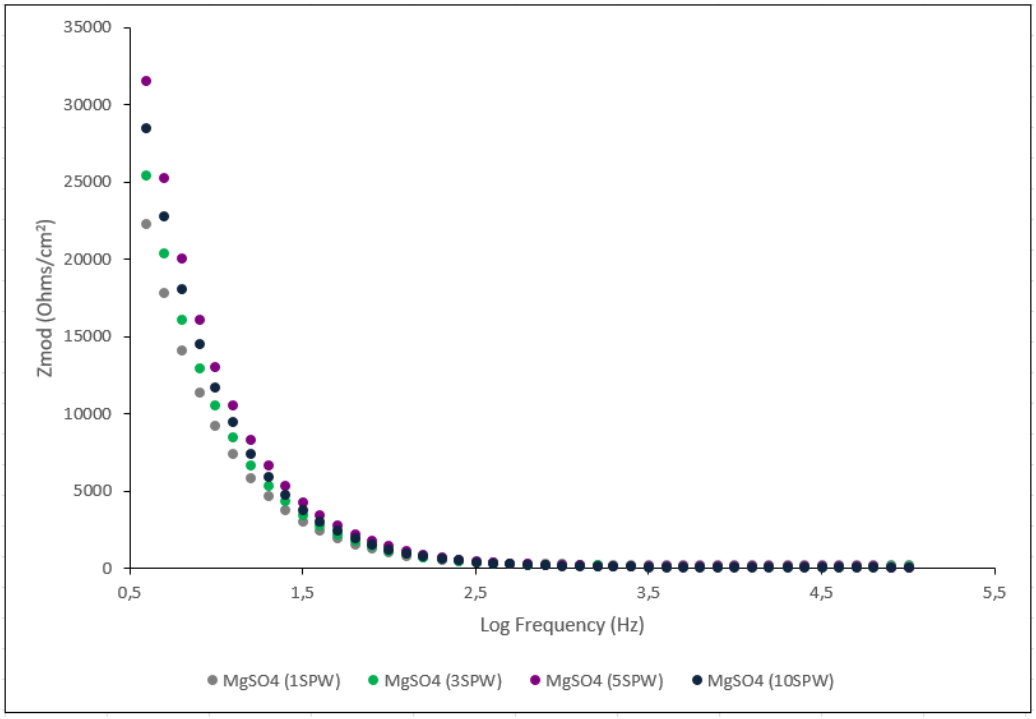

Figure 7.64: Bode plots of Z_{mod} (Ohms/cm^2) versus log frequency (Hz) for PdS in the presence of $MgSO_4$ at increasing ionic strength at a pH of 9.2 in O.O5 M $Na_2B_4O_7$.

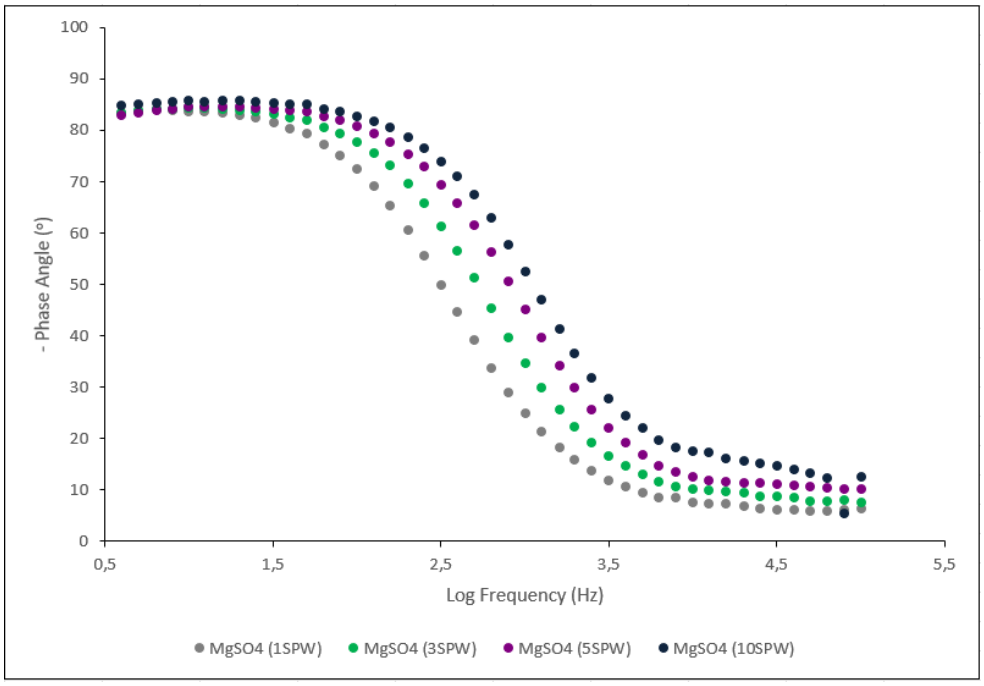

Figure 7.65: Bode plots of phase angle (°) versus log frequency for PdS in the presence of $MgSO_4$ at increasing ionic strength at a pH of 9.2 in O.O5 M $Na_2B_4O_7$.

Figures 7.63 to 7.65 depict Nyquist and Bode plots for PdS in the presence of $MgSO_4$ at increasing ionic strength. It is evident from the Nyquist plot in Figure 7.63 that the reactions that occurred on PdS in the presence of $MgSO_4$ were influenced by interfacial kinetics. It is observed that R_{ct} increased with an increase in ionic strength of $MgSO_4$. The larger R_{ct} could be ascribed to the formation of a higher number of oxidized species at higher ionic strengths. Furthermore, it is clear that R_s decreased with an increase in ionic strength of $MgSO_4$.

Higher impedance values were obtained in Figure 7.64 at higher ionic strengths, which correspond to the higher R_{ct} obtained in Figure 7.63. The lower Z_{mod} values obtained at lower ionic strengths indicate a higher rate of adsorption of $MgSO_4$ of the PdS mineral surface. Higher impedance values indicate lower capacitive behaviour of PdS in higher ionic strengths of $MgSO_4$. This denotes the formation of a thicker oxide layer or a layer with a smaller dielectric constant.

A typical response of a resistor to an AC with high frequency which resembles Rs, is illustrated by very low and relatively constant impedance values in the Bode plot, accompanied by phase angle values that decreased, approaching zero. Between the low and medium frequency range, it is shown that the relationship between impedance and frequency was inversely proportional, and the phase angles were determined to be – 85°, which is typical capacitive behavior of an electrical double layer at the mineral/solution interface.

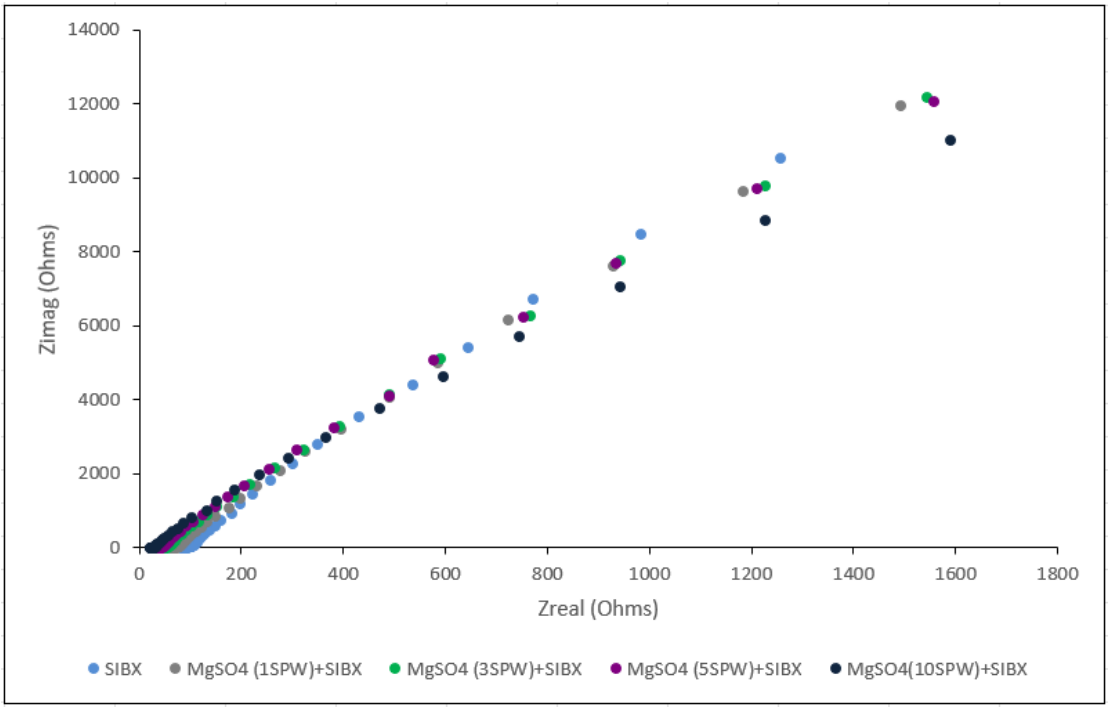

Figure 7.66: Nyquist plots for PdS in the absence and presence of $MgSO_4$ at increasing ionic strength with SIBX at a pH of 9.2 in O.O5 M $Na_2B_4O_7$.

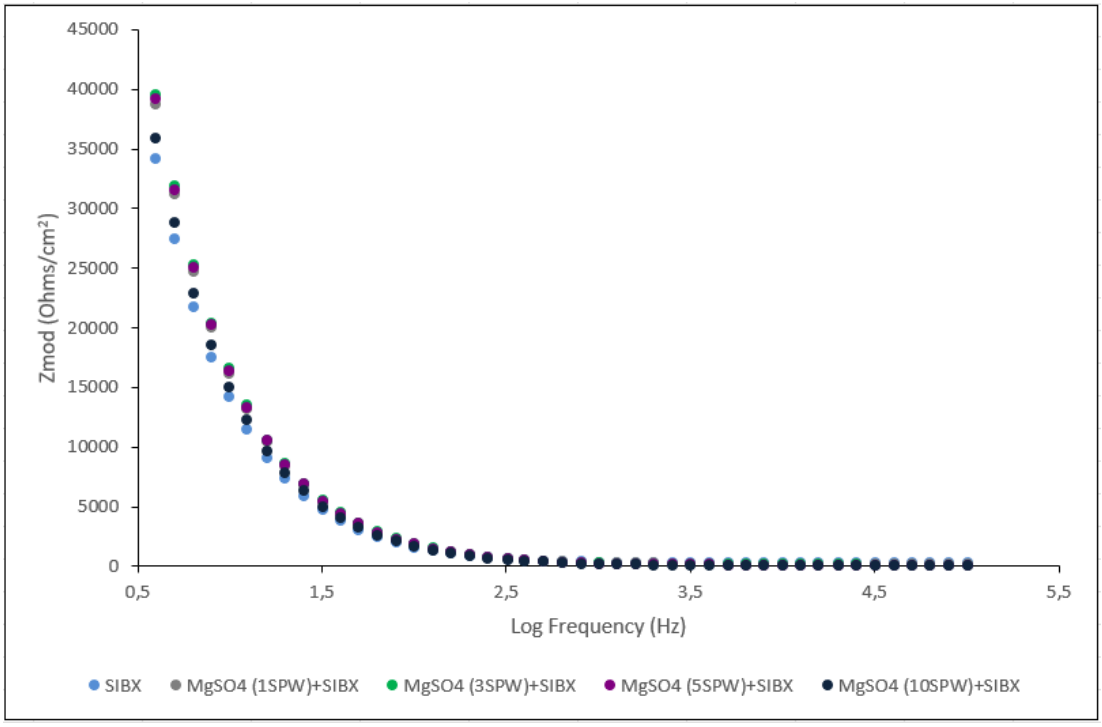

Figure 7.67: Bode plots of Z_{mod} (Ohms/cm^2) versus log frequency (Hz) for PdS in the absence and presence of $MgSO_4$ at increasing ionic strength with SIBX at a pH of 9.2 in O.O5 M $Na_2B_4O_7$.

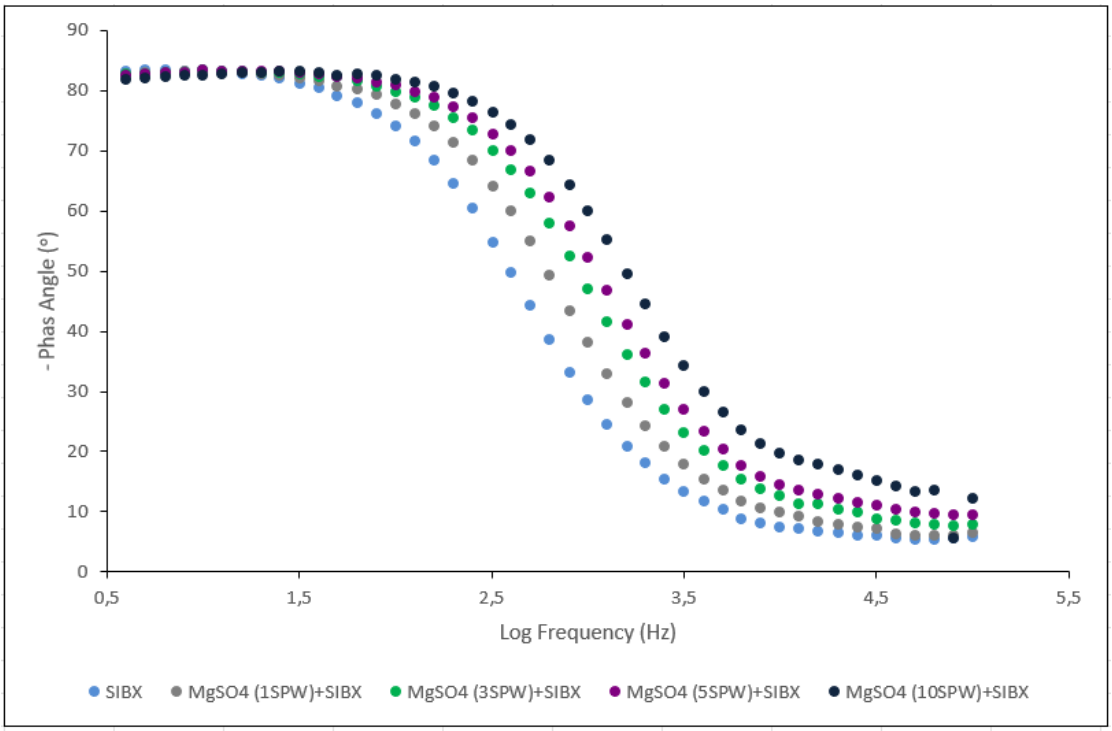

Figure 7.68: Bode plots of phase angle (°) versus log frequency for PdS in the absence and presence of $MgSO_4$ at increasing ionic strength with SIBX at a pH of 9.2 in O.O5 M $Na_2B_4O_7$.

Figures 7.66 to 7.68 illustrate Nyquist and Bode plots in the presence of $MgSO_4$ at increasing ionic strength in SIBX. It is visible from the Nyquist plot that R_{ct} for all conditions investigated in SIBX was found to be higher than in the absence of SIBX. Furthermore, the Nyquist plot shows an incomplete semicircle, which indicates the oxidation of PdS and SIBX adsorption are mainly controlled by charge transfer. Additionally, it is evident that R_s decreases with an increase in ionic strength.

It can be discerned from Figure 7.67 that the Z_{mod} values both in the absence and presence of $MgSO_4$ in SIBX were not significantly different, thereby implying that the rate of adsorption of SIBX both in the absence and presence of $MgSO_4$ did not differ significantly. This indicates that the formation of continuous surface layers on PdS, due to the adsorption of SIBX and the formation of dixanthogen was not significant under all conditions investigated. Moreover, the capacitive behaviour of the electrical double layer is demonstrated by the phase angles that were observed to be approximately – 85°.

7.4.3 Effect of salts at 1 SPW

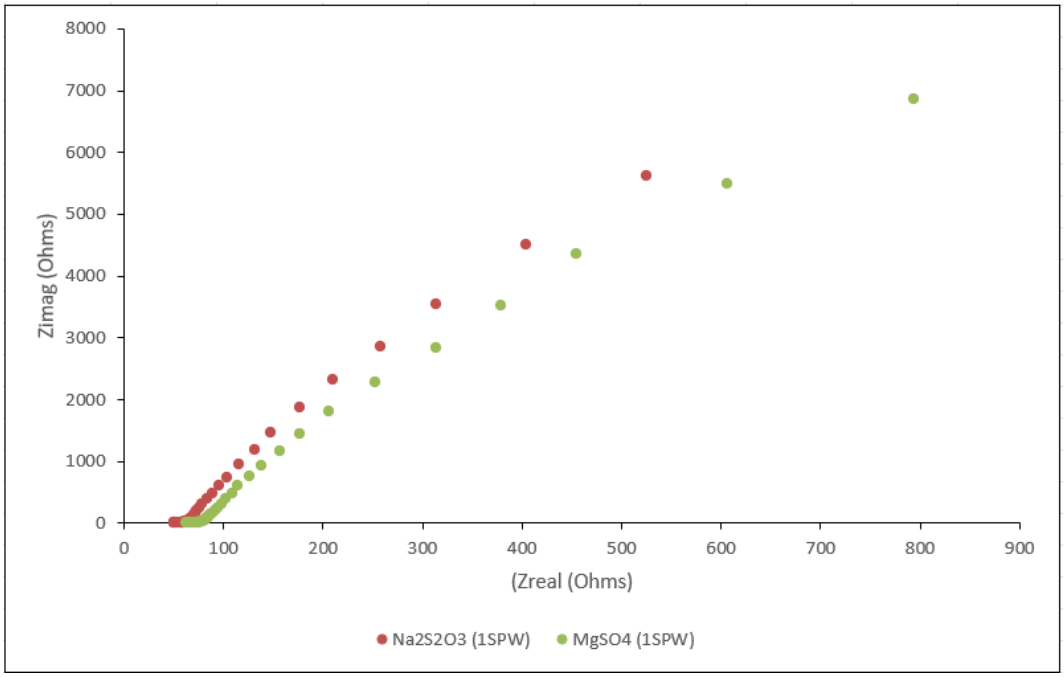

Figure 7.69: Nyquist plots for PdS in the presence of $Na_2S_2O_3$ and $MgSO_4$ at 1 SPW at a pH of 9.2 in O.O5 M $Na_2B_4O_7$.

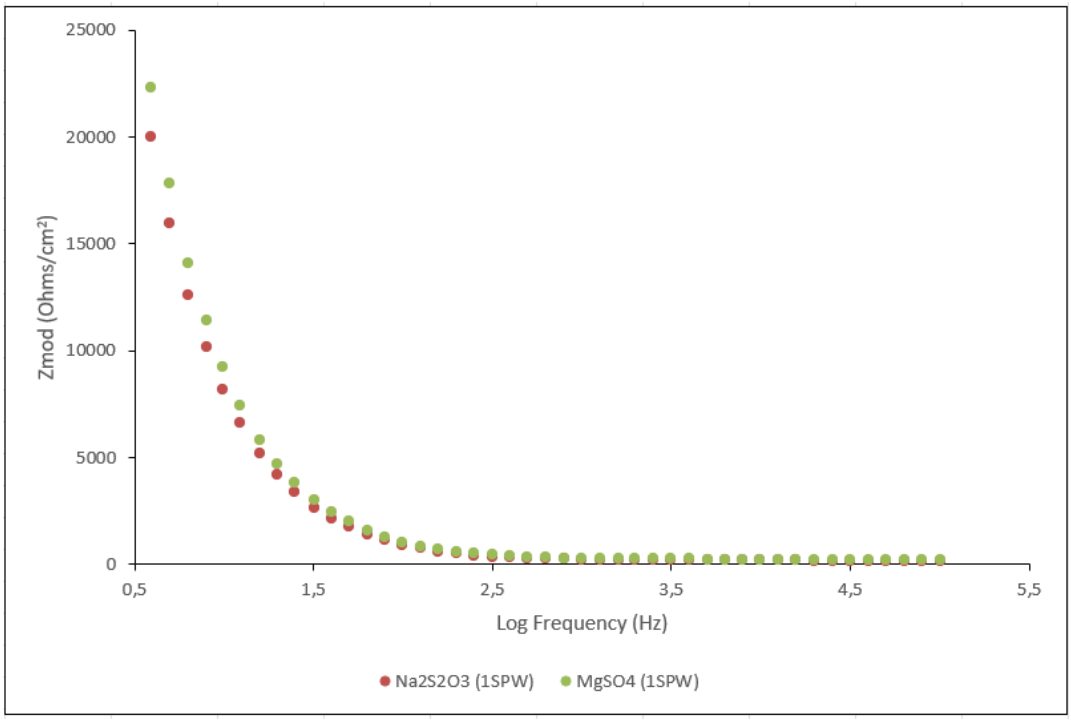

Figure 7.70: Bode plots of Z_{mod} (Ohms/cm^2) versus log frequency (Hz) for PdS in the presence of $Na_2S_2O_3$ and $MgSO_4$ at 1 SPW at a pH of 9.2 in O.O5 M $Na_2B_4O_7$.

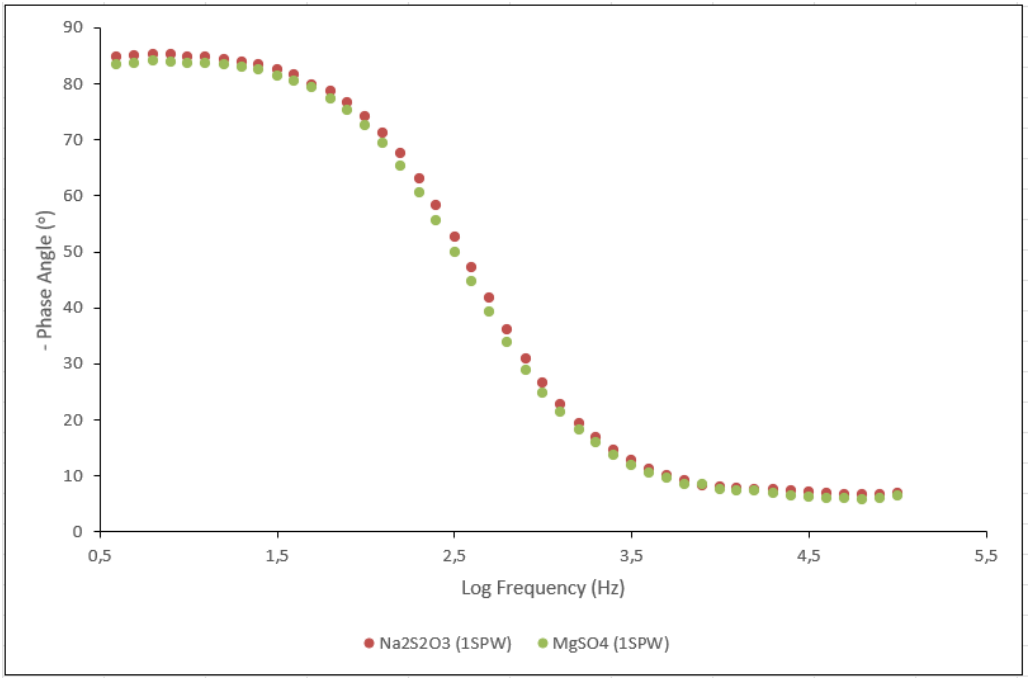

Figure 7.71: Bode plots of phase angle (°) versus log frequency for PdS in the presence of $Na_2S_2O_3$ and $MgSO_4$ at 1 SPW at a pH of 9.2 in O.O5 M $Na_2B_4O_7$.

Figures 7.69 to 7.71 convey Nyquist and Bode plots in the presence of $Na_2S_2O_3$ and $MgSO_4$ at 1 SPW. It is shown in the Nyquist plot in Figure 7.69 that the incomplete semicircle observed, which indicates that the adsorption of $Na_2S_2O_3$ and $MgSO_4$ was mainly attributed by the interfacial charge transfer kinetics process.

Moreover, it is noticeable that the Z_{mod} values from the Bode plot for PdS in the two salts were not significantly different. However, a slight decrease in Z_{mod} values is observed in the presence of $Na_2S_2O_3$, revealing that the rate of adsorption of $Na_2S_2O_3$ on PdS was slightly faster than that of $MgSO_4$. Additionally, it is evident that the phase angles that were observed to be approximately – 85°, are consistent with the capacitive behaviour caused by the electrical double layer at the PdS/solution interface.

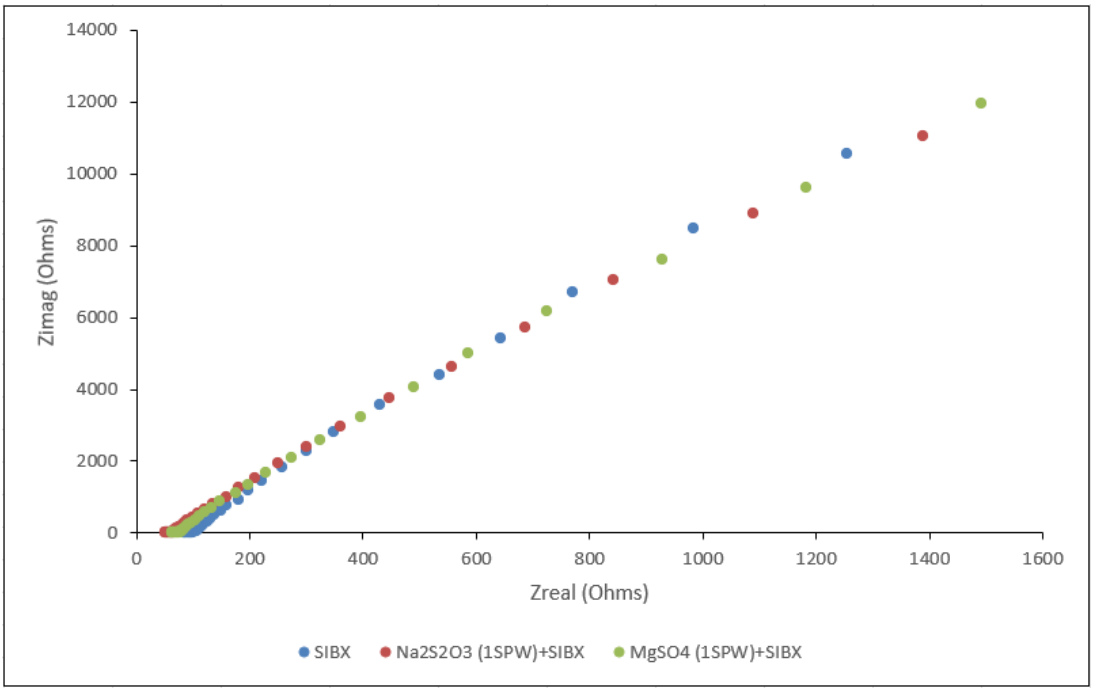

Figure 7.72: Nyquist plots for PdS in the absence and presence of Na2S2O3 and $MgSO_4$ at 1 SPW with SIBX at a pH of 9.2 in O.O5 M $Na_2B_4O_7$.

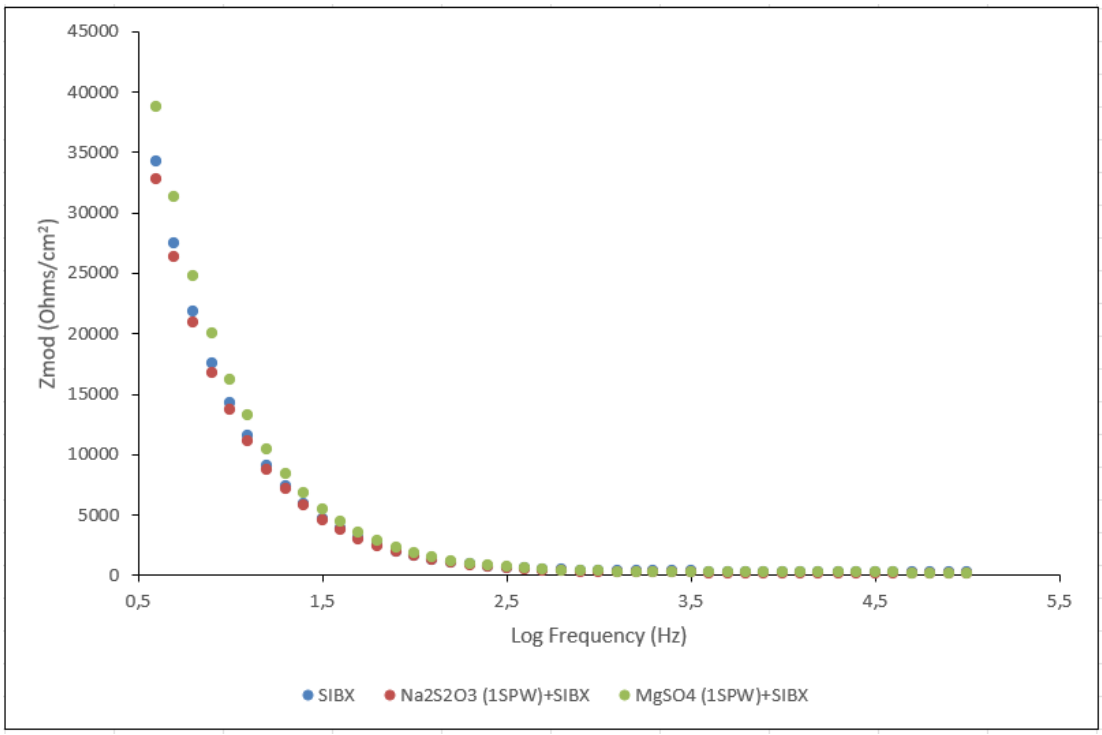

Figure 7.73: Bode plots of Z_{mod} (Ohms/cm^2) versus log frequency (Hz) for PdS in the absence and presence of $Na_2S_2O_3$ and $MgSO_4$ at 1 SPW with SIBX at a pH of 9.2 in O.O5 M $Na_2B_4O_7$.

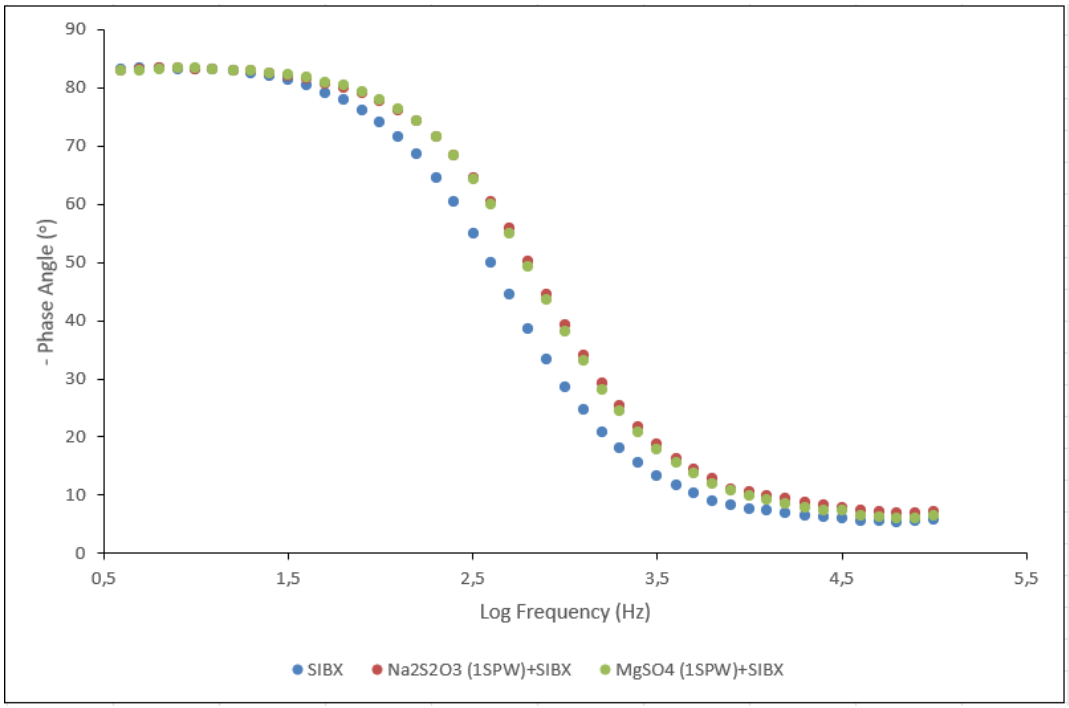

Figure 7.74: Bode plots of phase angle (°) versus log frequency for PdS in the absence and presence of $Na_2S_2O_3$ and $MgSO_4$ at increasing ionic strength with SIBX at a pH of 9.2 in O.O5 M $Na_2B_4O_7$.

Figures 7.72 to 7.74 exhibit Nyquist and Bode plots in the presence of $Na_2S_2O_3$ and $MgSO_4$ at 1 SPW in SIBX. It is observed in Figure 7.72 that generally R_{ct} for PdS in the presence of the two salts investigated in SIBX were higher than in the absence of SIBX. Higher surface resistance indicates lower capacitance hence lower current flow in the electrochemical reactions transpiring on the mineral surface. This is due to lower dielectric constants displayed by xanthate collectors.

The Bode plot demonstrates that the Z_{mod} values observed at lower frequencies both in the absence and presence of salts in SIBX, were not significantly different. However, a slight decrease in the Z_{mod} values was observed to occur in the order $MgSO_4$+SIBX > SIBX > $Na_2S_2O_3$+SIBX, implying that the rate of adsorption of $Na_2S_2O_3$+SIBX was slightly higher than other conditions investigated. Moreover, it is presumed that the rate of formation of continuous surface layers on PdS due to the adsorption and oxidation of SIBX to dixanthogen was almost similar for all the conditions investigated. Ultimately, the phase angles were found to be approximately – 85°, thereby displaying capacitive behaviour caused by the electrical double layer.

7.4.4 Effect of salts at 3 SPW

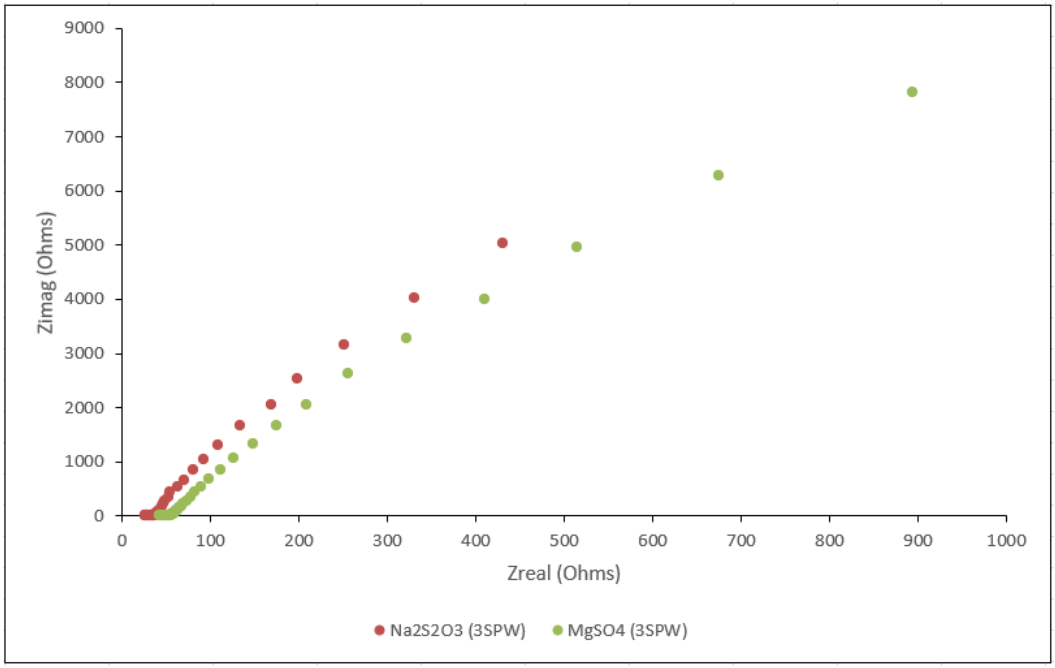

Figure 7.75: Nyquist plots for PdS in the presence of $Na_2S_2O_3$ and $MgSO_4$ at 3 SPW at a pH of 9.2 in O.O5 M $Na_2B_4O_7$.

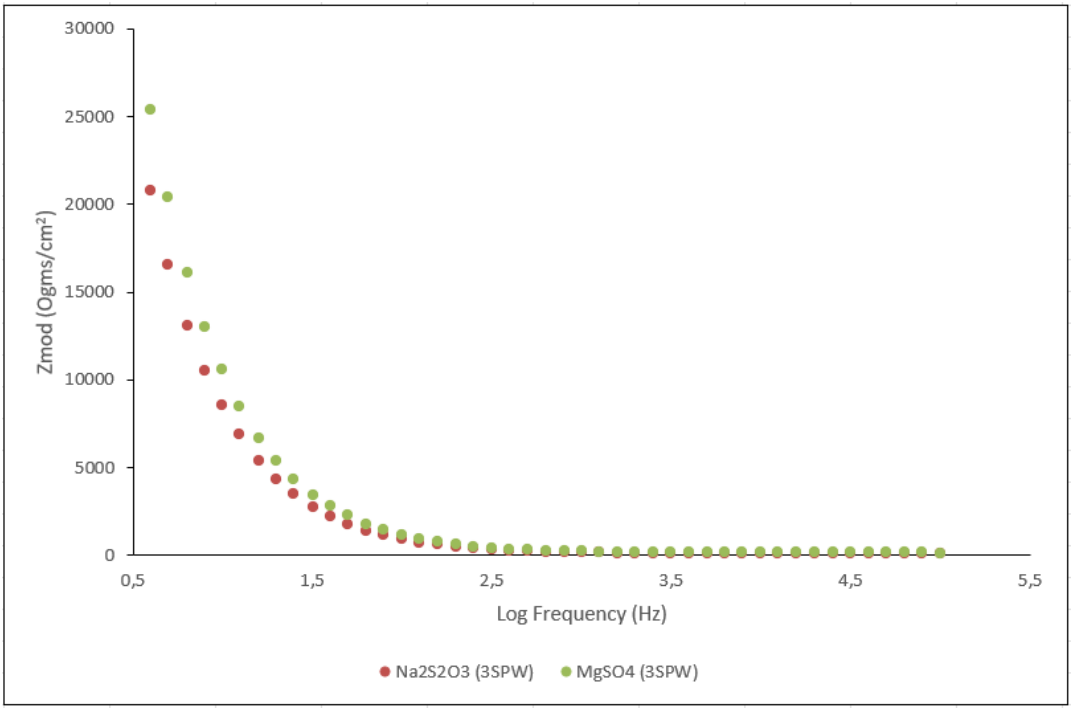

Figure 7.76: Bode plots of Z_{mod} (Ohms/cm^2) versus log frequency (Hz) for PdS in the presence of $Na_2S_2O_3$ and $MgSO_4$ at 3 SPW at a pH of 9.2 in O.O5 M $Na_2B_4O_7$.

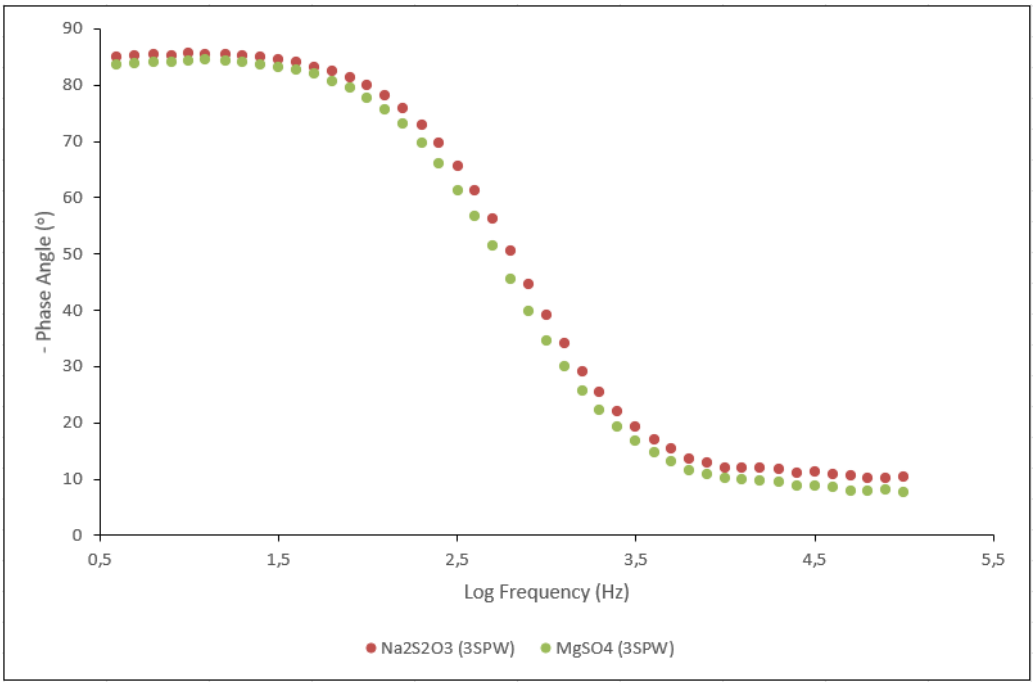

Figure 7.77: Bode plots of phase angle (o) versus log frequency for PdS in the presence of $Na_2S_2O_3$ and $MgSO_4$ at 3 SPW at a pH of 9.2 in O.O5 M $Na_2B_4O_7$.

Figures 7.75 to 7.77 convey Nyquist and Bode plots in the presence of $Na_2S_2O_3$ and $MgSO_4$ at 3 SPW. The Nyquist plot in Figure 7.76 exhibits incomplete semicircles for PdS in the presence of $Na_2S_2O_3$ and $MgSO_4$. This observation indicates that the adsorption of $Na_2S_2O_3$ and $MgSO_4$ on the mineral surface is mainly controlled by interfacial charge transfer kinetics. It was revealed that the R_s for $Na_2S_2O_3$ is less than that for $MgSO_4$. Higher R_{ct} is demonstrated in the presence of $MgSO_4$, denoting lower rate of electrochemical reactions. Hence, the lower R_{ct} obtained in the presence of $Na_2S_2O_3$ indicates a higher rate of electrochemical reactions taking place on the mineral surface.

The Bode plot in Figure 7.76 shows a lower Z_{mod} values in the lower frequency range for $Na_2S_2O_3$, implying a higher rate of adsorption on PdS in the presence of $Na_2S_2O_3$ than in $MgSO_4$ at 3 SPW. Higher Z_{mod} values displayed in the presence of $MgSO_4$ correspond to the higher R_{ct} obtained in the Nyquist plot. Higher impedance values demonstrate lower capacitive behaviour due to lower current flow for the electrochemical reactions transpiring on the PdS mineral surface. Furthermore, the Bode plot in Figure 7.77 display phase angles of approximately – 85° in the presence of both salts, thereby indicating a capacitive behaviour attributable to the electrical double layer at the mineral/solution interface.

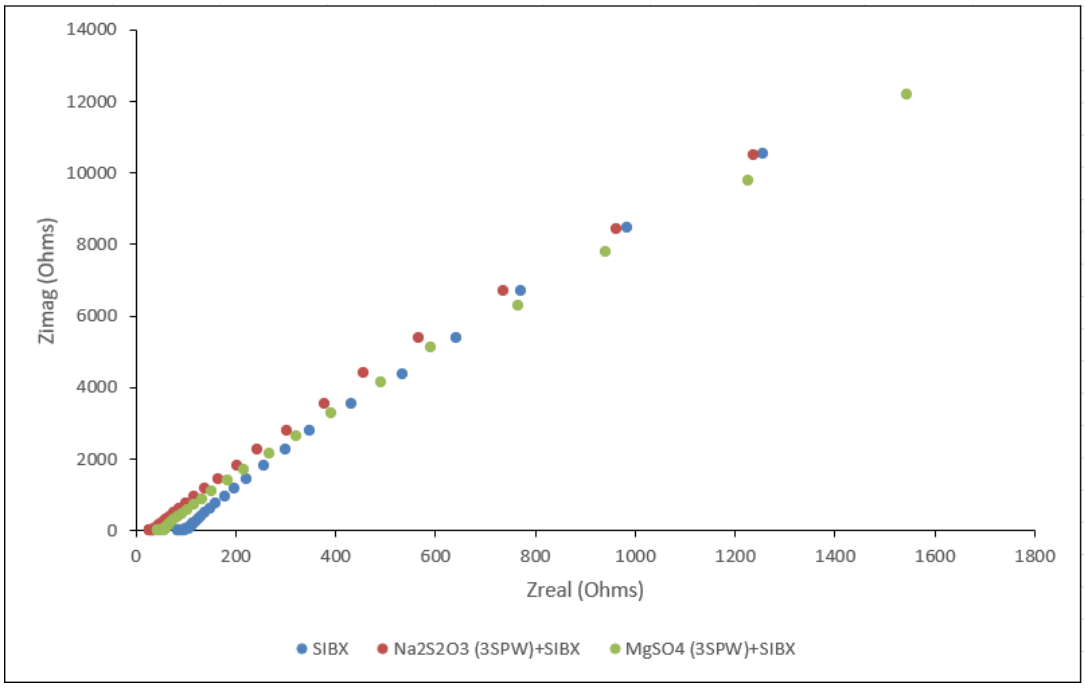

Figure 7.78: Nyquist plots for PdS in the absence and presence of $Na_2S_2O_3$ and $MgSO_4$ at 3 SPW with SIBX at a pH of 9.2 in O.O5 M $Na_2B_4O_7$.

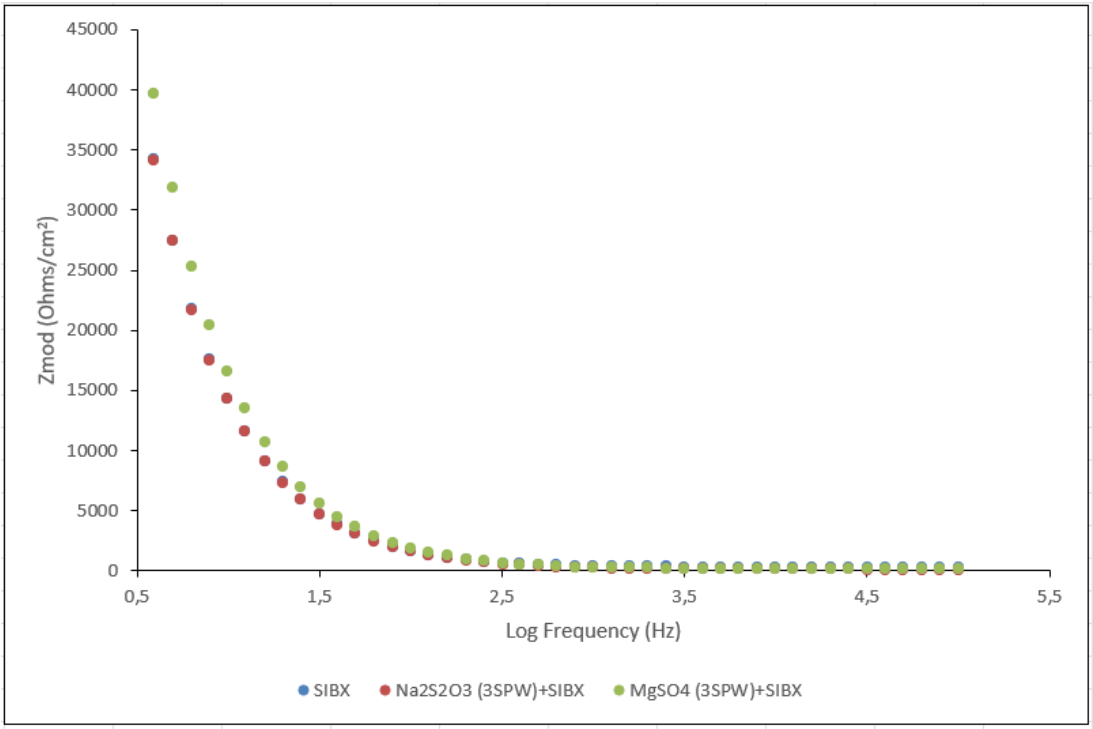

Figure 7.79: Bode plots of Z_{mod} (Ohms/cm^2) versus log frequency (Hz) for PdS in the absence and presence of $Na_2S_2O_3$ and $MgSO_4$ at 3 SPW with SIBX at a pH of 9.2 in O.O5 M $Na_2B_4O_7$.

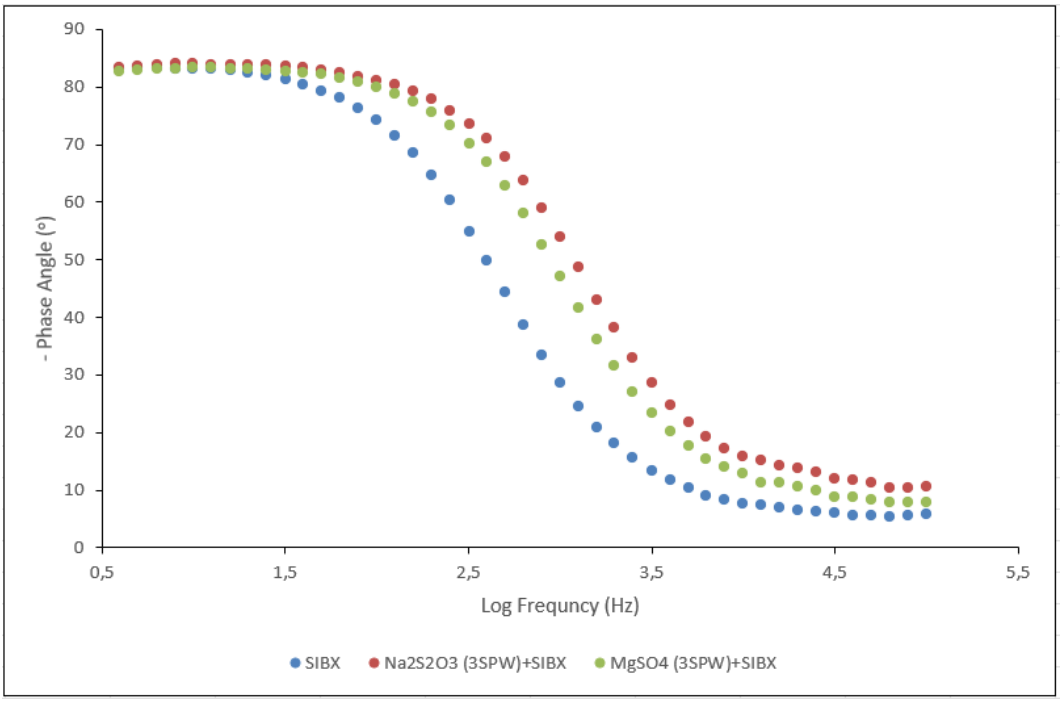

Figure 7.80: Bode plots of phase angle (°) versus log frequency for PdS in the absence and presence of $Na_2S_2O_3$ and $MgSO_4$ at 3 SPW with SIBX at a pH of 9.2 in O.O5 M $Na_2B_4O_7$.

Figures 7.78 to 7.80 demonstrate Nyquist and Bode plots in the presence of $Na_2S_2O_3$ and $MgSO_4$ at 3 SPW in SIBX. It is evident that the R_{ct} values of PdS in the presence of each salt in SIBX were higher than in the absence of SIBX, indicating surface coverage by stable and electrochemically passive oxidation layers of SIBX. Higher resistance corresponds to lower capacitance and lower current flow due to significantly small dielectric constants for xanthate collectors. Upon the adsorption of SIBX on the mineral surface, a decrease in the dielectric constant on the mineral/solution interface, consequently, decreases the capacitance value.

Figure 7.79 clearly shows that in the lower frequency domain, the rate of adsorption on PdS is faster in the presence of $Na_2S_2O_3$ in SIBX, as displayed by the lower Z_{mod} values. The remarkable change in impedance values in the low frequency range denotes the formation of continuous surface layers on the mineral surface, owing to the adsorption of xanthate ions and the oxidation of SIBX to dixanthogen. Moreover, the Bode plots in Figures 7.79 and 7.80 display low impedance values and phase angles that approach zero, which is typically a common response of a resistor to an AC with high frequency.

7.4.5 Effect of salts at 5 SPW

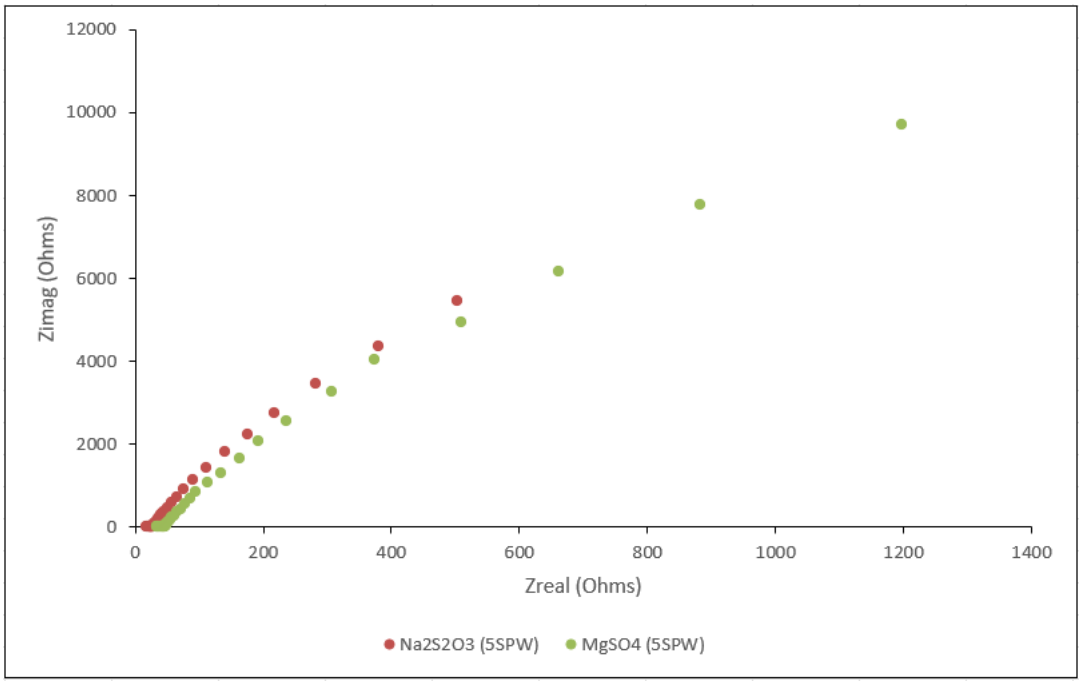

Figure 7.81: Nyquist plots for PdS in the presence of $Na_2S_2O_3$ and $MgSO_4$ at 5 SPW at a pH of 9.2 in O.O5 M $Na_2B_4O_7$.

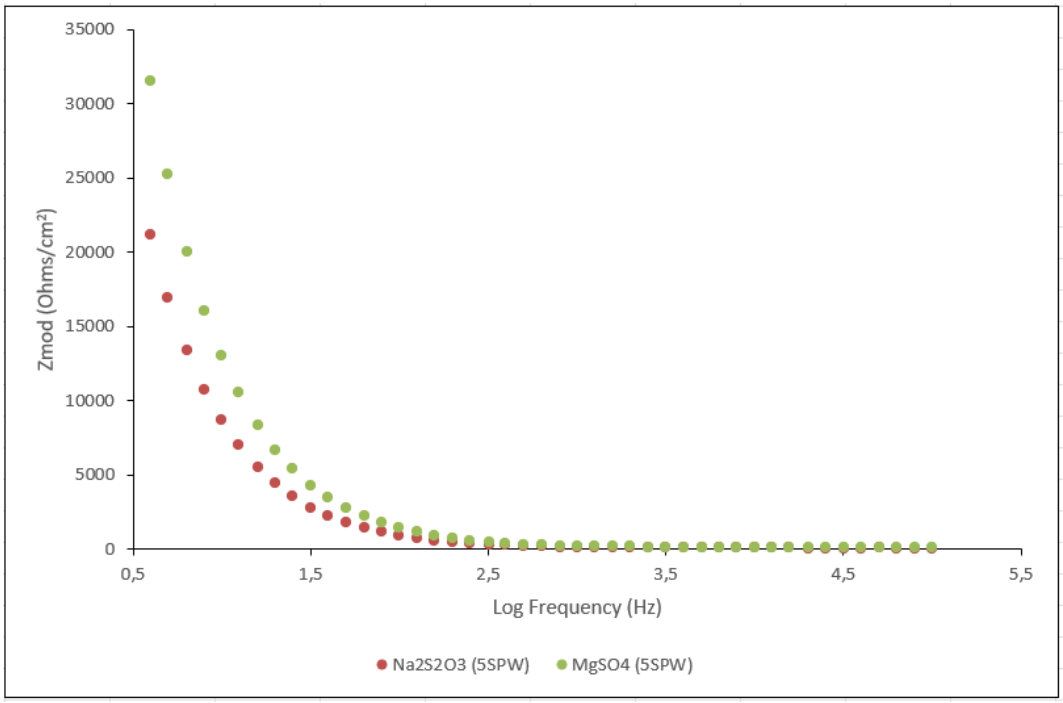

Figure 7.82: Bode plots of Z_{mod} (Ohms/cm^2) versus log frequency (Hz) for PdS in the presence of $Na_2S_2O_3$ and $MgSO_4$ at 5 SPW at a pH of 9.2 in O.O5 M $Na_2B_4O_7$.

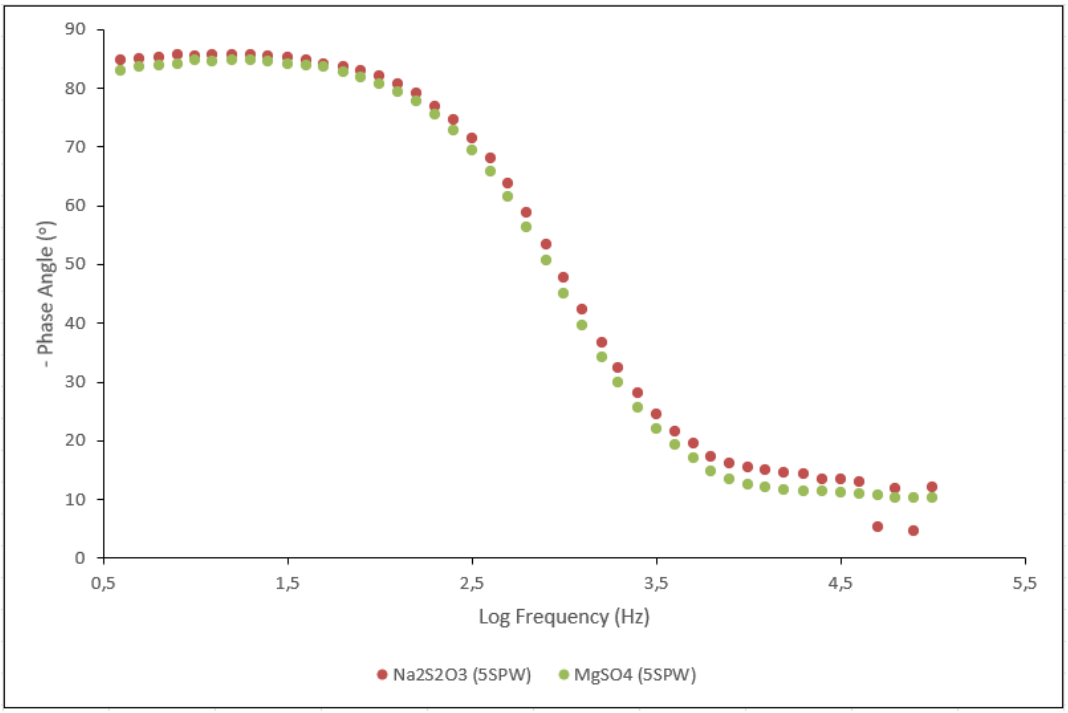

Figure 7.83: Bode plots of phase angle (o) versus log frequency for PdS in the presence of $Na_2S_2O_3$ and $MgSO_4$ at 5 SPW at a pH of 9.2 in O.O5 M $Na_2B_4O_7$.

Figures 7.81 to 7.83 show Nyquist and Bode plots for PdS in the presence of $Na_2S_2O_3$ and $MgSO_4$ at 5 SPW. It is apparent that the reactions occurring on the PdS mineral surface in the presence of $Na_2S_2O_3$ and $MgSO_4$ were most likely influenced by interfacial kinetics. $MgSO_4$ displayed higher R_{ct} than $Na_2S_2O_3$. Thereby, implying that the rate of reaction is faster on PdS in the presence of $Na_2S_2O_3$ at 5 SPW than in the presence of $MgSO_4$ at 5 SPW.

The Bode plot in Figure 7.82 displays significantly lower Z_{mod} values in the presence of $Na_2S_2O_3$, suggesting a higher rate of adsorption of $Na_2S_2O_3$ on PdS. The lower impedance values indicate higher capacitance due to high current flow for the electrochemical reactions occurring on the mineral surface. Moreover, a capacitive behaviour displayed probably by the electrical double layer at the mineral/solution interface is displayed by the phase angles that were determined to be approximately – 85°.

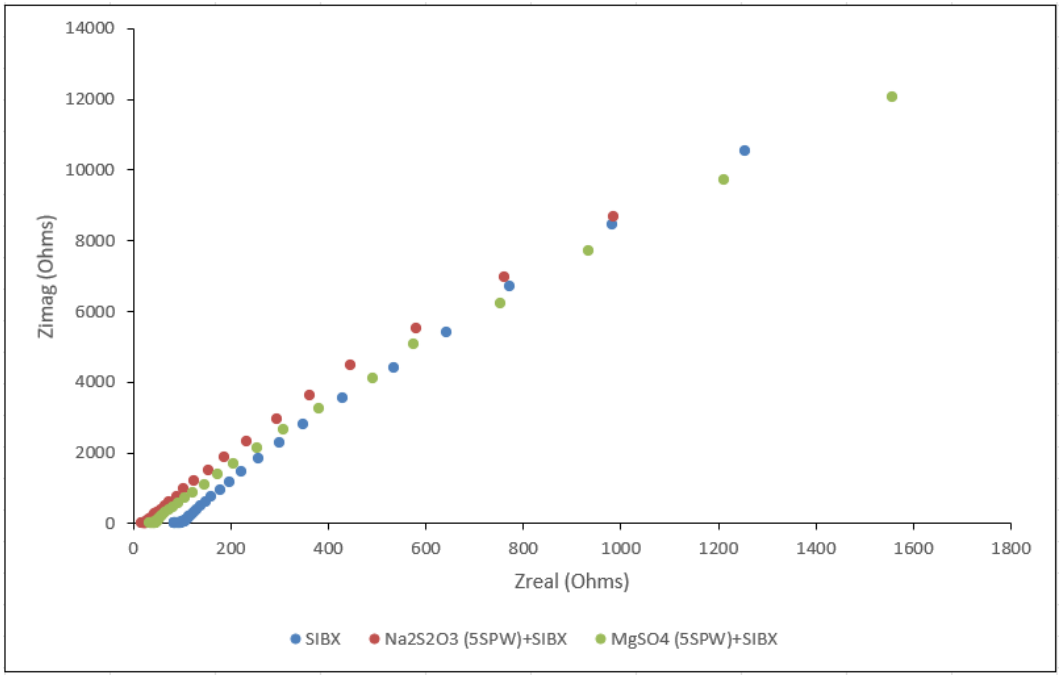

Figure 7.84: Nyquist plots for PdS in the absence and presence of $Na_2S_2O_3$ and $MgSO_4$ at 5 SPW with SIBX at a pH of 9.2 in O.O5 M $Na_2B_4O_7$.

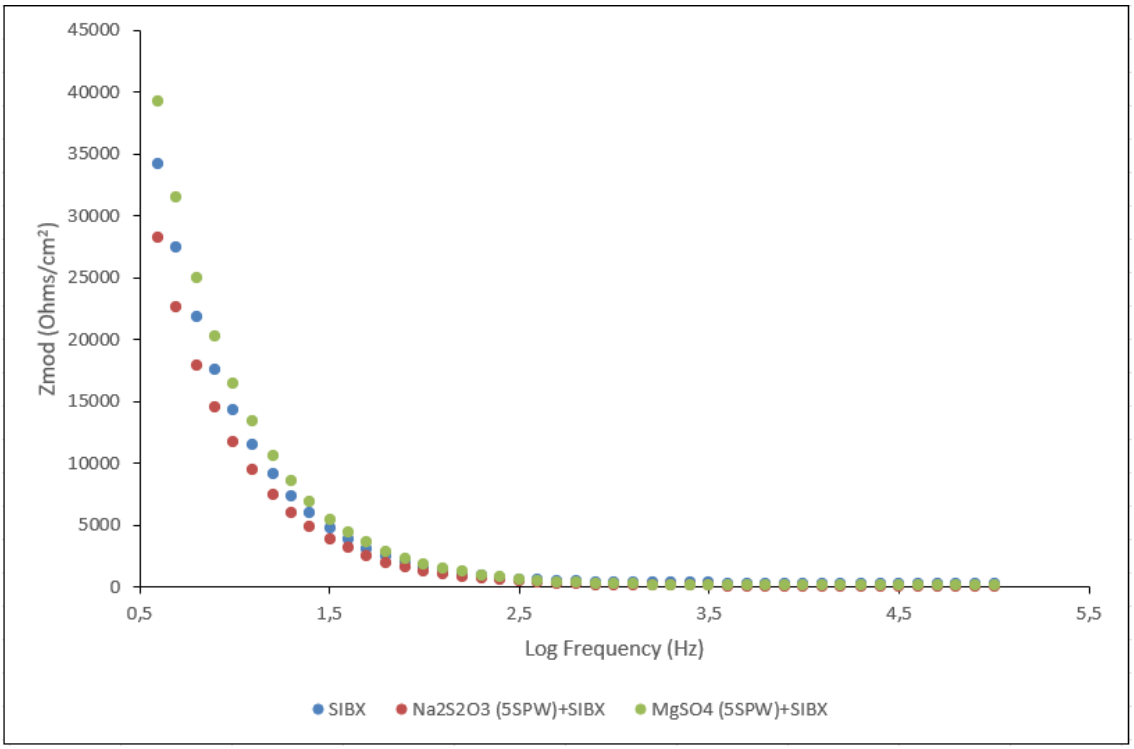

Figure 7.85: Bode plots of Z_{mod} (Ohms/cm^2) versus log frequency (Hz) for PdS in the absence and presence of $Na_2S_2O_3$ and $MgSO_4$ at 5 SPW with SIBX at a pH of 9.2 in O.O5 M $Na_2B_4O_7$.

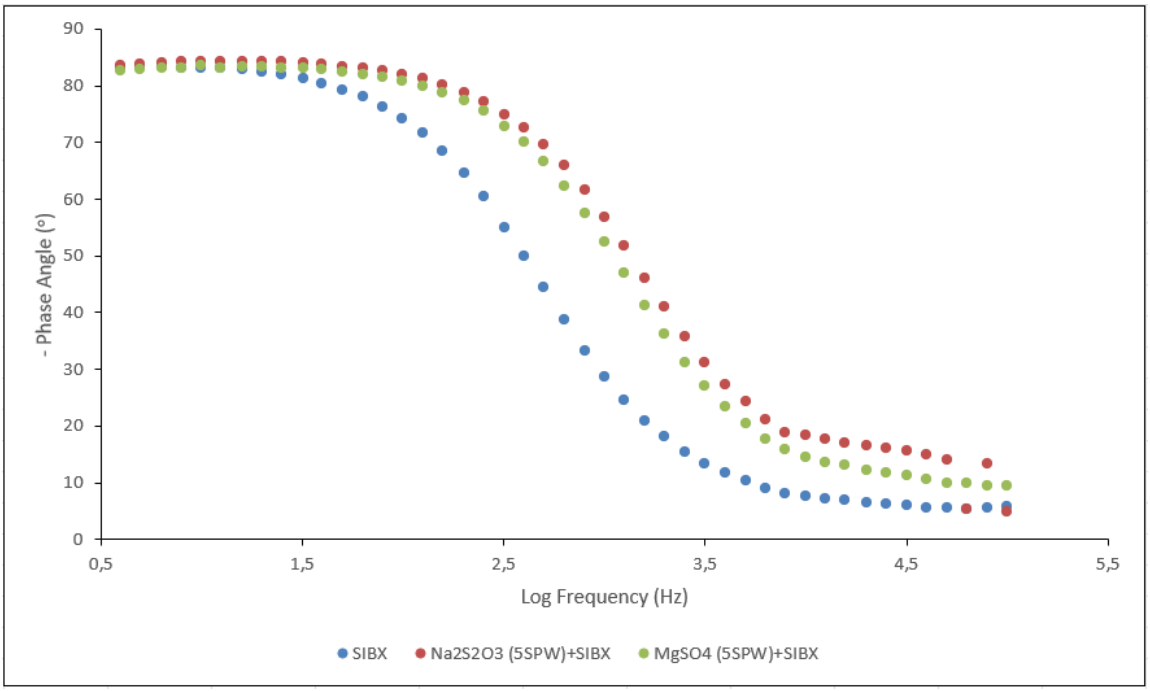

Figure 7.86: Bode plots of phase angle (°) versus log frequency for PdS in the absence and presence of $Na_2S_2O_3$ and $MgSO_4$ at 5 SPW with SIBX at a pH of 9.2 in O.O5 M $Na_2B_4O_7$.

Figures 7.84 to 7.86 illustrate Nyquist and Bode plots in the presence of $Na_2S_2O_3$ and $MgSO_4$ at 5 SPW in SIBX. It is evident that R_{ct} increased significantly in the presence of SIBX as depicted in Figure 7.84 than in Figure 7.81. A higher resistance resembles lower capacitance, owing to lower current flow for the electrochemical reactions. This observation occurs as a result of the smaller dielectric constant for xanthates that is estimated to be approximately 4 – 8.

The Bode plot in Figure 7.85 interestingly displays a decrease in Z_{mod} values in the lower frequency range in the order $Na_2S_2O_3$+SIBX < SIBX < $MgSO_4$+SIBX. Accordingly, it is predicted that the adsorption of $Na_2S_2O_3$+SIBX occurs at a faster rate on the mineral surface than in the presence of SIBX only and $MgSO_4$+SIBX. It is further observed that SIBX adsorbs faster on the mineral surface than in the presence of $MgSO_4$. Furthermore, the significant change in impedance in the low frequency domain indicates the formation of continuous surface layers at different rates for the conditions investigated. The surface layers were formed due to the adsorption of $Na_2S_2O_3$, $MgSO_4$ and the formation of hydrophilic species and the simultaneous adsorption of SIBX and its oxidation to dixanthogen. Additionally, R_s is depicted by the low impedance values and a decrease in phase angles to zero obtained at a higher frequency range. A capacitive behaviour at the

mineral/solution interface was demonstrated by phase angles that were determined to be approximately – 85°.

7.4.6 Effect of salts at 10 SPW

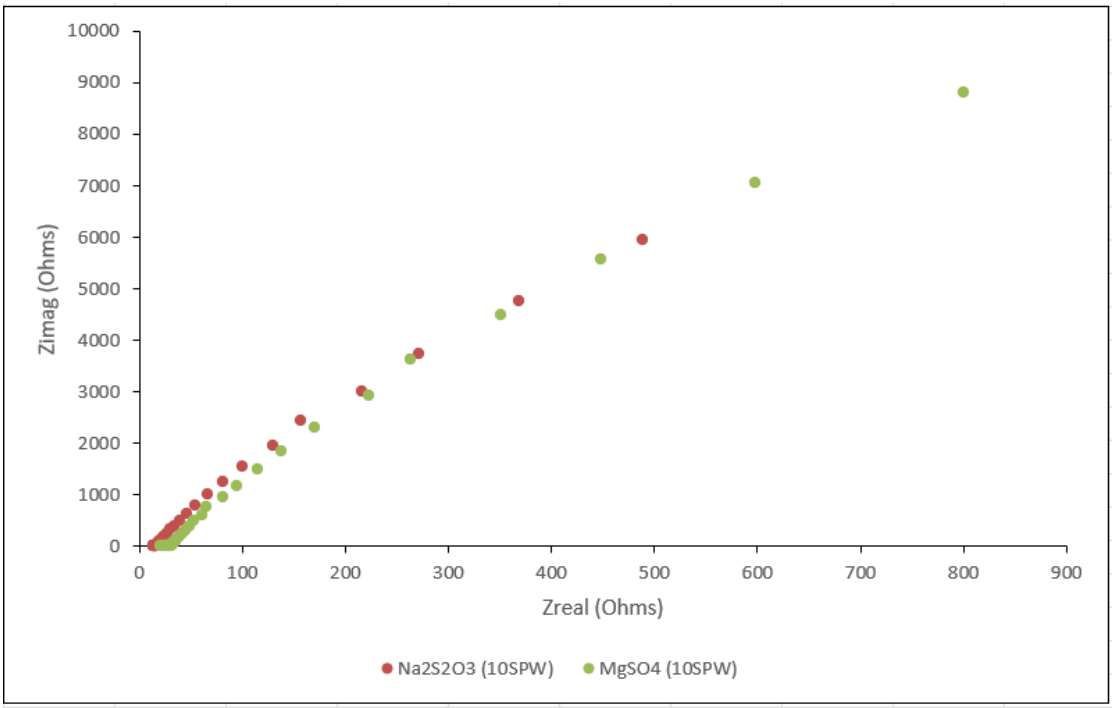

Figure 7.87: Nyquist plots for PdS in the presence of $Na_2S_2O_3$ and $MgSO_4$ at 10 SPW at a pH of 9.2 in O.O5 M $Na_2B_4O_7$.

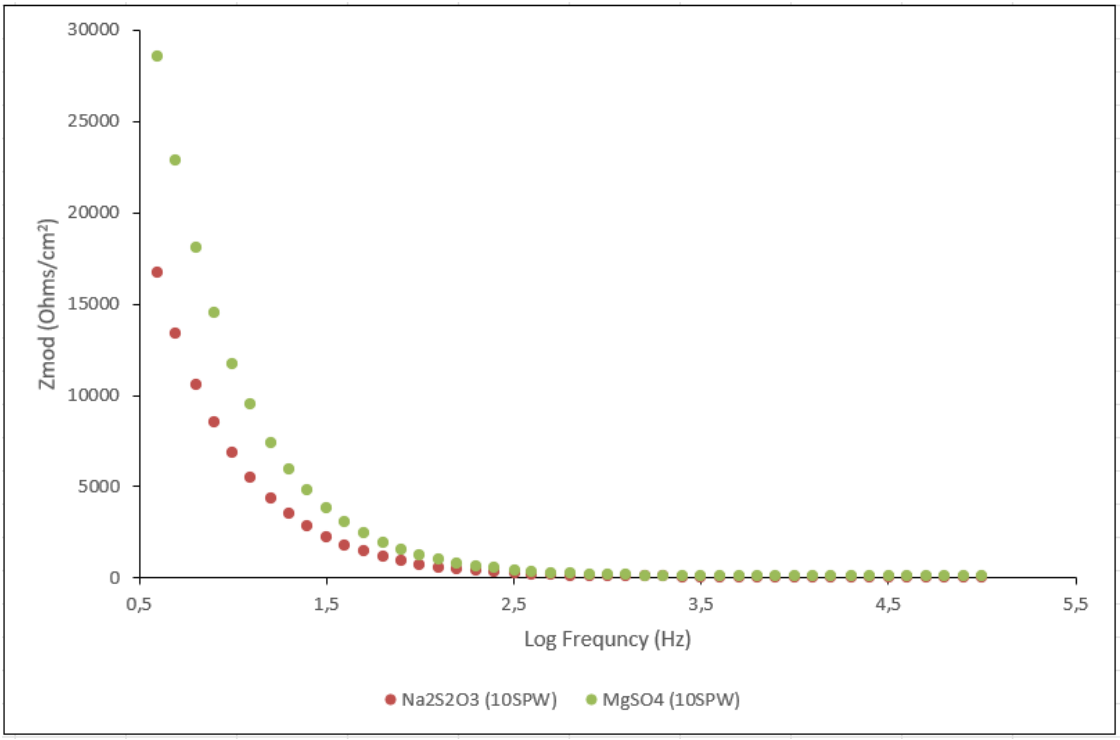

Figure 7.88: Bode plots of Z_{mod} (Ohms/ cm^2) versus log frequency (Hz) for PdS in the presence of $Na_2S_2O_3$ and $MgSO_4$ at 10 SPW at a pH of 9.2 in O.O5 M $Na_2B_4O_7$.

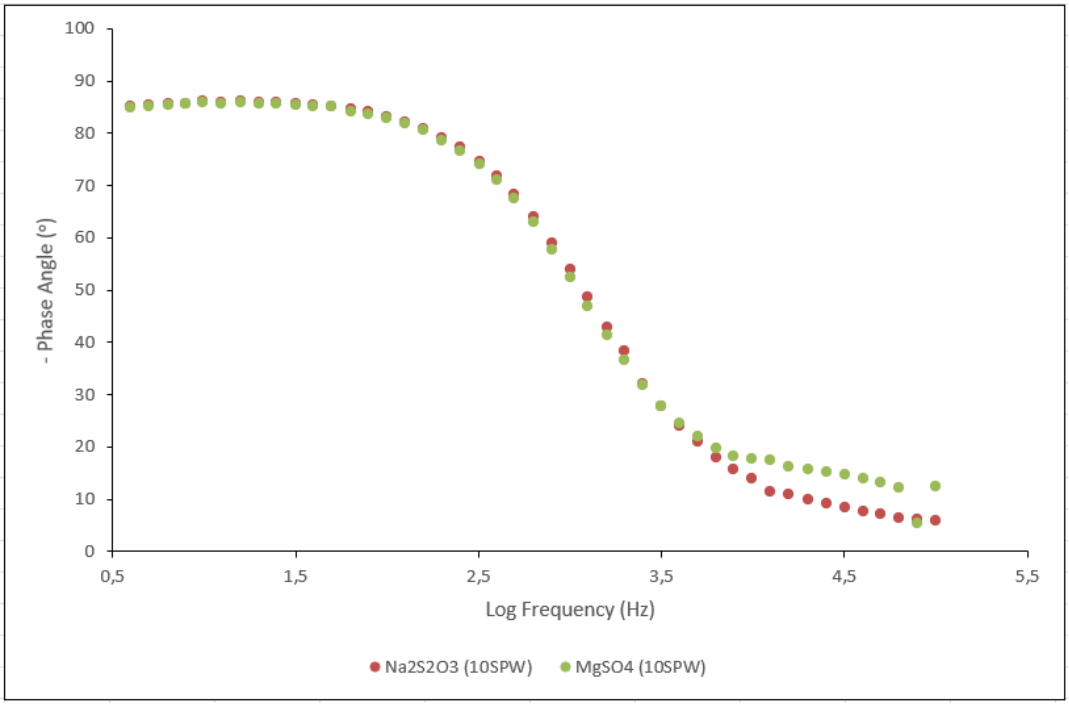

Figure 7.89: Bode plots of phase angle (o) versus log frequency for PdS in the presence of $Na_2S_2O_3$ and $MgSO_4$ at 10 SPW at a pH of 9.2 in O.O5 M $Na_2B_4O_7$.

Figures 7.87 to 7.89 show Nyquist and Bode plots for PdS in the presence of $Na_2S_2O_3$ and $MgSO_4$ at 10 SPW. It is evident in the Nyquist plot in Figure 7.87 that the electron transfer reactions taking place on PdS in the presence of $Na_2S_2O_3$ and $MgSO_4$ could be attributed to interfacial charge transfer kinetics. It is further observed that the R_s is smaller in the presence of $Na_2S_2O_3$ than in the presence of $MgSO_4$ at 10 SPW.

The Bode plot in Figure 7.88 shows an appreciable difference in Z_{mod} values in the presence of $Na_2S_2O_3$ and $MgSO_4$, in the lower frequency domain. The lower impedance values in the presence of $Na_2S_2O_3$, indicate a lower R_{ct} which corresponds to a high rate of adsorption of $Na_2S_2O_3$ and a high rate of reaction on the mineral surface. Moreover, the notable difference in impedance in the low frequency range could be associated with the formation of continuous surface layers due to the adsorption of $Na_2S_2O_3$ and $MgSO_4$ ions on the mineral surface. In addition, lower impedance values reveal higher capacitance due to a high current flow. This therefore suggests the formation of a thicker oxidation layer or a layer with a smaller dielectric constant. Ultimately, in the low frequency range, an inverse relationship was observed between impedance and frequency and phase angles were observed to be approximately – 85°, indicating a capacitive behaviour by the electrical double layer.

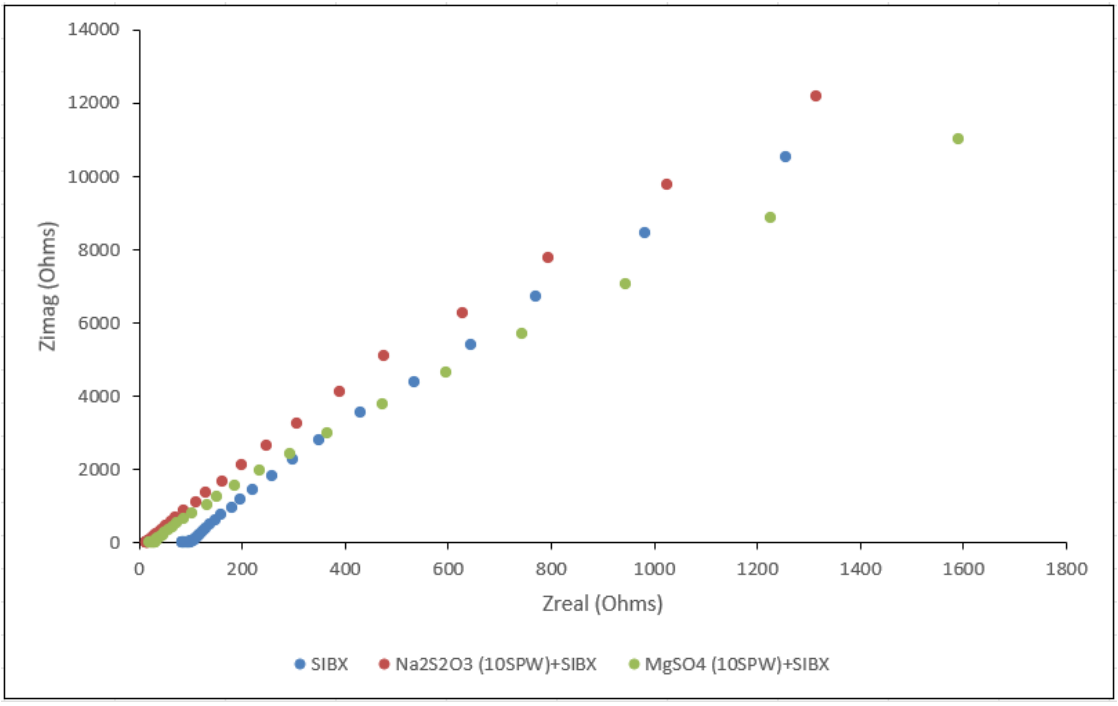

Figure 7.90: Nyquist plots for PdS in the absence and presence of $Na_2S_2O_3$ and $MgSO_4$ at 10 SPW with SIBX at a pH of 9.2 in O.O5 M $Na_2B_4O_7$.

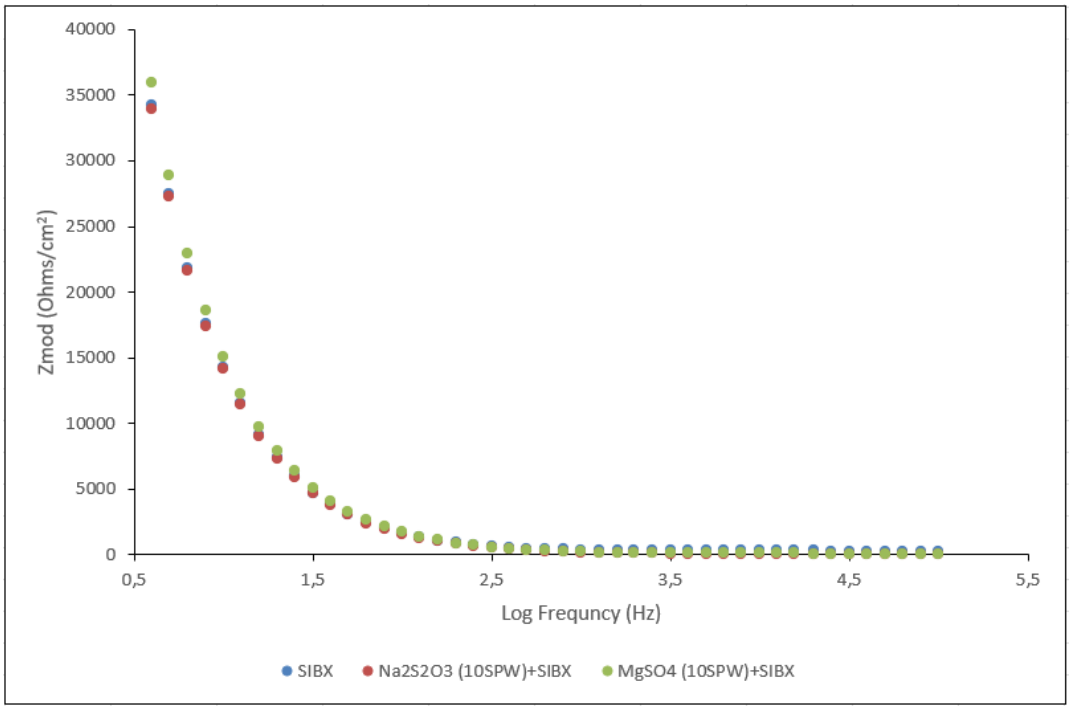

Figure 7.91: Bode plots of Z_{mod} (Ohms/ cm^2) versus log frequency (Hz) for PdS in the absence and presence of $Na_2S_2O_3$ and $MgSO_4$ at 10 SPW with SIBX at a pH of 9.2 in O.O5 M $Na_2B_4O_7$.

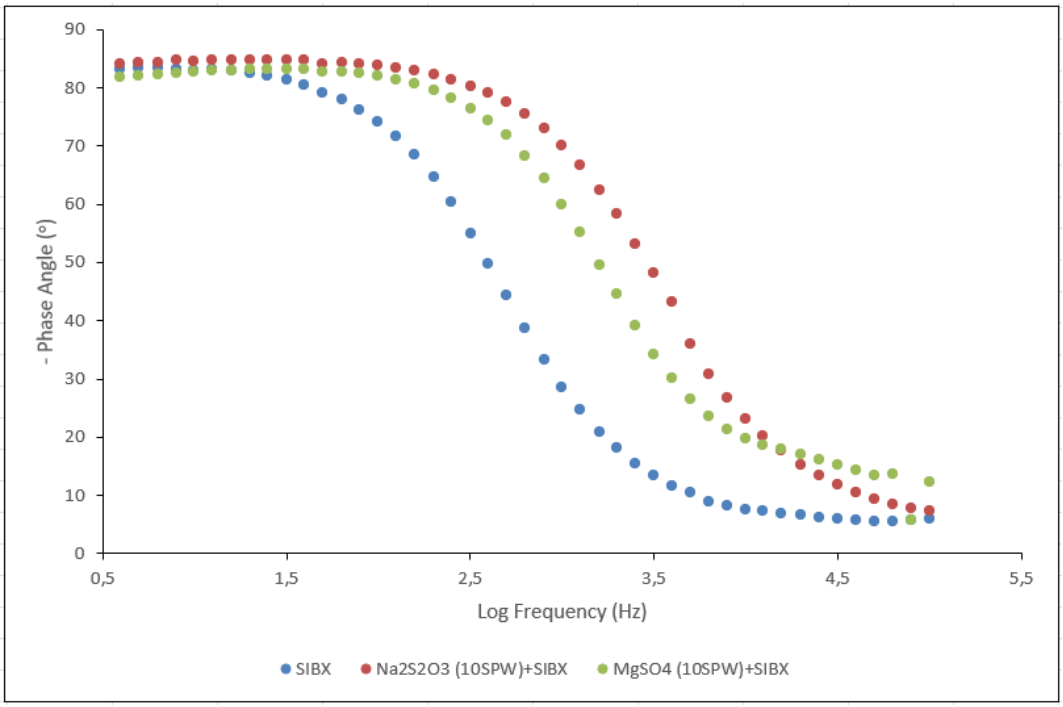

Figure 7.92: Bode plots of phase angle (o) versus log frequency for PdS in the absence and presence of $Na_2S_2O_3$ and $MgSO_4$ at 10 SPW with SIBX at a pH of 9.2 in O.O5 M $Na_2B_4O_7$.

Figures 7.90 to 7.92 plot Nyquist and Bode graphs in the presence of $Na_2S_2O_3$ and $MgSO_4$ at 10 SPW in SIBX. It is evident in Figure 7.90 that higher R_{ct} values were obtained in the presence of SIBX than in the absence of SIBX, Figure 7.87. A higher resistance is generally associated with

lower capacitance, due to the significantly smaller dielectric constant for SIBX. However, R_{ct} decreased in the order $Na_2S_2O_3$+SIBX > SIBX > $MgSO_4$+SIBX, thus indicating a higher rate of reaction on the mineral surface, in the presence of $MgSO_4$+SIBX. Furthermore, it is observed that the impedance for all conditions investigated in Figure 7.91 was probably attributed to mainly interfacial kinetics.

It is interesting to note that the rate of adsorption of $Na_2S_2O_3$+SIBX, $MgSO_4$+SIBX and SIBX only on PdS were found to be similar. This also suggests a similar rate in the formation of continuous layers on the mineral surface due to the adsorption of $Na_2S_2O_3$, $MgSO_4$ and SIBX and the subsequent formation of oxidation layers.

Additionally, it is observed on the Bode plots that at higher frequency domain, the impedance values obtained were relatively constant and were very low, whilst the phase angles decreased to zero. This is a normal response of a resistor to an AC with high frequency, which correlates to R_s. Moreover, a capacitive behaviour caused by the electrical double layer is displayed by phase angles of approximately – 85°.

7.5 Modelling of EIS data

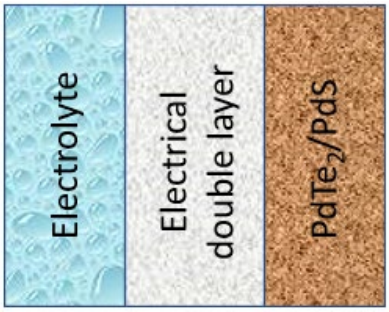

Figure 7.93: Physical model of palladium minerals in an electrolyte solution.

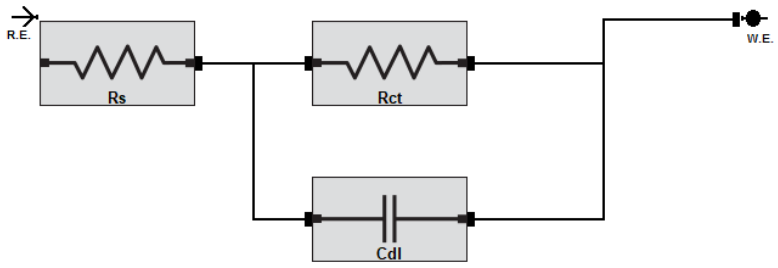

Figure 7.94: Equivalent circuit model for fitting EIS data in the presence of salts.

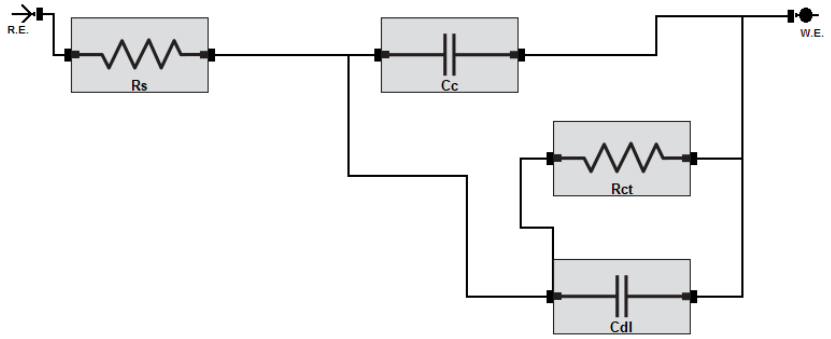

Figure 7.95: Equivalent circuit model for fitting EIS data in the presence of salts and SIBX.

Figure 7.93 displays a physical model of the palladium electrodes in an electrolyte. Based on the EIS results obtained, two equivalent circuit models are proposed for the electrochemical system to fit the experimental data by the simplex method using Echem analyst. The equivalent circuit in Figure 7.94, represents an electrochemical system that consists of the salts at the mineral surface. It consists of a resistor, R_s, in series with a parallel circuit that consists of a capacitor, C_{dl} (capacitance of the electrical double layer) and a resistor, R_{ct}. Figure 7.95 represents the electrochemical system that contains both the salts and SIBX. The equivalent circuit comprises of a resistor, R_s, in series with a parallel circuit consisting of a capacitor, C_c (capacitance of the coating layer from SIBX), a resistor, R_{ct} and a capacitor, C_{dl}.

7.6 Key Findings

Table 7.1: Key findings for EIS results

$PdTe_2$	PdS
• Generally, R_s decreased with an increase in ionic strength of the salts investigated.	• R_s decreased with an increase in ionic strength of the salts investigated.
• All conditions investigated showed that impedance was attributable to interfacial kinetics except for $Na_2S_2O_3$ at 1 SPW, $MgSO_4$ at 3 SPW and 5 SPW, and NaCl at 5 SPW and 10 SPW, which displayed diffusion-controlled processes at lower frequencies.	• All conditions displayed that impedance was influenced by interfacial kinetics except $Na_2S_2O_3$ at all ionic strengths with SIBX.
• $Na_2S_2O_3$ adsorbed the least among other salts.	• $Na_2S_2O_3$ adsorbs faster on PdS than $MgSO_4$.
• All salts investigated were adsorbed at a faster rate on the mineral surface at lower ionic strengths, except for $Na_2S_2O_3$ which adsorbed faster at higher ionic strengths.	• $Na_2S_2O_3$ demonstrated higher rates of adsorption with higher ionic strength. $MgSO_4$ displayed higher rates of adsorption at lower ionic strengths.
• Higher R_{ct} was exhibited with an increase in ionic strength in the case of $MgCl_2$, $CaCl_2$ and NaCl. Lower R_{ct} was displayed with an increase in ionic strength in the case of $Na_2S_2O_3$.	• Higher R_{ct} was conveyed at higher ionic strengths of the salts investigated.
• Phase angles of approximately – 80° were obtained, indicating capacitive behaviour at the mineral/solution interface.	• Phase angles of approximately – 85° were determined, implying capacitive behaviour at the mineral/solution interface.
• Adsorption of SIBX was inhibited by all salts investigated.	

8. Discussion

This chapter considers an integration of the rest potential, cyclic voltammetry and electrochemical impedance spectroscopy results obtained from this study. The results were analyzed to determine the mechanisms of interaction for $Na_2S_2O_3$, $NaCl_2$, $CaCl_2$, $MgSO_4$ and $MgCl_2$ at increasing ionic strength on $PdTe_2$ and PdS with and without SIBX. All potentials in this chapter are discussed according to SHE.

For the precise evaluation of the adsorption behaviour of SIBX in the presence of $Na_2S_2O_3$, $NaCl_2$, $CaCl_2$, $MgSO_4$ and $MgCl_2$ at increasing ionic strength, EIS data were fitted to the equivalent circuits Figures 7.94 and 7.95. This is further discussed in Section 8.8 of this Chapter.

8.1 Reactions of Palladium minerals in the absence of salts and SIBX

8.1.1 Reactions of PdS

On the anodic scan during cyclic voltammetry the current response of PdS in the buffer solution, without any salt, sets in above 0.3 V. This suggests the slow oxidation of PdS to SO_4^{2-} and PdO. This is due to the less negative potential (Equation 8.1), which implies that PdS will be slightly affected by oxidation. The reaction in Equation 8.1 is supported by the Pourbaix diagram in Figure 2.9, which illustrates the formation of PdO and SO_4^{2-} ions within the potential range investigated in this study.

$$PdS + 5H_2O \leftrightarrow PdO + SO_4^{2-} + 10H^+ + 8e^- \qquad E^0 = -0.04\,V \qquad \text{(Eqn. 8.1)}$$

On the negative sweep, a pronounced cathodic peak that developed within the potential range of – 0.1 V to – 0.6 V, depicts the reduction of more than one oxidized species. The reduction peak could be associated with the reduction of oxygen (Equation 2.28) and the reduction of the oxidized species formed on the mineral surface (Equations 8.2 and 8.3).

$$PdO + SO_4^{2-} + 8e^- + 10H^+ \rightarrow PdS + 5H_2O \qquad E = -0.07\,V \qquad \text{(Eqn. 8.2)}$$

$$Pd^{2+} + SO_4^{2-} + 8e^- + 8H^+ \rightarrow PdS + 4H_2O \qquad E = 0.048\,V \qquad \text{(Eqn. 8.3)}$$

8.1.2 Reactions of $PdTe_2$

The oxidation of $PdTe_2$ is illustrated by two anodic current peaks generated above the potential of 0.2 V. It is proposed that the oxidation of $PdTe_2$ in alkaline conditions might have formed any or all of the oxidized species, TeO_2 as demonstrated in Equation 2.10, and/or PdO, TeO_3^{2-}, $Pd(OH)_2$ as shown in Equations 2.22-2.26 (Mishra et al., 1990, Elvy and Williams, 1996, Tadie, 2015, D'Olimpio et al., 2019). It is presumed that the presence of Te on a $PdTe_2$ mineral, makes the mineral surface unstable against surface oxidation, therefore, Te is perceived to migrate to the mineral surface hence forming a stable overlayer of TeO_2. Thermodynamically, it is depicted in Figure 2.11, the Pourbaix diagram for a Te-O-H system, that under standard pressure and temperature, TeO_3^{2-} is the most stable species that form over a wide range of potential and pH. Furthermore, the thermodynamic feasibility of the oxidation of Te^0 to TeO_3^{2-} was practically proven by an extensive electrochemical investigation on the oxidation of Te ions by Mishra et al. (1990). Suggesting that whilst it is not a tellurium oxide initially on the mineral surface, the end speciation is the oxide species.

Moreover, Elvy and Williams (1996) reported on the incongruent surface oxidation of a Pd-Te-Bi system (PdTe, PdTeBi and PdBi), where it was proposed that Bi and/or Te migrate to the surface, where they are readily oxidized to form an overlayer of Bi_2O_3 or TeO_2 on the palladium-rich substrate. In addition, it was revealed that the reactivity of the Pd-Te-Bi system occurs in the order PdTe < PdTeBi < PdBi where it was suggested that though Te does not readily oxidize at ambient temperatures, the Te in PdTe and PdTeBi is much more reactive. Furthermore, Vermaak et al. (2004) observed that the oxidation of a Pd-Te-Bi system in the absence of a xanthate collector occurred at potentials above 300 mV. They further surmised that $PdTe_2$ should be more resistant to oxidation than PdBiTe, owing to the high tellurium content. However, it was determined in this work that $PdTe_2$ oxidizes at potentials above 200 mV. This suggests that $PdTe_2$ oxidizes at a lower potential than that reported for a Pd-Te-Bi system. It is important to note that the conditions of Vermaak et al. (2004) and this work were similar. Additionally, the findings of this work are in disagreement with those of Vermaak et al. (2004). The results obtained in this study, therefore, correspond to the reactivity series for non-metallic elements for Te and Bi on the periodic table, where it is expected that Te is more reactive than Bi.

Additionally, on the cathodic scan, a broad cathodic current peak was observed within the potential range of 0 V to – 0.2 V and the cathodic current peak that emerged above – 0.4 V could be associated with the reduction of more than one component of oxidation products formed on the

$PdTe_2$ mineral surface. The observed cathodic peaks could be a result of the reduction of palladium oxides/hydroxides and/or the reduction of TeO_3^{2-} to lower oxidation states of Te^{2-}, as displayed in Equations 2.17 and 2.18.

8.2 Reactions of Palladium minerals with SIBX

8.2.1 Reactions of PdS with SIBX

The extent of interaction of SIBX with PdS in the absence of salts is displayed in Figure 5.4. It is observed that the extent of interaction of SIBX with PdS is relatively high compared with other conditions investigated. Furthermore, it is shown that the final rest potential is approximately 139 mV, which is further away from the equilibrium potential of dixanthogen (80 mV) under these conditions. It is evident that the final rest potential for the baseline case was the highest among all other conditions investigated. Thus, indicating that the formation of dixanthogen is favourable and presumably, a faster rate of dixanthogen formation on the mineral surface may have transpired. This observation suggests that upon the adsorption of SIBX on PdS, SIBX oxidizes to dixanthogen as illustrated in Equation 2.9. The rest potential measurements obtained, corresponded to the cyclic voltammetry responses attained, where an appreciable anodic peak was generated above 0.2 V (200 mV), above the equilibrium potential of dixanthogen formation. Additionally, it has been proposed that the adsorption products on mineral surfaces are highly determined by the semiconductor type of minerals (Zhang, 2021). Considering that PdS is an n-type semiconductor (Ferrer et al., 2007), it is therefore expected that dixanthogen is formed on the mineral surface (Zhang, 2021). This assumption conforms to the findings of this study.

In electrochemical processes where the formation of a dimer is favoured, the mineral surface is not directly involved in any of the oxidation reactions but instead provides a pathway for electrons to be transferred from the active site where a xanthate collector oxidizes to the active site where the cathodic reaction involving the reduction of oxygen occurs. The mechanisms involved are firstly the electrochemical adsorption of the xanthate collector as demonstrated in Equation 2.29 followed by its oxidation as depicted in Equation 2.34.

Impedance data revealed that the adsorption of SIBX on PdS occurs through charge transfer kinetics (Figure 7.60). This is in agreement with the findings of Woods (1971), who proposed that the adsorption of xanthate collectors involves the transfer of charge from the collector to the mineral surface and a simultaneous reduction of oxygen takes place, where the charge is returned into the solution. Furthermore, it is discerned from Figure 7.62 that a phase angle of approximately

– 85° was obtained, owing to the capacitive behaviour of the electrical double layer and/or the coating layer exhibited by SIBX on the mineral surface.

Moreover, upon the cathodic scan, no cathodic peaks appeared. This suggests that the dixanthogen species formed on PdS might be soluble or electrochemically inactive within the potential region investigated in this study or the oxidation products formed could be loosely bound (Vermaak et al., 2007) to the mineral surface. However, it is highly unlikely to be due to soluble products because heavy metal xanthates are known to have a low solubility due to a covalent bond that exists between the metal and sulphur atoms (Sheikh, 1972).

8.2.2 Reactions of $PdTe_2$ with SIBX

It is observed in Figure 5.5 that despite the relatively high interactions between SIBX and $PdTe_2$, the final rest potential yielded was below the equilibrium potential of dixanthogen formation. This indicates that possibly two alternative reactions occurred on the mineral surface. Possibly a chemisorption reaction transpired as in Equation 2.29, which is a thermodynamically favoured reaction in the interaction of minerals and xanthate collectors. It is known to occur at lower potentials than the formation of the corresponding dixanthogen (Buckley and Woods, 1997). Alternatively, the formation of a metal xanthate was possibly favoured (Equation 8.4) (Figure 8.1). Though Pd forms a rare accumulation of n-type metal to semiconductor with Te, the effect of tellurium as a p-type doped narrow-band gap semiconductor (Qiu et al., 2019), makes the mineral more inclined to the formation of a metal xanthate.

$$PdTe_2 + 2X^- + 6H_2O \leftrightarrow PdX_2 + 2TeO_3^{2-} + 12H^+ + 10e^- \qquad E^o = 0.658 \qquad \text{(Eqn. 8.4)}$$

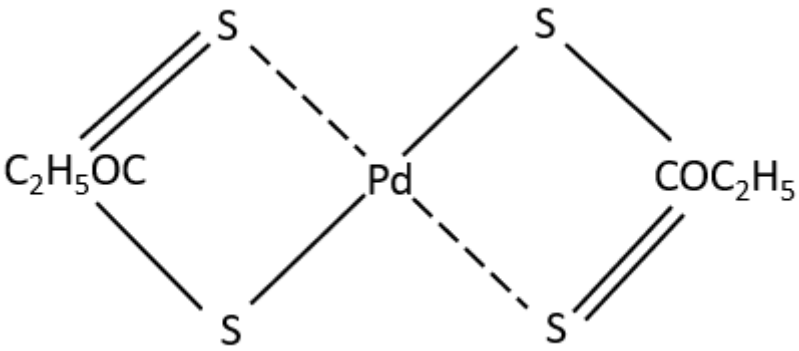

Figure 8.1: Divalent palladium xanthate

It is proposed in this study that the interaction of $PdTe_2$ and SIBX occurs through chemical and electrochemical mechanisms:

i. Chemisorption reaction (does not involve the transfer of electrons). This process has been associated with previous studies using K_{sp} values (Basilio and Yoon, 1992, Pecina et al., 2006). The K_{sp} of a metal-xanthate compound has been established to control the chemical step such that it determines the precipitation of a metal-xanthate compound. The K_{sp} value for PdX_2 has been determined in literature to be very low, 3.03×10^{-43} (Tadie, 2015). The low K_{sp} value of PdX_2, therefore, indicates that the precipitation of the metal-xanthate is likely to occur even if $PdTe_2$ is only slightly oxidized. Hence, the mechanisms of formation of $PdTe_2$ are proposed to occur as in Equations 8.5 to 8.8.

$$Pd^{2+}_{surface} + 2X^{-}_{aqueous} \leftrightarrow [Pd(X_2)]_{surface} \quad \text{(Eqn. 8.5)}$$

$$[PdTe_2, OH^-]_{surface} + X^{-}_{aqueous} \leftrightarrow [PdTe_2, X^-]_{surface} + OH^- \quad \text{(Eqn. 8.6)}$$

$$[PdOH^+]_{surface} + X^{-}_{aqueous} \leftrightarrow [Pd(X)^+]_{surface} + OH^- \quad \text{(Eqn. 8.7)}$$

$$[Pd(OH_2)]_{surface} + 2X^{-}_{aqueous} \leftrightarrow [Pd(X)_2]_{surface} + 2OH^- \quad \text{(Eqn. 8.8)}$$

A similar mechanism was proposed by Pecina et al. (2006) for the interaction between galena and DTPINa, a chelating agent, where it was suggested that the mechanism of DTPINa adsorption onto galena initiates with a chemisorption reaction of DTPINa through processes that do not involve electron transfer.

ii. On the anodic scan for SIBX only, at a potential above 0.3 V (Figure 6.25), an electrochemical reaction occurred between the xanthate ions and the active metallic sites on the $PdTe_2$ surface to form the metal-xanthate compound.

The overall mechanism:

$$2X^- + PdTe_2 \leftrightarrow Pd(X)_2 + 2Te + 2e^- \quad \text{(Eqn. 8.9)}$$

Moreover, the greater difference in rest potential obtained with $PdTe_2$ than with PdS conveys a greater rate of reduction of $PdTe_2$ in the presence of SIBX. Furthermore, the proposed anodic reactions justify the broad cathodic peak (Figure 6.26), which was observed to develop between a potential range of 0 to – 0.2 V. The reduction of more than one component of oxidation products was observed by the broad cathodic peak that was generated above – 0.4 V.

Additionally, EIS data from Figures 7.7 to 7.9 display higher R_{ct} in the case of SIBX only. This suggests lower capacitance due to lower current flow. Lower capacitive behaviour is attributable to the formation of a layer on the mineral surface with a smaller dielectric constant. Hence, the dielectric constant for xanthate collectors is known to be around 4 - 8 (Mu et al., 2015). Ultimately, a phase angle of approximately – 80° was exhibited, which demonstrates the capacitive behaviour. The capacitance effect is contributed by the double-layer charging effect (Cd) and possible surface layers (Cs). The latter could be associated with the adsorption of SIBX and the formation of oxidation products on the mineral surface. Furthermore, the electrode capacitance is demonstrated as the series combination of both effects as depicted in Equation 8.10. It is conveyed in Equation 8.10 that the formation of a surface layer, with a finite value of C_s will subsequently decrease the capacitance of the electrode (Vermaak et al., 2004). Owing to the predominance of lower potential species formed on the mineral surface.

$$\frac{1}{C} = \frac{1}{C_D} + \frac{1}{C_S} \qquad \text{(Eqn. 8.10)}$$

8.2.3 Surface coverage of SIBX on $PdTe_2$

Figure 8.2 plots the fractional surface coverage of SIBX on $PdTe_2$ in the absence and presence of the salts investigated at an increase in ionic strength. Thiol adsorption was established by integrating cathodic peaks from voltammograms for each condition investigated. Thereafter, the ratio between the number of moles of dixanthogen covering the mineral surface to the total surface coverage of a monolayer of xanthate was determined. Fractional coverage calculations were only performed for $PdTe_2$. The electrochemical responses generated in voltammograms for PdS did not allow for the determination of charge transferred in the reduction peaks, due to the absence of cathodic peaks. Detailed calculations are presented in Appendix C.

Notwithstanding the fact that surface coverages for SIBX were calculated for $PdTe_2$ only, it is presumed that SIBX formed a more uniform layer on the $PdTe_2$ and PdS mineral surfaces. The postulated uniform layer was formed as a result of the long hydrocarbon chain of SIBX, hence, increased lateral hydrophobic attraction forces between the hydrocarbon chains (Zhang, 2021). Furthermore, it was surmised that the cathodic currents from which the surface coverages were calculated, were due to SIBX only.

The fractional surface coverages of SIBX on $PdTe_2$ are discussed in detail under each salt investigated.

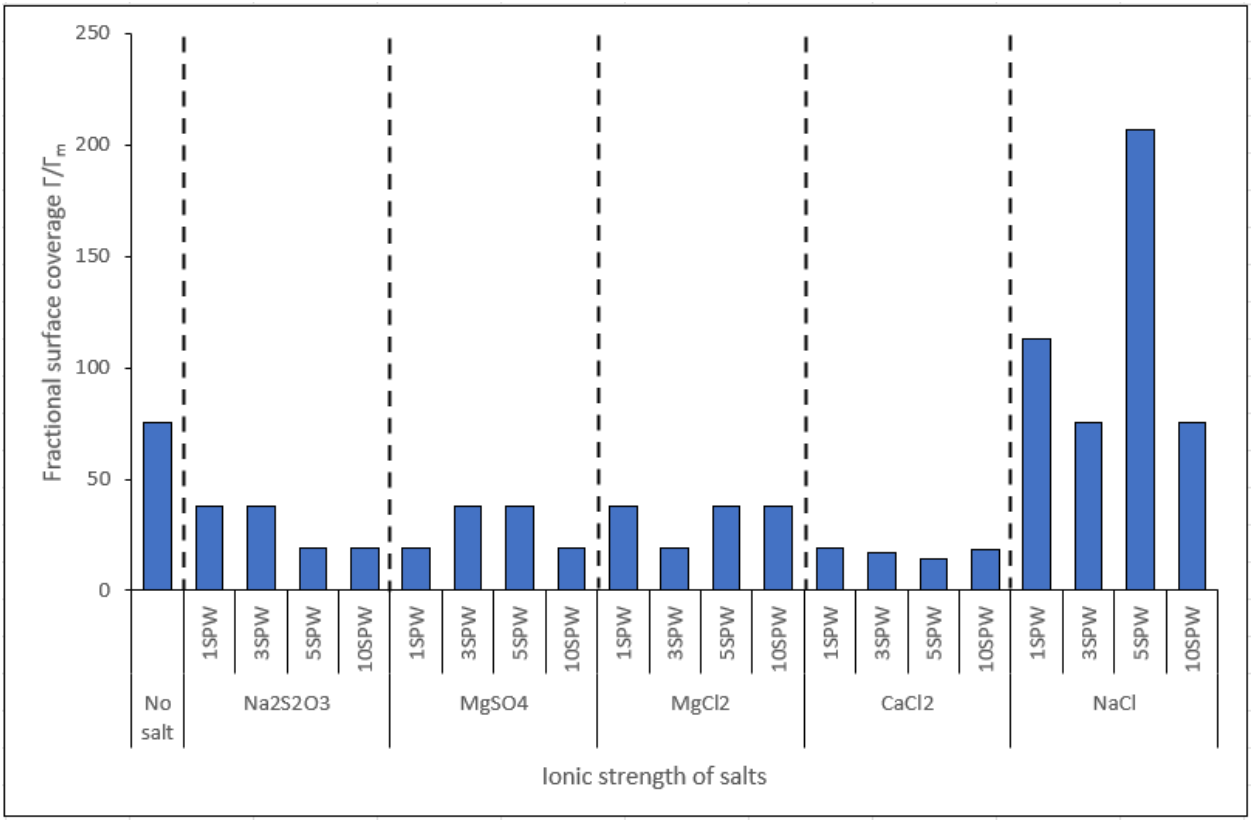

Figure 8.2: Fractional coverage of SIBX on $PdTe_2$ in the absence and presence of salts at increasing ionic strength.

8.3 Effect of $Na_2S_2O_3$ on adsorption of SIBX on palladium minerals

It can be discerned in the rest potential measurements (Figures 5.4 and 5.5) that $S_2O_3^{2-}$ ions interacted with PdS and $PdTe_2$ in a similar mechanism. However, the interaction between $S_2O_3^{2-}$ ions and PdS was high whereas the interaction between $S_2O_3^{2-}$ ions and $PdTe_2$ occurred to a lesser extent. Moreover, an increase in the extent of interaction between the palladium minerals and $S_2O_3^{2-}$ ions was observed to increase with increasing ionic strength. Considering that $S_2O_3^{2-}$ ions are surface-active ions, the increase in ionic strength would suggest an increase in surface activity through solvation and chemisorption. Thereby implying that $S_2O_3^{2-}$ ions occupied more metal active surface sites at higher ionic strengths. This is supported by Figure 8.3, which shows the higher rate of adsorption on $PdTe_2$ at higher ionic strengths.

It has been reported that the chelation of bivalent Pt forms stable complexes $[Pt(S_2O_3)_2]^{2-}$, $[Pt(S_20_3)_3]^{4-}$ and $[Pt(S_2O_3)_4]^{6-}$ (Livingstone, 1965, Anthony and Williams, 1993). Pt and Pd have been found to display similar behaviour (Tadie, 2015), owing to similar crystal structures and valence groups. It is therefore expected in this study that similar chelate-type complexes to those reported

for Pt by Livingstone (1965), would form in the case of Pd. $[Pd(S_2O_3)_2]^{2-}$ has been determined to be a highly stable palladium-thiosulphate complex with a stability constant of $K_{stab} = 3.66 \times 109$ ($logK_{stab} = 9.56$) (Tyutyunnik et al., 2016). However, it can be surmised that in the chelate complexes, ligands such as S and Te will bind through one sulphur and one oxygen atom as cis and trans isomers through similar mechanisms. The cyclic voltammetric response of PdS in the presence of $Na_2S_2O_3$ (Figure 6.5), displayed strong anodic currents above 0.1 V, thereby presenting an exponential dependence to potential. Similarly, an enhanced oxidation effect of $PdTe_2$ was observed in the presence of $Na_2S_2O_3$ (Figure 6.25). Analogous to previous studies, the strong anodic currents observed for both palladium minerals could be associated with the formation of the $[Pd(S_2O_3)_2]^{2-}$ complex. It can be speculated that this reaction occurs through an ion exchange reaction between the non-metallic atom attached to the palladium ion and the $S_2O_3^{2-}$ ions. Upon the cathodic scan, one reduction peak was observed in the case of PdS. This peak could be associated with the reduction of $[Pd(S_2O_3)_2]^{2-}$. Moreover, the three reduction peaks were displayed with $PdTe_2$, which could be assigned to the reduction of $[Pd(S_2O_3)_2]^{2-}$, TeO_3^{2-}, PdO and/or the reduction of Pd hydroxide to the metal (Equation 8.11).

$$Pd(OH)_2 + 2e^- \leftrightarrow Pd^o + 2OH^- \qquad \text{(Eqn. 8.11)}$$

It is evident in the rest potential measurements that the interactions of $S_2O_3^{2-}$ ions with palladium minerals, subsequently interfered with the manner in which SIBX interacted with the minerals. It is revealed that SIBX interacted with PdS to a lesser extent than with $PdTe_2$. However, a decrease in the extent of interaction between SIBX and the palladium minerals was observed with an increase in ionic strength. These findings agree with the Bode plots in Figures 8.4 and 8.5, where a high rate of adsorption of $Na_2S_2O_3$ was demonstrated on both $PdTe_2$ and PdS, at the highest ionic strength, as indicated by lower Zmod value. Hence, it is expected that the $Na_2S_2O_3$ ions interact more at higher ionic strengths and bind to the mineral surfaces prior to the interaction and adsorption of SIBX. Consequently, these observations are justified by Figure 8.2, which shows a decrease in surface coverage of SIBX on $PdTe_2$ with an increase in ionic strength. Additionally, Figure 8.3 shows an appreciable difference between the rate of adsorption of $Na_2S_2O_3$ on PdS and that of SIBX and PdS. It is clear that the adsorption of $Na_2S_2O_3$ occurred at a faster rate whereas that of SIBX itself proceeded at a much slower rate. On the contrary, Figure 8.4 displays almost similar rates of adsorption in the presence of SIBX and $Na_2S_2O_3$ at lower ionic strengths. The insignificant rates of adsorption on the $PdTe_2$ mineral surface will allow xanthate ions to occupy more active sites compared to PdS, hence the higher interactions obtained between $PdTe_2$ and SIBX in Figure 5.5.

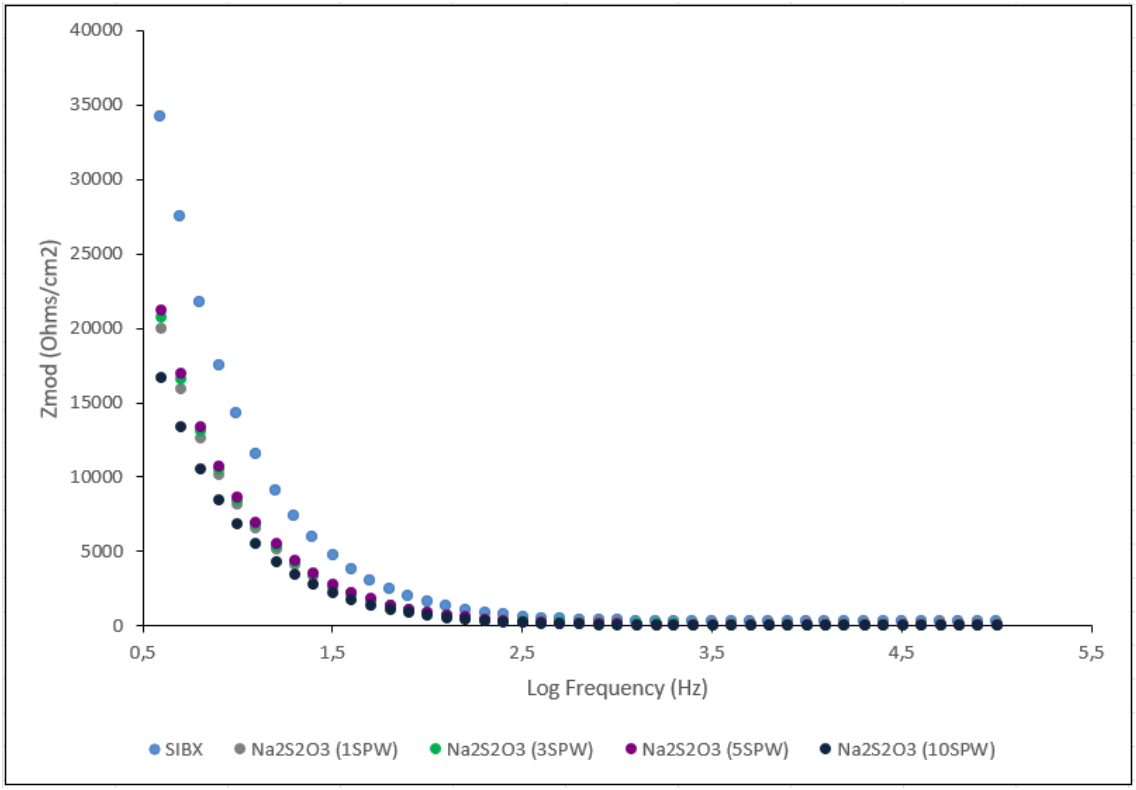

Figure 8.3: Bode plots of Z_{mod} (Ohms/cm^2) versus log frequency (Hz) for PdS in the presence of SIBX only and $Na_2S_2O_3$ at increasing ionic strength at a pH of 9.2 in O.O5 M $Na_2B_4O_7$.

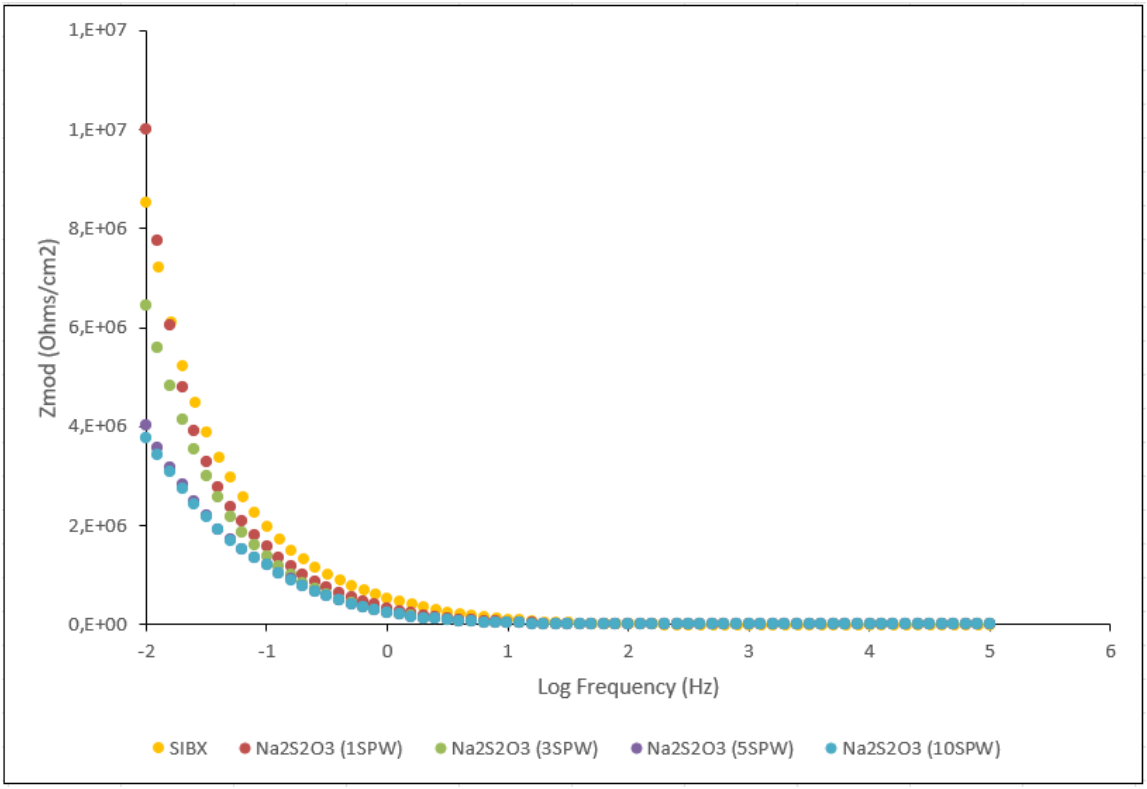

Figure 8.4: Bode plots of Z_{mod} (Ohms/cm^2) versus log frequency (Hz) for $PdTe_2$ in the presence of SIBX only and $Na_2S_2O_3$ at increasing ionic strength at a pH of 9.2 in O.O5 M $Na_2B_4O_7$.

Furthermore, the final rest potentials for $PdTe_2$ at all ionic strengths investigated developed below the equilibrium potential of dixanthogen formation. Hence, it is likely that the formation of a metal-xanthate is more favourable. The chemisorption mechanism can be illustrated by substitution reactions that occur for xanthate collectors (Equations 8.5 to 8.8). Moreover, it is probable that a Te-xanthate formed in addition to the Pd-xanthate species (Equation 8.9). Concerning PdS, the formation of dixanthogen at 1 SPW (Equation 2.34), is accepted in this study. However, at 3 SPW, 5 SPW and 10 SPW, final rest potentials that were below the equilibrium potential of dixanthogen formation were observed. This suggests that the formation of metal-xanthate is most likely favoured. Therefore, it follows the chemisorption reactions in Equations 8.12 to 8.15.

$$Pd^{2+}_{surface} + 2X^{-}_{aqueous} \leftrightarrow [Pd(X_2)]_{surface} \quad \text{(Eqn. 8.12)}$$

$$[PdS, OH^{-}]_{surface} + X^{-}_{aqueous} \leftrightarrow [PdS, X^{-}]_{surface} + OH^{-} \quad \text{(Eqn. 8.13)}$$

$$[PdOH^{+}]_{surface} + X^{-}_{aqueous} \leftrightarrow [Pd(X)^{+}]_{surface} + OH^{-} \quad \text{(Eqn. 8.14)}$$

$$[Pd(OH_2)]_{surface} + 2X^{-}_{aqueous} \leftrightarrow [Pd(X)_2]_{surface} + 2OH^{-} \quad \text{(Eqn. 8.15)}$$

Thereafter, the formation of a metal-xanthate compound occurs. The mechanism involves a two-step mechanism which involves equation 8.16 followed by the reaction in Equation 8.12.

$$PdS + 2OH^{-} \leftrightarrow Pd(OH)_2 + S + 2e^{-} \quad \text{(Eqn. 8.16)}$$

The overall mechanism:

$$2X^{-} + PdS \leftrightarrow PdX_2 + S^{o} + 2e^{-} \quad \text{(Eqn. 8.17)}$$

The rest potential results obtained (Figure 5.4) are in accordance with the cyclic voltammograms attained in Figure 6.6. It is observable that an additional anodic peak appeared after 0.1 V. This peak could be ascribed to the chemisorption of SIBX on the mineral surface. The absence of the reduction peaks could be associated with the irreversibility of the metal-xanthate process or probably the oxidation products formed were not electrochemically active within the potential range investigated or possibly the oxidation products formed were loosely bound (Vermaak et al., 2007) to the mineral surface. Furthermore, Figure 6.25 shows diminished reduction peaks in the presence of SIBX, thereby denoting the adsorption of xanthate ions on the mineral surface.

Comparatively, the Nyquist plots obtained in Figures 7.06 and 7.60 indicate that $S_2O_3^{2-}$ ions and xanthate ions adsorb onto palladium minerals through an ion exchange charge transfer mechanism. Moreover, the adsorption of xanthate ions on the palladium minerals is exhibited by an increase in R_{ct} in the presence of SIBX. This indicates lower capacitance due to the formation of continuous surface layers formed as a result of the adsorption of SIBX and consequently, the formation of dixanthogen or a metal-xanthate complex. Comparably, a shift in phase angles to the higher frequency range from the baseline case also denotes a decrease in capacitance owing to the very small dielectric constant demonstrated by xanthate collectors. Furthermore, the capacitive behaviour displayed by both minerals presumably indicates the existence of the electrical double layer and a coating layer generated by the presence of $S_2O_3^{2-}$ ions.

8.4 Effect of $CaCl_2$ on adsorption of SIBX on palladium minerals

It is apparent in Figure 5.4 that the rate at which PdS is reduced in the presence of Ca^{2+} ions is relatively high compared with other salts. The high decrease in rest potentials can be associated with a coating on the electrode surface that is generated by calcium ions (Moslemi et al., 2011). Moreover, Ca^{2+} ions are considered as surface active inorganic ions that specifically adsorb in the Stern layer through simple electrostatic attraction forces and simple forces of interaction. The adsorption density of such ions can be defined by Equation 8.18 (Fuerstenau, 1984).

$$\frac{\theta}{1-\theta} = \frac{c}{55.5} \exp\left(\frac{-\Delta G^{O}_{ads}}{RT}\right) \qquad \text{(Eqn. 8.18)}$$

Where θ represents the fractional coverage, c/55.5 is the mole fraction of solute in the aqueous phase and ΔG^{o}_{ads} represents the standard free energy of adsorption.

Hence, it is presumed that the coverage for Ca^{2+} ions on PdS increases with an increase in ionic strength and subsequently reduces the interaction between PdS and SIBX. This suggests that more active surface sites on PdS were occupied by Ca^{2+} ions as the ionic strength increased thereby hindering the interaction between xanthate ions and PdS. The Pourbaix diagram in Figure 8.5 illustrates the presence of Ca^{2+} ions in a Ca-O-H system within the alkaline pH range. Calcium ions have been accepted in literature to precipitate into $CaCO_3$ in alkaline conditions (Ikumapayi et al., 2012). Similarly, in this study, a white precipitate was observed in the buffer solution upon the addition of $CaCl_2$, hence suggesting the formation of $CaCO_3$. Additionally, it is presumed that $PdCO_3$ and $CaCO_3$ formed on the PdS mineral surface. Ca^{2+} and CO_3^{2-} ions may form on a mineral surface in addition to a partially oxidized surface demonstrating the presence of surface hydroxyl,

sulfoxyl and carbonate species, in which the composition is pH dependent (Ikumapayi et al., 2012). The existence of such bonds consequently decreases the number of active sites available for the interaction between xanthate ions and the mineral surface. The findings of this work agree with the work of (Ikumapayi et al., 2012), where an increase in band intensities of metal carbonate and calcium carbonate have been observed in alkaline conditions by the use of Diffuse reflectance FTIR spectroscopy and X-ray photoelectron spectroscopy (XPS). Additionally, a subsequent decrease in the intensity of xanthate bands was reported in the presence of Ca^{2+} ions (Ikumapayi et al., 2012).

It can be conjectured from this study that $CaCl_2$ probably dissociates in solution, with the calcium atom losing electrons to form the hydroxo and carbonate complexes which precipitate in their interaction with the active sites of the palladium mineral surface sites.

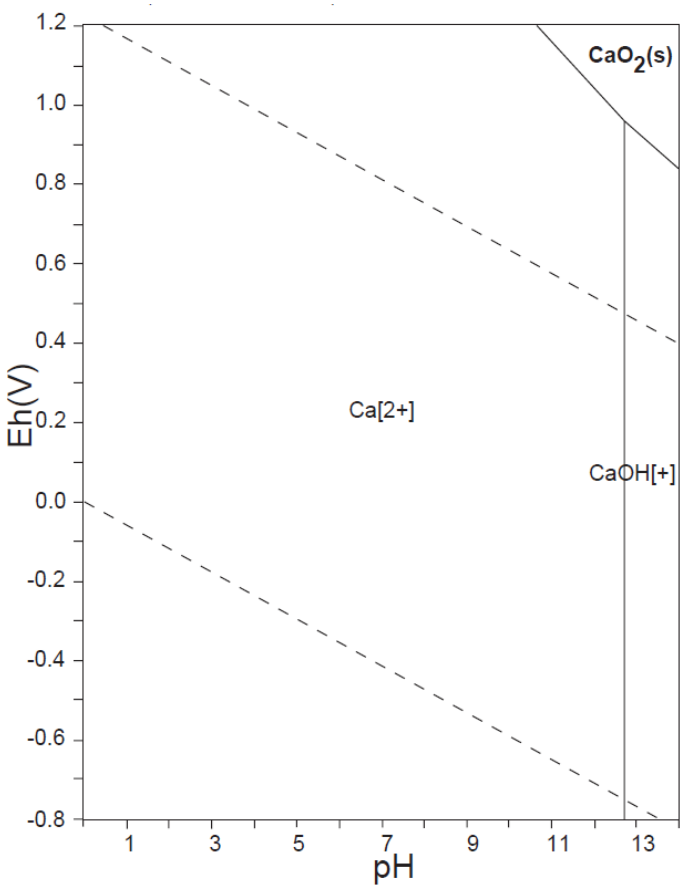

Figure 8.5: Eh-pH diagrams of a Ca-O-H system. ∑ Ca = 10^{-10}, 298.15 K, 10^{5} Pa (Takeno, 2005).

Moreover, it has been observed in Figure 5.4 that the interaction between Ca^{2+} ions and PdS, increased with an increase in ionic strength. This subsequently, resulted in a decrease in the rate at

which dixanthogen (Equation 2.34) formed on the mineral surface. Interestingly, at 1 SPW, the most favourable oxidation product of SIBX formed was most likely metal xanthate (Equation 6.16).

On the contrary, it is evident in Figure 5.5 that Ca^{2+} ions interacted with $PdTe_2$ in a different mechanism than PdS. Ca^{2+} ions exhibited increased rest potentials for $PdTe_2$. This effect increased with an increase in ionic strength and consequently enhanced the interaction between xanthate ions and $PdTe_2$. Considering that the final rest potentials obtained at all ionic strengths of $CaCl_2$ were above the equilibrium potential of dixanthogen formation, it is evident that the formation of dixanthogen is favoured on $PdTe_2$. Though the rest potential measurements show a high interaction between xanthate ions and $PdTe_2$, the surface coverage for SIBX in the presence of Ca^{2+} ions shown in Figure 8.2 is the lowest amongst other salts investigated. Possibly, this suggests that not all dixanthogen was reduced back to xanthate on the reduction peaks upon the cathodic scan (Figure 6.31).

The voltammetric responses of both PdS and $PdTe_2$ as displayed in Figures 6.12 and 6.30 convey that Ca^{2+} ions alter the rate of oxidation of both palladium minerals. It is evident that Ca^{2+} ions suppress the oxidation of the palladium minerals, with a greater extent of suppression being exhibited by $PdTe_2$. However, the rate of oxidation of the palladium minerals is suppressed more with an increase in the ionic strength of Ca^{2+} ions. The change in oxidation rate is attributed to the amounts of the oxidation products of calcium. It is proposed that in the case of PdS, calcium oxidation products such as $Ca(OH)_2$ adsorb especially on the sulphide sites, thereby suppressing further oxidation on the mineral surface (Equation 8.19). Sulphidic sites act as active sites for reagent adsorption. Additionally, Ca^{2+} ions have been postulated to replace metal ions, due to the initial change in surface stoichiometry (Hodgson and Agar, 1989).

$$S_2^{2-} + Ca(OH)^+ \rightarrow S_2(Ca(OH))^+ + e^- \qquad \text{(Eqn. 8.19)}$$

The pronounced cathodic peaks formed in the presence of calcium ions on PdS, as illustrated in Figure 6.12 possibly demonstrate the reverse of the process described in Equation 8.19, as well as the reduction of palladium hydroxide to the metal (Equation 8.11).

On the cathodic scan, no reduction peaks were observed, which demonstrated the reduction of the oxidation products formed. This suggests that the oxidation products formed could be electrochemically inactive within the potential region investigated or possibly the products formed were loosely bound (Vermaak et al., 2007) to the mineral surface. In contrast, cathodic peaks were

generated for $PdTe_2$ in the presence of Ca^{2+} ions and SIBX. It is interesting to note that there was no change in the reduction peaks in the presence of Ca^{2+} ions with and without SIBX. This indicates that possibly the interaction of SIBX in the presence of Ca^{2+} ions did not involve the direct adsorption of xanthate on the mineral surface.

Figure 8.6 denotes Bode plots of $PdTe_2$ in $CaCl_2$ at increasing ionic strength and SIBX. This figure was plotted to determine the adsorption rates of Ca^{2+} ions and SIBX on $PdTe_2$. It is clear that Ca^{2+} ions adsorb at a faster rate on the mineral surface than xanthate ions. However, an increase in the adsorption rate is observed with a decrease in ionic strength. Moreover, the Figure shows that the adsorption of Ca^{2+} ions on the mineral surface hinders the adsorption of xanthate ions on the mineral surface. Comparing Figures 7.22, without SIBX and Figure 7.25, where SIBX was present in the system, it is clear that no significant continuous surface layers formed on the mineral surface owing to the adsorption of xanthate ions. The insignificant change in impedance values observed denotes an insignificant change in capacitance values. These observations are consistent with the cyclic voltammograms obtained in Figures 6.30 and 6.31, where no additional features were observed for the reduction peaks of $PdTe_2$ in the presence of Ca^{2+} ions with and without SIBX. This, therefore, justifies the minimum surface coverage of SIBX in the presence of Ca^{2+} ions as denoted in Figure 8.5. Conclusively, it was observed in Figure 7.24 that the R_{ct} for SIBX itself was higher than the R_{ct} values of SIBX in the presence of Ca^{2+} ions. This implies that a higher amount of oxidized species were formed in the presence of SIBX than in the case where Ca^{2+} ions were present. This observation correlates to the results obtained for rest potential measurements, where it was determined that dixanthogen possibly formed under the conditions investigated. However, the lower R_{ct} values obtained in the presence of calcium ions demonstrate that the reactions resulting in the coating layer that formed on the mineral surface, occurred at a faster rate.

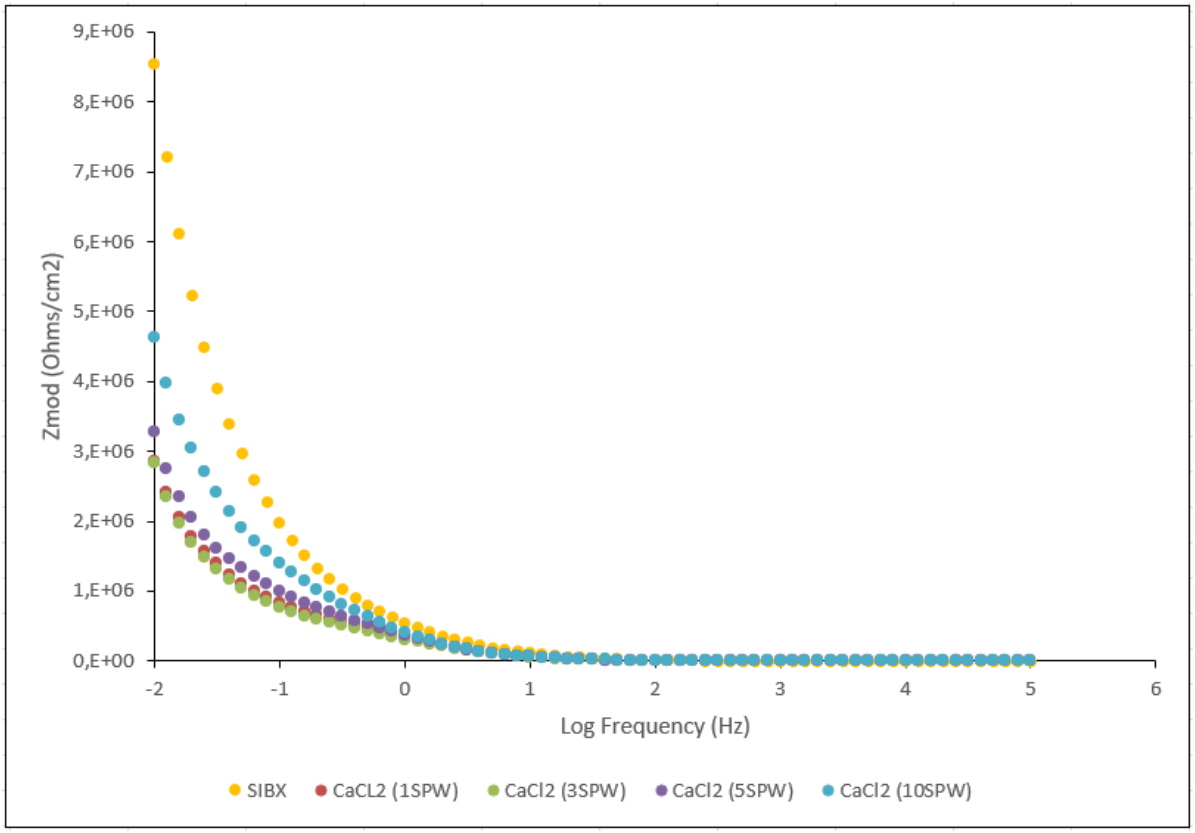

Figure 8.6: Bode plots of Z_{mod} (Ohms/cm^2) versus log frequency (Hz) for $PdTe_2$ in the presence of SIBX only and $CaCl_2$ at increasing ionic strength at a pH of 9.2 in O.O5 M $Na_2B_4O_7$.

8.5 Effect of $MgCl_2$ on adsorption of SIBX on palladium minerals

Figures 5.4 and 5.5 demonstrate that Mg^{2+} ions interact and adsorb onto PdS and $PdTe_2$ mineral surfaces through different mechanisms. It is apparent that Mg^{2+} ions display a decrease in rest potential for PdS and contrarily an increase in the rest potential for $PdTe_2$. Notwithstanding the different mechanisms exhibited by Mg^{2+} ions on both minerals, an increase in the extent of interactions is perceptible with an increase in ionic strength. Mg^{2+} ions are considered surface active ions, which adsorb in the stern layer through electrostatic interactions. The adsorption density of Mg^{2+} ions can be calculated using Equation 8.18 (Fuerstenau, 1984). It is postulated that $MgCl_2$ is most likely dissociated in solution, with the Mg^{2+} losing electrons and possibly precipitated to $Mg(OH)_2$ in their interaction with the palladium mineral surfaces (Equation 8.20). It is proposed that this coating subsequently inhibited the extent of interactions between SIBX and PdS. This assumption is in correspondence to the evidence given by the magnesium speciation diagram in Figure 8.7, where $Mg(OH)_2$ species are likely to form under alkaline conditions. Therefore, it is proposed that the anodic peak developed in Figures 6.10 and 6.28 (voltammograms) for each condition investigated could be associated with the precipitation of $Mg(OH)_2$. Furthermore, the

decrease in current densities generated in the presence of Mg^{2+} ions conveys the presence of a $Mg(OH)_2$ passivation layer, thus hindering further oxidation of the palladium minerals.

$$Mg(OH)_{2(aq)} \leftrightarrow Mg^{2+}_{(aq)} + 2OH^{-}_{(aq)} \qquad K = 10^{-0.019} \qquad \text{(Eqn. 8.20)}$$

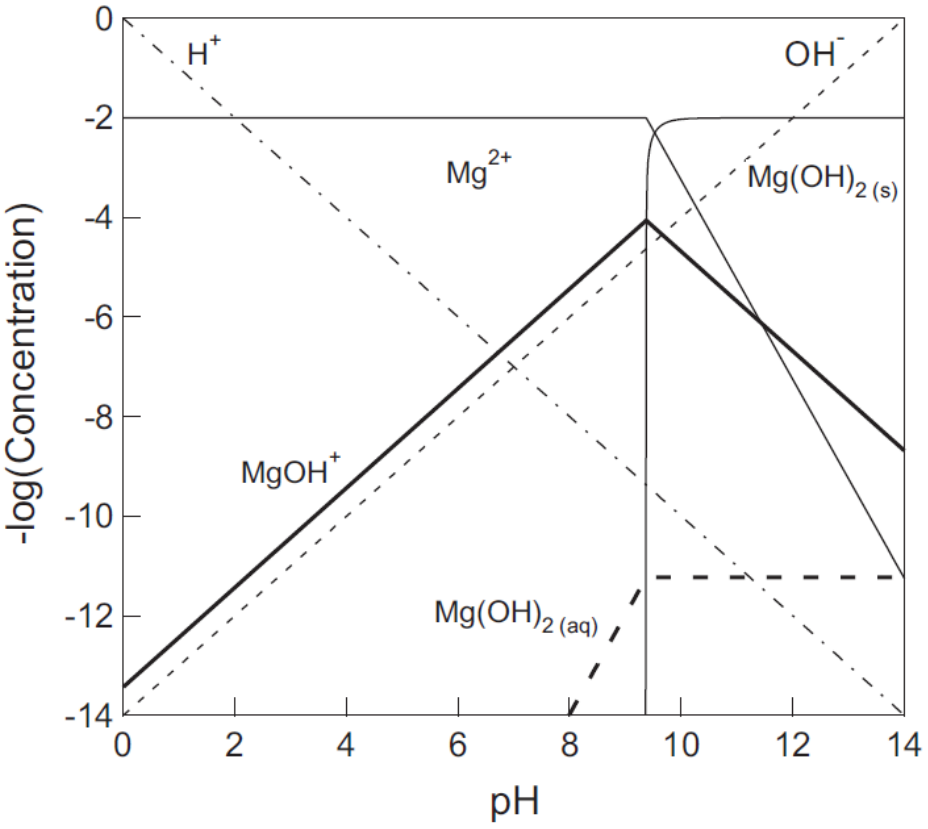

Figure 8.7: Magnesium species diagram at 10^{-2} M (Hirajima et al., 2016).

The diminished cathodic peaks illustrated in Figure 6.28, in the presence of $MgCl_2$, indicate that $Mg(OH)_2$ possibly inhibited further oxidation and reduction of the palladium mineral. Additionally, the passivation layer of $Mg(OH)_2$ prevents the oxidation products on the mineral surface from diffusing into the solution phase during the cathodic scan, thus retarding the reduction of these oxidized species.

Despite the different mechanisms in which Mg^{2+} ions interacted with the palladium minerals, it is evident from the rest potential measurements that the addition of SIBX significantly decreases the rest potentials of PdS and $PdTe_2$. Xanthate is a reductant, implying that it donated electrons to the palladium mineral surfaces on which it was oxidized to dixanthogen at the conditions investigated in this study. The decline in rest potentials denotes the adsorption of SIBX following an electrochemical process. Presumably, more xanthate adsorbed and oxidized on $PdTe_2$, and liberated more electrons, hence lower rest potentials in the presence of SIBX than for PdS.

It is illustrated in Figure 8.8 (Bode plots) that the rate of adsorption of Mg^{2+} ions on $PdTe_2$ differs to a great extent from the rate at which SIBX adsorbed on the mineral surface. However, it is displayed that Mg^{2+} ions adsorb faster than xanthate ions on $PdTe_2$. The increase in the adsorption rate of Mg^{2+} ions was found to be inversely proportional to the ionic strength of $MgCl_2$. Furthermore, it is interesting to note that the impedance values at different ionic strengths of $MgCl_2$ did not differ considerably in the lower frequency range. This suggests that the formation of continuous surface layers on $PdTe_2$ did not differ significantly with an increase in ionic strength. This conforms to the rest potential measurements in Figure 5.5, which show that the interactions of SIBX with $PdTe_2$ did not vary substantially in the presence of Mg^{2+} ions with an increase in ionic strength. Additionally, Figure 8.2 corresponds to these observations, as it was observed that the surface coverages for SIBX did not vary significantly with an increase in ionic strength.

In addition, the final rest potentials in the case of $PdTe_2$ show that the formation of dixanthogen is most likely favoured at 1 SPW, 3 SPW and 5 SPW. However, it is noticeable that the rate of formation of dixanthogen is slow under the aforementioned conditions. Furthermore, the formation of metal-xanthate is presumably favoured at 10 SPW. With respect to PdS, Figure 5.4 illustrates the formation of dixanthogen at all ionic strengths, though the lowest rate of dixanthogen formation is depicted at 1 SPW and 10 SPW. Moreover, the highest rate of dixanthogen formation is depicted in the intermediate ionic strengths.

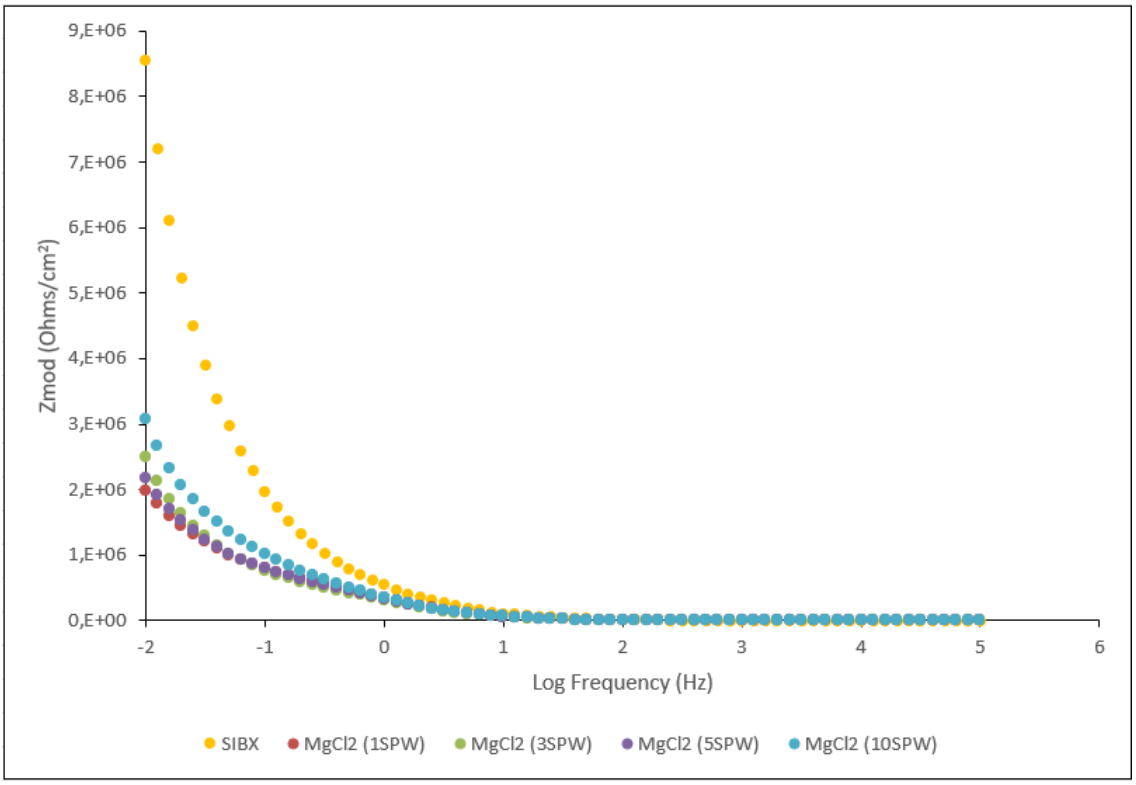

Figure 8.8: Bode plots of Z_{mod} (Ohms/cm^2) versus log frequency (Hz) for $PdTe_2$ in the presence of SIBX only and $MgCl_2$ at increasing ionic strength at a pH of 9.2 in O.O5 M $Na_2B_4O_7$.

The cyclic voltammograms in Figure 6.29 show significantly diminished anodic peaks for $PdTe_2$ in the presence of both Mg^{2+} ions and SIBX, in comparison to SIBX itself. This occurrence indicates that less dixanthogen was formed on the $PdTe_2$ mineral surface in the presence of Mg^{2+} ions. Additionally, the smaller reduction peaks developed in the presence of Mg^{2+} ions, suggest that xanthate ions were adsorbed and not all dixanthogen was reduced back to xanthate. Moreover, it was observable that due to the smaller reduction peaks, it was difficult to reduce the mineral surface in the presence of Mg^{2+} ions. Comparatively, the Bode plot in Figure 7.19, depicts that the adsorption of Mg^{2+} ions on $PdTe_2$ inhibits the adsorption and oxidation of SIBX. Consequently, the presence of $Mg(OH)_2$ shifted the anodic peaks for SIBX oxidation (Figure 6.29) to the anodic direction and generally lower current densities were obtained.

Figure 6.11 demonstrates pronounced anodic peaks, due to the oxidation of SIBX on PdS. It is shown that the area under the anodic peaks decreases with an increase in the ionic strength of $MgCl_2$, thereby implying that less dixanthogen was formed with an increase in ionic strength. These observations correlate well with the rest potential measurements, where a decrease in the extent of interactions between SIBX and PdS was observed to occur with an increase in ionic strength. Additionally, on the cathodic scan, no reduction peaks were observed presumably due to the formation of oxidation products that were electrochemically inactive within the potential range

investigated or the formation of loosely bound products (Vermaak et al., 2007) on the mineral surface.

Moreover, it is illustrated in Figure 7.18 that the presence of SIBX generated a remarkable increase in R_{ct} compared to Figure 7.15. The increase in R_{ct} in the presence of SIBX is due to the significantly smaller dielectric constant exhibited by organic compounds. The appreciable change in impedance values (Figure 7.19), in the lower frequency range, demonstrates a decrease in capacitance with a decrease in ionic strength. The existence of SIBX between the electrode/electrolyte interface decreases the dielectric constant of the double-layer capacitor. Furthermore, the interaction, adsorption and oxidation of SIBX on $PdTe_2$ presumably resulted in a decrease in capacitance, as denoted by the shift of phase angles to the higher frequency range (Figure 7.20). Therefore, the decrease in capacitance is caused by the formation of continuous surface layers as a result of the adsorption and formation of dixanthogen on $PdTe_2$. Ultimately, it is evident that the rate of reaction increases with an increase in the ionic strength of $MgCl_2$, in the presence of SIBX (Figures 7.18 and 7.19).

8.6 Effect of $MgSO_4$ on adsorption of SIBX on palladium minerals

It is shown in Figures 5.4 and 5.5 that SO_4^{2-} ions interact with both PdS and $PdTe_2$ in a similar mechanism. The SO_4^{2-} ions generally demonstrated an increase in rest potentials for both palladium minerals except for $MgSO_4$ at 1SPW, where the ions exhibited a decrease in rest potentials for PdS. It is perceptible that the increase in rest potentials increased with an increase in the ionic strength of $MgSO_4$. SO_4^{2-} ions are considered as potential determining ions that promptly pass between solid and liquid phases. They have been accepted in literature to generate a surface charge, σ_o and govern the magnitude of surface potential, ψ_o. The magnitude of surface charge is therefore dominated by the extent of substitution. Furthermore, EIS data obtained in this study shows that the double-layer model exists in the system investigated. This is demonstrated by the phase angle measurements obtained. Hence, in the double layer, the surface potential is regarded as zero at the point of zero surface charge (PZC), with its value at any activity of potential determining electrolyte, a^+, is regulated by Equation 8.21 (Fuerstenau, 1984).

$$\varphi_o = \left({}^{RT}/_{z_+F}\right)\ln\left({}^{a^+}/_{a^+_{pzc}}\right) \qquad \text{(Equation 8.21)}$$

It is evident from the Pourbaix diagram in Figure 8.9 that SO_4^{2-} ions may exist on the palladium mineral surfaces in alkaline conditions. SO_4^{2-} ions have been presumed to complex with available metal ions in solution. $MgSO_4$ may decompose in water as in Equation 8.22.

$$MgSO_4 \leftrightarrow Mg^{2+} + SO_4^{2-} \quad \text{(Equation 8.22)}$$

It is therefore postulated that the SO_4^{2-} ions present in the solution possibly complex up with the Pd^{2+} ions as in Equation 8.23. A similar reaction was reported in the case of pyrite and pyrrhotite, where Fe^{2+} ions were proposed to complex with SO_4^{2-} ions (Moslemi et al., 2011). In accordance with the formation of a metal-sulphate complex, Ikumapayi et al. (2012) observed a decrease in band intensities for sulphate ions in process water at alkaline conditions. It has been accepted in this study that the SO_4^{2-} ions possibly go through an ion exchange reaction with the non-metallic atom attached to the palladium atoms to form $PdSO_4$.

$$Pd^{2+} + SO_4^{2-} \rightarrow PdSO_4 \quad \text{(Equation 8.23)}$$

Unlike in this study, SO_4^{2-} ions were found to decrease the rest potentials for pyrite and pyrrhotite, where it was presumed that the sulphate complexes deplete the iron ions in solution. Hence, disturbing the solid, metal ions balance in solution. In order to reach this balance, the oxidation of the mineral surface should be greater, thus the ferro iron ions should be generated in higher quantities (Moslemi et al., 2011). Therefore, the opposite is true in the case of this study.

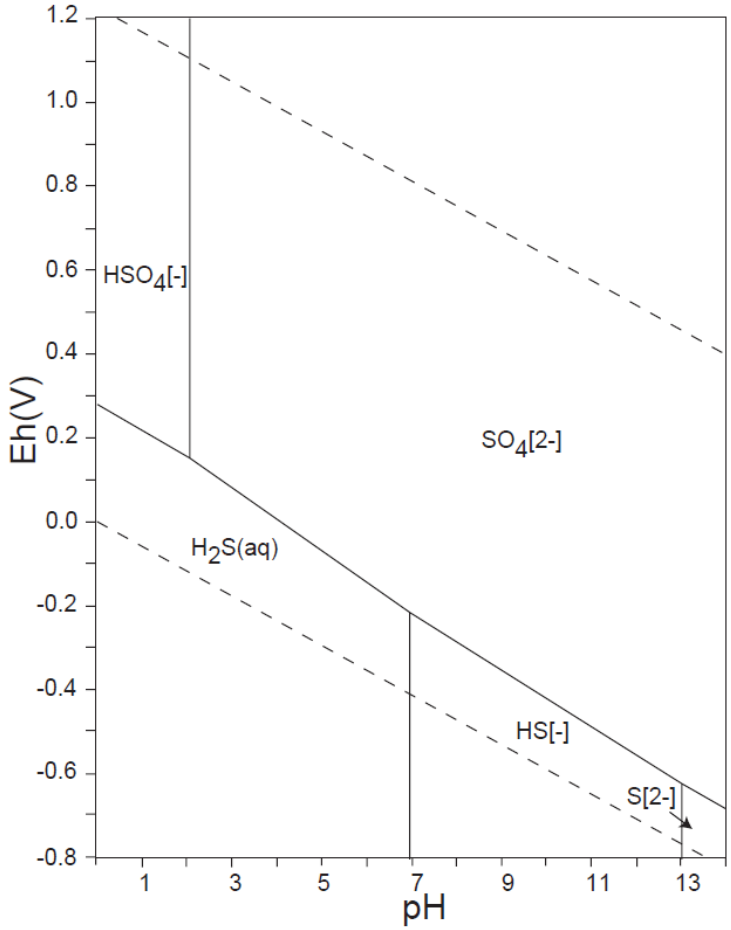

Figure 8.9: Eh-pH diagrams of a S-O-H system. $\sum S = 10^{-10}$, 298.15K, 10^5 Pa (Takeno, 2005).

The voltammetric responses of $PdTe_2$ (Figure 6.26), show that in the presence of SO_4^{2-} ions a decrease in the anodic peak, with respect to the anodic peak generated in the absence of the SO_4^{2-} ions, was observed. This behaviour could be attributed to the formation of a $PdSO_4$ passivation layer that hinders further oxidation on the mineral surface. Whilst the pronounced reduction peak in the range 0.1 V to - 0.3 V could be associated with the reduction of the oxidation products formed for $PdTe_2$ in the absence of SO_4^{2-} ions, the diminished cathodic peak in the presence of SO_4^{2-} ions could be attributed to the reduction of a $PdSO_4$ passivation layer. The smaller reduction peaks indicate that it is harder to reduce a sulphate coated $PdTe_2$ mineral surface than $PdTe_2$ itself.

In comparison with other salts, it can be discerned in Figure 5.4 that the presence of SO_4^{2-} ions on PdS resulted in the highest extent of xanthate interactions with the mineral surface. Similarly, relatively high interactions between SIBX and $PdTe_2$ were observed in the presence of SO_4^{2-} ions. It is evident from the rest potential measurements that the final rest potentials for both PdS and $PdTe_2$ in the presence of both SO_4^{2-} and xanthate ions yielded potentials that were more positive than the reversible potential of the X^-/X_2 couple. It is therefore proposed that the formation of

dixanthogen is favoured under these conditions (Equation 2.34). It is presumed that the electrochemical interactions of SIBX in the presence of SO_4^{2-} ions, could result in improved flotation recoveries for PdS and $PdTe_2$. However, it is noticeable that in the presence of SIBX, no reduction peaks were formed in the case of PdS, probably owing to the formation of electrochemically inactive products within the potential region investigated in this study or possibly the oxidation products formed were loosely bound (Vermaak et al., 2007) to the mineral surface. With regard to $PdTe_2$, almost insignificant reduction peaks formed in the presence of SIBX, owing to the adsorption of xanthate ions on the mineral surface. Furthermore, it is clear that the reduction peaks formed in the absence of SIBX, due to mineral oxidation, were significantly diminished upon the adsorption of xanthate ions on $PdTe_2$. However, it is presumed that not all dixanthogen formed is reduced back to xanthate.

The Bode plot in Figure 8.10 displays that the rate of adsorption of SO_4^{2-} ions on PdS does not differ significantly from the adsorption of SIBX itself. However, an increase in the rate of adsorption of SO_4^{2-} ions was observed with a decrease in ionic strength. In contrast, Figure 8.11 conveys the significantly fast adsorption of SO_4^{2-} ions on $PdTe_2$ in comparison with the adsorption of SIBX. Moreover, it is shown that the lowest and highest ionic strengths display the highest adsorption rate on the mineral surface compared to the intermediate ionic strengths. These findings conform to the results obtained on the surface coverages of SIBX on $PdTe_2$. It was observed that SIBX displayed higher surface coverages on $PdTe_2$ at 3 SPW and 5 SPW, owing to the slow adsorption of SO_4^{2-} ions on the mineral surface. Nonetheless, lower surface coverages of SIBX were obtained at 1 SPW and 10 SPW due to the fast adsorption of SO_4^{2-} ions on $PdTe_2$.

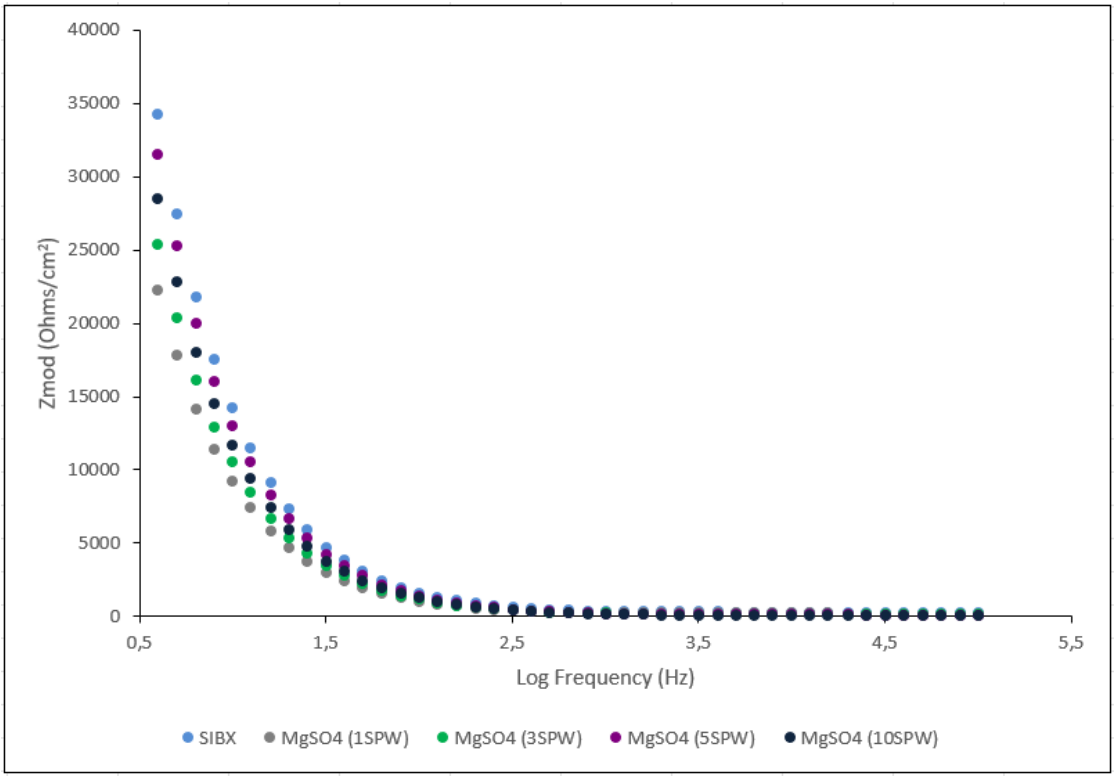

Figure 8.10: Bode plots of Z_{mod} (Ohms/cm^2) versus log frequency (Hz) for PdS in the presence of SIBX only and $MgSO_4$ at increasing ionic strength at a pH of 9.2 in O.O5 M $Na_2B_4O_7$.

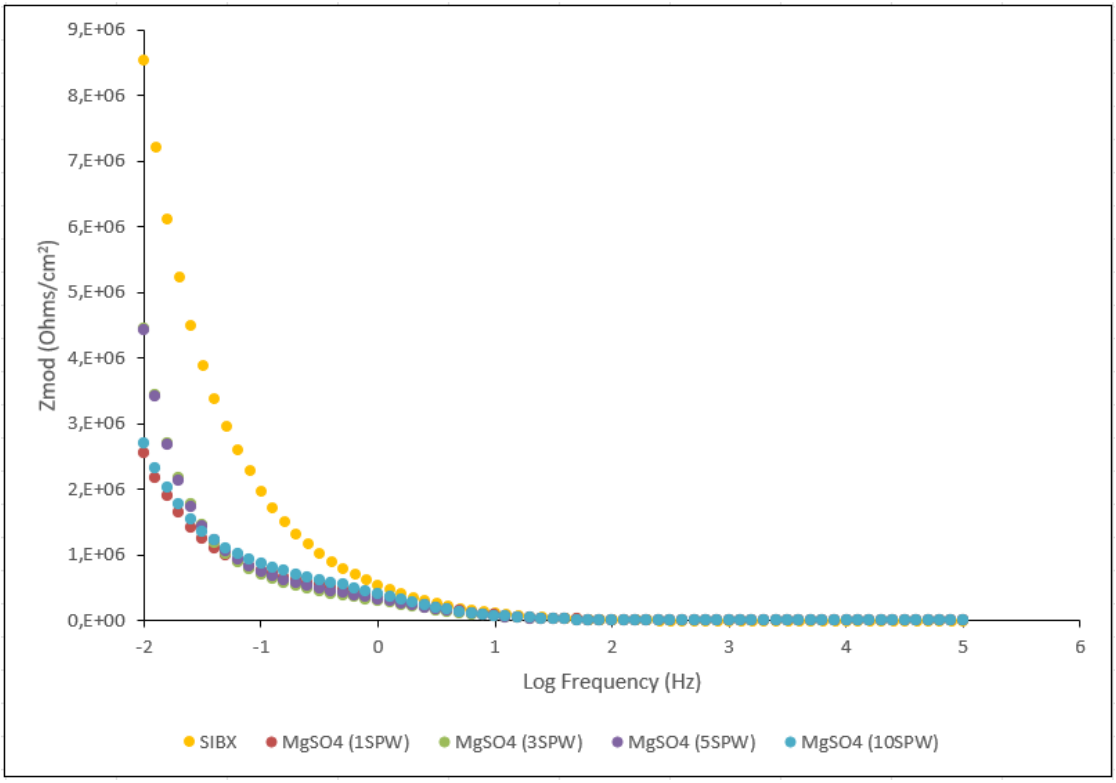

Figure 8.11: Bode plots of Z_{mod} (Ohms/cm^2) versus log frequency (Hz) for $PdTe_2$ in the presence of SIBX only and $MgSO_4$ at increasing ionic strength at a pH of 9.2 in O.O5 M $Na_2B_4O_7$.

The results obtained for impedance measurements were in good correlation with cyclic voltammetry and rest potential measurements. It was observable in the Nyquist plots in Figures 7.12 and 7.66 that R_{ct} increased in the presence of both SO_4^{2-} ions and SIBX, due to the formation of higher amounts of oxidized products. Additionally, a slight shift of the phase angles to high frequencies indicates lower capacitance values due to the smaller dielectric constant exhibited by SIBX. Lowering of the capacitance value suggests the interaction, adsorption and oxidation of SIBX to dixanthogen on the palladium mineral surfaces, at potentials more positive than the reversible potential of the xanthate-dixanthogen couple. It is important to note that the impedance values did not vary substantially with an increase in the ionic strength of $MgSO_4$, thereby implying that the formation of continuous layers in the presence of SO_4^{2-} ions did not vary considerably with an increase in ionic strength. This, therefore, enhances the interaction between SIBX and the palladium minerals. Furthermore, it has been accepted in literature that the anodic peak area demonstrates the amount of oxidized product formed on a mineral surface (You et al., 2013). The decrease in anodic peaks (Figure 6.27), in the presence of SO_4^{2-} ions of increasing ionic strength, implies that less dixanthogen was formed on the mineral surface. This phenomenon is consistent with Figure 8.2, which shows a higher surface coverage of SIBX in the absence of SO_4^{2-} ions than in conditions with SO_4^{2-} ions present.

Most work that has focused on the effects of SO_4^{2-} ions in flotation studies has highlighted their detrimental effects on valuable minerals (Ikumapayi et al., 2012, Sinche-Gonzalez and Fornasiero, 2021). However, Boujounoui et al. (2015) reported that 200 - 6000 mg/l of SO_4^{2-} ions have an enhanced effect on the flotation of valuable minerals. It is important to note that the concentrations investigated in this study ranged from the concentrations used by Boujounoui et al. (2015) to five times their maximum concentrations. Moreover, the enhanced flotation recoveries could be ascribed to the cleaning effect of SO_4^{2-} ions on mineral surfaces. Additionally, Boujounoui et al. (2015) attributed the positive effect of SO_4^{2-} ions on flotation recoveries to the formation of heavy metal sulphite salts, which are slightly soluble in water. The interactions of SO_4^{2-} ions on the active sites of mineral surfaces are regulated by the electrostatic charge on the mineral surface. Both of these are influenced by the concentration and the inherent binding affinities of SO_4^{2-} ions in a particular system (Wu et al., 2002, Lefevre and Fedoroff, 2006). Similarly, the formation of heavy metal xanthate sulphite salts possibly transpired in this work, considering that Pd is a known heavy metal.

8.7 Effect of NaCl on adsorption of SIBX on palladium minerals

Rest potential measurements in Figures 5.4 and 5.5 show that NaCl interacts with PdS and $PdTe_2$, respectively, through different mechanisms. The salt is demonstrated to have a slightly decreased rest potential for PdS, whereas it slightly increased the rest potential of $PdTe_2$. The interactions of NaCl with the palladium minerals have been demonstrated to be very minimal compared with the other ions investigated. This could be ascribed to the fact that Na^+ ions are considered to be non-surface active ions, that exist in the diffuse double layer and their role is to maintain electrostatic neutrality (Fuerstenau, 1984). Similarly, sodium chloride was observed by Moslemi et al. (2011) to reduce rest potentials for pyrite, pyrrhotite and steel. The magnitude of decrease in rest potential was revealed to increase with pH and this observation was associated with the presence of OH^- ions in solution. The decomposition of the ions in water is depicted in Equation 8.24. Additionally, the chloride ions from the sodium chloride have been accepted to decompose and dissolve any metal-oxide layer formed on the mineral surfaces.

$$NaCl \leftrightarrow Na^+ + Cl^- \qquad \text{(Eqn. 8.24)}$$

The presence of Na^+ on the palladium mineral surfaces is illustrated by the Na-O-H system in Figure 8.12. It is surmised in this study that NaCl dissociates in the alkaline solution and the sodium atom loses an electron to form Na^+ ions which do not significantly alter the mineral surfaces.

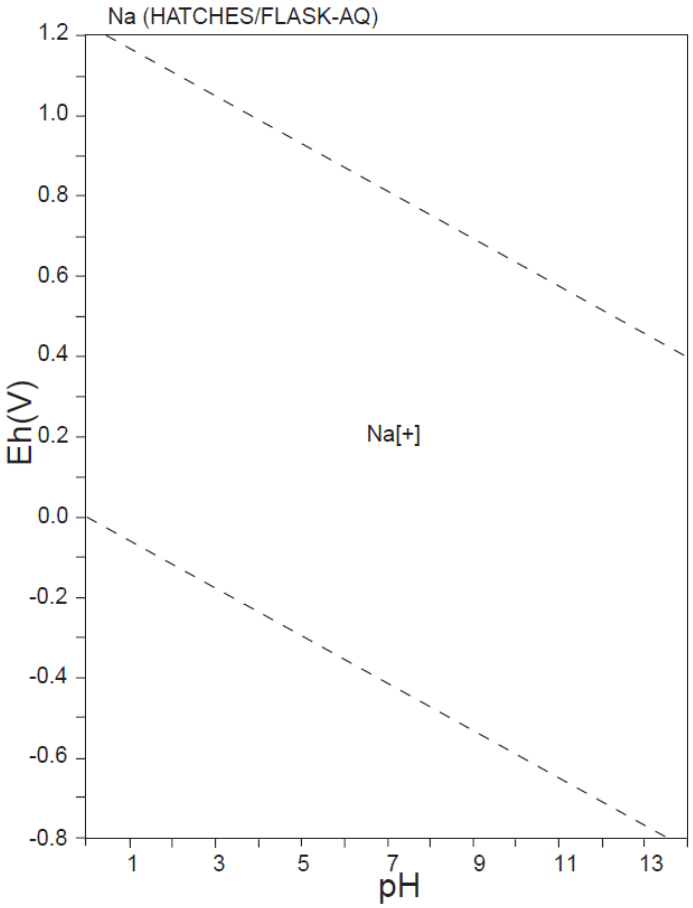

Figure 8.12: Eh-pH diagram illustrating a Na-O-H system. ∑ Na= 10^{-10}, 298.15 K, 10^{5} Pa (Takeno, 2005).

The minimum interactions between NaCl and the palladium minerals subsequently resulted in relatively high interactions between SIBX and the palladium minerals. These observations correspond to the very high surface coverages of SIBX on $PdTe_2$ (Figure 8.2). The optimum surface coverage of SIBX was obtained at 5 SPW after which a decrease is observed at 10 SPW, due to an increase in the concentration of the Na^+ ions present. The pronounced decrease in rest potentials in the presence of SIBX is due to the presence of xanthate ions which reduce the mineral surfaces of PdS and $PdTe_2$, by donating electrons to the palladium surfaces. Hence, an appreciable decrease in rest potentials indicates that SIBX adsorbed onto the mineral surfaces following electrochemical processes that occurred. Additionally, the insignificant effect on the interactions of NaCl with the mineral surfaces can be attributed to the small molecular size of NaCl, which makes it possible for them to enter the layer spacing of the minerals, thereby increasing the dipole-dipole forces between the palladium minerals and SIBX. It has been presumed that NaCl exhibits a salt effect on anionic collectors, which helps to promote the flotation of valuable minerals (Chaojun et al., 2020). Moreover, it is noticeable that the final rest potentials for $PdTe_2$ were

observed to be lower than those of PdS. This suggests that more SIBX was adsorbed and oxidized on $PdTe_2$, as indicated by the higher interactions. Hence, SIBX subsequently released more electrons on the mineral surface. The charge transfer between $PdTe_2$ and xanthate ions was easier due to the formation of presumably less oxidized species on the mineral surface. However, it is speculated from the final rest potentials in Figure 5.5 that the formation of dixanthogen is favourable at 1 SPW, whereas the formation of metal xanthate (Equations 6.5 to 6.9) is likely favoured at 3 SPW, 5 SPW and 10 SPW. Regarding PdS, it is clear that the final rest potentials were observed to be above the equilibrium potential of dixanthogen formation at all ionic strengths. This suggests that the formation of dixanthogen on the mineral surface was favourable.

Furthermore, the beneficial effect of NaCl on flotation recoveries have been associated with their insignificant effect on the surface charge of mineral surfaces and their adsorption behaviour. Though it was observed in this study in Figure 8.13 that the adsorption rate of Na^+ ions was higher than that of SIBX, the minimum interactions between the Na^+ ions and the palladium allow the xanthate ions to interact, adsorb and oxidize on the mineral surfaces. However, the rate of adsorption of Na^+ ions on the mineral surface was determined to decrease with an increase in ionic strength.

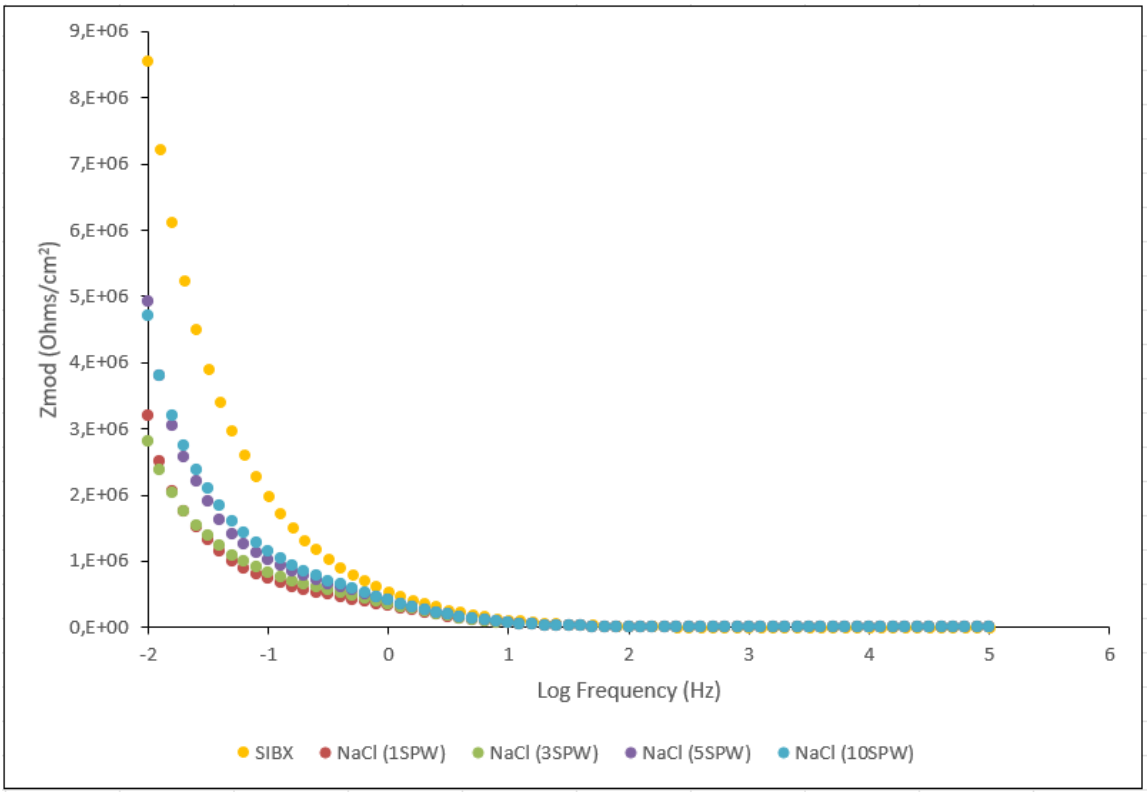

Figure 8.13: Bode plots of Z_{mod} (Ohms/cm^2) versus log frequency (Hz) for $PdTe_2$ in the presence of SIBX only and NaCl at increasing ionic strength at a pH of 9.2 in O.O5 M $Na_2B_4O_7$.

The Nyquist plots in Figure 7.30 show that R_{ct} decreases in the presence of NaCl and with an increase in ionic strength. This is in accordance with the higher activity of $PdTe_2$ in the cyclic voltammograms obtained in Figure 6.33 and the impedance data plotted in Figure 7.31. The higher impedance values of SIBX only can be ascribed to smaller capacitance, presumably owing to the formation of a continuous surface layer that consists mostly of dixanthogen that formed as a result of the adsorption and oxidation of xanthate ions on $PdTe_2$.

The contribution of capacitance to impedance is a maximum at intermediate frequencies (Figure 7.32). It is depicted in Figure 7.31 that the difference in impedance values in the absence and presence of salts with SIBX, is quite insignificant. The insignificant change in impedance values denotes an insignificant change in capacitance, hence implying no formation of continuous layers in the intermediate frequency range. However, it is observed that the formation of surface layers in the presence of SIBX and NaCl at increasing ionic strength occurs in the lower range frequency, where it is observed that the formation of continuous layers does not differ significantly at all conditions investigated. Based on the final rest potentials obtained, the continuous layers formed on the palladium surfaces could be associated mainly with the formation of dixanthogen (Equation 2.34). Moreover, it is displayed in Figures 6.32 and 6.33 that the reduction peaks in the presence

of SIBX shifted in the cathodic direction, implying that the interaction of xanthate ions with $PdTe_2$ was most likely a direct chemisorption reaction.

8.8 Equivalent circuit

The impedance for the equivalent circuits (Figures 7.94 and 7.95), can be expressed in the form of Equation 8.25 (Mu et al., 2015).

$$Z = R_s + \frac{R_{ct}}{1+j\omega C R_{ct}} \qquad \text{(Eqn. 8.25)}$$

Where ω is the angular frequency (ω = 2πf) of AC voltage and j is the imaginary unit. Therefore, in the high frequency range, the capacitor, originating from the electrical double layer and/or coating layer from ions, acts as a passageway for electricity and the impedance is equivalent to R_s. The equation further indicates that in the low frequency domain, the capacitor acts as an open circuit, hence hindering the passage of electricity. Accordingly, the impedance is equivalent to the sum of R_{ct} and R_s.

8.9 Summary

This study has demonstrated that $S_2O_3^{2-}$, SO_4^{2-}, Mg^{2+}, Ca^{2+} and Na^+ ions interact and adsorb onto $PdTe_2$ and PdS mineral surfaces. $S_2O_3^{2-}$, Mg^{2+}, Ca^{2+} and Na^+ ions displayed a decrease in rest potentials for PdS whilst, amongst other salts, only $S_2O_3^{2-}$ exhibited a decrease in rest potentials on $PdTe_2$. It is depicted that the divalent ions resulted in a greater extent of decrease in rest potentials for PdS than the monovalent ions. The rate at which PdS was reduced in the presence of the ions investigated followed the order $S_2O_3^{2-} > Ca^{2+} > Mg^{2+} > Na^+$. Moreover, the extent of interaction between these ions and PdS was inversely proportional to the extent of interaction between xanthate ions and PdS. However, SO_4^{2-} exhibited an increase in rest potentials for both PdS and $PdTe_2$. Alternatively, SO_4^{2-}, Mg^{2+}, Ca^{2+} and Na^+ conveyed an increase in rest potentials on $PdTe_2$. The extent of interaction, therefore, proceeded in the order $Ca^{2+} > SO_4^{2-} > Mg^{2+} > Na^+$. The divalent ions were observed to display a greater extent of interaction on $PdTe_2$ than the monovalent ion. Ions that resulted in an increase in rest potentials for both PdS and $PdTe_2$ allowed xanthate ions to interact to a greater extent with the palladium minerals. Whilst it was postulated in this study that the interaction of SIBX in the presence of $S_2O_3^{2-}$ ions presumably favoured the formation of a metal-xanthate, all other salts investigated favoured the formation of dixanthogen at all ionic strengths. Nevertheless, it was observed that the rate of formation of dixanthogen was

decreased in the presence of the salts than in SIBX itself. Despite the high interactions displayed between SIBX and $PdTe_2$, most conditions demonstrated that the formation of a metal xanthate is favoured more than the formation of dixanthogen. Unlike for PdS, the interaction between $PdTe_2$ and SIBX in the absence of the salts investigated favoured the formation of a metal-xanthate. Additionally, it was found that the manner in which ions interacted with $PdTe_2$ correlated well with the surface coverages observed for SIBX on $PdTe_2$.

It is proposed in this study that $S_2O_3^{2-}$ and SO_4^{2-} ions possibly form complexes with palladium minerals whereas Mg^{2+} and Ca^{2+} ions have been speculated to replace the metal ions on the mineral surfaces to form ion hydroxides. Hence, a decrease in current densities in the presence of salts, owing to the formation of passivation layers that hinder further oxidation on the palladium mineral surfaces. Furthermore, Na^+ ions generally displayed insignificant interactions and effects on the palladium minerals. Moreover, on the cathodic scan, it was observed that no reduction peaks were formed on PdS in the presence of SIBX and the ions investigated. It was therefore surmised that possibly the oxidation products formed in the presence of SIBX were electrochemically inactive within the potential range investigated or were loosely bound to the mineral surface or in some instances as that of $S_2O_3^{2-}$ ions, the absence of the reduction peaks could be assigned to the irreversibility of the metal-xanthate process. In the case of $PdTe_2$, reduction peaks were observed to diminish in the presence of SIBX, hence indicating the adsorption of SIBX on the mineral surface.

The impedance data obtained in this work indicates that $S_2O_3^{2-}$, SO_4^{2-}, Mg^{2+}, Ca^{2+}, Na^+ and SIBX interact with PdS and $PdTe_2$ through a charged transfer mechanism. Moreover, $S_2O_3^{2-}$, SO_4^{2-}, Mg^{2+}, Ca^{2+} and Na^+ adsorb at a faster rate on the palladium minerals than SIBX itself. The rate of adsorption was dependent on the type of ion, its concentration and the mineral type. In addition, higher R_{ct} values were displayed in the presence of SIBX. Considering that the double-layer capacitance is dependent upon the dielectric property and thickness of the electrical double layer, higher impedance values will consequently decrease the capacitance. This is due to the considerably smaller dielectric constant exhibited by xanthate collectors. A change in impedance values was observed in the lower frequency range for all ions investigated and SIBX. This change denoted the formation of continuous surface layers on the palladium minerals. Hence, the rate of formation of passivation layers on the mineral surfaces was fully dependent upon the ion type, its concentration, and the type of palladium mineral. Overall, it was shown that the palladium minerals displayed a capacitive behaviour in the presence of $S_2O_3^{2-}$, SO_4^{2-}, Mg^{2+}, Ca^{2+}, Na^+ and SIBX. This observation denotes the existence of the electrical double layer and/or coating layer on the palladium minerals.

An illustration of a summary of the findings of this work is shown in Figures 8.14 and 8.15.

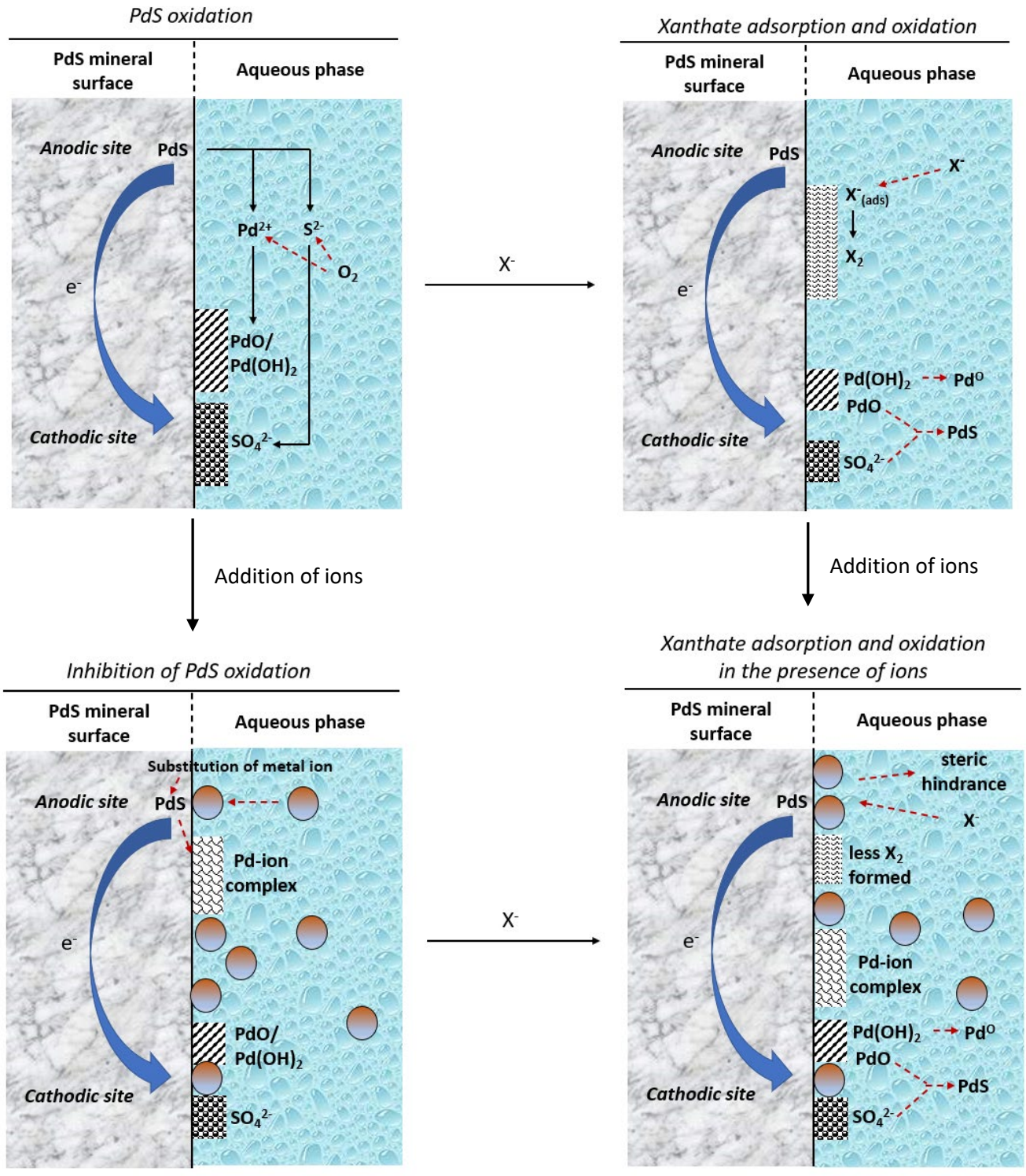

Figure 8.14: An illustration of the mechanisms of interaction of ions and xanthate collectors on PdS. Where ● represents the ions investigated in this study.

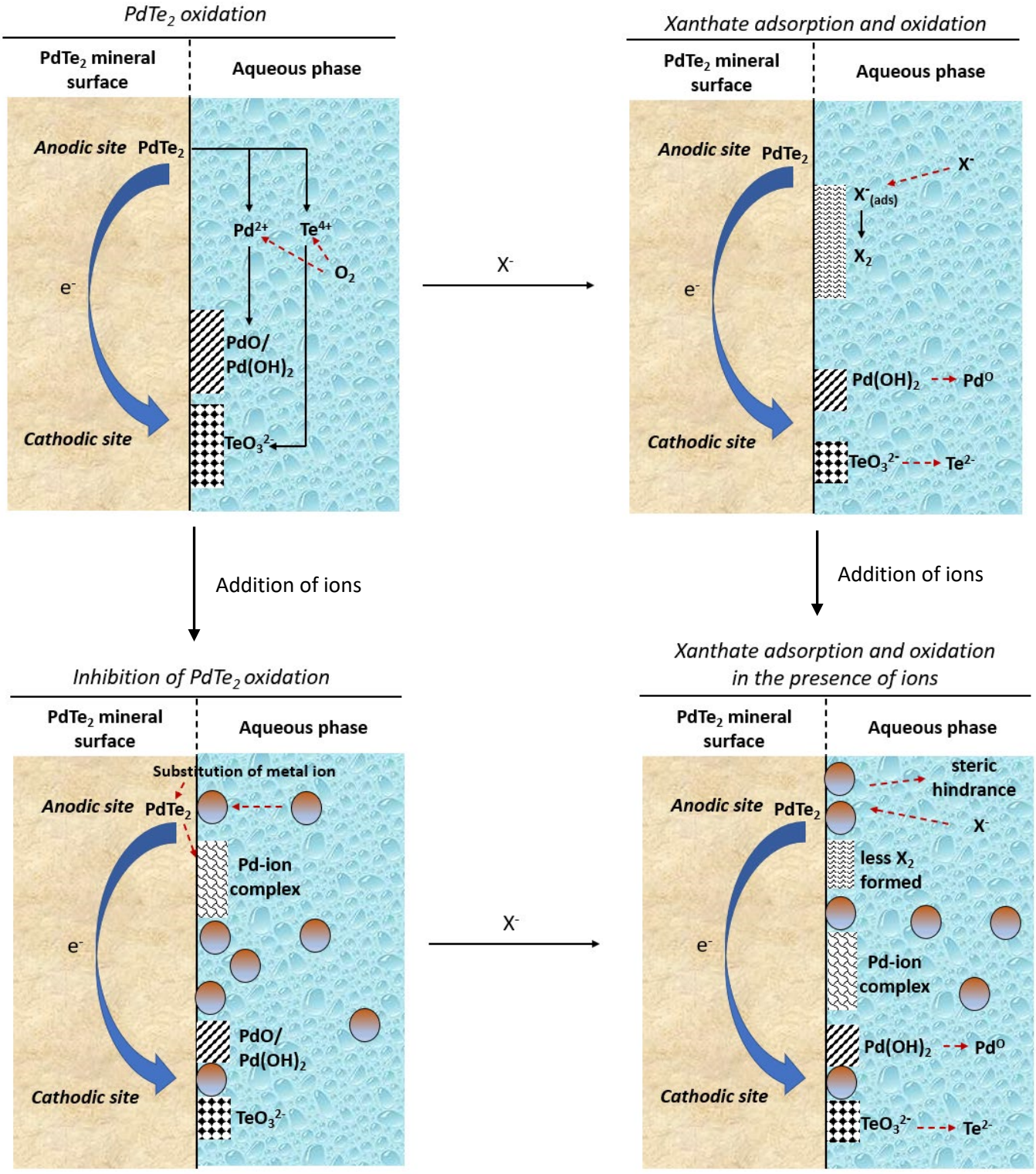

Figure 8.15: An illustration of the mechanisms of interaction of ions and xanthate collectors on $PdTe_2$. Where ● represents the ions investigated in this study.

9. Conclusions

This study investigated the mechanisms of interfacial interactions between SIBX and palladium minerals (PdS and $PdTe_2$) in the absence and presence of salts at increasing ionic strength. The electrochemical nature of mineral-salt and/or xanthate collector interactions implies that it is feasible to explore their mechanisms of interactions by electrochemical techniques. Rest potential, cyclic voltammetry and electrochemical impedance measurements were employed to answer the key questions developed in Chapter 3, to validate the conjectured hypotheses. This work provides answers in the field of water quality on the speculations made by previous studies about the interactions of xanthates with mineral surfaces in the presence of inorganic salts. Hence, in-depth knowledge of the mechanisms of interactions between PGM mineral surfaces with xanthates, in the presence of salts, has been established.

1) **How do single salts at increasing ionic strength interact with palladium minerals?**

It has been shown in this study that the extent of interaction between ions ($S_2O_3^{2-}$, SO_4^{2-}, Ca^{2+}, Mg^{2+} and Na^+) and the palladium minerals increased with an increase in ionic strength. However, the divalent ions, $S_2O_3^{2-}$ and Ca^{2+} displayed higher interactions with PdS than with other ions investigated. Moreover, $S_2O_3^{2-}$ and Ca^{2+}, Mg^{2+} and Na^+ decreased the rest potential for PdS, whereas SO_4^{2-} ions at higher ionic strengths of 3 SPW, 5 SPW and 10 SPW, exhibited an increase in rest potential for PdS. Alternatively, SO_4^{2-}, Ca^{2+}, Mg^{2+} and Na^+ ions conveyed an increase in rest potential for $PdTe_2$, whilst $S_2O_3^{2-}$ demonstrated a decrease in rest potential for the $PdTe_2$ mineral surface. Similar to PdS, the divalent ions generally displayed higher interactions compared to monovalent ions. This study, therefore, demonstrates that the mechanism of adsorption of ions on mineral surfaces is dominated by the type of mineral surface onto which the ions adsorb. Conversely, the extent of interaction of ions with mineral surfaces is fully dependent upon the mineral and salt type, and the ionic strength of the salt.

2) **How does SIBX interact with palladium minerals in the presence of single salts at increasing ionic strength?**

On PdS, increasing the ionic strength of the salts, significantly decreased the extent to which SIBX interacted with the mineral surface. Hence, decreasing the rate of dixanthogen formation on the mineral surface. Generally, the presence of salts decreased the rate of dixanthogen formation on PdS compared to the absence of salts in the system. Interestingly, though SIBX was revealed to

interact more with $PdTe_2$, at increasing ionic strengths, mostly the formation of a metal xanthate or dixanthogen at a lower rate was favoured.

3) **What are the adsorption mechanisms involved upon the interaction of SIBX with palladium minerals in the absence and presence of single salts with an increase in ionic strength?**

It has been established that the rate of adsorption of the salts investigated was mainly dependent upon the salt and mineral type. However, it has been determined that the salts investigated displayed faster adsorption kinetics than SIBX itself. Thereby, implying that $S_2O_3^{2-}$, SO_4^{2-}, Ca^{2+}, Mg^{2+} and Na^+ ions adsorb and occupy the metal active sites before the adsorption and oxidation of SIBX. The rate of adsorption of $S_2O_3^{2-}$ was determined to occur at a faster rate in higher ionic strengths, whereas the rate of adsorption of SO_4^{2-}, Ca^{2+}, Mg^{2+} and Na^+ ions occurred faster at lower ionic strengths. These findings suggest that the adsorption kinetics of salts on mineral surfaces is not determined by their ionic strength. In addition, it has been revealed that the adsorption of the ions investigated and/or SIBX occur via interfacial charge transfer kinetics, which involves an ion exchange mechanism in the case of the divalent anions whereas, with the divalent cations, their dissociation in solution and precipitation with hydroxides and/or carbonates was presumed to occur.

In the case of PdS, the formation of dixanthogen was favoured in the absence of salts, in the presence of SO_4^{2-}, Mg^{2+} and Na^+ ions at all ionic strengths, in $S_2O_3^{2-}$ ions at 1 SPW and in the presence of Ca^{2+} ions at 3 SPW, 5 SPW and 10 SPW. With respect to $PdTe_2$, the formation of dixanthogen was favoured in the presence of Ca^{2+}, SO_4^{2-}, at all ionic strengths, Mg^{2+} ions at 1 SPW, 3 SPW and 10 SPW and in Na^+ ions at 1 SPW. The formation of the dimer is presumed to proceed through a chemisorption reaction, which is thermodynamically favoured. After which the adsorbed xanthate ions will oxidize, forming a stable surface specie, dixanthogen. Additionally, the metal-xanthate specie was favoured on PdS with Ca^{2+} ions at 1 SPW and $S_2O_3^{2-}$ at 3 SPW, 5 SPW and 10 SPW only. Whereas, with $PdTe_2$, the metal-xanthate specie was favoured in the presence of $S_2O_3^{2-}$ ions at all ionic strengths investigated, Mg^{2+} ions at the highest ionic strength and Na^+ ions at ionic strengths of 3 SPW, 5 SPW and 10 SPW. The formation of a metal-xanthate could be associated with a chemisorption mechanism that is demonstrated by substitution reactions that occur for xanthate ions on the palladium mineral surfaces, as proposed in Chapter 8 of this study. Ultimately, the final step which involves the formation of the metal-xanthate may be illustrated by a two-step mechanism which involves the oxidation of the palladium surface and subsequently, the bonding of a xanthate ion with a metal ion.

This study has shown that the oxidation product formed after xanthate oxidation is heavily influenced by the type of mineral, the type of salt and its ionic strength. However, it was observed that higher ionic strengths mostly favoured the formation of a metal-xanthate whereas lower ionic strengths mostly favoured the formation of dixanthogen.

4) **How do different salts affect the interaction between SIBX and palladium minerals?**

It has been presumed that the presence of $S_2O_3^{2-}$ ions resulted in the formation of a $[Pd(S_2O_3)_2]^{2-}$ complex which passivated the palladium mineral surfaces. Hence, the significant decrease in interaction between SIBX and the palladium minerals; and a subsequent decrease in surface coverage of SIBX, with an increase in ionic strength.

In the presence of Ca^{2+} ions, the formation of $PdCO_3$, $CaCO_3$ and $Ca(OH)_2$ oxidation products was proposed. The rate at which PdS was reduced in the presence of Ca^{2+} ions increased with an increase in ionic strength and on the contrary the rate at which $PdTe_2$ was oxidized increased with an increase in ionic strength of Ca^{2+} ions. The manner in which the ions interacted with the palladium minerals affected the way in which SIBX interacted with each palladium mineral. The presence of Ca^{2+} ions was generally found to inhibit the oxidation of the palladium minerals. The rate of oxidation was determined to be suppressed more with an increase in ionic strength. Consequently, Ca^{2+} ions significantly decreased the interaction between SIBX and PdS whereas the interaction between the xanthate ions and $PdTe_2$ was enhanced. Interestingly, the least surface coverage of SIBX on $PdTe_2$ was obtained in the presence of Ca^{2+} ions amongst other salts.

It was determined that PdS was reduced in the presence of Mg^{2+} ions and alternatively $PdTe_2$ was oxidized. However, the formation of a passivation layer of $Mg(OH)_2$ was proposed, which inhibited the oxidation of the palladium surfaces and retarded the reduction of oxidized species. Additionally, it was observed that the presence of Mg^{2+} ions decreased the extent of interaction between SIBX and PdS, with an increase in ionic strength. On the contrary, the interactions of SIBX and $PdTe_2$ did not vary significantly in the presence of Mg^{2+} ions at all ionic strengths investigated. Accordingly, the surface coverage of SIBX in the presence of Mg^{2+} ions at all ionic strengths did not differ substantially. Moreover, the Mg^{2+} ions were found to enhance the interaction between xanthate ions and $PdTe_2$.

SO_4^{2-} ions were observed to interact with both palladium minerals in a similar mechanism. Both palladium minerals were oxidized in the presence of SO_4^{2-} ions. Therefore, this study proposed the formation of a $PdSO_4$ complex on PdS and $PdTe_2$ mineral surfaces, in the presence of SO_4^{2-} ions.

It was determined that the interaction of SIBX with the palladium minerals was enhanced in the presence of SO_4^{2-} ions. This suggests that the formation of the complex $PdSO_4$ most likely played a role in facilitating the interactions of xanthate ions with the palladium minerals. In contrast with what has been reported in literature, SO_4^{2-} ions have been determined in this study to enhance the interaction of xanthate ions with palladium mineral surfaces. Therefore, it is expected that they should have a beneficial effect on the flotation recoveries of PdS and $PdTe_2$.

As expected, Na^+ ions, being non-surface-active ions, interacted the least amongst other salts, with the palladium minerals. It was determined that Na^+ ions promoted the interaction between SIBX and the palladium mineral surfaces. In agreement with previous studies, it is expected that Na^+ ions had an insignificant effect on the surface charge of the palladium mineral surfaces and their adsorption behaviour. Hence, it is expected that Na^+ ions should have beneficial effects on the flotation recoveries of PdS and $PdTe_2$ minerals.

5) **Which electrical circuit elements represent the mineral-water interface of the palladium mineral systems?**

The EIS data obtained in this study suggest that the electrochemical system that consists of the salts at the palladium mineral surfaces may best be represented by a resistor representing R_s, in series with a parallel circuit of a capacitor, C_{dl}, denoting the presence of an electrical double layer and a resistor representing R_{ct} (Figure 7.94). Additionally, in the presence of both salts and SIBX, it has been accepted that an equivalent circuit for this system comprises a resistor, R_s, in series with a parallel circuit consisting of a capacitor, C_c (denoting a coating layer formed due to the adsorption and oxidation of SIBX) and a capacitor, C_{dl} (Figure 7.95).

10. Recommendations

Following the results obtained and conclusions made in the study, it is recommended that future work should consider:

- Complimenting such studies with batch flotation/micro-flotation tests and surface chemistry techniques.
- Exploring more mineral commodities. This will give a broader understanding of the interactions of such commodities with flotation reagents in the presence of salts.
- Examining the mechanisms of interfacial interactions between other collector types and possibly various surface-active flotation reagents with mineral surfaces. This will give an in-depth understanding of the extent to which the interactions of flotation reagents are possibly affected by the presence of salts in process water.
- The findings of this study could be further explored at pilot scale.

References

ACKERMAN, P. K., HARRIS, G. H., KLIMPEL, R. R. & APLAN, F. F. 1986. Evaluation of Flotation Collectors for Copper Sulfides and Pyrite I. Common Sulfhydryl Collectors. *International Journal of Mineral Processing,* 21, 105-127.

ACORD, K. 2021. *Electrochemical Impedance Spectroscopy* [Online]. Davis: University of California. Available: https://eng.libretexts.org/Bookshelves/Materials_Science/Supplemental_Modules_(Materials_Science)/Insulators/Electrochemical_Impedance_Spectroscopy [Accessed].

ALLISON, S. A. & FINKELSTEN, N. P. 1971. A study of the products of reaction between galena and aqueous xanthate solutions. *Trans. Instn Min. Metall,* 80, C235-C239.

ALLISON, S. A., GOOLD, L., NICOL, M. & GRANVILLE, A. 1972. A determination of the products of reaction between various sulphide minerals and aqueous xanthate solution, and a correlation of the products with electrode rest potentials. *Metallurgical and materials transactions. A, Physical metallurgy and materials science,* 3, 2613-2618.

AMETEK SCIENTIFIC INSTRUMENTS 2015. Application Note AC-1: Basics of Electrochemical Impedance Spectroscopy *In:* RESEARCH, P. A. (ed.) *Electrochemical Impedance Spectroscopy Overview.*

AMEZAGA, J. M., ROTTING, T. S., YOUNGER, P. L., NAIRN, R. W., NOLES, A. J., OYARZUN, R. & QUINTANILLA, J. 2011. A rich vein? Mining and the pursuit of sustainability. Environmental Science and Technology Feature, 45, 21-26.

ANTHONY, E. Y. & WILLIAMS, P. A. 1993. Thiosulfate Complexing of Platinum Group Elements. *Environmental Geochemistry of Sulfide Oxidation.*

APLAN, F. F. & CHANDER, S. 1988. *Reagents in Mineral Technology,* New York.

ATKIN, R., CRAIG, V. S. J. & BIGGS, S. 2001. Adsorption kinetics and structural arrangements of cetylpyridinium bromide at the silica-aqueous interface. *American Chemical Society,* 17, 6155-6163.

BARNES, S.-J., MAIER, W. D. & ASHWAL, L. D. 2004. Platinum-group element distribution in the Main Zone and Upper Zone of the Bushveld Complex, South Africa. *Chemical Geology,* 208, 293-317.

BARSOUKOV, E. & MACDONALD, J. R. 2005. *Impedance spectroscopy theory, experiment and applications,* New Jersey, John Wiley & sons, inc.

BASILIO, C. & YOON, R. H. 1992. Mechanism of TCB adsoption on copper and chalcocite. *In:* WOODS, R. & RICHARDSON, P. E. (eds.) *Electrochemistry in mineral and metal processing III.* The Electrochemical Society.

BOHINC, K., KRALJ-IGLIC, V. & IGLIC, A. 2001. Thickness of electrical double layer. Effect of ion size. *Electrochimica Acta,* 46, 3033-3040.

BOUJOUNOUI, K., ABIDI, A., BACAOUI, A., AMARI, K. E. & YAACOUBI, A. 2015. The influence of water quality on the flotation performance of complex sulphide ores- case study at Hajar Mine, Morocco. *The Journal of the Southern African Institute of Mining and Metallury,* 115, 1243-1251.

BOWDEN, J. L. 2016. Xanthate chemisorption at copper and chalcopyrite surfaces. *Journal of the Southern African Institute of Mining and Metallurgy,* 116, 503-508.

BRADSHAW, D. 1997. *Synergistic effects between thiol collectors used in the flotation of pyrite.* PhD, University of Cape Town.

BUCKLEY, A. N. 1996. Relaxation of the lead-deficient sulfide layer on oxidized galena. *Journal of Applied Electrochemistry,* 26, 899-907.

BUCKLEY, A. N. & WOODS, R. 1997. Chemisorption- the thermodynamically favoured process in the interaction of thiol collectors with sulphide minerals. *International Journal of Mineral Processing,* 51, 15-26.

BUCKLEY, A. N., GOH, S. W., LAMB, R. N. & WOODS, R. 2003. Interaction of thiol collectors with pre-oxidised sulfide minerals. *International Journal of Mineral Processing,* 72, 163-174.

CABRI, L. J., LAFLAMME, J. H. G., STEWART, J. M., TURNER, K. & SKINNER, B. J. 1978. On cooperite, braggite and vysotskite. *American Mineralogist,* 633**,** 832-839.

CAWTHORN, R. G. 1999. Tha platinum and palladium resources of the Bushveld Complex. *South African Journal of Science,* 95, 481-489.

CAWTHORN, R. G. 2010. The Platinum Group Element Deposits of the Bushveld Complex in South Africa. *Platinum Metals Review,* 54, 205-215.

CHANDER, S. 1988. Electrochemistry of sulphide mineral flotation. *Minerals and Metallurgical Processing*, 104-114.

CHANG, Z., CHEN, X. & PENG, Y. 2018. The adsorption behavior of surfactants on mineral surfaces in the presence of electrolytes – A critical review. *Minerals Engineering,* 121, 66-76.

CHAOJUN, F., YU, S., PENG, H., DNEG, X. & WANG, J. 2020. Ionic effect of NaCl and KCl on the flotation of diaspore and kaolinite using sodium oleate as collector. *In:* TOMSETT, A. (ed.) *TMS Annual Meeting and Exhibition.* San Diego, CA, United States: Springer.

CLARKE, P., FORNASIERO, D., RALSTON, J. & SMART, R. S. C. 1995. A study of the removal of oxidation products from sulphide mineral surfaces. *Minerals Engineering* 8, 1347-1357.

CLEMENTE, F., ARPAIA, P. & MANNA, C. 2013. Characterization of human skin impedance after electrical treatment for transdermal drug delivery. *Measurement,* 46, 3494-3501.

CORIN, K. C., REDDY, A., MIYEN, L., WIESE, J. G. & HARRIS, P. J. 2011. The effect of ionic strength of plant water on valuable mineral and gangue recovery in a platinum bearing ore from the Merensky reef. *Minerals Engineering,* 24, 131-137.

DALTRY, V. D. C. & WILSON, A. H. 1997. Review of platinum-group mineralogy: compositions and elemental associations of the PR-minerals and unidentified PGE-phases. . *Mineralogy and Petrology,* 60, 185-229.

DE WET, J. R., HODGKINSON, G., PISTORIUS, P. C., PRINSLOO, L. C. & SANDENBERGH, R. F. 1995. The influence of cyanide on the flotation of pyrite from Witwatersrand gold leach residues. *Minerals Engineering,* 8, 1333-1345.

D'OLIMPIO, G., GUO, C., KUO, C. N., EDLA, R., LUE, C. S., OTTAVIANO, L., TORELLI, P., WANG, L., BOUKHVALOV, D. W. & POLITANO, A. 2019. PdTe2 Transition-Metal Dichalcogenide: Chemical Reactivity, Thermal Stability, and Device Implementation. *Advanced Functional Materials,* 30, 1-12.

EKMEKÇI, Z., BECKER, M., TEKES, E. B. & BRADSHAW, D. 2010a. An impedance study of the adsorption of CuSO4 and SIBX on pyrrhotite samples of different provenances. *Minerals Engineering,* 23, 903-907.

EKMEKÇI, Z., BECKER, M., TEKES, E. B. & BRADSHAW, D. 2010b. The relationship between the electrochemical, mineralogical and flotation characteristics of pyrrhotite samples from different Ni Ores. *Journal of Electroanalytical Chemistry,* 647, 133-143.

ELIZONDO-ÁLVAREZ, M. A., FLORES-ÁLVAREZ, J. M., DÁVILA-PULIDO, G. I. & URIBE-SALAS, A. 2017. Interaction mechanism between galena and calcium and sulfate ions. *Minerals Engineering,* 111, 116-123.

ELVY, S. B. & WILLIAMS, P. A. 1996. XPS evidence for the incongruent surface oxidation of minerals in the Pd-Te-Bi system. *Surface and Interface Analysis,* 24, 641-646.

ERTEKIN, Z., PEKMEZ, K. & EKMEKÇI, Z. 2016. Evaluation of collector adsorption by electrochemical impedance spectroscopy. *International Journal of Mineral Processing,* 154, 16-23.

FERRER, I. J., DÍAZ-CHAO, P., PASCUAL, A. & SÁNCHEZ, C. 2007. An investigation on palladium sulphide (PdS) thin films as a photovoltaic material. *Thin Solid Films,* 515, 5783-5786.

FLORES-ÁLVAREZ, J. M., ELIZONDO-ÁLVAREZ, M. A., DÁVILA-PULIDO, G. I., GUERRERO-FLORES, A. D. & URIBE-SALAS, A. 2017. Electrochemical behavior of galena in the presence of calcium and sulfate ions. *Minerals Engineering,* 111, 158-166.

FUERSTENAU, D. W. 1984. Adsorption and electrical double layer phenomena at mineral-water interfaces. *AIP* American Institute of Physics and Chemistry of Porous Media-Schlumberger-Doll Research.

GAMRY INSTRUMENTS. 1989. *Basics of Electrochemical Impedance Spectroscopy* [Online]. Available: https://www.gamry.com/application-notes/EIS/basics-of-electrochemical-impedance-spectroscopy/ [Accessed].

GARDNER, J. R. & WOODS, R. 1979. A study of the surface oxidation of galena using cyclic voltammetry. *J. Electroanal. Chem*, 447-459.

GASKELL, T. F. 1936. The structure of braggite and palladium sulphide. *Patterson, J. Phys. Chem. Soc.*, 203-213.

GATOS, H. C. 1962. Crystalline structure and surface reactivity. *American Association for the Advancement of Science,* 137, 311-322.

GROSSI, M. & RICCÒ, B. 2017. Electrical impedance spectroscopy (EIS) for biological analysis and food characterization: a review. *Journal of Sensors and Sensor Systems,* 6, 303-325.

HIRAJIMA, T., SUYANTARA, G. P. W., ICHIKAWA, O., ELMAHDY, A. M., MIKI, H. & SASAKI, K. 2016. Effect of Mg 2+ and Ca 2+ as divalent seawater cations on the floatability of molybdenite and chalcopyrite. *Minerals Engineering,* 96-97, 83-93.

HODGSON, M. & AGAR, G. E. 1989. Electrochemical Investigations into the Flotation Chemistry of Pentlandite and Pyrrhotite: Process Water and Xanthate Interactions. *Canadian Metallurgical Quarterly,* 28, 189-198.

HU, Y., SUN, W. & WANG, D. 2009. *Electrochemistry of Flotation of Sulphide Minerals.*, Tsinghua University Press and Springer-Verlag Berlin Heidelberg.

HUAI, Y., PLACKOWSKI, C. & PENG, Y. 2018. The galvanic interaction between gold and pyrite in the presence of ferric ions. *Minerals Engineering,* 119, 236-243.

IKUMAPAYI, F., MAKITALO, M., JOHANSSON, B. & RAO, K. H. 2012. Recycling of process water in sulphide flotation: Effect of calcium and sulphate ions on flotation of galena. *Minerals Engineering,* 39, 77-88.

IKUMAPAYI, F. & RAO, K. H. 2015. Recycling Process Water in Complex Sulfide Ore Flotation: Effect of Calcium and Sulfate on Sulfide Minerals Recovery. *Mineral Processing and Extractive Metallurgy Review,* 36, 45-64.

IQBAL, M. Z. & RAFIUDDIN 2016. Preparation, characterization, electrical conductivity and dielectric studies of Na2SO4 and V2O5 composite solid electrolytes. *Measurement,* 81, 102-112.

JANETSKI, N. D., WOODBURN, S. I. & WOODS, R. 1977. An electrochemical investigation of pyrite flotation and depression. *International Journal of Mineral Processing,* 4, 227-239.

JONES, R. T. 1999. Platinum in South Africa. *South African Journal of Science,* 95, 525-534.

KHAN, A. & KELEBEK, S. 2004. Electrochemical aspects of pyrrhotite and pentlandite in relation to their flotation with xanthate. Part I: Cyclic voltammetry and rest potential measurements. *Journal of Applied Electrochemistry,* 34, 849-856.

KIRJAVAINEN, V., SCHREITHOFER, N. & HEISKANEN, K. 2002. Effect of calcium and thiosulphate ions on flotation selectivity of nickel copper ores. 15, 1-5.

KOCABAĞ, D. & GÜLER, T. 2007. Two-liquid flotation of sulphides: An electrochemical approach. *Minerals Engineering,* 20, 1246-1254.

LASCELLES, D., FINCH, J. A. & SUI, C. 2001. Depressant action of Ca and Mg on flotation of Cu activated sphalerite. *Canadian Metallurgical Quarterly,* 42, 133-140.

LASIA, A. 2014. *Electrochemical Impedance Spectroscopy and its applications.*, Springer Science+Business Media New York.

LATYPOV, R., CHISTYAKOVA, S., PAGE, A. & HORNSEY, R. 2015. Field Evidence for theIn Situ Crystallization of the Merensky Reef. *Journal of Petrology,* 56, 2341-2372.

LEFEVRE, G. & FEDOROFF, M. 2006. Sorption of sulfate ions onto hematite studied by attenuated total reflection-infrared spectroscopy: Kinetics and competition with other ions. *Physics and Chemistry of the earth,* 31, 499-504.

LEPPINEN, J. O. 1990. FTIR and flotation investigation of the adsorption of ethyl xanthate on activetd and non-activated sulfide minerals. *International Journal of Mineral Processing,* 30, 245-263.

LEPPINEN, J., LAAJALEHTO, K., KARTIO, I. & SOUNINEN, E. Proceedings of the 19th International Mineral Processing Congress, October 22-27 1995 San Francisco, USA. 35.

LIVINGSTONE, S. E. 1965. Metal complexes of ligands containing sulphur, selenium or tellurium as donor atoms. *Quarterly Reviews, Chemical Society.*

LOTTER, N. O. & BRADSHAW, D. J. 2010. The formulation and use of mixed collectors in sulphide flotation. *Minerals Engineering,* 23, 945-951.

MABOTT, G. A. 1983. An introduction to Cyclic Voltammetry. *Chemical education,* 60, 697-702.

MALATI, M. A. 1967. Activation of quartz by alkaline earth cations in oleate flotation. *Journal of Applied Chemistry,* 17, 209-212.

MANONO, M. S., CORIN, K. C. & WIESE, J. G. 2016. The influence of electrolytes present in process water on the flotation behaviour of a Cu-Ni containing ore. *Minerals Engineering,* 96-97, 99-107.

MANONO, M., CORIN, K. C. & WIESE, J. G. 2018. Water quality in a sulphide PGM ore implications for froth stability and gangue management. *Physicochemical Problems of Mineral Processing,* 54, 1253-1265.

MANYERUKE, T. D. & MAIER, W. D. 2005. Major and trace element geochemistry of the Platreef on the farm Townlands, nothern Bushveld Complex. *Geological Society of South Africa,* 108, 381-396.

MARAPE, G. & VERMAAK, M. K. G. 2012. Fundamentals of pentlandite mineralogy and its effect on its electrochemical behaviour. *Minerals Engineering,* 32, 60-67.

MCDONALD, I., HOLWELL, D. A. & ARMITAGE, P. E. B. 2005. Geochemistry and mineralogy of the Platreef and "Critical Zone" of the northern lobe of the Bushveld Complex, South Africa: implications for Bushveld stratigraphy and the development of PGE mineralisation. *Mineralium Deposita,* 40, 526-549.

MHONDE, N., SCHREITHOFER, N., CORIN, K. & MÄKELÄ, M. 2020. Assessing the Combined Effect of Water Temperature and Complex Water Matrices on Xanthate Adsorption Using Multiple Linear Regression. *Minerals,* 10.

MISHRA, K. K., HAM, D. & RAJESHWAR, K. 1990. Anodic oxidation of telluride ions in aqueous base: A rotating ring-disk electrode study. *J. Electrochem. Soc.,* 137.

MOSLEMI, H. & GHARABAGHI, M. 2016. A review on electrochemical behavior of pyrite in the froth flotation process. *Journal of Industrial and Engineering Chemistry,* 47, 1-18.

MOSLEMI, H., SHAMSI, P. & HABASHI, F. 2011. Pyrite and pyrrhotite open circuit potentials study: Effects on flotation. *Minerals Engineering,* 24, 1038-1045.

MU, Y., PENG, Y. & LAUTEN, R. A. 2015. Electrochemistry aspects of pyrite in the presence of potassium amyl xanthate and a lignosulfonate-based biopolymer depressant. *Electrochimica Acta,* 174, 133-142.

MUZENDA, E. 2010. An investigation into the effect of water quality on flotation perfomance. International Journal of Chemical and Molecular Engineering, 4.

OCTOBER, L. L., CORIN, K. C., MANONO, M. S., SCHREITHOFER, N. & WIESE, J. G. 2020. A fundamental study considering specific ion effects on the attachment of sulfide minerals to air bubbles. *Minerals Engineering,* 151.

OCTOBER, L. L., MANONO, M. S., CORIN, K. C., SCHREITHOFER, N. & WIESE, J. G. 2021. The Influence of Specific Ions and Oxyhydroxo Species in Plant Water on the Bubble-Particle Attachment of Pyrrhotite. *ACS Omega,* 6, 28496-28506.

OFOR, O. 1996. Effect of inorganic ions on oleate adsorption at a Nigerain hematite-water interface. *J. Colloid Interface Sci.,* 180, 323-328.

OH, S. Y., LEUNG, L., BOMMANNAN, D., GUY, R. H. & POTTS, R. O. 1993. Effect of current, ionic strenght and temperature on the electrical properties of skin. *Journal of Controlled Release,* 27, 115-125.

PARK, S.-J. & SEO, M.-K. 2011. Intermolecular Force. *Interface Science and Composites.*

PECINA, E. T., URIBE, A., FINCH, J. A. & NAVA, F. 2006. Mechanism of di-isobutyl dithiophosphinate adsorption onto galena and pyrite. *Minerals Engineering,* 19, 904-911.

PELL, M. A., MIRONOV, Y. V. & IBERS, J. A. 1996. PdTe2. *Acta Crystallographica Section C: Crystal Structure Communications,* 52, 1331-1332.

PENBERTHY, C. J., OOSTHUYZEN, E. J. & MERKLE, R. K. W. 2000. The recovery of platinum-group elements from the UG-2 chromitite, Bushveld Complex- a mineralogical perspective. *Mineralogy and Petrology,* 68, 213-222.

PERSSON, I. 1994. Review: Adsorption of Ions and Molecules to Solid Surfaces in Connection with Flotation of Sulphide Minerals. *Journal of Coordination Chemistry,* 32, 261-342.

POTAPOVA, E., GRAHN, M., HOLMGREN, A. & HEDLUND, J. 2010. The effect of calcium ions and sodium silicate on the adsorption of a model anionic flotation collector on magnetite studied by ATR-FTIR spectroscopy. *J Colloid Interface Sci,* 345, 96-102.

QIU, G., HUANG, S., SEGOVIA, M., VENUTHURUMILLI, P. K., WANG, Y., WU, W., XU, X. & YE, P. D. 2019. *Thermoelectric Performance of 2D Tellurium with Accumulation Contacts*. Nano Lett, 19, 1955-1962.

RAO, F., LÁZARO, I. & IBARRA, L. A. 2016. Solution chemistry of sulphide mineral flotation in recycled water and sea water: a review. *Mineral Processing and Extractive Metallurgy*, 126, 139-145.

REVENTOS, M. M., RIUS, J. & AMIGO, J. M. 2012. Mineralogy and geology- The role of crystallography since the discovery of x-ray diffraction in 1912. *Revista de la Sociedad Geologica de Espana,* 25, 133-143.

RIBEIRO, D. V., SOUZA, C. A. C. & ABRANTES, J. C. C. 2015. Use of Electrochemical Impedance Spectroscopy (EIS) to monitoring the corrosion of reinforced concrete. *Revista IBRACON de Estruturas e Materiais,* 8, 529-546.

RICHARDSON, P. E. 1995. *Surface chemistry of sulfide flotation*, Chapman and Hall.

RICHARDSON, P. E., STOUT III, J. V., PROCTOR, C. L. & WALKER, G. W. 1984. Electrochemical flotation of sulphides: Chalcocite-ethylxanthate interactions. *International Journal of Mineral Processing,* 12, 73-93.

RIDOUTT, G. B. & PFISTER, S. 2010. Reducing humanity's water footprint. *Environmental Science and Technology Viewpoint*, 44, 6019-6021.

RIJSBERMAN, F. R. 2006. Water scarcity: Fact or fiction? *Agricultural Water Management*, 80, 5-22.

SCHOUWSTRA, R. P., KINLOCH, E. D. & LEE, C. A. 2000. A short Geological Review of the Bushveld Complex. *Platinum Metals Review,* 44, 33-39.

SHACKLETON, N. J. 2007. *Surface characterisation and flotation behaviour of the platinum and palladium arsenide, telluride and sulphide mineral species*. PhD, University of Cape Town.

SHACKLETON, N. J., MALYSIAK, V. & O'CONNOR, C. T. 2007. Surface characteristics and flotation behaviour of platinum and palladium tellurides. *Minerals Engineering,* 20, 1232-1245.

SHEIKH, N. 1972. *Chemical stability of heavy metal xanthates*. PhD, University of British Columbia.

SHIMIZU, K. & BOILY, J.-F. 2014. Electrochemical Properties and Relaxation Times of the Hematite/Water Interface. *Langmuir,* 30, 9591-9598.

SHUEY, R. T. 1975. *Semiconducting ore minerals,* Amsterdam and New York, Elsevier Sci. Publ. Co.

SINCHE-GONZALEZ, M. & FORNASIERO, D. 2021. Understanding the effect of sulphate in mining-process water on sulphide flotation. *Minerals Engineering*, 165, 1-10.

TADIE, M. 2015. An electrochemical investigaton of Platinum Group Minerals. PhD, University of Cape Town.

TADIE, M., CORIN, K. C., WIESE, J. G., NICOL, M. & O'CONNOR, C. T. 2015a. An investigation into electrochemical interactions between platinum group minerals and xanthate: Voltammetric study. *Minerals Engineering,* 70, 148-155.

TADIE, M., CORIN, K. C., WIESE, J. G., NICOL, M. & O'CONNOR, C. T. 2015b. An investigation into the electrochemical interactions between platinum group minerals and sodium ethyl xanthate and sodium diethyl dithiophosphate collectors: Mixed potential study. *Minerals Engineering,* 83, 44-52.

TAKENO, N. 2005. Atlas of Eh-pH diagrams.: National Institute of Advanced Industrial Science and Technology.

TYUTYUNNIK, O. A., KUBRAKOVA, I. V. & PRYAZHNIKOV, D. V. 2016. Formation and sorption behavior of the palladium thiosulfate complexes under natural conditions (model experiments). *Geochemistry International*, 54, 85-91.

USUL, A. H. & TOLUN, R. 1974. Electrochemical study of the pyrite-oxygen-xanthate system. *International Journal of Mineral Processing,* 1, 135-140.

VENTER, J. A. & VERMAAK, M. K. G. 2008. EIS measurements of dithiocarbonate and trithiocarbonate interactions with pyrite and copper. *Minerals Engineering,* 21, 559-567.

VERMAAK, M. K. G. 1995. *Platinum-group Metals: A global perspective*, Mintek.

VERMAAK, M. K. G., VENTER, J. A. & PISTORIUS, P. C. 2004. Electrochemical studies of the interaction of ethyl xanthate with Pd-Bi-Te. *The Journal of the Southern African Institute of Mining and Metallury*, 661-666.

VERMAAK, M. K. G. 2005. *Fundamentals of the flotation behaviour of palladium bismuth tellurides.* PhD, University of Pretoria.

VERMAAK, M. K. G., PISTORIUS, P. C. & VENTER, J. A. 2005. Electrochemical and Raman spectroscopic studies of the interaction of ethyl xanthate with Pd–Bi–Te. *Minerals Engineering,* 18, 575-584.

VERMAAK, M. K. G., VENTER, J. A. & PISTORIUS, P. C. 2004. Electrochemical studies of the interaction of ethyl xanthate with Pd-Bi-Te. *The Journal of the Southern African Institute of Mining and Metallury*, 661-666.

WANG, J., XIE, L., LIU, Q. & ZENG, H. 2015. Effects of salinity on xanthate adsorption on sphalerite and bubble–sphalerite interactions. *Minerals Engineering,* 77, 34-41.

WANG, X.-H. & FORSSBERG, K. S. E. 1991. Mechanisms of pyrite flotation with xanthates. *International Journal of Mineral Processing,* 33, 275-290.

WEBMINERAL. Available: http://www.webmineral.com [Accessed].

WESTLAND, A. 1981. Inorganic chemistry of the platinum-group elements. Platinum-Group Elements: Mineralogy. geology, recovery. *Canadian Institute of Mining , Metallurgy and Petroleum, Special,* 23, 5-18.

WHITE, J. A. The Potgietersrus prospect- geology and exploration history. In: Anhausser CR (ed) Proceedings XVth CMMI Congresss, 1994 S Afr Inst Min Metall, Johannesburg. 173-181.

WIESE, J., HARRIS, P. & BRADSHAW, D. 2005. The influence of the reagent suite on the flotation of ores from the Merensky reef. *Minerals Engineering,* 18, 189-198.

WILLS, B. A. & NAPIER-MUNN, T. 2006. *Will's Mineral Processing Technology- An introduction to the practical aspects of ore treatment and mineral recovery*, Elsevier Science & Technology Books.

WOODS, R. 1971. The oxidation of ethyl xanthate on Platinum, Gold, Copper and Galena electrodes. Relation to the mechanism of mineral flotation. *The Journal of Physical Chemistry,* 75, 354-362.

WOODS, R. 1996. Chemisorption of thiols on metals and metal sulphides. *In:* BOCKRIS, J. O. M. P. P. (ed.) *Modern Aspects of Electrochemistry.* New York.

WU, C.-H., KUO, C.-Y., LIN, C.-F. & LO, S.-L. 2002. Modeling competitive adsorption of molybdate, sulfate, selenate and selenite using Freunndlich-type multi-component isotherm. *Chemosphere*, 47, 283-292.

YOU, G.-X., YU, C.-C., LU, Y. & DANG, Z. 2013. Evaluation of the protective effect of polysiloxane coating on pyrite with electrochemical techniques. *Electrochimica Acta*, 93, 65-71.

ZETA-METER INC. Zeta Potential: A Complete Course in 5 Minutes *The double layer* [Online]. Available: http://www.zeta-meter.com/5min.pdf.

ZHANG, J. 2021. An Investigation of the Adsorption of Xanthate on Bornite in Aqueous Solutions Using an Atomic Force Microscope. *Minerals*, 11.

ZIENTEK, M. L., CAUSEY, J. D., PARKS, H. L. & MILLER, R. J. 2010. Platinum Group elements in Southern Africa- Mineral Inventory and an Assessment of Undiscovered Mineral Resources. *In:* ZIENTEK, M. L., HAMMARSTROM, J. M. & JOHNSON, K. M. (eds.) *Global Mineral Resource Assessment.*

APPENDICES

Appendix A

Rest potential measurements for PdS

Time	PdS-NaCl-1SPW	PdS-NaCl-3SPW	PdS-NaCl-5SPW	PdS-NaCl-10SPW
	AVE/SHE	AVE/SHE	AVE/SHE	AVE/SHE
5,01	0,258675	0,252475	0,26212	0,260535
10,02	0,258675	0,25247	0,26213	0,260535
15,03	0,258695	0,25245	0,26212	0,260535
20,04	0,258765	0,252395	0,26205	0,260525
25,05	0,258885	0,2523	0,26186	0,26052
30,06	0,25904	0,252195	0,261545	0,260495
35,07	0,25919	0,252085	0,26118	0,26039
40,08	0,25929	0,251985	0,26083	0,260175
45,09	0,259325	0,251885	0,2605	0,259855
50,1	0,259295	0,25178	0,260195	0,259425
55,11	0,25925	0,25168	0,259895	0,25885
60,12	0,25922	0,2516	0,259575	0,25811
65,13	0,25919	0,251525	0,259205	0,257265
70,14	0,259135	0,25144	0,25878	0,25642
75,15	0,259035	0,25135	0,25836	0,255595
80,16	0,25888	0,251245	0,257985	0,25469
85,17	0,25868	0,25114	0,257645	0,25354
90,18	0,258485	0,25103	0,25734	0,25216
95,19	0,25836	0,25092	0,257055	0,25071
100,2	0,258315	0,25083	0,25674	0,24933
105,2	0,258305	0,250765	0,25637	0,248055
110,2	0,258285	0,25072	0,25599	0,246875
115,2	0,25822	0,25068	0,25568	0,245805
120,2	0,258095	0,250635	0,255435	0,24483
125,3	0,257945	0,25057	0,255195	0,243935
130,3	0,25781	0,250505	0,2549	0,243115
135,3	0,25771	0,250415	0,25459	0,242315
140,3	0,25765	0,25031	0,2543	0,24151
145,3	0,25758	0,25019	0,25404	0,240705
150,3	0,257505	0,25007	0,25381	0,2399
155,3	0,25744	0,249965	0,25361	0,239095
160,3	0,257395	0,24988	0,253385	0,238305
165,3	0,257355	0,249785	0,25312	0,237565
170,3	0,257295	0,24967	0,25282	0,23692
175,4	0,25721	0,24955	0,252495	0,236415

180,4	0,257115	0,24943	0,252155	0,2361
185,4	0,257015	0,24935	0,251805	0,236
190,4	0,25692	0,249295	0,251475	0,236015
195,4	0,2568	0,24925	0,251195	0,235895
200,4	0,256665	0,24919	0,250925	0,235435
205,4	0,25653	0,24913	0,250655	0,234675
210,4	0,256385	0,249065	0,250425	0,23376
215,4	0,256245	0,248995	0,250255	0,232865
220,4	0,256085	0,24892	0,25013	0,232105
225,4	0,255915	0,24885	0,249995	0,23154
230,5	0,25577	0,248775	0,249855	0,231125
235,5	0,255675	0,248725	0,24973	0,230775
240,5	0,2556	0,2487	0,249595	0,23046
245,5	0,2555	0,24867	0,24942	0,230165
250,5	0,255375	0,248625	0,249165	0,229855
255,5	0,25525	0,248555	0,248895	0,229505
260,5	0,25514	0,248485	0,24871	0,22914
265,5	0,25504	0,248425	0,24864	0,22884
270,5	0,25495	0,24836	0,2486	0,2286
275,5	0,254855	0,24829	0,248505	0,228315
280,6	0,25475	0,248215	0,248355	0,227955
285,6	0,254635	0,248145	0,24822	0,227585
290,6	0,25453	0,24808	0,24809	0,22721
295,6	0,254455	0,24803	0,247925	0,22679
300,6	0,2544	0,248	0,24767	0,22658
305,6	0,25434	0,24803	0,247415	0,2277
310,6	0,25421	0,24819	0,24742	0,231085
315,6	0,25394	0,248535	0,247975	0,235385
320,6	0,25342	0,248855	0,248875	0,23795
325,6	0,25261	0,24871	0,24925	0,23804
330,7	0,251605	0,24793	0,24851	0,236965
335,7	0,25065	0,24677	0,24697	0,235755
340,7	0,249945	0,2456	0,245305	0,23454
345,7	0,249545	0,24462	0,24395	0,23328
350,7	0,24933	0,24388	0,243005	0,232125
355,7	0,24914	0,24333	0,242385	0,231215
360,7	0,24892	0,24292	0,24195	0,230555
365,7	0,24864	0,24259	0,241585	0,23006
370,7	0,248335	0,242325	0,24123	0,229665
375,8	0,248005	0,242095	0,240915	0,229355
380,8	0,247615	0,24189	0,240645	0,229125
385,8	0,24711	0,241725	0,24043	0,228965
390,8	0,24651	0,24158	0,24024	0,22884
395,8	0,245955	0,24145	0,24007	0,22873
400,8	0,24558	0,241325	0,239925	0,22859
405,8	0,24538	0,2412	0,23979	0,228435

410,8	0,24527	0,241095	0,239635	0,228265
415,8	0,245165	0,24102	0,239445	0,22807
420,8	0,245045	0,24097	0,23925	0,227865
425,9	0,24495	0,240925	0,239055	0,22767
430,9	0,24495	0,240885	0,238875	0,22753
435,9	0,245075	0,24085	0,238705	0,22743
440,9	0,245215	0,2408	0,238555	0,227345
445,9	0,24525	0,24075	0,238415	0,22728
450,9	0,24519	0,24071	0,23829	0,227235
455,9	0,24509	0,240685	0,238155	0,22717
460,9	0,24495	0,24067	0,23803	0,22708
465,9	0,244845	0,24066	0,23792	0,226995
470,9	0,244855	0,24065	0,23782	0,22693
476	0,24495	0,24064	0,237675	0,226895
481	0,24503	0,240615	0,237495	0,22688
486	0,24504	0,240575	0,23729	0,22685
491	0,24498	0,240535	0,237105	0,22679
496	0,24483	0,240495	0,236935	0,226675
501	0,244575	0,240475	0,2368	0,226505
506	0,244275	0,240465	0,236705	0,226295
511	0,24404	0,24048	0,236655	0,226065
516	0,24391	0,240495	0,236605	0,225835
521	0,243795	0,24051	0,23653	0,225655
526	0,24363	0,24053	0,23642	0,22557
531,1	0,24344	0,24054	0,23629	0,22558
536,1	0,24328	0,240545	0,236175	0,225645
541,1	0,24317	0,24055	0,23608	0,225725
546,1	0,243135	0,240555	0,236025	0,225785
551,1	0,243145	0,24056	0,236	0,22582
556,1	0,24314	0,240565	0,235975	0,2258
561,1	0,243075	0,24057	0,23594	0,22573
566,1	0,24298	0,24059	0,235875	0,225655
571,1	0,24287	0,24062	0,235795	0,2256
576,2	0,24274	0,24066	0,235705	0,22558
581,2	0,24257	0,240695	0,23561	0,22556
586,2	0,242375	0,240705	0,235505	0,22555
591,2	0,24225	0,24071	0,235405	0,225545
596,2	0,24224	0,240715	0,235295	0,225565
601,2	0,24233	0,240715	0,23515	0,22557
606,2	0,24089	0,23925	0,23453	0,224555
611,2	0,2321	0,23028	0,2310925	0,217733
616,2	0,209325	0,206227	0,221075	0,1976155
621,2	0,1735725	0,168905	0,202685	0,163665
626,3	0,13474	0,13142	0,177	0,127015
631,3	0,104055	0,10555	0,1470635	0,10005
636,3	0,0865	0,0931	0,11898	0,08605

641,3	0,07995	0,08935	0,099245	0,0813
646,3	0,0793	0,0894	0,08945	0,08075
651,3	0,0807	0,09025	0,08665	0,08135
656,3	0,08225	0,091	0,08695	0,08195
661,3	0,08345	0,0914	0,0879	0,08235
666,3	0,0843	0,09165	0,08875	0,08255
671,3	0,085	0,0918	0,08935	0,0827
676,3	0,08555	0,092	0,08975	0,0829
681,4	0,0861	0,09215	0,09005	0,08305
686,4	0,0866	0,0923	0,09035	0,08325
691,4	0,08705	0,0925	0,0905	0,08345
696,4	0,08745	0,09265	0,0907	0,0836
701,4	0,08785	0,09275	0,09075	0,0837
706,4	0,0882	0,09285	0,09085	0,08385
711,4	0,0885	0,093	0,09095	0,084
716,4	0,08885	0,0931	0,091	0,08415
721,4	0,08915	0,0932	0,09115	0,0843
726,5	0,08945	0,0933	0,09135	0,08445
731,5	0,0897	0,0934	0,0915	0,08455
736,5	0,09	0,0935	0,09165	0,08465
741,5	0,0902	0,09355	0,09175	0,08475
746,5	0,09045	0,0936	0,09195	0,0849
751,5	0,09065	0,0937	0,09205	0,085
756,5	0,0908	0,09375	0,0921	0,08515
761,5	0,091	0,0938	0,09215	0,0853
766,5	0,0912	0,0939	0,0921	0,0854
771,5	0,09135	0,09395	0,09215	0,08555
776,5	0,0915	0,094	0,09225	0,0857
781,6	0,0916	0,09405	0,09235	0,08585
786,6	0,09165	0,0941	0,0924	0,08595
791,6	0,09175	0,09415	0,09245	0,08605
796,6	0,0918	0,0942	0,09255	0,0862
801,6	0,09195	0,09425	0,09265	0,0863
806,6	0,092	0,0943	0,09275	0,08645
811,6	0,0921	0,09435	0,0929	0,0865
816,6	0,09215	0,09435	0,09305	0,0866
821,6	0,0922	0,0944	0,0932	0,0867
826,7	0,0923	0,09445	0,093185	0,08675
831,7	0,0924	0,09445	0,093165	0,08685
836,7	0,0925	0,0945	0,0931	0,0869
841,7	0,0926	0,0945	0,093085	0,08695
846,7	0,0927	0,09455	0,09306	0,087
851,7	0,09275	0,09455	0,093025	0,08705
856,7	0,0928	0,09465	0,092985	0,08715
861,7	0,0929	0,09465	0,09295	0,08715
866,7	0,09295	0,09465	0,09292	0,08725

871,7	0,09305	0,09465	0,092895	0,08725
876,8	0,0931	0,09465	0,092965	0,08735
881,8	0,09315	0,0947	0,093015	0,08735
886,8	0,09325	0,0947	0,093	0,0874
891,8	0,09325	0,0947	0,093095	0,08745
896,8	0,0933	0,0947	0,093165	0,08745
901,8	0,09335	0,0947	0,093155	0,0875
906,8	0,09335	0,09475	0,0931	0,08755
911,8	0,09345	0,09475	0,092995	0,08755
916,8	0,09345	0,0948	0,092935	0,08755
921,8	0,09355	0,0948	0,09292	0,0876
926,8	0,0936	0,0948	0,09289	0,08755
931,9	0,09365	0,0948	0,092855	0,0876
936,9	0,0938	0,09475	0,09281	0,08765
941,9	0,09395	0,09475	0,09277	0,08765
946,9	0,09405	0,09475	0,09278	0,08775
951,9	0,09415	0,09475	0,09274	0,0878
956,9	0,09425	0,09475	0,092745	0,08785
961,9	0,09425	0,09475	0,09269	0,08785
966,9	0,0943	0,09475	0,09269	0,0879
971,9	0,0943	0,09475	0,0926	0,08795
977	0,09425	0,0948	0,092565	0,08795
982	0,0943	0,0948	0,09253	0,08805
987	0,0943	0,0948	0,09249	0,08805
992	0,09425	0,0948	0,0924	0,08805
997	0,09425	0,0948	0,092305	0,08805
1002	0,09425	0,0948	0,092205	0,08805
1007	0,0943	0,0948	0,0922	0,0881
1012	0,09435	0,0948	0,09225	0,0881
1017	0,0944	0,0948	0,09235	0,08815
1022	0,0944	0,0948	0,09241	0,08815
1027	0,0944	0,0948	0,09252	0,08815
1032	0,0944	0,09475	0,09258	0,08815
1037	0,0944	0,09475	0,092625	0,08815
1042	0,09435	0,09475	0,092565	0,0882
1047	0,09435	0,09475	0,09246	0,0882
1052	0,09435	0,09475	0,092365	0,08825
1057	0,09435	0,09475	0,092335	0,0883
1062	0,0944	0,09475	0,092405	0,0883
1067	0,0944	0,09475	0,09247	0,0883
1072	0,0944	0,0947	0,092485	0,0883
1077	0,0944	0,0947	0,09249	0,08835
1082	0,0944	0,0947	0,092495	0,08835
1087	0,0944	0,0947	0,09245	0,0884
1092	0,0944	0,0947	0,09245	0,0884
1097	0,09445	0,0947	0,09251	0,0884

1102	0,0945	0,0947	0,092525	0,0884
1107	0,0945	0,09465	0,092485	0,0884
1112	0,0945	0,09465	0,092445	0,0884
1117	0,0945	0,09465	0,09245	0,0884
1122	0,0945	0,09465	0,0925	0,0884
1127	0,0945	0,09465	0,092505	0,0885
1132	0,0945	0,0946	0,092515	0,0885
1137	0,0945	0,0946	0,09252	0,0885
1142	0,0945	0,0946	0,09262	0,08855
1147	0,09455	0,0946	0,092725	0,0885
1152	0,09455	0,0946	0,09282	0,0885
1157	0,09455	0,09455	0,092715	0,0885
1162	0,0945	0,09455	0,092555	0,08845
1167	0,0945	0,09455	0,092395	0,08845
1172	0,0945	0,0945	0,092235	0,0885
1177	0,09455	0,0945	0,092125	0,0885
1182	0,0945	0,0945	0,09201	0,0885
1187	0,09455	0,09445	0,091845	0,0885
1192	0,09455	0,09445	0,09168	0,0885
1197	0,0946	0,09445	0,091585	0,0885
1202	0,0946	0,09445	0,0915	0,0885

Time	PdS-$MgSO_4$-1SPW	PdS-$MgSO_4$-3SPW	PdS-$MgSO_4$-5SPW	PdS-$MgSO_4$-10SPW
	AVE/SHE	AVE/SHE	AVE/SHE	AVE/SHE
5,01	0,27015	0,2749	0,26203	0,26742
10,02	0,270155	0,2749	0,262045	0,26742
15,03	0,27016	0,274915	0,262115	0,26743
20,04	0,27019	0,274955	0,262345	0,26747
25,05	0,27028	0,275025	0,26278	0,267535
30,06	0,27048	0,275105	0,263375	0,26763
35,07	0,27078	0,275205	0,26397	0,267745
40,08	0,2711	0,27531	0,26445	0,26787
45,09	0,271315	0,27541	0,26476	0,268015
50,1	0,27135	0,27549	0,264825	0,26818
55,11	0,271255	0,275565	0,26463	0,268345
60,12	0,271145	0,275635	0,26438	0,268545
65,13	0,271125	0,275725	0,264325	0,268805
70,14	0,27123	0,275825	0,264495	0,269105
75,15	0,27138	0,275915	0,264755	0,269415
80,16	0,271525	0,27597	0,264935	0,2697
85,17	0,271675	0,27599	0,26492	0,26994
90,18	0,271855	0,275985	0,26472	0,27013
95,19	0,272035	0,27599	0,26452	0,270305
100,2	0,27214	0,275995	0,26455	0,27049
105,2	0,272145	0,27599	0,26484	0,270685
110,2	0,27205	0,27597	0,26521	0,27087
115,2	0,27185	0,27596	0,26547	0,27102
120,2	0,271595	0,27597	0,265565	0,271105
125,3	0,271395	0,275985	0,265465	0,271175
130,3	0,271345	0,276	0,265195	0,27127
135,3	0,27144	0,276005	0,26508	0,27142
140,3	0,27163	0,27598	0,26538	0,27157
145,3	0,27187	0,275935	0,26593	0,271715
150,3	0,272115	0,275885	0,266355	0,27188
155,3	0,272305	0,27586	0,26647	0,272115
160,3	0,27241	0,27586	0,266375	0,272375
165,3	0,272375	0,27587	0,26624	0,27259
170,3	0,27221	0,27589	0,266195	0,272745
175,4	0,271925	0,275905	0,26631	0,272885
180,4	0,27156	0,275915	0,26652	0,27299
185,4	0,271115	0,27591	0,26669	0,273
190,4	0,27067	0,275885	0,26664	0,272935
195,4	0,27037	0,275855	0,26633	0,272855
200,4	0,27034	0,275815	0,26594	0,2728
205,4	0,27051	0,27576	0,265785	0,272875
210,4	0,270725	0,2757	0,265995	0,273135
215,4	0,270885	0,27564	0,26642	0,27354
220,4	0,270955	0,275585	0,266855	0,273975

225,4	0,27092	0,27553	0,2671	0,27432
230,5	0,270795	0,27548	0,26711	0,274505
235,5	0,270635	0,275435	0,26703	0,2745
240,5	0,270525	0,27541	0,266985	0,274355
245,5	0,270495	0,275395	0,266995	0,274175
250,5	0,270495	0,275385	0,267155	0,274085
255,5	0,27041	0,27537	0,26743	0,274165
260,5	0,270215	0,275335	0,267555	0,27437
265,5	0,27001	0,27528	0,26736	0,2746
270,5	0,26999	0,275215	0,266915	0,274765
275,5	0,27028	0,27515	0,26641	0,274835
280,6	0,27082	0,27509	0,266015	0,27486
285,6	0,271225	0,27504	0,26579	0,27493
290,6	0,27118	0,27499	0,265665	0,275075
295,6	0,270805	0,27495	0,265505	0,27523
300,6	0,27031	0,274895	0,265225	0,27537
305,6	0,26992	0,274865	0,265	0,275535
310,6	0,2702	0,275015	0,2654	0,27612
315,6	0,271305	0,27568	0,267075	0,278105
320,6	0,27236	0,277135	0,27003	0,282235
325,6	0,27249	0,279185	0,273475	0,287845
330,7	0,271725	0,281265	0,27646	0,293295
335,7	0,27063	0,2829	0,27842	0,297535
340,7	0,26965	0,28395	0,279355	0,300435
345,7	0,26892	0,284445	0,27965	0,30226
350,7	0,268385	0,28443	0,27981	0,303455
355,7	0,267945	0,28401	0,28019	0,30445
360,7	0,267565	0,2834	0,280855	0,305415
365,7	0,26723	0,28264	0,28162	0,306245
370,7	0,266915	0,281655	0,282285	0,306855
375,8	0,26662	0,280625	0,282755	0,307245
380,8	0,266415	0,279845	0,283075	0,30745
385,8	0,26631	0,279405	0,283355	0,307495
390,8	0,266235	0,27919	0,283685	0,3075
395,8	0,26613	0,27911	0,284075	0,307475
400,8	0,26602	0,27921	0,284525	0,30742
405,8	0,26594	0,279415	0,285	0,30737
410,8	0,26588	0,279465	0,285445	0,30736
415,8	0,265815	0,27928	0,285825	0,307435
420,8	0,265735	0,279035	0,286105	0,307495
425,9	0,26566	0,27884	0,286215	0,30756
430,9	0,26563	0,278635	0,286165	0,307635
435,9	0,265605	0,2783	0,28614	0,30776
440,9	0,265535	0,277875	0,28632	0,30783
445,9	0,26539	0,277515	0,28668	0,307945
450,9	0,265175	0,277285	0,287055	0,308

455,9	0,26494	0,27716	0,287305	0,3081
460,9	0,264765	0,277065	0,28743	0,308095
465,9	0,26465	0,276965	0,28752	0,30813
470,9	0,264555	0,2769	0,28764	0,308115
476	0,26446	0,27697	0,28778	0,30809
481	0,264355	0,277245	0,287905	0,308065
486	0,26426	0,277665	0,28801	0,308
491	0,264165	0,27813	0,28811	0,307935
496	0,264055	0,278605	0,288205	0,30786
501	0,263955	0,279045	0,288245	0,307815
506	0,26388	0,279355	0,28821	0,3077
511	0,26385	0,27946	0,28816	0,30756
516	0,263835	0,279345	0,28813	0,30747
521	0,263845	0,27899	0,28817	0,30736
526	0,263855	0,278445	0,28826	0,30734
531,1	0,26384	0,27789	0,288365	0,307345
536,1	0,263815	0,27755	0,288455	0,30731
541,1	0,263795	0,277475	0,28851	0,30727
546,1	0,26376	0,27748	0,28855	0,30723
551,1	0,263665	0,277365	0,28859	0,30719
556,1	0,263505	0,27707	0,288605	0,30715
561,1	0,263315	0,27673	0,28856	0,307165
566,1	0,26307	0,27648	0,28845	0,30713
571,1	0,26275	0,276345	0,288335	0,307085
576,2	0,262395	0,276305	0,28823	0,307035
581,2	0,26211	0,276295	0,28806	0,306975
586,2	0,26198	0,276275	0,28773	0,306855
591,2	0,26202	0,276235	0,287245	0,306785
596,2	0,262175	0,276205	0,28676	0,30672
601,2	0,262355	0,2762	0,286395	0,306655
606,2	0,2598	0,27402	0,284945	0,30495
611,2	0,245055	0,261105	0,27575	0,29384
616,2	0,209285	0,228059	0,247655	0,26175
621,2	0,15919	0,179411	0,1993665	0,208905
626,3	0,113925	0,133395	0,14746	0,153675
631,3	0,08645	0,10411	0,11065	0,11499
636,3	0,07585	0,092	0,0936	0,09675
641,3	0,07495	0,0902	0,08985	0,09205
646,3	0,07735	0,0922	0,09175	0,0929
651,3	0,08	0,09465	0,09465	0,09505
656,3	0,08195	0,0965	0,097	0,09685
661,3	0,0833	0,0978	0,0986	0,09815
666,3	0,08435	0,0988	0,09985	0,09905
671,3	0,0852	0,09955	0,10085	0,0998
676,3	0,086	0,1003	0,1017	0,10045
681,4	0,08665	0,10085	0,1024	0,10105

686,4	0,0872	0,1014	0,103	0,1015
691,4	0,08775	0,1019	0,1036	0,1019
696,4	0,08825	0,10225	0,10405	0,1022
701,4	0,0887	0,1026	0,10446	0,1025
706,4	0,08905	0,10285	0,104845	0,1028
711,4	0,0894	0,1031	0,10506	0,10315
716,4	0,08975	0,10335	0,10527	0,10345
721,4	0,09005	0,10355	0,1055	0,10365
726,5	0,09025	0,10375	0,10575	0,10385
731,5	0,09045	0,10395	0,10605	0,104
736,5	0,0906	0,104155	0,10626	0,1043
741,5	0,0907	0,104345	0,106425	0,10455
746,5	0,0909	0,104475	0,1067	0,10475
751,5	0,09115	0,104645	0,10699	0,1049
756,5	0,0914	0,104755	0,107295	0,105
761,5	0,0916	0,104865	0,107435	0,105
766,5	0,09175	0,105025	0,107595	0,10515
771,5	0,0919	0,105135	0,10777	0,10525
776,5	0,09205	0,105295	0,107995	0,1053
781,6	0,09225	0,1054	0,10814	0,10535
786,6	0,0924	0,105505	0,108255	0,1055
791,6	0,0926	0,10561	0,108265	0,1056
796,6	0,09275	0,105715	0,108315	0,10565
801,6	0,0929	0,105815	0,10829	0,10575
806,6	0,09305	0,105905	0,108265	0,1058
811,6	0,0932	0,10594	0,108085	0,10586
816,6	0,0933	0,10602	0,10794	0,105825
821,6	0,0934	0,106045	0,107855	0,105755
826,7	0,0934	0,106125	0,107985	0,105805
831,7	0,09325	0,1062	0,10828	0,10579
836,7	0,0931	0,106225	0,108575	0,10561
841,7	0,09295	0,1063	0,1087	0,105405
846,7	0,093	0,106325	0,108605	0,105315
851,7	0,09325	0,106345	0,108415	0,10547
856,7	0,09345	0,106415	0,108345	0,10572
861,7	0,0936	0,10643	0,108445	0,10584
866,7	0,0937	0,106445	0,10848	0,10579
871,7	0,0937	0,106465	0,108525	0,10565
876,8	0,09375	0,10653	0,10854	0,10555
881,8	0,09375	0,106545	0,1084	0,1055
886,8	0,0937	0,10656	0,108125	0,10561
891,8	0,09375	0,106625	0,107875	0,10573
896,8	0,09385	0,10663	0,1079	0,10578
901,8	0,09385	0,10664	0,10826	0,10582
906,8	0,09385	0,106645	0,1087	0,105815
911,8	0,0939	0,106655	0,10898	0,1058

916,8	0,0939	0,10666	0,10907	0,10584
921,8	0,0939	0,10672	0,10911	0,105855
926,8	0,09385	0,106725	0,109165	0,105875
931,9	0,09365	0,10673	0,10942	0,105905
936,9	0,0935	0,106735	0,10965	0,105925
941,9	0,09345	0,106735	0,10985	0,105985
946,9	0,0935	0,10674	0,110005	0,10593
951,9	0,09365	0,10679	0,110095	0,105885
956,9	0,09375	0,106795	0,11017	0,10582
961,9	0,09385	0,106825	0,110015	0,105765
966,9	0,094	0,106895	0,109735	0,105675
971,9	0,0941	0,106995	0,10944	0,10558
977	0,0941	0,10708	0,10937	0,10527
982	0,09415	0,107175	0,109485	0,104875
987	0,0942	0,107175	0,109565	0,104475
992	0,0943	0,10715	0,109135	0,104325
997	0,0943	0,10716	0,108165	0,104385
1002	0,0943	0,107115	0,107185	0,1046
1007	0,0942	0,10707	0,106995	0,104765
1012	0,0942	0,107035	0,1075	0,1049
1017	0,0942	0,107	0,108265	0,1049
1022	0,0943	0,106975	0,1089	0,104925
1027	0,09435	0,106955	0,109295	0,10493
1032	0,09445	0,10694	0,10948	0,10498
1037	0,09455	0,106935	0,10952	0,10497
1042	0,09465	0,106935	0,10939	0,10495
1047	0,0947	0,106935	0,109275	0,10493
1052	0,09475	0,10693	0,10926	0,10491
1057	0,09485	0,106925	0,10933	0,104845
1062	0,09485	0,10692	0,10932	0,104735
1067	0,0948	0,106915	0,10926	0,104625
1072	0,09475	0,10691	0,10926	0,10447
1077	0,0948	0,106905	0,10921	0,10422
1082	0,0948	0,1069	0,109065	0,103965
1087	0,09485	0,106845	0,10903	0,10373
1092	0,09495	0,106835	0,109115	0,103455
1097	0,09495	0,106825	0,1093	0,10311
1102	0,09495	0,106815	0,10926	0,1027
1107	0,09495	0,106805	0,108865	0,10232
1112	0,0949	0,10679	0,108425	0,102035
1117	0,0949	0,10678	0,108235	0,10169
1122	0,09485	0,10677	0,108495	0,10139
1127	0,0948	0,10671	0,108945	0,10118
1132	0,0947	0,1067	0,10937	0,10116
1137	0,0943	0,106695	0,109565	0,10119
1142	0,09375	0,106685	0,10948	0,101375

1147	0,0933	0,106675	0,10927	0,101565
1152	0,09315	0,106665	0,10915	0,10181
1157	0,0933	0,106655	0,10921	0,102045
1162	0,09355	0,106595	0,10926	0,102225
1167	0,0938	0,106585	0,109245	0,10235
1172	0,09395	0,10658	0,109215	0,10237
1177	0,09405	0,10657	0,10923	0,10239
1182	0,09415	0,106565	0,109335	0,10247
1187	0,09425	0,106515	0,10941	0,10255
1192	0,0943	0,10651	0,10944	0,102635
1197	0,09425	0,10646	0,10946	0,10266
1202	0,0941	0,106455	0,10948	0,10266

Time	PdS-$Na_2S_2O_3$-1SPW	PdS-$Na_2S_2O_3$-3SPW	PdS-$Na_2S_2O_3$-5SPW	PdS-$Na_2S_2O_3$-10SPW
	AVE/SHE	AVE/SHE	AVE/SHE	AVE/SHE
5,01	0,27105	0,269285	0,26404	0,26912
10,02	0,271075	0,269305	0,264085	0,269145
15,03	0,271215	0,26941	0,264365	0,26932
20,04	0,27159	0,269705	0,2651	0,269835
25,05	0,27224	0,27021	0,266295	0,2708
30,06	0,273085	0,27092	0,267735	0,27207
35,07	0,27403	0,271775	0,269155	0,27338
40,08	0,27499	0,27268	0,27042	0,274565
45,09	0,27594	0,273535	0,271505	0,275625
50,1	0,27684	0,274295	0,27246	0,276585
55,11	0,27766	0,274945	0,27332	0,277455
60,12	0,278375	0,27548	0,274095	0,27822
65,13	0,278995	0,275895	0,274785	0,27886
70,14	0,279505	0,27625	0,27541	0,279395
75,15	0,279905	0,27656	0,27599	0,279905
80,16	0,2802	0,276835	0,27655	0,280415
85,17	0,280435	0,27707	0,27708	0,28094
90,18	0,28064	0,27726	0,277575	0,281455
95,19	0,28084	0,27743	0,278025	0,28194
100,2	0,281045	0,277565	0,278405	0,282365
105,2	0,28124	0,277655	0,278675	0,28276
110,2	0,281435	0,27769	0,278815	0,283135
115,2	0,28164	0,27772	0,278865	0,283485
120,2	0,281875	0,27778	0,27887	0,28378
125,3	0,282115	0,27789	0,278915	0,283975
130,3	0,282345	0,278035	0,279055	0,28405
135,3	0,282535	0,278165	0,2793	0,284065
140,3	0,2827	0,27825	0,27959	0,284135
145,3	0,28285	0,278315	0,27982	0,284305
150,3	0,282975	0,278395	0,279935	0,28449
155,3	0,28304	0,278525	0,27997	0,284625
160,3	0,28307	0,278665	0,28	0,284715
165,3	0,2831	0,27878	0,280085	0,284725
170,3	0,283125	0,278875	0,28023	0,28462
175,4	0,283135	0,279005	0,280425	0,28454
180,4	0,28311	0,279205	0,280645	0,284705
185,4	0,28305	0,279435	0,28087	0,28512
190,4	0,28298	0,279605	0,28108	0,285625
195,4	0,282935	0,279685	0,281255	0,286
200,4	0,28294	0,27972	0,2814	0,286125
205,4	0,28299	0,279745	0,28152	0,286035
210,4	0,28305	0,27977	0,28164	0,28592
215,4	0,28312	0,279795	0,281765	0,28594
220,4	0,28321	0,27981	0,28187	0,286075

225,4	0,283335	0,27983	0,281965	0,286245
230,5	0,28351	0,27988	0,28204	0,286395
235,5	0,28372	0,27999	0,282105	0,28655
240,5	0,28393	0,280125	0,28214	0,286715
245,5	0,284085	0,28025	0,28219	0,286875
250,5	0,28418	0,280305	0,28227	0,287015
255,5	0,28426	0,280285	0,282365	0,287095
260,5	0,284335	0,280205	0,282435	0,28714
265,5	0,284425	0,280095	0,28248	0,287195
270,5	0,284525	0,280005	0,282535	0,28731
275,5	0,28463	0,279945	0,2826	0,287455
280,6	0,28471	0,279875	0,28266	0,28754
285,6	0,28476	0,279795	0,28271	0,287525
290,6	0,284775	0,27971	0,28276	0,28742
295,6	0,28478	0,27967	0,28279	0,287315
300,6	0,28481	0,279625	0,28282	0,28735
305,6	0,28311	0,277875	0,28163	0,28494
310,6	0,273675	0,26855	0,27448	0,271545
315,6	0,251535	0,24583	0,25567	0,24097
320,6	0,22187	0,2129555	0,226265	0,2012365
325,6	0,1963215	0,1812	0,195215	0,167615
330,7	0,181505	0,15953	0,17127	0,14746
335,7	0,176145	0,14912	0,157155	0,138505
340,7	0,1759	0,146115	0,15073	0,13564
345,7	0,177325	0,146305	0,148715	0,135075
350,7	0,178735	0,14735	0,148705	0,135065
355,7	0,179715	0,14854	0,149385	0,13517
360,7	0,180365	0,14977	0,150185	0,13542
365,7	0,18087	0,1509	0,15089	0,135755
370,7	0,18132	0,151755	0,15146	0,135965
375,8	0,181715	0,1523	0,15191	0,135905
380,8	0,182035	0,152625	0,152285	0,13567
385,8	0,182255	0,15284	0,152625	0,135405
390,8	0,182375	0,15303	0,15297	0,13516
395,8	0,18245	0,153225	0,153305	0,134885
400,8	0,182525	0,15346	0,153545	0,134485
405,8	0,182595	0,15375	0,15363	0,133895
410,8	0,18266	0,154065	0,153505	0,13322
415,8	0,18272	0,154375	0,153215	0,132595
420,8	0,18278	0,154675	0,15292	0,132065
425,9	0,182875	0,15495	0,15273	0,131615
430,9	0,182985	0,1552	0,15266	0,131245
435,9	0,183105	0,15542	0,15272	0,13093
440,9	0,183195	0,15568	0,15294	0,1306
445,9	0,18314	0,156095	0,15328	0,13023
450,9	0,182875	0,156645	0,15357	0,129935

455,9	0,182465	0,15717	0,153695	0,12983
460,9	0,18205	0,157475	0,15373	0,129915
465,9	0,181765	0,157455	0,15382	0,13004
470,9	0,181645	0,157215	0,15392	0,130025
476	0,18166	0,15693	0,153875	0,12979
481	0,18173	0,15665	0,15364	0,12944
486	0,18185	0,156315	0,15337	0,12916
491	0,181985	0,155835	0,15321	0,12907
496	0,18208	0,155135	0,15314	0,129095
501	0,18208	0,15424	0,153045	0,12907
506	0,182005	0,15328	0,152845	0,12886
511	0,18191	0,152425	0,152495	0,128475
516	0,18178	0,151735	0,15207	0,128085
521	0,181605	0,151255	0,151605	0,127845
526	0,18141	0,15102	0,151195	0,12778
531,1	0,18124	0,151035	0,15093	0,12776
536,1	0,18108	0,15126	0,15085	0,12764
541,1	0,18092	0,151645	0,150915	0,12738
546,1	0,180755	0,152165	0,151025	0,12709
551,1	0,18062	0,15275	0,151045	0,12691
556,1	0,18054	0,15329	0,15094	0,12681
561,1	0,18056	0,153595	0,150825	0,12668
566,1	0,18063	0,153545	0,150825	0,12653
571,1	0,180665	0,15311	0,15095	0,126465
576,2	0,180635	0,15244	0,151115	0,12648
581,2	0,18065	0,15175	0,151225	0,126455
586,2	0,180745	0,151265	0,15128	0,12631
591,2	0,18084	0,15098	0,15126	0,12603
596,2	0,18079	0,1508	0,151145	0,125645
601,2	0,182115	0,150645	0,150905	0,125275
606,2	0,179125	0,149205	0,14956	0,12414
611,2	0,16727	0,14205	0,143645	0,11896
616,2	0,14302	0,125695	0,12974	0,10704
621,2	0,113775	0,104295	0,110155	0,0913
626,3	0,09135	0,08655	0,09215	0,07815
631,3	0,0804	0,0768	0,08095	0,0708
636,3	0,07785	0,0736	0,07645	0,0683
641,3	0,08025	0,0736	0,0757	0,06825
646,3	0,08155	0,07445	0,0763	0,0689
651,3	0,08255	0,07505	0,07685	0,06955
656,3	0,0832	0,07545	0,0771	0,0699
661,3	0,0836	0,0755	0,0771	0,07
666,3	0,0845	0,0755	0,077	0,07
671,3	0,0849	0,07545	0,07695	0,06995
676,3	0,0853	0,07555	0,0767	0,0698
681,4	0,0856	0,0757	0,0764	0,06965

686,4	0,08585	0,0759	0,0762	0,0692
691,4	0,0862	0,07605	0,076	0,0686
696,4	0,08645	0,07605	0,0758	0,0678
701,4	0,08665	0,07605	0,07555	0,06715
706,4	0,08685	0,0759	0,07535	0,06685
711,4	0,087	0,0758	0,07535	0,06685
716,4	0,0872	0,07575	0,0755	0,06695
721,4	0,0873	0,0757	0,07565	0,06695
726,5	0,08735	0,07565	0,0756	0,06655
731,5	0,08745	0,0758	0,07535	0,06595
736,5	0,08755	0,0761	0,075	0,0652
741,5	0,08775	0,07655	0,07465	0,06465
746,5	0,08795	0,0769	0,0743	0,06445
751,5	0,088	0,0771	0,07395	0,0645
756,5	0,08795	0,07705	0,07365	0,06465
761,5	0,0878	0,0769	0,0735	0,06465
766,5	0,08765	0,07665	0,0734	0,0645
771,5	0,08765	0,07635	0,07315	0,06435
776,5	0,0877	0,07615	0,07285	0,06415
781,6	0,08785	0,0761	0,0726	0,06405
786,6	0,08795	0,0761	0,0725	0,0639
791,6	0,0881	0,0761	0,07235	0,0637
796,6	0,08815	0,0761	0,0723	0,0635
801,6	0,0882	0,07605	0,0722	0,0633
806,6	0,08815	0,0759	0,07215	0,063
811,6	0,08805	0,07585	0,07205	0,06255
816,6	0,08795	0,07575	0,0719	0,0619
821,6	0,0878	0,0757	0,0718	0,0609
826,7	0,0877	0,0757	0,0717	0,05985
831,7	0,0876	0,0757	0,0716	0,05915
836,7	0,0876	0,07575	0,0714	0,05885
841,7	0,08765	0,07575	0,07115	0,05865
846,7	0,0877	0,07575	0,0708	0,05835
851,7	0,0877	0,07575	0,0704	0,0579
856,7	0,0876	0,07565	0,06995	0,0574
861,7	0,0874	0,07545	0,06945	0,05705
866,7	0,08735	0,0752	0,06885	0,05675
871,7	0,08725	0,075	0,06825	0,0564
876,8	0,0871	0,07495	0,0676	0,05605
881,8	0,0869	0,07505	0,06705	0,0557
886,8	0,08655	0,07515	0,0663	0,05545
891,8	0,0863	0,07515	0,0656	0,0553
896,8	0,0862	0,0751	0,06505	0,0553
901,8	0,0862	0,075	0,06485	0,05525
906,8	0,0863	0,07475	0,0648	0,0551
911,8	0,0864	0,0746	0,06465	0,0549

916,8	0,0865	0,07435	0,0644	0,0546
921,8	0,0865	0,07405	0,06415	0,05425
926,8	0,0864	0,07365	0,0641	0,0537
931,9	0,086	0,0732	0,0642	0,0531
936,9	0,08555	0,07285	0,0642	0,0525
941,9	0,0851	0,07225	0,06405	0,05205
946,9	0,08495	0,07125	0,06345	0,05175
951,9	0,08495	0,07015	0,0626	0,0516
956,9	0,08515	0,06945	0,0614	0,05155
961,9	0,08545	0,06925	0,0604	0,05165
966,9	0,0859	0,06935	0,05985	0,05175
971,9	0,08625	0,0696	0,0601	0,0519
977	0,0865	0,0698	0,0609	0,05195
982	0,0867	0,06995	0,0618	0,0518
987	0,0869	0,06985	0,06255	0,0515
992	0,0871	0,0697	0,0632	0,051
997	0,0873	0,06955	0,0639	0,0505
1002	0,0874	0,06955	0,0647	0,05035
1007	0,08745	0,0696	0,06535	0,05055
1012	0,0875	0,0695	0,06595	0,0509
1017	0,08755	0,06935	0,0664	0,0513
1022	0,08745	0,0691	0,0667	0,0515
1027	0,0871	0,06895	0,0669	0,05165
1032	0,08645	0,06875	0,06705	0,05165
1037	0,0858	0,0684	0,0672	0,0516
1042	0,0853	0,06825	0,06725	0,05155
1047	0,085	0,06815	0,06745	0,05145
1052	0,08505	0,0681	0,0676	0,0514
1057	0,0852	0,06805	0,0676	0,0513
1062	0,0854	0,0676	0,06745	0,0513
1067	0,0856	0,06665	0,06715	0,0512
1072	0,0856	0,0654	0,06685	0,05115
1077	0,0856	0,0642	0,0666	0,0511
1082	0,08565	0,0634	0,0664	0,0511
1087	0,08575	0,06305	0,0661	0,05115
1092	0,08595	0,06305	0,0658	0,0512
1097	0,0861	0,0634	0,06555	0,05125
1102	0,08615	0,0639	0,0653	0,0512
1107	0,08615	0,0644	0,06525	0,05115
1112	0,08605	0,0648	0,0653	0,05105
1117	0,08595	0,0651	0,06545	0,051
1122	0,08585	0,0654	0,0655	0,05085
1127	0,08585	0,0657	0,06555	0,05085
1132	0,0859	0,066	0,06545	0,05095
1137	0,08595	0,0662	0,06535	0,051
1142	0,0859	0,06645	0,0653	0,0511

1147	0,08595	0,06665	0,0653	0,05115
1152	0,086	0,06705	0,0654	0,0512
1157	0,08605	0,06765	0,0656	0,05125
1162	0,08615	0,0684	0,0658	0,05125
1167	0,08635	0,06915	0,0659	0,0513
1172	0,0868	0,0698	0,0658	0,0512
1177	0,0872	0,07015	0,0656	0,0507
1182	0,08745	0,07035	0,0654	0,05
1187	0,08745	0,0706	0,0652	0,04945
1192	0,087	0,0709	0,0652	0,0493
1197	0,08635	0,0711	0,06535	0,04945
1202	0,0857	0,07125	0,0655	0,0498

Time	PdS-$CaCl_2$-1SPW	PdS-$CaCl_2$-3SPW	PdS-$CaCl_2$-5SPW	PdS-$CaCl_2$-10SPW
	AVE/SHE	AVE/SHE	AVE/SHE	AVE/SHE
5,01	0,245845	0,248315	0,254405	0,261385
10,02	0,24583	0,2483	0,254415	0,261395
15,03	0,245755	0,248265	0,254495	0,26145
20,04	0,245595	0,248205	0,254705	0,26156
25,05	0,24542	0,24817	0,255065	0,261685
30,06	0,2453	0,248205	0,25549	0,261785
35,07	0,245275	0,2483	0,255895	0,26189
40,08	0,24533	0,24844	0,25627	0,26203
45,09	0,24544	0,24858	0,256595	0,26219
50,1	0,245575	0,24868	0,25684	0,262365
55,11	0,24571	0,24875	0,257	0,26255
60,12	0,24582	0,248795	0,257105	0,262705
65,13	0,245895	0,248825	0,25719	0,26281
70,14	0,245955	0,24887	0,25722	0,26289
75,15	0,24601	0,248935	0,257165	0,262995
80,16	0,245985	0,24905	0,257095	0,26315
85,17	0,24586	0,249215	0,257135	0,263315
90,18	0,245745	0,24938	0,257325	0,263475
95,19	0,245775	0,249515	0,257585	0,26364
100,2	0,245935	0,24962	0,25784	0,2638
105,2	0,24609	0,249705	0,258055	0,2639
110,2	0,246195	0,249785	0,258225	0,263905
115,2	0,24631	0,249865	0,258355	0,26396
120,2	0,246465	0,249945	0,25842	0,26418
125,3	0,24661	0,250035	0,25838	0,26453
130,3	0,24674	0,25013	0,258235	0,264895
135,3	0,24686	0,250185	0,25805	0,265215
140,3	0,24699	0,25019	0,25795	0,265435
145,3	0,24708	0,25014	0,25799	0,26555
150,3	0,24714	0,250095	0,258125	0,265615
155,3	0,24719	0,250075	0,25828	0,26572
160,3	0,24723	0,250065	0,258415	0,265905
165,3	0,247275	0,25004	0,258545	0,26614
170,3	0,247325	0,25001	0,25866	0,26634
175,4	0,24735	0,24999	0,25872	0,266485
180,4	0,24733	0,250005	0,258705	0,266595
185,4	0,247295	0,250025	0,258645	0,2667
190,4	0,247295	0,25002	0,258675	0,266785
195,4	0,247325	0,249985	0,258855	0,266855
200,4	0,24734	0,24993	0,25911	0,26694
205,4	0,247335	0,24986	0,2593	0,267015
210,4	0,24737	0,249825	0,259335	0,26707
215,4	0,247475	0,249865	0,25926	0,267095
220,4	0,247595	0,249995	0,259155	0,26713

225,4	0,247675	0,250175	0,25908	0,26722
230,5	0,24773	0,250345	0,25908	0,267395
235,5	0,247785	0,250465	0,259175	0,26762
240,5	0,24782	0,2505	0,259395	0,267855
245,5	0,247815	0,25046	0,259665	0,26804
250,5	0,24779	0,2504	0,259915	0,26814
255,5	0,24778	0,25031	0,26013	0,26817
260,5	0,247805	0,250215	0,26031	0,26819
265,5	0,247875	0,2502	0,260415	0,26822
270,5	0,247975	0,25028	0,26039	0,26828
275,5	0,24806	0,250365	0,260235	0,26835
280,6	0,248075	0,2504	0,26008	0,26842
285,6	0,24801	0,25038	0,260185	0,268485
290,6	0,24792	0,25036	0,26067	0,26854
295,6	0,247865	0,25037	0,26137	0,26853
300,6	0,24788	0,250415	0,261995	0,26837
305,6	0,24795	0,25044	0,26237	0,268085
310,6	0,247635	0,249575	0,26109	0,26701
315,6	0,245015	0,244565	0,253315	0,26176
320,6	0,237255	0,23136	0,23415	0,247625
325,6	0,22399	0,210323	0,2058975	0,2244645
330,7	0,208767	0,187365	0,17741	0,1985135
335,7	0,195965	0,168895	0,1562	0,176965
340,7	0,187555	0,157375	0,14406	0,16294
345,7	0,18297	0,151595	0,138665	0,15559
350,7	0,18064	0,14914	0,136765	0,152715
355,7	0,17931	0,14817	0,13603	0,15236
360,7	0,17841	0,14768	0,135375	0,1531
365,7	0,177685	0,14716	0,134685	0,154025
370,7	0,17686	0,14648	0,13418	0,154405
375,8	0,17586	0,145755	0,133915	0,15362
380,8	0,174915	0,14516	0,133765	0,1518
385,8	0,17421	0,14476	0,13362	0,14976
390,8	0,17362	0,144515	0,13345	0,148145
395,8	0,17306	0,14431	0,133215	0,147095
400,8	0,172655	0,14413	0,132895	0,14655
405,8	0,172435	0,143965	0,132565	0,146415
410,8	0,172175	0,143785	0,132295	0,14665
415,8	0,171815	0,143525	0,132105	0,14709
420,8	0,17152	0,14319	0,13193	0,147375
425,9	0,1713	0,142925	0,13174	0,14737
430,9	0,171035	0,142815	0,13156	0,14727
435,9	0,170735	0,142735	0,13141	0,147275
440,9	0,17042	0,142555	0,131295	0,14731
445,9	0,17008	0,142315	0,1312	0,147275
450,9	0,16974	0,142105	0,131075	0,14716

455,9	0,169425	0,141975	0,130895	0,147095
460,9	0,169075	0,14187	0,13068	0,147075
465,9	0,168755	0,141795	0,1305	0,14694
470,9	0,168605	0,1418	0,1304	0,1466
476	0,168555	0,141855	0,13036	0,146
481	0,168325	0,141855	0,13033	0,145055
486	0,167845	0,141755	0,13027	0,143905
491	0,16735	0,141615	0,13017	0,142945
496	0,16709	0,14152	0,13013	0,14243
501	0,167065	0,1415	0,1302	0,14223
506	0,167075	0,141485	0,130285	0,14208
511	0,166905	0,1414	0,13027	0,141785
516	0,16652	0,141245	0,130155	0,141335
521	0,16608	0,14109	0,13009	0,14086
526	0,16577	0,14101	0,13016	0,140515
531,1	0,165585	0,14103	0,130275	0,14035
536,1	0,165335	0,14107	0,130315	0,140315
541,1	0,164935	0,14099	0,130305	0,140285
546,1	0,1646	0,140815	0,130315	0,140245
551,1	0,164485	0,14067	0,130355	0,140255
556,1	0,164485	0,14063	0,130365	0,14027
561,1	0,16451	0,140655	0,130345	0,140185
566,1	0,164605	0,140705	0,13032	0,13994
571,1	0,16469	0,140735	0,130245	0,139625
576,2	0,164635	0,14072	0,130085	0,13936
581,2	0,164325	0,140695	0,12991	0,139145
586,2	0,16375	0,14068	0,129795	0,13896
591,2	0,16312	0,140645	0,12975	0,13884
596,2	0,162775	0,140545	0,12973	0,13884
601,2	0,162785	0,140375	0,129725	0,13896
606,2	0,162795	0,14019	0,12876	0,13892
611,2	0,15998	0,139035	0,12307	0,136325
616,2	0,147355	0,13373	0,109005	0,12569
621,2	0,12135	0,121805	0,090245	0,10495
626,3	0,09065	0,10514	0,07645	0,0817
631,3	0,06815	0,08861	0,0727	0,0661
636,3	0,05835	0,07655	0,0763	0,061
641,3	0,05745	0,07155	0,0822	0,0627
646,3	0,0602	0,07255	0,08705	0,06655
651,3	0,0634	0,07665	0,0903	0,07015
656,3	0,066	0,0811	0,0922	0,0728
661,3	0,06785	0,08475	0,0935	0,0747
666,3	0,06915	0,08735	0,09445	0,07605
671,3	0,0702	0,0892	0,09535	0,0771
676,3	0,071	0,0906	0,0961	0,07785
681,4	0,07165	0,09174	0,09675	0,0785

686,4	0,07225	0,092685	0,09735	0,07915
691,4	0,0728	0,093575	0,09785	0,0797
696,4	0,07325	0,094345	0,09835	0,08015
701,4	0,0735	0,095015	0,0987	0,08055
706,4	0,07365	0,09559	0,09915	0,0809
711,4	0,07385	0,096135	0,09945	0,0812
716,4	0,0742	0,096595	0,09975	0,0815
721,4	0,07475	0,09706	0,10005	0,08175
726,5	0,07545	0,097495	0,10025	0,08205
731,5	0,076	0,097855	0,10049	0,08225
736,5	0,07635	0,09826	0,10067	0,0824
741,5	0,0764	0,098615	0,100845	0,0825
746,5	0,0764	0,09896	0,101005	0,0825
751,5	0,07645	0,099245	0,101155	0,08255
756,5	0,0767	0,09947	0,101295	0,0826
761,5	0,07705	0,099725	0,10138	0,08275
766,5	0,07745	0,10002	0,10151	0,0828
771,5	0,0777	0,100255	0,101635	0,0829
776,5	0,07775	0,10048	0,101755	0,0829
781,6	0,07775	0,1007	0,10192	0,083
786,6	0,0777	0,100915	0,102075	0,083
791,6	0,0778	0,10113	0,10218	0,0831
796,6	0,0779	0,101295	0,10233	0,0832
801,6	0,07805	0,101505	0,102425	0,0833
806,6	0,07815	0,101665	0,102515	0,0833
811,6	0,07825	0,10182	0,102605	0,08335
816,6	0,07835	0,102015	0,102695	0,08345
821,6	0,0785	0,102205	0,10278	0,08355
826,7	0,0787	0,102335	0,102815	0,0836
831,7	0,0789	0,102515	0,102845	0,08365
836,7	0,07915	0,102645	0,10287	0,0837
841,7	0,0793	0,10283	0,10294	0,08375
846,7	0,0795	0,102965	0,10291	0,0838
851,7	0,07965	0,103035	0,102885	0,0838
856,7	0,07985	0,103155	0,102855	0,08385
861,7	0,08015	0,10328	0,102775	0,0839
866,7	0,0805	0,10342	0,10269	0,0839
871,7	0,08085	0,103515	0,102605	0,08385
876,8	0,0812	0,103665	0,102515	0,0838
881,8	0,0815	0,10381	0,102475	0,0837
886,8	0,08175	0,103955	0,102435	0,0837
891,8	0,082	0,10405	0,10235	0,0837
896,8	0,08215	0,10414	0,102315	0,08365
901,8	0,08225	0,104275	0,10228	0,08365
906,8	0,08235	0,1044	0,10219	0,08365
911,8	0,0824	0,10452	0,1021	0,08365

916,8	0,08255	0,10468	0,102005	0,0836
921,8	0,08265	0,104795	0,10191	0,08365
926,8	0,08275	0,10491	0,101865	0,0836
931,9	0,08285	0,10508	0,10182	0,08365
936,9	0,0829	0,105205	0,101775	0,08365
941,9	0,08285	0,105375	0,101775	0,0836
946,9	0,08275	0,105495	0,101825	0,0836
951,9	0,0826	0,105655	0,101925	0,08365
956,9	0,0826	0,105765	0,10208	0,0836
961,9	0,0827	0,10588	0,102235	0,0836
966,9	0,08285	0,105995	0,10239	0,0836
971,9	0,08305	0,106115	0,102495	0,0836
977	0,08315	0,10628	0,102555	0,0836
982	0,0833	0,106395	0,10256	0,08365
987	0,0833	0,106505	0,102565	0,08375
992	0,0833	0,106615	0,102515	0,0839
997	0,0832	0,106725	0,102465	0,08395
1002	0,083	0,106835	0,102415	0,084
1007	0,08285	0,10695	0,10242	0,08405
1012	0,0827	0,10706	0,10242	0,0841
1017	0,0826	0,107115	0,10242	0,08405
1022	0,0826	0,107215	0,10242	0,08395
1027	0,0826	0,107255	0,102465	0,0839
1032	0,08275	0,107295	0,102405	0,0839
1037	0,08285	0,1074	0,102345	0,0838
1042	0,0829	0,10746	0,10229	0,0837
1047	0,0829	0,107525	0,102235	0,0837
1052	0,0828	0,107585	0,10218	0,0836
1057	0,08275	0,107635	0,10218	0,08355
1062	0,08275	0,10768	0,10218	0,0836
1067	0,08285	0,10768	0,102175	0,08355
1072	0,083	0,107735	0,102175	0,0835
1077	0,08305	0,10778	0,102125	0,0835
1082	0,08305	0,107815	0,102125	0,0835
1087	0,083	0,10779	0,102125	0,0835
1092	0,083	0,107825	0,102075	0,0835
1097	0,08295	0,107815	0,102075	0,08345
1102	0,08285	0,10786	0,10202	0,08345
1107	0,0826	0,10791	0,102015	0,0834
1112	0,0824	0,107915	0,10201	0,0833
1117	0,08225	0,107975	0,102	0,0833
1122	0,0821	0,10799	0,10205	0,08325
1127	0,08205	0,108055	0,101995	0,08325
1132	0,082	0,10818	0,101945	0,08325
1137	0,082	0,10825	0,10184	0,08325
1142	0,0819	0,108315	0,10179	0,08325

1147	0,0817	0,108425	0,101685	0,08325
1152	0,0814	0,108485	0,101635	0,08325
1157	0,08105	0,108535	0,101585	0,0832
1162	0,0807	0,10859	0,10153	0,08315
1167	0,0803	0,108645	0,10153	0,08315
1172	0,07985	0,108705	0,101525	0,0831
1177	0,0794	0,108765	0,10157	0,0831
1182	0,07905	0,108875	0,101615	0,08305
1187	0,0787	0,10893	0,10161	0,08305
1192	0,07815	0,10899	0,101655	0,0831
1197	0,0775	0,109055	0,10165	0,0831
1202	0,0768	0,109055	0,101595	0,08315

Time	PdS-$MgCl_2$-1SPW	PdS-$MgCl_2$-3SPW	PdS-$MgCl_2$-5SPW	PdS-$MgCl_2$-10SPW
	AVE/SHE	AVE/SHE	AVE/SHE	AVE/SHE
5,01	0,26227	0,267385	0,260215	0,255665
10,02	0,262295	0,26741	0,260215	0,25569
15,03	0,262435	0,267545	0,260215	0,255865
20,04	0,262835	0,26792	0,260215	0,256355
25,05	0,26351	0,268545	0,26021	0,257205
30,06	0,26436	0,26932	0,26023	0,258285
35,07	0,26527	0,270125	0,26026	0,25941
40,08	0,266155	0,27092	0,260275	0,260455
45,09	0,26692	0,27171	0,260245	0,261365
50,1	0,26752	0,272465	0,260175	0,26213
55,11	0,26797	0,27317	0,2601	0,26278
60,12	0,26833	0,273785	0,26004	0,26337
65,13	0,26863	0,274325	0,26002	0,263975
70,14	0,26888	0,274825	0,26004	0,26468
75,15	0,269105	0,27531	0,26012	0,265505
80,16	0,269355	0,275785	0,260245	0,266325
85,17	0,26971	0,27624	0,260405	0,266985
90,18	0,2702	0,27667	0,26056	0,267425
95,19	0,27079	0,27707	0,26068	0,26772
100,2	0,27138	0,27743	0,26075	0,26797
105,2	0,27184	0,27776	0,260765	0,26825
110,2	0,27217	0,278045	0,26073	0,268585
115,2	0,272545	0,278295	0,260685	0,26895
120,2	0,27308	0,278505	0,26066	0,269245
125,3	0,273705	0,27868	0,26065	0,26945
130,3	0,274275	0,278855	0,26065	0,26961
135,3	0,274745	0,27905	0,26065	0,269785
140,3	0,27512	0,279265	0,260655	0,270015
145,3	0,275435	0,279445	0,260665	0,270315
150,3	0,275695	0,27961	0,260715	0,270665
155,3	0,275895	0,279795	0,260805	0,271005
160,3	0,27606	0,280015	0,26091	0,2713
165,3	0,27622	0,28024	0,26101	0,27153
170,3	0,27638	0,280455	0,261085	0,271705
175,4	0,276555	0,280645	0,261145	0,27186
180,4	0,276715	0,28078	0,261195	0,27199
185,4	0,276745	0,28087	0,261255	0,27212
190,4	0,27659	0,280965	0,261345	0,27225
195,4	0,27645	0,2811	0,261445	0,272365
200,4	0,27658	0,28125	0,26157	0,272445
205,4	0,276955	0,28137	0,26171	0,272485
210,4	0,277345	0,281445	0,26186	0,272485
215,4	0,277615	0,281525	0,261985	0,272455
220,4	0,277775	0,28162	0,26208	0,27241

225,4	0,27791	0,28173	0,262135	0,272395
230,5	0,278065	0,28182	0,262165	0,272405
235,5	0,2782	0,28186	0,26218	0,272415
240,5	0,27829	0,281885	0,262195	0,27242
245,5	0,27839	0,28198	0,26223	0,27242
250,5	0,278565	0,28216	0,26228	0,272415
255,5	0,278845	0,282355	0,262285	0,27239
260,5	0,279205	0,282495	0,26221	0,272355
265,5	0,27957	0,28257	0,262075	0,27232
270,5	0,2799	0,282595	0,26198	0,27235
275,5	0,28018	0,28259	0,261995	0,272435
280,6	0,280405	0,28257	0,262105	0,27255
285,6	0,280605	0,28254	0,26224	0,272665
290,6	0,28077	0,282535	0,26232	0,272735
295,6	0,28088	0,28253	0,262315	0,272775
300,6	0,28094	0,28243	0,262255	0,27276
305,6	0,281	0,28218	0,26227	0,272875
310,6	0,28119	0,28187	0,262425	0,273505
315,6	0,281305	0,281695	0,26234	0,27438
320,6	0,28073	0,281605	0,26124	0,27386
325,6	0,27917	0,281265	0,25876	0,27036
330,7	0,277085	0,280375	0,255395	0,264045
335,7	0,27522	0,27905	0,25188	0,25649
340,7	0,27393	0,27763	0,248705	0,249495
345,7	0,273215	0,27645	0,24606	0,244255
350,7	0,2729	0,275555	0,244005	0,240915
355,7	0,272815	0,274815	0,242495	0,23887
360,7	0,2728	0,274125	0,241405	0,237435
365,7	0,272805	0,27356	0,24058	0,23635
370,7	0,27286	0,27325	0,239925	0,23553
375,8	0,272955	0,273305	0,2394	0,234855
380,8	0,27305	0,273645	0,23898	0,234165
385,8	0,273125	0,27407	0,23862	0,23343
390,8	0,273185	0,274425	0,23826	0,232695
395,8	0,27325	0,274675	0,237815	0,232045
400,8	0,2733	0,27479	0,23721	0,23152
405,8	0,273365	0,274745	0,23647	0,23113
410,8	0,273475	0,274605	0,235705	0,230783
415,8	0,27359	0,2745	0,23499	0,230389
420,8	0,273665	0,274505	0,234355	0,2299455
425,9	0,27369	0,274605	0,233795	0,229505
430,9	0,27367	0,274745	0,23331	0,2290795
435,9	0,27358	0,274885	0,23291	0,2287035
440,9	0,273405	0,27496	0,2326	0,228394
445,9	0,273175	0,274955	0,232315	0,2281225
450,9	0,272985	0,274965	0,232035	0,227845

455,9	0,27293	0,27511	0,231745	0,2275845
460,9	0,27302	0,27543	0,231435	0,227363
465,9	0,27321	0,27584	0,23113	0,2271735
470,9	0,27345	0,27625	0,230905	0,2269655
476	0,27369	0,27658	0,23079	0,226695
481	0,27391	0,27681	0,23072	0,2263705
486	0,27405	0,27696	0,23066	0,226032
491	0,274045	0,277065	0,23059	0,2256879
496	0,273885	0,27714	0,230485	0,2253299
501	0,273645	0,277195	0,23034	0,224961
506	0,27346	0,277255	0,23022	0,224594
511	0,27345	0,277325	0,230125	0,2241965
516	0,27356	0,277415	0,230045	0,2237205
521	0,273615	0,27756	0,22999	0,2231505
526	0,273485	0,27778	0,229995	0,222582
531,1	0,273155	0,278035	0,23005	0,2221485
536,1	0,272755	0,278285	0,230095	0,221826
541,1	0,272425	0,278445	0,2301	0,22151
546,1	0,27228	0,278505	0,230055	0,2211395
551,1	0,27229	0,2785	0,229965	0,2207175
556,1	0,27236	0,278505	0,229875	0,220265
561,1	0,27239	0,278555	0,229855	0,2198
566,1	0,27236	0,2786	0,22994	0,219335
571,1	0,272285	0,27861	0,230065	0,2189
576,2	0,2722	0,27859	0,230135	0,21856
581,2	0,272165	0,27854	0,23011	0,218445
586,2	0,272215	0,27847	0,229985	0,218565
591,2	0,272325	0,278425	0,22981	0,218695
596,2	0,272475	0,278445	0,22966	0,21858
601,2	0,272655	0,27848	0,2296	0,218225
606,2	0,27151	0,27714	0,2291985	0,217705
611,2	0,263045	0,26779	0,2243775	0,214435
616,2	0,23786305	0,240155	0,20581	0,200615
621,2	0,19414	0,194035	0,16999	0,171585
626,3	0,144285	0,145655	0,129425	0,136
631,3	0,104935	0,112225	0,100665	0,10788
636,3	0,08345	0,09745	0,0883	0,09265
641,3	0,07625	0,0949	0,0869	0,0872
646,3	0,0764	0,09725	0,0897	0,0864
651,3	0,07885	0,10025	0,09285	0,0869
656,3	0,08125	0,1026	0,0951	0,08735
661,3	0,08305	0,10429	0,09665	0,08755
666,3	0,08445	0,105515	0,09765	0,08755
671,3	0,08555	0,106545	0,0984	0,08755
676,3	0,08645	0,10744	0,09905	0,0876
681,4	0,0873	0,10818	0,0996	0,0876

686,4	0,08795	0,10887	0,1001	0,08765
691,4	0,08855	0,10942	0,1005	0,0877
696,4	0,0891	0,10988	0,1008	0,0878
701,4	0,08955	0,11029	0,10105	0,08785
706,4	0,09	0,110595	0,101265	0,08795
711,4	0,0905	0,11087	0,10143	0,0879
716,4	0,09085	0,11118	0,10153	0,08785
721,4	0,09115	0,111525	0,10167	0,08775
726,5	0,09125	0,11181	0,10175	0,0877
731,5	0,0913	0,112095	0,10187	0,0876
736,5	0,09135	0,112375	0,10193	0,08755
741,5	0,0915	0,1126	0,10203	0,08755
746,5	0,09175	0,11282	0,10213	0,08755
751,5	0,09205	0,112985	0,102235	0,087535
756,5	0,0923	0,11315	0,10234	0,087535
761,5	0,0926	0,113315	0,102385	0,087465
766,5	0,0929	0,113485	0,10242	0,08739
771,5	0,09315	0,113555	0,102445	0,087205
776,5	0,0934	0,11365	0,102465	0,087015
781,6	0,09365	0,113775	0,10253	0,086825
786,6	0,0939	0,11393	0,102645	0,086635
791,6	0,0941	0,11409	0,102805	0,08645
796,6	0,0943	0,114235	0,102915	0,086285
801,6	0,0945	0,114345	0,102965	0,08619
806,6	0,0947	0,114425	0,10306	0,08611
811,6	0,09495	0,11451	0,10311	0,086035
816,6	0,0951	0,11464	0,10312	0,085915
821,6	0,0953	0,114845	0,1032	0,085805
826,7	0,0955	0,115085	0,10329	0,085635
831,7	0,09565	0,11527	0,10338	0,085475
836,7	0,0958	0,115345	0,103505	0,085335
841,7	0,09585	0,11534	0,103605	0,085185
846,7	0,096	0,115355	0,10369	0,08512
851,7	0,0961	0,115465	0,10377	0,08508
856,7	0,0962	0,115655	0,10385	0,08506
861,7	0,09635	0,11589	0,103885	0,08503
866,7	0,0965	0,116105	0,10393	0,085025
871,7	0,09665	0,116295	0,10394	0,08501
876,8	0,0968	0,11646	0,104005	0,08501
881,8	0,09685	0,11661	0,104125	0,08512
886,8	0,09695	0,11673	0,1042	0,085155
891,8	0,09695	0,11683	0,10431	0,08527
896,8	0,09705	0,116915	0,10441	0,085355
901,8	0,09705	0,116985	0,104545	0,08552
906,8	0,0971	0,11704	0,10463	0,08583
911,8	0,09715	0,11707	0,10473	0,08613

916,8	0,0972	0,11704	0,10485	0,086365
921,8	0,0972	0,11692	0,104975	0,0865
926,8	0,09725	0,116755	0,10509	0,086645
931,9	0,0973	0,116665	0,105185	0,086725
936,9	0,09735	0,11673	0,10532	0,086825
941,9	0,0974	0,116915	0,10541	0,086935
946,9	0,09755	0,117165	0,105505	0,087035
951,9	0,09765	0,11741	0,105605	0,087115
956,9	0,09775	0,11761	0,105715	0,087195
961,9	0,09785	0,117755	0,105765	0,087235
966,9	0,09795	0,117845	0,105815	0,087345
971,9	0,09805	0,11788	0,105865	0,08746
977	0,0981	0,11788	0,105915	0,08752
982	0,09815	0,11786	0,10596	0,08761
987	0,0982	0,117825	0,10605	0,087695
992	0,0983	0,117775	0,10608	0,087775
997	0,09835	0,117705	0,10615	0,08791
1002	0,0984	0,117655	0,10612	0,08803
1007	0,0984	0,11767	0,106135	0,088075
1012	0,0984	0,11772	0,106095	0,088105
1017	0,09845	0,11776	0,10605	0,088195
1022	0,0985	0,117785	0,10606	0,088255
1027	0,09845	0,117795	0,106075	0,088365
1032	0,0985	0,117825	0,106155	0,088535
1037	0,09855	0,117875	0,10624	0,088705
1042	0,09855	0,117885	0,10628	0,088855
1047	0,0986	0,117835	0,10632	0,08899
1052	0,09855	0,11776	0,106365	0,089095
1057	0,09855	0,117755	0,106355	0,089295
1062	0,0985	0,11785	0,10639	0,08942
1067	0,0985	0,118005	0,10643	0,08959
1072	0,0985	0,118135	0,10649	0,089745
1077	0,09855	0,11822	0,106615	0,089905
1082	0,0986	0,118255	0,106755	0,090105
1087	0,09855	0,11828	0,10689	0,090245
1092	0,0986	0,118275	0,106955	0,09032
1097	0,0986	0,11823	0,10699	0,090345
1102	0,09865	0,118145	0,107005	0,090375
1107	0,09865	0,117985	0,10695	0,090425
1112	0,0987	0,11776	0,106935	0,09041
1117	0,0986	0,11747	0,10692	0,09042
1122	0,09845	0,11715	0,10692	0,090485
1127	0,0984	0,11686	0,106935	0,09048
1132	0,09845	0,1167	0,10692	0,09055
1137	0,0986	0,1167	0,106965	0,090555
1142	0,0987	0,11683	0,106965	0,090655

1147	0,09875	0,117015	0,107065	0,090725
1152	0,09885	0,117215	0,107125	0,090775
1157	0,09885	0,117405	0,10718	0,09084
1162	0,0989	0,117575	0,107235	0,09088
1167	0,0989	0,11775	0,107335	0,090895
1172	0,099	0,1179	0,107385	0,0909
1177	0,099	0,118045	0,107435	0,090915
1182	0,09905	0,1182	0,10747	0,090885
1187	0,099	0,11834	0,107455	0,09087
1192	0,099	0,118435	0,10739	0,09086
1197	0,0989	0,11846	0,10739	0,090805
1202	0,0989	0,11839	0,107345	0,09084

Appendix B

Cyclic voltammetry measurements

B1: Raw data for cyclic voltammograms for $PdTe_2$- $Na_2S_2O_3$ (5SPW)

Buffer		SIBX		$Na_2S_2O_3$-5SPW		$Na_2S_2O_3$-5SPW+SIBX	
Potential/V	Current density/µA/cm^2	Potential/V	Current density/µA/cm^2	Potential/V	Current density/µA/cm^2	Potential/V	Current density/µA/cm^2
3,17E-02	-3,71E+01	-1,36E-01	-3,47E+01	-8,85E-03	-2,55E+01	-1,55E-01	-3,13E+01
3,37E-02	-3,80E+01	-1,34E-01	-3,31E+01	-6,90E-03	-2,34E+01	-1,53E-01	-3,04E+01
3,58E-02	-3,67E+01	-1,32E-01	-3,45E+01	-4,80E-03	-2,58E+01	-1,51E-01	-2,94E+01
3,77E-02	-3,82E+01	-1,30E-01	-3,37E+01	-2,74E-03	-2,55E+01	-1,49E-01	-2,93E+01
3,97E-02	-3,62E+01	-1,28E-01	-3,30E+01	-8,46E-04	-2,47E+01	-1,47E-01	-2,90E+01
4,16E-02	-3,60E+01	-1,26E-01	-3,21E+01	1,21E-03	-2,59E+01	-1,45E-01	-2,85E+01
4,37E-02	-3,65E+01	-1,24E-01	-3,10E+01	3,22E-03	-2,51E+01	-1,43E-01	-2,92E+01
4,57E-02	-3,63E+01	-1,22E-01	-3,08E+01	5,29E-03	-2,33E+01	-1,41E-01	-2,96E+01
4,77E-02	-3,63E+01	-1,20E-01	-2,97E+01	7,23E-03	-2,49E+01	-1,39E-01	-2,84E+01
4,96E-02	-3,67E+01	-1,18E-01	-3,09E+01	9,25E-03	-2,38E+01	-1,37E-01	-2,92E+01
5,17E-02	-3,58E+01	-1,16E-01	-2,93E+01	1,13E-02	-2,49E+01	-1,35E-01	-2,85E+01
5,37E-02	-3,60E+01	-1,14E-01	-3,02E+01	1,32E-02	-2,40E+01	-1,33E-01	-2,69E+01
5,57E-02	-3,54E+01	-1,12E-01	-3,07E+01	1,51E-02	-2,37E+01	-1,31E-01	-2,75E+01
5,77E-02	-3,42E+01	-1,10E-01	-3,00E+01	1,71E-02	-2,49E+01	-1,29E-01	-2,75E+01
5,97E-02	-3,49E+01	-1,08E-01	-3,05E+01	1,92E-02	-2,47E+01	-1,27E-01	-2,62E+01
6,17E-02	-3,35E+01	-1,06E-01	-3,07E+01	2,12E-02	-2,56E+01	-1,25E-01	-2,63E+01
6,37E-02	-3,29E+01	-1,04E-01	-3,00E+01	2,31E-02	-2,50E+01	-1,23E-01	-2,60E+01
6,56E-02	-3,19E+01	-1,02E-01	-3,06E+01	2,51E-02	-2,38E+01	-1,21E-01	-2,73E+01
6,76E-02	-3,16E+01	-1,00E-01	-2,95E+01	2,72E-02	-2,47E+01	-1,19E-01	-2,61E+01
6,97E-02	-3,09E+01	-9,80E-02	-3,09E+01	2,92E-02	-2,33E+01	-1,17E-01	-2,63E+01
7,16E-02	-3,04E+01	-9,60E-02	-3,17E+01	3,12E-02	-2,24E+01	-1,15E-01	-2,62E+01
7,36E-02	-2,85E+01	-9,40E-02	-3,08E+01	3,32E-02	-2,47E+01	-1,13E-01	-2,70E+01
7,57E-02	-2,89E+01	-9,20E-02	-3,22E+01	3,52E-02	-2,32E+01	-1,11E-01	-2,60E+01
7,77E-02	-2,81E+01	-9,00E-02	-3,09E+01	3,72E-02	-2,46E+01	-1,09E-01	-2,63E+01
7,97E-02	-2,76E+01	-8,80E-02	-2,96E+01	3,91E-02	-2,45E+01	-1,07E-01	-2,54E+01
8,16E-02	-2,70E+01	-8,60E-02	-2,96E+01	4,10E-02	-2,32E+01	-1,05E-01	-2,41E+01
8,37E-02	-2,78E+01	-8,41E-02	-3,07E+01	4,32E-02	-2,34E+01	-1,03E-01	-2,42E+01
8,57E-02	-2,71E+01	-8,20E-02	-2,96E+01	4,52E-02	-2,32E+01	-1,01E-01	-2,40E+01
8,77E-02	-2,56E+01	-8,01E-02	-3,20E+01	4,71E-02	-2,32E+01	-9,89E-02	-2,27E+01
8,96E-02	-2,48E+01	-7,80E-02	-3,21E+01	4,91E-02	-2,28E+01	-9,69E-02	-2,27E+01
9,16E-02	-2,31E+01	-7,60E-02	-3,15E+01	5,12E-02	-2,16E+01	-9,48E-02	-2,23E+01
9,36E-02	-2,17E+01	-7,40E-02	-3,08E+01	5,32E-02	-2,30E+01	-9,29E-02	-2,15E+01
9,56E-02	-2,01E+01	-7,20E-02	-3,09E+01	5,51E-02	-2,11E+01	-9,09E-02	-2,35E+01

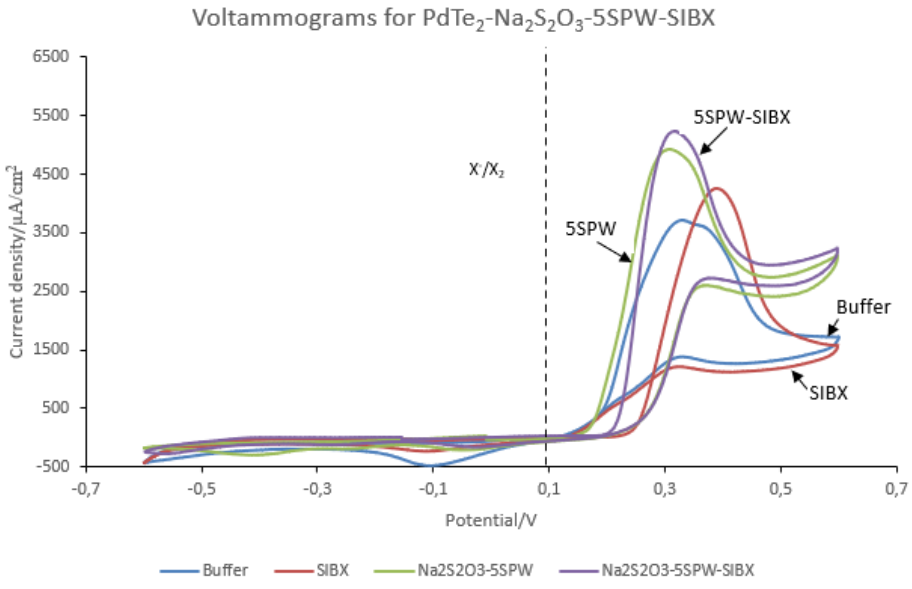

B2: Voltammograms for $PdTe_2$-$Na_2S_2O_3$ (5SPW)

Appendix C

Calculations for surface coverage of SIBX on $PdTe_2$

The area under the reduction peaks for the cyclic voltammograms generated in this study, were integrated using the Gamry software, Echem Analyst 2. The limits of integration are defined by the equation below:

$$\frac{Q}{A_{mineral}} = \int_0^t Current\ density\ dt$$

Where Q represents charge transfer in Coulombs and $A_{mineral}$ represents the surface area of mineral surface ($PdTe_2$) in cm^2.

- The collector coverage is determined by the formula Γ/Γ_m

Where **Γ** is the number of moles covering the surface, which is calculated by the formula:

$$\Gamma = Q/nF$$

Where n represents the number of electrons transferred from the collector molecule to the mineral surface and F is the Faraday's constant 9.6485×10^{-4} C/mol.

Γ_m is the total surface coverage of a monolayer. It is represented by the formula:

$$\Gamma_m = A_{mineral}/(A_{collector} * Avogadro's\ number)$$

Where $A_{mineral}$ represents the area of the mineral surface = 0.140 cm^2, $A_{collector}$ represents the area covered by a single collector molecule, in the case of SIBX = 42.3 $Å^2$ = 42.3×10^{-16} cm^2 and the $Avogadro's\ number$ 6.02214×10^{23} mol^{-1}.

C1: Surface coverages of SIBX on $PdTe_2$ in the absence and presence of salts at various ionic strengths

Condition	Charge (μC)	Γ (mols)	Coverage ($^{\Gamma}/_{\Gamma_m}$)
SIBX only	-875.7	4×10^{-9}	**82.57**
$Na_2S_2O_3$ (1SPW)+SIBX	-452.2	2×10^{-9}	**37.59**
$Na_2S_2O_3$ (3SPW)+SIBX	-400.2	2×10^{-9}	**37.59**
$Na_2S_2O_3$ (5SPW)+SIBX	-259.5	1×10^{-9}	**18.80**
$Na_2S_2O_3$ (10SPW)+SIBX	-277.2	1×10^{-9}	**18.80**
$CaCl_2$ (1SPW)+SIBX	-238.1	1×10^{-9}	**18.80**
$CaCl_2$ (3SPW)+SIBX	-173.3	8.98×10^{-10}	**16.88**
$CaCl_2$ (5SPW)+SIBX	-143.6	7.44×10^{-10}	**13.99**
$CaCl_2$ (10SPW)+SIBX	-185.4	9.61×10^{-10}	**18.06**
$MgSO_4$ (1SPW)+SIBX	-340.1	1×10^{-9}	**18.80**
$MgSO_4$ (3SPW)+SIBX	-470.4	2×10^{-9}	**37.59**
$MgSO_4$ (5SPW)+SIBX	-458.6	2×10^{-9}	**37.59**
$MgSO_4$ (10SPW)+SIBX	-368.4	1×10^{-9}	**18.80**
$MgCl_2$ (1SPW)+SIBX	-401.5	2×10^{-9}	**37.59**
$MgCl_2$ (3SPW)+SIBX	-347.9	1×10^{-9}	**18.80**
$MgCl_2$ (5SPW)+SIBX	-401.3	2×10^{-9}	**37.59**
$MgCl_2$ (10SPW)+SIBX	-490.7	2×10^{-9}	**37.59**
NaCl (1SPW)+SIBX	-1226.2	6×10^{-9}	**112.78**
NaCl (3SPW)+SIBX	-798.4	4×10^{-9}	**75.19**
NaCl (5SPW)+SIBX	-2197	1.1×10^{-8}	**206.77**
NaCl (10SPW)+SIBX	-854	4×10^{-9}	**75.19**

Appendix D

Electrochemical Impedance Spectroscopy:

D1: Impedance for $PdTe_2$ in all salts investigated at 10SPW+SIBX

	Zmod (Ohms/cm2)					
Log Frequency (Hz)	SIBX	Na2S2O3 (10SPW)+SIBX	MgSO4 (10SPW)+SIBX	MgCl2 (10SPW)+SIBX	CaCl2 (10SPW)+SIBX	NaCl (10SPW)+SIBX
5,000434077	850	159,0714286	198,5714286	151,1428571	146,7142857	205,2857143
4,900093902	864,2857	157,7857143	206,1428571	146,5	156	150
4,800304578	880,7143	168,5714286	220,4285714	156,8571429	154,2142857	220,0714286
4,700703717	899,2857	172,6428571	236,1428571	157,1428571	161	179,6428571
4,600864036	919,2857	183,3571429	254,9285714	160,7857143	168,5	200,5714286
4,500236475	944,2857	201	276,6428571	172,7857143	179,7142857	224,4285714
4,400883216	969,2857	226,7857143	297,7142857	182,8571429	192,8571429	250,1428571
4,301464073	997,1429	255,5	325,8571429	199,7857143	223,6428571	279,5714286
4,201123897	1022,143	289,9285714	353,4285714	220,5	249,4285714	315,2142857
4,100715087	1047,857	334,5	384,8571429	241,4285714	284,3571429	355,7142857
4,003460532	1077,857	385	421,4285714	267,6428571	322,3571429	402,3571429
3,903957709	1107,857	453,5714286	467,9285714	301,6428571	373,9285714	461,5
3,80126647	1147,857	544,7142857	527,7857143	336,4285714	444,3571429	544,1428571
3,700357528	1192,143	657,9285714	607,8571429	384,7142857	528,7857143	645,6428571
3,60031933	1259,286	802,1428571	711,5	442,7857143	634,1428571	770
3,501196242	1367,143	983,5714286	840,7142857	516,5714286	767,8571429	934,2857143
3,40277707	1460,714	1205,714286	1006,428571	605,8571429	933,5714286	1139,285714
3,29578694	1663,571	1500,714286	1234,285714	723,5714286	1139,285714	1407,142857
3,198106999	1850	1646,428571	1515,714286	860	1406,428571	1693,571429
3,102433706	2165,714	2263,571429	1749,285714	1022,142857	1721,428571	2065,714286
2,999261071	2537,857	2831,428571	2379,285714	1227,857143	2107,857143	2679,285714
2,901403827	2979,286	3485	2761,428571	1412,142857	2614,285714	3170,714286
2,797821311	3535	4123,571429	3346,428571	1787,142857	3248,571429	3879,285714
2,70372116	4280	5222,857143	4073,571429	2131,428571	3932,857143	4694,285714
2,599883072	5220,714	6474,285714	5028,571429	2601,428571	4857,857143	5787,142857
2,498999364	6356,429	7964,285714	6167,857143	3138,571429	5959,285714	7087,142857
2,402089351	7700	9714,285714	7507,142857	3762,857143	7242,857143	8607,142857
2,297979244	9464,286	12000	9242,857143	4577,857143	8935,714286	10571,42857
2,199755177	11514,29	14635,71429	11264,28571	5509,285714	10864,28571	12835,71429
2,098989639	14078,57	17878,57143	13757,14286	6656,428571	13242,85714	15635,71429
2,001733713	17071,43	21664,28571	16678,57143	7985,714286	16035,71429	18857,14286
1,897627091	21007,14	26507,14286	20428,57143	9700	19607,14286	23035,71429
1,801678059	25407,14	31828,57143	24642,85714	11614,28571	23585,71429	27592,85714
1,697839368	31092,86	38485,71429	30042,85714	14121,42857	28892,85714	33478,57143
1,59900924	37785,71	46300	36121,42857	16871,42857	34464,28571	40142,85714
1,500648063	45650	55157,14286	43485,71429	20192,85714	41235,71429	47957,14286
1,396722279	55635,71	65957,14286	52635,71429	24378,57143	49750	57928,57143
1,297979244	67300	78357,14286	62921,42857	29171,42857	59450	68871,42857
1,199755177	80357,14	91928,57143	74571,42857	34635,71429	70557,14286	81785,71429
1,093421685	97285,71	108714,2857	90000	41600	84928,57143	98500
0,996992982	115000	126785,7143	106071,4286	49571,42857	101142,8571	115785,7143
0,900093902	136357,1	146000	124285,7143	58242,85714	118357,1429	136071,4286
0,800510877	163142,9	169000	147285,7143	68185,71429	139785,7143	159142,8571
0,69966432	193357,1	196142,8571	173428,5714	80285,71429	164928,5714	187428,5714
0,596157081	228642,9	227071,4286	204214,2857	94500	194571,4286	220214,2857
0,499549626	266357,1	260357,1429	236571,4286	109428,5714	227714,2857	256285,7143
0,398634325	311428,6	300142,8571	276071,4286	127500	266142,8571	297571,4286
0,300595484	359357,1	343500	319500	146285,7143	309357,1429	344714,2857
0,200029267	415357,1	394214,2857	368928,5714	167857,1429	359785,7143	396714,2857
0,102776615	474642,9	449071,4286	424928,5714	190928,5714	413428,5714	455000
-0,000434512	544928,6	515642,8571	487857,1429	218214,2857	476285,7143	523285,7143
-0,101110344	623071,4	590928,5714	561000	248928,5714	541500	592642,8571
-0,198321941	704500	670071,4286	638357,1429	281714,2857	615928,5714	667071,4286
-0,297569464	799285,7	765714,2857	714214,2857	320642,8571	700214,2857	751428,5714
-0,397289055	905714,3	872857,1429	814285,7143	358071,4286	783571,4286	835714,2857
-0,499351937	1030714	977142,8571	920714,2857	406571,4286	880000	931428,5714
-0,598599459	1177143	1110000	1018571,429	465928,5714	987857,1429	1026428,571
-0,698319051	1321429	1237142,857	1141428,571	527928,5714	1122857,143	1138571,429
-0,798876103	1512143	1403571,429	1264285,714	608714,2857	1227142,857	1271428,571
-0,899629455	1725000	1590000	1421428,571	701642,8571	1382142,857	1389285,714
-0,999132278	1976429	1755000	1582857,143	806428,5714	1525000	1531428,571
-1,099906098	2286429	1974285,714	1782857,143	934285,7143	1712857,143	1677857,143
-1,199489123	2600714	2202142,857	1985714,286	1099285,714	1939285,714	1850000
-1,299902295	2975714	2457857,143	2220714,286	1229285,714	2170000	2037857,143
-1,399789694	3392143	2702857,143	2605000	1481428,571	2433571,429	2278571,429
-1,499900808	3892857	3021428,571	2995000	1736428,571	2745714,286	2577142,857
-1,599980365	4496429	3374285,714	3437142,857	1930714,286	3123571,429	2947142,857
-1,699839463	5229286	3757142,857	3962857,143	2285000	3459285,714	3330000
-1,799970733	6116429	4157142,857	4647142,857	2660000	3999285,714	3874285,714
-1,89997427	7214286	4570714,286	5398571,429	3097142,857	4520714,286	4470000
-2	8550000	5059285,714	6107857,143	3515714,286	5111428,571	5190714,286

D2: Phase angles for $PdTe_2$ in all salts investigated at 10SPW+SIBX

	Phase Angle (°)					
Log Frequency (Hz)	SIBX	Na2S2O3 (10SPW)+SIBX	MgSO4 (10SPW)+SIBX	MgCl2 (10SPW)+SIBX	CaCl2 (10SPW)+SIBX	NaCl (10SPW)+SIBX
5,000434077	5,972	14,8	21,06	10,44	13,62	12,09
4,900093902	7,454	19,77	23,03	14,35	14,44	32,72
4,800304578	8,361	21,09	25,86	14,54	19,19	16,63
4,700703717	9,332	26,93	28,2	19,13	22,66	37,27
4,600864036	10,24	31,16	30,42	21,66	26,59	39,09
4,500236475	11,11	52,14	32,05	24,86	31,11	41,02
4,400883216	12,15	53,29	34,13	27,78	35,34	42,46
4,301464073	12,86	54,82	35,92	44,58	55,19	45,51
4,201123897	14,08	57,03	38,14	45,12	56,55	45,46
4,100715087	15,52	59,86	40,82	45,88	58,06	48,81
4,003460532	17,08	62,75	43,9	47,67	60,62	51,11
3,903957709	19,48	65,82	47,66	50,08	63,28	54,06
3,80126647	22,49	69,53	51,8	52,25	66,01	57,34
3,700357528	25,87	71,33	56,07	54,79	68,61	60,87
3,60031933	29,34	73,67	60,03	57,63	70,87	63,93
3,501196242	33,21	75,84	63,63	59,83	72,9	66,6
3,40277707	38,42	76,93	66,69	62,07	74,48	68,81
3,29578694	44,31	77,7	69,76	64,16	75,99	70,99
3,198106999	49,24	78,29	74,47	65,75	76,71	73,68
3,102433706	54,18	78,88	73,58	67,2	77,53	72,92
2,999261071	58,37	78,89	75,33	68,62	82,69	74,34
2,901403827	61,71	80,14	75,08	69,97	79,3	75,17
2,797821311	64,76	79,93	76,53	70,01	79,04	75
2,70372116	67,47	79,7	76,89	70,77	78,76	75,81
2,599883072	69,6	79,38	77,12	71,34	78,65	75,93
2,498999364	71,23	78,94	77,18	71,62	78,41	75,94
2,402089351	72,44	78,43	77,07	71,81	78,09	75,88
2,297979244	73,35	77,76	76,83	71,9	77,71	75,65
2,199755177	73,97	77,02	76,47	71,88	77,23	75,43
2,098989639	74,33	76,13	76,03	71,76	76,67	75,09
2,001733713	74,47	75,22	75,45	71,62	76,04	74,74
1,897627091	74,43	74,08	74,82	71,27	75,41	74,24
1,801678059	74,24	72,87	74,12	70,88	74,69	73,74
1,697839368	74,12	71,37	72,89	70,2	73,66	73,68
1,59900924	73,31	70,15	72,36	69,83	73,12	72,54
1,500648063	72,64	68,69	71,35	69,23	72,23	71,88
1,396722279	71,79	67,2	70,36	68,43	71,41	71,06
1,297979244	70,68	65,79	69,18	67,25	70,79	70,2
1,199755177	69,81	64,25	67,95	66,57	69,82	69,15
1,093421685	69	62,77	66,52	65,46	68,61	68,39
0,996992982	67,24	61,36	65,81	64,28	67,98	66,94
0,900093902	66,05	59,57	64,2	63,11	66,29	65,89
0,800510877	64,46	58,75	62,8	61,71	65,51	64,95
0,69966432	62,86	57,52	61,47	60,28	64,38	63,64
0,596157081	61,17	56,57	60,03	58,62	63,2	62,08
0,499549626	59,44	55,69	58,49	57,08	61,79	60,64
0,398634325	57,61	54,73	57,02	55,5	60,37	58,84
0,300595484	55,74	53,67	55,56	53,66	58,74	57,14
0,200029267	53,98	52,73	53,89	52,17	57,29	55,32
0,102776615	52,28	51,82	52,25	50,39	55,57	53,15
-0,000434512	50,57	50,54	50,43	49,1	53,13	50,58
-0,101110344	48,93	49,38	48,09	46,65	51,09	48,64
-0,198321941	47,21	48,11	46,34	45,94	49,17	46,06
-0,297569464	45,85	46,85	43,96	44,94	46,99	43,52
-0,397289055	44,51	45,35	41,95	43,64	44,88	41,3
-0,499351937	42,9	43,59	40,01	41,69	42,48	38,96
-0,598599459	41,54	41,45	37,19	41,55	41,41	36,95
-0,698319051	40,04	39,49	35,62	40,73	38,44	34,6
-0,798876103	38,9	37,2	34,25	39,25	37,51	32,2
-0,899629455	37,08	35,11	32,52	38,76	35,33	31,11
-0,999132278	35,84	33,1	29,97	37,6	33,72	29,63
-1,099906098	34,36	31,53	27,67	37,07	32,69	27,83
-1,199489123	32,76	29,28	25,98	36,03	31,61	25,86
-1,299902295	31,59	27,04	24,92	36,8	29,83	24,75
-1,399789694	29,98	25,17	23,51	33,72	28,5	23,36
-1,499900808	28,54	23,34	22,21	34,86	27,95	22,22
-1,599980365	27,05	21,63	20,98	32,2	26,95	20,59
-1,699839463	26,01	19,98	19,54	31,72	24,86	18,99
-1,799970733	24,33	18,05	18,14	29,96	22,99	17,64
-1,89997427	23,21	16,47	16,86	27,14	20,79	16,35
-2	22,03	14,6	15,44	25,35	18,82	15,01